DIABETES, HYPERTENSION AND CARDIOVASCULAR DISEASES

EDITED BY: Soo-Kyoung Choi, Modar Kassan and Asunción Morán Morán
PUBLISHED IN: Frontiers in Cardiovascular Medicine and Frontiers in Physiology

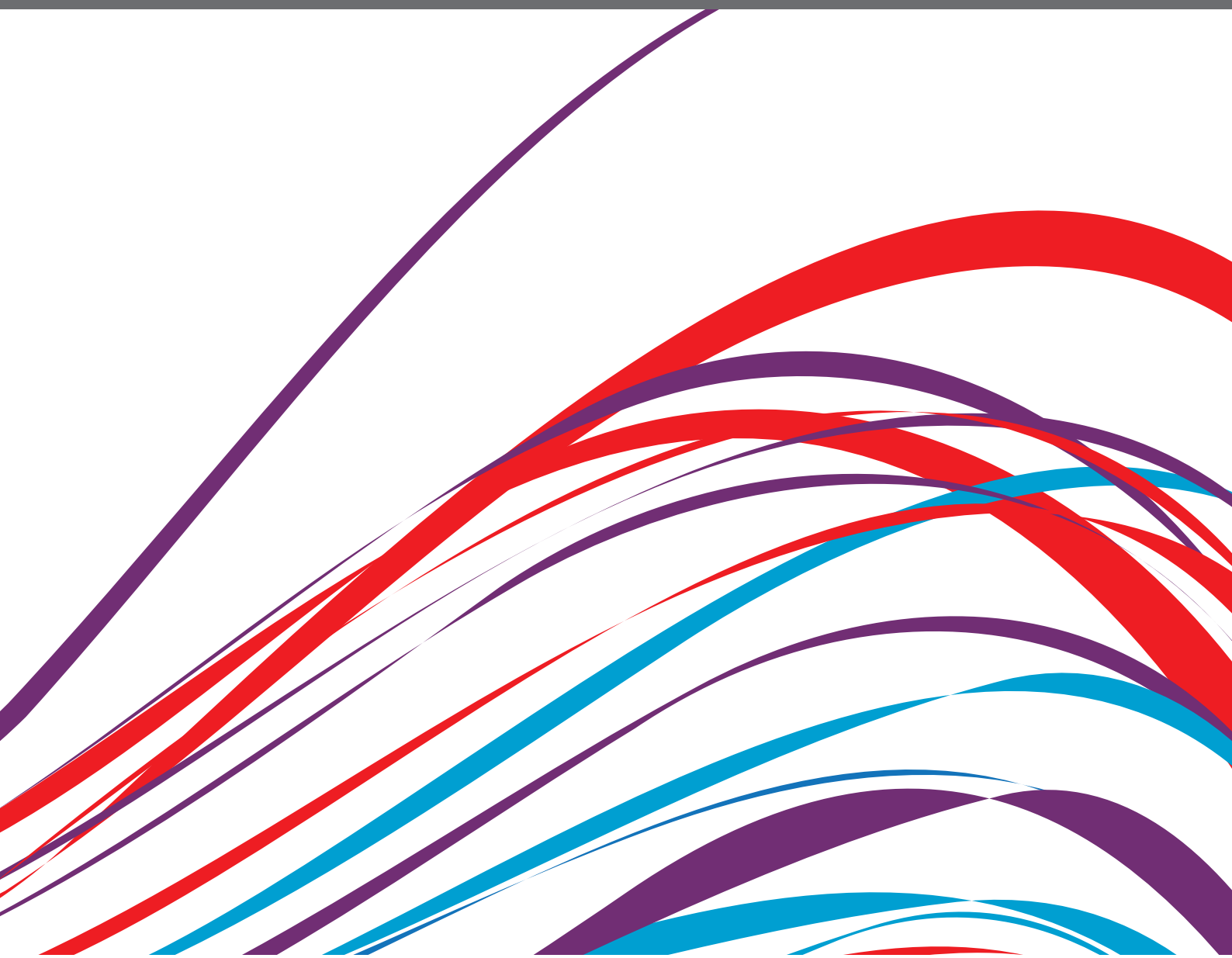

frontiers Research Topics

frontiers

ISSN 1664-8714
ISBN 978-2-88971-865-8
DOI 10.3389/978-2-88971-865-8

About Frontiers

Frontiers is more than just an open-access publisher of scholarly articles: it is a pioneering approach to the world of academia, radically improving the way scholarly research is managed. The grand vision of Frontiers is a world where all people have an equal opportunity to seek, share and generate knowledge. Frontiers provides immediate and permanent online open access to all its publications, but this alone is not enough to realize our grand goals.

Frontiers Journal Series

The Frontiers Journal Series is a multi-tier and interdisciplinary set of open-access, online journals, promising a paradigm shift from the current review, selection and dissemination processes in academic publishing. All Frontiers journals are driven by researchers for researchers; therefore, they constitute a service to the scholarly community. At the same time, the Frontiers Journal Series operates on a revolutionary invention, the tiered publishing system, initially addressing specific communities of scholars, and gradually climbing up to broader public understanding, thus serving the interests of the lay society, too.

Dedication to Quality

Each Frontiers article is a landmark of the highest quality, thanks to genuinely collaborative interactions between authors and review editors, who include some of the world's best academicians. Research must be certified by peers before entering a stream of knowledge that may eventually reach the public - and shape society; therefore, Frontiers only applies the most rigorous and unbiased reviews.
Frontiers revolutionizes research publishing by freely delivering the most outstanding research, evaluated with no bias from both the academic and social point of view. By applying the most advanced information technologies, Frontiers is catapulting scholarly publishing into a new generation.

What are Frontiers Research Topics?

Frontiers Research Topics are very popular trademarks of the Frontiers Journals Series: they are collections of at least ten articles, all centered on a particular subject. With their unique mix of varied contributions from Original Research to Review Articles, Frontiers Research Topics unify the most influential researchers, the latest key findings and historical advances in a hot research area! Find out more on how to host your own Frontiers Research Topic or contribute to one as an author by contacting the Frontiers Editorial Office: frontiersin.org/about/contact

DIABETES, HYPERTENSION AND CARDIOVASCULAR DISEASES

Topic Editors:
Soo-Kyoung Choi, Yonsei University College of Medicine, South Korea
Modar Kassan, University of Tennessee Health Science Center (UTHSC), United States
Asunción Morán Morán, University of Salamanca, Spain

Citation: Choi, S.-K., Kassan, M., Morán, A. M., eds. (2021). Diabetes, Hypertension and Cardiovascular Diseases. Lausanne: Frontiers Media SA.
doi: 10.3389/978-2-88971-865-8

Table of Contents

frontiers in Physiology

EDITORIAL
published: 22 October 2021
doi: 10.3389/fphys.2021.765767

Editorial: Diabetes, Hypertension and Cardiovascular Diseases

*Soo-Kyoung Choi**

Department of Physiology, Yonsei University College of Medicine, Seoul, South Korea

Keywords: diabetes, hypertension, type 2 diabetes, cardiovascular diseases, cardiovascular dysfunction

Editorial on the Research Topic

Diabetes, Hypertension and Cardiovascular Diseases

Hypertension and diabetes are common comorbidities and associated with risk of life-threatening cardiovascular diseases (CVD). The prevalence of type 2 diabetes (T2D) continues to increase worldwide. According to World Health Organization (WHO), the number of cases of T2D has risen from 108 million in 1980 to 422 million in 2014 and is expected to grow to 642 million by 2040. Hypertension is more common, rising in prevalence with a recent estimate of 1.39 billion cases. Diabetes and hypertension are both associated with microvascular and macrovascular diseases and closely related due to similar risk factors such as endothelial dysfunction, vascular inflammation, arterial remodeling, atherosclerosis, dyslipidemia, and obesity. The aim of this special issue was to provide novel perspectives to the pathophysiological features of cardiovascular complications associated with diabetes and hypertension. We encouraged researchers to submit the articles approaching the topic in basic, translational and clinical aspects. Indeed, this special Research Topic collates 13 articles (10 original research articles, 2 review articles, and 1 opinion) showing the relevance between cardiovascular diseases, diabetes and hypertension in various perspectives.

The topic includes two articles that deal with pathophysiology in different animal model of diabetes (genetic and chemically induced model) which are streptozotocin (STZ)—induced diabetic mice and db^{-}/db^{-} mice. The original article by Guerrero et al. showed that STZ-induced diabetic mice had higher urinary α-ketoglutarate (α-KG) and pro-renin receptor (PRR) expression along with augmented urinary angiotensin II (AngII) level and Na^{+} retention. They found that STZ-induced diabetic mice treated with montelukast (ML), receptor of α-KG (OXGR1) antagonist, did not show all these effects. They also reported that primary cultured inner medullary collecting duct (CD) cells treated with high glucose (HG) showed increased PRR expression, while OXGR1 antagonist prevented this effect. Their findings suggest this signaling pathway contributes to intratubular generation of AngII impacting on Na^{2+} handling.

Diabetic cardiomyopathy is characterized by structural and functional alterations of the heart. In this special issue, Pappritz et al. reported that $CD362^{+}$ mesenchymal stromal cell (MSC) application decreased cardiomyocyte stiffness and increased arteriole density, which correlated with increased myocardial nitric oxide (NO) and cyclic guanosine monophosphate (cGMP) levels in leptin receptor deficient db^{-}/db^{-} mice. However, the degree in improvement of cardiomyocyte

OPEN ACCESS

Edited and reviewed by:
Gerald A. Meininger,
University of Missouri, United States

***Correspondence:**
Soo-Kyoung Choi
skchoi@yuhs.ac

Specialty section:
This article was submitted to Vascular Physiology, a section of the journal Frontiers in Physiology

Received: *27 August 2021*
Accepted: *27 September 2021*
Published: *22 October 2021*

Citation:
Choi S-K (2021) Editorial: Diabetes, Hypertension and Cardiovascular Diseases. Front. Physiol. 12:765767. doi: 10.3389/fphys.2021.765767

stiffness following $CD362^{+}$ MSC application was insufficient to improve diastolic function. These findings could contribute to understand the mechanism of diabetic cardiomyopathy.

Hypertension is one of the most important risk factors in heart failure. Pressure overload-induced cardiac hypertrophy is one of the main characteristics of cardiac remodeling which contributes to development of heart failure. The transverse aortic constriction model is well-known disease model to study pressure overload-induced cardiac hypertrophy and heart failure. In the present topic, Deng et al. showed mice subjected to 27G transverse aortic constriction (TAC) had severe cardiac dysfunction, severe cardiac fibrosis, and exhibited characteristics of heart failure at 4 weeks post-TAC. Compared with 27G TAC mice, 26G TAC mice showed a much milder response in cardiac dysfunction and cardiac fibrosis, and a very small fraction of the 26G TAC group exhibited characteristics of heart failure. They concluded that different degrees of TAC induce distinct phenotypes in C57BL/6N mice. Their results will provide important reference value especially for researchers who conduct pressure overload–induced cardiac hypertrophy studies using C57BL/6N mice or genetically modified mice with a C57BL/6N background. Endothelial dysfunction is closely associated with diabetes and hypertension. Thus, understanding the mechanism of endothelial dysfunction could contribute to identifying the targets for these diseases. In the special issue, Osman et al. reported that endoplasmic reticulum (ER) stress-generated microparticles (MPs) impaired angiogenic capacity of human umbilical endothelial cells (HUVECs) and reduced nitric oxide (NO) release, indicating an impaired endothelial function. These findings are clinically relevant as they will help in the process of identifying new therapeutic targets against MPs produced in conditions characterized by the activation of ER stress such as diabetes, obesity and metabolic syndrome.

On the other hand, Cho et al. reported the role of thromboxane A2 receptor-mediated signaling in the pathophysiology of pulmonary arterial hypertension (PAH) in this special issue. They showed the attenuation of nitric oxide (NO)/ cyclic guanosine mono phosphate (cGMP) signaling and the upregulation of (ROCK2) increase the sensitivity to thromboxane A2 (TXA2) in the pulmonary arterial hypertension (PAH) animal, which might have pathophysiological implications in patients with PAH. Their findings provide valuable information to understand the mechanism of pulmonary hypertension.

In this special issue, we tried to show various studies in different point of view regarding the topic, we even showed gestational diabetes mellitus (GDM) and hypertensive disorders (HDP) in HIV infected pregnant women. In the review article, Phoswa described that HIV/AIDS is associated with the pathophysiology of gestational diabetes and hypertensive disorders in of pregnancy. The highly active antiretroviral therapy (HAART) usage increased risk of gestational diabetes in HIV infected pregnancies due to diabetogenic effect by causing dysregulation of progesterone and prolactin and predispose HIV infected women to GDM. This review article helps on improving therapeutic management and understanding of the pathophysiology of GDM and HDP in the absence as well as in the presence of HIV infection by reviewing studies reporting on these mechanisms.

In this special issue, we introduced articles provide various statistical information about risk and prevalence of hypertension. Zhang, et al. reported that lower birth weight is nonlinearly correlated with higher risk of hypertension, and birth weight between 3.43 and 3.80 kg might represent an intervention threshold. Moreover, lower birth weight may interact with adult obesity to significantly increase hypertension risk. Liu et al. reported subclinical atherosclerosis (SCA) was highly prevalent in the hypertension population and the thoracic aorta was the most frequently affected vascular site. Elevated serum uric acid (SUA) concentration was significantly associated with the prevalence and severity of SCA regardless of territories. Ye et al. described the prevalence and associated factors of hypertension and phenotypes in Chinese children and adolescents during 1991–2015. They reported that from 1991 to 2015, the age-standardized prevalence of hypertension and phenotypes in Chinese children and adolescents increased dramatically. Sex and age disparities were found in the prevalence of childhood hypertension and phenotypes. For adolescents aged 13–17 years, general obesity and central obesity were positively associated with hypertension, whereas the South region was a negatively related factor. For diastolic hypertension (IDH), sex, age, location (urban or rural), region (north or south), body mass index (BMI), waist circumference (WC), general obesity, and central obesity were associated factors. Older age group, general obesity and central obesity were related to the increased prevalence of isolated systolic hypertension (ISH), and only general obesity associate with the elevated prevalence of IDH. It provides novel insights into several aspects of the national challenge of childhood hypertension in China. On the other hand, Lin et al. determined that whether long-term intensity of glycemic exposure (IGE) during young adulthood is associated with multiple target organs function at midlife independent of single fasting glucose (FG) measurement. They included 2,859 participants, aged 18–30 years at Y0, in the coronary artery risk development in young adults (CARDIA) Study. They found that higher intensity of glycemic exposure during young adulthood was independently associated with subclinical alterations of target organs function at midlife. Their findings highlight the importance of early screening and management of IGE in youth. Enhanced external counterpulsation (EECP) can improve carotid circulation in patients with coronary artery disease. Zhang et al. investigated the acute effect of EECP on the hemodynamic parameters in the carotid arteries before, during, and immediately after EECP in patients with hypertension, hyperlipidemia, and type 2 diabetes. They found that enhanced EECP created an acute reduction in end-diastolic velocity (EDV), peak systolic velocity (PSV), and systolic/diastolic flow velocity ratio (VS/VD) and an immediate increase in the resistance index (RI), flow rate (FR), and mean inner diameter (ID) of common carotid arteries (CCA) in patients. Additionally, EECP induced the different hemodynamic responses in in

patients with different cardiovascular risk factors, which may provide theoretical guidance for making personalized plans in patients.

The opinion piece by Simko and Baka listed pleiotropic effects of ivabradine. They described that ivabradine has heart rate (HR)- and potential blood pressure (BP) reducing effects associated with target organ protection and the lack of undesirable metabolic and behavioral consequences (often seen with beta-blockers). They suggested ivabradine as a potential treatment for hypertensive patients with elevated HR, especially for those co-afflicted with metabolic disorders.

Recently, fibroblast growth factor-23 (FGF-23) has been identified as a new trigger of cardiac dysfunction. In this special issue, Vázquez-Sánchez et al. provide a review article summarizes current understandings of FGF-23 and focuses on emerging areas of FGF-23 in human cardiac events and its intracellular pathways in cardiomyocytes and fibroblasts. They described that significant changes in FGF-23 secretion induce detrimental effects on cardiac tissue and blocking these effects could be the possible new therapeutic opportunities.

Although this Research Topic has shed some insights on the relevance between cardiovascular diseases, diabetes and hypertension, we regret that we have not provided sufficient knowledge of this field. We currently re-launched the second collection of the articles with the same Research Topic. We hope that the next issue will also cover important studies as the first issue of this topic.

AUTHOR CONTRIBUTIONS

The author confirms being the sole contributor of this work and has approved it for publication.

ACKNOWLEDGMENTS

We sincerely thank all authors, reviewers, and Frontiers editorial staff for their efforts and valuable contributions.

Conflict of Interest: The author declares that the research was conducted in the absence of any commercial or financial relationships that could be construed as a potential conflict of interest.

Publisher's Note: All claims expressed in this article are solely those of the authors and do not necessarily represent those of their affiliated organizations, or those of the publisher, the editors and the reviewers. Any product that may be evaluated in this article, or claim that may be made by its manufacturer, is not guaranteed or endorsed by the publisher.

frontiers in Cardiovascular Medicine

ORIGINAL RESEARCH
published: 10 December 2020
doi: 10.3389/fcvm.2020.584791

Endoplasmic Reticulum (ER) Stress-Generated Extracellular Vesicles (Microparticles) Self-Perpetuate ER Stress and Mediate Endothelial Cell Dysfunction Independently of Cell Survival

*Aisha Osman[1], Heba El-Gamal[1], Mazhar Pasha[1], Asad Zeidan[2], Hesham M. Korashy[1], Shahenda S. Abdelsalam[1], Maram Hasan[1], Tarek Benameur[3] and Abdelali Agouni[1]**

[1] Department of Pharmaceutical Sciences, College of Pharmacy, QU Health, Qatar University, Doha, Qatar, [2] Department of Basic Sciences, College of Medicine, QU Health, Qatar University, Doha, Qatar, [3] College of Medicine, King Faisal University, Al-Ahsa, Saudi Arabia

Circulating extracellular vesicles (EVs) are recognized as biomarkers and effectors of endothelial dysfunction, the initiating step of cardiovascular abnormalities. Among these EVs, microparticles (MPs) are vesicles directly released from the cytoplasmic membrane of activated cells. MPs were shown to induce endothelial dysfunction through the activation of endoplasmic reticulum (ER) stress. However, it is not known whether ER stress can lead to MPs release from endothelial cells and what biological messages are carried by these MPs. Therefore, we aimed to assess the impact of ER stress on MPs shedding from endothelial cells, and to investigate their effects on endothelial cell function. EA.hy926 endothelial cells or human umbilical vein endothelial cells (HUVECs) were treated for 24 h with ER stress inducers, thapsigargin or dithiothreitol (DTT), in the presence or absence of 4-Phenylbutyric acid (PBA), a chemical chaperone to inhibit ER stress. Then, MPs were isolated and used to treat cells (10–20 μg/mL) for 24–48 h before assessing ER stress response, angiogenic capacity, nitric oxide (NO) release, autophagy and apoptosis. ER stress (thapsigargin or DDT)-generated MPs did not differ quantitatively from controls; however, they carried deleterious messages for endothelial function. Exposure of endothelial cells to ER stress-generated MPs increased mRNA and protein expression of key ER stress markers, indicating a vicious circle activation of ER stress. ER stress (thapsigargin)-generated MPs impaired the angiogenic capacity of HUVECs and reduced NO release, indicating an impaired endothelial function. While ER stress (thapsigargin)-generated MPs altered the release of inflammatory cytokines, they did not, however, affect autophagy or apoptosis in HUVECs. This work enhances the general understanding of the deleterious effects carried out by MPs in medical conditions where ER stress is sustainably activated such as diabetes and metabolic syndrome.

Keywords: extracellular vesicles (EVs), microparticles (MPs), endothelial function (dysfunction), apoptosis, cardiovascular disease, ER stress

OPEN ACCESS

Edited by:
Modar Kassan,
The University of Iowa, United States

Reviewed by:
Piyali Chatterjee,
Central Texas Veterans Health Care System, United States
Rabah Iratni,
United Arab Emirates University, United Arab Emirates
Georges Daoud,
American University of Beirut, Lebanon

****Correspondence:***
Abdelali Agouni
aagouni@qu.edu.qa
orcid.org/0000-0002-8363-1582

Specialty section:
This article was submitted to Hypertension, a section of the journal Frontiers in Cardiovascular Medicine

Received: *18 July 2020*
Accepted: *09 November 2020*
Published: *10 December 2020*

Citation:
Osman A, El-Gamal H, Pasha M, Zeidan A, Korashy HM, Abdelsalam SS, Hasan M, Benameur T and Agouni A (2020) Endoplasmic Reticulum (ER) Stress-Generated Extracellular Vesicles (Microparticles) Self-Perpetuate ER Stress and Mediate Endothelial Cell Dysfunction Independently of Cell Survival. Front. Cardiovasc. Med. 7:584791. doi: 10.3389/fcvm.2020.584791

INTRODUCTION

Maintaining optimal vascular homeostasis balance is very critical for the integrity of the cardiovascular tree to prevent the development of cardiovascular co-morbidities particularly prevalent with metabolic diseases such as obesity and diabetes. Achieving balance between relaxing and contracting factors, and between antithrombotic and prothrombotic factors is important for the normal function of the vascular system. These functions are maintained by the endothelium, a thin layer of endothelial cells that line the entire vasculature. Perturbation of endothelial functions in diseases such as diabetes and insulin resistance states disturb this balance leading to a state of endothelial dysfunction, the early step in the process of atherogenesis, resulting in cardiovascular complications in patients with cardiovascular risk factors such as obesity, diabetes and metabolic syndrome (1). Features of endothelial dysfunction in include: (i) impairment of vascular function indicated by reduced nitric oxide (NO) bioavailability, impaired endothelium-dependent smooth muscle relaxation and perturbated angiogenesis; (ii) induction of vascular inflammation marked by increased production of inflammatory mediators and adhesion molecules; and (iii) activation of a prothrombotic state by increasing the production of procoagulant factors and enhancing platelet aggregation.

The mechanisms underlying the development of endothelial dysfunction are not yet fully understood. However, in recent decade, circulating extracellular vesicles (EVs) have emerged as useful biomarkers, predictors and effectors of endothelial dysfunction that is known to be associated with metabolic abnormalities including obesity, diabetes and metabolic syndrome. EVs are typically classified in the literature according to their size and mechanism of biogenesis and release from the cell. The main EVs subtypes are exosomes, apoptotic bodies and microparticles (MPs). Exosomes range in size from 40 to 120 nm and are released from cells by fusion of multivesicular bodies (MVBs) with cell membrane and then MVBs release exosomes to the extracellular environment by exocytosis (2). While apoptotic bodies (size $>$ 1,000 nm) and MPs (size 100–1,000 nm) appear to have similar mechanisms of release which is outward blebbing and shedding of vesicles directly from the plasma membrane of apoptotic or activated cells, respectively (2, 3).

EVs levels, particularly large-sized EVs (MPs) originating from endothelial cells, were found to be altered in patients with metabolic and cardiovascular co-morbidities. Esposito et al. (4) have found CD31+/CD42b– endothelial MPs (EMPs) and CD31+/CD42b+ platelet MPs (PMPs) to be significantly elevated in obese women with concomitant reduction of endothelium-dependent flow mediated vasodilation. EMPs were reported as independent predictors of endothelial dysfunction (4). EMPs (5), and circulating MPs from diabetic patients (6), were found to be deleterious for endothelial cell function. EMPs were reported to be elevated in diabetic patients compared to healthy controls (7). Furthermore, a significant positive correlation between EMPs and glycated hemoglobin (HbA1c) levels was observed, and EMPs were identified as independent predictors of endothelial dysfunction (reduced flow-mediated dilation of brachial artery and elevated brachial ankle pulse wave velocity) in diabetic patients (7). Feng et al. (8) and Ishida et al. (9) showed significantly elevated levels of circulating MPs from endothelial origin in streptozotocin-induced diabetic rats, compared to non-diabetic rats (8, 9).

EVs are key molecular effectors in endothelial dysfunction. In metabolic syndrome patients, endothelial, procoagulant, platelet, and erythrocyte MPs were significantly elevated compared to healthy individuals (10, 11). Agouni et al. (10) reported that EVs derived from metabolic syndrome patients were able to induce endothelial dysfunction both *in vitro* and *in vivo*. Treatment of endothelial cells with metabolic syndrome MPs decreased NO production and increased the phosphorylation of endothelial NO synthase (eNOS) at the inhibitory site (Thr495), while injection of these MPs into mice attenuated vasodilation in response to acetylcholine in aortas (10) and caused a vascular hyporeactivity (12). However, the molecular and cellular mechanisms underpinning the deleterious actions of MPs on endothelial function are still poorly understood.

In recent years, the endoplasmic reticulum (ER) stress response has been identified as a strong molecular bridging link between insulin resistance, inflammation and endothelial dysfunction. The ER is the site for posttranslational folding and synthesis of secretory and transmembrane proteins. Upon various physiological or pathological disturbances that increase protein demand, the accumulation of misfolded or unfolded proteins can occur within the ER lumen, leading to the activation of an adaptive signaling cascade called unfolded protein response (UPR). The UPR is activated to attenuate protein synthesis, increase protein folding capacity and promote degradation of irreversibly misfolded proteins in an attempt to restore ER homeostasis (13). If ER homeostasis is not restored, ER stress response ensues which triggers signaling pathways involved in inflammation and cell apoptosis. Three transmembrane sensors located at the ER membrane: protein kinase R (PKR)-like ER kinase (PERK), inositol-requiring enzyme (IRE)-1α and activating transcription factor (ATF)-6, are activated following their dissociation from the major ER chaperone: immunoglobulin binding protein also known as glucose-regulated protein 78 (BiP/GRP78). BiP becomes thus available in the ER lumen to bind to and correct the misfolded and unfolded polypeptide chains; while the activated transmembrane sensors are involved in UPR downstream signaling pathways (13, 14). Collectively, UPR is a defensive mechanism activated to restore the proper function of the ER. However, upon its prolonged activation, a state of ER stress takes place. ER stress response by itself can result in endothelial dysfunction through various underlying molecular mechanisms including apoptosis, cellular inflammation and oxidative stress (15, 16). ER stress has been shown to be involved in endothelial dysfunction in models of diabetes and insulin resistance (15). Moreover, ER stress is linked to atherosclerosis as it was found to be activated in all stages of atherosclerosis (17). ER stress activation is closely associated with cell death which contributes to endothelial dysfunction (16, 18). ER stress-mediated cell death is linked to the activation of c-Jun N terminal kinase (JNK) and subsequent production of reactive oxygen species and activation of the autophagy (19). More recently, Safiedeen et al. (20) have shown a role for the

activation of ER stress in endothelial dysfunction induced by MPs. Exposure of human aortic endothelial cells to MPs derived from metabolic syndrome patients or apoptotic T-lymphocytes enhanced the expression of several markers associated with the three arms of ER stress (PERK, IRE-1α, and ATF-6) and reduced NO bioavailability. Furthermore, MPs impaired endothelium-dependent vasodilation *in vivo* in mice. All of these actions in cultured cells and mice were reversed in the presence of tauroursodeoxycholic acid (TUDCA), a chemical chaperone known to inhibit ER stress, indicating the strong involvement of ER stress in MP-induced endothelial dysfunction (20).

Although evidence is available about the involvement of ER stress in endothelial cell dysfunction mediated by MPs (20), it is still not known whether the activation of ER stress response is a cause or a consequence of MPs generation. Also, the effects mediated by ER stress-generated MPs on endothelial cell function still need to be investigated. Therefore, the aim of this study was to assess the impact of ER stress activation on MP shedding from endothelial cells, and to investigate their effects on the activation of ER stress itself and endothelial function with special focus on angiogenic capacity, NO release and possible implication of ER stress-mediated cell death and autophagy in the process.

MATERIALS AND METHODS

All experimental work was conducted in line with Qatar University Institutional Biohazard Committee (IBC) policies and guidelines.

Cell Culture and Maintenance

EA.hy926 endothelial cells (ATCC® CRL-2922™, Manassas, USA) were cultured in high glucose (25 mM) Dulbecco's Modified Eagle's Medium (DMEM) (Pan biotech, Aidenbach, Germany) supplemented with 10% fetal bovine serum (FBS; Gibco, Carlsbad, USA), 1% penicillin/ streptomycin (P/S; Gibco), 1% L-glutamine (Gibco) and 1% sodium pyruvate (Gibco). Cells were incubated at 37 and 5% Carbon dioxide (CO_2) in humidified conditions.

Primary Umbilical Vein Endothelial Cells; Normal, Human (HUVECs) (ATCC® PCS100010™) were cultured in Medium 200 (Gibco) supplemented with 2% Low Serum Growth Supplement (LSGS; Gibco) and 1% P/S. Cells were incubated at 37 and 5% Carbon dioxide (CO_2) in humidified conditions. HUVECs were used in experiments up to passage 6.

Cell Treatments

To pharmacologically induce ER stress, cells were either incubated with thapsigargin (TG) (300 nM, 24 h) (ThermoScientific, Waltham, USA), or Dithiothreitol (DTT) (Sigma-Aldrich, Hamburg, Germany) (2 mM, 24 h). The concentrations used in this study for TG and DTT were previously shown to induce ER stress in endothelial cells (18, 21). TG is an inhibitor of sarcoplasmic reticulum/endoplasmic reticulum Ca^{+2}-ATPase (SERCA); SERCA allows the transfer of Ca^{+2} from the cytoplasm to the lumen of the ER. By inhibiting SERCA with TG, the ER will be depleted from Ca^{+2} along with increasing the cytoplasmic Ca^{+2} levels. Ca^{+2} depletion results in losing the activity of Ca^{+2}-dependent chaperones that fix the misfolded and unfolded proteins (22). DTT is a reducing agent that works by reducing disulfide bonds of proteins, thus contributing to ER stress and activation of UPR. To harness the role of ER stress, a chemical chaperone was used to increase ER homeostasis and block ER stress, 4-Phenylbutyric Acid (PBA) (10 mM; Sigma-Aldrich). PBA, at this concentration, was shown to alleviate pharmacologically induced ER stress in endothelial cells (18). For MPs treatments, naïve EA.hy926 and HUVECs cells were stimulated with generated MPs from respective cell line at the concentrations of 10 or 20 μg/ml of medium for 24 or 48 h. Concentrations of MPs used were based on previously published reports (6, 23).

MPs Isolation and Quantification

MPs were isolated from culture media of treated cells (TG or DTT in the presence or absence of PBA) by serial centrifugations at 21,000 × *g* for 45 min at 4°C as described previously by us (23–25). Briefly, first, culture media were collected, and centrifuged at 1,500 × *g* for 20 min at room temperature to remove cell debris. Second, supernatants were aliquoted in Eppendorf tubes after discarding pellets and then centrifuged at 21,000 × *g* for 45 min at 4°C. Third, the supernatants were discarded, and pellets pooled from all tubes from the same treatment condition and transferred to 1 single tube, and then suspended in 1 ml of sterile and cold Phosphate Buffer Saline (PBS). Then, the suspended pellet was washed by two serial centrifugations at 21,000 × *g* for 45 min at 4°C with PBS changed each time to ensure no traces of medium are left. Finally, the supernatant was discarded and the pellet (MPs) was suspended in 300 µl of PBS and stored at 4°C until subsequent use (storage duration did not exceed 1 month for each batch). MPs were quantified indirectly by measuring the total protein content using Bicinchoninic acid (BCA) protein assay (ThermoScientific, Waltham, USA) according to the manufacturer's recommendations using a bovine serum albumin (BSA) standard curve. Each set of experiments was done using at least three different batches of MPs preparations.

Western Blot Analysis

Following treatments, cells were washed once in PBS to remove left-over medium, and then whole-protein lysates were extracted in cold Radioimmunoprecipitation Assay (RIPA) lysis buffer [0.5 M Tris pH 6.8, 20% Sodium dodecyl sulfate (SDS) and a cocktail of protease and phosphatase inhibitors]. Protein concentrations were determined using the BCA method (ThermoScientific, Waltham, USA). Equal amounts of proteins (10–20 µg) were resolved on SDS-PAGE gels (8–12% based on the molecular weights of targets). After transfer and blocking for 1 h in tris-buffered saline (TBS) and 0.1% of Tween 20 (Sigma-Aldrich, Hamburg, Germany) (T-TBS) and 5% dry milk, the blots were washed in T-TBS and incubated overnight with respective primary antibodies. Immunoblotting was done using primary antibodies against: BiP, p-p42/44 mitogen-activated protein kinase (MAPK) (Thr202/204), p42/44 MAPK, p-c-JUN (Ser73), p-p38 (Thr180), autophagy marker light chain 3 (LC-3 I/II) (1:1,000) (Cell Signaling Technology, Danvers, USA), or

TABLE 1 | List of human primers used for qPCR analysis.

Target Gene	Forward Primer	Reverse Primer
β-actin	CATGTACGTTGCTATCCAGGC	CTCCTTAATGTCACGCACGAT
BiP	CATCACGCCGTCCTATGTCG	CGTCAAAGACCGTGTTCTCG
CHOP	GAACGGCTCAAGCAGGAAATC	TTCACCATTCGGTCAATCAGAG
ATF-4	CCCTTCACCTTCTTACAACCTC	TGCCCAGCTCTAAACTAAAGGA
GRP94	GCTGACGATGAAGTTGATGTGG	CATCCGTCCTTGATCCTTCTCTA
TRIB3	AAGCGGTTGGAGTTGGATGAC	CACGATCTGGAGCAGTAGGTG
ATG-3	CCAACATGGCAATGGGCTAC	ACCGCCAGCATCAGTTTTGG
Beclin-1	TGAGGGATGGAAGGGTCTAAG	GCCTGGGCTGTGGTAAGTAATC
IL-10	ACTTTAAGGGTTACCTGGGTTGC	TCACATGCGCCTTGATGTCTG
eNOS	TGATGGCGAAGCGAGTGAAG	ACTCATCCATACACAGGACCC
VEGF-A	AGGGCAGAATCATCACGAAGT	AGGGTCTCGATTGGATGGCA
FGF-2	AGAAGAGCGACCCTCACATCA	CGGTTAGCACACACTCCTTTG

mouse anti-β-actin (1:5,000) (Santa Cruz Biotechnology, Dallas, USA). After washing in T-TBS, membranes were incubated with appropriate secondary antibodies (horseradish peroxidase-conjugated) (1:10,000) and chemiluminescence signal was visualized using Enhanced chemiluminescence (ECL) reagent (Abcam, Cambridge, UK) using FluorChem M imaging system (Protein Simple, San Jose, USA) and protein band intensities were analyzed using AlphaView software (Protein Simple).

Total RNA Isolation and Gene Expression Analysis

Following treatments, cells were washed in PBS (ThermoScientific, Waltham, USA), total RNA was extracted using the innuPREP RNA Mini kit (Analytikjena, Berlin, Germany) by following the supplier recommendations. RNA concentration and quality preparations were determined using a NanoDrop 2000 (ThermoScientific). cDNA synthesis was performed in of total RNA (500 ng) using the RevertAid reverse transcription kit (ThermoScientific) and an oligo$(dT)_{12-18}$ primer according to the supplier's instructions. Target genes were then amplified using GoTaq qPCR Master Mix (Promega, Madison, USA) in Applied Biosystems 7500 fast Real-Time PCR System (ThermoScientific).

All experiments were performed independently with at least three biological repeats and technical replicates. Data were analyzed by the comparative Ct method, and expressed as fold change relative to control group. The pairs of primers for human target genes were sourced from Primer bank and synthesized by Sigma-Aldrich (Hamburg, Germany). Sequences of human primers used in the study are summarized in **Table 1**.

Assessment of Apoptosis

Apoptosis in HUVECs treated with MPs (20 μg/ml for 48 h) generated from untreated HUVECs (CTL MPs) or cells treated with TG, TG + PBA or PBA, was assessed using Tali® apoptosis kit (ThermoScientific, Waltham, USA) according to the manufacturer's instructions. After treatments, culture medium was collected from the 6-well plates and transferred into 15-ml tubes. Then, cells were detached with trypsin and transferred to respective 15-ml tubes containing the old media. Media was then centrifuged at 1,500 × *g* for 5 min at 4°C, and the pellet was resuspended in 100 μl 1X Annexin Binding Buffer (ABB). Then, 5 μl of Annexin V solution were mixed to each sample and incubated at room temperature for 20 min in the dark. Samples were centrifuged again, and the pellet was resuspended in 100 μl of fresh 1X ABB. Lastly, 1 μl of propidium iodide (100 μg/ml) was added, and samples were incubated for 10 min in the dark. The samples were analyzed by loading the stained cells (25 μl) into the Tali Cellular Analysis Slides (ThermoScientific) and imaging using Tali Image-based Cytometer (ThermoScientific) following the kit protocol. The analysis included the percentages of live cells, dead cells and apoptotic cells in each cell preparation.

Endothelial Cell Tube-Like Structures Formation Assay

In vitro angiogenesis assay using Geltrex™ Matrigel matrix (ThermoScientific, Waltham, USA) was followed to assess the ability of endothelial cells to form tube-like structures, an indication of their angiogenic capacity. HUVECs were seeded into 6-well plates with a seeding density of 150,000 cells/well. Next day, cells were treated with MPs (20 μg/ml) derived from untreated HUVECs (CTL MPs) and those treated with TG, TG + PBA, or PBA. Untreated cells (no MPs treatment) were used as controls. Cells were left to incubate for 48 h. Geltrex™ (ThermoScientific) was thawed in the refrigerator (4°C) overnight before use. On the day of the experiment, Geltrex™ (100 μl) was added into 48-well plates then the plate was shacked gently for a uniform layer of the gel. The gel-coated wells were incubated at 37°C for 30 min until the gel solidified. Meanwhile, treated cells were washed with PBS and detached with trypsin. The cell suspension was then centrifuged at 1,500 × *g* for 5 min. The pellet was resuspended in 100 μl of medium and counted using hemocytometer. Cells were then loaded into gel-coated wells with a seeding density of 50,000 cells/well and cell suspension volume of 100 μl. The plate was incubated at 37°C and 5% CO_2 for 4 h. Following this, the formed tube-like structures were visualized by the phase contrast inverted microscope and images were taken (Optika, Ponteranica, Italy). Semi-quantitative image analysis was performed using WimTube software from Wimasis Image Analysis (Onimagin Technologies SCA, Cordoba, Spain) (26). Total tube lengths were counted in five blind fields per condition, averaged, and then compared across the experimental groups.

Enzyme-Linked Immunosorbent Assay (ELISA)

HUVECs were seeded into 6-well plates with at the density of 150,000 cells/well. The following day, cells were incubated for further 48 h with MPs (20 μg/ml) derived from untreated HUVECs (CTL MPs) and those treated with TG or TG + PBA. Untreated cells (no MPs treatment) were used as a negative control. Culture media were then collected from all conditions and interleukin (IL)-6 concentration (pg/ml) was

determined using a commercial ELISA colorimetric kit following the manufacturer's instructions (R&D Systems, Minneapolis, USA). Samples and IL-6 standards were loaded on a pre-coated microplate. Absorbance was then read at 450 nm with a reference wavelength correction set to 570 nm using a H1 synergy microplate reader (BioTek Instruments, Winooski, USA).

Indirect NO Quantification (Griess Assay)

HUVECs were seeded into 6-well plates with at the density of 150,000 cells/well. The following day, cells were incubated for further 48 h with MPs (20 μg/ml) derived from untreated HUVECs (CTL MPs) and those treated with TG or TG + PBA. Untreated cells (no MPs treatment) were used as a negative control. Then, the concentration of NO stable metabolites, nitrite and nitrate, were quantified using Griess assay following the manufacturer's recommendations (R&D Systems, Minneapolis, USA). Nitrite and nitrate concentration in culture media of cells reflect the levels of NO produced by cells. After treatments, culture media were collected, centrifuged to remove any debris. Nitrates in the samples were converted to nitrites by applying nitrate reductase. Finally, nitrite concentrations were determined by following the supplier instructions using a standard curve with nitrite. The concentration of the nitrite formed was proportional to the amount of NO produced by the cells when measured at 540 nm with wavelength correction at 690 nm using H1 synergy microplate reader (BioTek Instruments, Winooski, USA).

STATISTICAL ANALYSIS

Results are expressed as mean ± SEM, and n represents the number of biological repeats. Statistical analyses were performed with GraphPad Prism® 7.01e software for MAC using either one-way ANOVA or two-way ANOVA followed by Tukey's or Bonferroni multiple comparison *post hoc* tests, respectively. A two-tailed $P \leq 0.05$ was considered as statistically significant.

RESULTS

ER Stress Induction Did Not Cause Quantitative Differences in MPs Generated

Treatment of EA.hy926 endothelial cells with DTT (2 mM) for 24 h resulted in enhanced mRNA expression of ER stress target markers; *BiP*, *CHOP, GRP94 and ATF-4* (**Figure 1**). Treatment of HUVECs with TG (300 nM) for 24 h resulted in an increase in mRNA expression of *BiP*, *CHOP* and *TRIB3* (**Figures 2A–C**), while their incubation with DTT (2 mM; 24 h) caused an increase in mRNA expression of *BiP*, *CHOP, ATF-4,* and *TRIB3* (**Figures 2D–G**), indicating the successful induction of ER stress in both cell lines. As shown in **Figure 2H**, the treatment of HUVECs with TG for 24 h caused an increase in protein expression of BiP (**Figure 2H**). Interestingly, pre-treatment of cells with PBA (10 mM) partially, but significantly, prevented the increase in BiP protein expression caused by TG (**Figure 2H**).

Analysis of MPs isolated from various conditions showed no differences in amount of proteins associated with MPs isolated from EA.hy926 cells treated with DTT in the presence or absence of PBA (**Figure 3A**) or from HUVECs incubated with TG in the in the presence or absence of PBA (**Figure 3B**). These data suggest that ER stress induction while caused shedding of MPs, it did not increase its release compared to control conditions.

ER Stress-Generated MPs Activated ER Stress in a Vicious Circle in Both EA.hy926 Cells and HUVECs

EA.hy926 cells were treated with ER stress-generated MPs for 24 h, at MPs concentration of 10 μg/ml. As shown in **Figure 4**, treatment of cells with DTT-generated MPs caused an increase in mRNA expression of *CHOP* (**Figure 4A**) and *ATF-4* (**Figure 4B**), while no significant changes were observed for *GRP94* (**Figure 4C**) and *BiP* (**Figure 4D**) compared to control MPs, indicating activation of ER stress response. Interestingly, MPs generated from EA.hy926 cells stimulated with TG in presence of PBA (TG+PBA MPs) did not cause any changes in mRNA expression of ER stress markers studied compared to control MPs (CTL MPs) (**Figure 4**).

On the other hand, the treatment of HUVECs with TG-generated MPs at the concentration of 10 μg/ml caused an increase in mRNA expression of *BiP* (**Figure 5C**) and a trend for increase for *CHOP* (**Figure 5D**) after 48 h incubation, while incubation of cells for 24 h (**Figures 5A,B**) did not show differences compared to control MPs. MPs generated from HUVECs stimulated with TG in presence of PBA (TG + PBA MPs) did not cause any changes in mRNA expression of ER stress markers studied compared to control MPs (CTL MPs) (**Figure 5**). The stimulation of HUVECs with TG-generated MPs at a higher concentration of 20 μg/ml for both 24 and 48 h also caused an increase in mRNA expression of *BiP, ATF-4* and *CHOP* compared to control MPs at both time points (**Figure 6**).

Altogether, these data indicate that MPs generated under ER stress conditions can induce and self-perpetuate ER stress response in naïve endothelial cells, suggesting a vicious circle between shedding of MPs and activation of ER stress response.

ER Stress-Generated MPs Impaired Tube-Like Structures Formation in HUVECs

HUVECs were incubated with MPs generated under ER stress conditions (TG MPs) for 48 h before collecting the cells and growing them on Matrigel matrix for further 4 h to allow formation of tube-like structures, a marker of angiogenic capacity. As shown in **Figure 7A**, TG-generated MPs were able to impair tube-like structures formation on a Matrigel matrix, compared to control (no MPs), CTL MPs or PBA MPs (**Figure 7A**). Of note, MPs generated from cells treated with TG in presence of PBA (TG + PBA MPs) did not affect angiogenic capacity of HUVECs compared to control (no MPs), CTL MPs or PBA MPs (**Figure 7A**). These data support that ER stress-generated MPs can cause endothelial dysfunction as evidenced by reduced capacity to form tube-like structures when grown on a Matrigel three-dimensional matrix.

To further harness the effects of MPs on angiogenic capacity, we evaluated mRNA expression of 2 pro-angiogenic factors, Vascular endothelial growth factor A (*VEGF-A*) and basic fibroblast growth factor (*FGF-β* or *FGF-2*). As shown in **Figure 7B**, TG MPs and TG + PBA MPs reduced mRNA expression of *VEGF-A* compared to control (no MPs) and CTL

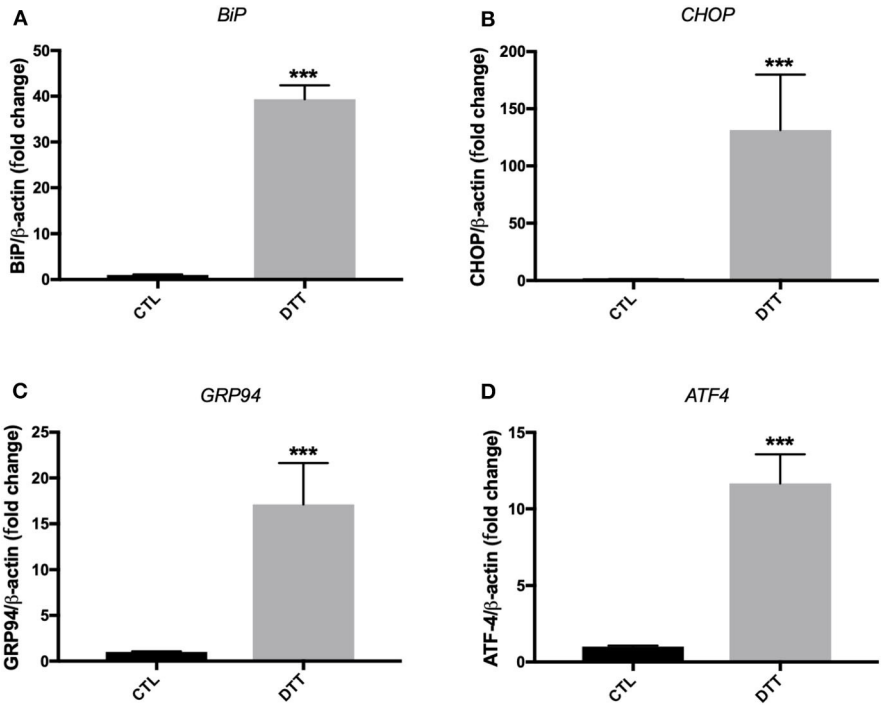

FIGURE 1 | ER stress induction with pharmacological inducer of ER stress, DTT, in EA.hy926 endothelial cells. Relative mRNA expression by RT-qPCR of ER stress markers: *BiP* **(A)**, *CHOP* **(B)**, *GRP94* **(C)**, and *ATF-4* **(D)** normalized against housekeeping gene *β-actin.* Dithiothreitol (DTT) was used in concentration of 2 mM for 24 h to induce ER stress ($n = 3$–4). Data are presented as mean ± SEM. Data were analyzed by one-way ANOVA and Tukey's multiple comparison test. ***$P < 0.001$ vs. control (CTL).

MPs; however, this decrease was compensated by an increase in *FGF-2* mRNA expression only in the group of cells treated with TG + PBA MPs (**Figure 7C**).

Given the importance of NO in the regulation of multiple functions of endothelial cells including angiogenesis, the levels of NO release were assessed in HUVECs exposed to MPs using the Griess assay. As shown in **Figure 8A**, treatment of cells with TG MPs (20 μg/ml for 48 h) caused a significant reduction in the concentration of nitrites while cells incubated with MPs generated from HUVECs treated with PBA alone or TG+PBA did not cause such a reduction (**Figure 8A**). This effect was not associated with any changes in mRNA expression of *eNOS* (**Figure 8B**).

Endothelial cell dysfunction is closely associated with cellular inflammation. As shown in **Figure 8C**, TG MPs caused an increase in the release of inflammatory cytokine IL-6 compared to CTL MPs and control (no MPs) groups. Simultaneously, cells treated with TG MPs showed a decrease in mRNA expression of anti-inflammatory cytokine *IL-10* while such decrease was not observed in cells treated with TG+PBA MPs (**Figure 8D**).

ER Stress-Generated MPs Did Not Affect Cell Survival in HUVECs

Apoptosis is an important molecular mechanism underpinning ER stress-mediated endothelial dysfunction and impaired angiogenic capacity (15, 18). We have therefore assessed the impact of ER stress activation by TG-generated MPs on cell survival of HUVECs. Cells were treated for 48 h with 20 μg/ml MPs, and apoptosis was then detected by Tali image-based cytometry. As shown in **Figure 9**, HUVECs treated with TG-generated MPs exhibited only 5% of apoptotic cells showing no statistical difference compared to control MPs-treated cells or all other treatment groups. These data indicate that impaired angiogenic capacity caused by TG-generated MPs was independent of an effect on cell survival.

Differential Effects Between TG and TG-generated MPs on the Regulation of Inflammatory and Survival Signaling Pathways and Autophagy

To further harness the intercellular signaling pathways associated with the effects of TG-generated MPs on endothelial cells, we have compared the effects of TG and TG-generated MPs on the activation of key cellular pathways associated with cell survival and apoptosis and known to be activated during ER stress response in addition to autophagy.

As shown in **Figure 10A**, the treatment of HUVECs with TG caused a decrease in the phosphorylation of c-JUN, an indicator of the activation of JNK pathway that was not rescued by PBA; however, the treatment of cells with TG-generated MPs did not affect p-cJUN expression (**Figure 10B**). On the other hand, while TG caused a trend to increase in the phosphorylation of

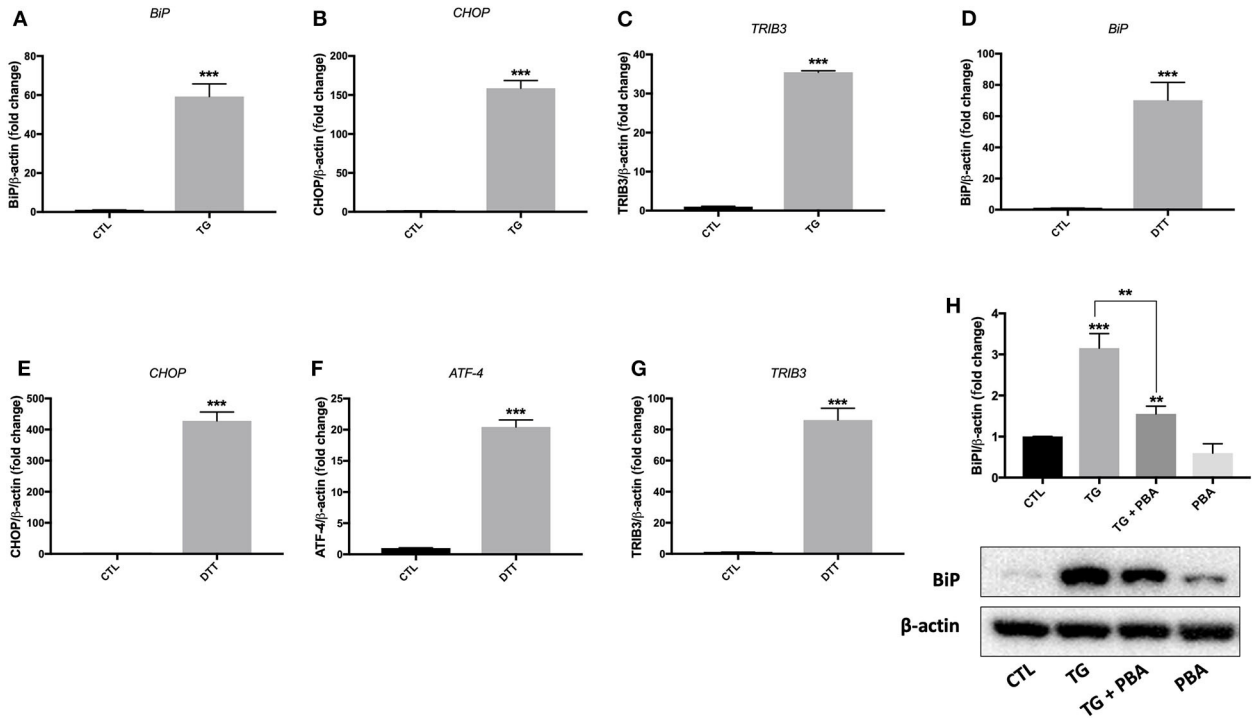

FIGURE 2 | ER stress was activated by TG and DTT in HUVECs. Relative mRNA expression by qPCR of ER stress markers: *BiP* **(A)**, *CHOP* **(B)**, and *TRIB3* **(C)** in HUVECs treated with thapsigargin (TG; 300 nM, 24 h) and *BiP* **(D)**, *CHOP* **(E)**, *ATF-4* **(F)** and *TRIB3* **(G)** in HUVECs treated with Dithiothreitol (DTT; 2M, 24 h) normalized against housekeeping gene *β-actin* ($n = 3$–4). **(H)**, Western blot of protein expression of BiP in HUVECs treated with thapsigargin (TG; 300 nM, 24 h) in the presence or absence of PBA (10 mM). Bars represent pooled densitometry data normalized to total amount of β-actin loading control expressed as fold change compared to control (CTL) ($n = 4$ per group). Data are presented as mean ± SEM. Data were analyzed by one-way ANOVA followed with Tukey's multiple comparison test. $^{**}P < 0.01$, $^{***}P < 0.001$ vs. control (CTL) or vs. indicated group.

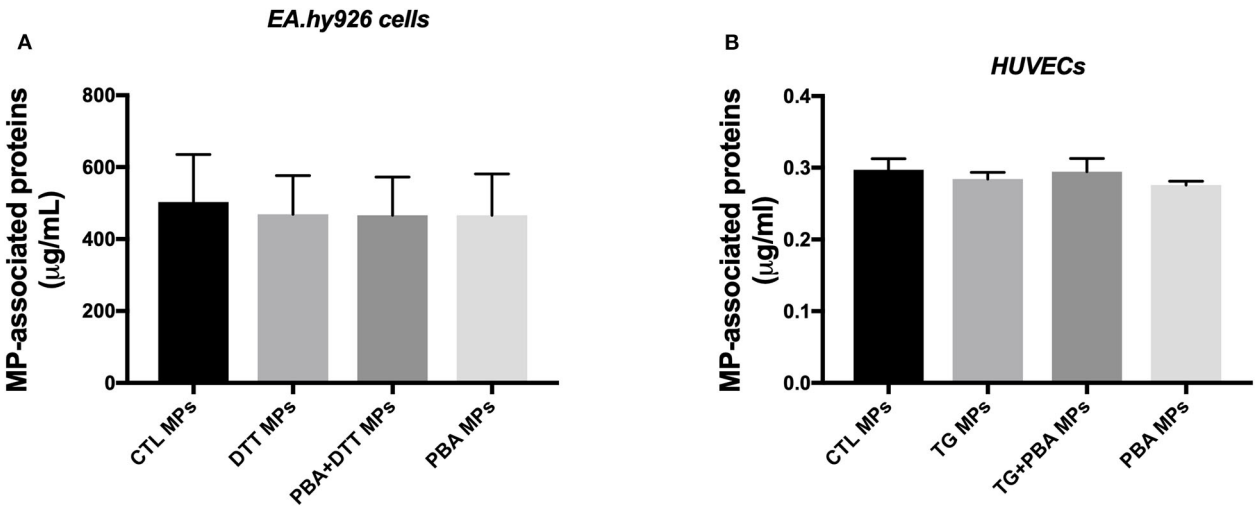

FIGURE 3 | Quantification of MPs-associated proteins generated from endothelial cells. **(A)**, Concentration of total proteins (μg/ml) associated with MPs derived from EA.hy926 endothelial cells treated with DTT (DTT MPs), DTT + PBA (DTT + PBA MPs) and PBA (PBA MPs); MPs were collected after 24 h of treatment ($n = 4$ per group). **(B)**, Concentration of proteins (μg/ml) associated with MPs derived from HUVECs treated with TG (TG MPs) and TG + PBA (TG + PBA MPs) and PBA (PBA MPs); MPs were collected after 24 h of TG treatment ($n = 9$ per group). Data are presented as mean ± SEM and analyzed by one-way ANOVA followed by Tukey's multiple comparison test.

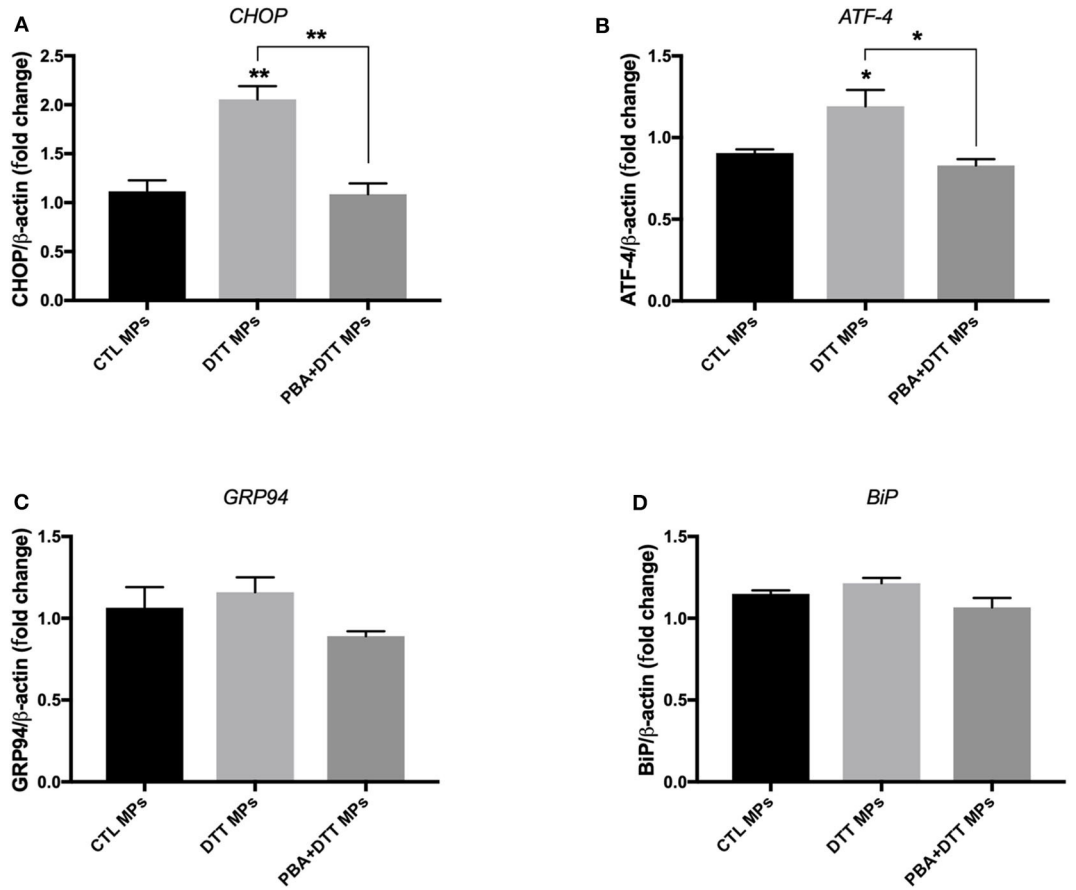

FIGURE 4 | ER stress-generated MPs activated ER stress in EA.hy926 endothelial cells. Relative mRNA expression levels of ER stress markers of *BiP* **(A)**, *ATF-4* **(B)**, *GRP94* **(C)**, and *BiP* **(D)** in EA.hy926 endothelial cells after treatment with MPs (10 μg/ml for 24 h) normalized against housekeeping gene *β-actin* ($n = 3$ per group). Data are presented as mean ± SEM and were analyzed by one-way ANOVA followed with Tukey's multiple comparison test. $^{*}P < 0.05$, $^{**}P < 0.01$ vs. CTL MPs or vs. indicated groups.

p38 MAPK (**Figure 10C**), TG-generated MPs showed a trend for decrease (**Figure 10D**). With regards to the activation of proliferative p42/44 MAPK pathway, TG treatment caused a significant reduction in phosphorylation and hence activation of p42/44 MAPK, an effect that was not prevented by incubation of cells with PBA (**Figure 10E**). However, the treatment of HUVECs with TG-generated MPs did not affect the activation of p42/44 MAPK signaling response (**Figure 10F**).

As shown in **Figure 11**, there was a differential effect of TG and TG-generated MPs on the activation of autophagy. TG caused a significant increase in autophagic rate as indicated by the increase in the ratio between LC3-II and LC3-I (indicative of the conversion of LC3-I into LC3-II) (**Figure 11A**). However, the treatment of HUVECs with TG-generated MPs did not affect the ratio between LC3-II and LC3-I (**Figure 11B**). The analysis of mRNA expression of *Beclin-1* (**Figure 11C**) and *autophagy related (ATG)-3* (**Figure 11D**), two additional makers of autophagy, revealed that treatment of HUVECs with MPs did not affect their expression levels corroborating protein expression results of LC3-I/II, indicating the absence of autophagy induction, at the concentrations and time exposure used for MPs.

Altogether, these data indicate that ER stress-generated MPs caused endothelial dysfunction in a mechanism that is independent from cell survival and autophagy despite their capacity to induce and hence self-perpetuate ER stress response.

DISCUSSION

Understanding the molecular mechanisms underlying endothelial dysfunction, an important contributing factor to the initiation of atherosclerosis that progresses to vascular complications, is warranted to identify targets for therapy and/or prevention. The underlying mechanisms of endothelial dysfunction are not fully clear; however, ER stress activation was shown to be implicated *in vitro* (18, 27) and *in vivo* (28, 29) in impaired endothelial cell functions. MPs have strongly emerged as biomarkers and mediators of endothelial dysfunction in diabetes and very seldom evidence is showing the implication

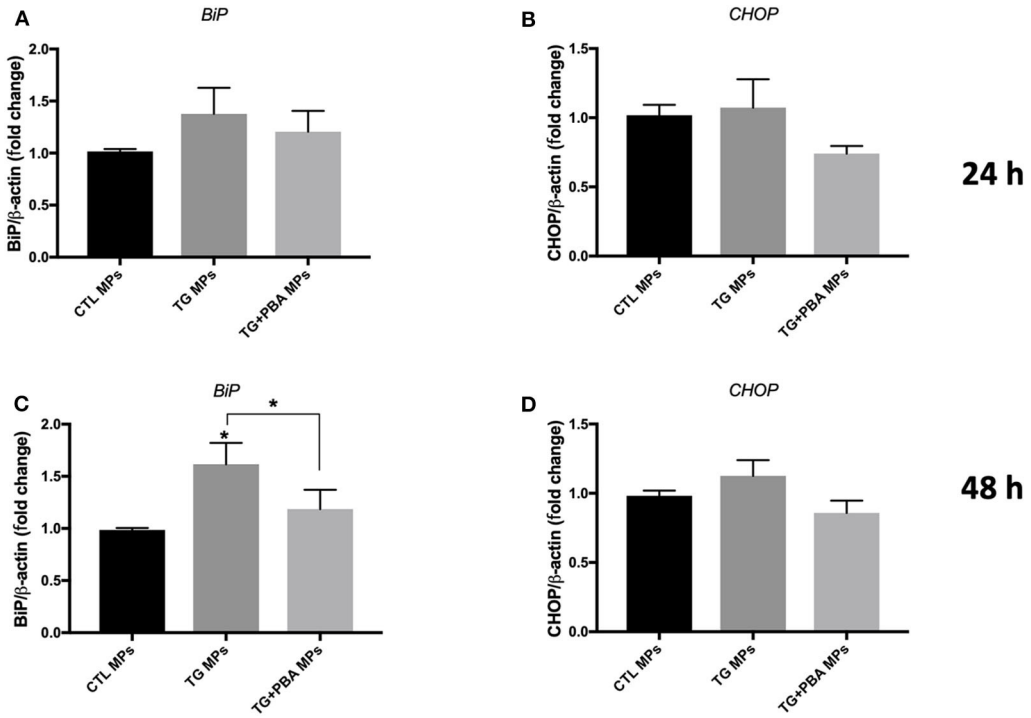

FIGURE 5 | ER stress-generated MPs (10 μg/ml) activated ER stress in HUVECs. Relative mRNA expression levels of ER stress markers of *BiP* **(A,C)** and *CHOP* **(B,D)** in HUVECs treated with CTL MPs, TG MPs and TG + PBA MPs at a concentration of 10 μg/ml for 24 and 48 h ($n = 4$ for each group) normalized against house-keeping gene *β-actin*. Data are presented as mean ± SEM and were analyzed by one-way ANOVA followed with Tukey's multiple comparison test. $^*P < 0.05$ vs. CTL MPs or vs. indicated groups.

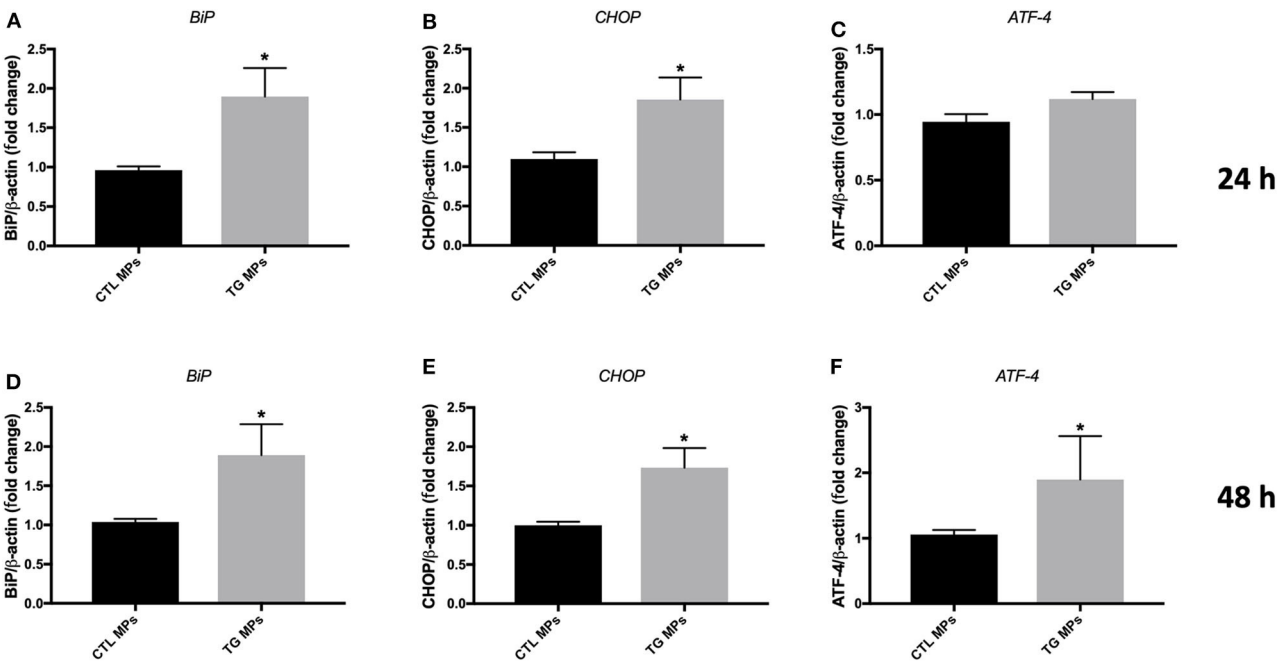

FIGURE 6 | ER stress-generated MPs (20 μg/ml) activated ER stress in HUVECs. Relative mRNA expression levels of ER stress markers *BiP* **(A,D)**, *CHOP* **(B,E)**, and *ATF-4* **(C,F)** in HUVECs treated with CTL MPs, TG MPs at a concentration of 20 μg/ml for 24 and 48 h ($n = 4$ in each group), normalized against housekeeping gene β-actin. Data are presented as mean ± SEM and were analyzed by one-way ANOVA followed with Tukey's multiple comparison test. $^*P < 0.05$ vs. CTL MPs.

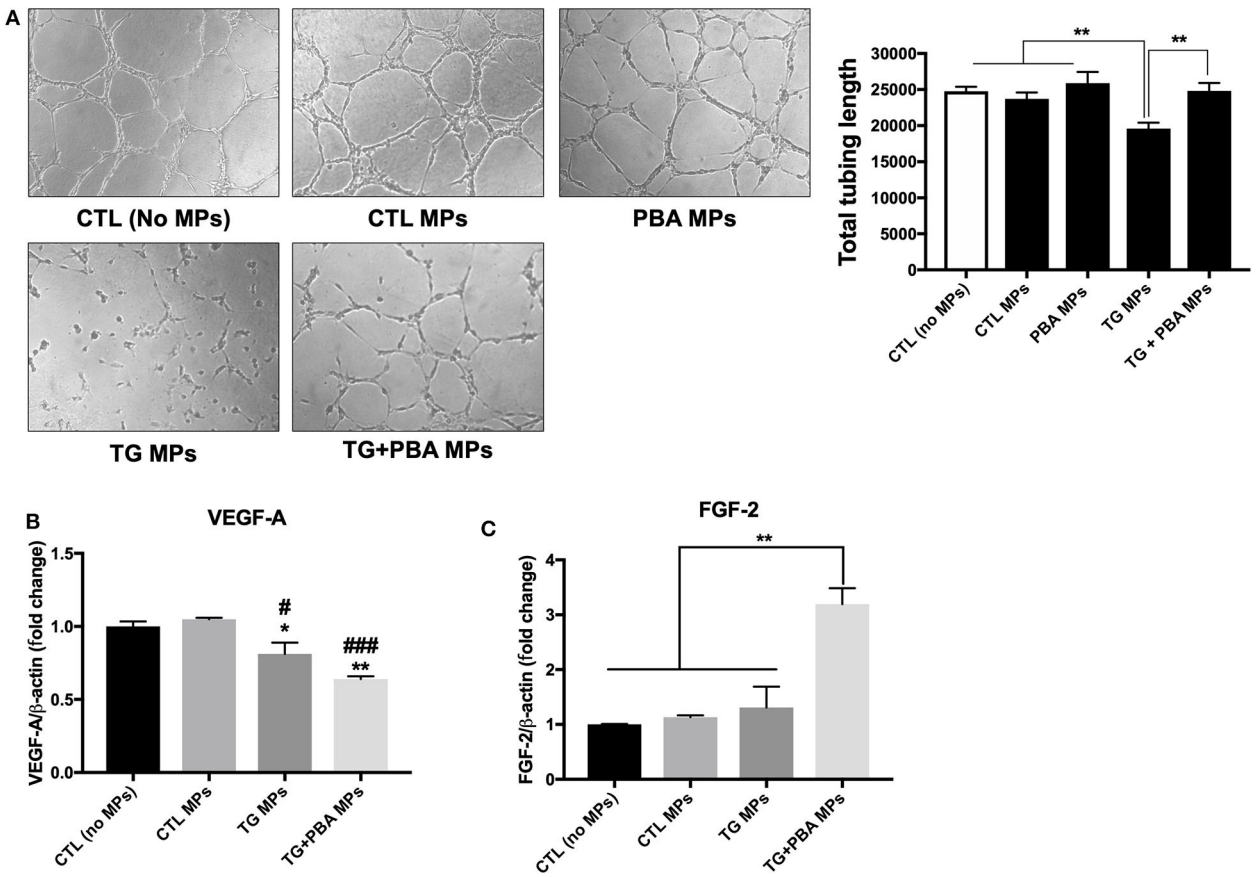

FIGURE 7 | ER stress-generated MPs impaired angiogenic capacity in HUVECs. **(A)**, HUVECs were incubated in complete M200 medium (CTL or no MPs), or in complete culture medium after treatment with CTL MPs, TG MPs, TG+PBA MPs or PBA MPs (20 μg/ml for 48 h). Angiogenic capacity of HUVECs was assessed by Matrigel-based tube formation assay. Images are representative of three independent experiments; images were taken after 4 h. To quantify angiogenesis, the length of tubes formed was counted in five random fields for each well using WimTube software from Wimasis Image Analysis. Bars represent the pooled data expressed as the total length of tubes formed in each condition. **(B,C)**, relative mRNA expression levels of angiogenic factors *VEGF-A* **(B)** and *FGF-2* **(C)** after treatment with MPs (20 μg/ml for 48 h), normalized against housekeeping gene β-actin ($n = 3$ per group). Data are presented as mean ± SEM and were analyzed by one-way ANOVA followed with Tukey's multiple comparison test. $^{*}P < 0.05$, $^{**}P < 0.01$ vs. CTL (No MPs) or vs. indicated groups; $\#\#P < 0.01$, $\#\#\#P < 0.001$ vs. CTL MPs.

of ER stress activation in MP-induced endothelial dysfunction (20, 30, 31).

In this project, we investigated the effects of MPs generated from endothelial cells under ER stress conditions on endothelial cell function. We confirmed here, for the first time, that subjecting endothelial cells to ER stress caused shedding of MPs and that ER stress-generated MPs were capable themselves of causing activation of ER stress in healthy endothelial cells in a vicious circle between ER stress activation and production of MPs. Previously, only one study reported that MPs from metabolic syndrome patients and apoptotic T-lymphocytes, induced endothelial dysfunction, partly, through the activation of ER stress response (20). Here, we showed that ER stress-generated MPs from endothelial cells, impaired angiogenic capacity *in vitro,* a feature of endothelial dysfunction, independently of cell survival. Our study contributes to the general understanding of the deleterious effects mediated by MPs. MPs exert their effects through their biological content. Therefore, future studies of the composition of MPs and determining the exact role of the biological materials in MPs-mediated pathological effects will aid further in identifying more specific therapeutic targets.

In our study, ER stress induction by TG or DTT for 24 h did not increase MPs production from endothelial cells compared to control. Our study is the first to report the effects of pharmacological ER stress induction on MP release in endothelial cells. In another cell type, smooth muscle cells (SMCs), it has been reported that shear stress-mediated ER stress caused a significant increase in the release of MPs compared to control (32). Unlike our study, Jia et al. (32) observed an increase in MPs shed from SMCs subjected to shear stress-mediated ER stress. The differences in cell types used (HUVECs vs. SMCs) and ER stress stimuli (shear stress for 48 h vs. DTT or TG) may explain differences in the impact of ER stress activation on MP shedding in the two cell types. Importantly, in our study, we observed that ER stress-generated MPs were different in relation to their effects

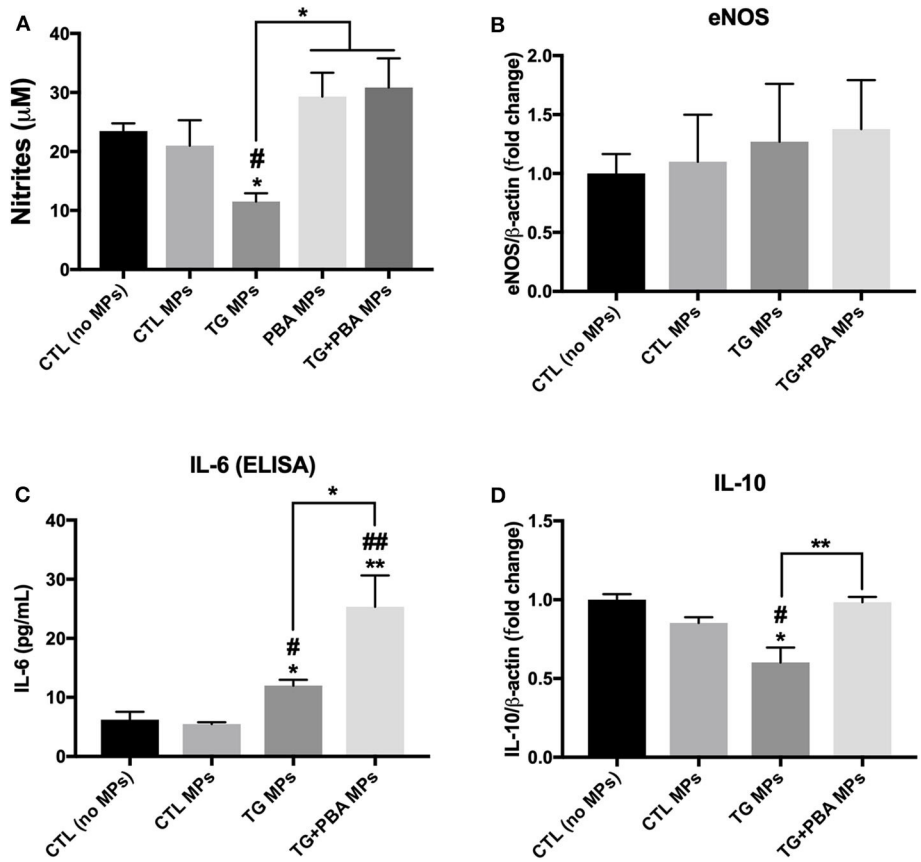

FIGURE 8 | Effects of TG-generated MPs on inflammatory cytokines and NO release. **(A)**, Nitrites concentration (μM), indicator of NO levels, in culture media from untreated HUVECs (CTL, no MPs) and cells treated with CTL MPs, TG MPs, TG+PBA MPs or PBA MPs at a concentration of 20 μg/ml for 48 h ($n = 6$ per group). **(B)**, Relative mRNA expression of *eNOS* in HUVECs after treatment with MPs (20 μg/ml for 48 h) normalized against housekeeping gene β-*actin* ($n = 3$ per group). **(C)**, IL-6 concentrations (pg/ml) determined by ELISA in culture media from control (No MPs) HUVECs and those treated with CTL MPs, TG MPs, TG + PBA MPs or PBA MPs at a concentration of 20 μg/ml for 48 h ($n = 3$). **(D)**, Relative mRNA expression levels of *IL-10* in HUVECs after treatment with MPs (20 μg/ml for 48 h) normalized against housekeeping gene β-*actin* ($n = 3$ per group). Data are presented as mean ± SEM. One-way ANOVA test was used for analysis and Tukey's multiple comparison test was used as a *post-hoc* test. $^*P < 0.05$, $^{**}P < 0.01$ vs. control (No MPs) or vs. indicated groups; $\#P < 0.05$, $\#\#P < 0.01$ vs. CTL MPs.

exerted on normal endothelial cells compared to the control MPs, indicating that although quantitatively there were no differences, ER stress-shed MPs were qualitatively different as they carried out deleterious biological messages against endothelial function as evidenced by impaired angiogenic capacity.

In our study, we reported, for the first time, that there is a vicious circle between ER stress activation in endothelial cells and generation of deleterious MPs that can themselves activate ER stress in naïve endothelial cells. Only one study was found in the literature showing the implication of ER stress in MPs-induced endothelial dysfunction (20); however, authors did not investigate the impact of ER stress on MP release. Our novel findings here harness the link between ER stress and MPs and improve our current understanding of cellular responses underpinning the release and action of MPs in disease. As noted in **Figures 4**–**6**, there were differences in the potency of ER stress induction caused by TG and DTT-generated MPs in EA.hy926 cells and HUVECs. DTT-generated MPs, used at the concentration of 10 μg/ml (24 h), were more potent in causing ER stress in EA.hy926 cells compared to the effects of TG-generated MPs in HUVECs used at the same concentration and incubation duration (24 h). This differential response of ER stress-generated MPs was observed although both TG and DTT were very potent in inducing ER stress in EA.hy926 cells and HUVECs (**Figure 1**). This can be explained by the differences in the mechanisms of ER stress activation by TG (intracellular calcium stores depletion) and DTT (reducing inter- and intra-protein disulfide bonds) that led to the shedding of MPs in addition to differences in the nature of cells where HUVECs are primary cells and EA.hy926 are immortalized cells. One limitation, however, to be highlighted here is that the effects of TG- and DTT-generated MPs were not tested in both cell types. We further support here that the qualitative content, which reflects the nature of the biological messages transferred to target cells, is more important than quantity of MPs in the initiation and maintenance of disease processes.

Angiogenesis involves cell migration and proliferation. Treatment of naïve HUVECs with ER stress-generated MPs

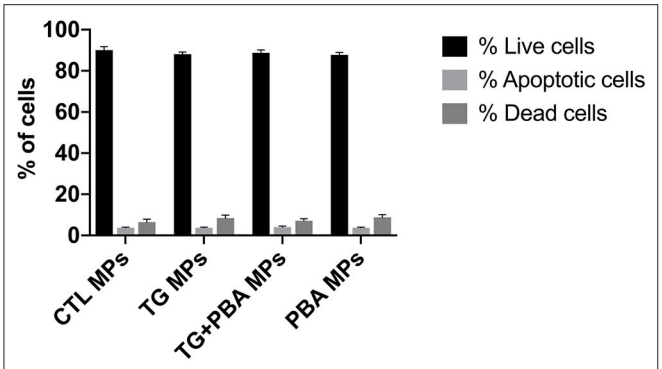

FIGURE 9 | Apoptosis in HUVECs treated with ER stress-generated MPs. Assessment of apoptosis in HUVECs treated with CTL MPs, TG MPs, TG + PBA MPs or PBA MPs at a concentration of 20 μg/ml for 48 h ($n = 3$). Apoptosis was analyzed by Tali® Image-based Cytometry. Bars represent pooled data for live, apoptotic and dead cells expressed as percentage of total number of cells. Data are presented as mean ± SEM. Two-way ANOVA test was used to analyze data followed with Bonferroni multiple comparison test.

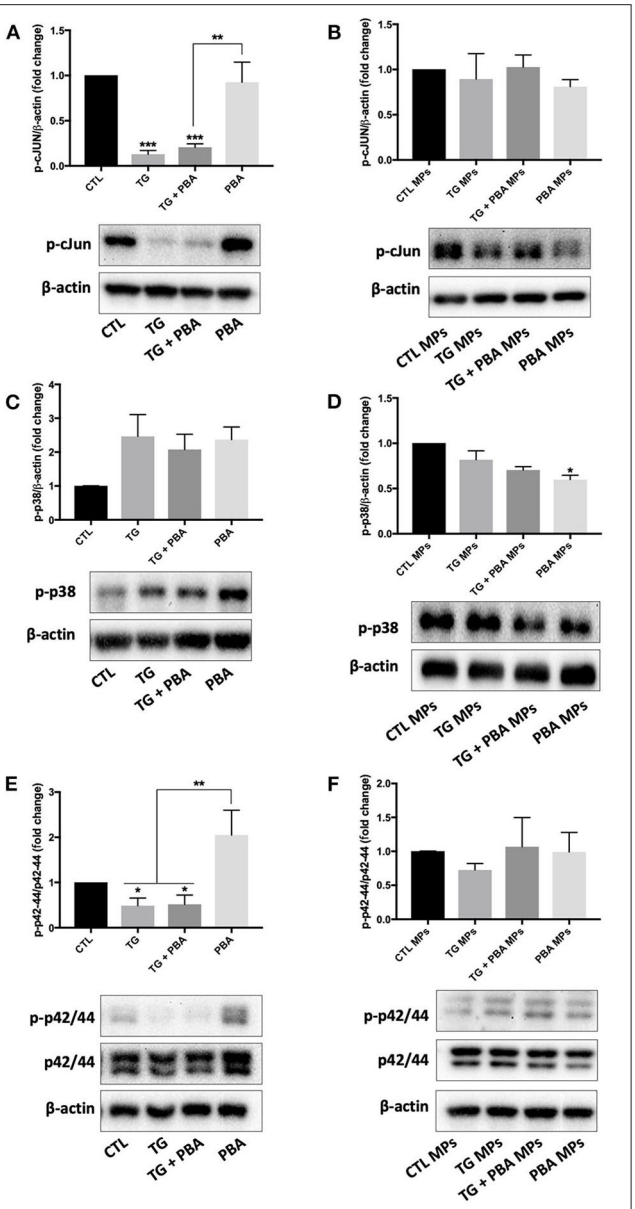

FIGURE 10 | Differential effects between TG and TG-generated MPs on the regulation of inflammatory and survival signaling pathways. Western blot analysis of protein expression of ER p-cJUN **(A,B)**, p-p38 **(C,D)**, and p-42/44 **(E,F)** in HUVECs treated with TG (300 nM, 24 h) in the presence or absence of PBA (10 mM) or treated with CTL MPs, TG MPs, TG + PBA MPs or PBA MPs at a concentration of 20 μg/ml for 48 h ($n = 3$–6 per group). Representative images from more than three independent experiments are shown. Bars represent pooled densitometry data normalized to total amount of β-actin loading control or total p42/44 expressed as fold change compared to control (CTL or CTL MPs) ($n = 4$ per group). Data are presented as mean ± SEM. One-way ANOVA test was used for analysis and Tukey's multiple comparison test was used as a *post-hoc* test. $^{*}P < 0.05$, $^{**}P < 0.01$, $^{***}P < 0.001$ vs. CTL or CTL MPs or vs. indicated groups.

impaired their capacity to form tube-like structures on a three-dimensional Matrigel matrix but did not affect apoptosis or protein expression of major pro-apoptotic (p-cJun) and proliferative (p-p38 and p-p42/44 MAPK) signals. This may indicate that impaired angiogenic effect is mediated through the inhibition of cell migration but not proliferation and cell survival. Future studies are warranted to determine the exact role of ER stress-generated MPs on endothelial cell migration. The reduction in angiogenic capacity caused by TG MPs was associated with a decrease in mRNA expression of *VEGF-A* and *FGF-2*, which may contribute to the deleterious effect of TG MPs on angiogenesis, while cells exposed to TG + PBA MPs showed an enhanced mRNA expression of *FGF-2*. Importantly, the treatment of HUVECs with TG MPs significantly reduced NO release unlike cells exposed to PBA MPs or TG + PBA MPs. Reduced NO bioavailability is a major contributor to impaired angiogenesis (15, 18).

It was noted that the mother cells from which MPs were derived showed differential effects of TG on the activation of antioxidants and pro-apoptotic and survival pathways studied in addition to autophagy, when compared to cells treated with ER stress-generated MPs. Of note, in contrast to TG-treated cells, where expression of p-cJUN was lower, TG-generated MPs did not affect the activation of JNK pathway. Similarly, TG-treated cells showed a reduced activation of the proliferative pathway p42/44 MAPK, while TG-generated MPs did not affect this signaling response. Furthermore, unlike TG-treated cells, the autophagic ratio (LC3-II/LC3-I) was not affected by treatment with ER stress-generated MPs. This was further confirmed by the absence of changes in mRNA expression of 2 other markers of autophagy, *Beclin-1* and *ATG-3*, in cells treated with MPs. ER stress activates autophagy under the control of IRE-1α which mediates the activation of MAPK leading at the end to the activation of autophagy (33). These data indicate a dissociation between the implications of the pharmacological- or MPs- induction of ER stress in endothelial cells. The effects of pharmacological ER stress appear to be driven by an impairment

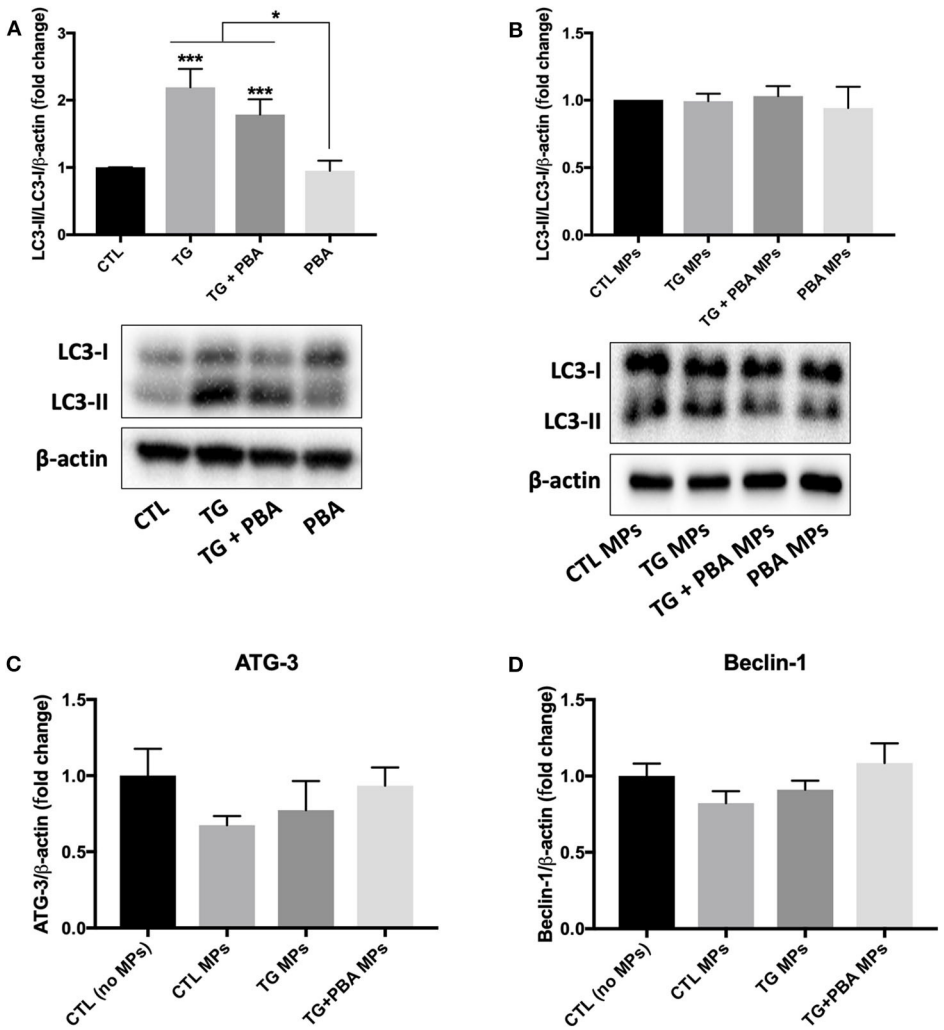

FIGURE 11 | Differential effects between TG and TG-generated MPs on autophagy activation. **(A,B)**, Western blot analysis of autophagy marker (LC3 I/II) in HUVECs treated with TG (300 nM, 24 h) in the presence or absence of PBA (10 mM) **(A)** or treated with CTL MPs, TG MPs, TG+PBA MPs or PBA MPs at a concentration of 20 μg/ml for 48 h **(B)** ($n = 3$–6 per group). Bars represent autophagic rate expressed as the ratio of densitometry signal for LC3-II normalized to LC3-I and to total amount of β-actin loading control expressed as fold change compared to control (CTL or CTL MPs) ($n = 4$–6 per group). **(C,D)**, relative mRNA expression levels of *ATG-3* **(C)** and *Beclin-1* **(D)** after treatment with MPs (20 μg/ml for 48 h) normalized against housekeeping gene *β-actin* ($n = 3$ per group). Data are presented as mean ± SEM. One-way ANOVA test was used for analysis and Tukey's multiple comparison test was used as a *post-hoc* test. $^*P < 0.05$, $^{***}P < 0.001$ vs. CTL or vs. indicated groups.

in cell survival, while ER stress-generated MPs mediate their effects on endothelial cells via a subtler regulation of intracellular signaling responses that are independent from apoptosis and cell survival. It is important to note that ER stress-generated MPs were used up to the concentration of 20 μg/ml and up to 48 h; longer exposure and/or higher concentration may affect cell survival and viability of endothelial cells; however, higher concentrations may not be relevant patho-physiologically because we have reported previously that circulating endothelial MPs metabolic syndrome patients for example represent only 2–3% of total MPs (10). Maamoun et al. (18) found that high glucose concentrations impaired angiogenesis in HUVECs through ER stress-mediated cell death in a mechanism involving proapoptotic pathway JNK that is closely linked to sustained ER stress. Moreover, they found that treatment of endothelial cells with PBA reduced apoptosis indicating that endothelial cell death was mediated by ER stress (18). In our study, ER stress-generated MPs induced ER stress and impaired angiogenesis in endothelial cells without affecting apoptosis, autophagy or antioxidant production involving probably other mechanisms linked to ER stress such as oxidative stress (15). Of note, we observed that MPs generated from cells exposed to TG and those exposed to TG + PBA MPs increased release of inflammatory cytokine IL-6 as assessed by ELISA, which can contribute to

the impairment of angiogenic capacity. Interestingly, mRNA expression of *IL-10*, a major anti-inflammatory cytokine, was reduced in cells treated with TG MPs, but preserved in cells incubated with TG+PBA MPs, which may contribute to counterbalancing the effects of increased IL-6 release in cells treated with TG+PBA MPs.

In conclusion, this study demonstrated that subjecting endothelial cells to ER stress resulted in the production of MPs, which were able to activate ER stress themselves in naïve endothelial cells in a vicious circle. TG-generated MPs, at the concentrations used, were able to reduce the capacity of HUVECs to form tube-like structures on a three-dimensional reconstituted basement membrane, without affecting autophagy or cell survival. This work enhances the general understanding of the deleterious effects carried out by MPs in medical conditions where ER stress is sustainably activated such as diabetes, obesity and metabolic syndrome. Our findings are clinically relevant as they will help in the process of identifying new therapeutic targets against MPs produced in conditions characterized by the activation of ER stress such as diabetes. MPs production in conditions with underlying ER stress were shown to initiate endothelial dysfunction. Therefore, MPs can be targeted by controlling their release from the cells, inhibiting their cellular uptake by the receipt cell or modulating their cargo content. For instance, several antidiabetics were reported to modulate the release of MPs in diabetic patients (34–36).

DATA AVAILABILITY STATEMENT

The raw data supporting the conclusions of this article will be made available by the authors, without undue reservation.

AUTHOR CONTRIBUTIONS

AA conceptualized and designed the study, administered the project and supervised the students and research associates, curated the data, and secured resources and funding. AO, HE-G, MP, SA, and MH performed experimental work. AA and AO performed the formal analysis, wrote the original draft of the manuscript, and prepared figures. HK, AZ, and TB contributed to analysis, discussion, reviewed, and edited the manuscript. All authors contributed to the article and approved the submitted version.

FUNDING

This research was made possible by Qatar University grants (QUCG-CPH-20/21-3; IRCC-2019-006; QUST-2-CPH-2017-19; QUST-1-CPH-2018-1) and award UREP24-016-3-004 from Qatar National Research Fund (a member of Qatar Foundation). SA is supported by a graduate assistantship from the office of graduate studies (Qatar University). The findings achieved and statements made herein are solely the responsibility of the authors.

REFERENCES

1. Cade WT. Diabetes-related microvascular and macrovascular diseases in the physical therapy setting. *Phys Ther.* (2008) 88:1322–35. doi: 10.2522/ptj.20080008
2. Heijnen HFG, Schiel AE, Fijnheer R, Geuze HJ, Sixma JJ. Activated platelets release two types of membrane vesicles: microvesicles by surface shedding and exosomes derived from exocytosis of multivesicular bodies and alpha-granules. *Blood.* (1999) 94:3791. doi: 10.1182/blood.V94.11.3791
3. Théry C, Boussac M, Véron P, Ricciardi-Castagnoli P, Raposo G, Garin J, et al. Proteomic analysis of dendritic cell-derived exosomes: a secreted subcellular compartment distinct from apoptotic vesicles. *J Immunol.* (2001) 166:7309. doi: 10.4049/jimmunol.166.12.7309
4. Schisano B, Giannetti G, Sardelli L, Ciotola M, Gualdiero R, Giugliano D, et al. Endothelial microparticles correlate with endothelial dysfunction in obese women. *J Clin Endocrinol Metab.* (2006) 91:3676–9. doi: 10.1210/jc.2006-0851
5. Brodsky SV, Zhang F, Nasjletti A, Goligorsky MS. Endothelium-derived microparticles impair endothelial function in vitro. *Am J Physiol Heart Circ Physiol.* (2004) 286:H1910–H5. doi: 10.1152/ajpheart.01172.2003
6. Martin S, Tesse A, Hugel B, Martínez MC, Morel O, Freyssinet J-M, et al. Shed membrane particles from T lymphocytes impair endothelial function and regulate endothelial protein expression. *Circulation.* (2004) 109:1653–9. doi: 10.1161/01.CIR.0000124065.31211.6E
7. Feng B, Chen Y, Luo Y, Chen M, Li X, Ni Y. Circulating level of microparticles and their correlation with arterial elasticity and endothelium-dependent dilation in patients with type 2 diabetes mellitus. *Atherosclerosis.* (2010) 208:264–9. doi: 10.1016/j.atherosclerosis.2009.06.037
8. Feng Q, Stork CJ, Xu S, Yuan D, Xia X, LaPenna KB, et al. Increased circulating microparticles in streptozotocin-induced diabetes propagate inflammation contributing to microvascular dysfunction. *J Physiol.* (2019) 597:781–98. doi: 10.1113/JP277312
9. Ishida K, Taguchi K, Hida M, Watanabe S, Kawano K, Matsumoto T, et al. Circulating microparticles from diabetic rats impair endothelial function and regulate endothelial protein expression. *Acta Physiol.* (2016) 216:211–20. doi: 10.1111/apha.12561
10. Agouni A, Lagrue-Lak-Hal AH, Ducluzeau PH, Mostefai HA, Draunet-Busson C, Leftheriotis G, et al. Endothelial dysfunction caused by circulating microparticles from patients with metabolic syndrome. *Am J Pathol.* (2008) 173:1210–9. doi: 10.2353/ajpath.2008.080228
11. Arteaga RB, Chirinos JA, Soriano AO, Jy W, Horstman L, Jimenez JJ, et al. Endothelial microparticles and platelet and leukocyte activation in patients with the metabolic syndrome. *Am J Cardiol.* (2006) 98:70–4. doi: 10.1016/j.amjcard.2006.01.054
12. Agouni A, Ducluzeau PH, Benameur T, Faure S, Sladkova M, Duluc L, et al. Microparticles from patients with metabolic syndrome induce vascular hypo-reactivity via Fas/Fas-ligand pathway in mice. *PLoS ONE.* (2011) 6:e27809. doi: 10.1371/journal.pone.0027809
13. Flamment M, Hajduch E, Ferré P, Foufelle F. New insights into ER stress-induced insulin resistance. *Trends Endocrinol Metab.* (2012) 23:381–90. doi: 10.1016/j.tem.2012.06.003
14. Battson ML, Lee DM, Gentile CL. Endoplasmic reticulum stress and the development of endothelial dysfunction. *Am J Physiol Heart Circ Physiol.* (2017) 312:H355–67. doi: 10.1152/ajpheart.00437.2016
15. Maamoun H, Benameur T, Pintus G, Munusamy S, Agouni A. Crosstalk between oxidative stress and endoplasmic reticulum (ER) stress in endothelial dysfunction and aberrant angiogenesis associated with diabetes: a focus on the protective roles of heme oxygenase (HO)-1. *Front Physiol.* (2019) 10:70. doi: 10.3389/fphys.2019.00070
16. Maamoun H, Abdelsalam SS, Zeidan A, Korashy HM, Agouni A. Endoplasmic reticulum stress: a critical molecular driver of endothelial dysfunction and cardiovascular disturbances associated with diabetes. *Int J Mol Sci.* (2019) 20:1658. doi: 10.3390/ijms20071658
17. Zhou J, Lhoták Š, Hilditch Brooke A, Austin Richard C. Activation of the unfolded protein response occurs at all stages of atherosclerotic lesion development in apolipoprotein E–deficient mice. *Circulation.* (2005) 111:1814–21. doi: 10.1161/01.CIR.0000160864.31351.C1

18. Maamoun H, Zachariah M, McVey JH, Green FR, Agouni A. Heme oxygenase (HO)-1 induction prevents endoplasmic reticulum stress-mediated endothelial cell death and impaired angiogenic capacity. *Biochem Pharmacol.* (2017) 127:46–59. doi: 10.1016/j.bcp.2016.12.009
19. Urano F, Wang X, Bertolotti A, Zhang Y, Chung P, Harding HP, et al. Coupling of stress in the ER to activation of JNK protein kinases by transmembrane protein kinase IRE1. *Science.* (2000) 287:664–6. doi: 10.1126/science.287.5453.664
20. Safiedeen Z, Rodríguez-Gómez I, Vergori L, Soleti R, Vaithilingam D, Douma I, et al. Temporal cross talk between endoplasmic reticulum and mitochondria regulates oxidative stress and mediates microparticle-induced endothelial dysfunction. *Antioxid Redox Signal.* (2016) 26:15–27. doi: 10.1089/ars.2016.6771
21. Roybal CN, Yang S, Sun CW, Hurtado D, Vander Jagt DL, Townes TM, et al. Homocysteine increases the expression of vascular endothelial growth factor by a mechanism involving endoplasmic reticulum stress and transcription factor ATF4. *J Biol Chem.* (2004) 279:14844–52. doi: 10.1074/jbc.M312948200
22. Sehgal P, Szalai P, Olesen C, Praetorius HA, Nissen P, Christensen SB, et al. Inhibition of the sarco/endoplasmic reticulum (ER) Ca(2+)-ATPase by thapsigargin analogs induces cell death via ER Ca(2+) depletion and the unfolded protein response. *J Biol Chem.* (2017) 292:19656–73. doi: 10.1074/jbc.M117.796920
23. Mostefai HA, Agouni A, Carusio N, Mastronardi ML, Heymes C, Henrion D, et al. Phosphatidylinositol 3-kinase and xanthine oxidase regulate nitric oxide and reactive oxygen species productions by apoptotic lymphocyte microparticles in endothelial cells. *J Immunol.* (2008) 180:5028–35. doi: 10.4049/jimmunol.180.7.5028
24. Agouni A, Mostefai HA, Porro C, Carusio N, Favre J, Richard V, et al. Sonic hedgehog carried by microparticles corrects endothelial injury through nitric oxide release. *FASEB J.* (2007) 21:2735–41. doi: 10.1096/fj.07-8079com
25. Ravindran S, Pasha M, Agouni A, Munusamy S. Microparticles as potential mediators of high glucose-induced renal cell injury. *Biomolecules.* (2019) 9:348. doi: 10.3390/biom9080348
26. Qiao K, Liu Y, Xu Z, Zhang H, Zhang H, Zhang C, et al. RNA m6A methylation promotes the formation of vasculogenic mimicry in hepatocellular carcinoma via Hippo pathway. *Angiogenesis.* (2020). doi: 10.1007/s10456-020-09744-8. [Epub ahead of print].
27. Bhatta M, Ma JH, Wang JJ, Sakowski J, Zhang SX. Enhanced endoplasmic reticulum stress in bone marrow angiogenic progenitor cells in a mouse model of long-term experimental type 2 diabetes. *Diabetologia.* (2015) 58:2181–90. doi: 10.1007/s00125-015-3643-3
28. Suganya N, Dornadula S, Chatterjee S, Mohanram RK. Quercetin improves endothelial function in diabetic rats through inhibition of endoplasmic reticulum stress-mediated oxidative stress. *Eur J Pharmacol.* (2018) 819:80–8. doi: 10.1016/j.ejphar.2017.11.034
29. Choi S-K, Lim M, Yeon S-I, Lee Y-H. Inhibition of endoplasmic reticulum stress improves coronary artery function in type 2 diabetic mice. *Exp Physiol.* (2016) 101:768–77. doi: 10.1113/EP085508
30. Benameur T, Osman A, Parray A, Ait Hssain A, Munusamy S, Agouni A. Molecular mechanisms underpinning microparticle-mediated cellular injury in cardiovascular complications associated with diabetes. *Oxid Med Cell Longev.* (2019) 2019:6475187. doi: 10.1155/2019/6475187
31. El-Gamal H, Parray AS, Mir FA, Shuaib A, Agouni A. Circulating microparticles as biomarkers of stroke: a focus on the value of endothelial- and platelet-derived microparticles. *J Cell Physiol.* (2019) 234:16739–54. doi: 10.1002/jcp.28499
32. Jia L-X, Zhang W-M, Li T-T, Liu Y, Piao C-M, Ma Y-C, et al. ER stress dependent microparticles derived from smooth muscle cells promote endothelial dysfunction during thoracic aortic aneurysm and dissection. *Clin Sci.* (2017) 131:1287–99. doi: 10.1042/CS20170252
33. Yang J, Yao S. JNK-Bcl-2/Bcl-xL-Bax/Bak pathway mediates the crosstalk between matrine-induced autophagy and apoptosis via interplay with Beclin 1. *Int J Mol Sci.* (2015) 16:25744–58. doi: 10.3390/ijms161025744
34. Esposito K, Maiorino MI, Di Palo C, Gicchino M, Petrizzo M, Bellastella G, et al. Effects of pioglitazone versus metformin on circulating endothelial microparticles and progenitor cells in patients with newly diagnosed type 2 diabetes—a randomized controlled trial. *Diabetes Obes Metab.* (2011) 13:439–45. doi: 10.1111/j.1463-1326.2011.01367.x
35. Nomura S, Omoto S, Yokoi T, Fujita S, Ozasa R, Eguchi N, et al. Effects of miglitol in platelet-derived microparticle, adiponectin, and selectin level in patients with type 2 diabetes mellitus. *Int J Gen Med.* (2011) 4:539–45. doi: 10.2147/IJGM.S22115
36. Shimazu T, Inami N, Satoh D, Kajiura T, Yamada K, Iwasaka T, et al. Effect of acarbose on platelet-derived microparticles, soluble selectins, and adiponectin in diabetic patients. *J Thromb Thrombolysis.* (2009) 28:429. doi: 10.1007/s11239-008-0301-3

Conflict of Interest: The authors declare that the research was conducted in the absence of any commercial or financial relationships that could be construed as a potential conflict of interest.

frontiers in Physiology

ORIGINAL RESEARCH
published: 03 February 2021
doi: 10.3389/fphys.2021.624967

Downregulation of Soluble Guanylate Cyclase and Protein Kinase G With Upregulated ROCK2 in the Pulmonary Artery Leads to Thromboxane A2 Sensitization in Monocrotaline-Induced Pulmonary Hypertensive Rats

*Suhan Cho[1], Hyun Namgoong[1], Hae Jin Kim[1,2], Rany Vorn[3], Hae Young Yoo[3] and Sung Joon Kim[1,2]**

[1] Department of Physiology, College of Medicine, Seoul National University, Seoul, South Korea, [2] Ischemic/Hypoxic Disease Institute, College of Medicine, Seoul National University, Seoul, South Korea, [3] Department of Nursing, Chung-Ang University, Seoul, South Korea

OPEN ACCESS

Edited by:
Soo-Kyoung Choi,
Yonsei University Health System,
South Korea

Reviewed by:
María Galán,
Sant Pau Institute for Biomedical Research, Spain
Young-Eun Cho,
The University of Iowa, United States

***Correspondence:**
Sung Joon Kim
physiolksj@gmail.com;
sjoonkim@snu.ac.kr

Specialty section:
This article was submitted to Vascular Physiology, a section of the journal Frontiers in Physiology

Received: 01 November 2020
Accepted: 13 January 2021
Published: 03 February 2021

Citation:
Cho S, Namgoong H, Kim HJ, Vorn R, Yoo HY and Kim SJ (2021) Downregulation of Soluble Guanylate Cyclase and Protein Kinase G With Upregulated ROCK2 in the Pulmonary Artery Leads to Thromboxane A2 Sensitization in Monocrotaline-Induced Pulmonary Hypertensive Rats. Front. Physiol. 12:624967. doi: 10.3389/fphys.2021.624967

Thromboxane A2 (TXA_2) promotes various physiological responses including pulmonary artery (PA) contraction, and pathophysiological implications have been suggested in cardiovascular diseases including pulmonary hypertension. Here, we investigated the role of TXA_2 receptor (TP)-mediated signaling in the pathophysiology of pulmonary arterial hypertension (PAH). The sensitivity of PA to the contractile agonist could be set by relaxing signals such as the nitric oxide (NO), soluble guanylate cyclase (sGC), and cGMP-dependent kinase (PKG) pathways. Changes in the TP agonist (U46619)-induced PA contraction and its modulation by NO/cGMP signaling were analyzed in a monocrotaline-induced PAH rat model (PAH-MCT). In the myograph study, PA from PAH-MCT showed higher responsiveness to U46619, that is decreased EC_{50}. Immunoblot analysis revealed a lower expression of eNOS, sGC, and PKG, while there was a higher expression of RhoA-dependent kinase 2 (ROCK2) in the PA from PAH-MCT than in the control. In PAH-MCT, the higher sensitivity to U46619 was reversed by 8-Br-cGMP, a membrane-permeable cGMP analog, but not by the NO donor, sodium nitroprusside (SNP 30 μM). In contrast, in the control PA, inhibition of sGC by its inhibitor (1H− [1,2,4] oxadiazolo [4,3−a] quinoxalin-1-one (ODQ), 10 μM) lowered the threshold of U46619-induced contraction. In the presence of ODQ, SNP treatment had no effect whereas the addition of 8-Br-cGMP lowered the sensitivity to U46619. The inhibition of ROCK by Y-27632 attenuated the sensitivity to U46619 in both control and PAH-MCT. The study suggests that the attenuation of NO/cGMP signaling and the upregulation of ROCK2 increase the sensitivity to TXA_2 in the PAH animal, which might have pathophysiological implications in patients with PAH.

Keywords: pulmonary hypertension, pulmonary artery smooth muscle, guanylate cyclase, protein kinase G, thromboxane A2 (TXA_2), monocrotaline

INTRODUCTION

Thromboxane A2 (TXA_2), a metabolic product of arachidonic acid, is involved in various physiological activities such as platelet aggregation, airway narrowing, and contraction of various types of arteries, including the pulmonary artery (PA). TXA_2 is synthesized by platelets and parenchymal cells of the intestine, kidney, and lung. In the pulmonary circulation system, TXA_2 appears to act as a physiological modulator of blood flow distribution. For instance, pretreatment with TXA_2 greatly facilitates hypoxic pulmonary vasoconstriction *in vitro* (Park et al., 2012; Yoo et al., 2012) and *in vivo* (Kylhammar and Rådegran, 2012).

Due to the short half-life (<30 s) of TXA_2, a stable synthetic analog U46619 is widely used to investigate its physiological and pathophysiological roles (Hamberg et al., 1975; Nakahata, 2008). TXA_2 and U46619 act through the thromboxane-prostanoid (TP) receptor which is a G-protein coupled receptor. The plasma TXA_2 levels correlated with the prevalence of cardiovascular diseases, including hypertension (Francois et al., 2004), atherosclerosis (Mehta et al., 1988), ischemic heart disease (Serneri et al., 1981), and stroke (Stier et al., 1988). In addition, increased TXA_2 activity was observed in pulmonary hypertension (Zamora et al., 1993).

Against the contractile signals in vascular smooth muscle cells (VSMCs) via phospholipase C (PLC)-coupled G-protein coupled receptors (GPCR) and voltage-operated L-type Ca^{2+} channels ($VOCC_L$), the tone of arteries is regulated by endothelium-derived relaxing factors (EDRFs) and endothelium-derived hyperpolarizing (EDH) mechanisms. Among EDRFs, the release of NO potently regulates vascular tone through the soluble guanylate cyclase (sGC)/cGMP/protein kinase G (PKG) pathway in VSMCs (Buvinic and Huidobro-Toro, 2001). The production of NO via an endothelial type of NO synthase (eNOS) occurs primarily through an increase in cytosolic Ca^{2+} concentration ($[Ca^{2+}]_c$) in the endothelium and Akt-dependent phosphorylation of eNOS (Zhao et al., 2015).

The stimulation of the TP receptor in vascular smooth muscle increases $[Ca^{2+}]_c$ via both stored Ca^{2+} release via PLC/IP_3 signaling and $VOCC_L$-dependent Ca^{2+} influx mechanisms including the activation of non-selective cation channels (Dorn and Becker, 1993; Nakahata, 2008; Yoo et al., 2012). In addition to the direct contractile signals to VSMCs, the stimulation of TP receptors in endothelial cells inhibited K^+ channels (e.g., SK_{Ca}) through an unknown mechanism, and thus reduced the EDH signals (Ellinsworth et al., 2014). $G\alpha_{12/13}$-dependent RhoA-mediated activation of kinase (ROCK) is activated by TP receptor-mediated signals that produce vascular contraction (Kozasa et al., 1998). The activation of ROCK increases the Ca^{2+}-sensitivity of smooth muscle via inhibition of myosin light chain phosphatase (MLCP) (Butler et al., 2013). The U46619-induced arterial contraction was significantly attenuated by Y-27632, an inhibitor of ROCK (Fu et al., 1998). In addition to contractile signaling, our recent study suggested that TP receptor-mediated stimulation of eNOS in the PA smooth muscle layer, counterbalances the potent vasoconstrictive effect of TXA_2 via the NO/cGMP-dependent signaling pathway (Kim et al., 2016).

NO dysregulation appears to be important in vascular tone regulation and PA remodeling in pulmonary arterial hypertension (PAH). Decreased NO availability is a common phenomenon in patients with PAH with impairment in the biosynthesis of NO (Klinger et al., 2013). In PAH, PA remodeling occurs along with changes in the molecular properties of smooth muscle cells (Schermuly et al., 2011). In cultured adult rat pulmonary arterial smooth muscle cells (PASMCs), downregulation of sGC and PKG expression occurred in parallel to phenotypic changes ranging from contractile to synthetic type, which might explain the PA remodeling in PAH (Lincoln et al., 2006). Interestingly, in a Sugen5416/hypoxia-induced PAH rat model, inhibition of NOS by NG-Nitro-L-arginine-methyl ester (L-NAME), revealed biphasic changes in NO availability, and decreased and increased in the early and late phase PAH, respectively. The latter change might counterbalance the excessive contractile tone of the chronic hypoxia-induced PAH arteries (Tanaka et al., 2017).

As a classical animal model of PAH, monocrotaline-injected rats (MCT-PAH) show typical medial thickening of PA with right ventricular hypertrophy. In PAH-MCT rats, a molecular biological investigation of PA tissue revealed increased expression of ROCK2 and decreased sGC (Lee et al., 2016). These changes may decrease the efficiency of the NO/cGMP pathway to enhance responsiveness to contractile agonists such as TXA_2. Taken together with the vasoactive signals of TXA_2 including eNOS activation in rat PA, we hypothesized that the putative downregulation of sGC in PAH-MCT might increase the responsiveness of PA to TXA_2. However, the functional changes, including the sensitivity to the relevant pharmacological agents, were not rigorously investigated in the remodeled PA. In the present study, the concentration-dependent contractile responses of rat PA to U46619 were analyzed using a Mulvany-type isometric tension recording system. In addition, an immunoblot assay was performed to confirm and further elucidate the changes in the levels of TP receptor, eNOS, sGC, and ROCK in PA from PAH-MCT.

MATERIALS AND METHODS

Animal Model

All experimental procedures were conducted with the approval of the Institutional Animal Care and Use Committee of Seoul National University (approval number: SNU-190408-3). Monocrotaline (Sigma, St. Louis, MO, United States) was dissolved in 2 mL of 1 M HCl and adjusted to pH 7.4 using 2 M NaOH solution. This aqueous solution was diluted to 17 mL with distilled water. Seven-week-old male Sprague-Dawley rats were randomly assigned and treated with a single intraperitoneal injection of monocrotaline (60 mg/kg) to induce the PAH-MCT model or an appropriate amount of saline. After 21 days, both the PAH-MCT rats and the age-matched control were sacrificed for further analysis, after measuring their body weight (b.w.).

Arterial Tissue Preparation

Lung tissues were excised and stored in ice-cold normal Tyrode's (NT) solution (140 mM of NaCl, 5.4 mM of KCl, 0.33 mM of NaH_2PO_4, 10 mM of HEPES, 10 mM of glucose, 1.8 mM of $CaCl_2$, and 1 mM of $MgCl_2$, pH 7.4 was adjusted with NaOH). The pulmonary artery bed was collected by removing the lung and bronchial tissues in NT solution. Excised pulmonary arteries were cleaned from perivascular adipose and other tissues under a microscope. Prepared arterial tissues were used for further analysis.

Isometric Tension Recordings

Isometric tension was measured using a dual-wire multi-channel myograph system (620 M; DMT, Aarhus, Denmark). Excised arteries were cut into 2 mm arterial ring segments and mounted with 25 μm tungsten wire on an NT solution-filled organ chamber for tension recording. For stabilization, mounted arteries were rested in physiological salt solution (PSS; 118 mM of NaCl, 4 mM of KCl, 24 mM of $NaHCO_3$, 1 mM of $MgSO_4$, 0.44 mM of NaH_2PO_4, 5.6 mM of glucose, and 1.8 mM of $CaCl_2$) for at least 15 min with a gas mixture (21% O_2, 5% CO_2, N_2 balance) after a basal tone was applied. The whole experiment was maintained at 37°C. For the experiment, 80 mM of KCl-PSS was used to induce contraction (80K) for the evaluation of vessel integrity, and the dose-dependent response of U46619 was evaluated with the application of differential dosages from 1 to 200 nM.

Histology

Pulmonary arterial ring segments were washed with phosphate-buffered saline (PBS) and fixed in 4% paraformaldehyde overnight. For histological analysis, paraffin-embedded tissues were cut and stained with hematoxylin and eosin (H&E) or Masson's trichrome (MT). Digital images of the stained sections were obtained at 200 × magnification using the Aperio ImageScope 12.3 software.

Western Blotting

Whole pulmonary arteries from the left lung were excised and homogenized with RIPA buffer (Millipore, United States) and protease/phosphatase inhibitor cocktail (Roche Diagnostics, Germany) for 1 h at 4°C. The samples were centrifuged at 13,000 ×*g* for 30 min at 4°C and the supernatant was collected. Protein concentration was determined using the Pierce™ BCA Protein Assay Kit (Thermo Fisher Scientific, United States). The loading samples were prepared with Laemmli sample buffer, resolved by 8% SDS-PAGE, and transferred to polyvinylidene difluoride membranes in 25 mM of Tris, 192 mM of glycine, 0.01% SDS, and 20% methanol. Membranes were blocked in 1 × TBS containing 1% Tween-20 and 5% skim milk (blocking solution) for 1 h at room temperature with gentle rocking and incubated overnight at 4°C with relevant primary antibodies for detecting protein expression. Mouse anti-eNOS monoclonal antibody 1:1000 (Abcam, ab76198,United Kingdom), rabbit anti-sGC-α polyclonal antibody 1:1000 (Cayman, 160895, United States), rabbit anti-sGC-β1 polyclonal antibody 1:1000 (Cayman, 160897, United States), rabbit anti-PKG monoclonal antibody 1:1000 (Cell signaling, 3248, United States), rabbit anti-ROCK1 monoclonal antibody 1:1000 (Abcam, ab45171, United Kingdom), rabbit anti-ROCK2 polyclonal antibody 1:1000 (Abcam, ab71598, United Kingdom), rabbit anti-TXA_2R polyclonal antibody 1:1000 (Abcam, ab233288, United Kingdom), and mouse anti-β-actin monoclonal antibody 1:10000 (Sigma, A1978, United States) were used. The signals were determined using ECL Plus Western blotting detection reagents (Amersham Biosciences, United Kingdom) and detected images were obtained by the Amersham™ Imager 600 (Amersham Biosciences, United Kingdom). The intensity of each band was measured using the ImageJ analysis software.

cGMP Concentration Measurement

cGMP concentration in the pulmonary arterial tissues was measured by a commercially available cGMP enzyme immunoassay (EIA) kit (Cayman). The excised pulmonary arteries were pulverized and homogenized with 5% trichloroacetic acid (TCA). The samples were centrifuged at 1,500 ×*g* for 30 min at 4°C and the supernatant was collected. The supernatants were analyzed according to the manufacturer's instructions.

Statistical Analysis

All data are expressed as mean ± SEM and the number of tested arteries is indicated as *n*. For all comparisons, arteries were obtained from at least three rats per protocol. Statistical differences between PAH-MCT and normal rats were analyzed using a two-sample T test. ANOVA was used to investigate more than two groups, and Tukey correction was performed for *post hoc* testing for significant differences. Two-way ANOVA was used to show the statistical differences in the concentration-dependent contractile response of U46619 between groups. Statistical differences were analyzed using SPSS Version 23 (IBM, SPSS, Chicago) and differences were considered when the *p*-value was less than 0.05.

RESULTS

Increased Contractile Sensitivity to U46619 in the PA of PAH-MCT

To characterize the PAH-MCT model, the b.w. changes, mass ratio of the right ventricle, and histological features of PA were analyzed. The b.w. on the 21st day after the MCT injection was lower in PAH-MCT than in CON (**Figure 1A**). The mass ratio of the right ventricles over the sum of the left ventricle and septum (RV/LV + S) was significantly higher in PAH-MCT than in CON (**Figure 1B**) (0.23 ± 0.006 vs. 0.57 ± 0.096; $p = 0.0012$). PA from PAH-MCT displayed a thicker medial layer than the PA from CON (**Figure 1C**, upper panel). MT staining revealed increased collagen deposition in the medial layer of PA from PAH-MCT (**Figure 1C**, lower panel).

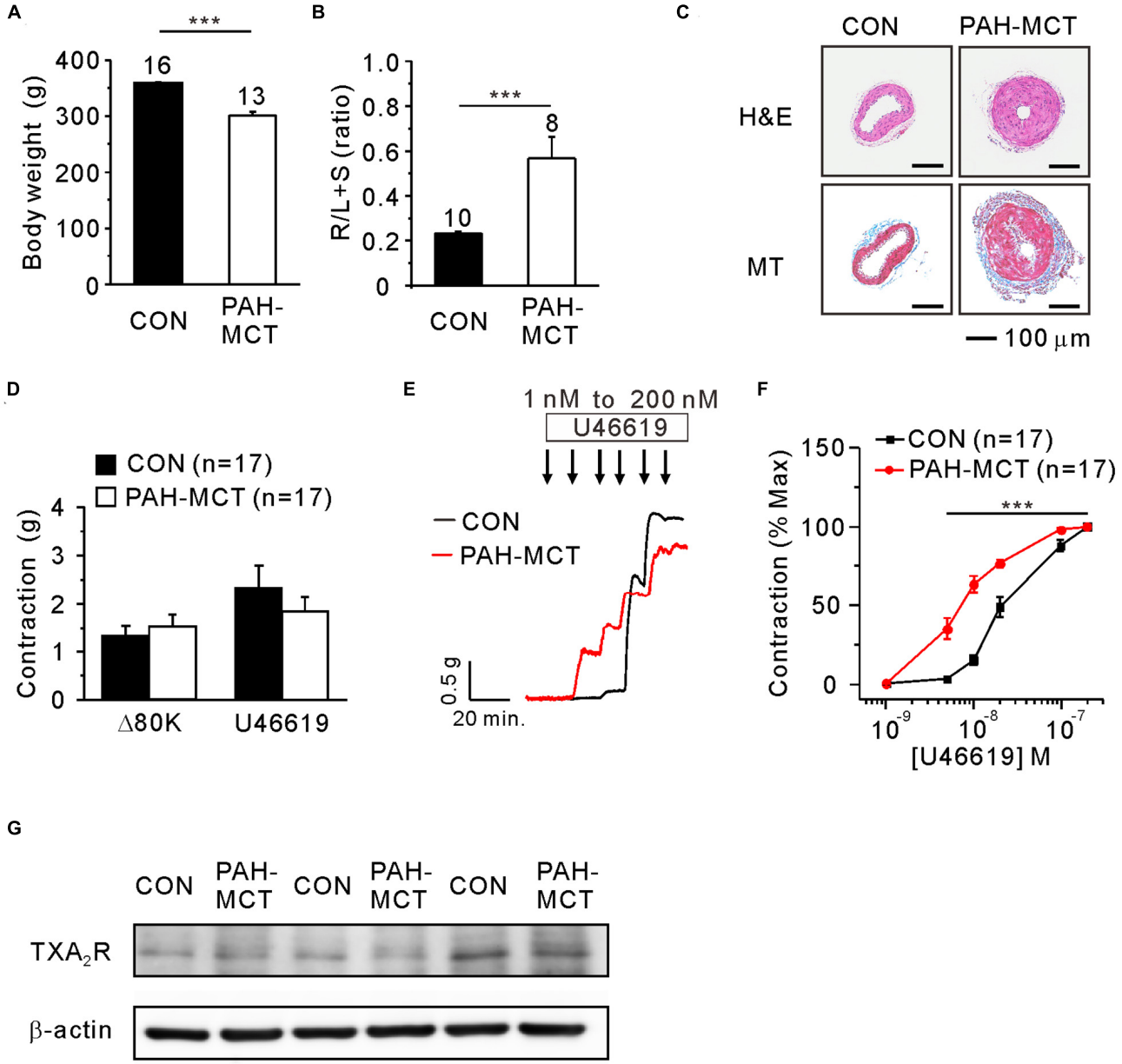

FIGURE 1 | Increased contractile responsiveness of PA to TXA_2 in PAH-MCT. Characteristics of PAH-MCT model with lower b.w. **(A)**, higher relative mass of the right ventricle (R/L + S mass ratio, **(B)**, and medial thickening of PA revealed by the H&E stained light microscopy [**(C)**, upper panel]. MT staining showed MCT-induced collagen deposition in PAH-MCT [**(C)**, lower panel, magnification of 200×. Scale bar: 100 μm]. Isometric tension recording of PA from CON and PAH-MCT rats. Contractile force of Δ80K and U46619 were represented with g **(D)**. The contractile responses to the stepwise increase in the concentration of U46619 **(E)**. The contractile responsiveness was analyzed with concentration-dependent contractile response curve [C-R curve, **(F)**]. The bar graphs represent the means ± SEMs. Statistical difference between groups are indicated as ***$P < 0.001$; bar graph with two sample *t*-test, and C-R curve with two-way ANOVA. **(G)** Representative three pairs of immunoblotting analyses comparing the expression of TP receptors in PAs between CON and PAH-MCT.

In each vessel, the contractile response to 80 mM of KCl (80K-contraction) was initially measured. The PA of PAH-MCT and CON did not show a significant difference at 80K-contraction (**Figure 1D**). To analyze the sensitivity to U46619, the concentration-dependent increase in contractile tone was measured with the isometric tension recording system (**Figure 1E**). The maximum contraction induced by 200 nM of U46619 was higher than that induced by 80K-contraction in CON. The U46619-induced maximum contraction showed a tendency of smaller amplitude in PAH-MCT, and statistical significance was not found owing to the cases with sizable amplitude (**Figure 1D**). When normalized to the maximum U46619-contraction, the concentration-dependent contractile response curve (C-R curve) showed significantly

higher sensitivity to U46619 in PAH-MCT than in CON. Notably, the contractile response at relatively low concentrations (5–20 nM) was more significant in PAH-MCT than in CON (**Figure 1F**). Despite the higher sensitivity to U46619 in PAH-MCT, the expression of TXA_2 receptor (TP) was not different between CON and PAH-MCT (**Figure 1G**).

Decreased Expression of NO/cGMP-Regulating Proteins and Increased Expression of ROCK2 in the PA of PAH-MCT

The sGC and PKG are known to mediate the relaxing signal from eNOS and NO to downstream proteins such as myosin light chain phosphatase (MLCP) and ROCK (**Figure 2A**). The immunoblot study showed decreased eNOS expression in PA of PAH-MCT (**Figure 2B**). sGC is a heterodimer composed of one alpha (sGC-α) and one heme-binding beta subunit (sGC-β). Immunoblot analysis of sGC showed a tendency of lower expression in PAH-MCT whereas statistical significance was found in the level of sGC-β1 (**Figures 2B,C**). The expression of PKG was also lower in PAH-MCT than in CON ($p = 0.030$). In contrast, the expression of ROCK2 was increased in PAH-MCT ($p = 0.043$), while the level of ROCK1 was not changed (**Figure 2C**). cGMP level in the PA tissues was lower in PAH-MCT than in CON (**Figure 2D**).

To investigate the contribution of relaxing signals distal to NO in the U46619-induced contraction, we analyzed the C-R curve after pretreatment with the NO donor sodium nitroprusside (SNP, 30 μM, 10 min). In the CON PA, the C-R curve was shifted to the right by SNP, implying lowered sensitivity to U46619 (**Figure 2E**). In contrast, the pretreatment with SNP did not affect the C-R curve in PAH-MCT (**Figure 2F**).

Pharmacological Regulation of eNOS, sGC, and ROCK in PAH-MCT and CON

To mimic the downregulation of eNOS and sGC proteins in the PAH-MCT, the PA of CON was pretreated with NOS inhibitor (L-NAME, 100 μM) or sGC inhibitor (ODQ, 10 μM). Both pharmacological inhibitors increased the sensitivity of PA to U46619 in CON, and the effect of L-NAME was relatively more prominent (**Figures 3A,B**). In the presence of L-NAME, the exogenous NO donor (SNP, 30 μM) shifted the C-R curve to the right, while SNP had no effect on the C-R curve in the presence of ODQ (**Figures 3C,D**). We compensated for sGC inhibition by using 8-bromoguanosine 3′, 5′-cyclic monophosphate (8-Br-cGMP), a membrane permeable analog of cGMP. The additional pretreatment with 5 μM of 8-Br-cGMP shifted the C-R curve to the right in the presence of ODQ (**Figures 3E,F**). Since the inhibition of ROCK2 was a plausible activity of PKG in the PA myocytes, we evaluated the effect of the ROCK inhibitor Y-27632. The additional pretreatment with 10 μM of Y-27632 also shifted the C-R curve to the right in the presence of ODQ (**Figures 3G,H**).

Next, the effects of the above pharmacological agents were tested in the PA of PAH-MCT. In contrast to the PA of CON, neither the inhibition of eNOS (L-NAME) nor sGC (ODQ) had an effect on the C-R curve of U46619 (**Figures 4A,B**). Despite the insignificant effect of L-NAME and ODQ, pretreatment with 8-Br-cGMP shifted the C-R curve to the right in the PA of PAH-MCT (**Figures 4C,D**). In addition, pretreatment with Y-27632 shifted the C-R curve to the right (**Figures 4E,F**).

Since the C-R curves shown above are normalized values (% contraction induced by 200 nM of U46619), the pretreatment with vasodilators such as 8-Br-cGMP and Y-27632 affected the maximum tone in the tested vessels. Since the initial 80K contraction was measured in the absence of the pharmacological agents, we compared the normalized maximum contraction (% of 80K contraction) in each tested condition (**Figure 5**). To investigate this, a single dose of U46619 (200 nM) was applied in the absence or presence of 8-Br-cGMP and ODQ. Pretreatment with 8-Br-cGMP did not affect the maximum contraction induced by U46619. Furthermore, the combined treatment with ODQ (8-Br-cGMP + ODQ) did not have a significant effect on maximum contraction (**Figure 5A**).

In contrast to the effect of 8-Br-cGMP, the direct inhibition of ROCK (Y-27632) largely suppressed the maximum contraction by U46619. However, when pretreated with both ODQ and Y-27632, the maximum contraction was restored to the control level in the PA from CON (**Figure 5B**, left panel). Interestingly, in the PA from PAH-MCT, neither pretreatment with Y-27632 alone nor the co-treatment with ODQ affected the maximum contraction by U46619 (**Figure 5B**, right panel).

The resistance to Y-27632 in the maximum contraction of PAH-MCT might be due to a hidden compensatory upregulation of contractile signaling pathways other than ROCK, such as voltage-operated L-type Ca^{2+} channels ($VOCC_L$) or protein kinase C (PKC). To test this possibility, we examined the effect of the $VOCC_L$ inhibitor (nifedipine, 1 μM) and an inhibitor of PKC (GF109203X, 10 μM). Both inhibitors decreased the maximum contraction by around 70% in PAH-MCT as well as in CON (**Figure 5C**).

DISCUSSION

The present study showed that the PA segments from rat with PAH-MCT are contracted by nanomolar ranges of the TXA_2 analog, which could be accounted for by the downregulation of NO-related signaling enzymes (eNOS, sGC, and PKG) and by the upregulation of ROCK2 (**Figure 6**). Although the membrane localization of TP receptors was not analyzed, the immunoblot analysis did not show changes in TP receptor expression (**Figure 1G**). Consistent with the schematic summary of the changes in PAH-MCT (**Figure 6**), the pharmacological inhibitors of eNOS and sGC shifted the C-R curves of CON PA in the rightward direction, but not in the PA from PAH-MCT (**Figures 3**, **4**). In PAH-MCT, the inhibition of ROCK effectively restored the C-R curve similar to that in CON (**Figure 4F**). Although the PKG level in PA was downregulated in PAH-MCT, the application of the PKG activator 8-Br-cGMP reversed the increased responsiveness to U46619 in PAH-MCT (**Figure 4D**). Taken together with the results of the immunoblotting assay, the analysis of the C-R curves appears to be an appropriate

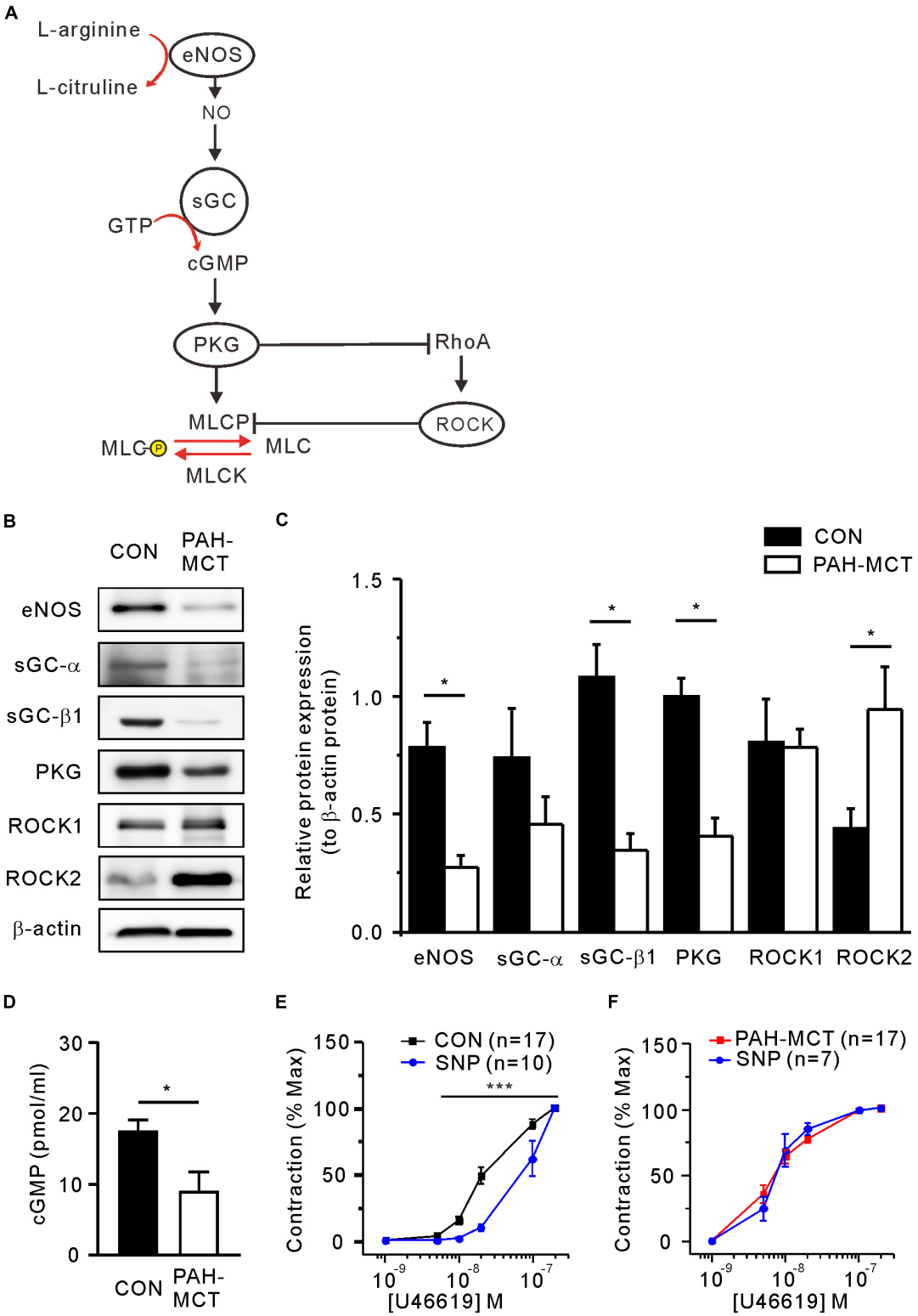

FIGURE 2 | Altered expression of NO/cGMP-regulating enzymes and ROCK in PAH-MCT. **(A)** Schematic drawing of NO/cGMP pathway molecules involved in the regulation of vascular smooth muscle contractility. **(B)** Representative western blot images of NO-sGC-cGMP pathway molecules with β-actin as a standard control. **(C)** Results of band intensity relative to β -actin ($n = 4$, respectively). **(D)** cGMP levels of PA tissues measured with EIA ($n = 4$). $^*P < 0.05$ vs. PAH-MCT; Mann-Whitney U test. **(E,F)** Effect of SNP (30 μM on the C-R curves of CON **(E)** and PAH-MCT **(F)**. $^{***}P < 0.001$; two-way ANOVA.

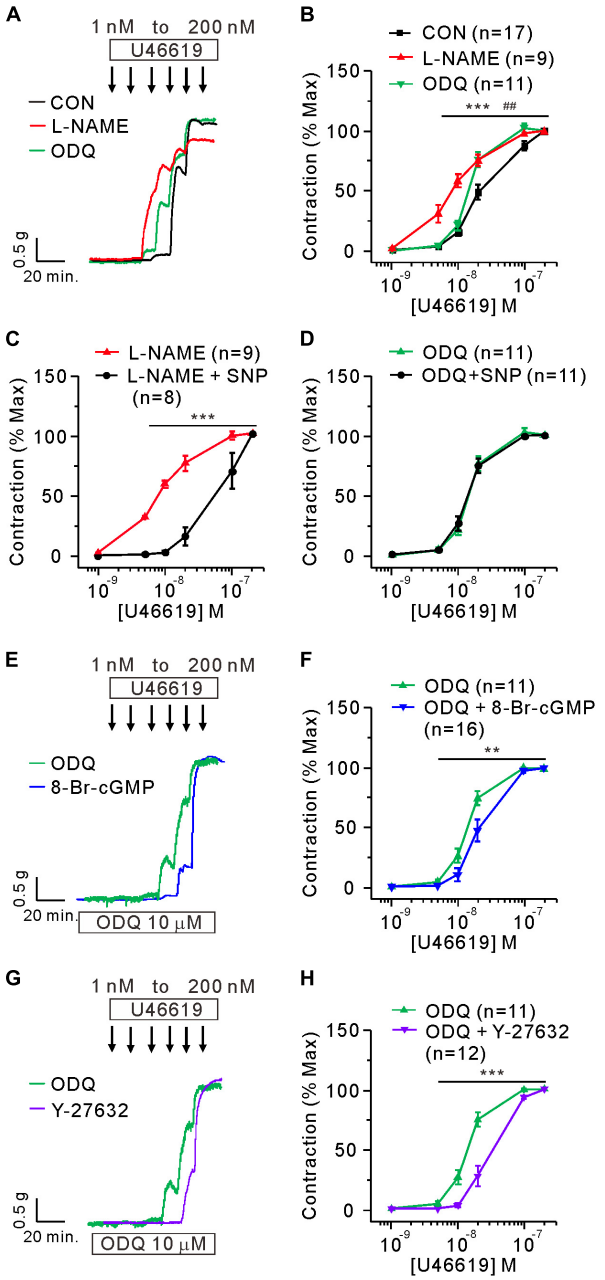

FIGURE 3 | Mimicking the functional changes in PAH-MCT by the inhibitors of eNOS and sGC in the PA of CON. **(A,B)** Effect of preincubation with L-NAME (100 μM) and ODQ (10 μM) on the C-R curves of CON. ***P < 0.001 L-NAME vs CON and ##P < 0.01 ODQ vs CON; two-way ANOVA. **(C,D)** Effect of SNP (30 μM on the sensitized C-R curves by L-NAME **(C)** or by ODQ **(D)**. **(E,F)** Effect of 8-Br-cGMP (30 μM) on the sensitized contraction and the C-R curve shifted by ODQ. **(G,H)** Effect of Y-27632 (10 μM) on the sensitized contraction and the C-R curve shifted by ODQ. Statistical difference between groups are indicated with **P < 0.01 or ***P < 0.001; two-way ANOVA.

approach to reveal the functional implication of the changes in the intracellular signals in PASMCs.

TP receptor signaling in the arterial contraction is mediated through $G\alpha_{12/13}$ to RhoA/ROCK or through $G\alpha_{q/11}$ to PLCβand $InsP_3$/diacylglycerol (DAG)/PKC signaling pathways. It is generally known that activated ROCK induces MLC2 phosphorylation indirectly, which is mediated by the inhibitory phosphorylation of Thr residues (T696 and T853) of MYPT that also prevent the stimulatory phosphorylation of neighboring Ser residues (S695 and S852) (Butler et al., 2013). MYPT1 is a member of the myosin phosphatase targeting protein (MYPT) family consisting of five genes, MYPT1, MYPT2, MBS85, MYPT3, and TIMAP, which function as targeting and regulatory subunits to confer substrate specificity and subcellular localization on the catalytic subunit of type 1δ protein serine/threonine phosphatase (PP1cδ) (Grassie et al., 2011). Taken together, we propose that the upregulation of ROCK along with downregulated sGC/PKG in PAH-MCT are responsible for the sensitized contractile response to TXA_2.

It was notable that the maximum contraction induced by 200 nM of U46619 was not affected by SNP or 8-Br-cGMP. In contrast, the inhibition of $VOCC_L$ and PKC significantly reduced the maximum contraction (**Figures 5A,C**). These results suggested that NO/cGMP-dependent signals have a modulatory role in MLC phosphorylation rather than a direct inhibition of Ca^{2+} signals and contractile mechanisms elicited by TP stimulation. The inhibition of ROCK showed differential effects on maximum contraction; Y-27632 significantly suppressed the maximum contraction in CON, but not in PAH-MCT. Interestingly, even in the PA of CON, Y-27632 did not decrease the maximum contraction in the presence of ODQ (**Figure 5B**). The results suggested a dominant relaxing signal from cGMP-PKG rather than a contractile signal via ROCK that converges on MYPT.

The phosphorylation states of Ser695/Ser852 and Thr696/Thr853 have mutually antagonistic effects on MYPT activity (Qiao et al., 2014). PKG phosphorylates and activates the Ser residues and induces translocation to MLC2, the dephosphorylation of which promotes vasorelaxation. In contrast, ROCK and other pro-contractile signals increase the phosphorylation of Thr residues in MYPT which induces membrane translocation and lowers the chances of interaction with MLC2 (Butler et al., 2013). In this scheme, the deficiency in cGMP-PKG signaling (e.g., ODQ treatment) would not allow for the control of MLC2 by MYPT, and the inhibitory effect of Y-27632 by preventing the interaction between MYPT and MLC2 could not be demonstrated. Since the downregulated eNOS/sGC/PKG in the PA of PAH-MCT would be equivalent to pharmacological inhibition, the effect of Y-27632 was not observed, especially in the conditions of maximum contraction.

Taken together, our present results could be interpreted based on the schematic model of the antagonistic influence on the MLCP activity between the sGC/cGMP/PKG and RhoA/ROCK pathways (**Figure 6**). The downregulation of sGC and PKG possibly minimized the role of MLCP, which is also the target of ROCK. Therefore, the pharmacological inhibition of ROCK might not affect the maximum level of contraction, while still shifting the C-R curve. Since the relative contribution from the other contractile signaling pathways was not altered in the

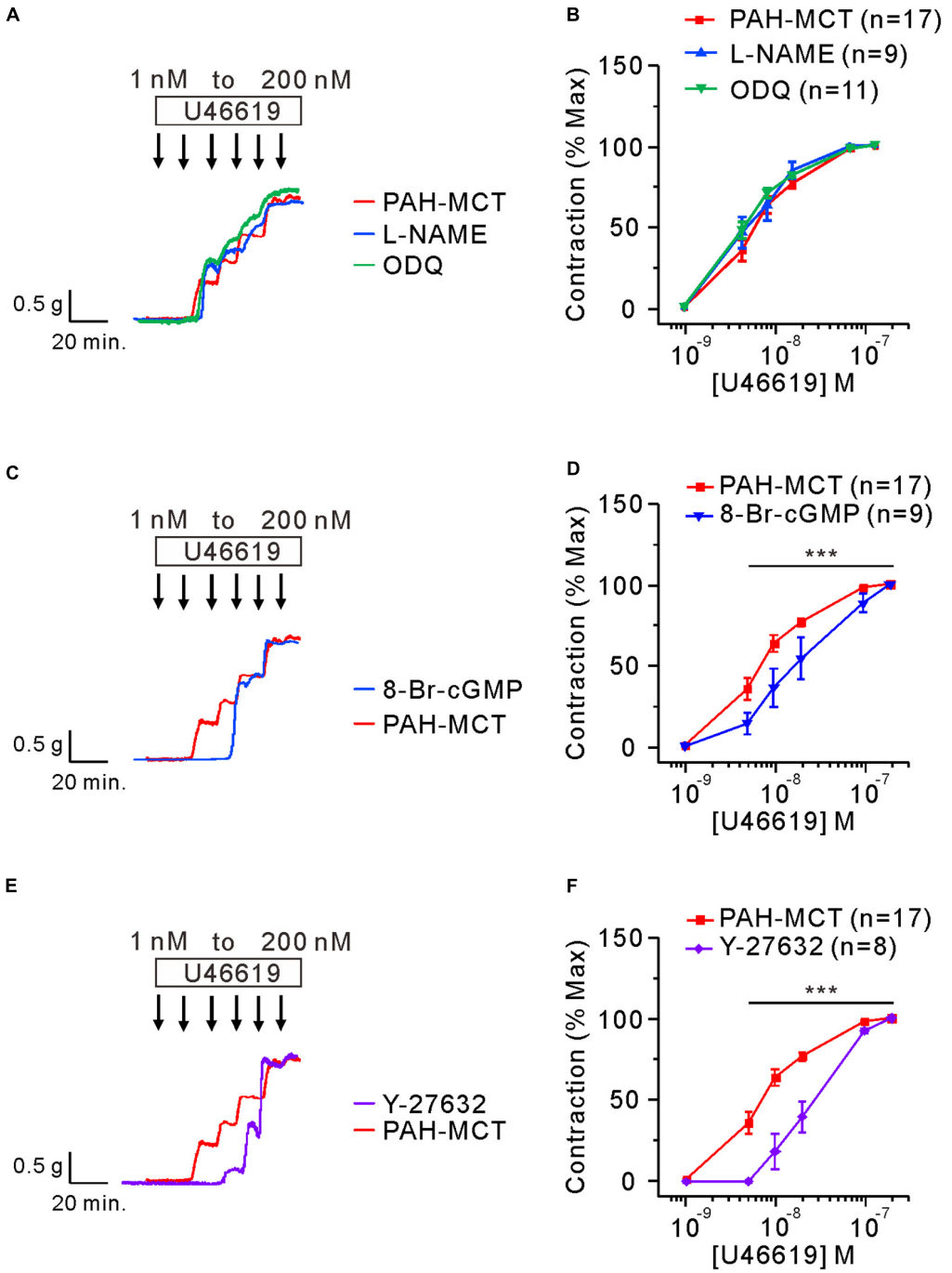

FIGURE 4 | Effects of the inhibitors of eNOS, sGC, and ROCK on the C-R curves of U46619 in the PA of PAH-MCT. **(A,B)** No significant effect of pretreatment with L-NAME (100 μM) and ODQ (10 μM) on the C-R curves of PAH-MCT. **(C,D)** Rightward shift of the C-R curve by 8-Br-cGMP (30 μM). **(E,F)** Rightward shift of the C-R curve by Y-27632 (10 μM). Statistical difference between groups are indicated with ***$P < 0.001$; two-way ANOVA.

PA from PAH-MCT (**Figure 5C**), we cautiously emphasized the critical counteractive regulatory effects of the eNOS-sGC-PKG and RhoA-ROCK pathways on MLCP in PA contraction by TP receptor stimulation. The altered expression of the above signaling molecules in the PASMCs would result in the dysregulation of vasodilation activity (**Figure 6B**).

The immunoblot assay revealed a significant decrease of eNOS expression in the PA of PAH-MCT. Downregulation of eNOS vascular endothelium is one of the major pathophysiological findings in cardiovascular diseases (Bauersachs et al., 1998; Chou et al., 1998; Kobayashi et al., 1999; Li et al., 2002; Lee et al., 2016). It is generally known that endothelial eNOS is

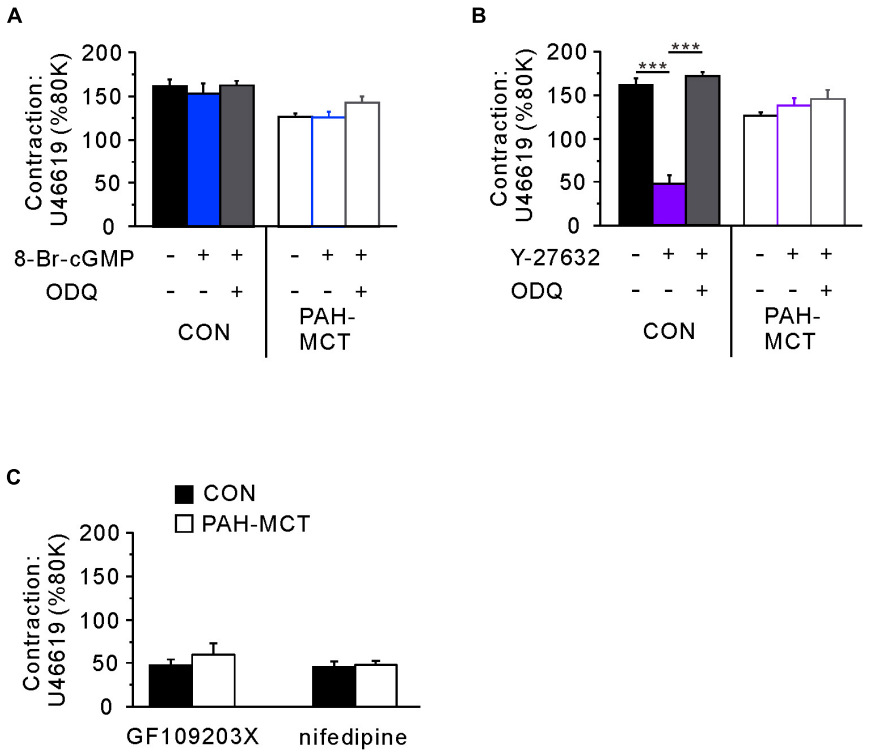

FIGURE 5 | Comparative analyzes of the signaling pathways determining the maximum tone of PA induced by 200 nM of U46619. **(A)** The pretreatment with 8-Br-cGMP alone or with ODQ did not affect the maximum contraction normalized to the 80K-contraction in each PA from CON and PAH-MCT. **(B)** Different effects of the pretreatment with Y27632 on the maximum tone of CON and PAH-MCT. Note that the inhibition by Y27632 was prevented by the co-treatment with ODQ in CON while not altered in PAH-MCT. **(C)** Effects of GF109203X (10 μM) and nifedipine (1 μM) on the maximum contraction induced by 200 nM of U46619. The bars represent the means ± SEMs. Statistical difference between groups are indicated as $^{***}P < 0.001$. Comparison of the effects of 8-Br-cGMP and Y27632.

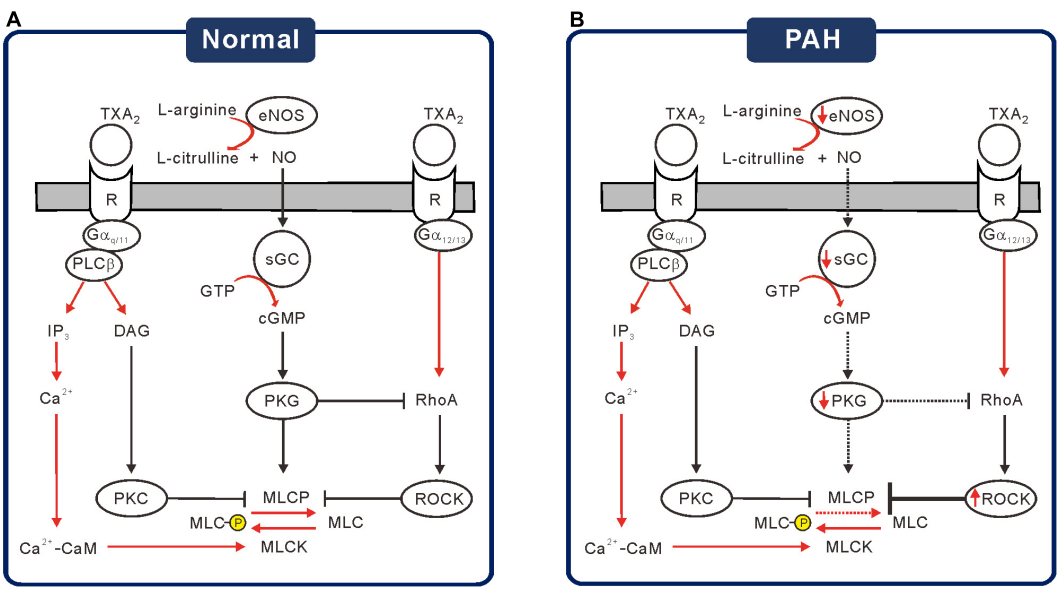

FIGURE 6 | Schematic diagrams of the altered signaling pathways suggested for the increased TXA_2 sensitivity in PAH-MCT. **(A)** Under the basal or stimulated signaling through NO-sGC-cGMP-PKG cascade, PKG activates MLCP but inhibits ROCK to prevent excessive contraction by TXA_2. **(B)** Under the pathological condition of PAH, decreased signaling via NO-sGC-cGMP-PKG would increase the MLC phosphorylation, resulting in increased responsiveness to TXA_2.

a major source of NO which diffuses to neighboring tissues to activate signaling cascades, including sGC. In rat PA, we have previously reported that the medial layer, most likely the smooth muscle cells also express eNOS. Although the level of eNOS expression in the PA medial layer is minute compared to the endothelium, TP stimulation could induce the muscular eNOS phosphorylation to partly contribute to the relaxing signals intrinsic to the myocytes (Kim et al., 2016). However, in the present study, the C-R curves were obtained in PA with an intact endothelium since the process of endothelium removal by mechanical abrasion generally induces unstable responses during U46619-induced contraction experiments. Considering the relatively minute expression of eNOS in the medial layer of PA, the decreased eNOS expression in the PAH-MCT would mostly reflect the downregulation in the endothelium (**Figure 2**).

Along with eNOS, the downregulation of the sGC subunit, especially sGC-β1, was a prominent and consistent finding in PAH-MCT. The critical role of sGC in the regulation of vascular contractility could be demonstrated by the effect of ODQ. In this respect, the abolished influence of ODQ treatment on the C-R curve of PA from PAH-MCT (**Figure 4B**) suggested that the downregulation of sGC was functionally crucial and could be underestimated when simply interpreted from the decreased expression level (**Figure 2C**). The downregulation of sGC and the decreased cGMP (**Figure 2D**) observed in the present study could be consistent with the rationale for the clinical application of PDE5 inhibitors for the treatment of PAH. In addition, a direct activator of sGC, riociguat, has been recently introduced for clinical studies (Montani et al., 2014). The concomitant partial decrease in PKG expression should be considered to interpret the functional changes under pathological conditions. Decreased PKG expression has also been reported in primary aortic vascular smooth muscle cells treated with inflammatory cytokines (Browner et al., 2004; Choi et al., 2018).

ROCK2 expression was increased in PA from PAH-MCT and the C-R curve was restored with ROCK inhibition. The pathophysiological role of ROCK-dependent signaling has also been found in systemic arteries. In the mesenteric artery of spontaneous hypertensive rats, H_2O_2 induces c-Src-dependent TXA_2 release and provokes vascular contractile responses through multiple signaling pathways, including ROCK (García-Redondo et al., 2015). Consistent with the pathophysiological implication of the TXA_2 pathway, both genetic and pharmacological suppression of TXA_2/TP signaling confers microvascular protection against oxidative injury in mesenteric arteries (Chiang, 2019).

In addition to the changes in PA contractility, increased synthesis of TXA_2 and local availability might also underlie the higher tension under pathological conditions. Experimentally, it was reported that a direct injection of U46619 induced a severe prolonged increase in systolic blood pressure, and death of the tested mice, which was not observed in the TP knockout mice (Sparks et al., 2013). Clinically, there is evidence that increased TXA_2 synthesis possibly contributes to increased vascular resistance in children with pulmonary hypertension and pregnancy-induced hypertension (Fitzgerald et al., 1990; Adatia et al., 1993). PAH patients showed higher TXA_2 synthesis with decreased prostacyclin (PGI_2) (Christman et al., 1992; Liel et al., 1993; Kazimierczyk and Kamiński, 2018) and platelet aggregation (Nakonechnicov et al., 1996; Varol et al., 2011), and increased thrombosis is one of the criteria for PAH (Farber and Loscalzo, 2004). Despite the repeatedly observed pathophysiological role of TXA_2 in PAH, the pharmacological antagonist of the TP receptor has not been clinically investigated yet. Instead, the administration of PGI_2 analog is one of the options for PAH treatment (Montani et al., 2014).

CONCLUSION

During the pathological condition of PAH, the combined increase in TXA_2 availability and contractile sensitivity to TXA_2 may worsen the burden of pulmonary circulation. Along with the functional changes, PA wall thickening dramatically increased peripheral resistance and right ventricular afterload in PAH. The markedly lowered threshold concentration of U46619 suggested vulnerability to collapse or uneven regional perfusion in the PAH lung. Since the C-R curves and their changes by pharmacological agents are consistent with the molecular biological findings than the simple comparison of maximum contraction levels, our present study emphasizes the implication of physiological parameters obtained from myography studies.

DATA AVAILABILITY STATEMENT

The original contributions presented in the study are included in the article/supplementary material, further inquiries can be directed to the corresponding author/s.

ETHICS STATEMENT

The animal study was reviewed and approved by the Institutional Animal Care and Use Committee (IACUC) of Seoul National University.

AUTHOR CONTRIBUTIONS

SC and SK: conception and design of study. SC, HN, and RV: conducting experiments, acquisition of data, analysis, and interpretation of data. SC, HY, and HK: drafting the manuscript. SK: revising the manuscript critically for important intellectual content. All authors contributed to the article and approved the submitted version.

FUNDING

This work was supported by the National Research Foundation of Korea (NRF) funded by the Ministry of Science and ICT of the Republic of Korea (grant nos. NRF-2018R1A5A2025964 and NRF-2018R1D1A1B07048998). In addition, this work was partly supported by the Education and Research Encouragement Fund of Seoul National University Hospital (2020).

REFERENCES

Adatia, I., Barrow, S., Stratton, P., Miall-Allen, V., Ritter, J., and Haworth, S. (1993). Thromboxane A2 and prostacyclin biosynthesis in children and adolescents with pulmonary vascular disease. *Circulation* 88, 2117–2122. doi: 10.1161/01.cir.88.5.2117

Bauersachs, J., Bouloumie, A., Mülsch, A., Wiemer, G., Fleming, I., and Busse, R. (1998). Vasodilator dysfunction in aged spontaneously hypertensive rats: changes in NO synthase III and soluble guanylyl cyclase expression, and in superoxide anion production. *Cardiovasc. Res.* 37, 772–779. doi: 10.1016/s0008-6363(97)00250-2

Browner, N. C., Sellak, H., and Lincoln, T. M. (2004). Downregulation of cGMP-dependent protein kinase expression by inflammatory cytokines in vascular smooth muscle cells. *Am. J. Physiol. Cell Physiol.* 287, C88–C96.

Butler, T., Paul, J., Europe-Finner, N., Smith, R., and Chan, E.-C. (2013). Role of serine-threonine phosphoprotein phosphatases in smooth muscle contractility. *Am. J. Physiol. Cell Physiol.* 304, C485–C504.

Buvinic, S., and Huidobro-Toro, J. P. (2001). Basal tonic release of nitric oxide coupled to cGMP production regulates the vascular reactivity of the mesenteric bed. *Eur. J. Pharmacol.* 424, 221–227. doi: 10.1016/s0014-2999(01)01165-7

Chiang, C.-Y. (2019). *Genetic Depletion of Thromboxane A2/Thromboxane-Prostanoid Receptor Signalling Prevents Microvascular Dysfunction in Ischaemia/Reperfusion Injury*. Taiwan: National Taiwan Normal University.

Choi, S., Park, M., Kim, J., Park, W., Kim, S., Lee, D.-K., et al. (2018). TNF-α elicits phenotypic and functional alterations of vascular smooth muscle cells by miR-155-5p–dependent down-regulation of cGMP-dependent kinase 1. *J. Biol. Chem.* 293, 14812–14822. doi: 10.1074/jbc.ra118.004220

Chou, T.-C., Yen, M.-H., Li, C.-Y., and Ding, Y.-A. (1998). Alterations of nitric oxide synthase expression with aging and hypertension in rats. *Hypertension* 31, 643–648. doi: 10.1161/01.hyp.31.2.643

Christman, B. W., McPherson, C. D., Newman, J. H., King, G. A., Bernard, G. R., Groves, B. M., et al. (1992). An imbalance between the excretion of thromboxane and prostacyclin metabolites in pulmonary hypertension. *N. Engl. J. Med.* 327, 70–75. doi: 10.1056/nejm199207093270202

Dorn, G.d., and Becker, M. W. (1993). Thromboxane A2 stimulated signal transduction in vascular smooth muscle. *J. Pharmacol. Exp. Ther.* 265, 447–456.

Ellinsworth, D. C., Shukla, N., Fleming, I., and Jeremy, J. Y. (2014). Interactions between thromboxane A2, thromboxane/prostaglandin (TP) receptors, and endothelium-derived hyperpolarization. *Cardiovasc. Res.* 102, 9–16. doi: 10.1093/cvr/cvu015

Farber, H. W., and Loscalzo, J. (2004). Pulmonary arterial hypertension. *N. Engl. J. Med.* 351, 1655–1665.

Fitzgerald, D., Rocki, W., Murray, R., Mayo, G., and FitzGerald, G. (1990). Thromboxane A2 synthesis in pregnancy-induced hypertension. *Lancet* 335, 751–754. doi: 10.1016/0140-6736(90)90869-7

Francois, H., Athirakul, K., Mao, L., Rockman, H., and Coffman, T. M. (2004). Role for thromboxane receptors in angiotensin-II–induced hypertension. *Hypertension* 43, 364–369. doi: 10.1161/01.hyp.0000112225.27560.24

Fu, X., Gong, M. C., Jia, T., Somlyo, A. V., and Somlyo, A. P. (1998). The effects of the Rho-kinase inhibitor Y-27632 on arachidonic acid-, GTPγ S-, and phorbol ester-induced Ca^{2+}-sensitization of smooth muscle. *FEBS Lett.* 440, 183–187. doi: 10.1016/s0014-5793(98)01455-0

García-Redondo, A. B., Briones, A. M., Martínez-Revelles, S., Palao, T., Vila, L., Alonso, M. J., et al. (2015). c-Src, ERK1/2 and Rho kinase mediate hydrogen peroxide-induced vascular contraction in hypertension: role of TXA2, NAD(P)H oxidase and mitochondria. *J. Hypertens.* 33, 77–87. doi: 10.1097/hjh.0000000000000383

Grassie, M. E., Moffat, L. D., Walsh, M. P., and MacDonald, J. A. (2011). The myosin phosphatase targeting protein (MYPT) family: a regulated mechanism for achieving substrate specificity of the catalytic subunit of protein phosphatase type 1δ. *Arch. Biochem. Biophys.* 510, 147–159. doi: 10.1016/j.abb.2011.01.018

Hamberg, M., Svensson, J., and Samuelsson, B. (1975). Thromboxanes: a new group of biologically active compounds derived from prostaglandin endoperoxides. *Proc. Natl. Acad. Sci. U.S.A.* 72, 2994–2998. doi: 10.1073/pnas.72.8.2994

Kazimierczyk, R., and Kamiński, K. (2018). The role of platelets in the development and progression of pulmonary arterial hypertension. *Adv. Med. Sci.* 63, 312–316. doi: 10.1016/j.advms.2018.04.013

Kim, H. J., Yoo, H. Y., Jang, J. H., Lin, H. Y., Seo, E. Y., Zhang, Y. H., et al. (2016). Wall stretch and thromboxane A2 activate NO synthase (eNOS) in pulmonary arterial smooth muscle cells via H_2O_2 and Akt-dependent phosphorylation. *Pflügers Arch. Eur. J. Physiol.* 468, 705–716. doi: 10.1007/s00424-015-1778-1

Klinger, J. R., Abman, S. H., and Gladwin, M. T. (2013). Nitric oxide deficiency and endothelial dysfunction in pulmonary arterial hypertension. *Am. J. Respirat. Crit. Care Med.* 188, 639–646. doi: 10.1164/rccm.201304-0686pp

Kobayashi, N., Kobayashi, K., Hara, K., Higashi, T., Yanaka, H., Yagi, S., et al. (1999). Benidipine stimulates nitric oxide synthase and improves coronary circulation in hypertensive rats. *Am. J. Hypertens.* 12, 483–491. doi: 10.1016/s0895-7061(98)00260-x

Kozasa, T., Jiang, X., Hart, M. J., Sternweis, P. M., Singer, W. D., Gilman, A. G., et al. (1998). p115 RhoGEF, a GTPase activating protein for Gα12 and Gα13. *Science* 280, 2109–2111. doi: 10.1126/science.280.5372.2109

Kylhammar, D., and Rådegran, G. (2012). Cyclooxygenase-2 inhibition and thromboxane A2 receptor antagonism attenuate hypoxic pulmonary vasoconstriction in a porcine model. *Acta Physiol.* 205, 507–519. doi: 10.1111/j.1748-1716.2012.02437.x

Lee, M.-Y., Tsai, K.-B., Hsu, J.-H., Shin, S.-J., Wu, J.-R., and Yeh, J.-L. (2016). Liraglutide prevents and reverses monocrotaline-induced pulmonary arterial hypertension by suppressing ET-1 and enhancing eNOS/sGC/PKG pathways. *Sci. Rep.* 6:31788.

Li, H., Wallerath, T., Münzel, T., and Förstermann, U. (2002). Regulation of endothelial-type NO synthase expression in pathophysiology and in response to drugs. *Nitric Oxide* 7, 149–164. doi: 10.1016/s1089-8603(02)00111-8

Liel, N., Nathan, I., Yermiyahu, T., Zolotov, Z., Lieberman, J., Dvilansky, A., et al. (1993). Increased platelet thromboxane A2/prostaglandin H2 receptors in patients with pregnancy induced hypertension. *Thrombosis Res.* 70, 205–210. doi: 10.1016/0049-3848(93)90126-9

Lincoln, T. M., Wu, X., Sellak, H., Dey, N., and Choi, C.-S. (2006). Regulation of vascular smooth muscle cell phenotype by cyclic GMP and cyclic GMP-dependent protein kinase. *Front. Biosci.* 11:356–367. doi: 10.2741/1803

Mehta, J. L., Lawson, D., Mehta, P., and Saldeen, T. (1988). Increased prostacyclin and thromboxane A2 biosynthesis in atherosclerosis. *Proc. Natl. Acad. Sci. U.S.A.* 85, 4511–4515. doi: 10.1073/pnas.85.12.4511

Montani, D., Chaumais, M.-C., Guignabert, C., Günther, S., Girerd, B., Jaïs, X., et al. (2014). Targeted therapies in pulmonary arterial hypertension. *Pharmacol. Ther.* 141, 172–191.

Nakahata, N. (2008). Thromboxane A2: physiology/pathophysiology, cellular signal transduction and pharmacology. *Pharmacol. Ther.* 118, 18–35. doi: 10.1016/j.pharmthera.2008.01.001

Nakonechnicov, S., Gabbasov, Z., Chazova, I., Popov, E., and Yu, B. (1996). Platelet aggregation in patients with primary pulmonary hypertension. *Blood Coagul. Fibrinol. Int. J. Haemostasis Thrombosis* 7, 225–227. doi: 10.1097/00001721-199603000-00029

Park, S. J., Yoo, H. Y., Kim, H. J., Kim, J. K., Zhang, Y.-H., and Kim, S. J. (2012). Requirement of pretone by thromboxane a2 for hypoxic pulmonary vasoconstriction in precision-cut lung slices of rat. *Kor. J. Physiol. Pharmacol.* 16, 59–64. doi: 10.4196/kjpp.2012.16.1.59

Qiao, Y. N., He, W. Q., Chen, C. P., Zhang, C. H., Zhao, W., Wang, P., et al. (2014). Myosin phosphatase target subunit 1 (MYPT1) regulates the contraction and relaxation of vascular smooth muscle and maintains blood pressure. *J. Biol. Chem.* 289, 22512–22523. doi: 10.1074/jbc.M113.525444

Schermuly, R. T., Ghofrani, H. A., Wilkins, M. R., and Grimminger, F. (2011). Mechanisms of disease: pulmonary arterial hypertension. *Nat. Rev. Cardiol.* 8:443.

Serneri, G. G. N., Gensini, G. F., Abbate, R., Mugnaini, C., Favilla, S., Brunelli, C., et al. (1981). Increased fibrinopeptide A formation and thromboxane A2 production in patients with ischemic heart disease: relationships to coronary pathoanatomy, risk factors, and clinical manifestations. *Am. Heart J.* 101, 185–194. doi: 10.1016/0002-8703(81)90665-7

Sparks, M. A., Makhanova, N. A., Griffiths, R. C., Snouwaert, J. N., Koller, B. H., and Coffman, T. M. (2013). Thromboxane receptors in smooth muscle promote hypertension, vascular remodeling, and sudden death. *Hypertension* 61, 166–173. doi: 10.1161/hypertensionaha.112.193250

Stier, C. Jr., Benter, I., and Levine, S. (1988). Thromboxane A2 in severe hypertension and stroke in stroke-prone spontaneously hypertensive rats. *Stroke* 19, 1145–1150. doi: 10.1161/01.str.19.9.1145

Tanaka, M., Abe, K., Oka, M., Saku, K., Yoshida, K., Ishikawa, T., et al. (2017). Inhibition of nitric oxide synthase unmasks vigorous vasoconstriction in established pulmonary arterial hypertension. *Physiol. Rep.* 5:e13537. doi: 10.14814/phy2.13537

Varol, E., Uysal, B. A., and Ozaydin, M. (2011). Platelet indices in patients with pulmonary arterial hypertension. *Clin. Appl. Thrombosis Hemostasis* 17, E171–E174.

Yoo, H. Y., Park, S. J., Seo, E.-Y., Park, K. S., Han, J.-A., Kim, K. S., et al. (2012). Role of thromboxane A2-activated nonselective cation channels in hypoxic pulmonary vasoconstriction of rat. *Am. J. Physiol. Cell Physiol.* 302, C307–C317.

Zamora, C. A., Baron, D. A., and Heffner, J. E. (1993). Thromboxane contributes to pulmonary hypertension in ischemia-reperfusion lung injury. *J. Appl. Physiol.* 74, 224–229. doi: 10.1152/jappl.1993.74.1.224

Zhao, Y., Vanhoutte, P. M., and Leung, S. W. (2015). Vascular nitric oxide: Beyond eNOS. *J. Pharmacol. Sci.* 129, 83–94. doi: 10.1016/j.jphs.2015.09.002

Conflict of Interest: The authors declare that the research was conducted in the absence of any commercial or financial relationships that could be construed as a potential conflict of interest.

frontiers in Cardiovascular Medicine

OPINION
published: 10 February 2021
doi: 10.3389/fcvm.2021.607998

Ivabradine and Blood Pressure Reduction: Underlying Pleiotropic Mechanisms and Clinical Implications

Fedor Simko [1,2,3]* *and Tomas Baka* [1]

[1] *Institute of Pathophysiology, Faculty of Medicine, Comenius University, Bratislava, Slovakia,* [2] *3rd Department of Internal Medicine, Faculty of Medicine, Comenius University, Bratislava, Slovakia,* [3] *Institute of Experimental Endocrinology, Biomedical Research Center, Slovak Academy of Sciences, Bratislava, Slovakia*

Keywords: ivabradine, blood pressure, endothelial dysfunction, vascular stiffness, neurohumoral activation

OPEN ACCESS

Edited by:
Modar Kassan,
University of Tennessee Health Science Center (UTHSC), United States

Reviewed by:
Sung Joon Kim,
Seoul National University, South Korea
Michel Burnier,
Centre Hospitalier Universitaire Vaudois (CHUV), Switzerland
Karima Ait-Aissa,
The University of Iowa, United States

***Correspondence:**
Fedor Simko
fedor.simko@fmed.uniba.sk

Specialty section:
This article was submitted to Hypertension, a section of the journal Frontiers in Cardiovascular Medicine

Received: *18 September 2020*
Accepted: *07 January 2021*
Published: *10 February 2021*

Citation:
Simko F and Baka T (2021) Ivabradine and Blood Pressure Reduction: Underlying Pleiotropic Mechanisms and Clinical Implications. Front. Cardiovasc. Med. 8:607998. doi: 10.3389/fcvm.2021.607998

INTRODUCTION

Elevated heart rate (HR) is a well-recognized but somewhat neglected risk factor among the healthy population and various cardiovascular pathologies (1). High HR is fraught with a spate of detrimental cardiovascular consequences including immense myocardial oxygen demand in reduced diastolic perfusion time (2) and low, oscillatory vascular shear stress with high tensile stress triggering endothelial dysfunction (3). Although beta-blockers (BBs) are considered to be the cornerstone treatment of elevated HR in various cardiovascular pathologies, they are associated with negative inotropy, a number of side effects, and undesirable metabolic actions limiting their usage (4, 5). Thus, new approaches to HR reduction are being continuously sought out.

The inhibition of the I_f current in the sinoatrial node (SAN) seems to offer a promising approach to the reduction of elevated HR. Indeed, the SAN's pacemaker cells are inherently capable of cyclic variations of the resting membrane potential necessary for spontaneous depolarization. The SAN's spontaneous slow diastolic depolarization is administered by a mixed sodium/potassium inward current, known as an I_f current, through the "funny" (f)-channel (6). Structurally, the f-channel belongs to hyperpolarization-activated, cyclic nucleotide-gated (HCN) channels and is activated by both hyperpolarization in the diastolic voltage range and intracellular cyclic adenosine monophosphate (7). Ivabradine selectively inhibits the I_f current, thus reducing the steepness of SAN's diastolic depolarization, ensuing diastole prolongation without affecting action potential duration or inducing negative inotropy (7, 8).

Several studies have assessed ivabradine's efficacy in clinical settings. In the SHIFT study, the investigation of 6,558 patients with systolic heart failure (HF) during a median 22.9 month follow-up period revealed that the addition of ivabradine to an established HF therapy significantly reduced the primary composite endpoint of hospital admission for worsening HF or cardiovascular death. Considering the results of the SHIFT study, ivabradine is recommended for patients with systolic HF and HR above 70 bpm despite an evidence-based optimal medical therapy (with or without BB) to reduce the composite endpoint of hospitalization and mortality (9, 10). The BEAUTIFUL study comprised 10,917 systolic HF patients with HR above 70 bpm suffering from stable coronary artery disease (CAD), and the primary endpoint was a composite of cardiovascular death and hospital admission for acute myocardial infarction or HF. Although neither the primary endpoint nor the cardiovascular death rate improved, ivabradine reduced the secondary endpoints

of hospital admissions for myocardial infarction and coronary revascularization (11). However, in the SIGNIFY study involving 19,102 patients with stable CAD but without HF, ivabradine did not reduce the compound primary endpoint of cardiovascular death and myocardial infarction (12).

Hypertension, however, is a substantially different condition, and data regarding ivabradine's effect on peripheral blood pressure (BP) in a hypertensive population are scanty. Yet ivabradine's interference with central BP (CBP) was indicated in several studies. Lopatin and Vitale (13) reviewed five studies analyzing ivabradine's effect on CBP in patients with CAD: two studies reported a neutral effect, while in two other studies and in one study, ivabradine decreased and increased CBP, respectively. In 12 normotensive patients with stable CAD and HR $\geq$ 70 bmp, a 3 week ivabradine treatment reduced brachial systolic and diastolic BP, while the HR reduction did not increase central aortic BP (14). Moreover, in patients with arterial hypertension and CAD treated with ivabradine, the increase in HR between resting conditions and early recovery post exercise showed a trend toward correlation with the radial augmentation index (15).

Besides ivabradine's HR-reducing action, which is considered to be a principal mechanism of its benefit, ivabradine exerts a number of pleiotropic effects, some of which may partly be HR independent (16, 17) and some of which are still emerging.

IVABRADINE AND BP REDUCTION

BBs have been a well-established means for HR reduction and the improvement of the energetic state of the myocardium in various cardiovascular diseases (18). The important advantage of ivabradine over BB seems to be its apparent independence from the sympathetic nervous system, thus avoiding negative inotropy or alpha-adrenoceptor-mediated coronary vasoconstriction (17).

According to generally accepted assumptions, ivabradine exerts a neutral effect on arterial BP in both experimental and clinical settings (8–12). However, based on several recent pieces of evidence, ivabradine could reduce BP under certain conditions:

- In an experiment with N^G-nitro-L-arginine methyl ester (L-NAME)-induced nitric oxide-deficient hypertension in rats, ivabradine (10 mg/kg/day) reduced HR and systolic BP measured by non-invasive tail-cuff plethysmography during a period of 4 weeks. Systolic BP was reduced from the first week by ivabradine treatment and continued to decrease each week. In the fourth week of the experiment, ivabradine reduced systolic BP by 15%, and the 4 week average systolic BP was decreased by 8% via ivabradine compared to that in the L-NAME group (19). In another study with L-NAME-induced hypertension, ivabradine reduced systolic BP not only in the L-NAME group (by 21%) but even in the control group (by 26%) (20).
- In a study that sought to improve non-dipping HR in a rat model of L-NAME-induced hypertension, daytime and nighttime systolic BP and HR were measured weekly after administration of the daily dose of ivabradine (10 mg/kg/day) at either daytime or nighttime during a period of 4 weeks. Interestingly, both daytime- and nighttime-dosed ivabradine decreased both daytime and nighttime systolic BP in hypertensive rats each week, reaching the largest 14% systolic BP decline during the last week of the experiment (21).
- In the three rat models of acute stress induced by handling (mild stress), restraint (moderate stress), or immobilization (severe stress), ivabradine (5 mg/kg) was administered intraperitoneally 30 min before stress exposure. In the groups pretreated with ivabradine, lower values of HR and mean arterial BP were observed in the baseline period, during exposure to stressors, as well as during the rest period following stress exposure in all three types of stressors applied and all intervals investigated (22).
- Two studies assessed the effect of acute or chronic ivabradine on HR and BP in spontaneously hypertensive rats and Wistar–Kyoto controls as measured by carotid catheterization under pentobarbital anesthesia. The acute administration of four consecutive ivabradine doses (1 mg/kg, i.v.) decreased systolic, diastolic, and mean BP in hypertensive rats and in controls (except for systolic BP, which remained unchanged) and increased pulse pressure in both rat strains (23). The chronic, 28 day administration of ivabradine (8.4 mg/kg/day via subcutaneous osmotic minipump) decreased systolic, diastolic, and mean BP and increased pulse pressure in both rat strains (24).
- In healthy volunteers treated with ivabradine (30 mg), propranolol (40 mg), or a placebo, hemodynamic parameters were investigated at rest and before and during tilt and exercise tests 2 and 5 h after drug intake. Ivabradine significantly reduced systolic BP at rest. However, during tilt and exercise tests, only propranolol but not ivabradine reduced systolic BP (25).

The mechanisms underlying the ambiguity of ivabradine's effect on BP in different conditions remain elusive. Yet the following two factors might be considered determining: (i) the pathophysiology of the ivabradine-treated disease, as in a rat model of isoproterenol-induced HF, ivabradine prevented detrimental systolic BP decline indicative of improved cardiac function (26), while in a rat model of L-NAME-induced hypertension, ivabradine decreased systolic BP by exerting antihypertensive properties (19); and (ii) concomitant therapy, as in pivotal clinical studies, e.g., SHIFT, BEAUTIFUL, or SIGNIFY, ivabradine was administered on top of the evidence-based optimal medical therapy, often including drugs modulating the sympathetic nervous system and/or renin–angiotensin–aldosterone system (8–12), thus presumably giving minimal space for ivabradine to exert an effect on BP. In clinical studies with HF patients, HR reduction without affecting BP was considered to be desirable, since the BP-reducing effect of well-established HF therapeutics such as BB, angiotensin-converting enzyme inhibitors (ACEis), angiotensin II type 1 receptor blockers (ARBs), or mineralocorticoid receptor antagonists (MRAs) can limit the achievement of the target doses. Interestingly, it has been shown that the efficacy and safety of ivabradine in HF patients were independent of systolic BP (27).

POTENTIAL MECHANISMS BEHIND IVABRADINE'S INTERFERENCE WITH BP

Although experimental data on ivabradine's BP-reducing effect are scarce and large prospective clinical studies featuring ivabradine and a hypertensive population are lacking, numerous potential mechanisms contributing to the BP reduction by ivabradine in experiments demonstrated in this study could be considered. Indeed, several pleiotropic effects of ivabradine, such as anti-inflammatory and antioxidant actions, the improvement of endothelium-dependent and endothelium-independent vascular relaxation, anti-atherosclerotic effects, and the attenuation of the neurohumoral activation, might individually or in concert contribute to BP reduction (**Figure 1**).

Ivabradine's Interference With Oxidative Stress, Inflammation, Endothelial Dysfunction, and Vascular Stiffness

Several plausible explanations for the potential BP-reducing effect of ivabradine are emerging. Besides HR reduction, ivabradine was shown to exert manifold pleiotropic effects within the vasculature in terms of inflammation and oxidative stress reduction and improvement of endothelial function and vascular elasticity (28). Indeed, in low-shear-stress-damaged isolated endothelial cells, ivabradine prevented inflammation and oxidative stress via the TOR/eNOS pathway (29). Ivabradine reduced reactive oxygen species levels in atherogenic diet-induced hypercholesterolemic rabbits (30). In apolipoprotein E-knockout mice, ivabradine reduced NADPH oxidase activity and prevented eNOS uncoupling (31); decreased monocyte chemotactic protein mRNA, markers of superoxide production and lipid peroxidation, and atherosclerotic plaque size (32); reduced the aortic mRNA expression of IL-6, TNF-α, and TGF-β (33); and downregulated pro-apoptotic and pro-inflammatory genes (23, 34). In hypercholesterolemic mice, ivabradine reduced the expression of pro-inflammatory VCAM-1 and enhanced the expression of anti-inflammatory eNOS on the inner surface of the aorta (35). These potentially protective effects of ivabradine could result in the improvement of aortic elasticity and endothelium-dependent relaxation (30, 33, 36). Indeed, ivabradine reduced neointimal hyperplasia and intima–media ratio in hypercholesterolemic rabbits (30) and attenuated aortic fibrosis and stiffness in diabetic mice (37). Ivabradine also inhibited the chemokine-induced migration of CD4-positive lymphocytes, thus potentially curbing atherosclerosis development (38). In clinical settings, ivabradine improved aortic elasticity and endothelial function in chronic systolic HF (36) and fostered the flow- and nitroglycerin-mediated dilation of the brachial artery in patients with CAD (39). Similarly, in patients with chronic stable CAD, HR reduction by ivabradine improved flow-mediated vasodilation and reduced the arterial stiffness of the brachial artery (40).

Increasing the magnitude of wall shear stress via HR reduction seems to be the underlying mechanism of ivabradine's arterial protection (35). Moreover, ivabradine increased the brain capillary density in mice with chronic mental stress (41), enhanced capillary formation in mice with myocardial infarction (42), and improved coronary reserve in rats afflicted with myocardial infarction potentially by the reduction of periarteriolar collagen (43). Taken together, these findings suggest that ivabradine may improve endothelium-dependent and endothelium-independent vascular relaxation, resulting in vasodilation along with improvement of microcirculation, thus contributing to BP reduction and improved organ perfusion.

Ivabradine was also shown to exert cardioprotection by the attenuation of both apoptosis and matrix metalloproteinase expression (44), to improve mitochondrial respiration, and to enhance ATP production and calcium retention capacity independent of HR reduction (16). Moreover, ivabradine showed a positive inotropic action induced by enhanced sarcoplasmic/endoplasmic reticulum calcium ATPase 2a (SERCA2a) activity (45). Thus, the vascular and cardiac protective pathways, along with HR reduction, may underlie ivabradine's effects of cardiovascular benefit.

Ivabradine Modifies Neurohumoral Pathways

The potential relation of ivabradine to neurohumoral systems should be taken into account. Although ivabradine is considered to exert its principal protection as a direct and selective HR reducer via inhibition of the I_f current in the SAN, its potential interaction with the sympathetic nervous system cannot be excluded. In the above-mentioned experiment with three acute stress rat models, the reduced BP in ivabradine-pretreated rats exposed to handling stress was associated with reduced adrenaline and noradrenaline release into the blood stream compared to placebo treatment (22). Furthermore, in Dahl salt-sensitive rats, chronic ivabradine treatment reduced mortality along with the reduction of urinary noradrenaline excretion (46). In a rat model of doxorubicin-induced HF, the measuring of HR variability indicated an ivabradine-induced improvement of the autonomic imbalance (47). In substudies of large clinical trials, the HR variability analysis has shown an ivabradine-mediated shift toward a parasympathetic tone (48, 49); and in hypertensive patients with metabolic syndrome, ivabradine reduced sympathetic activation (50).

Similarly, data regarding ivabradine's interaction with the renin–angiotensin–aldosterone system are emerging. In ApoE-deficient mice, ivabradine reduced the serum level of angiotensin II (Ang II) (51), reduced the mRNA expression and protein of the Ang II type 1 receptor (AT1 receptor) (33), and downregulated Ang II-regulated pro-inflammatory genes (34). Moreover, in rats with myocardial infarction, ivabradine reduced the myocardial protein expression of the AT1 receptor (43, 52) and tissue angiotensin-converting enzyme (52). In L-NAME-induced hypertension, along with BP reduction, ivabradine reduced the serum concentration of aldosterone and the aldosterone/Ang II ratio (19). Blunting the sympathetic nervous system or the renin–angiotensin–aldosterone system may contribute to the potential BP-reducing effect of ivabradine via the reduction of peripheral artery resistance or circulating volume.

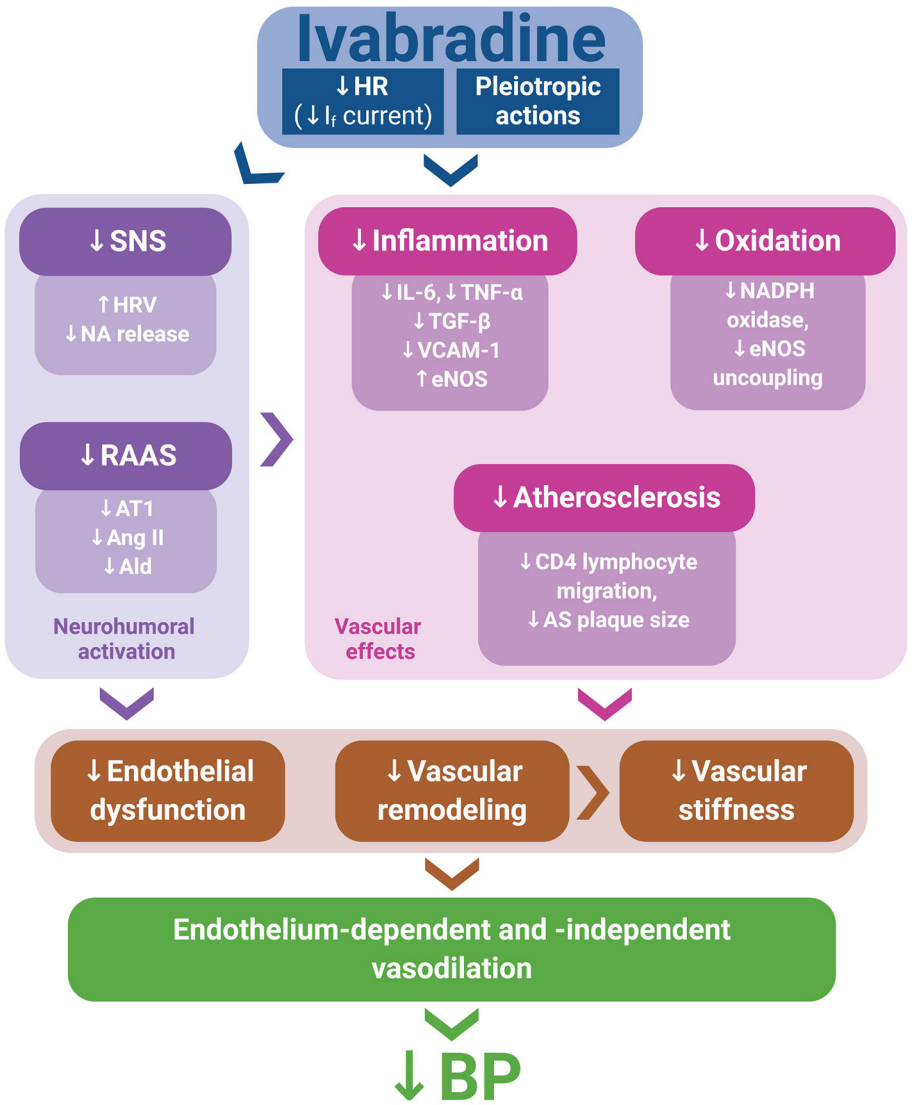

FIGURE 1 | Ivabradine's pleiotropic actions, along with heart rate (HR) reduction via I_f current inhibition, might mitigate neurohumoral activation, inflammation, oxidative stress, and atherosclerosis development, thus improving endothelial function and attenuating vascular remodeling and stiffness. These effects may contribute to endothelium-dependent and endothelium-independent vasodilation, potentially resulting in blood pressure (BP) reduction. Ald, aldosterone; Ang II, angiotensin II; AS, atherosclerotic; AT1, angiotensin II type 1 receptor; eNOS, endothelial nitric oxide synthase; HRV, heart rate variability; NA, noradrenaline; RAAS, renin–angiotensin–aldosterone system; SNS, sympathetic nervous system.

CONCLUDING REMARKS AND PERSPECTIVES

In the SHIFT study, ivabradine created hope for the treatment of HF patients with elevated HR. However, some studies with ivabradine were neutral and did not meet expectations. Thus, the indication for ivabradine should be considered carefully (53). On the other hand, the unique nature of ivabradine could be considered in several off-label indications (54), such as inappropriate sinus tachycardia (55) or postural orthostatic tachycardia syndrome (56). Ivabradine was recently shown to improve hypertensive heart function in rats with L-NAME-induced hypertension (19).

Hypertension with elevated HR might be another indication for ivabradine (57). Increased HR in hypertension is an undesirable condition that worsens the prognosis; thus, the decision regarding the optimal treatment of elevated HR in hypertension is an issue at the crossroads and has attracted professional attention for decades (1, 58). Ivabradine could become a candidate for this indication, considering a number of its pleiotropic effects:

- Based on several examples presented in this work, ivabradine might be able to reduce BP and could contribute to the reduction of the hemodynamic burden in hypertension. According to a scientific statement from the American Heart Association on the detection, evaluation, and management of resistant hypertension, the number of patients with resistant hypertension is expected to significantly increase (59, 60); therefore, seeking new approaches to BP control will be of utmost importance (61, 62).
- It has been previously shown that besides the increase in daily HR mean, insufficient HR decline during bedtime, i.e., non-dipping HR, increases cardiovascular risk (63–65). Moreover, non-dipping HR seems to be more frequent in hypertensive patients with chronic kidney disease than in the hypertensive population without kidney affliction (66). HR reduction with ivabradine reaches its peak effect in 3 to 4 h and lasts 8 to 12 h after ingestion (67), thus subjecting ivabradine to a flexible dosing scheme for targeting mean HR or nighttime HR. A well-tailored dosing of ivabradine might reverse non-dipping HR to a desirable HR dipping pattern (21, 57), thus presumably further reducing cardiovascular risk in hypertension.
- As opposed to BB (4, 5), ivabradine has not been observed to have negative metabolic effects (68, 69), which would be beneficial for hypertensive patients with metabolic syndrome prone to dyslipidemia, hyperuricemia, or diabetes mellitus.
- Ivabradine does not induce anxiety or other behavioral disorders in rats (70, 71), whereas BB therapy was shown to be associated with psychological disorders, such as nightmares (72, 73).
- Ivabradine was found to exert hypertensive heart protection. Indeed, in L-NAME-induced hypertension, ivabradine improved the systolic and diastolic dysfunctions of the remodeled left ventricle (LV) (19); and in a transverse aortic constriction mouse model, ivabradine reduced LV hypertrophy, fibrosis, and cardiomyocyte apoptosis and improved LV function (74). In a pig model of chronic Ang II infusion-induced hypertension and diastolic LV dysfunction, the acute administration of ivabradine improved LV filling parameters by an HR-independent mechanism (75). Moreover, ivabradine exerted an antihypertrophic effect on the aorta in spontaneously hypertensive rats (24) and renoprotection in rats with L-NAME-induced hypertension (76).

Taking into account ivabradine's HR- and (potential) BP-reducing effects associated with target organ protection and the lack of undesirable metabolic and behavioral consequences (often seen with BB), it appears reasonable to suggest the consideration of ivabradine for hypertensive patients with elevated HR, especially for those co-afflicted with metabolic disorders.

AUTHOR CONTRIBUTIONS

FS conceived and drafted the manuscript. TB revised the manuscript. Both authors participated in data analysis and interpretation and approved the submitted version.

FUNDING

This study was supported by research grants VEGA 1/0035/19 and VEGA 2/0112/19.

REFERENCES

1. Simko F, Baka T, Paulis L, Reiter RJ. Elevated heart rate and nondipping heart rate as potential targets for melatonin: a review. *J Pineal Res.* (2016) 61:127–37. doi: 10.1111/jpi.12348
2. Böhm M, Reil JC, Deedwania P, Kim JB, Borer JS. Resting heart rate: risk indicator and emerging risk factor in cardiovascular disease. *Am J Med.* (2015) 128:219–28. doi: 10.1016/j.amjmed.2014.09.016
3. Giannoglou GD, Chatzizisis YS, Zamboulis C, Parcharidis GE, Mikhailidis DP, Louridas GE. Elevated heart rate and atherosclerosis: an overview of the pathogenetic mechanisms. *Int J Cardiol.* (2008) 126:302–12. doi: 10.1016/j.ijcard.2007.08.077
4. Carella AM, Antonucci G, Conte M, Di Pumpo M, Giancola A, Antonucci E. Antihypertensive treatment with beta-blockers in the metabolic syndrome: a review. *Curr Diabetes Rev.* (2010) 6:215–21. doi: 10.2174/157339910791658844
5. Marketou M, Gupta Y, Jain S, Vardas P. Differential metabolic effects of beta-blockers: an updated systematic review of nebivolol. *Curr Hypertens Rep.* (2017) 19:22. doi: 10.1007/s11906-017-0716-3
6. Ide T, Ohtani K, Higo T, Tanaka M, Kawasaki Y, Tsutsui H. Ivabradine for the treatment of cardiovascular diseases. *Circ J.* (2019) 83:252–60. doi: 10.1253/circj.CJ-18-1184
7. DiFrancesco D, Borer JS. The funny current: cellular basis for the control of heart rate. *Drugs.* (2007) 67(Suppl. 2):15–24. doi: 10.2165/00003495-200767002-00003
8. Koruth JS, Lala A, Pinney S, Reddy VY, Dukkipati SR. The clinical use of ivabradine. *J Am Coll Cardiol.* (2017) 70:1777–84. doi: 10.1016/j.jacc.2017.08.038
9. Swedberg K, Komajda M, Böhm M, Borer JS, Ford I, Dubost-Brama A, et al. Ivabradine and outcomes in chronic heart failure (SHIFT): a randomised placebo-controlled study. *Lancet.* (2010) 376:875–85. doi: 10.1016/S0140-6736(10)61198-1
10. Ponikowski P, Voors AA, Anker SD, Bueno H, Cleland JGF, Coats AJS, et al. 2016 ESC Guidelines for the diagnosis treatment of acute chronic heart failure: the Task Force for the diagnosis treatment of acute chronic heart failure of the European Society of Cardiology (ESC)Developed with the special contribution of the Heart Failure Association (HFA) of the ESC. *Eur Heart J.* (2016) 37:2129–200. doi: 10.1093/eurheartj/ehw128
11. Fox K, Ford I, Steg PG, Tendera M, Ferrari R, BEAUTIFUL Investigators. Ivabradine for patients with stable coronary artery disease and left-ventricular systolic dysfunction (BEAUTIFUL): a randomised, double-blind, placebo-controlled trial. *Lancet.* (2008) 372:807–16. doi: 10.1016/S0140-6736(08)61170-8
12. Fox K, Ford I, Steg PG, Tardif JC, Tendera M, Ferrari R, et al. Ivabradine in stable coronary artery disease without clinical heart failure. *N Engl J Med.* (2014) 371:1091–9. doi: 10.1056/NEJMoa1406430
13. Lopatin YM, Vitale C. Effect of ivabradine on central aortic blood pressure in patients with stable coronary artery disease: what do we know? *Int J Cardiol.* (2016) 224:145–8. doi: 10.1016/j.ijcard.2016.09.054
14. Dillinger JG, Maher V, Vitale C, Henry P, Logeart D, Manzo Silberman S, et al. Impact of ivabradine on central aortic blood pressure and myocardial

perfusion in patients with stable coronary artery disease. *Hypertension.* (2015) 66:1138–44. doi: 10.1161/HYPERTENSIONAHA.115.06091
15. Fischer-Rasokat U, Honold J, Lochmann D, Liebetrau C, Leick J, Hamm C, et al. Ivabradine therapy to unmask heart rate-independent effects of β-blockers on pulse wave reflections. *Clin Res Cardiol.* (2014) 103:487–94. doi: 10.1007/s00392-014-0679-1
16. Kleinbongard P, Gedik N, Witting P, Freedman B, Klöcker N, Heusch G. Pleiotropic, heart rate-independent cardioprotection by ivabradine. *Br J Pharmacol.* (2015) 172:4380–90. doi: 10.1111/bph.13220
17. Heusch G. Pleiotropic action(s) of the bradycardic agent ivabradine: cardiovascular protection beyond heart rate reduction. *Br J Pharmacol.* (2008) 155:970–1. doi: 10.1038/bjp.2008.347
18. Bangalore S, Messerli FH, Kostis JB, Pepine CJ. Cardiovascular protection using beta-blockers: a critical review of the evidence. *J Am Coll Cardiol.* (2007) 50:563–72. doi: 10.1016/j.jacc.2007.04.060
19. Simko F, Baka T, Poglitsch M, Repova K, Aziriova S, Krajcirovicova K, et al. Effect of ivabradine on a hypertensive heart and the renin-angiotensin-aldosterone system in L-NAME-induced hypertension. *Int J Mol Sci.* (2018) 19:3017. doi: 10.3390/ijms19103017
20. Simko F, Repova K, Krajcirovicova K, Aziriova S, Paulis L, Baka T. Remodelling of the aorta and kidney in L-NAME-induced hypertension in rats: comparison of the protective effect of ivabradine with captopril and melatonin. *Diabetologia.* (2015) 58(Suppl. 1):S547.
21. Baka T, Simko F. Ivabradine reversed nondipping heart rate in rats with l-NAME-induced hypertension. *Clin Exp Pharmacol Physiol.* (2019) 46:607–10. doi: 10.1111/1440-1681.13075
22. Ondicova K, Hegedusova N, Tibensky M, Mravec B. Ivabradine reduces baseline and stress-induced increase of heart rate and blood pressure and modulates neuroendocrine stress response in rats depending on stressor intensity. *Gen Physiol Biophys.* (2019) 38:165–73. doi: 10.4149/gpb_2018046
23. Albaladejo P, Challande P, Kakou A, Benetos A, Labat C, Louis H, et al. Selective reduction of heart rate by ivabradine: effect on the visco-elastic arterial properties in rats. *J Hypertens.* (2004) 22:1739–45. doi: 10.1097/00004872-200409000-00018
24. Albaladejo P, Carusi A, Apartian A, Lacolley P, Safar ME, Bénétos A. Effect of chronic heart rate reduction with ivabradine on carotid and aortic structure and function in normotensive and hypertensive rats. *J Vasc Res.* (2003) 40:320–8. doi: 10.1159/000072696
25. Joannides R, Moore N, Iacob M, Compagnon P, Lerebours G, Menard JF, et al. Comparative effects of ivabradine, a selective heart rate-lowering agent, and propranolol on systemic and cardiac haemodynamics at rest and during exercise. *Br J Clin Pharmacol.* (2006) 61:127–37. doi: 10.1111/j.1365-2125.2005.02544.x
26. Simko F, Baka T, Repova K, Aziriova S, Krajcirovicova K, Paulis L, et al. Ivabradine improves survival and attenuates cardiac remodeling in isoproterenol-induced myocardial injury. *Fundam Clin Pharmacol.* (2020). doi: 10.1111/fcp.12620. [Epub ahead of print].
27. Komajda M, Böhm M, Borer JS, Ford I, Robertson M, Manolis AJ, et al. Efficacy and safety of ivabradine in patients with chronic systolic heart failure according to blood pressure level in SHIFT. *Eur J Heart Fail.* (2014) 16:810–6. doi: 10.1002/ejhf.114
28. Dominguez-Rodriguez A, Abreu-Gonzalez P. Ivabradine and the anti-inflammatory effects in patients with ischemic heart disease. *Int J Cardiol.* (2016) 221:627–8. doi: 10.1016/j.ijcard.2016.07.096
29. Li B, Zhang J, Wang Z, Chen S. Ivabradine prevents low shear stress induced endothelial inflammation and oxidative stress via mTOR/eNOS pathway. *PLoS ONE.* (2016) 11:e0149694. doi: 10.1371/journal.pone.0149694
30. Koniari I, Mavrilas D, Apostolakis E, Papadimitriou E, Papadaki H, Papalois A, et al. Inhibition of atherosclerosis progression, intimal hyperplasia, and oxidative stress by simvastatin and ivabradine may reduce thoracic aorta's stiffness in hypercholesterolemic rabbits. *J Cardiovasc Pharmacol Ther.* (2016) 21:412–22. doi: 10.1177/1074248415617289
31. Kröller-Schön S, Schulz E, Wenzel P, Kleschyov AL, Hortmann M, Torzewski M, et al. Differential effects of heart rate reduction with ivabradine in two models of endothelial dysfunction and oxidative stress. *Basic Res Cardiol.* (2011) 106:1147–58. doi: 10.1007/s00395-011-0227-3
32. Custodis F, Baumhäkel M, Schlimmer N, List F, Gensch C, Böhm M, et al. Heart rate reduction by ivabradine reduces oxidative stress, improves endothelial function, and prevents atherosclerosis in apolipoprotein E-deficient mice. *Circulation.* (2008) 117:2377–87. doi: 10.1161/CIRCULATIONAHA.107.746537
33. Custodis F, Fries P, Müller A, Stamm C, Grube M, Kroemer HK, et al. Heart rate reduction by ivabradine improves aortic compliance in apolipoprotein E-deficient mice. *J Vasc Res.* (2012) 49:432–40. doi: 10.1159/000339547
34. Aquila G, Morelli MB, Vieceli Dalla Sega F, Fortini F, Nigro P, Caliceti C, et al. Heart rate reduction with ivabradine in the early phase of atherosclerosis is protective in the endothelium of ApoE-deficient mice. *J Physiol Pharmacol.* (2018) 69:35–52. doi: 10.26402/jpp.2018.1.04
35. Luong L, Duckles H, Schenkel T, Mahmoud M, Tremoleda JL, Wylezinska-Arridge M, et al. Heart rate reduction with ivabradine promotes shear stress-dependent anti-inflammatory mechanisms in arteries. *Thromb Haemost.* (2016) 116:181–90. doi: 10.1160/TH16-03-0214
36. Bonadei I, Sciatti E, Vizzardi E, Fabbricatore D, Pagnoni M, Rossi L et al. Effects of ivabradine on endothelial function, aortic properties and ventricular-arterial coupling in chronic systolic heart failure patients. *Cardiovasc Ther.* (2018) 36:e12323. doi: 10.1111/1755-5922.12323
37. Reil JC, Hohl M, Reil GH, Granzier HL, Kratz MT, Kazakov A, et al. Heart rate reduction by If-inhibition improves vascular stiffness and left ventricular systolic and diastolic function in a mouse model of heart failure with preserved ejection fraction. *Eur Heart J.* (2013) 34:2839–49. doi: 10.1093/eurheartj/ehs218
38. Walcher T, Bernhardt P, Vasic D, Bach H, Durst R, Rottbauer W, et al. Ivabradine reduces chemokine-induced CD4-positive lymphocyte migration. *Mediators Inflamm.* (2010) 2010:751313. doi: 10.1155/2010/751313
39. Mangiacapra F, Colaiori I, Ricottini E, Balducci F, Creta A, Demartini C, et al. Heart Rate reduction by IVabradine for improvement of ENDothELial function in patients with coronary artery disease: the RIVENDEL study. *Clin Res Cardiol.* (2017) 106:69–75. doi: 10.1007/s00392-016-1024-7
40. Hohneck AL, Fries P, Ströder J, Schneider G, Wagenpfeil S, Schirmer SH, et al. Effects of heart rate reduction with ivabradine on vascular stiffness and endothelial function in chronic stable coronary artery disease. *J Hypertens.* (2019) 37:1023–31. doi: 10.1097/HJH.0000000000001984
41. Custodis F, Gertz K, Balkaya M, Prinz V, Mathar I, Stamm C, et al. Heart rate contributes to the vascular effects of chronic mental stress: effects on endothelial function and ischemic brain injury in mice. *Stroke.* (2011) 42:1742–9. doi: 10.1161/STROKEAHA.110.598607
42. Wu X, You W, Wu Z, Ye F, Chen S. Ivabradine promotes angiogenesis and reduces cardiac hypertrophy in mice with myocardial infarction. *Anatol J Cardiol.* (2018) 20:266–72. doi: 10.14744/AnatolJCardiol.2018.46338
43. Dedkov EI, Zheng W, Christensen LP, Weiss RM, Mahlberg-Gaudin F, Tomanek RJ. Preservation of coronary reserve by ivabradine-induced reduction in heart rate in infarcted rats is associated with decrease in perivascular collagen. *Am J Physiol Heart Circ Physiol.* (2007) 293:H590–8. doi: 10.1152/ajpheart.00047.2007
44. Chen SL, Hu ZY, Zuo GF, Li MH, Li B. I(f) current channel inhibitor (ivabradine) deserves cardioprotective effect via down-regulating the expression of matrix metalloproteinase (MMP)-2 and attenuating apoptosis in diabetic mice. *BMC Cardiovasc Disord.* (2014) 14:150. doi: 10.1186/1471-2261-14-150
45. Xie M, Huang HL, Zhang WH, Gao L, Wang YW, Zhu XJ, et al. Increased sarcoplasmic/endoplasmic reticulum calcium ATPase 2a activity underlies the mechanism of the positive inotropic effect of ivabradine. *Exp Physiol.* (2020) 105:477–88. doi: 10.1113/EP087964
46. Kakehi K, Iwanaga Y, Watanabe H, Sonobe T, Akiyama T, Shimizu S, et al. Modulation of sympathetic activity and innervation with chronic ivabradine and β-blocker therapies: analysis of hypertensive rats with heart failure. *J Cardiovasc Pharmacol Ther.* (2019) 24:387–96. doi: 10.1177/1074248419829168
47. El-Naggar AE, El-Gowilly SM, Sharabi FM. Possible ameliorative effect of ivabradine on the autonomic and left ventricular dysfunction induced by doxorubicin in male rats. *J Cardiovasc Pharmacol.* (2018) 72:22–31. doi: 10.1097/FJC.0000000000000586
48. Böhm M, Borer JS, Camm J, Ford I, Lloyd SM, Komajda M, et al. Twenty-four-hour heart rate lowering with ivabradine in chronic heart failure: insights from the SHIFT Holter substudy. *Eur J Heart Fail.* (2015) 17:518–26. doi: 10.1002/ejhf.258

49. Kurtoglu E, Balta S, Karakus Y, Yasar E, Cuglan B, Kaplan O, et al. Ivabradine improves heart rate variability in patients with nonischemic dilated cardiomyopathy. *Arq Bras Cardiol.* (2014) 103:308–14. doi: 10.5935/abc.20140109
50. Tsioufis KP, Dimitriadis K, Koutra E, Kalos T, Fragoulis C, Nikolopoulou L, et al. Effects of ivabradine on sympathetic overdrive and arterial stiffening in hypertensive patients with metabolic syndrome: a 6 month follow-up study. *J Am Coll Cardiol.* (2018) 71:1807. doi: 10.1016/S0735-1097(18)32348-9
51. Busseuil D, Shi Y, Mecteau M, Brand G, Gillis MA, Thorin E, et al. Heart rate reduction by ivabradine reduces diastolic dysfunction and cardiac fibrosis. *Cardiology.* (2010) 117:234–42. doi: 10.1159/000322905
52. Milliez P, Messaoudi S, Nehme J, Rodriguez C, Samuel JL, Delcayre C. Beneficial effects of delayed ivabradine treatment on cardiac anatomical and electrical remodeling in rat severe chronic heart failure. *Am J Physiol Heart Circ Physiol.* (2009) 296:H435–41. doi: 10.1152/ajpheart.00591.2008
53. McMurray JJ. It is BEAUTIFUL we should be concerned about, not SIGNIFY: is ivabradine less effective in ischaemic compared with non-ischaemic LVSD?. *Eur Heart J.* (2015) 36:2047–9. doi: 10.1093/eurheartj/ehv190
54. Oliphant CS, Owens RE, Bolorunduro OB, Jha SK. Ivabradine: a review of labeled and off-label uses. *Am J Cardiovasc Drugs.* (2016) 16:337–47. doi: 10.1007/s40256-016-0178-z
55. Cappato R, Castelvecchio S, Ricci C, Bianco E, Vitali-Serdoz L, Gnecchi-Ruscone T, et al. Clinical efficacy of ivabradine in patients with inappropriate sinus tachycardia: a prospective, randomized, placebo-controlled, double-blind, crossover evaluation. *J Am Coll Cardiol.* (2012) 60:1323–9. doi: 10.1016/j.jacc.2012.06.031
56. McDonald C, Frith J, Newton JL. Single centre experience of ivabradine in postural orthostatic tachycardia syndrome. *Europace.* (2011) 13:427–30. doi: 10.1093/europace/euq390
57. Simko F, Baka T. Chronotherapy as a potential approach to hypertensive patients with elevated heart rate? *Br J Clin Pharmacol.* (2019) 85:1861–2. doi: 10.1111/bcp.14020
58. Palatini P, Rosei EA, Casiglia E, Chalmers J, Ferrari R, Grassi G, et al. Management of the hypertensive patient with elevated heart rate: statement of the Second Consensus Conference endorsed by the European Society of Hypertension. *J Hypertens.* (2016) 34:813–21. doi: 10.1097/HJH.0000000000000865
59. Carey RM, Calhoun DA, Bakris GL, Brook RD, Daugherty SL, Dennison-Himmelfarb CR, et al. Resistant hypertension: detection, evaluation, and management: a scientific statement from the American Heart Association. *Hypertension.* (2018) 72:e53–90. doi: 10.1161/HYP.0000000000000084
60. Ruilope LM, Rodríguez-Sánchez E, Navarro-García JA, Segura J, Órtiz A, Lucia A, Ruiz-Hurtado G. Resistant hypertension: new insights and therapeutic perspectives. *Eur Heart J Cardiovasc Pharmacother.* (2020) 6:188–93. doi: 10.1093/ehjcvp/pvz057
61. Simko F, Reiter RJ, Paulis L. Melatonin as a rational alternative in the conservative treatment of resistant hypertension. *Hypertens Res.* (2019) 42:1828–31. doi: 10.1038/s41440-019-0318-3
62. Simko F, Pechanova O. Recent trends in hypertension treatment: perspectives from animal studies. *J Hypertens Suppl.* (2009) 27:S1–4. doi: 10.1097/01.hjh.0000358829.87815.d4
63. Baka T, Simko F. Nondipping heart rate: a neglected cardiovascular risk factor based on autonomic imbalance? *Auton Neurosci.* (2018) 210:83–4. doi: 10.1016/j.autneu.2018.02.001
64. Ben-Dov IZ, Kark JD, Ben-Ishay D, Mekler J, Ben-Arie L, Bursztyn M. Blunted heart rate dip during sleep and all-cause mortality. *Arch Intern Med.* (2007) 167:2116–21. doi: 10.1001/archinte.167.19.2116
65. Eguchi K, Hoshide S, Ishikawa J, Pickering TG, Schwartz JE, Shimada K, et al. Nocturnal nondipping of heart rate predicts cardiovascular events in hypertensive patients. *J Hypertens.* (2009) 27:2265–70. doi: 10.1097/HJH.0b013e328330a938
66. Biyik Z, Yavuz YC, Altintepe L, Celik G, Guney I, Oktar SF. Nondipping heart rate and associated factors in patients with chronic kidney disease. *Clin Exp Nephrol.* (2019) 23:1298–305. doi: 10.1007/s10157-019-01782-x
67. Choi HY, Noh YH, Cho SH, Ghim JL, Choe S, Kim UJ, et al. Evaluation of pharmacokinetic and pharmacodynamic profiles and tolerability after single (2.5, 5, or 10 mg) and repeated (2.5, 5, or 10 mg bid for 4.5 days) oral administration of ivabradine in healthy male Korean volunteers. *Clin Ther.* (2013) 35:819–35. doi: 10.1016/j.clinthera.2013.04.012
68. Borer JS, Tardif JC. Efficacy of ivabradine, a selective I(f) inhibitor, in patients with chronic stable angina pectoris and diabetes mellitus. *Am J Cardiol.* (2010) 105:29–35. doi: 10.1016/j.amjcard.2009.08.642
69. Vaillant F, Lauzier B, Ruiz M, Shi Y, Lachance D, Rivard ME, et al. Ivabradine and metoprolol differentially affect cardiac glucose metabolism despite similar heart rate reduction in a mouse model of dyslipidemia. *Am J Physiol Heart Circ Physiol.* (2016) 311:H991–1003. doi: 10.1152/ajpheart.00789.2015
70. Aziriova S, Repova K, Krajcirovicova K, Baka T, Zorad S, Mojto V, et al. Effect of ivabradine, captopril and melatonin on the behaviour of rats in L-nitro-arginine methyl ester-induced hypertension. *J Physiol Pharmacol.* (2016) 67:895–902.
71. Krajcirovicova K, Aziriova S, Baka T, Repova K, Adamcova M, Paulis L, et al. Ivabradine does not impair anxiety-like behavior and memory in both healthy and L-NAME-induced hypertensive rats. *Physiol Res.* (2018) 67(Suppl. 4):S655–64. doi: 10.33549/physiolres.934048
72. Brismar K, Mogensen L, Wetterberg L. Depressed melatonin secretion in patients with nightmares due to beta-adrenoceptor blocking drugs. *Acta Med Scand.* (1987) 221:155–8. doi: 10.1111/j.0954-6820.1987.tb01260.x
73. Gleiter CH, Deckert J. Adverse CNS-effects of beta-adrenoceptor blockers. *Pharmacopsychiatry.* (1996) 29:201–11. doi: 10.1055/s-2007-979572
74. Yu Y, Hu Z, Li B, Wang Z, Chen S. Ivabradine improved left ventricular function and pressure overload-induced cardiomyocyte apoptosis in a transverse aortic constriction mouse model. *Mol Cell Biochem.* (2019) 450:25–34. doi: 10.1007/s11010-018-3369-x
75. Melka J, Rienzo M, Bizé A, Jozwiak M, Sambin L, Hittinger L, et al. Improvement of left ventricular filling by ivabradine during chronic hypertension: involvement of contraction-relaxation coupling. *Basic Res Cardiol.* (2016) 111:30. doi: 10.1007/s00395-016-0550-9
76. Stanko P, Baka T, Repova K, Aziriova S, Krajcirovicova K, Barta A, et al. Ivabradine ameliorates kidney fibrosis in L-NAME-induced hypertension. *Front Med.* (2020) 7:325. doi: 10.3389/fmed.2020.00325

Conflict of Interest: The authors declare that the research was conducted in the absence of any commercial or financial relationships that could be construed as a potential conflict of interest.

frontiers in Physiology

REVIEW
published: 09 March 2021
doi: 10.3389/fphys.2021.632260

An Overview of FGF-23 as a Novel Candidate Biomarker of Cardiovascular Risk

Sara Vázquez-Sánchez[1], Jonay Poveda[1†], José Alberto Navarro-García[1†], Laura González-Lafuente[1], Elena Rodríguez-Sánchez[1], Luis M. Ruilope[1,2,3] and Gema Ruiz-Hurtado[1,2]*

[1] Cardiorenal Translational Laboratory, Institute of Research i+12, Hospital Universitario 12 de Octubre, Madrid, Spain, [2] CIBER-CV, Hospital Universitario 12 de Octubre, Madrid, Spain, [3] School of Doctoral Studies and Research, European University of Madrid, Madrid, Spain

OPEN ACCESS

Edited by:
Modar Kassan,
University of Tennessee Health Science Center (UTHSC), United States

Reviewed by:
Ebba Brakenhielm,
Institut National de la Santé et de la Recherche Médicale (INSERM), France
Akira Nishiyama,
Kagawa University, Japan

***Correspondence:**
Gema Ruiz-Hurtado
gemaruiz@h12o.es

[†] These authors have contributed equally to this work

Specialty section:
This article was submitted to Vascular Physiology, a section of the journal Frontiers in Physiology

Received: 22 November 2020
Accepted: 15 February 2021
Published: 09 March 2021

Citation:
Vázquez-Sánchez S, Poveda J, Navarro-García JA, González-Lafuente L, Rodríguez-Sánchez E, Ruilope LM and Ruiz-Hurtado G (2021) An Overview of FGF-23 as a Novel Candidate Biomarker of Cardiovascular Risk. Front. Physiol. 12:632260. doi: 10.3389/fphys.2021.632260

Fibroblast growth factor-23 (FGF)-23 is a phosphaturic hormone involved in mineral bone metabolism that helps control phosphate homeostasis and reduces 1,25-dihydroxyvitamin D synthesis. Recent data have highlighted the relevant direct FGF-23 effects on the myocardium, and high plasma levels of FGF-23 have been associated with adverse cardiovascular outcomes in humans, such as heart failure and arrhythmias. Therefore, FGF-23 has emerged as a novel biomarker of cardiovascular risk in the last decade. Indeed, experimental data suggest FGF-23 as a direct mediator of cardiac hypertrophy development, cardiac fibrosis and cardiac dysfunction via specific myocardial FGF receptor (FGFR) activation. Therefore, the FGF-23/FGFR pathway might be a suitable therapeutic target for reducing the deleterious effects of FGF-23 on the cardiovascular system. More research is needed to fully understand the intracellular FGF-23-dependent mechanisms, clarify the downstream pathways and identify which could be the most appropriate targets for better therapeutic intervention. This review updates the current knowledge on both clinical and experimental studies and highlights the evidence linking FGF-23 to cardiovascular events. The aim of this review is to establish the specific role of FGF-23 in the heart, its detrimental effects on cardiac tissue and the possible new therapeutic opportunities to block these effects.

Keywords: FGF-23, FGFR, heart, LVH, heart failure – pharmacological treatment – systolic dysfunction

INTRODUCTION

Cardiovascular disease remains the leading cause of morbidity and mortality worldwide, and heart failure (HF) has become a major public health problem in the industrialised world (Members et al., 2012). The prevalence of coronary artery disease in the general population is 7.3% (Enbergs et al., 2000), while it is around 15–20% for left ventricular hypertrophy (LVH) (Weber, 1991) and 3.9% for HF (Mosterd et al., 1999). Recent research provides evidence that a high plasma level of fibroblast growth factor-23 (FGF)-23 is a hallmark of cardiac damage resulting in deleterious remodelling and the induction of cardiac hypertrophy. In the last few years, FGF-23 has been identified as a new trigger of cardiac dysfunction (Seiler et al., 2011; Leifheit-Nestler et al., 2018b; Navarro-García et al., 2019). Therefore, it is essential to not only understand the mechanisms whereby FGF-23 signals are transduced but also the variables associated with the increase in FGF-23 so new therapeutic

strategies can be developed and applied in the near future (Chonchol et al., 2016; Rodelo-Haad et al., 2018).

FGF-23 is a hormone mainly synthesised by osteocytes and osteoblasts in long bones, although it can also be produced and secreted by different tissues, such as liver or even heart tissue under stress conditions (Hu et al., 2013). FGF-23 is involved in phosphate homeostasis and promotes renal phosphate excretion (Wolf, 2012; Mace et al., 2015), downregulation of 1,25-dihydroxyvitamin D (vitamin D) synthesis (Krajisnik et al., 2007; Mace et al., 2015; Navarro-García et al., 2018) and a decrease in parathyroid hormone (PTH) secretion (Navarro-García et al., 2018; von Jeinsen et al., 2019). FGF-23 is a 32 kDa protein encoded by the gene *fgf23* located in chromosome 12 and belongs to the FGF subfamily FGF19, which corresponds to the endocrine FGFs (Hu et al., 2013). It appears in the circulating blood in two forms: intact full-length proteins and C-terminal proteins resulting from the rupture of the entire molecule by furin-like enzymes (Tagliabracci et al., 2014). FGF receptors (FGFRs) mediate the effects of FGF-23 and have tyrosine-kinase activity (Farrell and Breeze, 2018). There are four isoforms (FGFR1–4), but FGF-23 has a low affinity for all FGFRs and requires a cofactor to promote its union (Kurosu and Kuro-o, 2009). FGFRs are widely expressed in various tissues, including bone, kidney and heart tissues. In the kidneys, FGF-23 binds to FGFR1 using protein Klotho as a cofactor (Kurosu and Kuro-o, 2009); however, in the heart, FGF-23 binds to FGFR4 independently of Klotho (Grabner et al., 2015; Faul, 2017). Therefore, whether FGF-23 exerts its effect on the heart through an unknown cofactor or it does not need the cofactor link remains unclear (Urakawa et al., 2006).

FGF-23 was originally identified through a gene mutation in patients with autosomal dominant hypophosphatemic rickets or X-linked hypophosphatemic rickets that results in elevated serum levels of FGF-23 (White et al., 2000). The discovery of FGF-23 has revolutionised our understanding of mineral metabolism. Multilevel feedback and the kinetics of hormone actions within the bone–kidney–parathyroid loops system allow the controlled expression or action of the mineral–bone components, such as phosphates, PTH and vitamin D (Blau and Collins, 2015). Changes in any of these components lead to a misbalance in the feedback loops, altering the circulating levels of all these components and affecting several organs, including off-target organs such as the heart (Navarro-García et al., 2018). For instance, in chronic kidney disease (CKD), as kidney excretion capacity decreases, serum phosphate levels increase and stimulate FGF-23 synthesis, causing a rise of PTH and a deficiency of vitamin D, which can lead to adverse cardiovascular events like LVH and HF (Faul et al., 2011; Mathew et al., 2014; Navarro-García et al., 2018).

Recent evidence from human and experimental studies points to a key role of FGF-23 in the development and progression of cardiac disease. Significant changes in FGF-23 secretion and its action on the heart may have broad health implications that need to be elucidated. This review summarises our current understanding of FGF-23 and focuses on emerging areas of FGF-23 in human cardiac events and its intracellular pathways in cardiomyocytes and fibroblasts.

CLINICAL VARIABLES AND CARDIAC EVENTS ASSOCIATED WITH HIGH CIRCULATING FGF-23 LEVELS

Systemic levels of FGF-23 are commonly analysed as an important biomarker for the diagnosis and prognosis of mineral bone disorders (MBD), and its measurement is recommended for patients with CKD. Currently, the extra-renal effects of this protein are becoming even more relevant, finding other targets such as the parathyroid gland and the cardiovascular and immune systems (Haffner and Leifheit-Nestler, 2017). The role of FGF-23 in cardiac disturbances is not clear or defined, especially the effects related not only to structural changes in the myocardium but also those related to cardiac dysfunction. High circulating levels of FGF-23 have been associated with cardiovascular pathophysiologic events, such as LVH, endothelial dysfunction and atherosclerosis (Lutsey et al., 2014). In addition, it remains unknown whether FGF-23 plays a detrimental role in cardiovascular events or if high plasma levels of FGF-23 are a simple consequence of cardiac disturbances. In this review, we identify the agreements and contradictions between clinical studies and put forward a scenario in which the specific role of FGF-23 in cardiovascular diseases can also be significantly harmful. Moreover, another unknown aspect that has arisen is the variability in FGF-23 levels according to different demographic variables, such as age, gender, ethnicity and clinical background. This issue is described in the following section.

FGF-23 and Demographic Variables: Age, Sex, and Ethnicity

High plasma levels of FGF-23 are associated with older age groups (>60 years) (Ix et al., 2012; Kestenbaum et al., 2014; Lutsey et al., 2014; Wright et al., 2014; Masson et al., 2015; Panwar et al., 2015; Speer et al., 2015; Souma et al., 2016; Ter Maaten et al., 2018; Huo et al., 2019), although some studies in younger populations have not found a significant correlation with age (Parker et al., 2010; Agarwal et al., 2014; di Giuseppe et al., 2014; Poelzl et al., 2014; Di Giuseppe et al., 2015; Chonchol et al., 2016; Takahashi et al., 2018). As age increases, metabolic disturbances are more prevalent; therefore, the lack of correlation with age may be due to the lack of metabolic changes. Another reason could be the low Klotho levels observed in older populations. Klotho is an anti-ageing factor, mainly expressed in the kidneys, which functions as a coreceptor of FGF-23 to increase the renal excretion of phosphates (Bian et al., 2014). As Klotho expression declines, serum phosphates increase and stimulate bone FGF-23 production, e.g., in CKD patients (Drew et al., 2017).

Interestingly, although the cardiovascular risk is higher in men, elevated FGF-23 levels are more commonly correlated with women (Parker et al., 2010; Seiler et al., 2011; Ix et al., 2012; Agarwal et al., 2014; di Giuseppe et al., 2014; Wright et al., 2014; Di Giuseppe et al., 2015; Masson et al., 2015; Panwar et al., 2015; Speer et al., 2015; Souma et al., 2016; Reindl et al., 2017; Ter Maaten et al., 2018; Cheng et al., 2020) than men (Kestenbaum et al., 2014; Chonchol et al., 2016; Huo et al., 2019). Nevertheless, some authors suggest that levels of FGF-23

could be independent of sex (Shibata et al., 2013; Lutsey et al., 2014; Poelzl et al., 2014; Koller et al., 2015). This discordance could be explained by the fact that most studies were carried out with older patients, including post-menopausal women. It is known that oestrogens diminish plasma FGF-23 levels, which might explain the increased FGF-23 levels in post-menopausal women compared to men (Ix et al., 2011). The physiological reason for the oestrogen effect on FGF-23 levels is that the oestrogen receptor regulates urinary phosphorus excretion at the proximal tubule, so in post-menopausal women, serum phosphorus levels are increased, thereby increasing FGF-23 secretion (Ix et al., 2011).

In contrast, the relationship between ethnicity and high plasma levels of FGF-23 is not yet clear. Some studies have associated greater levels of FGF-23 with Caucasian ethnicity (Ix et al., 2012; Chonchol et al., 2016; Patel et al., 2020), others with African American or Hispanic ethnicities (Lutsey et al., 2014; Wright et al., 2014), and others with none of them (Parker et al., 2010; Kestenbaum et al., 2014; Panwar et al., 2015; Robinson-Cohen et al., 2020). For instance, studies carried out in very diverse populations did not find any correlation with ethnicity variables (Kestenbaum et al., 2014). In this sense, Gutiérrez et al. (2010) demonstrated that a high level of serum phosphates, which leads to increased FGF-23 levels, is associated with low socioeconomic status independently of ethnicity. Some studies have even pointed to a relationship between FGF-23 levels and industrialisation, possibly due to different phosphate dietary intake through the addition of phosphates as food preservatives (Yuen et al., 2016). Therefore, future research and clinical studies should incorporate all these variables to achieve an intersectional perspective of the levels of FGF-23 in the general population (**Table 1**).

FGF-23 and Adverse Cardiac Events

FGF-23 is an early and complementary predictor of adverse cardiac events and could be suitable for improving risk assessment in vulnerable patients with HF or reduced ejection fraction (Koller et al., 2015). FGF-23 is positively correlated with but does not directly depend on the classical biomarkers of cardiac damage, such as N-terminal-pro-B-type natriuretic peptide (NT-proBNP) (Seiler et al., 2011; Shibata et al., 2013; Kestenbaum et al., 2014; Poelzl et al., 2014; Koller et al., 2015; Masson et al., 2015; Panwar et al., 2015; Speer et al., 2015; Wohlfahrt et al., 2015; Ter Maaten et al., 2018; von Jeinsen et al., 2019; Song et al., 2021), high-sensitive cardiac troponin T (hs-cTnT) (Kestenbaum et al., 2014; Masson et al., 2015; Song et al., 2021) and C-reactive protein (CRP) (Parker et al., 2010; Seiler et al., 2011; Ix et al., 2012; Lutsey et al., 2014; Panwar et al., 2015; Speer et al., 2015; Reindl et al., 2017; Song et al., 2021). Furthermore, it has already been demonstrated that the predictive value of the combination of these biomarkers on cardiovascular risk assessment is significantly greater than any of them alone (Wohlfahrt et al., 2015). In specific clinical circumstances, however, several authors have noted the relevance of FGF-23 as an independent biomarker. In this sense, Speer et al. (2015) demonstrated that the predictive value of FGF-23 for mortality and complications after cardiac surgery is comparable and even greater than the European System for Cardiac Operative Risk Evaluation (EuroSCORE II) and as good as that of NT-proBNP.

TABLE 1 | Demographic and clinical variables correlated with high plasma levels of FGF-23.

Variable	Condition	References
Demographic variables		
Age	Older > 60 years	Lutsey et al., 2014
		Panwar et al., 2015
		Masson et al., 2015
		Ix et al., 2012
		Wright et al., 2014
		Kestenbaum et al., 2014
		Speer et al., 2015
		Souma et al., 2016
		Ter Maaten et al., 2018
		Huo et al., 2019
	Not Correlated	Di Giuseppe et al., 2015
		di Giuseppe et al., 2014
		Parker et al., 2010
		Poelzl et al., 2014
		Agarwal et al., 2014
		Chonchol et al., 2016
		Takahashi et al., 2018
Sex	Women	Di Giuseppe et al., 2015
		Panwar et al., 2015
		Masson et al., 2015
		di Giuseppe et al., 2014
		Ix et al., 2012
		Wright et al., 2014
		Parker et al., 2010
		Speer et al., 2015
		Souma et al., 2016
		Ter Maaten et al., 2018
		Seiler et al., 2011
		Reindl et al., 2017
		Agarwal et al., 2014
		Cheng et al., 2020
	Men	Kestenbaum et al., 2014
		Chonchol et al., 2016
		Huo et al., 2019
	Not Correlated	Koller et al., 2015
		Lutsey et al., 2014
		Shibata et al., 2013
		Poelzl et al., 2014
Ethnicity	Caucasian	Ix et al., 2012
		Chonchol et al., 2016
		Patel et al., 2020
	African American or Hispanic	Lutsey et al., 2014
		Wright et al., 2014
	Not Correlated	Panwar et al., 2015
		Robinson-Cohen et al., 2020
		Parker et al., 2010
		Kestenbaum et al., 2014

Elevated systemic FGF-23 levels have been strongly associated with an increased risk of mortality, including cardiovascular mortality (Parker et al., 2010; Ix et al., 2012; Ärnlöv et al., 2013b; Poelzl et al., 2014; Masson et al., 2015; Speer et al., 2015; Chonchol et al., 2016; Ter Maaten et al., 2018; von Jeinsen et al., 2019). Indeed, several studies have shown that patients with high plasma levels of FGF-23 have a higher incidence of cardiovascular events and less survival (Parker et al., 2010; Masson et al., 2015; Speer et al., 2015). This fact could explain the increased mortality risk in these patients. In this sense, several authors have associated high plasma levels of FGF-23 with a greater risk of cardiovascular death than other causes of death (Ärnlöv et al., 2013a; Lutsey et al., 2014; Souma et al., 2016; Silva et al., 2019). Marthi et al. (2018) carried out a meta-analysis that looked at thirty-four studies: 17 with the general population, nine with CKD non-dialysis patients and eight with the dialysis population. Overall, when comparing participants classified by FGF-23 quartiles, in the top *versus* bottom third of baseline FGF-23 concentration there was a 70% increased risk of all-cause mortality and 42% increased risk of cardiovascular mortality (Marthi et al., 2018).

In general terms, the increased mortality risk associated with FGF-23 may be a consequence of the augmented incidence of cardiovascular events in patients with higher serum FGF-23 levels. LVH, HF, arrhythmias, myocardial infarction (MI) and vascular alterations such as stroke and vascular calcification are the most common adverse and fatal cardiac events studied in relation to FGF-23 (**Table 2**). It is important to highlight, however, that higher levels of FGF-23 have been associated not only with cardiovascular mortality but also with a significant increase in the risk of non-cardiovascular causes of death. Therefore, FGF-23 should be considered a relevant and specific predictor of mortality, and the relevance of FGF-23 as a predictor of mortality will most likely increase in the coming years.

FGF-23 and LVH

FGF-23 was associated with the development of LVH in CKD patients for the first time in 2009 by Gutiérrez et al. (2009), and this was corroborated by Faul et al. (2011). Currently, several studies have associated high plasma levels of FGF-23 with increased left ventricular mass (LVM), and consequently, with the degree of cardiac hypertrophy developed in the general population (Gutiérrez et al., 2008; Mirza et al., 2009; Seiler et al., 2011; Shibata et al., 2013; Agarwal et al., 2014; Kestenbaum et al., 2014; Masson et al., 2015; Panwar et al., 2015; Reindl et al., 2017; Silva et al., 2019; Cheng et al., 2020; Patel et al., 2020). In particular, FGF-23 has been linked to a greater risk of concentric hypertrophy, which is apparently a compensated cardiac hypertrophy that results in increased wall thickness without ventricular dilation (Mirza et al., 2009; Silva et al., 2019). In addition, it has been demonstrated that serum FGF-23 levels are associated with LVM and LVH in the older population (Mirza et al., 2009) and with less left ventricular ejection fraction and LVM in cardiology inpatients (Shibata et al., 2013). Therefore, the relationship between FGF-23 and cardiac hypertrophy, as well as the former's direct effect on cardiac remodelling through molecular pathways, has been well established and is discussed in the experimental section (section 3.2).

TABLE 2 | Risk of cardiac events and high plasma levels of FGF-23.

Adverse cardiac event	Association with	References
Mortality	Association with all-cause death	Masson et al., 2015
		Ix et al., 2012
		Parker et al., 2010
		Speer et al., 2015
		Chonchol et al., 2016
		Ter Maaten et al., 2018
		Ärnlöv et al., 2013b
		Poelzl et al., 2014
		von Jeinsen et al., 2019
	Association with cardiovascular death	Souma et al., 2016
		Ärnlöv et al., 2013a
		Lutsey et al., 2014
		Silva et al., 2019
LVH or LV mass	Association: Yes	Masson et al., 2015
		Silva et al., 2019
		Kestenbaum et al., 2014
		Shibata et al., 2013
		Agarwal et al., 2014
		Seiler et al., 2011
		Reindl et al., 2017
		Mirza et al., 2009
		Panwar et al., 2015
		Gutiérrez et al., 2008
		Patel et al., 2020
		Cheng et al., 2020
	Association: No	Wohlfahrt et al., 2015
Heart failure	Association: Yes	Lutsey et al., 2014
		Ix et al., 2012
		Parker et al., 2010
		Robinson-Cohen et al., 2020
		di Giuseppe et al., 2014
		Marthi et al., 2018
		Kestenbaum et al., 2014
		Andersen et al., 2016
		Ferreira et al., 2020
		Ferreira et al., 2019
		Cheng et al., 2020
	Association with LVEF < 40%	Seiler et al., 2011
		Shibata et al., 2013
		Poelzl et al., 2014
		von Jeinsen et al., 2019
		Agarwal et al., 2014
		Song et al., 2021
	Association with more severe NYHA class	Koller et al., 2015
		Wohlfahrt et al., 2015
		Ter Maaten et al., 2018
		Poelzl et al., 2014

(Continued)

TABLE 2 | Continued

Adverse cardiac event	Association with	References
Arrhythmias	Atrial fibrillation	Panwar et al., 2015
		Seiler et al., 2011
		Masson et al., 2015
		Ter Maaten et al., 2018
		Mathew et al., 2014
		Alonso et al., 2014
		Chua et al., 2019
		Dong et al., 2019
	Other arrhythmias	No evidence
Myocardial infarction	Association: Yes	Di Giuseppe et al., 2015
		Lutsey et al., 2014
		Ärnlöv et al., 2013b
		Marthi et al., 2018
		Takahashi et al., 2018
		Ferreira et al., 2020
	Association: No	Ix et al., 2012
		Parker et al., 2010
		Taylor et al., 2011
Stroke	Association: Yes	Di Giuseppe et al., 2015
		Panwar et al., 2015
		Wright et al., 2014
	Association: No	Kestenbaum et al., 2014
Vascular calcification	Association: Yes	Donate-Correa et al., 2019
		Silva et al., 2015
		Jimbo et al., 2014
		Dzgoeva et al., 2016
		Bortnick et al., 2019

For more details see each article which contains hazard ratio (HR) of specific variables with 95% confidence interval (CI).

FGF-23 and HF

It is well established that LVH causes pathologic changes in heart structure and function, increasing the risk of adverse cardiovascular events such as arrhythmias, coronary disease and HF. Indeed, elevations in circulating FGF-23 levels have been shown to have a strong relationship with HF (Parker et al., 2010; Kestenbaum et al., 2014; Lutsey et al., 2014; Ferreira et al., 2019, 2020; Cheng et al., 2020; Robinson-Cohen et al., 2020). HF is a clinical syndrome caused by a structural and/or functional cardiac abnormality and is characterised by the inability of the heart to supply the peripheral tissue with enough blood and oxygen (Atherton et al., 2016). It is one of the most common causes of morbidity and mortality (Ziaeian and Fonarow, 2016). Andersen et al. (2016) analysed serum FGF-23 in patients with HF *versus* healthy subjects and showed that FGF-23 levels were significantly higher in HF patients (1526 ± 1601 *versus* 55 ± 20 RU/mL, $p = 0.007$). Focusing on myocardial tissue, these authors also compared intracardiac FGF-23 expression levels between HF patients and healthy subjects but no differences were found (Andersen et al., 2016). These results suggest that increased plasma, but not cardiac FGF-23 levels might play an important role in the development of HF. However, as FGF-23 can be synthesised at the intracardiac level under pathological or stress circumstances such as MI, the contribution of cardiac FGF-23 should be further studied (Andrukhova et al., 2015).

In addition, Di Giuseppe et al. (2015) demonstrated that the relationship between FGF-23 levels and the development of HF was independent of other established risk factor markers, such as NT-proBNP. Ix et al. (2012) also showed that this relationship was stronger when kidney function was impaired, possibly due to the extremely high serum FGF-23 levels found in patients with kidney dysfunction (Wolf, 2010, 2012). Nevertheless, the meta-analysis by Marthi et al. (2018) did not find a trend across different levels of kidney function in the association between high FGF-23 and HF. From a cardiac functional point of view, many studies have correlated high plasma levels of FGF-23 with a reduced left ventricular ejected fraction (LVEF; <40%), which indicates that high FGF-23 levels are directly linked to systolic dysfunction (Seiler et al., 2011; Shibata et al., 2013; Agarwal et al., 2014; Poelzl et al., 2014; von Jeinsen et al., 2019; Song et al., 2021). Furthermore, high plasma levels of FGF-23 are also associated with albuminuria in CKD which is strongly associated with Heart Failure with reduced Ejection Fraction (HFrEF), but not with Heart Failure with preserved Ejection Fraction (HFpEF) (Nayor et al., 2017). However, several articles have shown that increased FGF-23 levels are associated with both types of HF, HFpEF (Almahmoud et al., 2018; van de Wouw et al., 2019; Kanagala et al., 2020; Roy et al., 2020) and HFrEF (Koller et al., 2015; Gruson et al., 2017). Thus, further studies are required to clarify the role of FGF-23 in each HF subtype. HF symptoms are graduated in the New York Heart Association (NYHA) functional classification based on the limitations to the physical activity of the patients caused by cardiac symptoms (Atherton et al., 2016). Importantly, elevations in FGF-23 levels have been associated with the most severe classes on the NYHA scale (Poelzl et al., 2014; Koller et al., 2015; Wohlfahrt et al., 2015; Ter Maaten et al., 2018; von Jeinsen et al., 2019) and, therefore, with more severe cardiac functional impairment and more serious stages of HF.

FGF-23 and Arrhythmia: Atrial Fibrillation

FGF-23 has been related to heart rate disturbances causing arrhythmias, which can be classified as extra beats, supraventricular tachycardia including atrial fibrillation (AF), ventricular arrhythmias and bradyarrhythmias. The vast majority of the clinical studies have correlated high plasma levels of FGF-23 with AF (Seiler et al., 2011; Alonso et al., 2014; Mathew et al., 2014; Masson et al., 2015; Panwar et al., 2015; Ter Maaten et al., 2018; Chua et al., 2019; Dong et al., 2019). According to Mathew et al. (2014), each two-fold increase in circulating FGF-23 increased the risk of AF by 41% in their multi-ethnic study of atherosclerosis and by 30% in their cardiovascular health study. There are several mechanisms by which high plasma levels of FGF-23 could cause AF. FGF-23 induces changes in the cardiac structure such as LVH and is also linked to vascular calcification (Mathew et al., 2014). Both factors modify filling pressures, thus increasing atrial size, the main risk factor for AF (Mathew et al., 2014). Evidence of other types of rhythm alterations, such as

those related to ventricular arrhythmia, is yet to be provided in a clinical setting, however.

FGF-23 and MI

Myocardial infarction is associated with severe complications, such as HF, pericarditis, arrhythmias, ventricular aneurysm and septal defects (Fox et al., 1979). The relationship between high plasma levels of FGF-23 and MI is controversial and requires further research to conclude whether high plasma levels of FGF-23 increase MI risk or not. Some authors have found a significant increase in the levels of FGF-23 after an MI (Ärnlöv et al., 2013b; Lutsey et al., 2014; Di Giuseppe et al., 2015; Takahashi et al., 2018; Ferreira et al., 2019); however, other authors have described a weak increase (Marthi et al., 2018) and some did not find any variation in FGF-23 at all (Parker et al., 2010; Taylor et al., 2011; Ix et al., 2012). At present, circulating FGF-23 levels in patients who have suffered an MI are being studied in three clinical trials that will shed light on this issue and lead to important future conclusions (reported at www.clinicaltrials.gov: NCT01971619, NCT02548364, and NCT03405207).

FGF-23 and Stroke

FGF-23 not only has a harmful effect on the heart but also on the vasculature, as shown by its relation to strokes (Parker et al., 2010; Ärnlöv et al., 2013b; Wright et al., 2014; Di Giuseppe et al., 2015; Marthi et al., 2018). Although Kestenbaum et al. (2014) found a non-significant relationship between elevated FGF-23 and all-cause stroke, Wright et al. (2014) found that elevated FGF-23 was a risk factor independent of CKD for overall stroke in a racially and ethnically diverse urban community. It is important to note that there are different types of strokes depending on the triggering cause: ischemic strokes, which include thrombotic strokes and cardioembolic strokes; haemorrhagic strokes; transient ischemic attacks; and cryptogenic strokes. A relationship has only been demonstrated between FGF-23 and haemorrhagic stroke (Di Giuseppe et al., 2015) and FGF-23 and cardioembolic stroke (Panwar et al., 2015), however. Therefore, although stroke is beyond the scope of this review, the harmful effects of FGF-23 on the vasculature deserve to be mentioned.

FGF-23 and Vascular Calcification

Vascular calcification is a major risk factor for cardiovascular disease which contributes to the high incidence of cardiovascular mortality (Pescatore et al., 2019). FGF-23, as a mineral metabolism factor, plays a direct role in calcification of tissues by modulating disturbances in calcium and phosphate balance (Donate-Correa et al., 2019). The relationship between increased systemic FGF-23 levels and vascular calcification has been shown experimentally in *in vitro* approaches (Jimbo et al., 2014), in patients with established cardiovascular disease (Donate-Correa et al., 2019), in pre-dialysis diabetic (Silva et al., 2015) and in CKD patients (Dzgoeva et al., 2016). Hence, FGF-23 outstands as a promising prognostic biomarker and therapeutic target in vascular calcification.

Consequently, FGF-23 may be considered as a biomarker and predictor of several important cardiac adverse events, but the mechanisms by which FGF-23 could have a harmful effect directly or indirectly on the heart remain misunderstood.

Other Disorders and Comorbidities Associated With High Plasma Levels of FGF-23

Finally, several clinical studies have linked the baseline characteristics of individuals with high plasma levels of FGF-23, discovering a direct correlation with bad health habits, MBD and CKD and with comorbidities such as diabetes and hypertension (**Table 3**).

FGF-23 and Lifestyle: Smoking, Poor Physical Activity, and Inadequate Food Intake

Many authors have found a relationship between high plasma levels of FGF-23 and smoking (Parker et al., 2010; Seiler et al., 2011; Ix et al., 2012; Agarwal et al., 2014; di Giuseppe et al., 2014; Di Giuseppe et al., 2015; Masson et al., 2015; Panwar et al., 2015; Souma et al., 2016; Patel et al., 2020), and only a few authors have failed to find this relationship (Ärnlöv et al., 2013a; Kestenbaum et al., 2014). Furthermore, patients with low levels of physical activity seem to have greater levels of FGF-23 (Ix et al., 2012; Kestenbaum et al., 2014; Masson et al., 2015). Gardinier et al. (2016) also demonstrated a significant increase in FGF-23 levels during exercise, mainly due to the response in osteocytes to the increased expression of PTH. Other studies have not found any changes in FGF-23 levels during exercise, however, even after demonstrating significantly increased Klotho levels and decreased PTH levels (Fakhrpour et al., 2020). A recent study comparing master athletes with age-matched controls showed a significantly better redox balance in athletes, with significantly higher Klotho levels possibly explaining the lower FGF-23 levels in people with higher physical activity (Rosa et al., 2020). It would be interesting to separate physical activity from inadequate food intake, however, as this could also influence FGF-23 levels. In this sense, food preserved with phosphate additives is associated with higher FGF-23 levels (Yuen et al., 2016; Pool et al., 2020). Thus, future studies should further explore the relationship between chronic dietary phosphate intake, FGF-23 levels and their specific association with cardiovascular risk. As smoking, low levels of physical activity and inadequate food intake are cardiovascular risk factors, these factors would enhance the role of FGF-23 in cardiovascular outcomes.

FGF-23 and MBD or Kidney Disease

Mineral bone disorders are usually the consequence of electrolyte imbalances, i.e., hyperphosphatemia, hyperkalaemia, or hypercalcemia (Navarro-García et al., 2018), which have been associated with high plasma levels of FGF-23. Indeed, elevated serum levels of FGF-23 are related to increased levels of phosphate (Parker et al., 2010; Seiler et al., 2011; Taylor et al., 2011; Shibata et al., 2013; Agarwal et al., 2014; Brandenburg et al., 2014; Kestenbaum et al., 2014; Lutsey et al., 2014; Poelzl et al., 2014; Wright et al., 2014; Panwar et al., 2015; Souma et al., 2016; Reindl et al., 2017), calcium (Ca^{2+}) (Parker et al., 2010; Wright et al., 2014; Di Giuseppe et al., 2015; Panwar et al., 2015; Reindl et al., 2017; Patel et al., 2020) and PTH (Taylor et al., 2011;

TABLE 3 | Other disorders and comorbidities correlated with high plasma levels of FGF-23.

Variable	Condition	References
Lifestyle		
Current smoker	Current smokers	Di Giuseppe et al., 2015
		Panwar et al., 2015
		Masson et al., 2015
		di Giuseppe et al., 2014
		Ix et al., 2012
		Parker et al., 2010
		Souma et al., 2016
		Seiler et al., 2011
		Agarwal et al., 2014
		Patel et al., 2020
	Not correlated	Kestenbaum et al., 2014
		Ärnlöv et al., 2013a
Physical activity	Worse	Masson et al., 2015
		Ix et al., 2012
		Kestenbaum et al., 2014
	Not correlated	Andersen et al., 2016
Inadequate food intake	Phosphate intake	Yuen et al., 2016
		Pool et al., 2020
Metabolic bone disorders and kidney disease		
Phosphate	Correlated positively	Di Giuseppe et al., 2015
		Lutsey et al., 2014
		Panwar et al., 2015
		Wright et al., 2014
		Parker et al., 2010
		Kestenbaum et al., 2014
		Poelzl et al., 2014
		Souma et al., 2016
		Seiler et al., 2011
		Shibata et al., 2013
		Taylor et al., 2011
		Reindl et al., 2017
		Agarwal et al., 2014
		Brandenburg et al., 2014
	Not correlated	Takahashi et al., 2018
Calcium	Correlated positively	Di Giuseppe et al., 2015
		Panwar et al., 2015
		Wright et al., 2014
		Parker et al., 2010
		Kestenbaum et al., 2014
		Reindl et al., 2017
		Patel et al., 2020
	Not correlated	Agarwal et al., 2014
		Takahashi et al., 2018
PTH	Correlated positively	Di Giuseppe et al., 2015
		Lutsey et al., 2014
		di Giuseppe et al., 2014
		Brandenburg et al., 2014
		Wright et al., 2014
		Souma et al., 2016
		Poelzl et al., 2014
		Taylor et al., 2011
		Sharma et al., 2020
	Not correlated	Shibata et al., 2013
Vitamin D	Correlated negatively	Souma et al., 2016
		Shibata et al., 2013
		Poelzl et al., 2014
		Chonchol et al., 2016
	Not correlated	Masson et al., 2015
		Kestenbaum et al., 2014
		Taylor et al., 2011
eGFR (<60 mL/min/1.73 m^2)	Correlated negatively	Koller et al., 2015
		Lutsey et al., 2014
		Panwar et al., 2015
		Ix et al., 2012
		Wright et al., 2014
		Parker et al., 2010
		Kestenbaum et al., 2014
		Speer et al., 2015
		Souma et al., 2016
		Wohlfahrt et al., 2015
		Ter Maaten et al., 2018
		Seiler et al., 2011
		Shibata et al., 2013
		Ärnlöv et al., 2013b
		Agarwal et al., 2014
		Ärnlöv et al., 2013a
		Poelzl et al., 2014
		Brandenburg et al., 2014
		Sharma et al., 2020
		Patel et al., 2020
		von Jeinsen et al., 2019
	Not correlated	Di Giuseppe et al., 2015
		Andersen et al., 2016
Albumin-to-creatinine ratio or creatine levels	Correlated positively	Koller et al., 2015
		Panwar et al., 2015
		Masson et al., 2015
		Ix et al., 2012
		Wright et al., 2014
		Kestenbaum et al., 2014
		Speer et al., 2015
		Souma et al., 2016
		Shibata et al., 2013
		Taylor et al., 2011
		Agarwal et al., 2014
		Ärnlöv et al., 2013a
		Sharma et al., 2020
		Song et al., 2021
	Not correlated	Reindl et al., 2017
		di Giuseppe et al., 2014
Comorbidities		
Diabetes	Higher prevalence	Lutsey et al., 2014
		Panwar et al., 2015

(Continued)

TABLE 3 | Continued

Variable	Condition	References
		Ix et al., 2012
		Wright et al., 2014
		Parker et al., 2010
		Kestenbaum et al., 2014
		Speer et al., 2015
		Wohlfahrt et al., 2015
		Agarwal et al., 2014
		Sharma et al., 2020
		Song et al., 2021
	Not correlated	Masson et al., 2015
		Ärnlöv et al., 2013a
Hypertension	Higher prevalence	Lutsey et al., 2014
		Masson et al., 2015
		Ix et al., 2012
		Kestenbaum et al., 2014
		Wright et al., 2014
		Agarwal et al., 2014
		Sharma et al., 2020
		Patel et al., 2020
	Not corelated	Parker et al., 2010
		Ärnlöv et al., 2013a

Brandenburg et al., 2014; di Giuseppe et al., 2014; Lutsey et al., 2014; Poelzl et al., 2014; Wright et al., 2014; Di Giuseppe et al., 2015; Souma et al., 2016; Sharma et al., 2020) and low levels of vitamin D (Shibata et al., 2013; Poelzl et al., 2014; Chonchol et al., 2016; Souma et al., 2016). Although it should also be noted that some authors did not find a relationship with Ca^{2+} (Agarwal et al., 2014), PTH (Shibata et al., 2013) or vitamin D (Taylor et al., 2011; Kestenbaum et al., 2014; Masson et al., 2015). It is well known that there is a complex network between FGF-23, PTH, vitamin D, calcium, phosphates and Klotho levels. This physiological network consists of a feedback mechanism through which disturbances in the level of one of these substances leads to changes in the levels of all the others (Navarro-García et al., 2018). Therefore, increased levels of PTH or vitamin D stimulate the synthesis of FGF-23 in the long bones and reduced renal Klotho expression increases serum phosphate load, which also induces FGF-23 synthesis. These mineral disturbances are classic complications in CKD, but in the last few decades, it has been shown that they also have a huge impact on cardiac tissue (**Figure 1**) because they have direct and indirect cardiotoxic effects, such as the development of LVH, HF or arrhythmias like AF (Navarro-García et al., 2018).

In relation to kidney disease, high plasma levels of FGF-23 have also been associated with impaired kidney function as represented by an estimated glomerular filtration rate (eGFR) < 60 mL/min/1.73 m^2 (Parker et al., 2010; Seiler et al., 2011; Ix et al., 2012; Shibata et al., 2013; Ärnlöv et al., 2013a,b; Agarwal et al., 2014; Brandenburg et al., 2014; Kestenbaum et al., 2014; Lutsey et al., 2014; Poelzl et al., 2014; Wright et al., 2014; Koller et al., 2015; Panwar et al., 2015; Speer et al., 2015; Wohlfahrt et al., 2015; Souma et al., 2016; Ter Maaten et al., 2018; von Jeinsen et al., 2019; Patel et al., 2020; Sharma et al., 2020) and high levels of creatinine (Taylor et al., 2011; Ix et al., 2012; Shibata et al., 2013; Ärnlöv et al., 2013a; Agarwal et al., 2014; Kestenbaum et al., 2014; Wright et al., 2014; Koller et al., 2015; Masson et al., 2015; Panwar et al., 2015; Speer et al., 2015; Souma et al., 2016; Sharma et al., 2020; Song et al., 2021). di Giuseppe et al. (2014); Andersen et al. (2016), and Reindl et al. (2017) did not find evidence of this association; however, the number of subjects they studied was limited. CKD is characterised by excessive plasma levels of phosphate; therefore, increased synthesis of FGF-23 is a compensatory mechanism that preserves phosphate homeostasis by increasing urinary excretion. FGF-23 decreases the activity of the sodium-phosphate cotransporter in the renal proximal tubule and reduces dietary absorption by down-regulating the expression of the enzyme responsible for synthesising calcitriol, 1α-hydroxylase (Gutiérrez et al., 2008; Wolf, 2012). Therefore, high plasma levels of FGF-23 are a good biomarker for impaired renal function.

Other Comorbidities Associated With High Plasma Levels of FGF-23.

Two of the major comorbidities that contribute to the development of cardiovascular disease are diabetes and hypertension, both of which now have a high prevalence (Ruilope, 2012; Strain and Paldanius, 2018). Recent studies have associated elevated plasma levels of FGF-23 with a higher prevalence of diabetes mellitus (Parker et al., 2010; Ix et al., 2012; Agarwal et al., 2014; Kestenbaum et al., 2014; Lutsey et al., 2014; Wright et al., 2014; Panwar et al., 2015; Speer et al., 2015; Wohlfahrt et al., 2015; Sharma et al., 2020; Song et al., 2021) and hypertension (Ix et al., 2012; Agarwal et al., 2014; Kestenbaum et al., 2014; Lutsey et al., 2014; Wright et al., 2014; Masson et al., 2015; Patel et al., 2020; Sharma et al., 2020). Some studies have demonstrated a reduction in soluble Klotho levels in patients with impaired fasting glucose (Zhang and Liu, 2018), together with increased levels of FGF-23 (Zaheer et al., 2017) in diabetic patients compared to healthy volunteers, even with preserved kidney function. In the field of hypertension, Liu et al. and other studies have found an association between FGF-23 and arterial stiffness after renal transplantation when renal function is restored (Feng et al., 2020; Liu et al., 2020). These comorbidities contribute to an increased risk of mortality and adverse outcomes and worsen the quality of life of patients and might be explained by the cardiovascular effects of FGF-23. Some studies did not support this association (Parker et al., 2010; Ärnlöv et al., 2013a; Masson et al., 2015), however. Further studies are needed to clarify the independence of hypertension and diabetes in elevating systemic levels of FGF-23.

In conclusion, high plasma levels of FGF-23 are associated with certain demographics, such as age and sex; with cardiovascular diseases like LVH, HF and AF; with clinical disturbances such as low eGFR, high phosphate and NT-pro-BNP; and with comorbidities like diabetes and hypertension. All these studies point to FGF-23 as an important and independent biomarker involved in several pathologic processes, including cardiovascular disease. This idea must be interpreted with

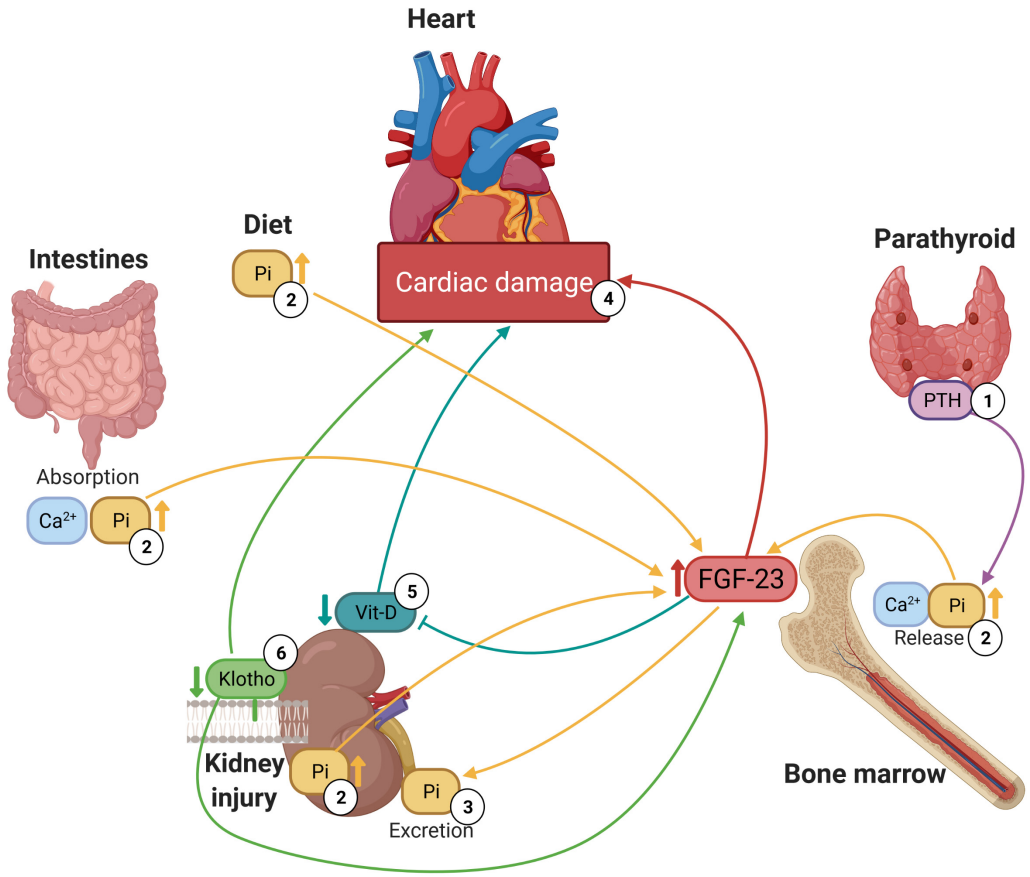

FIGURE 1 | Relationship between high plasma levels of FGF-23, mineral bone metabolism components and cardiac damage. (1) Parathyroid stimulates the release of phosphate and calcium from large calcium stores in the bones into the bloodstream. (2) High plasma levels of phosphate promote FGF-23 synthesis in bone marrow. (3) FGF-23 enhances the excretion of phosphate in kidneys. (4) High circulating FGF-23 levels are associated with several forms as cardiac damage including hypertrophy and HF. (5) FGF-23 reduces circulating 1,25(OH)2D, active form of vitamin D, and deficiency of vitamin D is associated with cardiac damage. (6) Low levels of Klotho are linked to both high plasma levels of FGF-23 and cardiac damage.

caution, however, as contradictions remain in the literature and a clear causal relationship is yet to be established, at least in a clinical setting. Hence, there is a need to experimentally address the relationship between high plasma levels of FGF-23 and cardiac disturbances to shed light on the origin of FGF-23 as a cause or consequence of cardiac damage and identify the specific FGF-23 downstream molecular pathways involved.

FGF-23 INDUCES CARDIAC DAMAGE: EXPERIMENTAL *IN VITRO* AND *IN VIVO* APPROACHES

As already mentioned, over the last decade, many studies have shown a significant and independent relationship between high plasma levels of FGF-23 and detrimental cardiac outcomes in a clinical setting (**Table 2**). In this cardiovascular setting, an urgent roadmap for further research has emerged, and experiments aimed at unravelling the role of FGF-23 in cardiac pathology are needed. To date, research studies have demonstrated that FGF-23 might induce cardiac dysfunction, hypertrophy and fibrosis in the heart.

FGF-23 Causes Cardiac Dysfunction

Correct heart function depends directly on the functional cells of the heart, that is, on the precise and coordinated contraction and relaxation cycle of cardiomyocytes (Fozzard, 1991). During contraction, intracellular Ca^{2+} levels of cardiomyocytes increase due to changes in the cardiomyocyte membrane action potential (AP) (Bers, 2002). AP is the reversible change in membrane potential as a consequence of the opening of different ion channels and leads to cardiomyocyte contraction in a process called excitation–contraction (EC) coupling, which represents the translation of electrical stimulation into mechanical work (Bers, 2002). Ca^{2+} is a key player in cardiac EC coupling (Fabiato and Fabiato, 1975) as a rise in free cytosolic Ca^{2+} is essential for the contraction of the cardiomyocytes (Bers, 2002). L-type calcium channels at the sarcolemma open due to the depolarisation of the AP, allowing the first Ca^{2+} influx into the cytoplasm (Fabiato and Fabiato, 1975). This Ca^{2+} influx activates

ryanodine receptors (RyRs), triggering a greater amount of Ca^{2+} release from the sarcoplasmic reticulum (SR) to the cytoplasm (Bers, 2006). The intracellular Ca^{2+} concentration increases and Ca^{2+} binds to troponin C at the myofilaments, starting the cardiomyocyte contraction (Bers, 2006).

To allow physiological relaxation, the Ca^{2+} levels should decrease in the same amount as the previous increase (Eisner et al., 2017). This reduction of cytosolic Ca^{2+} mostly takes place via two different processes: 92% of cytosolic Ca^{2+} is pumped back to the SR by the action of the SR–Ca^{2+}–adenosine triphosphatase 2a (SERCA) and, to a lesser extent (7%), Ca^{2+} is extruded from the cytoplasm to the extracellular medium by the Na^{+}–Ca^{2+} exchanger (Bers, 2006). This Ca^{2+} handling in the cardiomyocytes is a complex physiological process perfectly regulated by different proteins, and it is well known that calmodulin kinase II (CaMKII) and cAMP-dependent protein kinase (PKA) regulate the open probability of RyRs through several phosphorylations at different sites, increasing their activity (Bovo et al., 2017). In addition, CaMKII and PKA can also phosphorylate phospholamban (PLB), a SR membrane protein that regulates SERCA activity. PLB binds to SERCA and inhibits its activity in situations of dephosphorylation (Kranias and Hajjar, 2012).

In this context, it has been shown that FGF-23 is involved in this Ca^{2+} handling by increasing phosphorylation of regulator proteins such as CaMKII (Kao et al., 2014; Navarro-García et al., 2019), which could drive cardiomyocytes to develop a cellular phenotype related to contractile dysfunction and predisposition to arrhythmias (Curran et al., 2010) (**Figure 2**). Recent works have demonstrated that FGF-23 might induce pro-arrhythmogenic Ca^{2+} events by itself in isolated adult rat ventricular cardiomyocytes due to alterations in Ca^{2+} handling (Navarro-García et al., 2019). Direct acute perfusion of 100 ng/mL FGF-23 reduced systolic Ca^{2+} release and increased the spontaneous diastolic Ca^{2+} leak, increasing the incidence of arrhythmogenic Ca^{2+} events (Navarro-García et al., 2019). This phenotype is frequently observed in failing cardiomyocytes (Ruiz-Hurtado et al., 2015; Alvarado et al., 2017; Chen et al., 2020), which might explain the relationship between FGF-23 levels and HF incidence described previously in this review. The events observed in cells are strongly influenced by Ca^{2+} mishandling and could be induced by RyRs hyperactivity and a reduction in SERCA activity, both of which are responsible for reduced SR Ca^{2+} load (Navarro-García et al., 2019). These alterations would lead to impaired cardiomyocyte contraction, represented by less cell shortening (Navarro-García et al., 2019).

Similar results related to cardiac dysfunction and predisposition to ventricular arrhythmia were found in nephrectomised mice and homozygous Klotho-hypomorphic (*kl/kl*) mice, both of which are experimental animal models that have middle (∼300 pg/mL) or very high (∼400.000 pg/mL) circulating FGF-23 levels (Navarro-García et al., 2020). Interestingly, when these mice are treated with recombinant Klotho, cardiac dysfunction and pro-arrhythmogenic Ca^{2+} release events are prevented (Navarro-García et al., 2020). This highlights the possible protection of Klotho against the deleterious effects of FGF-23. Moreover, other studies reported that the cellular HL-1 line of atrial murine cardiomyocytes had a greater L-type Ca^{2+} current and greater Ca^{2+} transients and SR Ca^{2+} content after maintained FGF-23 (25 ng/mL) exposure during 24 h of treatment compared to control cells (Kao et al., 2014). This higher SR Ca^{2+} content may be a consequence of increased SERCA activity due to phosphorylation of PLB at the CaMKII-specific site (Thr^{17}) and not due to an intrinsic increase in the protein expression of SERCA or PLB (Kao et al., 2014). FGF-23 also dysregulated Ca^{2+} homeostasis, triggering delayed after depolarizations that have been related to the initiation of ventricular arrhythmias (Kao et al., 2014).

It is important to note that although both the cellular studies described above showed apparently different effects of FGF-23, the first showed the acute effect of FGF-23 on ventricular cardiomyocytes from a rat, while the second was carried out on an atrial cell line exposed to FGF-23 for longer periods. In both cases, the conclusion was that FGF-23 led to a greater predisposition to arrhythmias. Another effect of FGF-23 was described using mice ventricular muscle strips and showed that FGF-23 (9 ng/mL) was able to induce a significant increase in the peak isometric tension, slope and area of contractile waveforms (Touchberry et al., 2013). Therefore, in addition to the effect of FGF-23 on predisposition to cellular arrhythmia, it also could promote important alterations in cardiac function that regulate the contraction and relaxation process. It is well known that the main action of FGF-23, its phosphaturic action in the kidney, takes place via FGFR-binding; however, the FGFR isoform responsible for this effect of FGF-23 on cardiac function is yet to be identified, although some research has pointed to FGFR1 (Touchberry et al., 2013; Schumacher et al., 2019) or FGFR4 (Faul et al., 2011; Faul, 2017; Grabner et al., 2017).

Electrocardiogram (ECG) and echocardiography are two non-invasive methods used to estimate *in vivo* cardiac function. Ca^{2+} mishandling causes important changes in EC coupling, and this could also lead to pro-arrhythmogenic activity of cardiomyocytes, which is associated with abnormal heart rhythms. Indeed, a single-dose FGF-23 injection (40 μg/kg) in healthy mice was able to induce a significant increase (60%) in the occurrence of premature ventricular contractions recorded by ECG (Navarro-García et al., 2019). In addition, echocardiography allows the LV dimensions during systole and diastole, fractional shortening and ejection fraction to be measured. In general, mice with high circulating levels of FGF-23 had worse cardiac function than control mice, showing a lower percentage of fractional shortening, larger LV internal diameter in diastole, less cardiac output or higher LV diastolic pressure (Faul et al., 2011; Touchberry et al., 2013; Andrukhova et al., 2015; Hao et al., 2016; Han et al., 2020). Hence, FGF-23 could be an important factor causing changes in cardiac function and heart rhythm that can lead to the onset and worsening of cardiac disease.

FGF-23 Induces LVH

Ca^{2+} abnormalities, usually those related to Ca^{2+} overload, precede cardiac dysfunction, while LVH develops later (Li et al., 2019). LVH, which is present in 15–20% of the general population, is one of the main risk factors for the

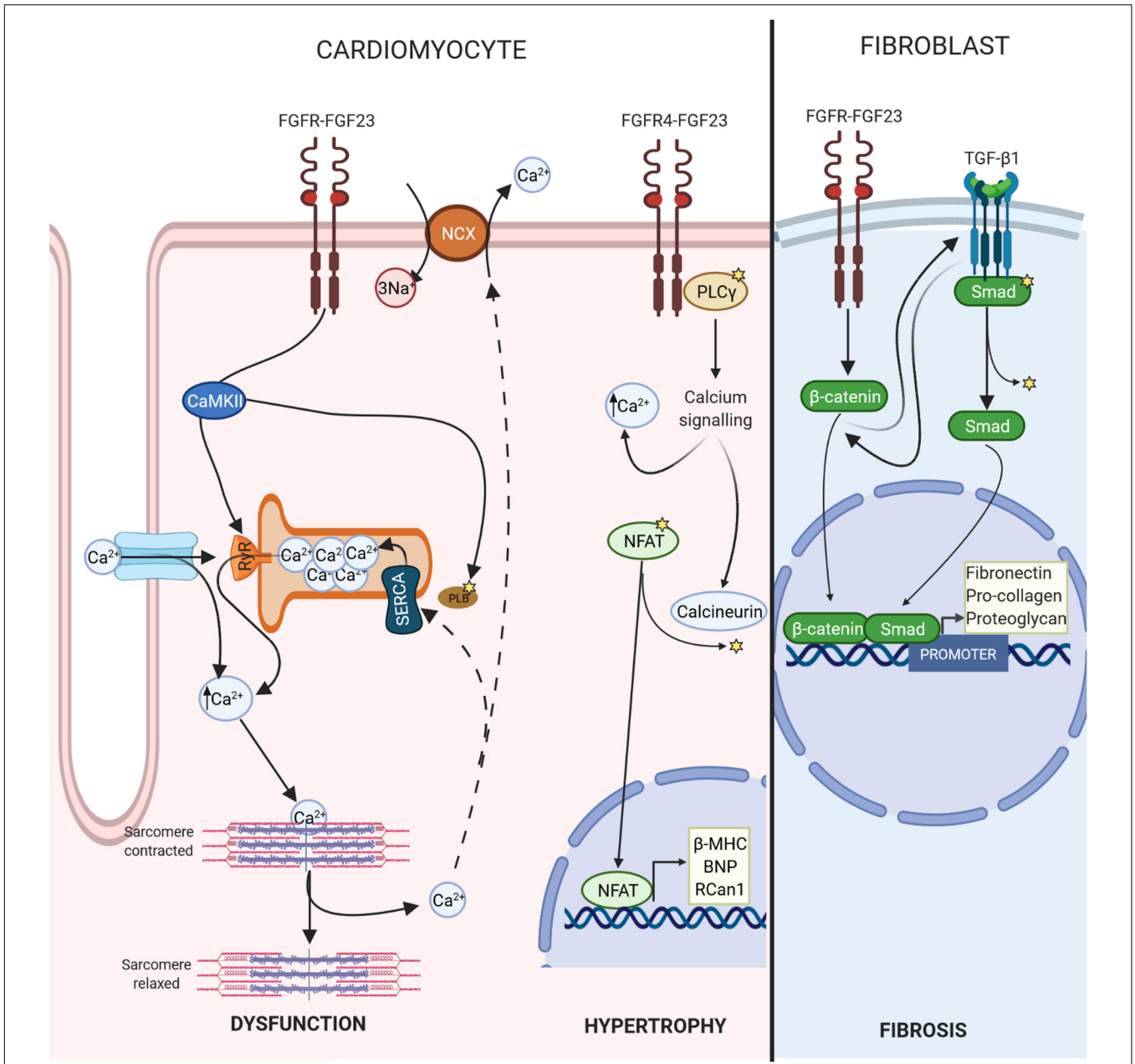

FIGURE 2 | FGF-23-FGFR signalling. FGF-23 binds to the extracellular domain of its receptor, causing autophosphorylation. In cardiomyocytes, this change leads to phosphorylate calcium regulatory proteins, such as CAMKII, which promotes Ca^{2+} mishandling and cardiac dysfunction. In addition, FGF-23/FGFR4 triggers calcium cascade and the activation of calcineurin, which dephosphorylate NFAT inducing transcription of pro-hypertrophic genes such as β-*MHC*, *BNP*, or *Rcan1*. In fibroblasts, FGF-23 promotes fibrosis through activation of β-catenin.

development of a variety of adverse cardiac events and is related to pathological cardiac remodelling (Weber, 1991). It has already been demonstrated that FGF-23 promotes cardiac hypertrophy directly by acting on FGFR4, which subsequently triggers the phospholipase (PLC)γ/calcineurin/nuclear factor of activated T-cells (NFAT) signalling pathway (Faul et al., 2011; Grabner et al., 2015; Leifheit-Nestler et al., 2018b; Han et al., 2020). FGF-23 binds to FGFR4, causing its auto-phosphorylation, which then induces PLCγ activation through the binding of PLCγ to a specific phosphorylated tyrosine residue within the FGFR4 cytoplasmic sequence (Vainikka et al., 1994). Activated PLCγ increases cytoplasmic Ca^{2+} levels and activates calcineurin, the main regulator of intracellular Ca^{2+} (Eswarakumar et al., 2005), with the subsequent dephosphorylation of NFAT (Molkentin, 2004). Dephosphorylated NFAT translocates to the nucleus, where it promotes the transcription of pro-hypertrophic genes, including regulator of calcineurin 1 (*Rcan1*), brain natriuretic peptide

(*BNP*), atrial natriuretic peptide (*ANP*) and β-myosin heavy chain (β-*MHC*) (Han et al., 2020) (**Figure 2**).

The hypertrophic effect of FGF-23 has been proven in *in vitro* and *in vivo* experiments. HL-1 atrial cells incubated with recombinant FGF-23 (rFGF-23) exhibited a higher cross-sectional surface area and an increase in pro-hypertrophic genes (Touchberry et al., 2013). Similarly, murine models with high levels of circulating FGF-23 showed greater mRNA levels of pro-hypertrophic genes, greater heart weight/body weight or heart weight/tibial length ratios and greater LV thickness (Faul et al., 2011; Andrukhova et al., 2015; Hao et al., 2016; Slavic et al., 2017; Leifheit-Nestler et al., 2018b; Han et al., 2020). Faul et al. (2011) published a large study where they demonstrated the hypertrophic effect of FGF-23. Cell surface area and expression of pro-hypertrophic genes in isolated neonatal rat ventricular myocytes (NRVM) increased after 48 h of treatment with FGF-23 (10, 25, and 100 ng/mL), while direct administration of rFGF-23 into the LV myocardium in mice caused cardiac hypertrophy after 14 days of treatment, even without an increase in circulating FGF-23 levels or other changes in mineral metabolism (Faul et al., 2011). Mice injected with FGF-23 showed greater heart weight/tibial length ratios and LV wall thickness in contrast to vehicle mice (Faul et al., 2011). This cardiac remodelling was also observed in mice after rFGF-23 (40 μg/kg) intravenous injections twice daily for 5 days, after which the immunohistochemistry and RT-PCR of pro-hypertrophic genes in the heart showed the presence of LVH development (Faul et al., 2011). Han et al. (2020) reported similar results in mice after intraperitoneal administration of rFGF-23 at 75 ng/g twice daily for 5 days. Leifheit-Nestler et al. (2018b) studied two different mouse strains: *kl/kl* mice and an experimental model for human X-linked hypophosphatemia with a mutation that inactivates the endopeptidases of the X chromosome (Hyp) mice. Both models showed high endogenous FGF-23 synthesis and elevated circulating FGF-23 levels compared to wild-type (WT) controls. *kl/kl* mice exhibited adverse cardiac remodelling, their heart weight/body weight ratios and cross-sectional areas of myocytes were higher than those of WT mice and the cardiac mRNA of their pro-hypertrophic genes was also increased. In the same way, experimental models of cardiac damage, such as post MI, ischemia reperfusion (I/R) and transversal aortic constriction, have been used to demonstrate that LVH is related to a profound increase in circulating levels of FGF-23, higher cardiac mRNA and protein expression of FGF-23 (Andrukhova et al., 2015; Hao et al., 2016; Slavic et al., 2017). All these data point to FGF-23 as a direct cause of LVH.

Furthermore, several studies have provided evidence that FGF-23 activates the PLCγ/calcineurin/NFAT signalling pathway. *In vivo*, healthy mice treated with rFGF-23 showed upregulated PLCγ protein levels compared to vehicle-treated mice (Han et al., 2020). In addition, *in vitro* treatment of rFGF-23 in NRVM activates PLCγ, and incubation with the PLCγ inhibitor U73122 blocks the hypertrophic effect of FGF-23 (Faul et al., 2011). Other evidence has been reported by Faul et al. (2011) and Grabner et al. (2015), who analysed NFAT activity after incubation with rFGF-23 in C2C12 myoblast (an immortalised mouse myoblast cell line) and in NRVM, respectively, and found that cells treated with FGF-23 showed a rise in NFAT activity compared to vehicle-treated cells. Also, Grabner et al. (2015) showed that this effect of FGF-23 was blocked by the calcineurin inhibitor cyclosporine A. In a study by Leifheit-Nestler et al. (2018b), qRT-PCR analysis revealed that cardiac FGFR4 mRNA expression was upregulated in both *kl/kl* and Hyp mice compared to their respective WT controls, but especially in *kl/kl* mice. In contrast, calcineurin protein levels were increased and NFAT phosphorylation was reduced only in *kl/kl* mice, therefore, the pro-hypertrophic genes were upregulated in *kl/kl* mice but not Hyp mice. There are two likely reasons for the differences observed between mouse strains. First, the circulating levels of FGF-23 are much higher in *kl/kl* mice. Second, the differences in Ca^{2+} and phosphate levels: *kl/kl* mice present with hyperphosphatemia and hypercalcemia, while Hyp mice have hypophosphatemia and normal levels of Ca^{2+}. Interestingly, this hypertrophic effect is also influenced by the absence of Klotho, as *kl/kl mice*, which is the experimental model with the highest systemic FGF-23 levels, show a greater degree of hypertrophy in a Klotho-deficient context. It is also important to mention that soluble Klotho could act as a circulating lure for FGF-23, impeding its binding to cardiac FGFRs; act as a coreceptor in cardiomyocytes, causing a switch in or even the blockade of the FGF-23 signalling pathway; or interact with an unknown receptor activating the cardiac protective signalling pathway. Thus, Klotho could block or reduce the hypertrophic effect of FGF-23 on the heart, as it does with the deleterious effect of FGF-23 on cardiac function (Navarro-García et al., 2019, 2020). Indeed, several authors have shown the cardioprotective action of recombinant supplementation with Klotho in several experimental models of direct or indirect cardiac damage (Xie et al., 2012; Hu et al., 2017; Liu et al., 2019; Navarro-García et al., 2019, 2020; Wright et al., 2019; Han et al., 2020).

FGFR4 expression is upregulated when FGF-23 levels are elevated, therefore, FGF-23 is considered to be an inducer of cardiac hypertrophy through FGFR4 (Grabner et al., 2015). Immunoprecipitated PLCγ-bound FGFR4 was elevated in isolated NRVM treated for 30 min with FGF-23 at 25 ng/mL compared to control cells and cells co-treated with FGF-23 plus anti-FGFR4 antibodies (Grabner et al., 2015). Although a high phosphate (2%) diet is known to induce LVH and FGF-23 synthesis (Hu et al., 2015), FGFR4 knockout (KO) mice did not show LVH after 12 weeks of a high phosphate diet. In this way, blocking FGFR4 could be potentially useful for avoiding deleterious FGF-23 cardiac actions in a clinical setting (Grabner et al., 2015). Grabner et al. (2017) attributed a substantial role in LVH pathogenesis to FGFR4 and claimed that FGF-23/FGFR4-mediated LVH could be reversible, at least in rodents. To validate this hypothesis, they carried out three types of experiments. The first found that the hypertrophic effect was reversible after incubation of NRVM with FGF-23 for 24 h and then with anti-FGFR4 antibodies. In addition, pre-treatment with anti-FGFR4 antibodies prevented FGF-23-induced hypertrophy. In the second experiment, LVH induced by 5/6 nephrectomy in rats, a model that presents high FGF-23 levels, did not progress in animals treated with anti-FGFR4 antibodies for 4 weeks after surgery compared with untreated nephrectomised rats.

In the third experiment, 18-month-old FGFR4 KO mice were protected from LVH (despite having high plasma levels of FGF-23) compared with WT mice, which, in normal conditions, at this age develop LVH (Grabner et al., 2017). Finally, a recent study using inducible FGFR4 KO mice in which FGFR4 was depleted only in the heart by tamoxifen treatment, found that they did not develop LVH after intraperitoneal injections of rFGF-23 at 75 ng/g twice daily for 5 days, unlike WT mice given the same treatment (Han et al., 2020). All these experimental studies show that FGF-23 activates cardiac PLCγ/calcineurin/NFAT signalling and development of LVH through FGFR4 (**Figure 2**).

FGF-23 Induces Cardiac Fibrosis

Fibrosis is a response aimed at protecting an organ from an injurious event; however, it leads to massive deposition of the extracellular matrix (ECM), disrupting the normal tissue architecture and inducing destruction of the parenchyma (Franklin, 1997). Tissue fibrosis is responsible for increased organ size; therefore, an increase in the heart's mass can be due to cellular hypertrophy or cardiac fibrosis or both. The cellular hypertrophic effect of FGF-23 has already been established (see section 3.2); however, the role of circulating and/or cardiac FGF-23 in the progression of cardiac fibrosis is not yet clear. Hao et al. (2016) suggested that FGF-23 promotes myocardial fibrosis through the activation of β-catenin, which is a profibrotic factor that cross-talks with transforming growth factor-β1 (TGF-β1) signalling, also an important fibrogenic agent. TGF-β1 receptors/Smad complexes stimulate chemotaxis in fibroblasts and increase the expression of collagen, fibronectin, and proteoglycans, the main components of the ECM (Leifheit-Nestler and Haffner, 2018). TGF-β1 signalling can induce the expression of β-catenin pathway members and *vice versa* (Guo et al., 2012). When β-catenin translocases into the nucleus, Smads and β-catenin form a complex at the promoter to coregulate specific gene expression and stimulate the transcription of fibrosis-related genes (Guo et al., 2012) (**Figure 2**). In adult myocardial fibroblasts, rFGF-23 induces proliferation in a dose-dependent manner (15, 25, and 50 ng/mL) through overexpression of profibrotic genes, such as β-catenin and procollagen I and II (Hao et al., 2016). Furthermore, FGF-23 increases the proliferation of neonatal rat cardiofibroblasts and expression of TGF-β1, TGF-β1 receptor/Smad complexes, connective tissue growth factor and collagen I (Leifheit-Nestler et al., 2018a; Böckmann et al., 2019). It has been shown that FGF-23 also intensifies the effect of TGF-B1 via FGFR1 promoting fibrosis, whereas cotreatment with an inhibitor of FGFR1 avoids this fibrosis (Kuga et al., 2020).

Böckmann et al. (2019) also hypothesised that FGF-23 might activate the local renin–angiotensin–aldosterone system, promoting fibrosis through increased cardiac mRNA expression levels of angiotensinogen, angiotensin-converting enzyme and angiotensin II receptor type 1. This hypothesis has already been demonstrated via the cotreatment of neonatal rat cardiofibroblasts with antihypertensive drugs like spironolactone, which prevented fibrotic development (Böckmann et al., 2019). Therefore, further studies are needed to unravel the different pathways through which FGF-23 induces cardiac fibrosis.

FGF-23-induced cardiac fibrosis has also been observed using *in vivo* experimental approaches. Leifheit-Nestler et al. (2018b) showed that *kl/kl* mice developed myocardial fibrosis due to a significant rise in the expression of collagen I and TGF-β1. Furthermore, Hu et al. (2015) showed that TGF-β1 is responsible for activating the extracellular signal-regulated kinase 1/2 pathway in *kl/kl* mice, which leads to cardiac hypertrophy and fibrosis. It has been demonstrated that direct damage to the myocardium raises cardiac levels of FGF-23 (Schumacher et al., 2019). In an MI mice model, FGF-23 and FGFR1 increased early in the myocardium (Schumacher et al., 2019). This cardiac FGF-23 could result from an increased uptake from the circulation or may be synthesised intrinsically in the heart (Schumacher et al., 2019). The main sources of FGF-23 in the heart are local fibroblasts, which increase fibroblast migration and the expression of fibronectin and collagen I (Schumacher et al., 2019). Hao et al. (2016) used adeno-associated virus-carrying FGF-23 injections in mice followed by MI or I/R. The treated mice showed significantly increased cardiac fibrosis compared to negative controls, and this effect was prevented by the inhibition of β-catenin (Hao et al., 2016). FGF-23 might have a positive role in healing after an MI by stimulating the fibroblasts to fill the empty area and produce ECM components (Schumacher et al., 2019); however, it induces pathologic fibrosis in the heart after long exposures and can also influence cardiac hypertrophy development.

STRATEGIES TO AVOID DELETERIOUS FGF-23 EFFECTS ON THE HEART

Various therapeutic approaches are currently being considered to avoid the harmful effects of FGF-23. The key aspects are listed here as follows: FGF-23 antibodies, blockers of FGFRs and phosphate binders. In addition, Klotho as a potential therapy has been included based on the relevant cardio-protection showed by the exogenous recombinant Klotho supplementation examined in several experimental studies.

FGF-23 Antibodies

FGF-23 antibodies could be considered as the first therapeutic option; however, it is important to point out that FGF-23 is a pleiotropic factor that regulates many physiological processes, such as phosphate excretion. These processes would also be blocked with the use of these antibodies. For example, chronic treatment with FGF-23 antibodies for 6 weeks in an experimental CKD rat model improved secondary hyperparathyroidism by decreasing PTH and increasing vitamin D, but phosphate levels, aortic calcification and even mortality were significantly increased (Shalhoub et al., 2012). Therefore, this therapeutic option can be dismissed as the negative impact of the side effects might be greater than the clinical benefits as in situations of renal dysfunction. Currently, these antibodies have only been validated for the treatment of X-linked hypophosphatemic rickets caused by high plasma levels of FGF-23 (Carpenter et al., 2014). There have been several studies in humans (Carpenter et al., 2014; Imel et al., 2015) and Hyp mice

(Yamazaki et al., 2008; Aono et al., 2009, 2011) that support the efficacy of FGF-23 antibodies in ameliorating biochemical, morphological, histological and clinical abnormalities associated with X-linked hypophosphatemia, but the safety of this treatment is still under investigation (Fukumoto, 2016) (reported at www.clinicaltrials.gov: NCT02163577 and NCT02312687).

FGFRs Blockers

FGF-23 exerts its action by binding to FGFRs 1–4, and several studies have proposed FGFR4 as the main FGFR isoform that mediates the effect of FGF-23 on the heart (Grabner et al., 2015, 2017; Leifheit-Nestler et al., 2016). Therefore, a useful therapeutic option currently being studied to impede FGF-23 effects on the heart consists of the specific blockage of FGFR4 (Grabner et al., 2017). This receptor has been related to the deleterious cardiovascular effect mediated by FGF-23, such as LVH inducing the overexpression of cardiac remodelling genes, including *BNP* and β-*MHC* (Leifheit-Nestler et al., 2018b). Moreover, the phosphaturic action of FGF-23 is mediated by FGFR1 in the kidneys. Therefore, blocking FGFR4 could prevent the adverse effects of FGF-23 on the heart without interfering in the other physiological functions of FGF-23, such as increased phosphate excretion in situations where the renal function has declined (Taylor et al., 2019). In support of this, Grabner et al. (2017) showed *in vitro* in NRVM that the hypertrophic effect of FGF-23 can be prevented by pre-treating these cells with anti-FGFR4. Furthermore, in the same study, LVH did not progress in 5/6 nephrectomised rats treated with anti-FGFR4 antibodies for 4 weeks after surgery compared with the control group (in which a further 28% increase in LVM was observed) (Grabner et al., 2017). These experimental results make FGFR4 an interesting therapeutic target, the safety of which has already been proven in clinical trials in cardiovascular diseases (reported at www.clinicaltrials.gov: NCT02476019). In addition, FGFR4 blockade is currently used in oncology trials as neoadjuvant chemotherapy to improve patients' response, since it has a beneficial anti-angiogenic effect (Xin et al., 2018; Gluz et al., 2020).

Phosphate Binders

High plasma levels of FGF-23 are correlated with high levels of phosphate, which are also considered to be a cause of cardiovascular adverse events (Zoccali et al., 2013). In this way, decreasing phosphate levels could improve the prognosis of patients with cardiovascular disease who have high plasma levels of FGF-23. There are three common types of phosphorus binders: Ca^{2+}-containing binders, aluminium-containing binders and non-Ca^{2+} or Ca^{2+}-free phosphate binders (Chan et al., 2017). These drugs are commonly used in the CKD population in combination with a dietary phosphate restriction (Ketteler and Biggar, 2013). Sharon et al. showed that patients with CKD and hyperparathyroidism treated with cinacalcet for 20 weeks had a 30% decrease in their levels of FGF-23 compared with the placebo group, and this was associated with a lower risk of cardiovascular events and mortality (Moe et al., 2015). In another study, Gonzalez-Parra et al. (2011) showed that treatment with the phosphate binder lanthanum carbonate in stage 3 CKD patients was associated with a decrease in serum FGF-23 levels and a decrease in the risk of adverse cardiovascular events. Nonetheless, the effect of these treatments is modest, and the levels of FGF-23 remain above the normal range despite the reported decreases (Zoccali et al., 2013).

Klotho as a Potential Therapeutic Option

Recent experimental research has pointed to Klotho as a potentially useful treatment for reducing or avoiding the harmful effects of FGF-23 on the heart. Indeed, Han et al. (2020) showed that the FGF-23/FGFR4 signalling is attenuated by intraperitoneal administration of soluble Klotho in mice, preventing FGF-23-induced LVH. Moreover, Hu et al. (2015) and Navarro-García et al. (2020) used a *kl/kl* mice to show that Klotho deficiency is a novel intermediate mediator of pathologic cardiac remodelling and dysfunction induced by high plasma levels of FGF-23. There are three hypothetical actions by which Klotho could prevent the effects of FGF-23 on the heart: by being a soluble lure for FGF-23 and impeding its binding to cardiac FGFR4; by acting as a coreceptor in cardiomyocytes, causing a switch in or even inhibition of the FGF-23 signalling pathway; or by interacting with an unknown receptor and activating the cardiac protective signalling pathway. To date, Klotho therapy has been studied only at the experimental level. Further research is needed to determine the ability of Klotho therapy to prevent the detrimental effects of FGF-23 in patients while maintaining the physiological phosphaturic FGF-23 action.

In summary, more experimental research and clinical data are required to identify which is the best option for controlling the deleterious effects of FGF-23, especially on the heart, while maintaining its physiological phosphaturic action. This option could involve blocking the FGF-23/FGFR4 axis or it could involve the promising therapies that use recombinant Klotho.

CONCLUDING REMARKS AND FUTURE PERSPECTIVES

In conclusion, FGF-23 has a direct association with the development and progression of several events related to high cardiovascular risk, such as LVH, HF and arrhythmias, and its value as a cardiovascular biomarker in humans has been clinically demonstrated. Furthermore, a variety of *in vitro* and *in vivo* experimental approaches have indicated that FGF-23/FGFR axis signalling, especially that of the FGF-23/FGFR4 axis, provides an important base for the development of cardiac dysfunction through Ca^{2+} mishandling and cardiac hypertrophy and cardiac fibrosis through increased expression of target genes and proteins. Therefore, this axis represents an excellent therapeutic target for interrupting the harmful cardiac effects of FGF-23. Indeed, diverse neutralising anti-FGF-23 or anti-FGFR blocking antibodies are being tested in human clinical trials to assess their utility and safety. Whether FGF-23/FGFR signalling *per se* can initiate changes in cardiac function and structure or whether it only modulates cardiac remodelling in

concert with other cardio-toxic factors remains unclear, however. Further research is needed to define whether FGF-23 effects are only deleterious or are dose- and/or time-dependent profitable effects, whether cardiomyocytes may themselves produce FGF-23, and the role of FGF-23 in myocardial damage. Therefore, it is essential to identify all the FGF-23-dependent pathways and their mediators that may have potential diagnostic, prognostic and therapeutic significance to cardiovascular diseases.

AUTHOR CONTRIBUTIONS

SV-S, JP, JAN-G, and GR-H wrote the manuscript with the contribution of LG-L, ER-S, and LR. All authors have read and agreed to the published version of the manuscript.

FUNDING

This work was supported by the Fundación Renal Íñigo Álvarez de Toledo (FRIAT) and by several projects at the Instituto de Salud Carlos III (PI17/01093, PI17/01193, and PI20/00763), and was co-funded by the European Regional Development Fund (Fondos FEDER).

ACKNOWLEDGMENTS

SV-S is an assistant researcher from the Education and Research Council of Madrid (PEJ-2019-AI/SAL-13521), ER-S is a PFIS Ph.D. student (FI18/00261), JP is a Sara Borrell researcher from ISCIII (CD19/00029) and GR-H is a Miguel Servet researcher from ISCIII (CP15/00129 and CPII20/00022).

REFERENCES

Agarwal, I., Ide, N., Ix, J. H., Kestenbaum, B., Lanske, B., Schiller, N. B., et al. (2014). Fibroblast growth factor–23 and cardiac structure and function. *J. Am. Heart Assoc.* 3:e000584.

Almahmoud, M. F., Soliman, E. Z., Bertoni, A. G., Kestenbaum, B., Katz, R., Lima, J. A. C., et al. (2018). Fibroblast growth factor-23 and heart failure with reduced versus preserved ejection fraction: MESA. *J. Am. Heart Assoc.* 7:e008334.

Alonso, A., Misialek, J. R., Eckfeldt, J. H., Selvin, E., Coresh, J., Chen, L. Y., et al. (2014). Circulating fibroblast growth factor-23 and the incidence of atrial fibrillation: the atherosclerosis risk in Communities study. *J. Am. Heart Assoc.* 3:e001082.

Alvarado, F. J., Chen, X., and Valdivia, H. H. (2017). Ablation of the cardiac ryanodine receptor phospho-site Ser2808 does not alter the adrenergic response or the progression to heart failure in mice. Elimination of the genetic background as critical variable. *J. Mol. Cell Cardiol.* 103, 40–47. doi: 10.1016/j.yjmcc.2017.01.001

Andersen, I. A., Huntley, B. K., Sandberg, S. S., Heublein, D. M., and Burnett, J. C. Jr. (2016). Elevation of circulating but not myocardial FGF23 in human acute decompensated heart failure. *Nephrol. Dial. Transplant.* 31, 767–772. doi: 10.1093/ndt/gfv398

Andrukhova, O., Slavic, S., Odörfer, K. I., and Erben, R. G. (2015). Experimental myocardial infarction upregulates circulating fibroblast growth factor-23. *J. Bone Mineral Res.* 30, 1831–1839. doi: 10.1002/jbmr.2527

Aono, Y., Hasegawa, H., Yamazaki, Y., Shimada, T., Fujita, T., Yamashita, T., et al. (2011). Anti-FGF-23 neutralizing antibodies ameliorate muscle weakness and decreased spontaneous movement of Hyp mice. *J. Bone Mineral Res.* 26, 803–810. doi: 10.1002/jbmr.275

Aono, Y., Yamazaki, Y., Yasutake, J., Kawata, T., Hasegawa, H., Urakawa, I., et al. (2009). Therapeutic effects of anti-FGF23 antibodies in hypophosphatemic rickets/osteomalacia. *J. Bone Mineral Res.* 24, 1879–1888. doi: 10.1359/jbmr.090509

Ärnlöv, J., Carlsson, A. C., Sundström, J., Ingelsson, E., Larsson, A., Lind, L., et al. (2013a). Higher fibroblast growth factor-23 increases the risk of all-cause and cardiovascular mortality in the community. *Kidney Int.* 83, 160–166. doi: 10.1038/ki.2012.327

Ärnlöv, J., Carlsson, A. C., Sundström, J., Ingelsson, E., Larsson, A., Lind, L., et al. (2013b). Serum FGF23 and risk of cardiovascular events in relation to mineral metabolism and cardiovascular pathology. *Clin. J. Am. Soc. Nephrol.* 8, 781–786. doi: 10.2215/cjn.09570912

Atherton, J. J., Bauersachs, J., Carerj, S., Ceconi, C., and Coca, A. (2016). Erol Ç, et al. 2016 ESC Guidelines for the diagnosis and treatment of acute and chronic heart failure. *Eur. J. Heart Fail.* 18, 891–975.

Bers, D. M. (2002). Cardiac excitation–contraction coupling. *Nature* 415, 198–205.

Bers, D. M. (2006). Altered cardiac myocyte Ca regulation in heart failure. *Physiology* 21, 380–387. doi: 10.1152/physiol.00019.2006

Bian, A., Xing, C., and Hu, M. C. (2014). Alpha Klotho and phosphate homeostasis. *J. Endocrinol. Invest.* 37, 1121–1126. doi: 10.1007/s40618-014-0158-6

Blau, J. E., and Collins, M. T. (2015). The PTH-Vitamin D-FGF23 axis. *Rev. Endocr. Metab. Disord.* 16, 165–174.

Böckmann, I., Lischka, J., Richter, B., Deppe, J., Rahn, A., Fischer, D.-C., et al. (2019). FGF23-mediated activation of local RAAS promotes cardiac hypertrophy and fibrosis. *Int. J.Mol. Sci.* 20:4634. doi: 10.3390/ijms20184634

Bortnick, A. E., Xu, S., Kim, R. S., Kestenbaum, B., Ix, J. H., Jenny, N. S., et al. (2019). Biomarkers of mineral metabolism and progression of aortic valve and mitral annular calcification: the multi-ethnic study of atherosclerosis. *Atherosclerosis* 285, 79–86. doi: 10.1016/j.atherosclerosis.2019.04.215

Bovo, E., Huke, S., Blatter, L. A., and Zima, A. V. (2017). The effect of PKA-mediated phosphorylation of ryanodine receptor on SR Ca2+ leak in ventricular myocytes. *J. Mol. Cell. Cardiol.* 104, 9–16. doi: 10.1016/j.yjmcc.2017.01.015

Brandenburg, V. M., Kleber, M. E., Vervloet, M. G., Tomaschitz, A., Pilz, S., Stojakovic, T., et al. (2014). Fibroblast growth factor 23 (FGF23) and mortality: the ludwigshafen risk and cardiovascular health study. *Atherosclerosis* 237, 53–59. doi: 10.1016/j.atherosclerosis.2014.08.037

Carpenter, T. O., Imel, E. A., Ruppe, M. D., Weber, T. J., Klausner, M. A., Wooddell, M. M., et al. (2014). Randomized trial of the anti-FGF23 antibody KRN23 in X-linked hypophosphatemia. *J. Clin. Invest.* 124, 1587–1597. doi: 10.1172/jci72829

Chan, S., Au, K., Francis, R. S., Mudge, D. W., Johnson, D. W., and Pillans, P. I. (2017). Phosphate binders in patients with chronic kidney disease. *Austr. Prescriber.* 40, 10–14.

Chen, J., Xu, S., Zhou, W., Wu, L., Wang, L., and Li, W. (2020). Exendin-4 reduces ventricular arrhythmia activity and calcium sparks-mediated sarcoplasmic reticulum Ca Leak in Rats with Heart failure. *Int. Heart J.* 61, 145–152. doi: 10.1536/ihj.19-327

Cheng, N., He, Y., Dang, A., Lv, N., Wang, X., and Li, H. (2020). Association between plasma fibroblast growth factor 23 and left ventricular mass index in patients with Takayasu arteritis. *Clin. Rheumatol.* 39, 1591–1599. doi: 10.1007/s10067-019-04895-6

Chonchol, M., Greene, T., Zhang, Y., Hoofnagle, A. N., and Cheung, A. K. (2016). Low vitamin D and high fibroblast growth factor 23 serum levels associate with infectious and cardiac deaths in the HEMO study. *J. Am. Soc.Nephrol.* 27, 227–237. doi: 10.1681/asn.2014101009

Chua, W., Purmah, Y., Cardoso, V. R., Gkoutos, G. V., Tull, S. P., Neculau, G., et al. (2019). Data-driven discovery and validation of circulating blood-based biomarkers associated with prevalent atrial fibrillation. *Eur. Heart J.* 40, 1268–1276. doi: 10.1093/eurheartj/ehy815

Curran, J., Brown, K. H., Santiago, D. J., Pogwizd, S., Bers, D. M., and Shannon, T. R. (2010). Spontaneous Ca waves in ventricular myocytes from failing hearts depend on Ca2+-calmodulin-dependent protein kinase II. *J. Mol. Cell. Cardiol.* 49, 25–32. doi: 10.1016/j.yjmcc.2010.03.013

di Giuseppe, R., Buijsse, B., Hirche, F., Wirth, J., Arregui, M., Westphal, S., et al. (2014). Plasma fibroblast growth factor 23, parathyroid hormone, 25-hydroxyvitamin D3, and risk of heart failure: a prospective, case-cohort study. *J. Clin. Endocrinol. Metab.* 99, 947–955. doi: 10.1210/jc.2013-2963

Di Giuseppe, R., Kühn, T., Hirche, F., Buijsse, B., Dierkes, J., Fritsche, A., et al. (2015). Plasma fibroblast growth factor 23 and risk of cardiovascular disease: results from the EPIC-Germany case-cohort study. *Eur. J. Epidemiol.* 30, 131–141. doi: 10.1007/s10654-014-9982-4

Donate-Correa, J., Martín-Núñez, E., Hernández-Carballo, C., Ferri, C., Tagua, V. G., Delgado-Molinos, A., et al. (2019). Fibroblast growth factor 23 expression in human calcified vascular tissues. *Aging* 11, 7899–7913. doi: 10.18632/aging.102297

Dong, Q., Li, S., Wang, W., Han, L., Xia, Z., Wu, Y., et al. (2019). FGF23 regulates atrial fibrosis in atrial fibrillation by mediating the STAT3 and SMAD3 pathways. *J. Cell Physiol.* 234, 19502–19510. doi: 10.1002/jcp.28548

Drew, D. A., Katz, R., Kritchevsky, S., Ix, J., Shlipak, M., Gutiérrez, O. M., et al. (2017). Association between soluble klotho and change in kidney function: the health aging and body composition study. *J. Am. Soc. Nephrol.* 28, 1859–1866. doi: 10.1681/asn.2016080828

Dzgoeva, F. U., Sopoev, M. Y., Bestaeva, T. L., Khamitsaeva, O. V., Ktsoeva, F. A., and Sageeva, R. O. (2016). [Role of fibroblast growth factor 23 in the development of cardiovascular diseases in patients with end-stage renal failure on programmed hemodialysis]. *Ter Arkh.* 88, 51–56. doi: 10.17116/terarkh2016881251-56

Eisner, D. A., Caldwell, J. L., Kistamás, K., and Trafford, A. W. (2017). Calcium and excitation-contraction coupling in the heart. *Circ. Res.* 121, 181–195. doi: 10.1016/b978-012436570-4/50007-8

Enbergs, A., Bürger, R., Reinecke, H., Borggrefe, M., Breithardt, G., and Kerber, S. (2000). Prevalence of coronary artery disease in a general population without suspicion of coronary artery disease: angiographic analysis of subjects aged 40 to 70 years referred for catheter ablation therapy. *Eur. Heart J.* 21, 45–52. doi: 10.1053/euhj.1999.1763

Eswarakumar, V., Lax, I., and Schlessinger, J. (2005). Cellular signaling by fibroblast growth factor receptors. *Cytokine Growth Factor Rev.* 16, 139–149.

Fabiato, A., and Fabiato, F. (1975). Contractions induced by a calcium-triggered release of calcium from the sarcoplasmic reticulum of single skinned cardiac cells. *J. Physiol.* 249, 469–495. doi: 10.1113/jphysiol.1975.sp011026

Fakhrpour, R., Hamid Tayebi Khosroshahi, H., Ebrahim, K., Ahmadizad, S., Abbasnejad, M., Mesgari Abbasi, M., et al. (2020). . Effect of sixteen weeks combined training on FGF-23, klotho, and fetuin-a levels in patients on maintenance hemodialysis. *Iran J. Kidney Dis.* 14, 212–218.

Farrell, B., and Breeze, A. L. (2018). Structure, activation and dysregulation of fibroblast growth factor receptor kinases: perspectives for clinical targeting. *Biochem. Soc. Trans.* 46, 1753–1770. doi: 10.1042/bst20180004

Faul, C. (2017). Cardiac actions of fibroblast growth factor 23. *Bone* 100, 69–79. doi: 10.1016/j.bone.2016.10.001

Faul, C., Amaral, A. P., Oskouei, B., Hu, M.-C., Sloan, A., Isakova, T., et al. (2011). FGF23 induces left ventricular hypertrophy. *J. Clin. Invest.* 121, 4393–4408.

Feng, S., Wang, H., Yang, J., Hu, X., Wang, W., Liu, H., et al. (2020). Kidney transplantation improves arterial stiffness in patients with end-stage renal disease. *Int. Urol. Nephrol.* 52, 877–884. doi: 10.1007/s11255-020-02376-3

Ferreira, J. P., Sharma, A., Mehta, C., Bakris, G., Rossignol, P., White, W. B., et al. (2020). Multi-proteomic approach to predict specific cardiovascular events in patients with diabetes and myocardial infarction: findings from the EXAMINE trial. *Clin. Res. Cardiol.* [Epub ahead of print].

Ferreira, J. P., Verdonschot, J., Collier, T., Wang, P., Pizard, A., Bär, C., et al. (2019). Proteomic Bioprofiles and mechanistic pathways of progression to heart failure. *Circ. Heart Fail.* 12:e005897.

Fox, A. C., Glassman, E., and Isom, O. W. (1979). Surgically remediable complications of myocardial infarction. *Prog. Cardiovasc. Dis.* 21, 461–484. doi: 10.1016/0033-0620(79)90026-4

Fozzard, H. A. (1991). *Excitation-Contraction Coupling in the Heart. Cellular and Molecular Mechanisms in Hypertension*. Berlin: Springer, 135–142.

Franklin, T. (1997). Therapeutic approaches to organ fibrosis. *Int. J. Biochem. Cell Biol.* 29, 79–89. doi: 10.1016/s1357-2725(96)00121-5

Fukumoto, S. (2016). FGF23-FGF receptor/Klotho pathway as a new drug target for disorders of bone and mineral metabolism. *Calcified Tissue Int.* 98, 334–340. doi: 10.1007/s00223-015-0029-y

Gardinier, J. D., Al-Omaishi, S., Morris, M. D., and Kohn, D. H. (2016). PTH signaling mediates perilacunar remodeling during exercise. *Matrix Biol.* 52-54, 162–175. doi: 10.1016/j.matbio.2016.02.010

Gluz, O., Kolberg-Liedtke, C., Prat, A., Christgen, M., Gebauer, D., Kates, R., et al. (2020). Efficacy of deescalated chemotherapy according to PAM50 subtypes, immune and proliferation genes in triple-negative early breast cancer: primary translational analysis of the WSG-ADAPT-TN trial. *Int. J. Cancer* 146, 262–271. doi: 10.1002/ijc.32488

Gonzalez-Parra, E., Gonzalez-Casaus, M. L., Galán, A., Martinez-Calero, A., Navas, V., Rodriguez, M., et al. (2011). Lanthanum carbonate reduces FGF23 in chronic kidney disease Stage 3 patients. *Nephrol. Dial. Transplant.* 26, 2567–2571. doi: 10.1093/ndt/gfr144

Grabner, A., Amaral, A. P., Schramm, K., Singh, S., Sloan, A., Yanucil, C., et al. (2015). Activation of cardiac fibroblast growth factor receptor 4 causes left ventricular hypertrophy. *Cell Metab.* 22, 1020–1032.

Grabner, A., Schramm, K., Silswal, N., Hendrix, M., Yanucil, C., Czaya, B., et al. (2017). FGF23/FGFR4-mediated left ventricular hypertrophy is reversible. *Sci. Rep.* 7, 1–12.

Gruson, D., Ferracin, B., Ahn, S. A., and Rousseau, M. F. (2017). Head to head comparison of intact and C-terminal fibroblast growth factor 23 in heart failure patients with reduced ejection fraction. *Int. J, Cardiol.* 248, 270–273. doi: 10.1016/j.ijcard.2017.06.129

Guo, Y., Xiao, L., Sun, L., and Liu, F. (2012). Wnt/β-catenin signaling: a promising new target for fibrosis diseases. *Physiol. Res.* 61, 337–346. doi: 10.33549/physiolres.932289

Gutiérrez, O. M., Anderson, C., Isakova, T., Scialla, J., Negrea, L., Anderson, A. H., et al. (2010). Low socioeconomic status associates with higher serum phosphate irrespective of race. *J. Am. Soc. Nephrol.* 21, 1953–1960. doi: 10.1681/asn.2010020221

Gutiérrez, O. M., Januzzi, J. L., Isakova, T., Laliberte, K., Smith, K., Collerone, G., et al. (2009). Fibroblast growth factor-23 and left ventricular hypertrophy in chronic kidney disease. *Circulation* 119, 2545–2552. doi: 10.1161/circulationaha.108.844506

Gutiérrez, O. M., Mannstadt, M., Isakova, T., Rauh-Hain, J. A., Tamez, H., Shah, A., et al. (2008). Fibroblast growth factor 23 and mortality among patients undergoing hemodialysis. *N. Engl. J. Med.* 359, 584–592.

Haffner, D., and Leifheit-Nestler, M. (2017). Extrarenal effects of FGF23. *Pediatr. Nephrol.* 32, 753–765. doi: 10.1007/s00467-016-3505-3

Han, X., Cai, C., Xiao, Z., and Quarles, L. D. (2020). FGF23 induced left ventricular hypertrophy mediated by FGFR4 signaling in the myocardium is attenuated by soluble Klotho in mice. *J. Mol. Cell. Cardiol.* 138, 66–74. doi: 10.1016/j.yjmcc.2019.11.149

Hao, H., Li, X., Li, Q., Lin, H., Chen, Z., Xie, J., et al. (2016). FGF23 promotes myocardial fibrosis in mice through activation of β-catenin. *Oncotarget* 7, 64649–64664. doi: 10.18632/oncotarget.11623

Hu, M. C., Shi, M., Cho, H. J., Adams-Huet, B., Paek, J., Hill, K., et al. (2015). Klotho and phosphate are modulators of pathologic uremic cardiac remodeling. *J. Am. Soc. Nephrol.* 26, 1290–1302. doi: 10.1681/asn.2014050465

Hu, M. C., Shi, M., Gillings, N., Flores, B., Takahashi, M., Kuro-o, M., et al. (2017). Recombinant α-Klotho may be prophylactic and therapeutic for acute to chronic kidney disease progression and uremic cardiomyopathy. *Kidney Int.* 91, 1104–1114. doi: 10.1016/j.kint.2016.10.034

Hu, M. C., Shiizaki, K., Kuro-o, M., and Moe, O. W. (2013). Fibroblast growth factor 23 and Klotho: physiology and pathophysiology of an endocrine network of mineral metabolism. *Annu. Revi. Physiol.* 75, 503–533. doi: 10.1146/annurev-physiol-030212-183727

Huo, Y. Y., Bai, X. J., Han, L. L., Wang, N., Han, W., and Sun, X. F. (2019). [Association of fibroblast growth factor 23 with age-related cardiac diastolic function subclinical state in a healthy Chinese population]. *Zhonghua Yi Xue Za Zhi.* 99, 1390–1396.

Imel, E. A., Zhang, X., Ruppe, M. D., Weber, T. J., Klausner, M. A., Ito, T., et al. (2015). Prolonged correction of serum phosphorus in adults with X-linked hypophosphatemia using monthly doses of KRN23. *J. Clin. Endocrinol. Metab.* 100, 2565–2573. doi: 10.1210/jc.2015-1551

Ix, J. H., Chonchol, M., Laughlin, G. A., Shlipak, M. G., and Whooley, M. A. (2011). Relation of sex and estrogen therapy to serum fibroblast growth factor 23, serum phosphorus, and urine phosphorus: the Heart and Soul Study. *Am. J. Kidney Dis.* 58, 737–745. doi: 10.1053/j.ajkd.2011.06.011

Ix, J. H., Katz, R., Kestenbaum, B. R., de Boer, I. H., Chonchol, M., Mukamal, K. J., et al. (2012). Fibroblast growth factor-23 and death, heart failure, and cardiovascular events in community-living individuals: CHS (Cardiovascular Health Study). *J. Am. Coll. Cardiol.* 60, 200–207. doi: 10.1016/j.jacc.2012.03.040

Jimbo, R., Kawakami-Mori, F., Mu, S., Hirohama, D., Majtan, B., Shimizu, Y., et al. (2014). Fibroblast growth factor 23 accelerates phosphate-induced vascular calcification in the absence of Klotho deficiency. *Kidney Int.* 85, 1103–1111. doi: 10.1038/ki.2013.332

Kanagala, P., Arnold, J. R., Khan, J. N., Singh, A., Gulsin, G. S., Eltayeb, M., et al. (2020). Fibroblast-growth-factor-23 in heart failure with preserved ejection fraction: relation to exercise capacity and outcomes. *ESC Heart Fail.* 7, 4089–4099. doi: 10.1002/ehf2.13020

Kao, Y. H., Chen, Y. C., Lin, Y. K., Shiu, R. J., Chao, T. F., Chen, S. A., et al. (2014). FGF-23 dysregulates calcium homeostasis and electrophysiological properties in HL-1 atrial cells. *Eur. J. Clin. Inves.* 44, 795–801. doi: 10.1111/eci.12296

Kestenbaum, B., Sachs, M. C., Hoofnagle, A. N., Siscovick, D. S., Ix, J. H., Robinson-Cohen, C., et al. (2014). Fibroblast growth factor-23 and cardiovascular disease in the general population: the multi-ethnic study of atherosclerosis. *Circ. Heart Fail.* 7, 409–417. doi: 10.1161/circheartfailure.113.000952

Ketteler, M., and Biggar, P. H. (2013). Use of phosphate binders in chronic kidney disease. *Curr. Opin. Nephrol. Hypertens.* 22, 413–420. doi: 10.1097/mnh.0b013e32836214d4

Koller, L., Kleber, M. E., Brandenburg, V. M., Goliasch, G., Richter, B., Sulzgruber, P., et al. (2015). Fibroblast growth factor 23 is an independent and specific predictor of mortality in patients with heart failure and reduced ejection fraction. *Circ. Heart Fail.* 8, 1059–1067. doi: 10.1161/circheartfailure.115.002341

Krajisnik, T., Björklund, P., Marsell, R., Ljunggren, O., Akerström, G., Jonsson, K. B., et al. (2007). Fibroblast growth factor-23 regulates parathyroid hormone and 1-hydroxylase expression in cultured bovine parathyroid cells. *J. Endocrinol.* 195, 125–131. doi: 10.1677/joe-07-0267

Kranias, E. G., and Hajjar, R. J. (2012). Modulation of cardiac contractility by the phopholamban/SERCA2a regulatome. *Circ. Res.* 110, 1646–1660. doi: 10.1161/circresaha.111.259754

Kuga, K., Kusakari, Y., Uesugi, K., Semba, K., Urashima, T., Akaike, T., et al. (2020). Fibrosis growth factor 23 is a promoting factor for cardiac fibrosis in the presence of transforming growth factor-β1. *PLoS One* 15:e0231905. doi: 10.1371/journal.pone.0231905

Kurosu, H., and Kuro-o, M. (2009). The Klotho gene family as a regulator of endocrine fibroblast growth factors. *Mol. Cell. Endocrinol.* 299, 72–78. doi: 10.1016/j.mce.2008.10.052

Leifheit-Nestler, M., Große Siemer, R., Flasbart, K., Richter, B., Kirchhoff, F., Ziegler, W. H., et al. (2016). Induction of cardiac FGF23/FGFR4 expression is associated with left ventricular hypertrophy in patients with chronic kidney disease. *Nephrol. Dial Transplant.* 31, 1088–1099. doi: 10.1093/ndt/gfv421

Leifheit-Nestler, M., and Haffner, D. (2018). Paracrine effects of FGF23 on the heart. *Front. Endocrinol.* 9:278. doi: 10.3389/fendo.2018.00278

Leifheit-Nestler, M., Kirchhoff, F., Nespor, J., Richter, B., Soetje, B., Klintschar, M., et al. (2018a). Fibroblast growth factor 23 is induced by an activated renin–angiotensin–aldosterone system in cardiac myocytes and promotes the pro-fibrotic crosstalk between cardiac myocytes and fibroblasts. *Nephrol. Dial. Transplant.* 33, 1722–1734. doi: 10.1093/ndt/gfy006

Leifheit-Nestler, M., Richter, B., Basaran, M., Nespor, J., Vogt, I., Alesutan, I., et al. (2018b). Impact of altered mineral metabolism on pathological cardiac remodeling in elevated fibroblast growth factor 23. *Front. Endocrinol.* 9:333. doi: 10.3389/fendo.2018.00333

Li, J., Kemp, B. A., Howell, N. L., Massey, J., Miñczuk, K., Huang, Q., et al. (2019). Metabolic changes in spontaneously hypertensive rat hearts precede cardiac dysfunction and left ventricular hypertrophy. *J. Am. Heart Assoc.* 8:e010926.

Liu, X., Niu, Y., Zhang, X., Zhang, Y., Yu, Y., Huang, J., et al. (2019). Recombinant α-klotho protein alleviated acute cardiorenal injury in a mouse model of lipopolysaccharide-induced septic cardiorenal syndrome type 5. *Anal. Cell. Pathol.* 2019:5853426.

Liu, Y. C., Tsai, J. P., Wang, L. H., Lee, M. C., and Hsu, B. G. (2020). Positive correlation of serum fibroblast growth factor 23 with peripheral arterial stiffness in kidney transplantation patients. *Clin. Chi.m Acta* 505, 9–14. doi: 10.1016/j.cca.2020.02.014

Lutsey, P. L., Alonso, A., Selvin, E., Pankow, J. S., Michos, E. D., Agarwal, S. K., et al. (2014). Fibroblast growth factor-23 and incident coronary heart disease, heart failure, and cardiovascular mortality: the atherosclerosis risk in communities study. *J. Am. Heart Assoc.* 3:e000936.

Mace, M. L., Gravesen, E., Hofman-Bang, J., Olgaard, K., and Lewin, E. (2015). Key role of the kidney in the regulation of fibroblast growth factor 23. *Kidney Int.* 88, 1304–1313. doi: 10.1038/ki.2015.231

Marthi, A., Donovan, K., Haynes, R., Wheeler, D. C., Baigent, C., Rooney, C. M., et al. (2018). Fibroblast growth factor-23 and risks of cardiovascular and noncardiovascular diseases: a meta-analysis. *J. Am. Soc. Nephrol.* 29, 2015–2027. doi: 10.1681/asn.2017121334

Masson, S., Agabiti, N., Vago, T., Miceli, M., Mayer, F., Letizia, T., et al. (2015). The fibroblast growth factor-23 and Vitamin D emerge as nontraditional risk factors and may affect cardiovascular risk. *J. Int. Med.* 277, 318–330. doi: 10.1111/joim.12232

Mathew, J. S., Sachs, M. C., Katz, R., Patton, K. K., Heckbert, S. R., Hoofnagle, A. N., et al. (2014). Fibroblast growth factor-23 and incident atrial fibrillation: the Multi-Ethnic Study of Atherosclerosis (MESA) and the Cardiovascular Health Study (CHS). *Circulation* 130, 298–307. doi: 10.1161/circulationaha.113.005499

Members, W. G., Roger, V. L., Go, A. S., Lloyd-Jones, D. M., Benjamin, E. J., Berry, J. D., et al. (2012). Heart disease and stroke statistics—2012 update: a report from the American Heart Association. *Circulation* 125, e2–e220.

Mirza, M. A., Larsson, A., Melhus, H., Lind, L., and Larsson, T. E. (2009). Serum intact FGF23 associate with left ventricular mass, hypertrophy and geometry in an elderly population. *Atherosclerosis* 207, 546–551. doi: 10.1016/j.atherosclerosis.2009.05.013

Moe, S. M., Chertow, G. M., Parfrey, P. S., Kubo, Y., Block, G. A., Correa-Rotter, R., et al. (2015). Cinacalcet, fibroblast growth factor-23, and cardiovascular disease in hemodialysis: the evaluation of cinacalcet HCl therapy to lower cardiovascular events (EVOLVE) trial. *Circulation* 132, 27–39. doi: 10.1161/circulationaha.114.013876

Molkentin, J. D. (2004). Calcineurin–NFAT signaling regulates the cardiac hypertrophic response in coordination with the MAPKs. *Cardiovasc. Res.* 63, 467–475. doi: 10.1016/j.cardiores.2004.01.021

Mosterd, A., Hoes, A., De Bruyne, M., Deckers, J., Linker, D., Hofman, A., et al. (1999). Prevalence of heart failure and left ventricular dysfunction in the general population. The Rotterdam Study. *Eur. Heart J.* 20, 447–455. doi: 10.1053/euhj.1998.1239

Navarro-García, J. A., Delgado, C., Fernández-Velasco, M., Val-Blasco, A., Rodríguez-Sánchez, E., Aceves-Ripoll, J., et al. (2019). Fibroblast growth factor-23 promotes rhythm alterations and contractile dysfunction in adult ventricular cardiomyocytes. *Nephrol. Dial. Transplant.* 34, 1864–1875. doi: 10.1093/ndt/gfy392

Navarro-García, J. A., Rueda, A., Romero-García, T., Aceves-Ripoll, J., Rodríguez-Sánchez, E., González-Lafuente, L., et al. (2020). Enhanced Klotho availability protects against cardiac dysfunction induced by uraemic cardiomyopathy by regulating Ca. *Br. J. Pharmacol.* 177, 4701–4719. doi: 10.1111/bph.15235

Navarro-García, J. A., Fernández-Velasco, M., Delgado, C., Delgado, J. F., Kuro-O, M., Ruilope, L. M., et al. (2018). PTH, vitamin D, and the FGF-23–klotho axis and heart: Going beyond the confines of nephrology. *Eur. J. Clin. Investigat.* 48:e12902. doi: 10.1111/eci.12902

Nayor, M., Larson, M. G., Wang, N., Santhanakrishnan, R., Lee, D. S., Tsao, C. W., et al. (2017). The association of chronic kidney disease and microalbuminuria with heart failure with preserved vs. reduced ejection fraction. *Eur. J. Heart Fail.* 19, 615–623. doi: 10.1002/ejhf.778

Panwar, B., Jenny, N. S., Howard, V. J., Wadley, V. G., Muntner, P., Kissela, B. M., et al. (2015). Fibroblast growth factor 23 and risk of incident stroke in community-living adults. *Stroke* 46, 322–328. doi: 10.1161/strokeaha.114.007489

Parker, B. D., Schurgers, L. J., Brandenburg, V. M., Christenson, R. H., Vermeer, C., Ketteler, M., et al. (2010). The associations of fibroblast growth factor 23 and uncarboxylated matrix Gla protein with mortality in coronary artery disease: the Heart and Soul Study. *Anna. Int. Med.* 152, 640–648. doi: 10.7326/0003-4819-152-10-201005180-00004

Patel, R. B., Ning, H., de Boer, I. H., Kestenbaum, B., Lima, J. A. C., Mehta, R., et al. (2020). Fibroblast growth factor 23 and long-term cardiac function: the multi-ethnic study of atherosclerosis. *Circ. Cardiovasc. Imaging* 13:e011925.

Pescatore, L. A., Gamarra, L. F., and Liberman, M. (2019). Multifaceted mechanisms of vascular calcification in aging. *Arterioscler. Thromb. Vasc. Biol.* 39, 1307–1316. doi: 10.1161/atvbaha.118.311576

Poelzl, G., Trenkler, C., Kliebhan, J., Wuertinger, P., Seger, C., Kaser, S., et al. (2014). FGF 23 is associated with disease severity and prognosis in chronic heart failure. *Eur. J. Clin. Invest.* 44, 1150–1158.

Pool, L. R., Kershaw, K. N., Gordon-Larsen, P., Gutiérrez, O. M., Reis, J. P., Isakova, T., et al. (2020). Racial differences in the associations between food insecurity and fibroblast growth factor 23 in the coronary artery risk development in young adults study. *J. Ren. Nutr.* 30, 509–517. doi: 10.1053/j.jrn.2020.01.020

Reindl, M., Reinstadler, S. J., Feistritzer, H.-J., Mueller, L., Koch, C., Mayr, A., et al. (2017). Fibroblast growth factor 23 as novel biomarker for early risk stratification after ST-elevation myocardial infarction. *Heart* 103, 856–862. doi: 10.1136/heartjnl-2016-310520

Robinson-Cohen, C., Shlipak, M., Sarnak, M., Katz, R., Peralta, C., Young, B., et al. (2020). Impact of race on the association of mineral metabolism with heart failure: the Multi-Ethnic Study of Atherosclerosis. *J. Clin. Endocrinol. Metab.* 105, e1144–e1151.

Rodelo-Haad, C., Rodríguez-Ortiz, M. E., Martin-Malo, A., Pendon-Ruiz de Mier , M. V., Agüera, M. L., Muñoz-Castañeda, J. R., et al. (2018). Phosphate control in reducing FGF23 levels in hemodialysis patients. *PLoS One* 13:e0201537. doi: 10.1371/journal.pone.0201537

Rosa, T. S., Neves, R. V. P., Deus, L. A., Sousa, C. V., da Silva Aguiar, S., de Souza , M. K., et al. (2020). Sprint and endurance training in relation to redox balance, inflammatory status and biomarkers of aging in master athletes. *Nitric Oxide* 102, 42–51. doi: 10.1016/j.niox.2020.05.004

Roy, C., Lejeune, S., Slimani, A., de Meester, C., Ahn As , S. A., Rousseau, M. F., et al. (2020). Fibroblast growth factor 23: a biomarker of fibrosis and prognosis in heart failure with preserved ejection fraction. *ESC Heart Fail.* 7, 2494–2507. doi: 10.1002/ehf2.12816

Ruilope, L. M. (2012). Current challenges in the clinical management of hypertension. *Nat. Rev. Cardiol.* 9, 267–275. doi: 10.1038/nrcardio.2011.157

Ruiz-Hurtado, G., Li, L., Fernández-Velasco, M., Rueda, A., Lefebvre, F., Wang, Y., et al. (2015). Reconciling depressed Ca2+ sparks occurrence with enhanced RyR2 activity in failing mice cardiomyocytes. *J. Gen. Physiol.* 146, 295–306. doi: 10.1085/jgp.201511366

Schumacher, D., Alampour-Rajabi, S., Ponomariov, V., Curaj, A., Wu, Z., Staudt, M., et al. (2019). Cardiac FGF23: New insights into the role and function of FGF23 after acute myocardial infarction. *Cardiovasc. Pathol.* 40, 47–54. doi: 10.1016/j.carpath.2019.02.001

Seiler, S., Cremers, B., Rebling, N. M., Hornof, F., Jeken, J., Kersting, S., et al. (2011). The phosphatonin fibroblast growth factor 23 links calcium–phosphate metabolism with left-ventricular dysfunction and atrial fibrillation. *Eur. Heart J.* 32, 2688–2696. doi: 10.1093/eurheartj/ehr215

Shalhoub, V., Shatzen, E. M., Ward, S. C., Davis, J., Stevens, J., Bi, V., et al. (2012). FGF23 neutralization improves chronic kidney disease–associated hyperparathyroidism yet increases mortality. *J. Clin. Invest.* 122, 2543–2553. doi: 10.1172/jci61405

Sharma, S., Katz, R., Bullen, A. L., Chaves, P. H. M., de Leeuw, P. W., Kroon, A. A., et al. (2020). Intact and C-Terminal FGF23 assays-do kidney function, inflammation, and low iron influence relationships with outcomes? *J. Clin. Endocrinol. Metab.* 105, e4875–e4885.

Shibata, K., Fujita, S.-I., Morita, H., Okamoto, Y., Sohmiya, K., Hoshiga, M., et al. (2013). Association between circulating fibroblast growth factor 23, α-Klotho, and the left ventricular ejection fraction and left ventricular mass in cardiology inpatients. *PLoS One* 8:e73184. doi: 10.1371/journal.pone.0073184

Silva, A. P., Gundlach, K., Büchel, J., Jerónimo, T., Fragoso, A., Silva, C., et al. (2015). Low magnesium levels and FGF-23 dysregulation predict mitral valve calcification as well as intima media thickness in predialysis diabetic patients. *Int. J. Endocrinol.* 2015:308190.

Silva, A. P., Mendes, F., Carias, E., Gonçalves, R. B., Fragoso, A., Dias, C., et al. (2019). Plasmatic Klotho and FGF23 Levels as Biomarkers of CKD-Associated Cardiac Disease in Type 2 Diabetic Patients. *Int. J. Mol. Sci.* 20:1536. doi: 10.3390/ijms20071536

Slavic, S., Ford, K., Modert, M., Becirovic, A., Handschuh, S., Baierl, A., et al. (2017). Genetic ablation of Fgf23 or klotho does not modulate experimental heart hypertrophy induced by pressure overload. *Sci. Rep.* 7, 1–12.

Song, T., Fu, Y., Wang, Y., Li, W., Zhao, J., Wang, X., et al. (2021). FGF-23 correlates with endocrine and metabolism dysregulation, worse cardiac and renal function, inflammation level, stenosis degree, and independently predicts in-stent restenosis risk in coronary heart disease patients underwent drug-eluting-stent PCI. *BMC Cardiovasc. Disord.* 21:24. doi: 10.1186/s12872-020-01839-w

Souma, N., Isakova, T., Lipiszko, D., Sacco, R. L., Elkind, M. S., DeRosa, J. T., et al. (2016). Fibroblast growth factor 23 and cause-specific mortality in the general population: the Northern Manhattan Study. *J. Clin. Endocrinol. Metab.* 101, 3779–3786. doi: 10.1210/jc.2016-2215

Speer, T., Groesdonk, H. V., Zapf, B., Buescher, V., Beyse, M., Duerr, L., et al. (2015). A single preoperative FGF23 measurement is a strong predictor of outcome in patients undergoing elective cardiac surgery: a prospective observational study. *Crit. Care* 19:190.

Strain, W. D., and Paldanius, P. (2018). Diabetes, cardiovascular disease and the microcirculation. *Cardiovasc. Diabetol.* 17:57.

Tagliabracci, V. S., Engel, J. L., Wiley, S. E., Xiao, J., Gonzalez, D. J., Appaiah, H. N., et al. (2014). Dynamic regulation of FGF23 by Fam20C phosphorylation, GalNAc-T3 glycosylation, and furin proteolysis. *Proc. Natl. Acad. Sci. U.S.A.* 111, 5520–5525. doi: 10.1073/pnas.1402218111

Takahashi, H., Ozeki, M., Fujisaka, T., Morita, H., Fujita, S. I., Takeda, Y., et al. (2018). Changes in serum fibroblast growth factor 23 in patients with acute myocardial infarction. *Circ. J.* 82, 767–774. doi: 10.1253/circj.cj-17-0826

Taylor, A., Yanucil, C., Musgrove, J., Shi, M., Ide, S., Souma, T., et al. (2019). FGFR4 does not contribute to progression of chronic kidney disease. *Sci. Rep.* 9, 1–6.

Taylor, E. N., Rimm, E. B., Stampfer, M. J., and Curhan, G. C. (2011). Plasma fibroblast growth factor 23, parathyroid hormone, phosphorus, and risk of coronary heart disease. *Am. Heart J.* 161, 956–962. doi: 10.1016/j.ahj.2011.02.012

Ter Maaten, J. M., Voors, A. A., Damman, K., van der Meer, P., Anker, S. D., Cleland, J. G., et al. (2018). Fibroblast growth factor 23 is related to profiles indicating volume overload, poor therapy optimization and prognosis in patients with new-onset and worsening heart failure. *Int. J. Cardiol.* 253, 84–90. doi: 10.1016/j.ijcard.2017.10.010

Touchberry, C. D., Green, T. M., Tchikrizov, V., Mannix, J. E., Mao, T. F., Carney, B. W., et al. (2013). FGF23 is a novel regulator of intracellular calcium and cardiac contractility in addition to cardiac hypertrophy. *Am. J. Physiol. Endocrinol. Metab.* 304, E863–E873.

Urakawa, I., Yamazaki, Y., Shimada, T., Iijima, K., Hasegawa, H., Okawa, K., et al. (2006). Klotho converts canonical FGF receptor into a specific receptor for FGF23. *Nature* 444, 770–774. doi: 10.1038/nature05315

Vainikka, S., Joukov, V., Wennström, S., Bergman, M., Pelicci, P. G., and Alitalo, K. (1994). Signal transduction by fibroblast growth factor receptor-4 (FGFR-4). Comparison with FGFR-1. *J. Biol. Chem.* 269, 18320–18326. doi: 10.1016/s0021-9258(17)32309-8

van de Wouw, J., Broekhuizen, M., Sorop, O., Joles, J. A., Verhaar, M. C., Duncker, D. J., et al. (2019). Chronic kidney disease as a risk factor for heart failure with preserved ejection fraction: a focus on microcirculatory factors and therapeutic targets. *Front. Physiol.* 10:1108. doi: 10.3389/fphys.2019.01108

von Jeinsen, B., Sopova, K., Palapies, L., Leistner, D. M., Fichtlscherer, S., Seeger, F. H., et al. (2019). Bone marrow and plasma FGF-23 in heart failure patients: novel insights into the heart–bone axis. *ESC Heart Fail.* 6, 536–544. doi: 10.1002/ehf2.12416

Weber, J. R. (1991). Left ventricular hypertrophy: its prevalence, etiology, and significance. *Clin. Cardiol.* 14(Suppl. 3), 13–17. doi: 10.1002/clc.4960140704

White, K. E., Evans, W. E., O'Riordan, J. L., Speer, M. C., Econs, M. J., Lorenz-Depiereux, B., et al. (2000). Autosomal dominant hypophosphataemic rickets is associated with mutations in FGF23. *Nat. Genet.* 26, 345–348. doi: 10.1038/81664

Wohlfahrt, P., Melenovsky, V., Kotrc, M., Benes, J., Jabor, A., Franekova, J., et al. (2015). Association of fibroblast growth factor-23 levels and angiotensin-converting enzyme inhibition in chronic systolic heart failure. *JACC: Heart Fail.* 3, 829–839. doi: 10.1016/j.jchf.2015.05.012

Wolf, M. (2010). Forging forward with 10 burning questions on FGF23 in kidney disease. *J. Am. Soc. Nephrol.* 21, 1427–1435. doi: 10.1681/asn.2009121293

Wolf, M. (2012). Update on fibroblast growth factor 23 in chronic kidney disease. *Kidney Int.* 82, 737–747. doi: 10.1038/ki.2012.176

Wright, C. B., Dong, C., Stark, M., Silverberg, S., Rundek, T., Elkind, M. S., et al. (2014). Plasma FGF23 and the risk of stroke: the Northern Manhattan Study (NOMAS). *Neurology* 82, 1700–1706. doi: 10.1212/wnl.0000000000000410

Wright, J. D., An, S. W., Xie, J., Lim, C., and Huang, C. L. (2019). Soluble klotho regulates TRPC6 calcium signaling via lipid rafts, independent of the FGFR-FGF23 pathway. *FASEB J.* 33, 9182–9193. doi: 10.1096/fj.201900321r

Xie, J., Cha, S.-K., An, S.-W., Kuro-o, M., Birnbaumer, L., and Huang, C.-L. (2012). Cardioprotection by Klotho through downregulation of TRPC6 channels in the mouse heart. *Nat. Commun.* 3, 1–11.

Xin, Z., Song, X., Jiang, B., Gongsun, X., Song, L., Qin, Q., et al. (2018). Blocking FGFR4 exerts distinct anti-tumorigenic effects in esophageal squamous cell carcinoma. *Thorac Cancer* 9, 1687–1698. doi: 10.1111/1759-7714.12883

Yamazaki, Y., Tamada, T., Kasai, N., Urakawa, I., Aono, Y., Hasegawa, H., et al. (2008). Anti-FGF23 neutralizing antibodies show the physiological role and structural features of FGF23. *J. Bone Mineral Res.* 23, 1509–1518. doi: 10.1359/jbmr.080417

Yuen, S. N., Kramer, H., Luke, A., Bovet, P., Plange-Rhule, J., Forrester, T., et al. (2016). Fibroblast growth factor-23 (FGF-23) levels differ across populations by degree of industrialization. *J. Clin. Endocrinol. Metab.* 101, 2246–2253. doi: 10.1210/jc.2015-3558

Zaheer, S., de Boer, I. H., Allison, M., Brown, J. M., Psaty, B. M., Robinson-Cohen, C., et al. (2017). Fibroblast growth factor 23, mineral metabolism, and adiposity in normal kidney function. *J. Clin. Endocrinol. Metab.* 102, 1387–1395. doi: 10.1210/jc.2016-3563

Zhang, L., and Liu, T. (2018). Clinical implication of alterations in serum Klotho levels in patients with type 2 diabetes mellitus and its associated complications. *J. Diabetes Complications* 32, 922–930. doi: 10.1016/j.jdiacomp.2018.06.002

Ziaeian, B., and Fonarow, G. C. (2016). Epidemiology and aetiology of heart failure. *Nat. Rev. Cardiol.* 13, 368–378.

Zoccali, C., Yilmaz, M. I., and Mallamaci, F. (2013). FGF23: a mature renal and cardiovascular risk factor? *Blood Purificat.* 36, 52–57. doi: 10.1159/000351001

Conflict of Interest: The authors declare that the research was conducted in the absence of any commercial or financial relationships that could be construed as a potential conflict of interest.

frontiers in Cardiovascular Medicine

ORIGINAL RESEARCH
published: 15 April 2021
doi: 10.3389/fcvm.2021.638992

The Prevalence, Distribution, and Extent of Subclinical Atherosclerosis and Its Relation With Serum Uric Acid in Hypertension Population

Fei Liu[1†], Simei Hui[1†], Tesfaldet H. Hidru[1], Yinong Jiang[1], Ying Zhang[1], Yan Lu[1], Haichen Lv[1], Sharen Lee[2], Yunlong Xia[1] and Xiaolei Yang[1*]*

[1] Department of Cardiology, First Affiliated Hospital of Dalian Medical University, Dalian, China, [2] Faculty of Medicine, Chinese University of Hong Kong, Hong Kong, China

OPEN ACCESS

Edited by:
Soo-Kyoung Choi,
Yonsei University College of Medicine,
South Korea

Reviewed by:
Luigi Petramala,
Sapienza University of Rome, Italy
Maddalena Illario,
University of Naples Federico II, Italy

***Correspondence:**
Xiaolei Yang
yangxl1012@yeah.net
Yunlong Xia
yunlong_xia@126.com

[†] These authors have contributed equally to this work and share first authorship

Specialty section:
This article was submitted to Hypertension, a section of the journal Frontiers in Cardiovascular Medicine

Received: 08 December 2020
Accepted: 25 March 2021
Published: 15 April 2021

Citation:
Liu F, Hui S, Hidru TH, Jiang Y, Zhang Y, Lu Y, Lv H, Lee S, Xia Y and Yang X (2021) The Prevalence, Distribution, and Extent of Subclinical Atherosclerosis and Its Relation With Serum Uric Acid in Hypertension Population. Front. Cardiovasc. Med. 8:638992. doi: 10.3389/fcvm.2021.638992

Background: Data are limited on the prevalence, distribution, and extent of subclinical atherosclerosis (SCA) in populations with primary hypertension and an in-depth evaluation is required to explore the impact of elevated serum uric acid (SUA) levels on the systemic extent of SCA.

Methods: A total of 1,534 individuals with blood pressure-controlled primary hypertension registered from January 1, 2015 to May 31, 2018 were included. The systemic extent and risk factors of SCA in the carotid, coronary, thoracic, and renal territories were investigated by Doppler ultrasound and computed tomography.

Results: SCA was present in 85.9% of patients. The proportion of focal, intermediate and generalized SCA was 17.9, 21.3, and 46.6%. Plaques were most common in the thoracic aorta (74%), followed by the coronary (55.3%), carotid (51.6%), and renal (45.8%) arteries, respectively. Participants were stratified into quartiles based on gender-specific SUA levels. Compared with patients in the first quartile, the Odds Ratio (OR) [95% confidence interval] for SCA in the second, third and fourth quartile were 1.647 (1.011–2.680), 3.013 (1.770–5.124), and 5.081 (3.203–10.496), respectively. Patients with elevated SUA levels at high 10-year Framingham risk had a higher likelihood of a more severe risk of SCA (95.8%). However, extensive SCA was also present in a substantial number of low 10-year-Framingham risk patients at the higher quartiles of SUA (53.8%).

Conclusions: SCA was highly prevalent in the hypertension population and the thoracic aorta was the most frequently affected vascular site. Elevated SUA concentration was significantly associated with the prevalence and severity of SCA regardless of territories.

Keywords: hypertension, subclinical atherosclerosis risk factor, uric acid, cardiovascular disease, risk factor

INTRODUCTION

Subclinical atherosclerosis (SCA) refers to the existing arteriosclerosis with no significant clinical symptoms of severe atherosclerotic stenosis, or SCA in arteries [coronary artery, cerebral artery, renal artery, and peripheral artery (1)]. Published documents revealed that SCA is prevalent in people with traditional cardiovascular risk factors such as high blood pressure, dyslipidemia,

obesity, diabetes, and smoking (2). However, currently there is only one published report to our knowledge that detailed the prevalence, vascular distribution, and multi-territorial extent of SCA among the general population (3). Hence, data is lacking among patients with hypertension.

Recent studies have found that high concentrations of serum uric acid (SUA) is associated with kidney, cardiovascular, cerebrovascular, and peripheral vascular target organ damages (4). Also, previous studies reported that high concentrations of SUA independently is associated with cardiovascular risk and events in both the general population and in patients with hypertension (5–7). However, other studies on uric acid and target organ damage reported no significant association between high levels of SUA and cardiovascular events (8, 9). Consequently, the association of high levels of SUA and SCA remains controversial and further studies are required.

The natural progress of atherosclerosis comprises a protracted subclinical phase, with the disease often diagnosed following a cardiovascular event or lately at an advanced stage (10). It is well-established that cardiovascular events are associated with poor health outcomes. Also, many deaths secondary to coronary artery disease occurs suddenly in patients with hypertension (11). Tangible scientific evidence on risk and identification of SCA is needed to improve the prevention and treatment of atherosclerotic diseases (12). In extension, it is of great significance to reduce the risk of cardiovascular events by strengthening the identification of patients with early atherosclerotic disease through non-invasive or minimally invasive methods. In this context, we sought to assess the prevalence, vascular distribution, and multi-territorial extent of SCA, and explore the relationship between SUA levels and SCA in hypertensive patients.

METHODS

Study Sample

We examined hospitalized patients with hypertension, aged 18–80 years, between January 1, 2015 and May 31, 2018 at the First Affiliated Hospital of Dalian Medical University. Those with secondary hypertension, uncontrolled blood pressure, prior cardiovascular disease including coronary disease, stroke/transient ischemic attack, and those patients missing key clinical covariates were excluded. A total of 1,534 patients were included in the present study. A brief description of the study participants is given in **Figure 1**. The study was conducted under the guidelines of the Helsinki declaration. All protocols described here were performed under the approved guidelines. The study was approved by the First Affiliated Hospital of the Dalian Medical University Institutional Review Board, and the requirement for informed consent was waived.

Definition of Explanatory Variables

Clinical characteristics, including age, sex, and major risk factors of hypertension (diabetes mellitus, arterial hypertension, dyslipidemia, smoking, family history of cardiovascular disease) were ascertained from electronic health records. Blood samples, regardless of fasting status, were collected, and all the biochemical parameters (glucose, triglyceride, low-density lipoprotein, total cholesterol, high-density lipoprotein, and creatinine levels) were performed at the First Affiliated Hospital of Dalian Medical University using the standard protocols. SUA levels were determined using the Uricase-Peroxidase method with an autoanalyzer (BECKMAN COULTER AU680 Chemistry Analyzer, USA). Diabetes mellitus was defined as fasting plasma glucose $\geq$126 mg/dL or treatment with insulin or oral hypoglycemic medication (13). Arterial hypertension was defined as systolic blood pressure $\geq$140 mmHg, diastolic blood pressure $\geq$90 mmHg, or current use of blood pressure-lowering medication (14). Dyslipidemia was defined as total cholesterol $\geq$240 mg/dL, low-density lipoprotein cholesterol $\geq$160 mg/dL, high density lipoprotein cholesterol $<$40 mg/dL, or use of lipid-lowering drugs (15, 16). Patients with a current history of smoking or reported a lifetime consumption of $>$100 cigarettes were defined as smokers (17, 18). The estimated glomerular filtration rate (eGFR) was calculated using the Modification of Diet in Renal Disease equation (19). Cardiovascular risk was evaluated by the 10-year risk of coronary heart disease of the Framingham Heart Study (FHS) (18, 20). FHS scores were classified as low ($<$10%), moderate (10–20%), or high ($>$20%) risk.

Identification of SCA

Patients were examined by cervical vascular color ultrasonic inspection, coronary computer tomography (CT), renal artery CT, and thoracic aorta CT to evaluate SCA.

Vascular Ultrasound Imaging

We examined the bilateral carotid artery by using Color Doppler Ultrasonic diagnostic instrument (Philips iU-22 Ultrasound System, Philips Medical Systems, Bothell, WA, USA). Carotid intima-media thickness (IMT) was quantified by carotid ultrasound (21, 22). The presence of a plaque can be identified by an IMT $\geq$1.5 mm, or by a focal increase in thickness by more than 0.5 mm or 50% of the surrounding carotid IMT-value (23). The degree of carotid stenosis was graded according to the internal carotid artery peak systolic velocity (ICA PSV): (i) Normal: ICA PSV is $<$125 cm/s and no plaque or intimal thickening is visible; (ii) Minimal: 50% stenosis when ICA PSV is $<$125 cm/s and plaque or intimal thickening is visible; (iii) Mild: 50–69% stenosis when ICA PSV is 125–230 cm/s and plaque is visible; (iv) Moderate: 70% stenosis to near occlusion when ICA PSV is $>$230 cm/s and visible plaque and lumen narrowing are seen; (v) Severe: near occlusion when there is a markedly narrowed lumen at color Doppler US; and (vi) Occluded: total occlusion when there is no detectable patent lumen at the gray-scale US and no flow at spectral, power, and color Doppler US (24).

Computed Tomography Angiography

We evaluated the coronary arteries, thoracic aorta, and renal arteries using dual-source cardiovascular CT (SOMATOM Definition AS, Siemens Healthineers, Forchheim, Germany). The degree of stenosis was graded according to the inner diameter of the lumen: Normal: absence of plaque and no luminal stenosis; Minimal: plaque with $<$25% stenosis; Mild: 25–49%

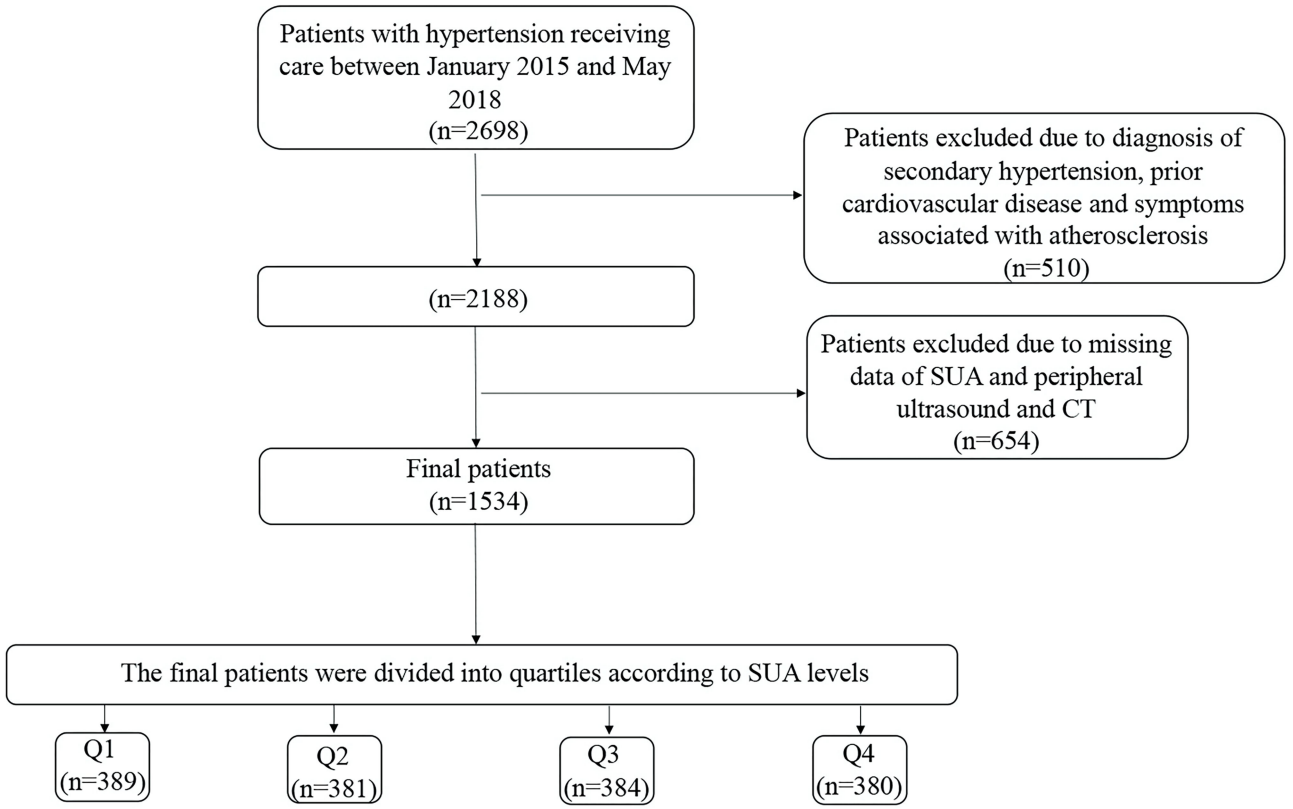

FIGURE 1 | Flow Chart of the participants. The quartiles of SUA concentration were calculated separately for men and women. SUA, serum uric acid; CT, Computed tomography.

stenosis; Moderate: 50–69% stenosis; Severe: 70–99% stenosis; Occluded (25).

Definition of Subclinical Atherosclerosis and Multi-Territorial Extent of Subclinical Atherosclerosis

SCA was defined as the availability of atherosclerotic plaques in the coronary, carotid, thoracic, and renal territories. The multi-territorial extent of SCA was defined according to the number of vascular sites affected. Patients were classified as disease-free (0 vascular sites affected), focal (1 site), intermediate (2 sites), or generalized (≥3 sites) SCA.

Statistical Analysis

Data processing, management and statistical analysis were performed using SPSS (version 23). The population studied was stratified into quartiles based on gender-specific levels of SUA. The respective cut-off of SUA values for Q1, Q2, Q3, and Q4 were ≤356.00, 356.01–412.00, 412.01–467.00, and ≥467.00 μmol/L in men. The cut-off of SUA values for Q1, Q2, Q3, and Q4 in women were ≤320.00, 320.01–369.00, 369.01–433.00, and ≥433.01 μmol/L, respectively. Continuous and categorical variables were summarized using mean ± SD and percentiles, respectively. Analysis of variance was employed to compare three groups or more. The χ^2-test was used to compare categorical variables. The likelihood of SCA associated with elevated SUA levels was calculated using a logistic regression model; SUA values were entered in the models as quartiles (with the first sex-specific quartile as the baseline reference) to assess the odds ratio (OR) and 95 percent confidence interval (95% CI). The logistic regression analysis was carried out in three models. Model 1 adjusted for age and sex. Model 2 adjusted for age, sex, eGFR, smoking, alcohol and diuretic use. Model 3 adjusted for age, sex, eGFR, smoking, alcohol intake, use of antihypertensive drugs, use of statins, blood pressure, diabetes and dyslipidemia. We further calculated OR and corresponding 95% CIs for the occurrence of SCA associated with 1 SD increase in SUA for patients who were classified according to FHS-10 year risk. All statistical analyses were two-sided, and a *P*-value of <0.05 was considered statistically significant.

RESULTS

Baseline Characteristics

This study included 1,534 patients (775 men and 759 women). The baseline characteristics of participants by SUA quartile (Q) are presented in **Table 1**. The values of the mean SUA, TG, creatinine and percentage of dyslipidemia were significantly higher in Q4 than in Q1–Q3. The values of the mean eGFR

TABLE 1 | Baseline characteristics of patients by serum uric acid (SUA) quartiles.

Variables	Total	Quartiles of serum uric acid (n = 1,534)				*P*-value
		Q1	Q2	Q3	Q4	
Number of subjects	1,534	389	381	384	380	
SUA, μmol/L	397.70 ± 87.85	296.37 ± 38.86	366.34 ± 24.65	418.93 ± 26.26	511.40 ± 58.49	<0.001
Male, *N* (%)	775 (50.5)	196 (50.4)	193 (50.7)	193 (50.3)	193 (50.8)	0.999
Age, years	60.11 ± 13.33	60.70 ± 13.98	60.02 ± 13.36	60.63 ± 13.453	59.09 ± 12.47	0.307
Smoking, *N* (%)	440 (28.7)	108 (27.8)	98 (25.7)	117 (30.5)	117 (30.8)	0.518
Alcohol use, *N* (%)	362 (23.6)	87 (22.4)	82 (21.5)	95 (24.7)	98 (25.8)	0.798
SBP, mm Hg	130.45 ± 9.31	130.40 ± 9.45	129.74 ± 9.10	130.29 ± 9.69	131.33 ± 8.93	0.125
DBP, mm Hg	80.79 ± 9.11	80.02 ± 9.35	80.71 ± 8.96	81.51 ± 9.27	80.92 ± 8.79	0.153
Diabetes, *N* (%)	424 (27.6)	92 (23.7)	109 (28.6)	108 (28.1)	115 (30.3)	0.201
Dyslipidemia, *N* (%)	1,219 (79.7)	296 (76.7)	290 (76.3)	321 (83.6)	312 (82.1)	0.020
Statins use, *N* (%)	1,077 (70.2)	251 (64.5)	267 (70.1)	290 (75.5)	269 (70.8)	0.010
TC, mg/dL	193.17 ± 40.57	193.25 ± 40.64	193.47 ± 39.70	193.17 ± 41.66	192.80 ± 40.39	0.997
TG, mg/dL	163.20 ± 131.46	151.90 ± 146.58	146.6 ± 92.16	161.29 ± 113.66	193.28 ± 158.12	<0.001
HDL-c, mg/dL	47.65 ± 10.98	49.451 ± 11.43	47.806 ± 10.722	47.26 ± 10.89	46.04 ± 10.63	<0.001
LDL-c, mg/dL	107.88 ± 27.30	107.07 ± 26.94	108.59 ± 27.16	108.38 ± 27.80	107.49 ± 27.36	0.849
Creatinine, μmol//L	71.09 ± 41.59	66.69 ± 38.79	67.10 ± 18.35	71.87 ± 19.28	79.09 ± 41.59	<0.001
eGFR (mL/min/1.73 m^2)	90.36 ± 21.00	94.87 ± 21.43	93.11 ± 18.91	88.51 ± 20.00	84.86 ± 22.07	<0.001
Diuretics use, *N* (%)	474 (30.9)	101 (26.0)	111 (29.1)	128 (33.3)	134 (35.3)	0.024
CCB use, *N* (%)	1,402 (91.4)	354 (91.0)	353 (92.7)	346 (90.1)	349 (91.8)	0.626
ACEI/ARB use, *N* (%)	501 (32.7)	116 (29.8)	101 (26.5)	138 (35.9)	146 (38.4)	0.001
β-blockers use, *N* (%)	758 (49.4)	174 (44.7)	183 (48.0)	192 (50.0)	209 (55.0)	0.037

Data were presented as mean ± SD for continuous variable and number (percentage) for category variables. The quartiles of SUA concentration were calculated separately for men and women. The cut-off of SUA levels in men was ≤356.00, 356.01–412.00, 412.01–467.00 and ≥467.01 μmol/L. The cut-off of SUA levels in women was ≤320.00, 320.01–369.00, 369.01–433.00 and ≥433.01 μmol/L. SUA, serum uric acid; SBP, systolic blood pressure; DBP, diastolic blood pressure; TC total cholesterol; TG, triglyceride; HDL-C, high-density lipoprotein cholesterol; LDL-C, low-density lipoprotein cholesterol; eGFR, estimated glomerular filtration rate; CCB, Calcium channel blocker; ACEI, angiotensin-converting enzyme inhibitor; ARB, angiotensin II receptor blocker.

levels were significantly higher in Q1 than in Q2–Q4. The proportion of participants, who were in diuretic and statin use was higher in the highest quartile (Q4) compared with lower quartiles.

The Prevalence, Vascular Distribution, and Extent of Subclinical Atherosclerosis Across the Serum Uric Acid Levels

According to **Table 2**, plaques were discovered by ultrasound and CT angiography in 85.9% of the patients (51.6% in the carotids, 55.3% in the coronary, 74% in the thoracic aorta, and 44% in the renal arteries). Patients with asymptomatic thoracic aorta atherosclerosis accounted for the highest proportion (74%). Classification of participants according to the extent of atherosclerosis showed focal SCA in 17.9%, intermediate SCA in 21.3%, and generalized SCA in 46.6%. Among those participants having generalized SCA, the thoracic aorta was the most likely territory to be affected. With an increase of uric acid levels, the proportion of patients with SCA were increased. The prevalence of SCA increased from 78.9 to 92.1% across Q1–Q4 of SUA levels. Regardless of the territory of the artery, the degree of SCA was increased with an increase in uric acid concentration ($P < 0.05$).

Elevated Serum Uric Acid Levels Increase the Risk of Subclinical Atherosclerosis

We used the logistic regression model to analyze the risk of SCA. The OR for SCA was analyzed in each SUA quartile, with the first quartile serving as the reference group. The association between SUA and the prevalence of SCA is presented in **Table 3** and **Supplementary Table 1**. Compared with patients in the first quartile, the ORs (95% CI) for SCA in Q2, Q3, and Q4 were 1.647 (1.011–2.680), 3.013 (1.770–5.124) and 5.081 (3.203–10.496), respectively (p for trend <0.05). Also, patients with hypertension with elevated SUA levels had a higher likelihood of an increased number of SCA sites. The ORs (95% CI) for the number of SCA sites among patients with hypertension in Q2, Q3, and Q4 were 2.246 (1.664–3.028), 2.748 (2.024–3.732) and 4.455 (3.235–6.135), respectively (p for trend <0.05). As shown in **Figure 2**, patients in the highest SUA quartile had a significantly increased risk of SCA in the carotid artery, coronary artery, thoracic aorta, and renal artery even after adjusting for potential confounding factors, including age, sex, eGFR, smoking, alcohol use, antihypertensive drugs use, statins use, hypertension, diabetes, and dyslipidaemia.

Similarly, patients in the highest quartile of SUA had a higher risk of severe SCA. For instance, the ORs (95% CI) for carotid atherosclerosis in those patients who were in Q2, Q3, and Q4

TABLE 2 | Prevalence of SCA according to quartiles of SUA levels.

		Quartiles of SUA (*N* = 1,534)				
	Total	**Q1 (*N* = 389)**	**Q2 (*N* = 381)**	**Q3 (*N* = 384)**	**Q4 (*N* = 380)**	***P*-value**
SUA, μmol/L	397.70 ± 87.85	296.37 ± 38.86	366.34 ± 24.65	418.93 ± 26.26	511.40 ± 58.49	<0.001
SCA, *N* (%)	1,317 (85.9)	307 (78.9)	318 (83.5)	342 (89.1)	350 (92.1)	<0.001
Number of SCA sites, *N* (%)						
0	217 (14.1)	82 (21.1)	83 (16.5)	42 (10.9)	30 (7.9)	<0.001
1	275 (17.9)	80 (20.6)	67 (17.6)	65 (16.9)	63 (16.6)	
2	327 (21.3)	87 (22.4)	67 (17.6)	89 (23.2)	84 (22.1)	
≥3	715 (46.6)	140 (36.0)	184 (48.3)	188 (49.0)	203 (53.4)	
Distribution of SCA, *N* (%)						
Carotid artery	792 (51.6)	157 (40.4)	202 (53.0)	215 (56.0)	218 (57.4)	<0.001
Coronary artery	848 (55.3)	158 (40.6)	208 (54.6)	215 (56.0)	267 (70.3)	<0.001
Thoracic aorta	1,135 (74.0)	273 (70.2)	272 (71.4)	290 (75.5)	300 (78.9)	0.022
Renal artery	702 (45.8)	147 (37.8)	174 (45.7)	199 (51.8)	182 (47.9)	0.001
Severity of arterial stenosis						
Carotid artery, *N* (%)						
Normal	743 (48.4)	232 (59.6)	179 (47.0)	169 (44.0)	163 (42.9)	<0.001
Minimal	763 (49.7)	152 (39.1)	198 (52.0)	207 (53.9)	206 (54.2)	
Mild-severe	28 (1.8)	5 (1.3)	4 (1.0)	8 (2.1)	11 (2.9)	
Coronary artery, *N* (%)						
Normal	686 (44.7)	231 (59.4)	173 (45.4)	169 (44.0)	113 (29.7)	<0.001
Minimal	539 (35.1)	117 (30.1)	145 (38.1)	126 (32.8)	151 (39.7)	
Mild	168 (11.0)	32 (8.2)	34 (8.9)	49 (12.8)	53 (13.9)	
Moderate-severe	141 (9.2)	9 (2.3)	29 (7.6)	40 (10.4)	63 (16.6)	
Thoracic aorta, *N* (%)						
Normal	399 (26.0)	116 (29.8)	109 (28.6)	94 (24.5)	80 (21.1)	0.043
Minimal	1,120 (73.0)	269 (69.2)	268 (70.3)	289 (75.3)	294 (77.4)	
Mild-severe	15 (1.0)	4 (1.0)	4 (1.0)	1 (0.3)	6 (1.6)	
Renal artery, *N* (%)						
Normal	832 (54.2)	242 (62.2)	207 (54.3)	185 (48.2)	198 (52.1)	0.003
Minimal	370 (24.1)	89 (22.9)	102 (26.8)	96 (25.0)	83 (21.8)	
Mild	248 (16.2)	47 (12.1)	56 (14.7)	74 (19.3)	71 (18.7)	
Moderate	46 (3.0)	5 (1.3)	10 (2.6)	16 (4.2)	15 (3.9)	
Severe	38 (2.5)	6 (1.5)	6 (1.6)	13 (3.4)	13 (3.4)	

Data were presented as mean ± SD for continuous variable and number (percentage) for categorical variables. SUA, serum uric acid; SCA, subclinical atherosclerosis.

were 1.996 (1.426–2.795), 2.195 (1.567–3.077), and 2.821 (1.998–3.987), respectively (p for trend <0.05). Patients in the higher quartiles were more likely to have severe coronary, thoracic and renal SCA than those in the first quartile. Compared with patients in the first quartile, the ORs (95% CI) for coronary, thoracic, and renal SCA in Q4 were 5.270 (3.881–7.156), 1.984 (1.318–2.983), and 2.614 (1.895–3.604), respectively (P for trend across quartiles for all SCA was <0.05).

Elevated Serum Uric Acid Levels Associated With the Risk of Subclinical Atherosclerosis in All Categories of FHS 10-Year Risk

Although the FHS 10-year risk was designed to assess the risk of cardiovascular events derived from atherosclerosis, not the presence of SCA, we aimed to complement these predictive models by comparing the presence and extent of subclinical disease across different risk categories. Most patients with an increased cardiovascular risk scale, 10-year FHS risk, had a higher prevalence of SCA (**Supplementary Table 2**). Patients classified at high 10-year FHS risk had the highest prevalence of SCA (95.8%), and 84% of the high-risk patients had SCA in two or more territories (84.2%). Among patients at moderate 10-year FHS risk, 79.8% had SCA. Also, extensive SCA was present in a substantial number of patients among the low-risk category (53.8%). **Figure 3A** describes the prevalence of SCA based on SUA quartiles in patients grouped by FHS-10 year risk. Compared to the patients at the lower quartiles of SUA, those patients at higher quartiles of SUA levels had a higher proportion of SCA, with high FHS-10 year risk patients in Q4 accounts for the highest risk of SCA (98.7%). However, substantial SCA

TABLE 3 | Risk of SCA according to baseline serum uric acid quartiles in adjusted models.

		Quartiles of SUA (*N* = 1,534)					
		Q2 (*N* = 381)		Q3 (*N* = 384)		Q4 (*N* = 380)	
	Q1 (*N* = 389)	OR (95%CI)	*P*-value	OR (95%CI)	*P*-value	OR (95%CI)	*P*-value
SCA	1.000 (ref.)	1.647 (1.011–2.680)	0.045	3.013 (1.770–5.124)	<0.001	5.081 (3.203–10.496)	<0.001
Number of SUA sites	1.000 (ref.)	2.246 (1.664–3.028)	<0.001	2.748 (2.024–3.732)	<0.001	4.455 (3.235–6.135)	<0.001
SCA in carotid artery	1.000 (ref.)	2.119 (1.504–2.986)	<0.001	2.289 (1.621–3.232)	<0.001	2.804 (1.970–3.991)	<0.001
SCA in coronary artery	1.000 (ref.)	2.149 (1.542–2.995)	<0.001	2.197 (1.575–3.062)	<0.001	5.596 (3.892–8.045)	<0.001
SCA in thoracic aorta	1.000 (ref.)	1.131 (0.754–1.697)	0.552	1.456 (0.962–2.203)	0.076	2.138 (1.381–3.310)	0.001
SCA in renal artery	1.000 (ref.)	1.927 (1.326–2.801)	0.001	2.724 (1.861–3.983)	<0.001	2.527 (1.723–3.706)	<0.001
Severity of carotid artery stenosis	1.000 (ref.)	1.996 (1.426–2.795)	<0.001	2.195 (1.567–3.077)	<0.001	2.821 (1.998–3.987)	<0.001
Severity of coronary stenosis	1.000 (ref.)	1.994 (1.480–2.686)	<0.001	2.319 (1.723–3.121)	<0.001	5.270 (3.881–7.156)	<0.001
Severity of thoracic aorta stenosis	1.000 (ref.)	1.096 (0.747–1.611)	0.638	1.290 (0.875–1.904)	0.199	1.984 (1.318–2.983)	0.001
Severity of renal artery stenosis	1.000 (ref.)	1.670 (1.215–2.293)	0.002	2.347 (1.714–3.212)	<0.001	2.614 (1.895–3.604)	<0.001

Adjusted for age, sex, eGFR, smoking, alcohol use, antihypertensive drugs use, statins use, blood pressure, diabetes, and dyslipidaemia. SUA, serum uric acid; SCA, subclinical atherosclerosis; OR, odds ratio; CI, Confidence Interval.

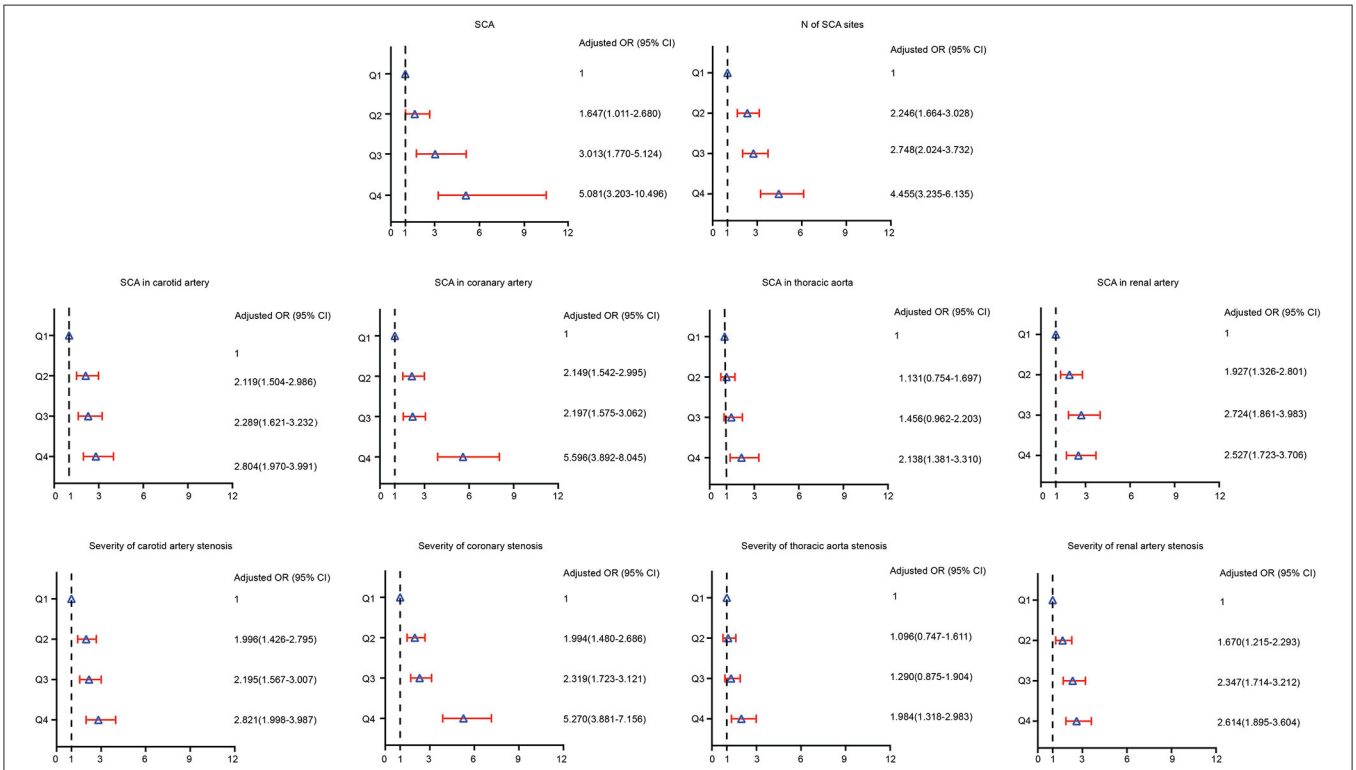

FIGURE 2 | Risk of prevalence and severity of SCA according to baseline serum uric acid quartiles in adjusted models.

risk was present among those patients in the highest quartile of SUA levels classified at the low-risk category. **Table 4** describes the adjusted odds ratios for SCA according to baseline serum uric acid quartile in patients grouped by FHS-10 year risk. The OR (CI) for SCA for patients in quartile four classified at low, moderate and high FSH risk were 4.036 (1.564, 10.416), 4.262 (1.689, 10.754), and 10.889 (3.034, 39.078), respectively. Also, an increase in one standard deviation of SUA (87.85 μmol/L) was significantly associated with SCA in those patients regardless of the different category of FHS 10-year risk (**Figure 3B**), with the ORs for SCA at low, moderate and high FHS risk groups were 1.873, 1.675, and 2.528, respectively.

TABLE 4 | Risk of SCA according to baseline serum uric acid quartile in adjusted models in patients grouped by FHS-10 year risk.

	Quartiles of SUA (*N* = 1,534)						
	Q1 (*N* = 389)	Q2 (*N* = 381)		Q3 (*N* = 384)		Q4 (*N* = 380)	
		OR (95%CI)	*P*-value	OR (95%CI)	*P*-value	OR (95%CI)	*P*-value
Low	1.000 (ref.)	2.271 (0.938, 5.496)	0.069	5.439 (2.025, 14.608)	0.001	4.036 (1.564, 10.416)	0.004
Moderate	1.000 (ref.)	0.795 (0.362, 1.748)	0.568	1.368 (0.616, 3.039)	0.442	4.262 (1.689, 10.754)	0.002
High	1.000 (ref.)	2.402 (1.032, 5.593)	0.042	3.602 (1.431, 9.07)	0.007	10.889 (3.034, 39.078)	<0.001

OR, odds ratio; CI, Confidence Interval.

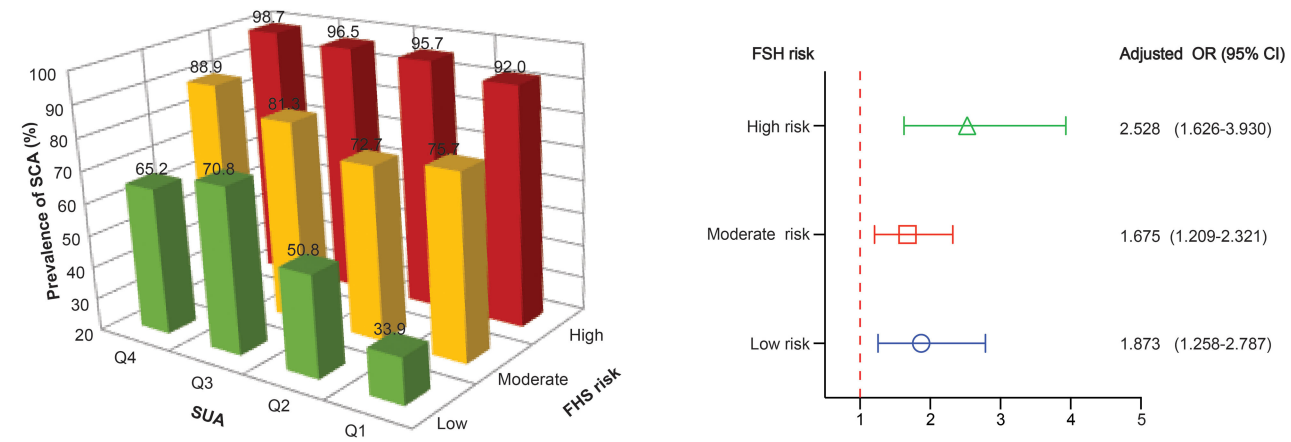

FIGURE 3 | (A) The prevalence of subclinical atherosclerosis based on SUA quartiles in patients grouped by FHS-10 year risk. **(B)** Adjusted odds ratios for subclinical atherosclerosis for 1 SD increase in SUA in patients grouped by FHS-10 year risk.

DISCUSSION

Using a multi-territorial evaluation, the present study discovers a high prevalence of SCA (85.9%) in patients with hypertension, with nearly half of patients classified as having generalized SCA (46.6%). Also, the findings of this cross-sectional analysis clarified the relationship between elevated SUA and the presence of SCA in the Chinese population with hypertension. Those participants who had a high concentration of SUA were more likely to have SCA. Even after adjustment for possible confounders, the association between elevated SUA concentrations and SCA remained significant. Similarly, most individuals classified at high risk by traditional scale (10-year FHS risk) had a higher prevalence, vascular distribution, and multi-territorial extent of SCA. However, extensive SCA was also present in a substantial number of low-risk patients at the higher quartiles of SUA classified at low FHS-10 year risk, suggesting elevated SUA associates with SCA risk to some extent regardless of FHS risk.

Uric acid is the final product of purine metabolism (26), mainly produced in the liver and gastrointestinal tract and excreted by the kidney (27). Epidemiological studies reported positive associations in blood pressure readings with an increase in SUA (28), whereas some documented evidence reported there exists a significant association between SUA and hypertension (29). Hypertension and plasma aldosterone concentration have been proved to be strongly associated with surrogate markers of SCA (30, 31) whereas other potential risk factors for SCA were rarely reported. In the present study, the proportion of patients with SCA were increased with an increase in SUA levels. Participants in the higher quartiles of SUA levels had a higher likelihood of having SCA. Importantly, the degree of atherosclerosis was found to increase with an increase in SUA levels. Atherosclerosis is the leading cause of cardiovascular death and disabilities such as sudden death, myocardial infarction, or stroke (32). Therefore, it is of great significance to take effective measures to intervene before individuals develop into the clinical phase or end-stage.

According to our present study, the thoracic aorta is the most frequently affected vascular site. However, the previous study reported a strong prevalence of SCA in the iliofemoral arteries (82%) among the low-risk population (3). In the present study, the iliofemoral region has not been studied therefore the comparison between the thoracic aorta and iliofemoral arteries cannot be done. Overall, among the 1,534 patients with hypertension included in the present study, 85.9% of patients were presented with SCA, which indicates a higher prevalence of subclinical atherosclerosis than the prevalence of SCA (63%) reported in the PESA study among the general population

(3). These differences in the prevalence of SCA is probably attributable to (i) the examination of different territories, which were not explored in earlier studies (for instance thoracic aorta), (ii) investigation of more territories, and (iii) examination of hypertension individuals who are already at higher risk of SCA. Given the high prevalence of SCA in the thoracic aorta (74%), SCA assessment tends to be more important. Thus, imaging of thoracic aorta may be a useful screening tool among the hypertension population for detecting atherosclerosis in its early stages.

Both the Asymptomatic Polyvascular Abnormalities Community study (APACS) (33) and the Brisighella Heart Study (34) reported a positive correlation between an increase in hyperuricemia rates and the risk of atherosclerosis. In the present study, the patients with hypertension in the higher quartiles of SUA had lower eGFR. Thus, its negative implication in compromising the predictive power of SUA may not be underestimated. Nevertheless, the present study indicated that patients with hypertension in the top quartile of SUA had an increased risk of SCA, even after adjusting for conventional risk factors for CVD, including the body mass index (BMI), eGFR, and dyslipidemia. Regardless of the FHS-10 year risk category, those patients at higher quartile of SUA levels had a higher OR for SCA. These findings suggest that individuals with high SUA levels, regardless of the status of their FHS 10-year risk, are remained at risk of SCA. Notably, the patients with low FHS-10 year risk in the Q3 (OR = 5.439), and Q4 (OR = 4.036) showed a tremendous risk of SCA, indicating the strong relationship between SUA level and SCA. Therefore, community health strategies aimed at SCA prevention among hypertension individuals, whose SUA levels and FHS 10 years risk score increased greater than the standard cut-off points should be accompanied by ultrasound or CT evaluations to improve the treatment outcomes and avoid serious complications of SCA.

This research connected elevated SUA with asymptomatic pre-clinical arterial atherosclerosis. The result of these findings gives novel insights into the overall distribution of SCA among the Chinese population with hypertension. Future studies are needed to investigate whether SUA modulation could delay or even prevent SCA. To our knowledge, this is the first study to investigate the relationship between the SUA and asymptomatic atherosclerosis rates in a Chinese population with hypertension. In our study, 79.7% of the population had dyslipidemia and 70% had statin use, which may mitigate the bias associated with the confounding effect of dyslipidemia. However, there are some drawbacks. Firstly, due to the limitations of cross-sectional nature, the cause-and-effect relationship between SUA and SCA was not discussed. Second, the present study does not include evidence on the underlying cause of stenosis, which makes the root of arterial stenosis difficult to categorize. Therefore, we propose an additional longitudinal study to provide epidemiological evidence for the relationship between elevated SUA and incident SCA among the hypertension population in China.

DATA AVAILABILITY STATEMENT

The raw data supporting the conclusions of this article will be made available by the authors, without undue reservation.

AUTHOR CONTRIBUTIONS

YX and XY designed the study. FL and SH contributed in the study protocol, literature searches, data collection, and statistical analysis and were involved in the final draft of the manuscript. TH, YJ, YZ, YL, HL, and SL contributed in the coordination of designing and analysis. All authors have read and approved the final manuscript.

FUNDING

This study was supported by grants from National Natural Science Foundation of China (81900439), Science Foundation of Education Department of Liaoning Province (LZ2019020), National Natural Science Foundation of China (81970286), Chang Jiang Scholars Program (T2017124) and program of Liaoning Distinguished Professor.

ACKNOWLEDGMENTS

We acknowledge all participants and Yiducloud (Beijing) Technology Ltd. for their assistance in data searching, extraction, and processing.

SUPPLEMENTARY MATERIAL

The Supplementary Material for this article can be found online at: https://www.frontiersin.org/articles/10.3389/fcvm.2021.638992/full#supplementary-material

REFERENCES

1. Herrington W, Lacey B, Sherliker P, Armitage J, Lewington S. Epidemiology of atherosclerosis and the potential to reduce the global burden of atherothrombotic disease. *Circ Res.* (2016) 118:535–46. doi: 10.1161/CIRCRESAHA.115.307611
2. Bian L, Xia L, Wang Y, Jiang J, Zhang Y, Li D, et al. Risk factors of subclinical atherosclerosis and plaque burden in high risk individuals: results from a community-based study. *Front Physiol.* (2018) 9:739. doi: 10.3389/fphys.2018.00739
3. Fernandez-Friera L, Penalvo JL, Fernandez-Ortiz A, Ibanez B, Lopez-Melgar B, Laclaustra M, et al. Prevalence, vascular distribution, and multiterritorial extent of subclinical atherosclerosis in a middle-aged cohort: the PESA (progression of early subclinical atherosclerosis) study. *Circulation.* (2015) 131:2104–13. doi: 10.1161/CIRCULATIONAHA.114.014310
4. Maloberti A, Maggioni S, Occhi L, Triglione N, Panzeri F, Nava S, et al. Sex-related relationships between uric acid and target organ damage in hypertension. *J Clin Hypertens (Greenwich).* (2018) 20:193–200. doi: 10.1111/jch.13136

5. Fang J, Alderman MH. Serum uric acid and cardiovascular mortality the NHANES I epidemiologic follow-up study, 1971-1992. *Natl Health Nutr Exam Survey JAMA.* (2000) 283:2404–10. doi: 10.1001/jama.283.18.2404
6. Niskanen LK, Laaksonen DE, Nyyssonen K, Alfthan G, Lakka HM, Lakka TA, et al. Uric acid level as a risk factor for cardiovascular and all-cause mortality in middle-aged men: a prospective cohort study. *Arch Intern Med.* (2004) 164:1546–51. doi: 10.1001/archinte.164.14.1546
7. Williams B, Mancia G, Spiering W, Agabiti Rosei E, Azizi M, Burnier M, et al. 2018 ESC/ESH Guidelines for the management of arterial hypertension. *Eur Heart J.* (2018) 39:3021–104. doi: 10.1093/eurheartj/ehy339
8. Campo C, Ruilope LM, Segura J, Rodicio JL, Garcia-Robles R, Garcia-Puig J. Hyperuricemia, low urine urate excretion and target organ damage in arterial hypertension. *Blood Press.* (2003) 12:277–83. doi: 10.1080/08037050310019418
9. Tsioufis C, Chatzis D, Vezali E, Dimitriadis K, Antoniadis D, Zervoudaki A, et al. The controversial role of serum uric acid in essential hypertension: relationships with indices of target organ damage. *J Hum Hypertens.* (2005) 19:211–7. doi: 10.1038/sj.jhh.1001810
10. Simon A, Megnien JL, Levenson J. Detection of preclinical atherosclerosis may optimize the management of hypertension. *Am J Hypertens.* (1997) 10:813–24. doi: 10.1016/S0895-7061(97)00118-0
11. Kannel WB, Castelli WP, Gordon T, McNamara PM. Serum cholesterol, lipoproteins, and the risk of coronary heart disease. *Framingham Study Ann Intern Med.* (1971) 74:1–12. doi: 10.7326/0003-4819-74-1-1
12. Fernandez-Ortiz A, Jimenez-Borreguero LJ, Penalvo JL, Ordovas JM, Mocoroa A, Fernandez-Friera L, et al. The progression and early detection of subclinical atherosclerosis (PESA) study: rationale and design. *Am Heart J.* (2013) 166:990–8. doi: 10.1016/j.ahj.2013.08.024
13. Pearson TA, Palaniappan LP, Artinian NT, Carnethon MR, Criqui MH, Daniels SR, et al. American Heart Association guide for improving cardiovascular health at the community level, 2013 update: a scientific statement for public health practitioners, healthcare providers, and health policy makers. *Circulation.* (2013) 127:1730–53. doi: 10.1161/CIR.0b013e31828f8a94
14. Williams B, Mancia G, Spiering W, Agabiti Rosei E, Azizi M, Burnier M, et al. 2018 Practice guidelines for the management of arterial hypertension of the European Society of Hypertension and the European Society of Cardiology: ESH/ESC task force for the management of arterial hypertension: erratum. *J Hypertens.* (2019) 37:456. doi: 10.1097/HJH.0000000000002026
15. Expert Panel on Detection Evaluation, Treatment of High Blood Cholesterol in Adults. Executive summary of the third report of the national cholesterol education program (NCEP) expert panel on detection, evaluation, and treatment of high blood cholesterol in adults (adult treatment panel III). *JAMA.* (2001) 285:2486–97. doi: 10.1001/jama.285.19.2486
16. Maloberti A, Giannattasio C, Bombelli M, Desideri G, Cicero AFG, Muiesan ML, et al. Hyperuricemia and risk of cardiovascular outcomes: the experience of the URRAH (uric acid right for heart health) project. *High Blood Press Cardiovasc Prev.* (2020) 27:121–8. doi: 10.1007/s40292-020-00368-z
17. Bild DE, Bluemke DA, Burke GL, Detrano R, Diez Roux AV, Folsom AR, et al. Multi-ethnic study of atherosclerosis: objectives and design. *Am J Epidemiol.* (2002) 156:871–81. doi: 10.1093/aje/kwf113
18. Ford ES, Giles WH, Mokdad AH. The distribution of 10-Year risk for coronary heart disease among US adults: findings from the national health and nutrition examination survey III. *J Am Coll Cardiol.* (2004) 43:1791–6. doi: 10.1016/j.jacc.2003.11.061
19. Ma YC, Zuo L, Chen JH, Luo Q, Yu XQ, Li Y, et al. Modified glomerular filtration rate estimating equation for Chinese patients with chronic kidney disease. *J Am Soc Nephrol.* (2006) 17:2937–44. doi: 10.1681/ASN.2006040368
20. Pencina MJ, D'Agostino RB, Sr., Larson MG, Massaro JM, Vasan RS. Predicting the 30-year risk of cardiovascular disease: the framingham heart study. *Circulation.* (2009) 119:3078–84. doi: 10.1161/CIRCULATIONAHA.108.816694
21. Nambi V, Chambless L, Folsom AR, He M, Hu Y, Mosley T, et al. Carotid intima-media thickness and presence or absence of plaque improves prediction of coronary heart disease risk: the ARIC (atherosclerosis risk in communities) study. *J Am Coll Cardiol.* (2010) 55:1600–7. doi: 10.1016/j.jacc.2009.11.075
22. Sehestedt T, Jeppesen J, Hansen TW, Wachtell K, Ibsen H, Torp-Pedersen C, et al. Risk prediction is improved by adding markers of subclinical organ damage to SCORE. *Eur Heart J.* (2010) 31:883–91. doi: 10.1093/eurheartj/ehp546
23. Williams B, Mancia G, Spiering W, Agabiti Rosei E, Azizi M, Burnier M, et al. 2018 ESC/ESH Guidelines for the management of arterial hypertension: the task force for the management of arterial hypertension of the European Society of Cardiology and the European Society of Hypertension: the task force for the management of arterial hypertension of the European Society of Cardiology and the European Society of Hypertension. *J Hypertens.* (2018) 36:1953–2041. doi: 10.1097/HJH.0000000000001940
24. Grant EG, Benson CB, Moneta GL, Alexandrov AV, Baker JD, Bluth EI, et al. Carotid artery stenosis: gray-scale and Doppler US diagnosis–Society of Radiologists in Ultrasound Consensus Conference. *Radiology.* (2003) 229:340–6. doi: 10.1148/radiol.2292030516
25. Leipsic J, Abbara S, Achenbach S, Cury R, Earls JP, Mancini GJ, et al. SCCT guidelines for the interpretation and reporting of coronary CT angiography: a report of the Society of Cardiovascular Computed Tomography Guidelines Committee. *J Cardiovasc Comput Tomogr.* (2014) 8:342–58. doi: 10.1016/j.jcct.2014.07.003
26. Kirça M, Oguz N, Çetin A, Uzuner F, Yeşilkaya A. Uric acid stimulates proliferative pathways in vascular smooth muscle cells through the activation of p38 MAPK, p44/42 MAPK and PDGFRβ. *J Recept Signal Transduct Res.* (2017) 37:167–73. doi: 10.1080/10799893.2016.1203941
27. Cicero AF, Rosticci M, Fogacci F, Grandi E, D'Addato S, Borghi C. High serum uric acid is associated to poorly controlled blood pressure and higher arterial stiffness in hypertensive subjects. *Eur J Intern Med.* (2017) 37:38–42. doi: 10.1016/j.ejim.2016.07.026
28. Allen NB, Siddique J, Wilkins JT, Shay C, Lewis CE, Goff DC, et al. Blood pressure trajectories in early adulthood and subclinical atherosclerosis in middle age. *JAMA.* (2014) 311:490–7. doi: 10.1001/jama.2013.285122
29. Kuwabara M, Hisatome I, Niwa K, Hara S, Roncal-Jimenez CA, Bjornstad P, et al. Uric acid is a strong risk marker for developing hypertension from prehypertension: a 5-year Japanese cohort study. *Hypertension.* (2018) 71:78–86. doi: 10.1161/HYPERTENSIONAHA.117.10370
30. Alatab S, Fakhrzadeh H, Sharifi F, Mostashfi A, Mirarefin M, Badamchizadeh Z, et al. Impact of hypertension on various markers of subclinical atherosclerosis in early type 2 diabetes. *J Diabetes Metab Disord.* (2014) 13:24. doi: 10.1186/2251-6581-13-24
31. Concistre A, Petramala L, Bisogni V, Mezzadri M, Olmati F, Saracino V, et al. Subclinical atherosclerosis due to increase of plasma aldosterone concentrations in essential hypertensive individuals. *J Hypertens.* (2019) 37:2232–9. doi: 10.1097/HJH.0000000000002170
32. Go AS, Mozaffarian D, Roger VL, Benjamin EJ, Berry JD, Borden WB, et al. Executive summary: heart disease and stroke statistics—2013 update: a report from the American Heart Association. *Circulation.* (2013) 127:143–52. doi: 10.1161/CIR.0b013e318282ab8f
33. Li Q, Zhou Y, Dong K, Wang A, Yang X, Zhang C, et al. The association between serum uric acid levels and the prevalence of vulnerable atherosclerotic carotid plaque: a cross-sectional study. *Sci Rep.* (2015) 5:10003. doi: 10.1038/srep10003
34. Cicero AF, Salvi P, D'Addato S, Rosticci M, Borghi C, Brisighella Heart Study Group. Association between serum uric acid, hypertension, vascular stiffness and subclinical atherosclerosis: data from the Brisighella heart study. *J Hypertens.* (2014) 32:57–64. doi: 10.1097/HJH.0b013e328365b916

Conflict of Interest: The authors declare that the research was conducted in the absence of any commercial or financial relationships that could be construed as a potential conflict of interest.

frontiers in Cardiovascular Medicine

ORIGINAL RESEARCH
published: 22 April 2021
doi: 10.3389/fcvm.2021.641272

Distinct Phenotypes Induced by Different Degrees of Transverse Aortic Constriction in C57BL/6N Mice

Haiyan Deng[1†], *Lei-Lei Ma*[2†], *Fei-Juan Kong*[3,4*] *and Zengyong Qiao*[1*]

[1] Department of Cardiovascular Medicine, Shanghai Jiao Tong University Affiliated Sixth People's Hospital South Campus, Shanghai, China, [2] Department of Cardiology, Shanghai Institute of Cardiovascular Diseases, Zhongshan Hospital, Fudan University, Shanghai, China, [3] Department of Endocrinology and Metabolism, Shanghai General Hospital, Shanghai Jiao Tong University School of Medicine, Shanghai, China, [4] Department of Endocrinology and Metabolism, Xuhui District Central Hospital of Shanghai, Shanghai, China

The transverse aortic constriction (TAC) model surgery is a widely used disease model to study pressure overload–induced cardiac hypertrophy and heart failure in mice. The severity of adverse cardiac remodeling of the TAC model is largely dependent on the degree of constriction around the aorta, and the phenotypes of TAC are also different in different mouse strains. Few studies focus on directly comparing phenotypes of the TAC model with different degrees of constriction around the aorta, and no study compares the difference in C57BL/6N mice. In the present study, C57BL/6N mice aged 10 weeks were subjected to sham, 25G TAC, 26G TAC, and 27G TAC surgery for 4 weeks. We then analyzed the different phenotypes induced by 25G TAC, 26G TAC, and 27G TAC in c57BL/6N mice in terms of pressure gradient, cardiac hypertrophy, cardiac function, heart failure situation, survival condition, and cardiac fibrosis. All C57BL/6N mice subjected to TAC surgery developed significantly hypertrophy. Mice subjected to 27G TAC had severe cardiac dysfunction, severe cardiac fibrosis, and exhibited characteristics of heart failure at 4 weeks post-TAC. Compared with 27G TAC mice, 26G TAC mice showed a much milder response in cardiac dysfunction and cardiac fibrosis compared to 27G TAC, and a very small fraction of the 26G TAC group exhibited characteristics of heart failure. There was no obvious cardiac dysfunction, cardiac fibrosis, and characteristics of heart failure observed in 25G TAC mice. Based on our results, we conclude that the 25G TAC, 26G TAC, and 27G TAC induced distinct phenotypes in C57BL/6N mice.

Keywords: cardiac hypertrophy, transverse aortic constriction, C57BL/6N mice, cardiac fibrosis, heart failure

OPEN ACCESS

Edited by:
Soo-Kyoung Choi,
Yonsei University College of Medicine, South Korea

Reviewed by:
Jane A. Leopold,
Brigham and Women's Hospital and Harvard Medical School, United States
Youngin Kwon,
Yonsei University, South Korea

****Correspondence:***
Zengyong Qiao
qiaozy6666@163.com
Fei-Juan Kong
kongfeijuan@163.com

† These authors have contributed equally to this work

Specialty section:
This article was submitted to Hypertension, a section of the journal Frontiers in Cardiovascular Medicine

Received: *14 December 2020*
Accepted: *23 February 2021*
Published: *22 April 2021*

Citation:
Deng H, Ma L-L, Kong F-J and Qiao Z (2021) Distinct Phenotypes Induced by Different Degrees of Transverse Aortic Constriction in C57BL/6N Mice. Front. Cardiovasc. Med. 8:641272. doi: 10.3389/fcvm.2021.641272

INTRODUCTION

Heart failure (HF) is still one of the leading causes of mortality worldwide, and the prevalence of HF continues to rise over time. Just between the years 2013 and 2016, there were about 6.2 million adults diagnosed with HF in America (1), which is a great loss to people's health and the economy. As a result, it is more important to better understand the development of HF and find new therapeutic targets. The development of HF is characterized by a process of adverse cardiac remodeling (2), and there

are three major patterns of cardiac remodeling: pressure overload–induced concentric hypertrophy, volume overload–induced eccentric hypertrophy, and mixed load–induced post-myocardial-infarct remodeling (3). Heart disease animal models play an important role in studying these remodeling processes as well as in preclinical studies. The validity and accuracy of animal models are necessary for the mechanism study of HF and for new drug development as well (4, 5).

Hypertension is one of the most important risk factors in the development of HF. To learn the mechanisms of pressure overload–induced cardiac hypertrophy, the transverse aortic constriction (TAC) model was first built by Rockman et al. (6). Over decades of development, several improved TAC models with minimal invasiveness and low mortality have been developed by other research groups (7–9), and this made the TAC model more effective and accurate. Animals subjected to TAC go through cardiac hypertrophy, cardiac fibrosis, a limited amount of inflammation, and eventually develop to cardiac dilation and HF. The severity of adverse cardiac remodeling induced by TAC largely relies on the degree of constriction of the aorta and the duration of aortic constriction correlated to the degree of adverse remodeling (10). The most common needle size for constriction in TAC is 27 gauge (27 G, outer diameter 0.41 mm) (4, 5, 10) although there are limited studies using 25-gauge (25 G, outer diameter 0.51 mm) (11) and 26-gauge (26 G, outer diameter 0.46 mm) needles (12). Compared with bigger size needles, smaller needles can create a narrower constriction loop, which induces severe adverse remodeling and higher mortality (13). Besides the severity of constriction, the species of animals and genetic background are also responsible for the variability of TAC response. Therefore, a better understanding of the accurate response of specific animal strains and specific constriction to TAC is very important for the research on HF. However, very few studies focus on the direct comparison of phenotypes of the TAC model induced by different needle sizes in great detail (13). Also, the phenotype comparison of TAC response induced by different needle sizes in C57BL/6N mice has not been reported to date. The potentially different adverse cardiac remodeling induced by varying degrees of pressure overload in C57BL/6N mice remains unknown.

In the present study, we compare the different response to TAC induced by 25 G, 26 G, and 27 G needles in C57BL/6N mice, and we analyze cardiac hypertrophy, cardiac function, and cardiac fibrosis changes in response to varying constriction degrees. Our study may provide deep insight for a pressure overload–induced heart failure study in C57BL/N mice.

METHODS

Animals

The male C57BL/6N mice used in this study were obtained from Shanghai Laboratory Animal Center (Chinese Academy of Sciences, Shanghai, China). All the animal experiments were conducted in compliance with the Guide for the Care and Use of Laboratory Animals published by the U.S. National Institutes of Health (the 8th edition, NRC 2011). All the *in vivo* experiments were approved by the Animal Care and Use Committee of Fudan University.

TAC Surgery

Thirty male C57BL/6N mice aged 10 weeks were randomly divided into four groups: Sham ($n = 6$), 25 G TAC ($n = 8$), 26 G TAC ($n = 8$), and 27 G TAC ($n = 8$). All TAC group mice were subjected to minimally invasive TAC surgery as described elsewhere (14). Mice were anesthetized with 1% pentobarbital sodium (50 mg/kg) through intraperitoneal injection. The hair on the neck and chest were removed using a depilatory agent, and then the surgery area was disinfected with betadine and alcohol. A 0.5–1.0 cm longitudinal skin incision was made at the level of the suprasternal notch, and then a 2–3 mm longitudinal sternum cut was made to locate the thymus and aorta. The aorta between the origin of the right innominate and left common carotid arteries was tied with a bent 25 G, 26 G, or 27 G needle with a 6-0 silk suture, and then the needle was quickly removed after ligation. The sham mouse surgery was under the same procedures except that the artery was not ligated. After surgery, the mice were allowed to fully recover on a warming pad and housed in standard housing condition.

Echocardiography

Echocardiography analysis was performed using the Vevo 2100 imaging system (VisualSonics, Canada) as described in a previous study (15). Briefly, the mice were anesthetized with isoflurane (0.5–4%), and parasternal long- and short-axis views in B- and M-Mode were recorded when the heart rate of the mice was maintained at 450–550 bpm. To access the peak pressure gradient induced by TAC, pulsed-wave Doppler was applied to the aortic arch as described elsewhere (16). The pulsed-wave Doppler was used to measure blood velocities in either TAC or sham mice. The peak pressure gradient was calculated with the pulsed-wave peaks by using the modified Bernoulli equation (Pressure gradient = 4^{*}velocity^{2}) (16). All measurements were averaged with three measurements per variable animal.

Tissue Collection

Mice were anesthetized with 5% isoflurane. After being fully anesthetized, the heart was quickly excised and washed with ice-cold PBS. After being weighed, the heart was cut into three parts. The middle part was put into 4% polyformaldehyde solution for histological analysis, and the top and bottom parts were quickly put into liquid nitrogen and transferred to a -80° freezer later. The lungs and tibia length were also weighed and measured.

Histological Staining

Cardiomyocyte size and extent of LV fibrosis were measured using hematoxylin and eosin (H&E) and Masson's trichrome staining, respectively. After being fixed with 4% polyformaldehyde, the heart was finally embedded into paraffin. The heart-embedded paraffin blocks were cut into 5-μm sections. Then, the sections were stained with H&E and Masson's trichrome. At least five sections of each heart were examined, and at least five random images were captured at each section.

The images were analyzed by using the Image-Pro Plus 5.0 image analysis system (Media Cybernetics, Rockville, MD).

Real-Time Polymerase Chain Reaction (RT-PCR)

The gene expression level of col-1, col-3, and TGF-β were measured using RT-PCR. Total RNA was extracted from frozen heart tissue by using the TRIzol reagent (Invitrogen, Carlsbad, CA), and 1 μg total RNA was used for reverse transcription to synthesize cDNA by using TOYOBO RT-PCR kit (TOYOBO, Japan). SYBR Premix Ex Taq kit (Cat#: RR420A, TaKaRa, Japan) was used in the RT-PCR reaction for relative quantification of RNA. The primers we used were synthesized by Sangon Biotech (Shanghai, China), and the sequences of the primers are as follows: col-1 (Forward: CAACCTCAAG AAGTCCCTGC, Reverse: AGGTGAATCGACTGTTGCCT), col-3 (Forward: CACCCCTCTCTTATTTTGGCAC, Reverse: AGACTCATAGGACTGACCAAGGTAGTT), TGF-β (Forward: GGCGGTGCTCGCTTTGTA, Reverse: GCGGGTGACTT CTTTGGC), ANP (Forward: CTGCTTCGGGGGTAGGATTG, Reverse: GCTCAAGCAGAATCGACTGC), BNP (Forward: GAGGTCACTCCATCCTCTGG, Reverse: GCCATTTCCTC CGACTTTTCTC), GAPDH (Forward: AACAAGCAACT GTCCCTGAGC, Reverse: GTAGACAGAAGGTGGCACAGA). GAPDH was used as a reference gene.

Western Blot

Total proteins were extracted from heart tissues and quantified by using the bicinchoninic acid protein assay. According to the molecular weight of the target proteins, the protein samples were separated in 10% SDS-PAGE and then transferred to Immobilon-P polyvinylidene fluoride (PVDF) membranes. After being blocked with Western blocking buffer, the membranes were incubated overnight at 4°C with primary antibodies: TGF-β (1:1,000), COL1A1 (1:1,000), phosphorylated ERK (1:5,000), and ERK (1:5,000) (Cell Signaling Technology, Danvers, MA, USA) and then incubated with horseradish peroxidase (HRP)-conjugated secondary antibodies (1:1,000) for 1 h at room temperature. After interaction with a Pro-Light chemiluminescent detection kit (Tiangen Biotech Inc., Beijing, China), the proteins of the membranes were detected using the LAS-3000 imaging system (FUJIFILM Inc., Tokyo, Japan), and the results were analyzed with ImageJ software (National Institutes of Health, Bethesda, MD, USA).

Statistical Analysis

All the data in the present study are expressed as mean ± standard error. All the data statistics analyses were performed by GraphPad Prism 8.0 (GraphPad Prism Software, CA, USA). For comparison of more than two groups, one-way ANOVA followed by Tukey's post-test was used. For two-factor design experiments, two-way ANOVA followed by Tukey's multiple comparisons test was performed. Statistical significance was presented by repeat symbols: a single symbol means $p \leq 0.05$; double symbols mean $p \leq 0.01$; triple symbols mean $p \leq 0.001$.

RESULTS

Pressure Gradient

To evaluate the outcomes of different needle sizes on TAC-induced pressure overload conditions, we measured the pressure gradient across the construction site in each group using pulse wave Doppler. The pressure gradient was measured 1 week after TAC surgery. Compared with sham mice (3.8 ± 0.4 mmHg), the pressure gradient was significantly increased by TAC surgery in 25 G TAC (44.5 ± 1.8 mmHg), 26 G TAC (55.7 ± 3.7 mmHg), and 27 G TAC (75.2 ± 6.1 mmHg) ($p < 0.001$; **Figures 1A,B**). Moreover, the pressure gradient was significantly higher in 27 G TAC compared with 25 G TAC ($p < 0.001$) and 26 G TAC ($p < 0.01$). Although there was no statistically significant difference between 25 and 26 G TAC, the pressure gradient in 26 G TAC was much higher than that in 25 G TAC. These results show that the different needle sizes have successfully induced different degrees of pressure overload conditions in C57BL/6N mice.

Cardiac Hypertrophy

Compared with sham mice, all mice subjected to TAC surgery successfully developed cardiac hypertrophy (**Figure 2**). The echocardiography results showed that the left ventricular anterior wall (LVAW) thickness in 25, 26, and 27 G TAC increased 25.2, 29.2, and 36.8%, respectively, compared with sham mice after 4 weeks of TAC (**Figure 2A**). Importantly, the LVAW thickness in 27 G TAC was much thicker than that in 26 ($p < 0.05$) and 25 G TAC ($p < 0.001$). Although there was no statistically significant difference in LVAW wall thickness between 25 and 26 G TAC, the LVAW thickness in 26 G TAC was increased by 3.8% compared with 25G TAC. Further *post-hoc* analysis showed a significant increase of LVAW thickness between all three TAC and sham mice after just 1 week of TAC surgery; however, there was no significant difference among the three TAC groups, whereas the significant difference between 25 and 27 G TAC emerged 2 and 3 weeks after TAC surgery, but this significant difference disappeared at 4 weeks after TAC surgery. Similar results about the left ventricular posterior wall (LVPW) thickness (**Figure 2B**) have been observed. LV mass normalized to body weight is one of the very important parameters of cardiac hypertrophy. Our results showed that LV mass increased 21.7, 29.3, and 49.2% in 25, 26, and 27 G TAC, respectively, compared with sham mice after 4 weeks of TAC surgery (**Figure 2C**). The mice subjected to 27 G TAC had more significant LV mass than 26 G TAC ($p < 0.001$), and 26 G TAC had more than that in 25 G TAC but with no statistical significance. Further *post-hoc* analysis showed that LV mass of the 27 G TAC mice significantly increased just 1 week after TAC surgery compared with sham mice; however, this significant difference appeared 2 weeks after TAC surgery in 26 G TAC and emerged 3 weeks after TAC in 25 G TAC mice.

In accordance with the echocardiographic data, the heart size was increased in 25, 26, and 27 G TAC compared with sham mice, and the heart size in 27 G TAC was bigger than that in 26 G TAC and the 26 G TAC bigger than that in 25 G TAC (**Figure 2D**). Similarly, the heart weight normalized to tibia length (HW/TL) and atrial weight normalized to tibia length (AW/TL) were all significantly increased in 25 ($p < 0.01$), 26 ($p < 0.001$), and 27 G

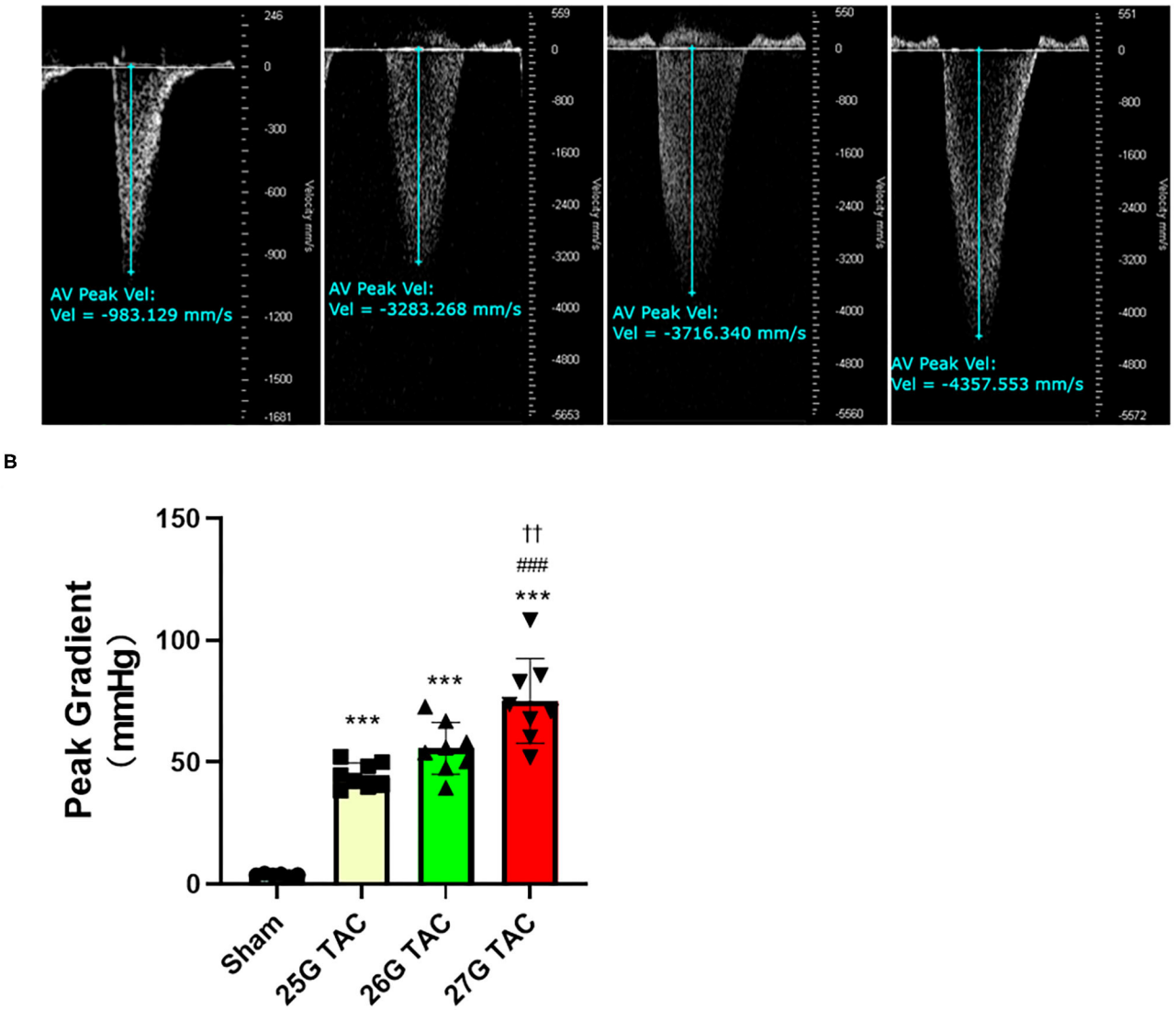

FIGURE 1 | Aortic pressure gradients following 1 week of TAC. **(A)** Representative pulsed wave Doppler images for sham, 25, 26, and 27 G TAC mice after 1 week. **(B)** Peak pressure gradients calculated from Doppler velocities after 1 week of TAC. $^{***}P < 0.001$ vs. sham, $^{\#\#\#}P < 0.001$ vs. 25 G TAC, $^{\dagger\dagger}P < 0.01$ vs. 26 G TAC by one-way ANOVA with Tukey's post-test.

TAC mice ($p < 0.001$) compared with sham mice (**Figures 2E,F**). Among the TAC mice, the HW/TL in 27 G TAC was significantly higher than that in 26 ($p < 0.05$) and 25 G TAC ($p < 0.001$); however, there was no significant difference between 25 and 26 G TAC. Accordingly, the cardiomyocyte area was significantly increased in 27 ($P < 0.001$) and 26 G TAC ($P < 0.05$) compared with sham mice, but the significant difference was absent in 25 G mice compared with sham mice (**Figures 2G,H**). What's more, the cardiomyocyte area in 27 G TAC mice was significantly larger than that in 25 ($p < 0.001$) and 26 G TAC mice ($p < 0.05$).

We also examined the expression of hypertrophic genes. Our results show that atrial natriuretic peptide (ANP) and B-type natriuretic peptides (BNP) gene expression was significantly increased in 25, 26, and 27 G TAC mice compared with sham mice, and the ANP and BNP gene expression in 27 G TAC was significantly higher than that in 26 and 25 G TAC; however, there was no significant difference between 25 and 26 G TAC (**Figures 2I,J**).

Taken together, these results show that 25, 26, and 27 G TAC successfully induced different degrees of cardiac hypertrophy.

Cardiac Function

To test the cardiac function change induced by different degrees of constriction in the TAC surgery, LV structure and systolic

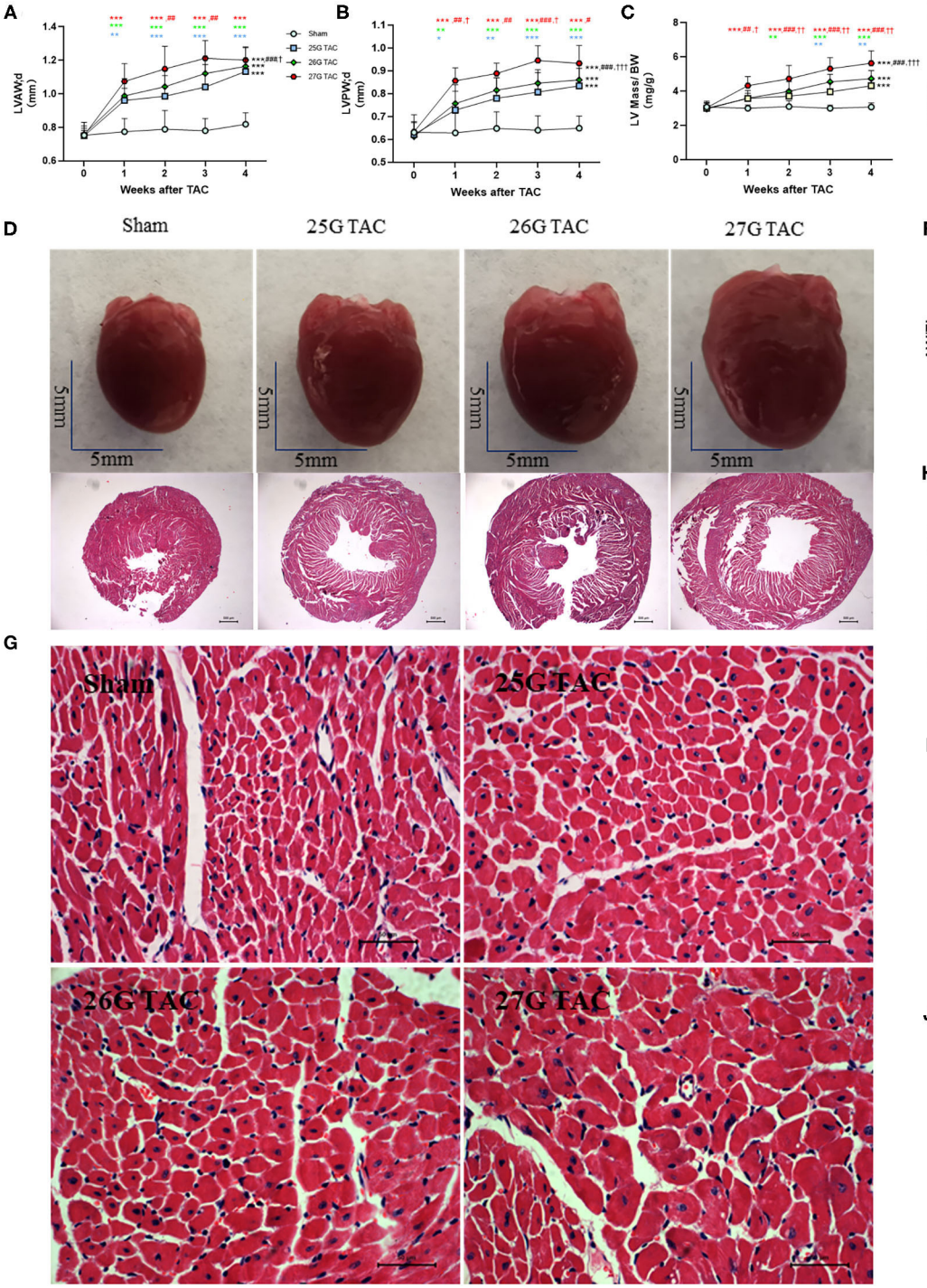

FIGURE 2 | 25, 26, and 27 G TAC induced different degrees of cardiac hypertrophy in C57BL/6N mice. The echocardiography-derived results of **(A)** the LVAW thickness, **(B)** LVPW thickness, and **(C)** LV mass normalized to body weight. **(D)** Representative heart pictures for sham, 25, 26, and 27 G TAC mice after 4 weeks of TAC and representative images of H&E staining of cross-heart sections; scale bars 500 um. **(E)** HW/TL and **(F)** AW/TL in sham, 25, 26, and 27 G TAC mice after 4 weeks of TAC. **(G)** Representative LV sections stained with H&E and DAPI (blue) for assessment of cardiomyocyte area. Scale bar= 50 μm. **(H)** Quantification of cardiomyocyte area. **(I,J)** RT-PCR analysis of ANP and BNP mRNA. $^{*}P < 0.05$, $^{**}P < 0.01$, and $^{***}P < 0.001$ vs. sham, $^{\#}P < 0.05$, $^{\#\#}p < 0.01$, $^{\#\#\#}p < 0.001$ vs. 25 G, $^{\dagger}P < 0.05$, $^{\dagger\dagger}P < 0.01$, and $^{\dagger\dagger\dagger}P < 0.001$ vs. 26 G TAC, TAC by two- **(A–C)** or one-way ANOVA **(E,F,H)** with Tukey's post-test. Colored symbols **(A–C)** indicate $^{*}P < 0.05$, $^{**}P < 0.01$, and $^{***}P < 0.001$ vs. sham, $^{\#}P < 0.05$, $^{\#\#}p < 0.01$, $^{\#\#\#}p < 0.001$ vs. 25 G, $^{\dagger}P < 0.05$, $^{\dagger\dagger}P < 0.01$ vs. 26 G TAC at the time point indicated.

function were analyzed presurgery and at 1, 2, 3, and 4 weeks after TAC surgery by using echocardiography. M-Mode analysis in the parasternal long axis detected a progressive decline in systolic function for mice subjected to 27 and 26 G TAC surgery from 2 to 4 weeks after TAC. There was a mild increasing trend at 1 week after TAC; however, there was no significant change in systolic function for mice subjected to 25 G TAC compared with sham mice (**Figures 3A–C**). The ejection fraction (EF) in 27 G TAC mice was significantly decreased at 3 weeks after TAC compared with sham mice, whereas this significant difference emerged in 26 G TAC mice at 4 weeks after TAC (**Figure 3B**). Importantly, the EF in 27 G TAC mice was much lower than that in 26 G TAC mice ($p < 0.01$) and in 25 G TAC mice ($p < 0.001$). Similar results were observed for the fractional shortening (FS) (**Figure 3C**). We also detected the end-diastolic LV diameter and volume, which are important parameters for LV dilation and cardiac dysfunction.

The end-diastolic LV diameter in mice subjected 27 G TAC was significantly decreased at 1 week after TAC surgery compared with sham mice and then progressively increased from 2 to 4 weeks after TAC and emerged with a significant difference at 4 weeks ($p < 0.05$) after TAC compared with sham mice (**Figure 3D**). Although the end-diastolic LV diameter in mice subjected to 26 G TAC had an increasing trend from 2 to 4 weeks after TAC, there was no statistically significant difference compared with sham mice. However, compared with 25 G TAC mice, the end-diastolic LV diameter in 27 G TAC mice was significantly higher at 3 weeks ($p < 0.01$) and 4 weeks ($p < 0.01$) after TAC. We observed similar results for the end-diastolic LV volume (**Figure 3E**). We also did the survival analysis after TAC surgery (**Figure 3F**). The mice subjected to 25 G TAC had 100% survival within 4 weeks after TAC, whereas one of eight mice (12.5%) subjected to 26 G TAC and two of eight mice (25%) subjected to 27 G TAC died 3–4 weeks after TAC. Moreover, we also analyzed the LW/TL to evaluate HF at 4 weeks after TAC (**Figure 3G**). The LW/TL was significantly increased in the mice subjected to 27 G TAC compared with sham mice ($p < 0.001$), 25 G TAC mice ($p < 0.001$), and 26 G TAC mice ($p < 0.001$). Although there was no statistically significant difference in LW/TL for 25 and 26 G TAC compared with sham, the LW/TL slightly increased 4.3 and 9.7% in 25 and 26 G TAC mice compared with sham mice, respectively.

Cardiac Fibrosis

To test the cardiac fibrosis induced by different degrees of constriction in TAC surgery in mice, Masson's trichrome staining was applied to heart tissue paraffin sections. Compared with sham mice, mice subjected to 25 ($p < 0.01$), 26 ($p < 0.001$), and 27 G TAC ($p < 0.001$) developed significant cardiac fibrosis (**Figures 4A,B**). Importantly, mice subjected to 27 G TAC had much severer cardiac fibrosis than in 25 ($p < 0.001$) and 26 G TAC mice ($p < 0.001$). Accordingly, we observed similar results from the analysis of heart tissue fibrosis gene expression. The col-1, col-3, and TGF-β gene expression in 27 G TAC mice was significantly increased compared with sham mice, and the col-1 and TGF-β gene expression in 26 G mice were significantly increased compared with sham mice (**Figures 4C–E**). The col-1 and TGF-β gene expression in 27 G TAC mice was significantly higher than that in 25 and 26 G TAC mice. We got similar results from analysis of col-1 and TGF-β protein expression (**Figures 4F–H**); the protein expression of col-1 and TGF-β in 27 G TAC mice was significantly higher than in 25 and 26 G TAC mice. Although not all data showed a significantly difference, the fibrosis gene expression showed a gradually increasing trend in the order of sham mice, 25 G TAC mice, 26 G TAC mice, and 27 G TAC mice.

DISCUSSION

In the present study, we directly compared the different cardiac remodeling phenotypes induced by different degrees of LV pressure overload in C57BL/6N mice. Specifically, we analyzed the different phenotypes induced by 25, 26, and 27 G TAC in c57BL/6N mice in terms of pressure gradient, cardiac hypertrophy, cardiac function, HF situation, survival condition, and cardiac fibrosis. All C57BL/6N mice subjected to TAC surgery developed significant hypertrophy. Mice subjected to 27 G TAC experienced a compensatory period to decompensatory period over 4 weeks after TAC, and 27 G TAC mice had severe cardiac dysfunction, severe cardiac fibrosis, and exhibited characteristics of heart failure at 4 weeks post-TAC. Whereas, mice subjected to 26 G TAC showed a much milder response in cardiac dysfunction, cardiac fibrosis compared to 27 G TAC, and a very small fraction of 26 G TAC mice exhibited characteristics of HF, which means 26 G TAC caused the transition from the LV hypertrophy to an early phase of cardiac dysfunction and HF in C57BL/6N mice. However, except for significant cardiac hypertrophy, there was no obvious cardiac dysfunction, cardiac fibrosis, and characteristics of HF observed in 25 G TAC mice. Based on our results, we conclude that the 25, 26, and 27 G TAC induced distinct phenotypes in C57BL/6N mice.

TAC surgery is one of the most popular pressure overload models for studying cardiac hypertrophy and cardiac remodeling, and it has been widely used and modified to be less invasive since it was first reported in 1991 (4, 6–9, 17, 18). There are many factors that affect the phenotype of TAC-induced cardiac remodeling, among which the constriction degree is the most important one. Besides this, species of animals, age, sex, and genetic background also affect the phenotype variability of TAC-induced cardiac remodeling. The widely phenotypic difference reported with this model has raised the question of how we can choose the proper condition of TAC surgery in a specific study. Unfortunately, very few studies focus on the direct comparison of different cardiac remodeling phenotypes induced by 25, 26, and 27 G TAC, and no one has compared this difference in C57BL/6N mice. C57BL/6N and C57BL/6J mice are two of the most commonly used C57BL/6 substrains, and they have been widely used as genetic background transgenic and gene knockout mice. Michelle and colleagues conducted a comparative phenotypic and genomic analysis of C57BL/6J and C57BL/6N mouse strains, and annotated 34 SNPs and two indels that distinguish C57BL/6J and C57BL/6N coding sequences (19).

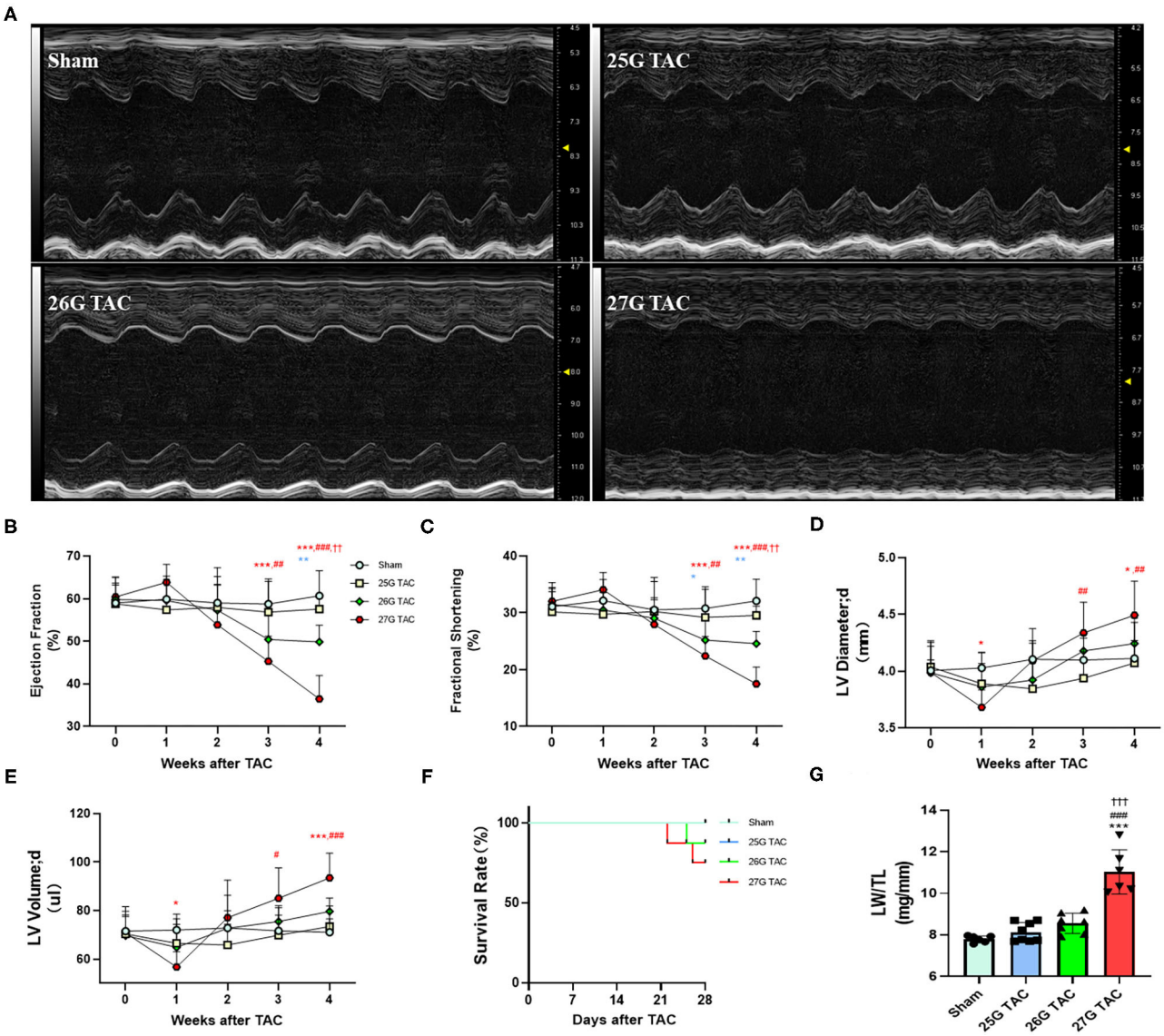

FIGURE 3 | 25, 26, and 27 G TAC induced different degrees of reduction of cardiac function in C57BL/6N mice. The echocardiography-derived results of **(A)** representative images of M-Mode images after 4 weeks of TAC show systolic dysfunction, **(B)** EF, **(C)** FS, **(D)** the end-diastolic LV diameter, and **(E)** the end-diastolic LV volume. **(F)** Kaplan–Meier survival curves. **(G)** LW/TL. $^{***}P < 0.001$ vs. sham, $^{###}p < 0.001$ vs. 25 G, $^{†††}P < 0.001$ vs. 26 G TAC by two- **(B–E)** or one-way ANOVA **(G)** with Tukey's post-test. Colored symbols **(A–C)** indicate $^{*}P < 0.05$, $^{**}P < 0.01$, and $^{***}P < 0.001$ vs. sham, $^{\#}P < 0.05$, $^{\#\#}p < 0.01$, $^{\#\#\#}p < 0.001$ vs. 25 G, $^{††}P < 0.01$ vs. 26 G TAC at the time point indicated.

Besides this, it is reported that there are phenotypic differences between C57BL/6J and C57BL/6N in many disease models, such as the diet-induced type 2 diabetes model (20), the non-alcoholic steatohepatitis model (21), influenza a virus induced inflammation-associated disease (22), and postnatal hypoxic-ischemic brain injury mouse model (23) as well as pressure overload–induced cardiac hypertrophy (24). Lorena and colleagues found that cardiac response to pressure overload is distinct between C57BL/6J and C57BL/6N mice, and the survival and cardiac function are significantly lower in C57BL/6N mice compared with C57BL/6J (24). However, to our knowledge, a direct comparison of pressure gradient, cardiac hypertrophy, cardiac function, and cardiac fibrosis phenotype changes among the 25, 26, and 27 TAC-induced cardiac remodeling have not been reported.

Cardiac hypertrophy is the consequence of the heart's response to a variety of extrinsic and intrinsic stimuli, which impose increased biomechanical stress (25). Initially, the development of hypertrophy is a compensatory mechanism, and contractile function is maintained. However, when the heart is subjected to excessive and/or persistent stress, cardiac function becomes maladaptive and decompensatory, eventually

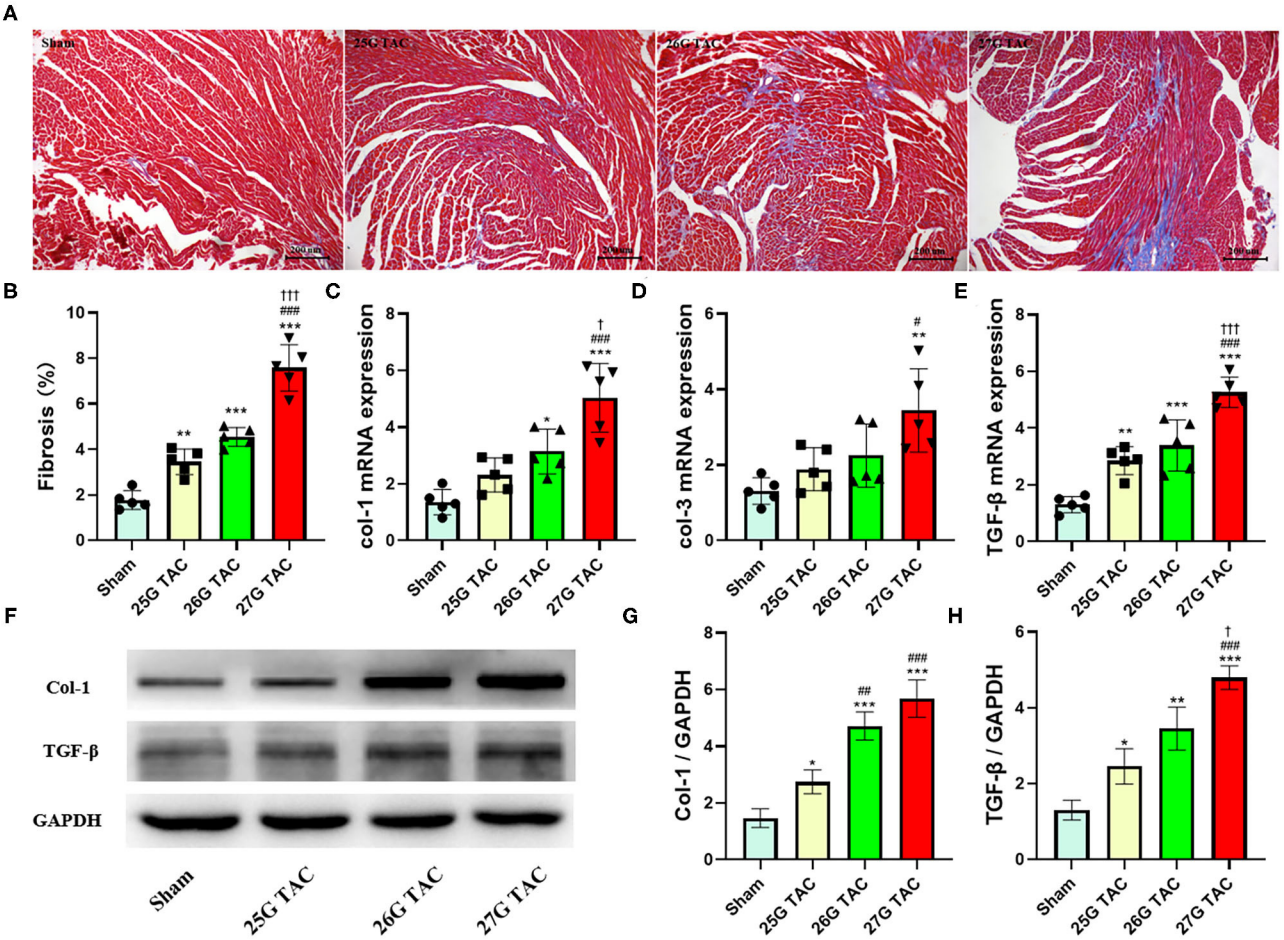

FIGURE 4 | 25, 26, and 27 G TAC induced different degrees of cardiac fibrosis in C57BL/6N mice. **(A)** Representative images for cardiac fibrosis. **(B)** Quantification of cardiac fibrosis. Apical left ventricular gene expression of **(C)** col-1, **(D)** col-3, **(E)** TGF-β. **(F–H)** Western blot analysis of col-1 and TGF-β. $^{*}P < 0.05$, $^{**}P < 0.01$, and $^{***}P < 0.001$ vs. sham, $^{\#}P < 0.05$, $^{\#\#}p < 0.01$, $^{\#\#\#}p < 0.001$ vs. 25 G, $^{\dagger}P < 0.05$, $^{\dagger\dagger\dagger}P < 0.001$ vs. 26 G TAC by one-way ANOVA with Tukey's post-test.

leading to HF (26). Constriction degree is an important factor that affects the development process of pressure overload–induced cardiac remodeling. In the present study, we directly compared the phenotypes of cardiac remodeling induced by 25, 26, and 27 G TAC in C57BL/6N mice. We found that mice subjected to 27 G TAC surgery had a short increasing trend of cardiac function at 1 week after TAC, then the cardiac function continuously decreased from 2 weeks after TAC surgery, and eventually developed HF characterized by significantly decreased cardiac function, significantly increased lung mass and atrial weight, and more mortality at 4 weeks after TAC. This data indicated that mice subjected to 27 G TAC surgery experienced both compensatory-phase and decompensatory-phase cardiac hypertrophy, which suggests 27 G TAC surgery in C57BL/6N mice is extremely useful in both mechanistic and drug studies aiming to improve or reverse the cardiac dysfunction in a pressure overload–induced heart failure model. Compared with 27 G TAC mice, mice subjected to 26 G TAC surgery had less cardiac dysfunction and only a very small fraction of mice showed signs of HF at 4 weeks after TAC surgery, which indicated that 26 G TAC mice were at the transition stage between compensated and decompensated heart failure. In this situation, adverse cardiac remodeling was still observed, but the mortality can be maintained at a low level, which probably makes 26 G TAC surgery more useful on the mice with more susceptibility to mortality, such as genetically modified mice. In contrast, mice subjected to 25 G TAC surgery were still at the compensatory cardiac hypertrophy stage without cardiac dysfunction and HF. Therefore, the 25 G TAC model could be very useful for studying hypertensive heart disease in mice.

Cardiac fibrosis is defined as the deposition of extracellular matrix proteins in the cardiac interstitium, and interstitial fibrosis plays an important role in the development and progression of HF via causing adverse electrical and mechanical disturbances in diseased hearts (27). Pressure overload–induced cardiac hypertrophy is invariably accompanied by the formation of cardiac fibrosis (28), and this cardiac fibrosis alters myocardial stiffness and consequently affects myocardial function, which

plays a major role in the progressive decompensation of the cardiac dysfunction (29, 30). Here, we also analyzed the cardiac fibrosis difference in C57BL/6N mice subjected to 25, 26, and 27 G TAC surgery. Mice subjected to 27 G TAC had severe cardiac fibrosis confirmed by the analysis of Masson's trichrome staining and fibrosis-related gene expression. Compared with 27 G TAC mice, the cardiac fibrosis in 26 G TAC mice was much milder. Although there was slight cardiac fibrosis in 25 G TAC mice, there was not much difference compared with sham mice. The cardiac fibrosis is consistent with the cardiac function changes in 25, 26, and 27 G TAC mice, respectively, which confirms the importance of cardiac fibrosis in the development and progression of HF.

The present study provides a comprehensive analysis of distinct phenotypes induced by 25, 26, and 27 G TAC surgery in C57BL/6N mice. However, there are still some limitations in the current study. First, all mice used in the present study were male C57BL/6N mice aged 10 weeks although the cardiac remodeling phenotypes induced by TAC surgery are affected by the sex and age of animals; therefore, the results in the present study may not apply to female or different age mice. Given the consideration of most previously published papers, we chose to focus our study within 4 weeks after TAC surgery although we got distinct phenotypes from 25, 26, and 27 G TAC mice at this time point in terms of cardiac hypertrophy, cardiac function, and cardiac fibrosis; however, we did not analyze the phenotype changes among the different degree TAC over 4 weeks after TAC, so whether these distinct phenotypes among the three different degrees of TAC group are magnified or blunted more than 4 weeks after TAC is still unknown. In addition, the mice subjected to 25 G TAC surgery in current study were still at the compensatory cardiac hypertrophy stage, so we have no idea about the specific timeline for the development of pressure overload–induced heart failure in 25 G TAC mice, and this question should be addressed in the future study.

In summary, in the present study, we directly compared the different phenotypes induced by 25, 26, and 27 G TAC surgery in the aspects of pressure gradient, cardiac hypertrophy, cardiac function, and HF and cardiac fibrosis. Importantly, this is the first time to conduct such a study in C57BL/6N mice, and our results will provide important reference value especially for researchers who conduct pressure overload–induced cardiac hypertrophy studies using C57BL/6N mice or genetically modified mice with a C57BL/6N background.

DATA AVAILABILITY STATEMENT

The original contributions presented in the study are included in the article/**Supplementary Material**, further inquiries can be directed to the corresponding author/s.

ETHICS STATEMENT

The animal study was reviewed and approved by Animal Care and Use Committee of Fudan University.

AUTHOR CONTRIBUTIONS

HD and L-LM performed the experiments and analyzed the data. HD wrote the manuscript. F-JK and ZQ designed and supervised the study and revised the manuscript. All authors contributed to the article and approved the submitted version.

FUNDING

This work was supported by Science and Technology Commission of Shanghai Municipality (19JC1415704), the Medical Research Project of Shanghai Xuhui District (SHXH201836), Clinical research project of health industry of Shanghai Municipal Health Commission (20194Y0181), and National Natural Science Foundation of China (81870290).

SUPPLEMENTARY MATERIAL

The Supplementary Material for this article can be found online at: https://www.frontiersin.org/articles/10.3389/fcvm.2021.641272/full#supplementary-material

Supplementary Figure 1 | Western blot analysis of p-Erk. **(A)** Representative images for p-Erk, t-Erk, and GAPDH. **(B)** Quantification of p-Erk/t-Erk. $^{*}P < 0.05$, $^{***}P < 0.001$ vs. sham, $^{\#\#}P < 0.01$, $^{\#\#\#}p < 0.001$ vs. 25 G, $^{\dagger\dagger}P < 0.01$ vs. 26 G TAC by one-way ANOVA with Tukey's post-test.

REFERENCES

1. Benjamin EJ, Muntner P, Alonso A, Bittencourt MS, Callaway CW, Carson AP, et al. Heart disease and stroke statistics-2019 update: a report from the American Heart Association. *Circulation.* (2019) 139:e56–28. doi: 10.1161/CIR.0000000000000659
2. Frantz S, Bauersachs J, Ertl G. Post-infarct remodelling: contribution of wound healing and inflammation. *Cardiovasc Res.* (2009) 81:474–81. doi: 10.1093/cvr/cvn292
3. Opie LH, Commerford PJ, Gersh BJ, Pfeffer MA. Controversies in ventricular remodelling. *Lancet*. (2006) 367:356–67. doi: 10.1016/S0140-6736(06)68074-4
4. Wang X, Ye Y, Gong H, Wu J, Yuan J, Wang S, et al. The effects of different angiotensin II type 1 receptor blockers on the regulation of the ACE-AngII-AT1 and ACE2-Ang(1-7)-Mas axes in pressure overload-induced cardiac remodeling in male mice. *J Mol Cell Cardiol.* (2016) 97:180–90. doi: 10.1016/j.yjmcc.2016.05.012
5. Yu Y, Hu Z, Li B, Wang Z, Chen S. Ivabradine improved left ventricular function and pressure overload-induced cardiomyocyte apoptosis in a transverse aortic constriction mouse model. *Mol Cell Biochem.* (2019) 450:25–34. doi: 10.1007/s11010-018-3369-x
6. Rockman HA, Ross RS, Harris AN, Knowlton KU, Steinhelper ME, Field LJ, et al. Segregation of atrial-specific and inducible expression of an atrial natriuretic factor transgene in an in vivo murine model of cardiac hypertrophy. *Proc Natl Acad Sci USA*. (1991) 88:8277–81. doi: 10.1073/pnas.88.18.8277
7. Eichhorn L, Weisheit CK, Gestrich C, Peukert K, Duerr GD, Ayub MA, et al. A closed-chest model to induce transverse aortic constriction in mice. *J Vis Exp*. (2018) e57397. doi: 10.3791/57397
8. Tavakoli R, Nemska S, Jamshidi P, Gassmann M, Frossard N. Technique of minimally invasive transverse aortic constriction in mice for induction of left ventricular hypertrophy. *J Vis Exp*. (2017) 56231. doi: 10.3791/56231
9. Zaw AM, Williams CM, Law HK, Chow BK. Minimally invasive transverse aortic constriction in mice. *J Vis Exp*. (2017) 55293. doi: 10.3791/55293

10. Bosch L, de Haan JJ, Bastemeijer M, van der Burg J, van der Worp E, Wesseling M, et al. The transverse aortic constriction heart failure animal model: a systematic review and meta-analysis. *Heart Fail Rev*. (2020). doi: 10.1007/s10741-020-09960-w. [Epub ahead of print].
11. Calamaras TD, Baumgartner RA, Aronovitz MJ, McLaughlin AL, Tam K, Richards DA, et al. Mixed lineage kinase-3 prevents cardiac dysfunction and structural remodeling with pressure overload. *Am J Physiol Heart Circ Physiol.* (2019) 316:H145–59. doi: 10.1152/ajpheart.00029.2018
12. Liu Y, Chien WM, Medvedev IO, Weldy CS, Luchtel DL, Rosenfeld ME, et al. Inhalation of diesel exhaust does not exacerbate cardiac hypertrophy or heart failure in two mouse models of cardiac hypertrophy. *Part Fibre Toxicol.* (2013) 10:49. doi: 10.1186/1743-8977-10-49
13. Furihata T, Kinugawa S, Takada S, Fukushima A, Takahashi M, Homma T, et al. The experimental model of transition from compensated cardiac hypertrophy to failure created by transverse aortic constriction in mice. *Int J Cardiol Heart Vasc.* (2016) 11:24–8. doi: 10.1016/j.ijcha.2016.03.007
14. Hu P, Zhang D, Swenson L, Chakrabarti G, Abel ED, Litwin SE. Minimally invasive aortic banding in mice: effects of altered cardiomyocyte insulin signaling during pressure overload. *Am J Physiol Heart Circ Physiol*. (2003). 285:H1261–9. doi: 10.1152/ajpheart.00108.2003
15. Wu J, Bu L, Gong H, Jiang G, Li L, Ma H, et al. Effects of heart rate and anesthetic timing on high-resolution echocardiographic assessment under isoflurane anesthesia in mice. *J Ultrasound Med.* (2010) 29:1771–8. doi: 10.7863/jum.2010.29.12.1771
16. Mohammed SF, Storlie JR, Oehler EA, Bowen LA, Korinek J, Lam CS, et al. Variable phenotype in murine transverse aortic constriction. *Cardiovasc Pathol.* (2012) 21:188–98. doi: 10.1016/j.carpath.2011.05.002
17. Martin TP, Robinson E, Harvey AP, MacDonald M, Grieve DJ, Paul A, et al. Surgical optimization and characterization of a minimally invasive aortic banding procedure to induce cardiac hypertrophy in mice. *Exp Physiol.* (2012) 97:822–32. doi: 10.1113/expphysiol.2012.065573
18. Schnelle M, Catibog N, Zhang M, Nabeebaccus AA, Anderson G, Richards DA, et al. Echocardiographic evaluation of diastolic function in mouse models of heart disease. *J Mol Cell Cardiol.* (2018) 114:20–8. doi: 10.1016/j.yjmcc.2017.10.006
19. Simon MM, Greenaway S, White JK, Fuchs H, Gailus-Durner V, Wells S, et al. A comparative phenotypic and genomic analysis of C57BL/6J and C57BL/6N mouse strains. *Genome Biol.* (2013) 14:R82. doi: 10.1186/gb-2013-14-7-r82
20. Rendina-Ruedy E, Hembree KD, Sasaki A, Davis MR, Lightfoot SA, Clarke SL, et al. A comparative study of the metabolic and skeletal response of C57BL/6J and C57BL/6N mice in a diet-induced model of type 2 diabetes. *J Nutr Metab.* (2015) 2015:758080. doi: 10.1155/2015/758080
21. Kawashita E, Ishihara K, Nomoto M, Taniguchi M, Akiba S. A comparative analysis of hepatic pathological phenotypes in C57BL/6J and C57BL/6N mouse strains in non-alcoholic steatohepatitis models. *Sci Rep.* (2019) 9:204. doi: 10.1038/s41598-018-36862-7
22. Eisfeld AJ, Gasper DJ, Suresh M, Kawaoka Y. C57BL/6J and C57BL/6NJ mice are differentially susceptible to inflammation-associated disease caused by influenza A virus. *Front Microbiol.* (2018) 9:3307. doi: 10.3389/fmicb.2018.03307
23. Wolf S, Hainz N, Beckmann A, Maack C, Menger MD, Tschernig T, et al. Brain damage resulting from postnatal hypoxic-ischemic brain injury is reduced in C57BL/6J mice as compared to C57BL/6N mice. *Brain Res.* (2016) 1650:224–31. doi: 10.1016/j.brainres.2016.09.013
24. Garcia-Menendez L, Karamanlidis G, Kolwicz S, Tian R. Substrain specific response to cardiac pressure overload in C57BL/6 mice. *Am J Physiol Heart Circ Physiol.* (2013) 305:H397–402. doi: 10.1152/ajpheart.00088.2013
25. Frey N, Olson EN. Cardiac hypertrophy: the good, the bad, and the ugly. *Annu Rev Physiol.* (2003) 65:45–79. doi: 10.1146/annurev.physiol.65.092101.142243
26. Osterholt M, Nguyen TD, Schwarzer M, Doenst T. Alterations in mitochondrial function in cardiac hypertrophy and heart failure. *Heart Fail Rev.* (2013) 18:645–56. doi: 10.1007/s10741-012-9346-7
27. Schelbert EB, Fonarow GC, Bonow RO, Butler J, Gheorghiade M. Therapeutic targets in heart failure: refocusing on the myocardial interstitium. *J Am Coll Cardiol.* (2014) 63:2188–98. doi: 10.1016/j.jacc.2014.01.068
28. Houser SR, Piacentino V III, Weisser J. Abnormalities of calcium cycling in the hypertrophied and failing heart. *J Mol Cell Cardiol.* (2000) 32:1595–607. doi: 10.1006/jmcc.2000.1206
29. Weber KT, Brilla CG. Pathological hypertrophy and cardiac interstitium. Fibrosis and renin-angiotensin-aldosterone system. *Circulation*. (1991) 83:1849–65. doi: 10.1161/01.CIR.83.6.1849
30. Weber KT, Janicki JS, Shroff SG, Pick R, Chen RM, Bashey RI. Collagen remodeling of the pressure-overloaded, hypertrophied nonhuman primate myocardium. *Circ Res.* (1988) 62:757–65. doi: 10.1161/01.RES.62.4.757

Conflict of Interest: The authors declare that the research was conducted in the absence of any commercial or financial relationships that could be construed as a potential conflict of interest.

frontiers in Cardiovascular Medicine

ORIGINAL RESEARCH
published: 11 May 2021
doi: 10.3389/fcvm.2021.627741

Trends in Prevalence of Hypertension and Hypertension Phenotypes Among Chinese Children and Adolescents Over Two Decades (1991–2015)

Xinxin Ye[1†], Qian Yi[1†], Jing Shao[2], Yan Zhang[3], Mingming Zha[4], Qingwen Yang[4], Wei Xia[5], Zhihong Ye[2] and Peige Song[1,6]*

[1] School of Public Health, Zhejiang University School of Medicine, Zhejiang University, Hangzhou, China, [2] School of Nursing, Zhejiang University School of Medicine, Zhejiang University, Hangzhou, China, [3] Faculty of Life Science and Medicine, Kings College London, London, United Kingdom, [4] Medical School Southeast University, Nanjing, China, [5] School of Nursing, Sun Yat-Sen University, Guangdong, China, [6] Women's Hospital, Zhejiang University School of Medicine, Zhejiang University, Hangzhou, China

OPEN ACCESS

Edited by:
Soo-Kyoung Choi,
Yonsei University College of Medicine, South Korea

Reviewed by:
Jane A. Leopold,
Brigham and Women's Hospital and Harvard Medical School, United States
Yi Song,
Peking University, China
Zhiyong Zou,
Peking University, China

***Correspondence:**
Peige Song
peigesong@zju.edu.cn

[†]These authors have contributed equally to this work

Specialty section:
This article was submitted to Hypertension, a section of the journal Frontiers in Cardiovascular Medicine

Received: 10 November 2020
Accepted: 08 April 2021
Published: 11 May 2021

Citation:
Ye X, Yi Q, Shao J, Zhang Y, Zha M, Yang Q, Xia W, Ye Z and Song P (2021) Trends in Prevalence of Hypertension and Hypertension Phenotypes Among Chinese Children and Adolescents Over Two Decades (1991–2015). Front. Cardiovasc. Med. 8:627741. doi: 10.3389/fcvm.2021.627741

Background: Hypertension is a leading cause of cardiovascular-related morbidity and mortality. Elevated blood pressure (BP) in children is related to long-term adverse health effects. Until recently, few studies have reported the secular trend and associated factors of hypertension phenotypes in Chinese children and adolescents.

Methods: From the China Health and Nutrition Survey (CHNS) 1991–2015, a total of 15,143 records of children aged 7–17 years old were included. Following definitions of hypertension from the Chinese Child Blood Pressure References Collaborative Group, we estimated the prevalence of prehypertension, hypertension, stage 1 hypertension, stage 2 hypertension and its phenotypes (ISH, isolated systolic hypertension; IDH, isolated diastolic hypertension; SDH, combined systolic and diastolic hypertension). General estimation equation was used to analyze the trends in the prevalence of hypertension and hypertension phenotypes, and a multivariable logistic regression was constructed to explore the associated factors.

Results: During 1991–2015, increasing trends were revealed in BP and hypertension prevalence ($P < 0.001$) in Chinese children and adolescents. For ISH, IDH and SDH, the age-standardized prevalence increased dramatically from 0.9 to 2.2%, from 6.2 to 14.1%, and from 1.4 to 2.9%, respectively (all $P < 0.001$). Adolescents aged 13–17 years (OR = 1.76, 95% CI: 1.56–1.97, $P < 0.001$), general obesity (OR = 2.69, 95% CI: 2.10-3.44, $P < 0.001$) and central obesity (OR = 1.49, 95% CI: 1.21–1.83, $P < 0.001$) were positively associated with hypertension, whereas the South region (OR = 0.65, 95% CI: 0.58–0.73, $P < 0.001$) was a negative factor. Furthermore, body mass index (BMI) and general obesity were linked to the presence of ISH, IDH and SDH. Age, waist circumference (WC) and central obesity were additionally associated with ISH, and sex, age, urban/rural setting, North/South region, WC and central obesity were additionally associated with IDH.

Conclusion: BP levels and prevalence of hypertension and phenotypes increased dramatically in Chinese children and adolescents from 1991 to 2015. Regional discrepancy, demographic features, BMI, WC and overweight/obesity status were associated factors of hypertension among youths.

Keywords: hypertension, hypertension phenotypes, China, children, adolescents, trends

INTRODUCTION

Hypertension, or elevated blood pressure (BP), is a highly prevalent chronic disease globally. Hypertension has been recognized as a primary modifiable contributor to cardiovascular and cerebrovascular diseases (1). In China, hypertension affects more than 270 million people, emerging as a major public health challenge (2–4). It was estimated that the direct costs caused by hypertension reached 210.3 billion Yuan in 2013, accounting for 6.61% of the total Chinese health-care expenditure (5). Hypertension is not a disorder that confines to adults, globally, millions of children were suffering from hypertension (6). Pathophysiologic and epidemiologic evidence has shown an association between childhood hypertension and long-term adverse health effects (7).

Unlike adulthood hypertension, whose definition has been upgraded to a universally diagnostic standard, the measurement of childhood hypertension is comparatively complicated (8). The cutoffs of childhood hypertension have been suggested as a systolic blood pressure (SBP) or a diastolic blood pressure (DBP) equal to or higher than 95th percentile by age, sex, and height (9). According to the fourth report from the National High Blood Pressure Education Program (NHBPEP) Working Group in the United States, BP in children and adolescents was suggested to be measured on at least three separate occasions at an interval of 2 weeks due to the apparent fluctuations (10). In 2017, the American Academy of Pediatrics (AAP) guidelines recommended the use of ambulatory BP monitoring in the diagnosis and management of hypertension in children (11).

China is the largest developing country across the world, where the emergence of hypertension has brought a heavy burden to the whole country (8, 10, 12, 13). A cohort study in China revealed that the hypertension prevalence was 17.00% in boys and 14.13% in girls aged 7–17 years (14), and it ranged from 5.2 to 7.8% in Italy among school-aged children (15, 16). Several previous studies have focused on the prevalence of hypertension, whereas studies on trends in different hypertension phenotypes were limited in China. Early identification of different hypertension phenotypes in youth is of significant importance in preventing cardiovascular events in adulthood (17). Compared with previous studies, we extended the study period to 1991–2015. We additionally assessed the prevalence of hypertension severity (stage one hypertension and stage two hypertension) and phenotypes (ISH, isolated systolic hypertension; IDH, isolated diastolic hypertension; SDH, systolic and diastolic hypertension) by age and sex, and explored the effects of demographic, geographic, anthropometric factors and obesity on childhood hypertension in China.

We herein hypothesized that the prevalence of hypertension and hypertension phenotypes in children increased gradually with years; the secular trends in childhood hypertension prevalence differed by age, sex, locations, and region; demographic, anthropometric, geographic factors, and general/central obesity were independently associated with increased BP and hypertension phenotypes in Chinese children and adolescents.

MATERIALS AND METHODS

Study Design and Study Population

Details about the study design of CHNS are available elsewhere (18, 19). In brief, CHNS is a longitudinal health and nutrition survey in China, beginning in 1989 and having been continuously conducted every 2 or 4 years. So far, CHNS has been conducted for 10 rounds (1989, 1991, 1993, 1997, 2000, 2004, 2006, 2009, 2011, and 2015) and covered a set of large provinces across China (the list and locations of investigated provinces are shown in **Supplementary Table 1** and **Supplementary Figure 1**). In each round, a multistage random-cluster sampling method was adopted to ensure a good representative of the general Chinese population. First, all counties and cities in each province were stratified into three groups (low-, middle- and high-income). Then, four counties (one low-, two middle-, and one high-income county) and two cities (usually the provincial capital and a lower-income city) were randomly selected. Third, one community and three rural villages within each selected county and two communities and two suburban villages within each selected city were randomly chosen. In each community or village, all members of 20 households were randomly selected (18, 19). A total of 15,143 records (7,423 subjects) aged 7–17 years old with complete data from 1991 to 2015 were included in this study, and the number of participants who participated twice or more was 4,865. The sample sizes of the nine rounds were 2,429 in 1991, 2,254 in 1993, 2,254 in 1997, 2,217 in 2000, 1,364 in 2004, 1,145 in 2006, 1,012 in 2009, 1,404 in 2011 and 1,064 in 2015 (the excluded and included records are shown in **Table 1**). CHNS was approved by the Institutional Review Committees of the University of North Carolina at Chapel Hill, the National Institute of Nutrition and Food Safety, the Chinese Center for Disease Control and Prevention, and the China-Japan Friendship Hospital, Ministry of Health. All respondents signed informed consent.

Data Collection

Data on demographics (age and sex) and geographic location (urban/rural and North/South region) were collected by trained interviewers using a structured questionnaire. BP, weight, height,

TABLE 1 | Comparison of demographic characteristics between the excluded and included subjects in CHNS 1991–2015.

Characteristic	1991–2015 combined			1991			1993			1997			2000		
	Excluded 3,460	Included 15,143	*p* value	Excluded 508	Included 2,429	*P* value	Excluded 527	Included 2,254	*p* value	Excluded 622	Included 2,254	*p* value	Excluded 660	Included 2,217	*P* value
AGE GROUP															
7–12 years	1,526 (44.10%)	8,783 (58.00%)	<0.001	229 (45.08%)	1,335 (54.96%)	<0.001	246 (46.68%)	1,285 (57.01%)	<0.001	271 (43.57%)	1,358 (60.25%)	<0.001	207 (31.36%)	1,207 (54.44%)	<0.001
13–17 years	1,934 (55.90%)	6,360 (42.00%)		279 (54.92%)	1,094 (45.04%)		281 (53.32%)	969 (42.99%)		351 (56.43%)	896 (39.75%)		453 (68.64%)	1,010 (45.56%)	
SEX															
Male	1,842 (53.24%)	7,947 (52.48%)	0.421	277 (54.53%)	1,251 (51.50%)	0.215	256 (48.58%)	1,175 (52.13%)	0.142	333 (53.54%)	1,192 (52.88%)	0.773	342 (51.82%)	1,176 (53.04%)	0.58
Female	1,618 (46.76%)	7,196 (47.52%)		231 (45.47%)	1,178 (48.50%)		271 (51.42%)	1,079 (47.87%)		289 (46.46%)	1,062 (47.12%)		318 (48.18%)	1,041 (46.96%)	
LOCATION															
Urban	866 (25.03%)	4,347 (28.71%)	<0.001	112 (22.05%)	620 (25.52%)	0.099	110 (20.87%)	566 (25.11%)	0.041	142 (23.00%)	659 (29.24%)	0.002	161 (24.39%)	609 (27.47%)	0.117
Rural	2,594 (74.97%)	10,796 (71.29%)		396 (77.95%)	1,809 (74.48%)		417 (79.13%)	1,688 (74.89%)		480 (77.00%)	1,595 (70.76%)		499 (75.61%)	1,608 (72.53%)	
REGION															
North	1,434 (41.45%)	5,286 (34.91%)	<0.001	226 (44.49%)	728 (29.97%)	<0.001	228 (43.26%)	698 (30.97%)	<0.001	221 (35.53%)	776 (34.43%)	0.609	266 (40.3%)	964 (43.48%)	0.147
South	2,026 (58.55%)	9,857 (65.09%)		282 (55.51%)	1,701 (70.03%)		299 (56.74%)	1556 (69.03%)		401 (64.47%)	1,478 (65.57%)		394 (59.70%)	1,253 (56.52%)	
BMI (kg/m^2)	17.42±4.63	17.69±3.25	0.040	15.4±1.86	17.38±2.78	<0.001	15.66±1.94	17.28±2.68	<0.001	15.66±2.05	17.43±2.78	<0.001	16.46±2.41	17.68±2.85	0.004
WC (cm)	59.01±12.85	62.87±9.9	<0.001	NA	NA		56.48±6.8	62.39±8.5	<0.001	55.98±6.45	61.39±8.17	<0.001	58.42±7.12	62.8±8.38	<0.001
GENERAL OBESITY															
Normal	568 (85.80%)	13,228 (88.06%)	0.08	83 (94.32%)	2,222 (92.20%)	0.47	86 (93.48%)	2,046 (91.96%)	0.60	101 (93.52%)	2,042 (91.12%)		44 (95.65%)	1,983 (90.05%)	0.21
Overweight/ Obesity	94 (14.20%)	1,794 (11.94%)		5 (5.68%)	188 (7.80%)		6 (6.52%)	179 (8.04%)		7 (6.48%)	199 (8.88%)	0.39	2 (4.35%)	219 (9.95%)	
CENTRAL OBESITY															
Normal	567 (91.60%)	10,571 (91.68%)	0.94	NA	NA		66 (95.65%)	1,217 (96.36%)	0.76	128 (96.24%)	2,078 (96.25%)	1.00	72 (94.74%)	2,068 (94.65%)	0.97
Central Obesity	52 (8.40%)	959 (8.32%)		NA	NA		3 (4.35%)	46 (3.64%)		5 (3.76%)	81 (3.75%)		4 (5.26%)	117 (5.35%)	

(Continued)

TABLE 1 | Continued

Characteristis	2004			2006			2009			2011			2015		
	Excluded 283	Included 1,364	*p* value	Excluded 153	Included 1,145	*P* value	Excluded 127	Included 1,012	*P* value	Excluded 88	Included 1,404	*p* value	Excluded 500	Included 1,064	*P* value
AGE GROUP															
7–12 years	158 (55.83%)	646 (47.36%)	0.009	74 (48.37%)	667 (58.25%)	0.02	63 (49.61%)	618 (61.07%)	0.013	42 (52.5%)	874 (62.25%)	0.081	236 (47.2%)	793 (74.53%)	<0.001
13–17 years	125 (44.17%)	718 (52.64%)		79 (51.63%)	478 (41.75%)		64 (50.39%)	394 (38.93%)		38 (47.5%)	530 (37.75%)		264 (52.8%)	271 (25.47%)	
Sex															
Male	154 (54.42%)	720 (52.79%)	0.617	85 (55.56%)	609 (53.19%)	0.581	72 (56.69%)	562 (55.53%)	0.804	41 (51.52%)	713 (50.78%)	0.935	282 (56.4%)	549 (51.60%)	0.047
Female	129 (45.58%)	644 (47.21%)		68 (44.44%)	536 (46.81%)		55 (43.31%)	450 (44.47%)		39 (48.75%)	691 (49.22%)		218 (43.6%)	515 (48.40%)	
LOCATION															
Urban	59 (20.85%)	408 (29.91%)	0.002	41 (26.80%)	343 (29.96%)	0.421	35 (27.56%)	274 (27.08%)	0.908	34 (42.50%)	530 (37.75%)	0.395	172 (34.40%)	338 (31.77%)	0.3
Rural	224 (79.15%)	956 (70.09%)		112 (73.20%)	802 (70.04%)		92 (72.44%)	738 (72.92%)		46 (57.50%)	874 (62.25%)		328 (66.00%)	726 (68.23%)	
REGION															
North	138 (48.76%)	556 (40.76%)	0.013	77 (50.33%)	445 (38.86%)	0.007	40 (31.50%)	375 (37.06%)	0.22	35 (43.75%)	442 (31.48%)	0.022	203 (40.60%)	302 (28.38%)	<0.001
South	145 (51.24%)	808 (59.24%)		76 (49.67%)	700 (61.14%)		87 (68.50%)	637 (62.94%)		45 (56.25%)	962 (68.52%)		297 (59.40%)	762 (71.62%)	
BMI, kg/m^2	16.54±2.71	18.1±2.92	<0.001	16.65±2.93	17.77±3.09	0.109	16.96±4.28	17.79±3.35	0.4368	15.57±2.14	18.35±3.8	0.0208	21.12±6.52	18.28±5.6	<0.001
WC, cm	57.73±8.53	64.1±9.47	<0.001	57.55±7.63	62.52±10.01	0.005	67.49±7.36	63.07±10.01	0.1273	55.57±7.21	64.49±11.96	0.0683	63.11±20.26	63.03±13.71	0.9487
GENERAL OBESITY															
Normal	87 (87.88%)	1,181 (87.35%)	0.88	14 (70.00%)	979 (87.49%)	0.02	9 (90.00%)	845 (83.83%)	0.60	10 (100.00%)	1,111 (79.13%)	0.11	134 (70.90%)	819 (77.19%)	0.06
Overweight/ Obesity	12 (12.12%)	171 (12.65%)		6 (30.00%)	140 (12.51%)		1 (10.00%)	163 (16.17%)		0 (0.00%)	293 (20.87%)		55 (29.10%)	242 (22.81%)	
CENTRAL OBESITY															
Normal	105 (94.59%)	1,243 (92.21%)	0.36	33 (100.00%)	1,047 (93.32%)	0.13	10 (83.33%)	898 (89.62%)	0.48	6 (100.00%)	1,168 (83.31%)	0.27	147 (82.12%)	852 (81.22%)	0.77
Central Obesity	6 (5.41%)	105 (7.79%)		0 (0.00%)	75 (6.68%)		2 (16.67%)	104 (10.38%)		0 (0.00%)	234 (16.69%)		32 (17.88%)	197 (18.78%)	

Data are presented as means ± standard deviations or n (%); BMI, Body Mass Index; WC, Waist Circumference.

TABLE 2 | Classification of blood pressure and definitions of hypertension and hypertension phenotypes in children and adolescents.

Category	Definition
Normal	SBP with DBP less the 90th percentile (for age, sex and height)
Prehypertension	An SBP and/or DBP between the 90th and 95th percentile (for age, sex and height) or ≥120/80 mm Hg
Hypertension	An SBP and/or DBP≥95th percentile (for age, sex and height) on ≥3 separate occasions
Stage 1	An SBP and/or DBP between 95th and 99th percentile plus 5 mmHg (for age, sex and height) on ≥3 separate occasions
Stage 2	An SBP and/or DBP above 99th percentile plus 5 mmHg (for age, sex and height) on ≥3 separate occasions
ISH	An SBP≥95th percentile (for age, sex, and height) but a DB*P* <95th percentile (for age, sex, and height) on ≥3 separate occasions
IDH	A DBP≥95th percentile (for age, sex, and height) but an SB*P* < 95th percentile (for age, sex, and height) on ≥3 separate occasions
SDH	An SBP and DBP≥95th percentile (for age, sex, and height) on ≥3 separate occasions

** SBP, systolic blood pressure; DBP, diastolic blood pressure; IDH, isolated diastolic hypertension; ISH, isolated systolic hypertension; SDH, systolic-diastolic hypertension.*

waist circumference (WC) and hip circumference (HC) were measured following standardized protocols from the World Health Organization (20). BP was calculated as the mean of three measurements with an interval of 3–5 min by standard mercury sphygmomanometer (11, 21, 22). Weight was measured without coats to the nearest 0.1 kg on a calibrated beam scale, and height was measured without shoes to the nearest 0.1 cm using a portable stadiometer. WC was taken at the end of expiratory period at the midpoint of the line between the lower rib and the upper iliac crest (23, 24). HC was measured at the level of maximal gluteal protrusion with a non-elastic tape. Body mass index (BMI) was calculated as weight divided by height squared (kg/m^2), waist to height ratio (WHtR) as WC divided by height, and waist to hip ratio (WHR) as WC divided by HC.

Definitions

Hypertension and Phenotypes

Conforming to the standard of the Chinese Child Blood Pressure References Collaborative Group, the definitions of childhood hypertension and phenotypes are listed in **Table 2** (25).

Demographics, Geographic Locations, General, and Central Obesity

Following the criteria of the 2017 AAP guidelines, we divided all participants into two age groups of 7–12 and 13–17 years (11). Residence was classified into South China (Shanghai, Jiangsu, Hubei, Hunan, Guangxi, Guizhou, and Chongqing in CHNS) and North China (Beijing, Liaoning, Heilongjiang, Shandong, and Henan in CHNS). Using the Working Group on Obesity in China criteria, a BMI between 85th and 95th percentile of sex and age group was defined as overweight, and ≥95th percentile as obesity. Central obesity was defined as a WC> 90th percentile in each sex and age group, or a WHtR ≥ 0.5, or a WHR ≥ 0.9 in boys or ≥0.85 in girls (26).

Statistical Analysis

In descriptive analyses, continuous variables were reported as mean and standard deviation (SD) and categorical data were presented as percentage (%) with 95% confidence interval (CI). Using the Chi-square test, we compared the age and sex distributions between the excluded and included groups. Given that the same participant might be included in different survey rounds, generalized estimating equation (GEE) was adopted (27, 28). Individual calendar year was selected as a single continuous variable and age were adjusted for in GEE models to examine the trends in the prevalence of childhood hypertension and phenotypes. Subgroup trend analyses from 1991 to 2015 were conducted by strata of age and sex. To estimate the associated factors of childhood hypertension and phenotypes, multivariable logistic regression was carried out. All statistical analyses were performed using Stata statistical software (version 14.0; Stata Corporation, College Station, TX, USA), and a $P < 0.05$ was considered as statistically significant in two-sided tests.

RESULTS

Characteristics of the Participants

A total of 18,603 records of children and adolescents were available from CHNS 1991 to 2015, of which 15,143 were with BP measurements. The basic characteristics (demographics, anthropometry and geography) are shown in **Table 3**. The flow chart of this study is shown in **Supplementary Figure 2**.

Trends in SBP, DBP, and Prevalence of Childhood Hypertension and Phenotypes

Table 4 shows the changes in age-standardized mean SBP and DBP by strata of age and sex. From 1991 to 2015, SBP and DBP values increased significantly from 96.18 mmHg (95% CI: 95.65–96.71) to 101.54 mmHg (95% CI: 100.78–102.30), and from 62.61 mmHg (95% CI: 62.22–63.01) to 66.65 mmHg (95% CI: 66.10–67.20), respectively (both *P*-values for age-adjusted trend< 0.001). Mean SBP and DBP values increased across age and sex groups during the same time period, with an average annual increase (AAI) ranging from 0.12 mmHg to 0.37 mmHg and an average relative increase (ARI) from 0.19 to 0.46%.

Table 5 presents the trends of age-standardized prevalence of childhood hypertension and phenotypes. For prehypertension, the age-standardized prevalence significantly increased from 7.0% (95% CI: 6.0–8.1) in 1991 to 13.00% (95% CI: 11.1–15.1) in 2015. Prehypertension was consistently more prevalent in boys (than in girls) and in teenagers aged 13–17 years (than in those aged 7–12 years). For childhood hypertension, the overall age-standardized prevalence rose from 8.5% (95% CI: 7.4–9.7) to 19.2% (95% CI: 16.9–21.7) across the same study time period, yielding a relative increasing rate of 5.3% ($P < 0.001$). The prevalence of childhood hypertension was generally higher in participants aged 13–17 years (than in the younger groups). Besides, the age-standardized prevalence of prehypertension

TABLE 3 | Characteristics of included subjects in CHNS 1991–2015.

Characteristic	1991–2015 combined (15,143)	1991 (2,429)	1993 (2,254)	1997 (2,254)	2000 (2,217)	2004 (1,364)	2006 (1,145)	2009 1,012	2011 (1,404)	2015 (1,064)
AGE GROUP										
7–12 years	8,783 (58.00)	1,335 (54.96)	1,285 (57.01)	1,358 (60.25)	1,207 (54.44)	646 (47.36)	667 (58.25)	618 (61.07)	874 (62.25)	793 (74.53)
13–17 years	6,360 (42.00)	1,094 (45.04)	969 (42.99)	896 (39.75)	1,010 (45.56)	718 (52.64)	478 (41.75)	394 (38.93)	530 (37.75)	271 (25.47)
SEX										
Male	7,947 (52.48)	1,251 (51.50)	1,175 (52.13)	1,192 (52.88)	1,176 (53.04)	720 (52.79)	609 (53.19)	562 (55.53)	713 (50.78)	549 (51.60)
Female	7,196 (47.52)	1,178 (48.50)	1,079 (47.87)	1,062 (47.12)	1,041 (46.96)	644 (47.21)	536 (46.81)	450 (44.47)	691 (49.22)	515 (48.40)
ANTHROPOMETRIC MEASURES										
Height, cm	144.65 ± 0.26	142.37 ± 0.64	142.11 ± 0.68	142.62 ± 0.65	146.41 ± 0.63	149.05 ± 0.86	146.04 ± 1.00	146.44 ± 0.99	146.47 ± 0.88	144.55 ± 0.97
Weight, kg	38.18 ± 0.21	36.39 ± 0.49	36.05 ± 0.50	36.55 ± 0.50	38.89 ± 0.50	41.33 ± 0.69	39.12 ± 0.77	39.29 ± 0.82	40.67 ± 0.77	39.35 ± 0.96
BMI, kg/m^2	17.69 ± 0.05	17.38 ± 0.11	17.28 ± 0.12	17.43 ± 0.11	17.68 ± 0.11	18.10 ± 0.15	17.77 ± 0.18	17.79 ± 0.20	18.35 ± 0.20	18.28 ± 0.34
WC, cm	62.87 ± 0.19	NA	62.39 ± 0.47	61.39 ± 0.35	62.80 ± 0.35	64.10 ± 0.50	62.52 ± 0.58	63.07 ± 0.62	64.49 ± 0.63	63.03 ± 0.83
BLOOD PRESSURE MEASURES										
SBP, mmHg	98.44 ± 0.20	96.18 ± 0.53	96.34 ± 0.54	97.18 ± 0.53	99.49 ± 0.54	101.53 ± 0.70	98.00 ± 0.73	99.83 ± 0.78	100.12 ± 0.65	101.54 ± 0.76
DBP, mmHg	64.57 ± 0.15	62.61 ± 0.39	63.25 ± 0.41	63.67 ± 0.40	65.15 ± 0.39	66.66 ± 0.51	64.74 ± 0.52	66.63 ± 0.57	65.36 ± 0.47	66.65 ± 0.55
SETTING										
Urban	4,347 (28.71)	620 (25.52)	566 (25.11)	659 (29.24)	609 (27.47)	408 (29.91)	343 (29.96)	274 (27.08)	530 (37.75)	338 (31.77)
Rural	10,796 (71.29)	1,809 (74.48)	1,688 (74.89)	1,595 (70.76)	1,608 (72.53)	956 (70.09)	802 (70.04)	738 (72.92)	874 (62.25)	726 (68.23)
REGION										
North	5,286 (34.91)	728 (29.97)	698 (30.97)	776 (34.43)	964 (43.48)	556 (40.76)	445 (38.86)	375 (37.06)	442 (31.48)	302 (28.38)
South	9,857 (65.09)	1,701 (70.03)	1,556 (69.03)	1,478 (65.57)	1,253 (56.52)	808 (59.24)	700 (61.14)	637 (62.94)	962 (68.52)	762 (71.62)

**Data are expressed as n (%) or mean ± SD; BMI, body mass index; WC, Waist circumference; SBP, systolic blood pressure; DBP, diastolic blood pressure. NA, Not available.*

TABLE 4 | Mean SBP and DBP in Chinese children and adolescents, CHNS 1991–2015.

Variable	1991 (*n* = 2,429)	1993 (*n* = 2,254)	1997 (*n* = 2,254)	2000 (*n* = 2,217)	2004 (*n* = 1,364)	2006 (*n* = 1,145)	2009 (*n* = 1,012)	2011 (*n* = 1,404)	2015 (*n* = 10,64)	AAI (%)	ARI (%)	P for age-adjusted trend
SBP (mmHg), mean (95% CI)												
Overall	96.18	96.34	97.18	99.49	101.53	98.00	99.83	100.12	101.54	0.22	0.23	<0.001
	(95.65–96.71)	(95.8–96.88)	(96.65–97.72)	(98.95–100.02)	(100.83–102.24)	(97.27–98.73)	(99.05–100.62)	(99.47–100.77)	(100.78–102.3)			
AGE GROUP												
7–12 years	90.47	91.59	92.65	95.14	95.27	92.98	96.54	96.24	99.23	0.37	0.40	<0.001
	(89.88–91.06)	(90.93–92.25)	(92.02–93.27)	(94.48–95.8)	(94.32–96.21)	(92.12–93.85)	(95.54–97.55)	(95.47–97)	(98.37–100.09)			
13–17 years	103.15	102.64	104.05	104.68	107.17	105.00	104.99	106.52	108.29	0.21	0.21	<0.001
	(102.4–103.9)	(101.91–103.37)	(103.29–104.82)	(103.92–105.44)	(106.34–108.01)	(104.02–105.97)	(103.93–106.06)	(105.57–107.46)	(106.94–109.65)			
SEX												
Male	96.51	96.67	97.19	100.32	102.48	98.76	100.20	101.24	102.90	0.27	0.28	<0.001
	(95.76–97.26)	(95.88–97.45)	(96.45–97.93)	(99.56–101.09)	(101.47–103.48)	(97.71–99.81)	(99.11–101.29)	(100.29–102.19)	(101.81–103.99)			
Female	95.83	95.99	97.17	98.54	100.48	97.13	99.37	98.96	100.09	0.18	0.19	<0.001
	(95.08–96.58)	(95.26–96.72)	(96.39–97.95)	(97.8–99.29)	(99.52–101.45)	(96.12–98.15)	(98.25–100.5)	(98.09–99.84)	(99.03–101.14)			
DBP (mmHg), mean (95% CI)												
Overall	62.61	63.25	63.67	65.15	66.66	64.74	66.63	65.36	66.65	0.17	0.27	<0.001
	(62.22–63.01)	(62.84–63.66)	(63.27–64.08)	(64.76–65.53)	(66.15–67.18)	(64.22–65.26)	(66.06–67.2)	(64.89–65.84)	(66.1–67.2)			
AGE GROUP												
7–12 years	58.99	60.23	60.77	62.49	63.09	61.52	64.77	62.95	65.49	0.27	0.46	<0.001
	(58.5–59.47)	(59.7–60.76)	(60.28–61.27)	(61.99–62.99)	(62.35–63.83)	(60.91–62.12)	(64.04–65.5)	(62.38–63.52)	(64.86–66.11)			
13–17 years	67.04	67.26	68.07	68.33	69.88	69.24	69.55	98.96	100.09	0.12	0.19	<0.001
	(66.5–67.58)	(66.7–67.82)	(67.49–68.65)	(67.78–68.87)	(69.26–70.5)	(68.48–70)	(68.71–70.38)	(68.64–70.07)	(68.97–71.09)			
SEX												
Male	62.66	63.43	63.58	65.55	67.13	65.14	66.67	66.36	67.46	0.20	0.32	<0.001
	(62.1–63.21)	(62.84–64.03)	(63.04–64.12)	(65.01–66.09)	(66.41–67.84)	(64.39–65.89)	(65.9–67.44)	(65.67–67.05)	(66.66–68.26)			
Female	62.57	63.06	63.78	64.69	66.15	64.29	66.58	64.34	65.78	0.13	0.21	<0.001
	(62.01–63.13)	(62.48–63.63)	(63.17–64.38)	(64.14–65.24)	(65.41–66.88)	(63.58–65.01)	(65.73–67.43)	(63.69–64.98)	(65.03–66.52)			

AAI, Average annual increase, AAI was computed by dividing the difference of blood pressure between 1991 and 2015 by the number of years covered; ARI = Average relative increase, ARI was calculated by dividing the average annual change by the baseline mean blood pressure in 1991; trends in mean blood pressure from 1991 to 2015 were assessed by the generalized-estimating-equation method and adjusted by age and sex.

TABLE 5 | Prevalence of hypertension and phenotypes in Chinese children and adolescents, CHNS 1991–2015.

Variable	1991 (*n* = 2,429)	1993 (*n* = 2,254)	1997 (*n* = 2254)	2000 (*n* = 2217)	2004 (*n* = 1,364)	2006 (*n* = 1,145)	2009 (*n* = 1,012)	2011 (*n* = 1404)	2015 (*n* = 1,064)	AAI (%)	ARI (%)	*P* for age-adjusted trend
Prehypertension (%, 95% CI)												
Overall	7.0 (6.0–8.1)	7.5 (6.4–8.6)	8.5 (7.4–9.7)	9.2 (8.0–10.4)	9.9 (8.4–11.6)	9.2 (7.6–11.0)	11.3 (9.5–13.4)	9.9 (8.4–11.6)	13.0 (11.1–15.1)	0.3	3.6	<0.001
AGE GROUP												
7–12 years	5.7 (4.6–7.1)	6.1 (5–7.6)	6.5 (5.3–7.9)	6.5 (5.3–8.1)	7.1 (5.4–9.1)	6.1 (4.6–8.2)	9.5 (7.5–12.1)	6.3 (4.9–8.1)	12.7 (10.6–15.2)	0.3	5.2	<0.001
13–17 years	8.6 (7.1–10.4)	9.2 (7.5–11.2)	11.6 (9.7–13.9)	12.3 (10.4–14.5)	12.4 (10.2–15.0)	13.4 (10.6–16.8)	14.0 (10.9–17.8)	15.8 (13.0–19.2)	13.7 (10.0–18.3)	0.2	2.5	<0.001
SEX												
Male	6.6 (5.3–8.1)	7.5 (6.1–9.1)	8.7 (7.2–10.5)	9.5 (8.0–11.3)	11.7 (9.5–14.2)	9.5 (7.4–12.1)	11.9 (9.5–14.9)	11.8 (9.6–14.4)	13.3 (10.7–16.4)	0.3	4.3	<0.001
Female	7.5 (6.1–9.1)	7.4 (6.0–9.1)	8.3 (6.8–10.1)	8.7 (7.2–10.6)	7.9 (6.1–10.3)	8.8 (6.6–11.5)	10.4 (7.9–13.6)	8.0 (6.2–10.2)	12.6 (10.0–15.8)	0.2	2.9	0.001
Hypertension (%, 95% CI)												
Overall	8.5 (7.4–9.7)	9.6 (8.5–10.9)	11.1 (9.9–12.5)	12.4 (11.1–13.8)	16.9 (15.0–18.9)	9.9 (8.3–11.7)	15.9 (13.8–18.3)	12.6 (11.0–14.4)	19.2 (16.9–21.7)	0.5	5.3	<0.001
AGE GROUP												
7–12 years	4.5 (3.5–5.7)	8.0 (6.7–9.6)	8.1 (6.8–9.7)	9.9 (8.3–11.7)	13.2 (10.8–16)	6.3 (4.7–8.4)	16.3 (13.6–19.5)	11.3 (9.4–13.6)	18.2 (15.6–21.0)	0.6	12.7	<0.001
13–17 years	13.3 (11.5–15.5)	11.8 (9.9–14.0)	15.7 (13.5–18.3)	15.3 (13.3–17.7)	20.2 (17.4–23.3)	14.9 (11.9–18.3)	15.2 (12.0–19.1)	14.7 (11.9–18.0)	22.1 (17.6–27.5)	0.4	2.8	<0.001
SEX												
Male	9.0 (7.5–10.7)	10.1 (8.5–12)	10.1 (8.5–11.9)	13.2 (11.4–15.2)	16.4 (13.9–19.3)	10.2 (8.8–12.8)	14.4 (11.7–17.6)	14.2 (11.8–16.9)	21.5 (18.3–25.1)	0.5	5.8	<0.001
Female	8.0 (6.6–9.7)	9.1 (7.5–11.0)	12.3 (10.5–14.5)	11.4 (9.6–13.5)	17.4 (14.7–20.5)	9.5 (7.3–12.3)	17.8 (14.5–21.6)	11.0 (8.9–13.6)	16.7 (13.7–20.2)	0.4	4.6	<0.001
Stage 1 hypertension (%, 95% CI)												
Overall	8.0 (7.0–9.2)	9.1 (8.0–10.4)	10.6 (9.4–11.9)	11.7 (10.5–13.1)	16.0 (14.1–18)	9.7 (8.1–11.5)	14.6 (12.6–16.9)	12.3 (10.6–14.1)	17.7 (15.5–20.1)	0.4	5.0	<0.001
AGE GROUP												
7–12 years	4.3 (3.3–5.5)	7.5 (6.2–9.1)	7.7 (6.4–9.3)	9.3 (7.8–11.1)	12.1 (9.8–14.8)	6.3 (4.7–8.4)	14.7 (12.1–17.7)	11.0 (9.1–13.2)	16.4 (14–19.1)	0.5	11.8	<0.001
13–17 years	12.6 (10.8–14.7)	11.1 (9.3–13.3)	14.8 (12.7–17.3)	14.7 (12.6–17.0)	19.5 (16.8–22.6)	14.4 (11.6–17.9)	14.5 (11.3–18.3)	14.3 (11.6–17.6)	21.4 (16.9–26.7)	0.4	2.9	<0.001
SEX												
Male	8.7 (7.3–10.4)	9.4 (7.9–11.3)	9.8 (8.3–11.6)	12.4 (10.6–14.4)	15.6 (13.1–18.4)	9.9 (7.7–12.5)	13.2 (10.6–16.2)	13.7 (11.4–16.5)	20.4 (17.2–24.0)	0.5	5.6	<0.001
Female	7.3 (5.9–8.9)	8.7 (7.2–10.5)	11.4 (9.6–13.4)	11.0 (9.2–13.0)	16.5 (13.8–19.5)	9.5 (7.3–12.3)	16.4 (13.3–20.2)	10.7 (8.6–13.2)	14.8 (11.9–18.1)	0.3	4.3	<0.001
Stage 2 hypertension (%, 95% CI)												
Overall	0.5 (0.3–0.8)	0.5 (0.3–0.9)	0.6 (0.3–1.0)	0.6 (0.4–1.1)	0.9 (0.5–1.5)	0.2 (0.0–0.7)	1.3 (0.7–2.2)	0.4 (0.1–0.9)	1.5 (0.9–2.4)	0.0	9.7	0.012
AGE GROUP												
7–12 years	0.2 (0.1–0.7)	0.5 (0.2–1.0)	0.4 (0.2–0.9)	0.6 (0.3–1.2)	1.1 (0.5–2.3)	0.0 (0.0–0.0)	1.6 (0.9–3.0)	0.3 (0.1–1.1)	1.8 (1.0–3.0)	0.06	28.6	<0.001
13–17 years	0.7 (0.4–1.5)	0.6 (0.3–1.4)	0.9 (0.4–1.8)	0.7 (0.3–1.4)	0.7 (0.3–1.7)	0.4 (0.1–1.7)	0.8 (0.2–2.3)	0.4 (0.1–1.5)	0.7 (0.2–2.9)	0.0	0.0	0.589
SEX												
Male	0.2 (0.1–0.7)	0.7 (0.3–1.4)	0.3 (0.1–0.8)	0.8 (0.4–1.5)	0.8 (0.4–1.8)	0.3 (0.1–1.3)	1.2 (0.6–2.6)	0.4 (0.1–1.3)	1.1 (0.5–2.4)	0.0	14.8	0.045
Female	0.7 (0.3–1.4)	0.4 (0.1–1.0)	0.9 (0.5–1.7)	0.5 (0.2–1.1)	0.9 (0.4–2.1)	0.0 (0.0–0.0)	1.3 (0.6–2.9)	0.3 (0.1–1.2)	1.9 (1.0–3.6)	0.1	7.8	0.110
ISH (%, 95% CI)												
Overall	0.9 (0.6–1.4)	0.8 (0.5–1.3)	1.6 (1.1–2.2)	1.4 (0.9–1.9)	2.1 (1.5–3.0)	1.1 (0.7–1.9)	1.6 (1.0–2.6)	1.1 (0.7–1.9)	2.2 (1.4–3.2)	0.1	5.4	0.001

(Continued)

TABLE 5 | Continued

Variable	1991 (n = 2,429)	1993 (n = 2,254)	1997 (n = 2254)	2000 (n = 2217)	2004 (n = 1,364)	2006 (n = 1,145)	2009 (n = 1,012)	2011 (n = 1404)	2015 (n = 1,064)	AAI (%)	ARI (%)	P for age-adjusted trend
AGE GROUP												
7–12 years	1 (0.6–1.8)	0.8 (0.4–1.5)	1.2 (0.7–2.0)	1.3 (0.8–2.1)	1.7 (0.9–2.9)	1.3 (0.7–2.6)	2.0 (1.1–3.5)	1.5 (0.9–2.8)	1.5 (0.7–2.9)	0.02	1.7	<0.001
13–17 years	0.8 (0.5–1.6)	0.8 (0.4–1.6)	2.0 (1.3–3.0)	1.4 (0.9–2.4)	2.6 (1.6–4.2)	0.9 (0.4–2.2)	1.1 (0.5–2.6)	0.7 (0.3–1.7)	2.9 (1.8–4.8)	0.1	10.1	0.932
SEX												
Male	0.3 (0.1–0.8)	0.5 (0.3–1.1)	1.0 (0.6–1.7)	1.3 (0.8–2.2)	1.1 (0.5–2.3)	1.2 (0.6–2.4)	1.9 (1.1–3.4)	1.3 (0.7–2.3)	2.0 (1.2–3.3)	0.1	23.9	0.027
Female	1.7 (1.1–2.7)	1.1 (0.6–2.0)	2.3 (1.5–3.6)	1.4 (0.8–2.3)	3.1 (2.0–4.6)	1.0 (0.4–2.5)	1.0 (0.4–2.7)	0.9 (0.4–2.2)	2.6 (1.2–5.3)	0.0	2.0	0.021
IDH (%, 95% CI)												
Overall	6.2 (5.3–7.2)	7.5 (6.5–8.7)	7.5 (6.5–8.7)	8.9 (7.8–10.1)	13.0 (11.3–14.9)	7.2 (5.8–8.8)	12.1 (10.2–14.2)	9.2 (7.8–10.8)	14.1 (12.1–16.3)	0.3	5.4	<0.001
AGE GROUP												
7–12 years	3.6 (2.7–4.7)	6.1 (4.9–7.5)	4.9 (3.9–6.2)	6.1 (4.9–7.6)	10.5 (8.4–13.1)	3.1 (2.1–4.8)	11.7 (9.3–14.4)	7.8 (6.2–9.8)	12.6 (10.5–15.1)	0.4	10.5	<0.001
13–17 years	9.3 (7.7–11.2)	9.5 (7.8–11.5)	11.4 (9.5–13.6)	12.2 (10.3–14.3)	15.2 (12.7–18)	12.8 (10.1–16.1)	12.7 (9.7–16.4)	11.5 (9.1–14.5)	18.5 (14.3–23.5)	0.4	4.1	<0.001
SEX												
Male	6.6 (5.4–8.2)	7.8 (6.4–9.5)	7.6 (6.3–9.3)	9.7 (8.1–11.5)	12.8 (10.5–15.4)	7.4 (5.6–9.8)	10.5 (8.2–13.3)	10.2 (8.2–12.7)	16.4 (13.5–19.7)	0.4	6.1	<0.001
Female	5.7 (4.5–7.2)	7.2 (5.8–8.9)	7.3 (5.9–9.1)	8.0 (6.5–9.8)	13.2 (10.8–16.0)	6.9 (5.0–9.4)	14.0 (11.1–17.5)	8.1 (6.3–10.4)	11.7 (9.1–14.7)	0.3	4.4	<0.001
SDH (%, 95% CI)												
Overall	1.4 (1.4–1.9)	1.3 (0.9–1.8)	2.1 (1.6–2.8)	2.1 (1.6–2.8)	1.8 (1.2–2.6)	1.6 (1.0–2.5)	2.3 (1.5–3.4)	2.3 (1.6–3.2)	2.9 (2.1–4.1)	0.1	4.8	0.001
AGE GROUP												
7–12 years	0.6 (0.3–1.2)	1.4 (0.9–2.2)	2.1 (1.5–3.1)	2.4 (1.7–3.4)	1.5 (0.8–2.9)	1.9 (1.1–3.3)	2.8 (1.7–4.4)	2.3 (1.5–3.5)	3.5 (2.4–5.1)	0.12	20.4	<0.001
13–17 years	2.3 (1.5–3.4)	1.1 (0.6–2.0)	2.0 (1.3–3.2)	1.8 (1.1–2.8)	1.9 (1.2–3.3)	1.0 (0.4–2.5)	1.5 (0.7–3.4)	2.3 (1.3–3.9)	1.1 (0.4–3.4)	−0.1	−2.2	0.632
SEX												
Male	1.3 (0.8–2.1)	1.5 (1.0–2.4)	1.3 (0.8–2.1)	2.2 (1.5–3.2)	1.9 (1.2–3.3)	1.5 (0.8–2.8)	2.0 (1.1–3.5)	2.4 (1.5–3.8)	3.6 (2.4–5.6)	0.1	7.7	0.002
Female	1.4 (0.9–2.3)	1.0 (0.6–1.8)	3.0 (2.1–4.2)	2.0 (1.3–3.1)	1.6 (0.8–2.9)	1.7 (0.9–3.2)	2.7 (1.5–4.6)	2.2 (1.3–3.6)	2.1 (1.2–3.8)	0.0	2.0	0.146

AAI, Average annual increase, AAI was computed by dividing the difference of prevalence between 1991 and 2015 by the number of years covered; ARI=Average relative increase, ARI was calculated by dividing the average annual change by the baseline prevalence in 1991; trends in prevalence from 1991 to 2015 were assessed by the generalized–estimating-equation method and adjusted by age and sex.

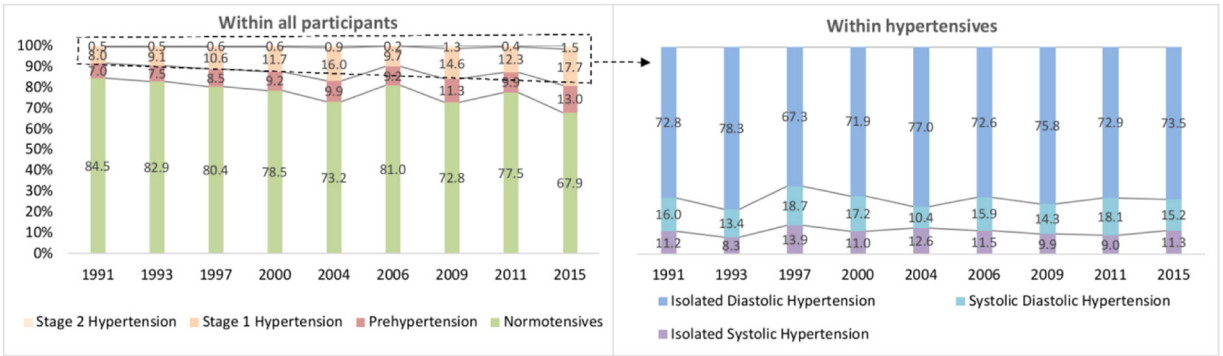

FIGURE 1 | The proportions of childhood hypertension and phenotypes, CHNS 1991–2015.

and hypertension increased in all age and sex subgroups ($P < 0.001$) and the prevalence of hypertension in children aged 7–12 years increased the most during the survey rounds (increased by 12.7%).

For stage 1 and stage 2 hypertension, the age-standardized prevalence increased from 8.0% (95% CI: 7.0–9.2) to 17.7% (95% CI: 15.5–20.1) and from 0.5% (95% CI: 0.3–0.8) to 1.5% (95% CI: 0.9–2.4), respectively. The prevalence of stage 1 hypertension was generally higher than that of stage 2 hypertension. Within this time frame, the ARI rates of both stage 1 and stage 2 hypertension were greater in 7–12 years old children (increased by 11.8% and 28.6%) than in older groups (increased by 2.9% and 0.0%). No statistically significant prevalence trend in stage 2 hypertension was observed among people aged 13–17 years and in girls ($P =$ 0.589 and 0.110, separately).

IDH accounted for the largest share of hypertension phenotypes (**Figure 1**). For ISH, the age-standardized prevalence increased significantly from 0.9% (95% CI: 0.6–1.4) to 2.2% (95% CI: 1.4–3.2) from CHNS 1991 to CHNS 2015. Upward trends were observed in all subgroups (males, females and 7–12 years), except in people aged 13–17 ($P = 0.932$). For IDH, the age-standardized prevalence increased from 6.2% to 14.1% (boys from 6.6 to 16.4%, girls from 5.7 to 11.7%) over 25 years. The prevalence of IDH in two age groups (7–12 and 13–17 years) increased by 10.5% and 4.1% (both age-adjusted $P < 0.001$). The age-standardized prevalence of SDH increased from 1.4% (95% CI: 1.4–1.9) in 1991 to 2.9% (95% CI: 2.1–4.1) in 2015. An increasing trend of SDH prevalence was revealed in the age group of 7–12 years (from 0.6 to 3.5%) and in boys (from 1.3 to 3.6%) (**Table 5**).

The Associations of Demographic, Geographic, Anthropometric Factors, and Obesity With Hypertension and Hypertension Phenotypes

Of the 15,143 records, 11,450 were with complete information on BP, weight, height, WC, HC, age, sex, setting and region. The demographic characteristics between the included ($n = 15,143$) group and excluded ($n = 3,460$) group were compared (**Table 1**). Of note, the included participants were relatively younger than the excluded individuals across all survey rounds ($P < 0.05$), except for in CHNS 2004 and 2011, where no sex difference was observed between the two groups (all $P > 0.05$).

Table 6 shows the associated demographic, geographic and anthropometric factors of hypertension and phenotypes. Age, region, BMI, WC, general obesity, and central obesity were found to be associated with hypertension ($P < 0.001$). Compared with children aged 7–12 years, those aged older than 13 years and above were more likely to suffer from prehypertension (OR = 2.08, 95%CI: 1.82–2.37, $P < 0.001$) and stage 1 hypertension (OR = 1.81, 95%CI: 1.61–2.03, $P < 0.001$). Girls (vs. boys) were less likely to be affected by prehypertension (OR = 0.83, 95%CI: 0.73–0.95, $P = 0.005$), whereas no sex difference was observed in the prevalence of stage 1 and 2 hypertension. BMI and WC were significantly correlated with the prevalence of different hypertension phenotypes (all ORs with 95%CI were >1 and $P < 0.05$, except for the SDH). For prehypertension, stage 1 hypertension and stage 2 hypertension, general obesity was a positive factor, with ORs of 2.00 (95%CI: 1.47–2.73, $P <$ 0.001), 2.62 (95%CI: 2.03–3.38, $P < 0.001$), and 3.68 (95%CI: 1.82–7.44, $P < 0.001$), respectively. Central obesity was linked to both stages of hypertension additionally (OR = 1.43, 95%CI: 1.16–1.78, $P = 0.001$ and 2.76, 95%CI: 1.48–5.14, 0.001). For IDH, advanced age (OR = 2.02, 95%CI: 1.77–2.31, $P < 0.001$), general obesity (OR = 1.83, 95%CI: 1.36–2.47, $P < 0.001$) and central obesity (OR = 1.50, 95%CI: 1.19–1.90, $P = 0.001$) were positively associated with higher odds, whereas females, rural residents and south region were negative factors (ORs=0.86, 0.86 and 0.59, all $P < 0.05$). Similar to IDH, three out of these factors (13–17 years age group, general obesity and central obesity) were related to the increased prevalence of ISH (ORs = 1.57, 3.56, and 2.43, all $P < 0.05$). However, only general obesity contributed to the elevated prevalence of SDH, with an OR of 7.27 (95%CI: 4.57–11.59, $P < 0.001$).

DISCUSSION

The current study describes the prevalence and associated factors of hypertension and phenotypes in Chinese children and adolescents during 1991–2015. It provides novel insights

TABLE 6 | Multivariable odds ratios of demographic, geographic, and anthropometric factors and obesity for childhood hypertension and phenotypes.

Characteristic	Prehypertension		Hypertension		Stage 1 hypertension		Stage 2 hypertension		ISH		IDH		SDH	
	OR (95%CI)	*P*	OR (95%CI)	*P*	OR (95%CI)	*P*	OR (95%CI)	*P*	OR (95%CI)	*P*	OR (95%CI)	*P*	OR (95%CI)	*P*
SURVEY YEAR														
1993	1	Ref	1	Ref	1	Ref	1	Ref	1	Ref	1	Ref	1	Ref
1997	1.17 (0.91–1.52)	0.226	1.09 (0.86–1.37)	0.484	1.11 (0.88–1.41)	0.380	0.74 (0.30–1.83)	0.517	1.93 (0.94–3.96)	0.073	0.97 (0.74–1.26)	0.800	1.25 (0.72–2.17)	0.428
2000	1.23 (0.96–1.59)	0.106	1.17 (0.93–1.46)	0.188	1.20 (0.95–1.51)	0.133	0.75 (0.31–1.82)	0.530	1.78 (0.86–3.68)	0.118	1.08 (0.83–1.40)	0.556	1.30 (0.75–2.27)	0.348
2004	1.33 (1.01–1.75)	0.043	1.61 (1.27–2.04)	<0.001	1.65 (1.30–2.10)	<0.001	1.00 (0.39–2.54)	1.000	2.73 (1.30–5.71)	0.008	1.58 (1.22–2.06)	0.001	1.13 (0.61–2.12)	0.695
2006	1.18 (0.88–1.58)	0.276	0.89 (0.68–1.17)	0.413	0.95 (0.72–1.26)	0.708	0.21 (0.05–0.97)	0.045	1.35 (0.58–3.14)	0.489	0.85 (0.62–1.16)	0.311	0.79 (0.40–1.57)	0.499
2009	1.61 (1.21–2.16)	0.001	1.60 (1.24–2.07)	<0.001	1.60 (1.23–2.08)	0.001	1.57 (0.67–3.68)	0.296	2.03 (0.93–4.45)	0.076	1.60 (1.20–2.13)	0.001	1.31 (0.69–2.49)	0.410
2011	1.35 (1.02–1.78)	0.035	1.12 (0.87–1.44)	0.377	1.18 (0.92–1.53)	0.192	0.33 (0.11–1.05)	0.060	1.19 (0.54–2.62)	0.666	1.11 (0.84–1.47)	0.475	1.10 (0.60–2.00)	0.754
2015	2.14 (1.62–2.85)	<0.001	2.08 (1.61–2.67)	<0.001	2.09 (1.61–2.71)	<0.001	1.53 (0.65–3.59)	0.327	2.48 (1.17–5.25)	0.018	2.16 (1.63–2.86)	<0.001	1.37 (0.73–2.55)	0.324
AGE GROUP														
7–12 years	1	Ref	1	Ref	1	Ref	1	Ref	1	Ref	1	Ref	1	Ref
13–17 years	2.08 (1.82–2.37)	<0.001	1.76 (1.56–1.97)	<0.001	1.81 (1.61–2.03)	<0.001	1.02 (0.63–1.63)	0.939	1.57 (1.15–2.14)	0.004	2.02 (1.77–2.31)	<0.001	0.92 (0.69–1.22)	0.553
SEX														
Male	1	Ref	1	Ref	1	Ref	1	Ref	1	Ref	1	Ref	1	Ref
Female	0.83 (0.73–0.95)	0.005	0.92 (0.82–1.03)	0.160	0.91 (0.81–1.03)	0.126	1.08 (0.69–1.70)	0.743	1.19 (0.87–1.63)	0.279	0.86 (0.75–0.98)	0.025	1.01 (0.77–1.33)	0.927
LOCATION														
Urban	1	Ref	1	Ref	1	Ref	1	Ref	1	Ref	1	Ref	1	Ref
Rural	1.08 (0.94–1.25)	0.283	0.94 (0.83–1.07)	0.358	0.94 (0.83–1.07)	0.346	1.03 (0.63–1.67)	0.918	1.42 (0.99–2.04)	0.055	0.86 (0.75–0.99)	0.042	1.16 (0.86–1.58)	0.328
REGION														
North	1	Ref	1	Ref	1	Ref	1	Ref	1	Ref	1	Ref	1	Ref
South	0.94 (0.82–1.08)	0.401	0.65 (0.58–0.73)	<0.001	0.65 (0.57–0.73)	<0.001	0.70 (0.44–1.12)	0.134	1.10 (0.78–1.55)	0.576	0.59 (0.52–0.68)	<0.001	0.76 (0.58–1.02)	0.063
BMI (kg/m^2)	1.06 (1.02–1.10)	0.003	1.10 (1.07–1.14)	<0.001	1.10 (1.07–1.14)	<0.001	1.04 (1.01–1.08)	0.014	1.05 (1.00–1.10)	0.044	1.08 (1.04–1.12)	<0.001	1.12 (1.01–1.24)	0.030
WC (cm)	1.02 (1.01–1.03)	<0.001	1.02 (1.01–1.03)	<0.001	1.02 (1.01–1.03)	<0.001	1.03 (1.01–1.06)	0.012	1.04 (1.02–1.06)	<0.001	1.02 (1.01–1.03)	<0.001	1.00 (0.98–1.02)	0.804
GENERAL OBESITY														
Normal	1	Ref	1	Ref	1	Ref	1	Ref	1	Ref	1	Ref	1	Ref
Overweight	1.26 (1.00–1.59)	0.051	1.66 (1.38–2.01)	<0.001	1.68 (1.39–2.04)	<0.001	1.25 (0.56–2.76)	0.584	1.48 (0.84–2.59)	0.172	1.54 (1.24–1.91)	<0.001	2.47 (1.62–3.77)	<0.001
Obesity	2.00 (1.47–2.73)	<0.001	2.69 (2.10–3.44)	<0.001	2.62 (2.03–3.38)	<0.001	3.68 (1.82–7.44)	<0.001	3.56 (2.03–6.22)	<0.001	1.83 (1.36–2.47)	<0.001	7.27 (4.57–11.59)	<0.001
CENTRAL OBESITY														
Normal	1	Ref	1	Ref	1	Ref	1	Ref	1	Ref	1	Ref	1	Ref
Central Obesity	1.18 (0.91–1.53)	0.203	1.49 (1.21–1.83)	<0.001	1.43 (1.16–1.78)	0.001	2.76 (1.48–5.14)	0.001	2.43 (1.48–3.99)	<0.001	1.50 (1.19–1.90)	0.001	1.08 (0.69–1.72)	0.728

**Values were odds ratio (95% confidence interval); Odds ratio for each variable was adjusted for all other variables in the table; Ref, reference; BMI, Body Mass Index; WC, Waist Circumference;The comparisons were between hypertension groups and normotensives; The multivariable generalized estimating equations (GEE) logistic regression adjusted all variables listed.*

into several aspects of the national challenge of childhood hypertension in China. From 1991 to 2015, the age-standardized prevalence of hypertension and phenotypes in Chinese children and adolescents increased dramatically. Sex and age disparities were found in the prevalence of childhood hypertension and phenotypes. For adolescents aged 13–17 years, general obesity and central obesity were positively associated with hypertension, whereas the South region was a negatively related factor. For IDH, sex, age, location (urban or rural), region (north or south), BMI, WC, general obesity and central obesity were associated factors. Older age group, general obesity and central obesity were related to the increased prevalence of ISH, and only general obesity associate with the elevated prevalence of IDH.

It is well-known that hypertension in children is associated with long-term adverse health effects (7). However, few studies reported the trends and related factors of childhood hypertension phenotypes. To the best of our knowledge, this study is the first to report the secular trends in the prevalence of hypertension phenotypes in such a large sample of Chinese children over more than two decades. Based on the stringent sampling approach and standardized procedures for BP measurements in CHNS, the quality of our results was largely ensured. In line with a national survey in the United States, significant increasing temporal trends in childhood BP and the prevalence of hypertension (from 8.5 to 19.2%) were revealed in our study (29). However, such an upward secular trend was not universally observed in some previous studies due to the heterogeneity in demographic characteristics and socioeconomic status in different settings. For example, the Youth Heart Project in Northern Ireland has reported that the DBP has decreased by about ten mmHg during the past decade (30). In addition, a survey-based study in the United States showed that both mean SBP and DBP declined by 0.7 and 4.3 mmHg among 17-year-old adolescents from 1999–2002 to 2009–2012 (31). Liang et al. successfully revealed increasing trends in the prevalence of prehypertension and hypertension in Chinese children and adolescents from 1991 to 2004 (32). Compared with their study, we extended the study period from 1991–2004 to 1991–2015, additionally assessed the prevalence of hypertension according to severity (stage 1 hypertension and stage 2 hypertension) and phenotype (ISH, IDH, and SDH), and explored the effects of demographic, geographic factors, and obesity on hypertension.

IDH plays a critical role in childhood hypertension, and the prevalence was estimated to be 6.2–14.1% in this study, accounting for 67.3–78.3% of all phenotypes of hypertension. IDH in children and adolescents was defined as a DBP $\geq$ 95th percentile and an SBP $<$ 95th percentile for each age, sex, and height subgroup (10). It has been discovered that DBP levels were regulated by the renin-angiotensin-aldosterone system (RAAs) and vasoactive substances (33). Disease and unhealthy lifestyles may affect the regulation of RAAs and lead to a rise in DBP values (34–36).

Our results showed that the prevalence of hypertension and its phenotypes by sex and age subgroups increased dramatically over the recent two decades. Compared with girls, boys were more vulnerable to prehypertension and IDH. The sex differences in hypertension prevalence have been generally recognized as a result of hormones occurring at puberty (37). It has been reported that estrogen was essential for the enhancement of endothelium-dependent vasodilation and regulation of smooth muscle cells (37, 38). Besides, unhealthy behaviors, such as alcohol intake, sedentary lifestyle and obesity were more common in boys than girls in China, which may contribute to a greater risk of hypertension (39, 40). In the current study, the prevalence of hypertension among teenagers aged 13–17 years (ranging from 11.8 to 22.1%) was higher than that in 7–12 years old children (ranging from 4.5 to 18.2%). According to clinical studies and animal experiments, the changes in vascular elasticity as children grow may partly explain the age disparities in the prevalence of hypertension among children (41, 42). Moreover, the prevalence of childhood hypertension differed in regions and locations. In comparison with urban children, rural children had a lower prevalence of IDH, which may be resulted from a better lifestyle and environment in rural settings, including more healthy eating patterns, more physical activities and fewer air pollutions (43, 44). Similarly, children living in South China were less likely to be affected by hypertension, stage 1 hypertension and IDH. It has been estimated that diary sodium intake in North China is higher than that in South China, which might have attributed to the differences across geographic regions (45).

It is widely acknowledged that obesity is one of the most important factors responsible for elevated BP in children and adolescents (46, 47). In accordance with a population-based study in Nigeria, where BMI and WC were revealed as risk factors for hypertension and prehypertension, we found that both general obesity and central obesity were associated factors of childhood hypertension (48). Previous studies also stated that the proportion of obese children suffering from hypertension was three times higher than that of non-obese children (49, 50). However, the mechanisms by which obesity directly influence BP is still unclear. It is reported that sympathicotonia and insulin resistance could regulate BP level through changing vascular reactivity and reduced-sodium excretion (51, 52). Besides, the accumulation of visceral adipose tissue triggers an immune response, resulting in an excessive amount of free fatty acids (FFA) (53). The high concentrated FFA in portal vein circulation inhibits the clearance of insulin and activates the production of angiotensinogen. In addition, the unbalanced angiotensinogen affects vasoconstriction and sodium reabsorption and, therefore, increases BP and develops hypertension (53).

Limitations

Several limitations should be considered when interpreting the results of this study. First, the national representativeness of CHNS could not be fully ensured, despite the large sample size and a wide range of economic and demographic variations. Second, BP was measured three times on a one-time visit rather than on three different occasions. The prevalence of hypertension might be overestimated (54). Third, people that were included at each study interval were not necessarily the same people, so the change in blood pressure over time may be related to sampling in each round. Fourth, several confounding factors, such as family economic level, family parent education, children's dietary patterns, comorbidities and medications were

not accounted for in our multivariable analyses due to the absence of relative information.

CONCLUSION

In conclusion, BP levels and prevalence of hypertension and phenotypes increased dramatically in Chinese children and adolescents from 1991 to 2015. Regional discrepancy, demographic features, BMI, WC, and overweight/obesity status were associated factors of hypertension among youths. Our findings call for actions to identify and prevent childhood hypertension in China.

DATA AVAILABILITY STATEMENT

The datasets presented in this study can be found in online repositories. The names of the repository/repositories and accession number(s) can be found in the article/**Supplementary Material**.

AUTHOR CONTRIBUTIONS

PS designed the study. XY, QY, WX, and PS managed and analyzed the data. XY and QY prepared the first draft. All authors were involved in revising the paper and gave final approval of the submitted versions.

SUPPLEMENTARY MATERIAL

The Supplementary Material for this article can be found online at: https://www.frontiersin.org/articles/10.3389/fcvm.2021.627741/full#supplementary-material

REFERENCES

1. Kokubo Y, Matsumoto C. Hypertension is a risk factor for several types of heart disease: review of prospective studies. *Adv Exp Med Biol.* (2017) 956:419–26. doi: 10.1007/5584_2016_99
2. Girndt M. Diagnostik und Therapie der chronischen Nierenerkrankung. *Der Internist.* (2017) 58:243–56. doi: 10.1007/s00108-017-0195-2
3. Griffin G. Antiplatelet therapy and anticoagulation in patients with hypertension. *Am Fam Physician.* (2005) 71:897–9. doi: 10.1001/jama.293.9.1123
4. Xiong X, Yang X, Liu Y, Zhang Y, Wang P, Wang J. Chinese herbal formulas for treating hypertension in traditional Chinese medicine: perspective of modern science. *Hypertens Res.* (2013) 36:570–9. doi: 10.1038/hr.2013.18
5. Center N C. *China Cardiovascular Disease Report 2015. First Edition Ed.* Beijing: China Encyclopedia press (2016). p. 13–24.
6. Song P, Zhang Y, Yu J, Zha M, Zhu Y, Rahimi K, et al. Global prevalence of hypertension in children. *Jama Pediatr.* (2019) 173:1154. doi: 10.1001/jamapediatrics.2019.3310
7. Rapsomaniki E, Timmis A, George J, Pujades-Rodriguez M, Shah AD, Denaxas S, et al. Blood pressure and incidence of twelve cardiovascular diseases: lifetime risks, healthy life-years lost, and age-specific associations in 1·25 million people. *Lancet.* (2014) 383:1899–911. doi: 10.1016/S0140-6736(14)60685-1
8. Hansen ML, Gunn PW, Kaelber DC. Underdiagnosis of hypertension in children and adolescents. *JAMA.* (2007) 298:874. doi: 10.1001/jama.298.8.874
9. Battistoni A, Canichella F, Pignatelli G, Ferrucci A, Tocci G, Volpe M. Hypertension in young people: epidemiology, diagnostic assessment and therapeutic approach. *High Blood Pressur Cardiovasc Prev.* (2015) 22:381–8. doi: 10.1007/s40292-015-0114-3
10. Adolescents NHBP. The fourth report on the diagnosis, evaluation, and treatment of high blood pressure in children and adolescents. *Pediatrics.* (2004) 114:555–76. doi: 10.1161/01.HYP.0000143545.54637.af
11. Flynn JT, Kaelber DC, Baker-Smith CM, Blowey D, Carroll AE, Daniels SR, et al. Clinical practice guideline for screening and management of high blood pressure in children and adolescents. *Pediatrics.* (2017) 140:e20171904. doi: 10.1542/peds.2017-1904
12. Burgner DP, Sabin MA, Magnussen CG, Cheung M, Sun C, Kähönen M, et al. Early childhood hospitalisation with infection and subclinical atherosclerosis in adulthood: The Cardiovascular Risk in Young Finns Study. *Atherosclerosis.* (2015) 239:496–502. doi: 10.1016/j.atherosclerosis.2015.02.024
13. Beckett LA, Rosner B, Roche AF, Guo S. Serial changes in blood pressure from adolescence into adulthood. *Am J Epidemiol.* (1992) 135:1166–77. doi: 10.1093/oxfordjournals.aje.a116217
14. Zhang Y, Wang S. Comparison of blood pressure levels among children and adolescents with different body mass index and waist circumference: study in a large sample in Shandong, China. *Eur J Nutr.* (2014) 53:627–34. doi: 10.1007/s00394-013-0571-1
15. Marcovecchio M L, Mohn A, Diddi G, Polidori N, Chiarelli F, Fuiano N. Longitudinal assessment of blood pressure in school-aged children: a 3-year follow-up study. *Pediatr Cardiol.* (2016) 37:255–61. doi: 10.1007/s00246-015-1271-9
16. Chiolero A, Cachat F, Burnier M, Paccaud F, Bovet P. Prevalence of hypertension in schoolchildren based on repeated measurements and association with overweight. *J Hypertens.* (2007) 25:2209–17. doi: 10.1097/HJH.0b013e3282ef48b2
17. Olsen MH, Angell SY, Asma S, Boutouyrie P, Burger D, Chirinos J A, et al. A call to action and a lifecourse strategy to address the global burden of raised blood pressure on current and future generations: the Lancet Commission on hypertension. *Lancet.* (2016) 388:2665–712. doi: 10.1016/s0140-6736(16)31134-5
18. Popkin BM, Du S, Zhai F. Cohort profile: the china health and nutrition survey—monitoring and understanding socio-economic and health change in China, 1989–2011. *Int J Epidemiol.* (2010) 39:1435–40. doi: 10.1093/ije/dyp322
19. Zhang B, Zhai FY, Du SF, Popkin BM. The China health and nutrition survey, 1989-2011. *Obes Rev.* (2014) 15:2–7. doi: 10.1111/obr.12119
20. Organization WH. Physical status: the use and interpretation of anthropometry. Report of a WHO Expert Committee. *WHO.* (1995) 854:1–452. doi: 10.1002/(sici)1520-6300(1996) 8:6<786::aid-ajhb11>3.0.co;2-i
21. Hui F, Yin-kun Y, Jie M. Establishing the user-friendly screening criteria for elevated blood pressure in Chinese children aged 3-17 years. *Chinese J Hypert.* (2017) 5:436–40. doi: 10.16439/j.cnki.1673-7245.2017.05.010
22. Sinha R, Saha A, Samuels J. American academy of pediatrics clinical practice guidelines for screening and management of high blood pressure in children and adolescents: what is new? *Indian Pediatr.* (2019) 56:317–21. doi: 10.1007/s13312-019-1523-5
23. Xi B, Liang Y, He T, Reilly KH, Hu Y, Wang Q, et al. Secular trends in the prevalence of general and abdominal obesity among Chinese adults, 1993-2009. *Obes Rev.* (2012) 13:287–96. doi: 10.1111/j.1467-789X.2011.00944.x
24. Song P, Li X, Bu Y, Ding S, Zhai D, Wang E, et al. Temporal trends in normal weight central obesity and its associations with cardiometabolic risk among Chinese adults. *Sci Rep-Uk.* (2019) 9:5411. doi: 10.1038/s41598-019-41986-5
25. Fan H, Yan Y, Mi J. Updating blood pressure references for Chinese children aged 3-17 years. *Chinese J Hypert.* (2017) 25:428–35. doi: 10.16439/j.cnki.1673-7245.2017.05.009

26. Commission NHAF. *Screening Criteria for Overweight and Obesity in School-Age Children and Adolescents.* WS /T 586-—2017. (2018). Available online at: http://ty.sx.gov.cn/art/2018/5/17/art_1489227_18292267.html.
27. Guerra MW, Shults J, Amsterdam J, Ten-Have T. The analysis of binary longitudinal data with time-dependent covariates. *Stats Med.* (2012) 31:931–48. doi: 10.1002/sim.4465
28. Zeger LSL. Longitudinal data analysis using generalized linear models. *Biometrika.* (1986) 73:13–22. doi: 10.1093/biomet/73.1.13
29. Din-Dzietham R, Liu Y, Bielo M, Shamsa F. High blood pressure trends in children and adolescents in national surveys, 1963 to 2002. *Circulation.* (2007) 116:1488–96. doi: 10.1161/CIRCULATIONAHA.106.683243
30. Watkins D, McCarron P, Murray L, Cran G, Boreham C, Robson P, et al. Trends in blood pressure over 10 years in adolescents: analyses of cross sectional surveys in the Northern Ireland Young Hearts project. *BMJ.* (2004) 329:139. doi: 10.1136/bmj.38149.510139.7C
31. Xi B, Zhang T, Zhang M, Liu F, Zong X, Zhao M, et al. Trends in elevated blood pressure among us children and adolescents: 1999–2012. *Am J Hypertens.* (2016) 29:217–25. doi: 10.1093/ajh/hpv091
32. Liang Y, Xi B, Hu Y, Wang C, Liu J, Yan Y, et al. Trends in blood pressure and hypertension among Chinese children and adolescents: China health and nutrition surveys 1991–2004. *Blood Press.* (2011) 20:45–53. doi: 10.3109/08037051.2010.524085
33. Mattson D L. Immune mechanisms of salt-sensitive hypertension and renal end-organ damage. *Nat Rev Nephrol.* (2019) 15:290–300. doi: 10.1038/s41581-019-0121-z
34. Franklin S S, Pio J R, Wong N D, Larson M G, Leip E P, Vasan R S, et al. Predictors of new-onset diastolic and systolic hypertension. *Circulation.* (2005) 111:1121–7. doi: 10.1161/01.CIR.0000157159.39889.EC
35. Gu M, Qi Y, Li M, Niu W. Association of body mass index and alcohol intake with hypertension subtypes among HAN chinese. *Clin Exp Hypertens.* (2011) 33:518–24. doi: 10.3109/10641963.2011.561899
36. Price A J, Crampin A C, Amberbir A, Kayuni-Chihana N, Musicha C, Tafatatha T, et al. Prevalence of obesity, hypertension, and diabetes, and cascade of care in sub-Saharan Africa: a cross-sectional, population-based study in rural and urban Malawi. *Lancet Diabetes Endocri.* (2018) 6:208–22. doi: 10.1016/S2213-8587(17)30432-1
37. White K, Johansen AK, Nilsen M, Ciuclan L, Wallace E, Paton L, et al. Activity of the estrogen-metabolizing enzyme cytochrome p450 1b1 influences the development of pulmonary arterial hypertension. *Circulation.* (2012) 126:1087–98. doi: 10.1161/CIRCULATIONAHA.111.062927
38. Zhu Y. Abnormal vascular function and hypertension in mice deficient in estrogen receptor beta. *Science.* (2002) 295:505–8. doi: 10.1126/science.1065250
39. Du T, Sun X, Yin P, Yuan G, Zhang M, Zhou X, et al. Secular trends in the prevalence of low risk factor burden for cardiovascular disease according to obesity status among Chinese adults, 1993–2009. *Bmc Public Health.* (2014) 14:961. doi: 10.1186/1471-2458-14-961
40. Millwood IY, Li L, Smith M, Guo Y, Yang L, Bian Z, et al. Alcohol consumption in 0.5 million people from 10 diverse regions of China: prevalence, patterns and socio-demographic and health-related correlates. *Int J Epidemiol.* (2017) 46:2103. doi: 10.1093/ije/dyx210
41. Amin-Hanjani S, Du X, Pandey D K, Thulborn K R, Charbel F T. Effect of age and vascular anatomy on blood flow in major cerebral vessels. *J Cerebral Blood Flow Metab.* (2015) 35:312–8. doi: 10.1038/jcbfm.2014.203
42. Sletner L, Mahon P, Crozier S R, Inskip H M, Godfrey K M, Chiesa S, et al. Childhood fat and lean mass. *Arterioscl Thromb Vasc Biol.* (2018) 38:2528–37. doi: 10.1161/ATVBAHA.118.311455
43. Fallah Z, Qorbani M, Motlagh ME, Heshmat R, Ardalan G, Kelishadi R. Prevalence of prehypertension and hypertension in a nationally representative sample of iranian children and adolescents: the CASPIAN-IV study. *Int J Prev Med.* (2014) 5 (Suppl. 1):S57–64.
44. Agyemang C, Redekop WK, Owusu-Dabo E, Bruijnzeels MA. Blood pressure patterns in rural, semi-urban and urban children in the Ashanti region of Ghana, West Africa. *BMC Public Health.* (2005) 5:114. doi: 10.1186/1471-2458-5-114
45. Huang L, Wang H, Wang Z, Wang Y, Zhang B, Ding G. Associations of dietary sodium, potassium, and sodium to potassium ratio with blood pressure—regional disparities in China. *Nutrients.* (2020) 12:366. doi: 10.3390/nu12020366
46. Moser DC, Giuliano IDCB, Titski ACK, Gaya AR, Coelho-e-Silva MJ, Leite N. Anthropometric measures and blood pressure in school children. *J Pediat-Brazil.* (2013) 89:243–9. doi: 10.1016/j.jped.2012.11.006
47. Ramesh V, Saraswat S, Choudhury N, Gupta RK. Relationship of serum alanine aminotransferase (ALT) to body mass index (BMI) in blood donors: the need to correct ALT for BMI in blood donor screening. *Transfusion Med.* (1995) 5:273–4. doi: 10.1111/j.1365-3148.1995.tb00213.x
48. Ononamadu CJ, Ezekwesili CN, Onyeukwu OF, Umeoguaju UF, Ezeigwe OC, Ihegboro GO. Comparative analysis of anthropometric indices of obesity as correlates and potential predictors of risk for hypertension and prehypertension in a population in Nigeria. *Cardiovasc J Afr.* (2017) 28:92–9. doi: 10.5830/CVJA-2016-061
49. Sorof JM, Poffenbarger T, Franco K, Bernard L, Portman RJ. Isolated systolic hypertension, obesity, and hyperkinetic hemodynamic states in children. *J Pediatrics.* (2002) 140:660–6. doi: 10.1067/mpd.2002.125228
50. Sorof J, Daniels S. Obesity hypertension in children: a problem of epidemic proportions. *Hypertension.* (2002) 40:441–7. doi: 10.1161/01.hyp.0000032940.33466.12
51. Anyaegbu E I, Dharnidharka V R. Hypertension in the teenager. *Pediatr Clin N Am.* (2014) 61:131–51. doi: 10.1016/j.pcl.2013.09.011
52. Palatini P. Sympathetic overactivity in hypertension: a risk factor for cardiovascular disease. *Curr Hypertens Rep.* (2001) 3:S3–9. doi: 10.1007/s11906-001-0065-z
53. Frayn K N. Visceral fat and insulin resistance–causative or correlative? *Br J Nutr.* (2000) 83 (Suppl. 1):S71–7. doi: 10.1017/s0007114500000982
54. Zhao Y, Wang L, Xue H, Wang H, Wang Y. Fast food consumption and its associations with obesity and hypertension among children: results from the baseline data of the childhood obesity study in china mega-cities. *BMC Public Health.* (2017) 17:933. doi: 10.1186/s12889-017-4952-x

Conflict of Interest: The authors declare that the research was conducted in the absence of any commercial or financial relationships that could be construed as a potential conflict of interest.

frontiers in Cardiovascular Medicine

REVIEW
published: 12 May 2021
doi: 10.3389/fcvm.2021.613930

The Role of HIV Infection in the Pathophysiology of Gestational Diabetes Mellitus and Hypertensive Disorders of Pregnancy

*Wendy N. Phoswa**

Department of Life and Consumer Sciences, University of South Africa (UNISA), Science Campus, Florida, South Africa

Purpose of the Review: The main objective of this study is to investigate mechanisms associated with gestational diabetes mellitus (GDM) and hypertensive disorders of pregnancy (HDP) in HIV infected pregnant women by looking how placental hormones such as (progesterone and prolactin) and basic haemostatic parameters are regulated in HIV infected pregnancies.

Recent Findings: HIV/AIDS are a major global obstetric health burden that lead to increased rate of morbidity and mortality. HIV/AIDS has been associated with the pathophysiology of GDM and HDP. Increased risk of GDM due to highly active antiretroviral therapy (HAART) usage has been reported in HIV infected pregnancies, which causes insulin resistance in both pregnant and non-pregnant individuals. HAART is a medication used for lowering maternal antepartum viral load and pre-exposure and post-exposure prophylaxis of the infant. In pregnant women, HAART induces diabetogenic effect by causing dysregulation of placental hormones such as (progesterone and prolactin) and predispose HIV infected women to GDM. In addition to HIV/AIDS and GDM, Studies have indicated that HIV infection causes haemostatic abnormalities such as hematological disorder, deregulated haematopoiesis process and the coagulation process which results in HDP.

Summary: This study will help on improving therapeutic management and understanding of the pathophysiology of GDM and HDP in the absence as well as in the presence of HIV infection by reviewing studies reporting on these mechanism.

Keywords: gestational diabetes, gestational hypertension, highly active antiretroviral therapy, human immune deficiency virus, hypertensive disorders of pregnancy, pre-eclampsia

OPEN ACCESS

Edited by:
Modar Kassan, University of Tennessee Health Science Center (UTHSC), United States

Reviewed by:
Marius Miglinas, Vilnius University, Lithuania
Alexis A. Gonzalez, Pontifical Catholic University of Valparaíso, Chile

***Correspondence:**
Wendy N. Phoswa
phoswawendy@gmail.com

Specialty section:
This article was submitted to Hypertension, a section of the journal Frontiers in Cardiovascular Medicine

Received: *04 October 2020*
Accepted: *19 April 2021*
Published: *12 May 2021*

Citation:
Phoswa WN (2021) The Role of HIV Infection in the Pathophysiology of Gestational Diabetes Mellitus and Hypertensive Disorders of Pregnancy. Front. Cardiovasc. Med. 8:613930. doi: 10.3389/fcvm.2021.613930

INTRODUCTION

Human immune deficiency virus and acquired immunodeficiency syndrome (HIV/AIDS) is the major global health burden affecting ∼36.9 million people in the world, including 1.8 million children. "About 25% people don't know their HIV status" (1). The prevalence of HIV infection is higher in low- and middle- income countries, with about 66% living in sub-Saharan Africa. Approximately "19.6 million people are living in East and Southern Africa" (2). In 2017, there were 800,000 new HIV infections in 2017 in the Southern Africa. About 66% adults and 59% children are on anti-retroviral therapy (3).

In the 1980s, the average life expectancy following HIV/AIDS diagnosis was ∼1 year. However, with improved medical care; Today, availability of highly active anti retro viral therapy (HAART) started early in the course of HIV infection, have been beneficial in suppressing HIV thus reducing mortality and improving life span of HIV infected individuals (4–6). Unfortunately these drugs lead to development of other adverse health outcomes such as metabolic disorders (Insulin resistance, diabetes mellitus, dyslipidemia, and lipodystrophy) (6, 7). Several studies have reported on the incidence of diabetes mellitus (DM) in HAART experienced individuals (8, 9). The prevalence of DM has been reported to be 10% in HIV individuals receiving medical care, nearly 3.8% higher than in the HIV uninfected population (10, 11).

"Several risk factors such as aging, male sex, obesity, African American, Hispanic, Indian ethnicity, family history, and hepatitis C coinfection, high body mass index (BMI), greater waist circumference, and lower socioeconomic class, have been associated with the development of DM in HIV-infected individuals" (12–18). HIV infection has reported to been linked more with type 2 diabetes mellitus (T2DM) rather than type 1 diabetes mellitus (12). Another type of diabetes that has been widely associated with HIV infection in pregnancy is gestational diabetes mellitus (GDM). Several studies have reported on the incidence of GDM in HIV infected pregnant women. It is speculated that this occurs as a result of HIV infection which causes alterations in the placental hormones which are associated with insulin resistance. Additionally, human immune deficiency virus (HIV) has also been observed as a risk factor for HDP (19). Multiple studies have reported that HIV predisposes pregnant women to HDP (19, 20). Although, the mechanism behind this remains to be ununderstood. It is believed that this occurs as a result of exposure to HAART. HAART "is a treatment given to non-pregnant and pregnant women to prevent viral replication and mother-to-child transmission" (21). This treatment has been reported to alter maternal haemostatic profile (22, 23).

Current literature provides enough evidence that there is a direct link between HIV infection and the pathophysiology of GDM as well HDP. Therefore, more research is required in order to understand association between HIV infection and these diseases. This will help the health care practitioners to improve diagnostic criteria's and care for HIV infected women who are suffering from GDM as well as HDP. And will also help better our knowledge and understanding on the pathophysiology of these conditions in order to improve therapeutic approaches. Hence, the main objective of this study is to investigate mechanisms associated with GDM and HDP in HIV infected pregnant women by looking how placental hormones such as (progesterone and prolactin) and basic haemostatic parameters are regulated in HIV infected pregnancies.

GESTATIONAL DIABETES MELLITUS

"Gestational diabetes mellitus (GDM), is defined as excessive glucose intolerance diagnosed during gestation" (24). This disease affects 14% of all pregnancies world-wide (25). The prevalence of GDM in high-income countries is 2–10% and 1.6–14% in low-middle-income countries (26, 27).

Normally, "pregnancy involves altered state of glucose metabolism and insulin sensitivity" (28). However, this change predisposes some pregnant women to GDM (18, 29). Pregnancies affected by GDM are associated with detrimental effects on maternal and fetal health. These effects include, "risk of cesarean and operative vaginal delivery, macrosomia, preterm birth, shoulder dystocia, microangiopathy, neonatal hypoglycemia and hyperbilirubinemia, pregnancy induced hypertension, and pre-eclampsia" (30, 31). Women with a previous history of GDM have increased risk of developing T2DM at an earlier stage in life and cardiovascular diseases (32). Risk factors for GDM include family history of diabetes, advanced maternal age, obesity, ethnicity (no white ethnicity), and previous pregnancy complications (17, 18, 29). "There is currently no cure for GDM, except lifestyle intervention (balanced diet and regular exercise)" (33).

The "prevalence of GDM in HIV uninfected pregnant women is 2–5% of all pregnancies in high income countries" (34, 35) and 2–7% in HIV-infected pregnant women (7, 36–45). "Increased risk of developing GDM in HIV infected women has been reported to be due to the use of HAART which induces insulin resistance in pregnant and non-pregnant individuals" (46). Currently, studies have outlined on the pathophysiology of GDM, however the association between GDM and HIV infection remain obscure.

PATHOPHYSIOLOGY OF GDM

Gestational diabetes result from hyperinsulinemia and insulin resistance leading to abnormal glucose intolerance. During the early stages of pregnancy, various metabolic changes occur in the order to promote adipose tissue accumulation. "These changes include increased insulin secretion and insulin sensitivity" (29). Some studies report that insulin sensitivity remain unchanged or decreased during early stages of pregnancy (47, 48). However, "In later stages of pregnancy, insulin sensitivity is reduced due to activation of a number of hormones such as placental lactogen, estrogen, leptin, progesterone, prolactin, cortisol, and adiponectin. It has been reported that insulin resistance plays a central role in the pathophysiology of GDM" (49, 50).

Placental Induced Insulin Resistance

In the placenta, insulin binds to insulin receptors (IRs) which are present in the placental cells (cytotrophoblasts), thus activating the signaling pathways such as the Ras-extracellular-signal-regulated kinase (Ras-ERK) and the IRS (IR substrate)-PI3K-Akt-mTOR pathway, which are important for placental cellular differentiation, proliferation and metabolism of nutrients (51–53). Insulin is not the only hormone responsible for activating these pathways, growth factors and placental hormones, also play a very important role in their activation (54–56).

During normal pregnancy development the placenta secretes several hormones such as human placental lactogen (hPL), human placental growth hormone (hPGH), progesterone, adiponectin, leptin, prolactin, and cortisol into the maternal blood systems (57). These hormones play a very crucial role

in fetoplacental development. However, over secretion as well as under secretion of these hormones has been associated with reduced insulin sensitivity during pregnancy (49, 57, 58).

Human Placental Lactogen or Human or Chorionic Somatomammotropin Hormone

Human placental lactogen (hPL) has been shown to "induce insulin secretion from the pancreases during pregnancy" (59). Various studies have documented that hPL can induce insulin resistance (60, 61). Additionally, other studies indicate that hPL can cause peripheral lipolysis insulin resistance (62, 63), although the results are debatable (64). A study conducted by Vasavada et al. (65) in Beta cells of transgenic mice showed that placental lactogen (PL) resulted in over secretion of plasma insulin. Interestingly they also observed increased (2-fold) insulin content in the pancreas. Similar findings were observed by Parsons et al. (66) where they found that placental lactogen secretion resulted in increased islet cell proliferation and insulin secretion. Although, studies have reported on the role of placental lactogen on insulin resistance, However very few studies have reported on human placenta (**Table 1**). Therefore, more studies looking at the role of human placental lactogen on insulin resistance in different ethnics groups are needed.

Human Placental Growth Hormone

The human placental growth hormone (hPGH) is found in the placental cells (syncytiotrophoblast), and is said to "replace pituitary growth hormone during pregnancy" (78). This hormone has also been implicated to induce diabetogenic effects result from increased glucose levels and insulin resistance (60, 79). A study conducted by Barbour et al. (68) showed that "hPGH may lead to insulin resistance by increasing the expression of the p85α monomer, which inhibits p85-p110 heterodimer from binding to insulin receptor substrate-1 (IRS-1) protein" (67) thus preventing further insulin signaling leading to substantially reduced glucose uptake (80, 81). "IRS-1 interacts with the p85-p110 heterodimer of phosphatidylinositide 3-kinase (PI3K) which then leads to the activation of this enzyme and subsequent stimulation of adenylate kinase 3 (Akt), resulting in enhanced glucose utilization, and increased glycogen and protein synthesis" (82, 83).

It has been reported that "GDM patients had decreased levels of IRS-1" (49) indicating that in DGM patients there is increased levels of insulin resistance.

Progesterone

According to Costrini and Kalkhoff (84) "Progesterone contribute to increased insulin secretion and plasma insulin sensitivity to glucose administration during pregnancy." Several studies have reported on the diabetogenic effect of progesterone (69–72, 85, 86). Rebarber et al. (87) observed that Administration of progesterone compound; prophylactic intramuscular 17α-Hydroxyprogesterone (17P) resulted in 12.9% incidence of GDM compared to 4.9% control groups. Implying that "17P is associated with an increased risk of GDM". In contrast a study done by Rosta et al. (88); evaluating the effect of vaginal administration of progesterone on the incident of GDM, showed that there was no significance difference on the incidence of GDM in progesterone treated and the control group. They further concluded that "the use of progesterone is not linked with an increased risk of GDM" (88).

Adiponectin

Adiponectin, "is an insulin-inducing hormone secreted by adipose tissue" (89). It is been associated with the pathogenesis of insulin resistance (90). Low levels of adiponectin lead to insulin resistance thus resulting in the pathophysiology of GDM (49, 91).

Studies have shown that the risk of GDM is higher in women with reduced adiponectin levels (92, 93). The general function of adiponectin is to "facilitates insulin action through binding to its receptors AdipoR1 and AdipoR2, thereby leading to induction of adenosine monophosphate dependent kinase (AMPK), PPAR-α" (94).

Adiponectin induces antidiabetic effects by stimulating glucose uptake *via* AMPK by "binding to its receptors AdipoR1 and AdipoR2" (95). "This reduces glucose production in the liver, which can account for the antidiabetic effects of adiponectin" (95). A case control study done by Mohammadi and Paknahad (73) showed decreased serum concentration levels of adiponectin in GDM women indicating adiponectin as a diagnostic tool for detecting the presence of GDM. Although, there are very few studies (96) that have reported on the role of adiponectin on the pathogenesis of insulin resistance in GDM (**Table 1**), more studies are needed in order to understand how adiponectin is regulated in GDM patients.

Leptin

"Is a hormone produced by adipocytes and in low levels by the gastric fundic intestine, placenta, skeletal muscle, and brain" (94, 97). Leptin is important for glucose homeostasis (94). Administration of leptin have been reported to lower insulin secretion (98–102).

A study done *in vitro* showed that "leptin can prevent glucose transporter 2 (GLUT2) phosphorylation, glucose transport, and intracellular adenosine triphosphate (ATP) levels" (98).

Leptin has also been shown to "reduce cyclic adenosine monophosphate (cAMP)-induced insulin secretion, *via* stimulation of phosphodiesterase-3B (PDE3B") (103–105). Leptin also inhibits protein kinase C (PKC)-induced insulin secretion (106).

The function of leptin is "mediated by the Janus kinase, signal transducer and activator of transcription (JAK-STAT) pathway" (94). "Leptin receptor-mediated JAK–STAT signaling is crucial for monitoring of food ingestion and body weight" (94). Leptin also stimulate PI3K which in turn stimulate IRS-1 followed which activate insulin secretion allowing glucose uptake by the cells (94).

The levels of leptin in diabetes are remain debatable. Several studies report higher plasma leptin levels diabetes mellitus (96, 107, 108). In contrast, Some studies report that reduced levels of leptin correlates with type 1 diabetes (109). However, some studies indicate that there is no correlation between plasma leptin levels and diabetes (110, 111). Interestingly, some research

TABLE 1 | A comprehensive list of studies in this review reporting on hormones associated with GDM.

Hormone investigated	Author	Country	Cohort type	Main findings
Human placental lactogen (hPL)	(66)	United States	Rat pancreatic cells (islets of Langerhans)	hPL increased insulin secretion.
Human placental lactogen (hPL)	(59)	United States	Rat, mouse, and human pancreatic cells (islets of Langerhans)	hPL induces insulin resistance during pregnancy.
Human placental lactogen (hPL)	(65)	United States	Mice	hPL increased plasma insulin and pancreatic insulin secretion.
Human placental growth hormone (hPGH)	(67)	United States	Mice	hPGH may contribute to the insulin resistance.
Progesterone	(68)	United States	Pregnant women	The use of 17alpha-hydroxyprogesterone caproate (17P) predisposes women to GDM.
Progesterone	(69)	United States	Pregnant women	Women receiving weekly intramuscular 17alpha-hydroxyprogesterone had increased prevalence of GDM.
Progesterone	(70)	Brazil	Rat pancreatic cells (islets of Langerhans)	Progesterone leads to pancreatic cells oxidative stress and may be associated with gestational diabetes in pregnancy.
Progesterone	(71)	United States	Pregnant women	In obese women, the use of 17alpha-hydroxyprogesterone caproate (17P) may increase their chances of developing GDM.
Progesterone	(72)	Iran	Pregnant women	The use of 17alpha-hydroxyprogesterone caproate (17P) may associated with increased risk of GDM in women who conceived *via* assisted reproductive technology.
Adiponectin	(73)	Iran	Pregnant women	Adiponectin is lower in gestational diabetic women.
Leptin	(74)	Austria	Pregnant women	Leptin is correlated with insulin resistance.
Leptin	(75)	Iran	Pregnant women	Leptin is higher in GDM.
Leptin	(76)	China	Pregnant women	Leptin is associated with GDM.
Prolactin	(77)	Australia	Pregnant women	High prolactin is associated with higher glucose and the pathogenesis on GDM.

findings report that diabetogenic effect of plasma leptin was only observed in men than women (96, 112, 113).

A study by Kautzky-Willer et al. (74) showed that "high serum leptin levels were correlated with insulin resistance in GDM." These findings were confirmed by Soheilykhah et al. (75) who observed similar correlation. More interestingly, a study conducted by Yang et al. (76) in Chinese population, investigating the "association between gestational diabetes and plasma leptin levels, leptin G2548, and leptin receptor Gln223Arg polymorphisms" showed that "GDM was only associated with high plasma leptin levels rather that leptin Gln223Arg and leptin receptor polymorphisms." Although, studies have reported on the association between plasma leptin levels and GDM, however, there are currently no studies that have reported on the association between leptin levels and GDM in the African population (**Table 1**). More studies are needed in order to see how plasma leptin levels, leptin, and leptin receptor gene polymorphisms are expressed in the African population.

Prolactin

Prolactin is a "hormone has also been shown to play role in maintaining glucose homeostasis" (114). Association between prolactin levels and the risk of GDM remain controversial. Some studies report that "excessive prolactin levels have been associated with insulin resistance in diabetes" (115), and some report that "high prolactin levels are associated with decreased risk of diabetes mellitus and impaired glucose tolerance" (116). A prospective study conducted by Wang et al. (117) showed that "high circulating prolactin levels are associated with reduced incident of diabetes mellitus." In contrast, Daimon et al. (118) showed that "high serum prolactin levels is associated with metabolic effect such as insulin insensitivity in Men."

Very few studies have associated the levels of prolactin with GDM. High prolactin levels have been linked to the pathogenesis of GDM (77). In contrast, Retnakaran et al. (119) documented that high prolactin levels indicate a sign of lower chances to develop diabetes. Therefore, more studies are needed to confirm how prolactin levels are regulated in GDM.

Cortisol

Other factors such as "increased levels of serum cortisol" (120), "Tumor necrosis factor α (TNF α, ILs e.g., IL-6), can interrupt the insulin signaling pathway and can lead to insulin resistance during normal pregnancy" (121).

PATHOPHYSIOLOGY OF GDM IN HIV ASSOCIATED PREGNANCIES

HIV/AIDS has been shown to be the global pandemic that lead both maternal and perinatal morbidity and mortality resulting from pregnancy related complications such as GDM. The placenta is believed to play a primary role in the pathogenesis of gestational diabetes. The placenta is a highly specialized organ that is responsible for normal pregnancy development. It allows feto-maternal exchange of gases and nutrients for fetal development and maintenance to occur. Various pathogens, such as bacterial, fungal, and virus infection (e.g., HIV) can disturb the normal performance of the placenta and lead to pregnancy related complications.

HAART usage during HIV infected pregnancies has been mentioned as the key factor that lead to pregnancy related complications (122–124). HAART-induced GDM is believed to result from the dysregulation of placental hormones during pregnancy. Several studies have reported on how these hormones are regulated in during HIV infection and in the duration of HAART.

Placenta development is regulated by progesterone (125, 126). Reduced levels of progesterone in HIV infection has been reported to disrupt normal pregnancy development (127).

Previous studies have shown that "progesterone levels are lower in HAART treated HIV-infected pregnant women" (128, 129), this explain why there is an increase rate of pregnancy complications in HIV associated pregnancies. A study conducted by Mohammadi et al. (130) on mice revealed that progesterone supplementation to HAART-treated mice improved their placental function. Currently, there are no studies that have reported on the levels of progesterone in HIV associated GDM women. Studies are needed in order to see how this hormone is regulated in HIV induced metabolic disorders.

Leptin is another hormone that has been reported in HIV associated metabolic disorders. This hormone is known for it anti-diabetogenic effects (131). Leptin levels are generally higher in females than in male population (132). In women, leptin levels increase drastically during pregnancy and decrease before or during labor (133).

There is contradictory data on levels of leptin in HIV associated studies. A previous study has reported that leptin levels are decreased in HIV/HAART-associated lipoatrophy (134). In contrast Haffejee et al. (135), observed that high leptin levels in HIV-infected HAART treated women is associated with the pathogenesis of a pregnancy complication (pre-eclampsia). To the best of our knowledge, no studies have reported on the levels of leptin in in HIV infected gestational diabetic women. More studies are needed evaluating the levels of leptin in HIV associated metabolic disorders.

Prolactin is also another hormone that has been found to be elevated during HIV infection (136, 137), but not correlated to HAART usage (138). In contrast, Okeke et al. (139) indicated that prolactin levels are suppressed in HIV infected pregnancy women and that HAART had no effect on the levels of prolactin. No studies have reported on how prolactin in regulated in the presence of HIV infection in GDM women. Therefore, studies are needed in order to understand the pathophysiology underlying GDM during HIV infection.

More interestingly, metabolic disturbance in HIV infected individuals has been correlated with increased serum cortisol. Collazos et al. (140), showed that HIV infected patients who initiated HAART had elevated serum cortisol levels. These findings confirmed the role of cortisol on the metabolic disorders induced by HAART during HIV infection.

In addition, a study evaluating the levels of hPGH showed that HIV status had no effect on the levels of this hormone. These findings were in accordance with the findings by Esemu et al. (141), who investigated the effect of HIV infection on insulin-like growth factor-1 (IGF-1) and angiogenic factors in Cameroonian pregnant women receiving HAART. They reported that "HIV infection did not alter the regulation of both factors" (141). Their findings also confirmed the important of HAART usage in maintaining IGF-1 during pregnancy (141). "IGF-1 is a primary mediator of growth hormone" and placental growth hormone (142). It is also involved in stimulating insulin signaling pathway *via* activation of PI3K-AKT pathway. However, more studies are still needed in order to validate how this hormone is regulated in the presence of HIV infection.

Apart from GDM, HIV infection and its association with increased risk of hypertensive disorders of pregnancy has been reported (19).

HYPERTENSIVE DISORDERS OF PREGNANCY

Affect up to 10% of all pregnancies globally (143). The "HDP comprise of gestational hypertension (GH), preeclampsia (PE) and eclampsia (E). A majority of HDP cases are from low and middle income countries" (144). In South Africa, "HDP are the most common direct cause of maternal mortality and account for 18% of all maternal deaths" (145, 146). Hypertensive disorders of pregnancy can also "affect the fetus and the newborn by leading to premature delivery, intrauterine growth retardation (IUGR), abruptio placentae and intrauterine death" (147). "Maternal complications include the HELLP syndrome (hemolyisis, elevated liver enzymes, low platelets), pulmonary edema, acute liver/renal failure, disseminated intravascular coagulopathy, adult respiratory distress syndrome, sepsis, and liver hemorrhage" (144). Despite extensive research on HDP, the pathophysiology of this disorder remains an egnima. Inflammation is one of the commonly reported factors that lead to the development of HDP (148). Among other factors reported to be involved in the pathophysiology of HDP is haemostatic (hematology and coagulation) profile. Studies have demonstrated that "neutrophil to lymphocyte ratios and platelet count may predict disease development, and may help in monitoring disease and the prognosis of HDP" (149–154).

Several risk factors are associated with the pathogenesis HDP. These factors include previous history of PE or GH, multiple pregnancies, polycystic ovarian syndrome, chronic kidney disease, hypertension, diabetes, and autoimmune disorders (155).

Recently, HIV has also been observed as a risk factor for HDP (19). Multiple studies have reported that HIV predisposes pregnant women to HDP (19, 20). Although, the mechanism behind this is still to be elucidated. It is believed that this occurs as a result of exposure to highly active antiretroviral therapy (HAART). HAART is a treatment given to non-pregnant and pregnant women to prevent viral replication and mother-to-child transmission (21). This treatment has been reported to induce maternal pro-inflammatory profile, thereby leading to hypertension related disorders of pregnancy (20, 156, 157). Although many studies have focused on the effect of HAART on inflammatory response as the primary cause of HDP in HIV infected individuals. To the best of our knowledge they are very few studies that have reported on the effect of this treatment on the haemostatic profile in association to HDP.

THE ROLE OF HIV INFECTION ON HAEMOSTATIC PROFILE AND HYPERTENSIVE DISORDERS OF PREGNANCY

HIV has been identified to be strongly linked with haemostatic abnormalities such as hematological disorder, dysregulated haematopoiesis process, and the coagulation process (22, 23). The pathophysiological mechanism behind this link is believed to be through endothelial dysfunction (23, 158). Endothelial dysfunction not only affects haemostatic profile, but is also widely associated with HDP (159, 160).

Endothelial Dysfunction in Hypertensive Disorders of Pregnancy

"The maternal vascular endothelium is a principal factor involved in the pathogenesis of HDP" (159, 161–165). Under normal conditions there is a balance in the endothelium relaxing and contractile factors that play a pivotal role in regulating arterial compliance, vascular resistance, and blood pressure. However, under abnormal conditions such as HDP, there is an imbalance of these factors. This results to damaged blood vessels which end results leads to endothelial dysfunction which is involved in the pathophysiology of HDP (161–163).

Markers of Endothelial Dysfunction Associated With the Pathophysiology of HDP

Several markers of endothelial dysfunction have been associated with HDP (166–168). These markers are "endothelin-1 (ET-1), soluble vascular adhesion molecule and interleukin-8, ELAM-, and endothelial leukocyte adhesion molecule-1. Endothelin-1 is widely reported to be associated with the pathophysiology of PE" (169–172). These studies have shown that "ET-1 is increased in PE" compared to normotensive pregnancies (168, 173–175). Interestingly, it has been reported that "endothelial dysfunction may also lead to diseases associated with maternal liver and brain" (176–178). Severe forms of PE affecting the liver include HELLP syndrome (hemolysis, elevated liver enzymes, low platelet count) (176). A study by Lind et al. (179) indicated that there is correlation between ET-1 and HELLP syndrome in PE. More interestingly, a study of hypertension in an animal model also revealed that there was a strong association between HELLP syndrome and ET-1 activation (180). Eclampsia is another sever form of PE which is accompanied by the presence of seizures (177, 178, 181). The pathophysiology of eclampsia is also reported to involve ET-1, however studies demonstrating this association are lacking. HIV infection has also been identified as a major factor contributing to endothelial dysfunction. Reports on the role of ET-1 on other HDP such as GH are also lacking. Therefore, more studies are needed in order to have a full understanding of the role of ET-1 on the pathophysiology of HDP. Apart from markers associated with endothelial dysfunction in HDP, HIV infection is another identified marker associated with endothelial dysfunction (182, 183).

The Role of HIV Infection on Endothelial Dysfunction

The role of HIV infection on endothelial dysfunction has been reported to result from "interaction of HIV with host cells that consist of the CD4 receptor, coreceptor chemokines ligand 4 (CXCR4), and chemokines receptor 5 (CCR5)" (184, 185). This interaction occurs with "the help of Glycoprotein 120 (gp120)" (184, 185). This leads to reduced nitric oxide expression followed by endothelial dysfunction (184, 185). Several studies have associated HIV infection with endothelial dysfunction (182, 183). Funderburg et al. (182) reported that "higher plasma HIV RNA levels associates with endothelial dysfunction in HIV-infected patients." Similarly, "a mouse model expressing HIV viral proteins env, tat, nef, vpu, vpr, and rev demonstrated aortic endothelial dysfunction and increased arterial stiffness" (183). Interestingly, a study by Solages et al. (186), demonstrated that HIV-infected patients had significantly impaired endothelial function, which result from disturbances in their coagulation system as demonstrated by vasoconstriction in comparison to the HIV-uninfected group.

Role of HIV Infection on Coagulation

"Endothelial cells produce different molecules that are involved in clotting and fibrinolysis process" (187). These molecules are "Willebrand factor (vWF), tissue plasminogen activator, plasminogen activator inhibitor, and protein S" (187). In HIV-infected individuals, "endothelial abnormality is a common disorder induced by the action of the virus and virus-associated inflammatory response" (188). Such endothelial abnormality "activates the coagulation system, leading to the consumption of coagulation factors" (188). Moreover, it is reported that the levels of vWF are increased in HIV (189). Similar findings have been reported in HDP (190, 191). Therefore, more research on vWF in HIV associated HDP is needed in order to provide possible association between the role of HIV infection in HDP.

CONCLUSION

The findings of this review indicate that placental hormones increases insulin resistance during pregnancy however there is very limited data on studies evaluating how these hormones

are regulated in HIV infected pregnant women more studies are needed especially from African countries since there is high prevalence of HIV infection as well as high incidences maternal and fetal complication.

STRENGTH OF THE STUDY

This manuscript highlights on the role of HIV infection in GDM and HDP by looking at hormones associated with GDM and haemostatic parameters associated with HDP in both HIV infected and uninfected pregnancies.

LIMITATION OF THE STUDY

Clinical or experimental data reporting on the pathophysiology of GDM induced by placental and peripheral hormones in low risk pregnancy vs. HIV infected pregnancy are needed. Also more studies reporting on the haemostatic parameters in HIV infected vs. HIV uninfected pregnancies are needed more especially in Sub Saharan Africa which is a highly affected by HIV infection.

AUTHOR CONTRIBUTIONS

WNP conceptualized, wrote, and proof read the manuscript.

REFERENCES

1. HIV/AIDS JUNPo. *Communities at the Centre: Global AIDS Update 2019*. Geneva: UNAIDS. (2019).
2. UNAIDS.AIDSinfo. *UNAIDS 2019 Estimates*. UNAIDS (2019).
3. HIV/AIDS JUNPo. Geneva: UNAIDS 2018. (cited December 19, 2018). Available online at: https://www.unaids.org/sites/default/files/media_asset/unaids-data-2018_en.pdf
4. Porter K, Babiker A, Bhaskaran K, Darbyshire J, Pezzotti P, Porter K, et al. Determinants of survival following HIV-1 seroconversion after introduction of HAART. *Lancet.* (2003) 362:1267–74. doi: 10.1016/S0140-6736(03)14570-9
5. Palella FJ Jr, Delaney KM, Moorman AC, Loveless MO, Fuhrer J, Satten GA, et al. Declining morbidity and mortality among patients with advanced human immunodeficiency virus infection. *N Engl J Med.* (1998) 338:853–60. doi: 10.1056/NEJM199803263381301
6. Dagogo-Jack S. New drugs and diabetes risk: antipsychotic and antiretroviral agents. *Clin Diabetes.* (2006) 569–81. doi: 10.1016/B978-1-4160-0273-4.50047-3
7. Watts DH, Balasubramanian R, Maupin RT Jr, Delke I, Dorenbaum A, Fiore S, et al. Maternal toxicity and pregnancy complications in human immunodeficiency virus–infected women receiving antiretroviral therapy: PACTG 316. *Am J Obstet Gynecol.* (2004) 190:506–16. doi: 10.1016/j.ajog.2003.07.018
8. Samaras K, Wand H, Law M, Emery S, Cooper D, Carr A. Prevalence of metabolic syndrome in HIV-infected patients receiving highly active antiretroviral therapy using International Diabetes Foundation and Adult Treatment Panel III criteria: associations with insulin resistance, disturbed body fat compartmentalization, elevated C-reactive protein, and hypoadiponectinemia. *Diabetes care.* (2007) 30:113–9. doi: 10.2337/dc06-1075
9. Takarabe D, Rokukawa Y, Takahashi Y, Goto A, Takaichi M, Okamoto M, et al. Autoimmune diabetes in HIV-infected patients on highly active antiretroviral therapy. *J Clin Endocrinol Metab.* (2010) 95:4056–60. doi: 10.1210/jc.2010-0055
10. Hernandez-Romieu AC, Garg S, Rosenberg ES, Thompson-Paul AM, Skarbinski J. Is diabetes prevalence higher among HIV-infected individuals compared with the general population? Evidence from MMP and NHANES 2009–2010. *BMJ Open Diabetes Res Care.* (2017) 5:e000304. doi: 10.1136/bmjdrc-2016-000304
11. Samad F, Harris M, Puskas CM, Ye M, Chia J, Chacko S, et al. Incidence of diabetes mellitus and factors associated with its development in HIV-positive patients over the age of 50. BMJ Open Diabetes Res Care. (2017) 5:e000457. doi: 10.1136/bmjdrc-2017-000457
12. Kalra S, Kalra B, Agrawal N, Unnikrishnan A. Understanding diabetes in patients with HIV/AIDS. *Diabetol Metab Syndr.* (2011) 3:2. doi: 10.1186/1758-5996-3-2
13. Glümer C, Carstensen B, Sandbæk A, Lauritzen T, Jørgensen T, Borch-Johnsen K. A Danish diabetes risk score for targeted screening: the Inter99 study. *Diabetes care.* (2004) 27:727–33. doi: 10.2337/diacare.27.3.727
14. Rasmussen LD, Mathiesen ER, Kronborg G, Gerstoft J, Obel N. Risk of diabetes mellitus in persons with and without HIV: a Danish nationwide population-based cohort study. *PLoS ONE.* (2012) 7:e44575. doi: 10.1371/journal.pone.0044575
15. Norris A, Dreher HM. Lipodystrophy syndrome: the morphologic and metabolic effects of antiretroviral therapy in HIV infection. *J Assoc Nurses AIDS Care.* (2004) 15:46–64. doi: 10.1177/1055329004271187
16. Fichtenbaum C, Hadigan C, Kotler D, Pierone JG, Sax P, Steinhart C, et al. Treatingmorphologic and metabolic complications in HIV-infected patients on antiretroviral therapy. A consensus statement of an advisory committee of the International Association of Physicians in AIDS Care. *IAPAC Mon.* (2005) 11:38–46.
17. Ben-Haroush A, Yogev Y, Hod M. Epidemiology of gestational diabetes mellitus and its association with Type 2 diabetes. *Diabet Med.* (2004) 21:103–13. doi: 10.1046/j.1464-5491.2003.00985.x
18. Macaulay S, Dunger DB, Norris SA. Gestational diabetes mellitus in Africa: a systematic review. *PLoS ONE.* (2014) 9:e97871. doi: 10.1371/journal.pone.0097871
19. Machado ES, Krauss MR, Megazzini K, Coutinho CM, Kreitchmann R, Melo VH, et al. Hypertension, preeclampsia and eclampsia among HIV-infected pregnant women from Latin America and Caribbean countries. *J Infect.* (2014) 68:572–80. doi: 10.1016/j.jinf.2013.12.018
20. Sebitloane HM, Moodley J, Sartorius B. Associations between HIV, highly active anti-retroviral therapy, and hypertensive disorders of pregnancy among maternal deaths in South Africa 2011–2013. *Int J Gynaecol Obstet.* (2017) 136:195–9. doi: 10.1002/ijgo.12038
21. Phoswa WN, Naicker T, Ramsuran V, Moodley J. Pre-eclampsia: the role of highly active antiretroviral therapy and immune markers. *Inflamm Res.* (2019) 68:47–57. doi: 10.1007/s00011-018-1190-3
22. Karpatkin S, Nardi M, Green D. Platelet and coagulation defects associated with HIV-1-infection. *Thromb Haemost.* (2002) 88:389–401. doi: 10.1055/s-0037-1613228
23. Friel TJ, Scadden DT, Leung L, Landaw SA. Hematologic manifestations of HIV infection: thrombocytopenia and coagulation abnormalities. *Med Update.* (2007) 46:1–12. doi: 10.5045/kjh.2011.46.4.253
24. Marathe PH, Gao HX, Close KL. American Diabetes Association standards of medical c are in diabetes (2017). *J Diabetes.* (2017) 9:320–4. doi: 10.1111/1753-0407.12524
25. Federation ID. *IDF Diabetes Atlas*. Brussels: International Diabetes Federation. (2013)
26. Jiwani A, Marseille E, Lohse N, Damm P, Hod M, Kahn JG. Gestational diabetes mellitus: results from a survey of country prevalence and practices. *J Matern Fetal Neonatal Med.* (2012) 25:600–10. doi: 10.3109/14767058.2011.587921
27. Seshiah V, Balaji V, Balaji MS, Paneerselvam A, Arthi T, Thamizharasi M, et al. Prevalence of gestational diabetes mellitus in South India (Tamil Nadu): a community based study. *JAPI.* (2008) 56:329–33.
28. Moore TR, Hauguel-De Mouzon S, Catalano P. Diabetes in pregnancy. In: *Maternal-Fetal Medicine: Principles and Practice*. 5th ed. Philadelphia: Saunders (2004). p. 1023–61.
29. Adams S, Rheeder P. Screening for gestational diabetes mellitus in a South African population: prevalence, comparison of diagnostic criteria and the role of risk factors. *S Afr Med J.* (2017) 107:523–7. doi: 10.7196/SAMJ.2017.v107i6.12043

30. Catalano Pa, Ehrenberg H. The short-and long-term implications of maternal obesity on the mother and her offspring. *BJOG.* (2006) 113:1126–33. doi: 10.1111/j.1471-0528.2006.00989.x
31. Jackson E. Glycosuria as an indication for glucose tolerance testing during pregnancy. *South Afr Med J.* (1979) 56:921–3.
32. Sacks DA, Hadden DR, Maresh M, Deerochanawong C, Dyer AR, Metzger BE, et al. Frequency of gestational diabetes mellitus at collaborating centers based on IADPSG consensus panel–recommended criteria: the Hyperglycemia and Adverse Pregnancy Outcome (HAPO) Study. *Diabetes care.* (2012) 35:526–8. doi: 10.2337/dc11-1641
33. Nasiri-Amiri F, Sepidarkish M, Shirvani MA, Habibipour P, Tabari NSM. The effect of exercise on the prevention of gestational diabetes in obese and overweight pregnant women: a systematic review and meta-analysis. *Diabetol Metabol Syndr.* (2019) 11:1–14. doi: 10.1186/s13098-019-0470-6
34. American College of Obstetricians and Gynecologists Committee on Practice Bulletins–Obstetrics. Management guidelines for obstetrician–gynecologists. *Gestational Diabetes Obstet Gynecol.* (2001) 98:525–38.
35. Kalus AA, Chien AJ, Olerud JE. Diabetes mellitus and other endocrine diseases. In: Gabbe SG, Niebyl JR, Simpson JL, editors. *Obstetrics: Normal and Problems Pregnancies*. 3rd ed. New York, NY: Churchill-Livingstone (1996). p. 1037–81.
36. González-Tomé M, Ramos Amador J, Guillen S, Solís I, Fernández-Ibieta M, Munoz E, et al. Gestational diabetes mellitus in a cohort of HIV-1 infected women. *HIV Med.* (2008) 9:868–74. doi: 10.1111/j.1468-1293.2008.00639.x
37. Walli R, Herfort O, Michl GM, Demant T, Jäger H, Dieterle C, et al. Treatment with protease inhibitors associated with peripheral insulin resistance and impaired oral glucose tolerance in HIV-1-infected patients. *AIDS.* (1998) 12:F167–73. doi: 10.1097/00002030-199815000-00001
38. Carr A, Samaras K, Burton S, Law M, Freund J, Chisholm DJ, et al. A syndrome of peripheral lipodystrophy, hyperlipidaemia and insulin resistance in patients receiving HIV protease inhibitors. *AIDS.* (1998) 12:F51–F8. doi: 10.1097/00002030-199807000-00003
39. Justman JE, Benning L, Danoff A, Minkoff H, Levine A, Greenblatt RM, et al. Protease inhibitor use and the incidence of diabetes mellitus in a large cohort of HIV-infected women. *J Acquir Immune Defic Syndr.* (2003). 32:298–302. doi: 10.1097/00126334-200303010-00009
40. Dubé MP. Disorders of glucose metabolism in patients infected with human immunodeficiency virus. *Clin Infect Dis.* (2000) 31:1467–75. doi: 10.1086/317491
41. Brambilla AM, Novati R, Calori G, Meneghini E, Vacchini D, Luzi L, et al. Stavudine or indinavir-containing regimens are associated with an increased risk of diabetes mellitus in HIV-infected individuals. *AIDS.* (2003) 17:1993–5. doi: 10.1097/00002030-200309050-00022
42. Palacios R, Santos J, Ruiz J, González M, Márquez M. Factors associated with the development of diabetes mellitus in HIV-infected patients on antiretroviral therapy: a case–control study. *AIDS.* (2003) 17:933–5. doi: 10.1097/00002030-200304110-00025
43. Aschkenazi S, Rochelson B, Bernasko J, Kaplan J. Insulin resistance complicating pregnancy in a human immunodeficiency virus–infected patient treated with protease inhibitors and corticosteroids. *Obstetr Gynecol.* (2003) 102:1210–2. doi: 10.1016/S0029-7844(03)00166-2
44. Hui DY. Effects of HIV protease inhibitor therapy on lipid metabolism. *Prog Lipid Res.* (2003) 42:81–92. doi: 10.1016/S0163-7827(02)00046-2
45. Monier PL, Wilcox R. Metabolic complications associated with the use of highly active antiretroviral therapy in HIV-1–infected adults. *Am J Med Sci.* (2004) 328:48–56. doi: 10.1097/00000441-200407000-00007
46. Jao J, Wong M, Van Dyke RB, Geffner M, Nshom E, Palmer D, et al. Gestational diabetes mellitus in HIV-infected and-uninfected pregnant women in Cameroon. *Diabetes Care.* (2013) 36:e141–2. doi: 10.2337/dc13-0968
47. Catalano PM, Huston L, Amini SB, Kalhan SC. Longitudinal changes in glucose metabolism during pregnancy in obese women with normal glucose tolerance and gestational diabetes mellitus. *Am J Obstetr Gynecol.* (1999) 180:903–16. doi: 10.1016/S0002-9378(99)70662-9
48. Catalano PM, Tyzbir ED, Wolfe RR, Calles J, Roman NM, Amini SB, et al. Carbohydrate metabolism during pregnancy in control subjects and women with gestational diabetes. *Am J Physiol.* (1993) 264:E60–7. doi: 10.1152/ajpendo.1993.264.1.E60
49. Barbour LA, McCurdy CE, Hernandez TL, Kirwan JP, Catalano PM, Friedman JE. Cellular mechanisms for insulin resistance in normal pregnancy and gestational diabetes. *Diabetes Care.* (2007) 30(Suppl. 2):S112–9. doi: 10.2337/dc07-s202
50. Ryan EA, Enns L. Role of gestational hormones in the induction of insulin resistance. *J Clin Endocrinol Metab.* (1988) 67:341–7. doi: 10.1210/jcem-67-2-341
51. Colomiere M, Permezel M, Riley C, Desoye G, Lappas M. Defective insulin signaling in placenta from pregnancies complicated by gestational diabetes mellitus. *Eur J Endocrinol.* (2009) 160:567–78. doi: 10.1530/EJE-09-0031
52. Jansson N, Rosario FJ, Gaccioli F, Lager S, Jones HN, Roos S, et al. Activation of placental mTOR signaling and amino acid transporters in obese women giving birth to large babies. *J Clin Endocrinol Metabol.* (2013) 98:105–13. doi: 10.1210/jc.2012-2667
53. Ruiz-Palacios M, Prieto-Sánchez MT, Ruiz-Alcaraz AJ, Blanco-Carnero JE, Sanchez-Campillo M, Parrilla JJ, et al. Insulin treatment may alter fatty acid carriers in placentas from gestational diabetes subjects. *Int J Mol Sci.* (2017) 18:1203. doi: 10.3390/ijms18061203
54. Araújo JR, Keating E, Martel F. Impact of gestational diabetes mellitus in the maternal-to-fetal transport of nutrients. *Curr Diab Rep.* (2015) 15:1. doi: 10.1007/s11892-014-0569-y
55. Mendoza MC, Er EE, Blenis J. The Ras-ERK and PI3K-mTOR pathways: cross-talk and compensation. *Trends Biochem Sci.* (2011) 36:320–8. doi: 10.1016/j.tibs.2011.03.006
56. Knöfler M, Sooranna S, Daoud G, Whitley GS, Markert U, Xia Y, et al. Trophoblast signalling: knowns and unknowns–a workshop report. *Placenta.* (2005) 26:S49–51. doi: 10.1016/j.placenta.2005.02.001
57. Kampmann U, Knorr S, Fuglsang J, Ovesen P. Determinants of maternal insulin resistance during pregnancy: an updated overview. *J Diabetes Res.* (2019) 2019:5320156. doi: 10.1155/2019/5320156
58. Catalano P. Trying to understand gestational diabetes. *Diabet Med.* (2014) 31:273–81. doi: 10.1111/dme.12381
59. Brelje TC, Scharp DW, Lacy PE, Ogren L, Talamantes F, Robertson M, et al. Effect of homologous placental lactogens, prolactins, and growth hormones on islet B-cell division and insulin secretion in rat, mouse, and human islets: implication for placental lactogen regulation of islet function during pregnancy. *Endocrinology.* (1993) 132:879–87. doi: 10.1210/endo.132.2.8425500
60. Barbour LA, Shao J, Qiao L, Pulawa LK, Jensen DR, Bartke A, et al. Human placental growth hormone causes severe insulin resistance in transgenic mice. *Am J Obstetr Gynecol.* (2002) 186:512–7. doi: 10.1067/mob.2002.121256
61. Lombardo MF, De Angelis F, Bova L, Bartolini B, Bertuzzi F, Nano R, et al. Human placental lactogen (hPL-A) activates signaling pathways linked to cell survival and improves insulin secretion in human pancreatic islets. *Islets.* (2011) 3:250–8. doi: 10.4161/isl.3.5.16900
62. Handwerger S. The growth hormone gene cluster: physiological actions and regulation during pregnancy. *Growth Genet Horm.* (2009) 25:1–8.
63. Rechler MM, Clemmons DR. Regulatory actions of insulin-like growth factor-binding proteins. *Trends Endocrinol Metabol.* (1998) 9:176–83. doi: 10.1016/S1043-2760(98)00047-2
64. Velegrakis A, Sfakiotaki M, Sifakis S. Human placental growth hormone in normal and abnormal fetal growth. *Biomed Rep.* (2017) 7:115–22. doi: 10.3892/br.2017.930
65. Vasavada RC, Garcia-Ocaña A, Zawalich WS, Sorenson RL, Dann P, Syed M, et al. Targeted expression of placental lactogen in the beta cells of transgenic mice results in beta cell proliferation, islet mass augmentation, and hypoglycemia. *J Biol Chem.* (2000) 275:15399–406. doi: 10.1074/jbc.275.20.15399
66. Parsons JA, Brelje TC, Sorenson RL. Adaptation of islets of Langerhans to pregnancy: increased islet cell proliferation and insulin secretion correlates with the onset of placental lactogen secretion. *Endocrinology.* (1992) 130:1459–66. doi: 10.1210/en.130.3.1459
67. Barbour LA, Shao J, Qiao L, Leitner W, Anderson M, Friedman JE, et al. Human placental growth hormone increases expression of the P85 regulatory unit of phosphatidylinositol 3-kinase and triggers severe insulin resistance in skeletal muscle. *Endocrinology.* (2004) 145:1144–50. doi: 10.1210/en.2003-1297

68. Barbour LA, Rahman SM, Gurevich I, Leitner JW, Fischer SJ, Roper MD, et al. Increased P85α is a potent negative regulator of skeletal muscle insulin signaling and induces in vivo insulin resistance associated with growth hormone excess. *J Biol Chem.* (2005) 280:37489–94. doi: 10.1074/jbc.M506967200
69. Waters TP, Schultz BA, Mercer BM, Catalano PM. Effect of 17α-hydroxyprogesterone caproate on glucose intolerance in pregnancy. *Obstetr Gynecol.* (2009) 114:45–9. doi: 10.1097/AOG.0b013e3181a9454b
70. Nunes V, Portioli-Sanches E, Rosim MP, Araujo MdS, Praxedes-Garcia P, Valle MMR, et al. Progesterone induces apoptosis of insulin-secreting cells: insights into the molecular mechanism. *J Endocrinol.* (2014) 221:273–84. doi: 10.1530/JOE-13-0202
71. Egerman R, Ramsey R, Istwan N, Rhea D, Stanziano G. Maternal characteristics influencing the development of gestational diabetes in obese women receiving 17-alpha-hydroxyprogesterone caproate. *J Obes.* (2014) 2014:563243. doi: 10.1155/2014/563243
72. Kouhkan A, Khamseh ME, Moini A, Pirjani R, Valojerdi AE, Arabipoor A, et al. Predictive factors of gestational diabetes in pregnancies following assisted reproductive technology: a nested case–control study. *Arch Gynecol Obstet.* (2018) 298:199–206. doi: 10.1007/s00404-018-4772-y
73. Mohammadi T, Paknahad Z. Adiponectin concentration in gestational diabetic women: a case-control study. *Clin Nutr Res.* (2017) 6:267–76. doi: 10.7762/cnr.2017.6.4.267
74. Kautzky-Willer A, Pacini G, Tura A, Bieglmayer C, Schneider B, Ludvik B, et al. Increased plasma leptin in gestational diabetes. *Diabetologia.* (2001) 44:164–72. doi: 10.1007/s001250051595
75. Soheilykhah S, Mojibian M, Rahimi-Saghand S, Rashidi M, Hadinedoushan H. Maternal serum leptin concentration in gestational diabetes. *Taiwan J Obstet Gynecol.* (2011) 50:149–53. doi: 10.1016/j.tjog.2011.01.034
76. Yang M, Peng S, Li W, Wan Z, Fan L, Du Y. Relationships between plasma leptin levels, leptin G2548A, leptin receptor Gln223Arg polymorphisms and gestational diabetes mellitus in Chinese population. *Sci Rep.* (2016) 6:1–6. doi: 10.1038/srep23948
77. Ekinci EI, Torkamani N, Ramchand SK, Churilov L, Sikaris KA, Lu ZX, et al. Higher maternal serum prolactin levels are associated with reduced glucose tolerance during pregnancy. *J Diabetes Investig.* (2017) 8:697–700. doi: 10.1111/jdi.12634
78. Lacroix MC, Guibourdenche J, Frendo JL, Muller F, Evain-Brion D. Human placental growth hormone–a review. *Placenta.* (2002) 23 Suppl A:S87–94. doi: 10.1053/plac.2002.0811
79. Higgins MF, Russell NE, Crossey PA, Nyhan KC, Brazil DP, McAuliffe FM. Maternal and fetal placental growth hormone and IGF axis in type 1 diabetic pregnancy. *PLoS ONE.* (2012) 7:e29164. doi: 10.1371/journal.pone.0029164
80. Heitritter SM, Solomon CG, Mitchell GF, Skali-Ounis N, Seely EW. Subclinical inflammation and vascular dysfunction in women with previous gestational diabetes mellitus. *J Clin Endocrinol Metabol.* (2005) 90:3983–8. doi: 10.1210/jc.2004-2494
81. Winzer C, Wagner O, Festa A, Schneider B, Roden M, Bancher-Todesca D, et al. Plasma adiponectin, insulin sensitivity, and subclinical inflammation in women with prior gestational diabetes mellitus. *Diabetes Care.* (2004) 27:1721–7. doi: 10.2337/diacare.27.7.1721
82. Cusi K, Maezono K, Osman A, Pendergrass M, Patti ME, Pratipanawatr T, et al. Insulin resistance differentially affects the PI 3-kinase–and MAP kinase–mediated signaling in human muscle. *J Clin Invest.* (2000) 105:311–20. doi: 10.1172/JCI7535
83. Grimmsmann T, Levin K, Meyer M, Beck-Nielsen H, Klein H. Delays in insulin signaling towards glucose disposal in human skeletal muscle. *J Endocrinol.* (2002) 172:645–51. doi: 10.1677/joe.0.1720645
84. Costrini N, Kalkhoff R. Relative effects of pregnancy, estradiol, and progesterone on plasma insulin and pancreatic islet insulin secretion. *J Clin Invest.* (1971) 50:992–9. doi: 10.1172/JCI106593
85. Straub SG, Sharp GW, Meglasson MD, De Souza CJ. Progesterone inhibits insulin secretion by a membrane delimited, non-genomic action. *Biosci Rep.* (2001) 21:653–66. doi: 10.1023/A:1014773010350
86. Rouholamin S, Zarean E, Sadeghi L. Evaluation the effect of 17-alpha hydroxyprogesterone caproate on gestational diabetes mellitus in pregnant women at risk for preterm birth. *Advan Biomed Res.* (2015) 4:242. doi: 10.4103/2277-9175.168609
87. Rebarber A, Istwan NB, Russo-Stieglitz K, Cleary-Goldman J, Rhea DJ, Stanziano GJ, et al. Increased incidence of gestational diabetes in women receiving prophylactic 17α-hydroxyprogesterone caproate for prevention of recurrent preterm delivery. *Diabetes Care.* (2007) 30:2277–80. doi: 10.2337/dc07-0564
88. Rosta K, Ott J, Kelemen F, Temsch W, Lahner T, Reischer T, et al. Is vaginal progesterone treatment associated with the development of gestational diabetes? A retrospective case–control study. *Arch Gynecol Obstet.* (2018) 298:1079–84. doi: 10.1007/s00404-018-4895-1
89. Chandran M, Phillips SA, Ciaraldi T, Henry RR. Adiponectin: more than just another fat cell hormone? *Diabetes Care.* (2003) 26:2442–50. doi: 10.2337/diacare.26.8.2442
90. Ziemke F, Mantzoros CS. Adiponectin in insulin resistance: lessons from translational research. *Am J Clin Nutr.* (2010) 91:258S−61S. doi: 10.3945/ajcn.2009.28449C
91. Karpe F. Insulin resistance by adiponectin deficiency: is the action in skeletal muscle? *Diabetes.* (2013) 62:701–2. doi: 10.2337/db12-1519
92. Carpenter MW. Gestational diabetes, pregnancy hypertension, and late vascular disease. *Diabetes Care.* (2007) 30(Suppl. 2):S246–S50. doi: 10.2337/dc07-s224
93. Retnakaran R, Hanley AJ, Raif N, Connelly PW, Sermer M, Zinman B. Reduced adiponectin concentration in women with gestational diabetes: a potential factor in progression to type 2 diabetes. *Diabetes Care.* (2004) 27:799–800. doi: 10.2337/diacare.27.3.799
94. Yadav A, Kataria MA, Saini V, Yadav A. Role of leptin and adiponectin in insulin resistance. *Clin Chim Acta.* (2013) 417:80–4. doi: 10.1016/j.cca.2012.12.007
95. Yamauchi T, Kamon J, Minokoshi Ya, Ito Y, Waki H, Uchida S, et al. Adiponectin stimulates glucose utilization and fatty-acid oxidation by activating AMP-activated protein kinase. *Nat Med.* (2002) 8:1288. doi: 10.1038/nm788
96. Söderberg S, Zimmet P, Tuomilehto J, Chitson P, Gareeboo H, Alberti K, et al. Leptin predicts the development of diabetes in Mauritian men, but not women: a population–based study. *Int J Obes.* (2007) 31:1126. doi: 10.1038/sj.ijo.0803561
97. Zhang Y, Proenca R, Maffei M, Barone M, Leopold L, Friedman JM. Positional cloning of the mouse obese gene and its human homologue. *Nature.* (1994) 372:425. doi: 10.1038/372425a0
98. Lam NT, Lewis JT, Cheung AT, Luk CT, Tse J, Wang J, et al. Leptin increases hepatic insulin sensitivity and protein tyrosine phosphatase 1B expression. *Mol Endocrinol.* (2004) 18:1333–45. doi: 10.1210/me.2002-0193
99. Seufert J, Kieffer TJ, Habener JF. Leptin inhibits insulin gene transcription and reverses hyperinsulinemia in leptin-deficient ob/ob mice. *Proc Nat Acad Sci.* (1999) 96:674–9. doi: 10.1073/pnas.96.2.674
100. Stephens TW, Basinski M, Bristow PK, Bue-Valleskey JM, Burgett SG, Craft L, et al. The role of neuropeptide Y in the antiobesity action of the obese gene product. *Nature.* (1995) 377:530. doi: 10.1038/377530a0
101. Weigle DS, Bukowski TR, Foster DC, Holderman S, Kramer JM, Lasser G, et al. Recombinant ob protein reduces feeding and body weight in the ob/ob mouse. *J Clin Invest.* (1995) 96:2065–70. doi: 10.1172/JCI118254
102. Kulkarni RN, Wang Z-L, Wang R-M, Hurley JD, Smith DM, Ghatei MA, et al. Leptin rapidly suppresses insulin release from insulinoma cells, rat and human islets and, *in vivo*, in mice. *J Clin Invest.* (1997) 100:2729–36. doi: 10.1172/JCI119818
103. Poitout V, Rouault C, Guerre-Millo Ml, Briaud I, Reach GR. Inhibition of insulin secretion by leptin in normal rodent islets of Langerhans. *Endocrinology.* (1998) 139:822–6. doi: 10.1210/endo.139.3.5812
104. Zhao AZ, Bornfeldt KE, Beavo JA. Leptin inhibits insulin secretion by activation of phosphodiesterase 3B. *J Clin Invest.* (1998) 102:869–73. doi: 10.1172/JCI3920
105. Ahren B, Havel PJ. Leptin inhibits insulin secretion induced by cellular cAMP in a pancreatic B cell line (INS-1 cells). *Am J Physiol.* (1999) 277:R959–66. doi: 10.1152/ajpregu.1999.277.4.R959
106. Lee JW, Swick AG, Romsos DR. Leptin constrains phospholipase C-protein kinase C-induced insulin secretion *via* a phosphatidylinositol 3-kinase-dependent pathway. *Exp Biol Med.* (2003) 228:175–82. doi: 10.1177/153537020322800207

107. Wannamethee SG, Lowe GD, Rumley A, Cherry L, Whincup PH, Sattar N. Adipokines and risk of type 2 diabetes in older men. *Diabetes Care.* (2007) 30:1200–5. doi: 10.2337/dc06-2416
108. Bandaru P, Shankar A. Association between plasma leptin levels and diabetes mellitus. *Metab Syndr Relat Disord.* (2011) 9:19–23. doi: 10.1089/met.2010.0037
109. Soliman AT, Omar M, Assem HM, Nasr IS, Rizk MM, El Matary W, et al. Serum leptin concentrations in children with type 1 diabetes mellitus: relationship to body mass index, insulin dose, and glycemic control. *Metabolism.* (2002) 51:292–6. doi: 10.1053/meta.2002.30502
110. Haffner SM, Stern MP, Miettinen H, Wei M, Gingerich RL. Leptin concentrations in diabetic and non-diabetic Mexican-Americans. *Diabetes.* (1996) 45:822–4. doi: 10.2337/diab.45.6.822
111. Maahs DM, Hamman RF, D'Agostino R Jr, Dolan LM, Imperatore G, Lawrence JM, et al. The association between adiponectin/leptin ratio and diabetes type: the SEARCH for Diabetes in Youth Study. *J Pediatr.* (2009) 155:133–5.e1. doi: 10.1016/j.jpeds.2008.12.048
112. Welsh P, Murray HM, Buckley BM, De Craen AJ, Ford I, Jukema JW, et al. Leptin predicts diabetes but not cardiovascular disease: results from a large prospective study in an elderly population. *Diabetes Care.* (2009) 32:308–10. doi: 10.2337/dc08-1458
113. Mcneely MJ, Boyko EJ, Weigle DS, Shofer JB, Chessler SD, Leonnetti DL, et al. Association between baseline plasma leptin levels and subsequent development of diabetes in Japanese Americans. *Diabetes Care.* (1999) 22:65–70. doi: 10.2337/diacare.22.1.65
114. Bhattacharya S, Kalra S, Dutta D, Khandelwal D, Singla R. The interplay between pituitary health and diabetes mellitus–the need for 'Hypophyseo-vigilance'. *Eur Endocrinol.* (2020) 16:25. doi: 10.17925/EE.2020.16.1.25
115. Park S, Kim DS, Daily JW, Kim SH. Serum prolactin concentrations determine whether they improve or impair β-cell function and insulin sensitivity in diabetic rats. *Diabetes Metab Res Rev.* (2011) 27:564–74. doi: 10.1002/dmrr.1215
116. Wang T, Lu J, Xu Y, Li M, Sun J, Zhang J, et al. Circulating prolactin associates with diabetes and impaired glucose regulation: a population-based study. *Diabetes Care.* (2013) 36:1974–80. doi: 10.2337/dc12-1893
117. Wang T, Xu Y, Xu M, Ning G, Lu J, Dai M, et al. Circulating Prolactin and Risk of Type 2 Diabetes: A Prospective Study. *Am J Epidemiol.* (2016) 184:295–301. doi: 10.1093/aje/kwv326
118. Daimon M, Kamba A, Murakami H, Mizushiri S, Osonoi S, Yamaichi M, et al. Association between serum prolactin levels and insulin resistance in non-diabetic men. *PLoS ONE.* (2017) 12:e0175204. doi: 10.1371/journal.pone.0175204
119. Retnakaran R, Ye C, Kramer CK, Connelly PW, Hanley AJ, Sermer M, et al. Maternal serum prolactin and prediction of postpartum β-cell function and risk of prediabetes/Diabetes. *Diabetes Care.* (2016) 39:1250–8. doi: 10.2337/dc16-0043
120. Krishnaveni GV, Veena SR, Jones A, Srinivasan K, Osmond C, Karat SC, et al. Exposure to maternal gestational diabetes is associated with higher cardiovascular responses to stress in adolescent indians. *J Clin Endocrinol Metab.* (2015) 100:986–93. doi: 10.1210/jc.2014-3239
121. Kirwan JP, Hauguel-De Mouzon S, Lepercq J, Challier J-C, Huston-Presley L, Friedman JE, et al. TNF-α is a predictor of insulin resistance in human pregnancy. *Diabetes.* (2002) 51:2207–13. doi: 10.2337/diabetes.51.7.2207
122. Fowler MG, Qin M, Fiscus SA, Currier JS, Flynn PM, Chipato T, et al. Benefits and risks of antiretroviral therapy for perinatal HIV prevention. *N Engl J Med.* (2016) 375:1726–37. doi: 10.1056/NEJMoa1511691
123. Sibiude J, Warszawski J, Tubiana R, Dollfus C, Faye A, Rouzioux C, et al. Premature delivery in HIV-infected women starting protease inhibitor therapy during pregnancy: role of the ritonavir boost? *Clin Infect Dis.* (2012) 54:1348–60. doi: 10.1093/cid/cis198
124. Van Dyke RB, Chadwick EG, Hazra R, Williams PL, Seage GR III. The PHACS SMARTT study: assessment of the safety of in utero exposure to antiretroviral drugs. *Front Immunol.* (2016) 7:199. doi: 10.3389/fimmu.2016.00199
125. Kim M, Park HJ, Seol JW, Jang JY, Cho YS, Kim KR, et al. VEGF-A regulated by progesterone governs uterine angiogenesis and vascular remodelling during pregnancy. *EMBO Mol Med.* (2013) 5:1415–30. doi: 10.1002/emmm.201302618
126. Chen JZ-J, Wong MH, Brennecke SP, Keogh RJ. The effects of human chorionic gonadotrophin, progesterone and oestradiol on trophoblast function. *Mol Cell Endocrinol.* (2011) 342:73–80. doi: 10.1016/j.mce.2011.05.034
127. Amirhessami-Aghili N, Spector SA. Human immunodeficiency virus type 1 infection of human placenta: potential route for fetal infection. *J Virol.* (1991) 65:2231–6. doi: 10.1128/JVI.65.5.2231-2236.1991
128. Papp E, Balogun K, Banko N, Mohammadi H, Loutfy M, Yudin MH, et al. Low prolactin and high 20-α-hydroxysteroid dehydrogenase levels contribute to lower progesterone levels in HIV-infected pregnant women exposed to protease inhibitor–based combination antiretroviral therapy. *J Infect Dis.* (2016) 213:1532–40. doi: 10.1093/infdis/jiw004
129. Papp E, Mohammadi H, Loutfy MR, Yudin MH, Murphy KE, Walmsley SL, et al. HIV protease inhibitor use during pregnancy is associated with decreased progesterone levels, suggesting a potential mechanism contributing to fetal growth restriction. *J Infect Dis.* (2014) 211:10–8. doi: 10.1093/infdis/jiu393
130. Mohammadi H, Papp E, Cahill L, Rennie M, Banko N, Pinnaduwage L, et al. HIV antiretroviral exposure in pregnancy induces detrimental placenta vascular changes that are rescued by progesterone supplementation. *Sci Rep.* (2018) 8:6552. doi: 10.1038/s41598-018-24680-w
131. Oral EA, Simha V, Ruiz E, Andewelt A, Premkumar A, Snell P, et al. Leptin-replacement therapy for lipodystrophy. *N Engl J Med.* (2002) 346:570–8. doi: 10.1056/NEJMoa012437
132. van Crevel R, Karyadi E, Netea MG, Verhoef H, Nelwan RH, West CE, et al. Decreased plasma leptin concentrations in tuberculosis patients are associated with wasting and inflammation. *J Clin Endocrinol Metab.* (2002) 87:758–63. doi: 10.1210/jcem.87.2.8228
133. Hardie L, Trayhurn P, Abramovich D, Fowler P. Circulating leptin in women: a longitudinal study in the menstrual cycle and during pregnancy. *Clin Endocrinol.* (1997) 47:101–6. doi: 10.1046/j.1365-2265.1997.2441017.x
134. Nagy GS, Tsiodras S, Martin LD, Avihingsanon A, Gavrila A, Hsu WC, et al. Human immunodeficiency virus type 1-related lipoatrophy and lipohypertrophy are associated with serum concentrations of leptin. *Clin Infect Dis.* (2003) 36:795–802. doi: 10.1086/367859
135. Haffejee F, Naicker T, Singh M, Moodley J. Placental leptin in HIV-associated preeclampsia. *Eur J Obstetr Gynecol Reprod Biol.* (2013) 171:271–6. doi: 10.1016/j.ejogrb.2013.09.027
136. Montero A, Bottasso OA, Luraghi MaR, Giovannoni AG, Sen L. Association between high serum prolactin levels and concomitant infections in HIV-infected patients. *Hum Immunol.* (2001) 62:191–6. doi: 10.1016/S0198-8859(00)00245-7
137. Raushaniya B, Tatyana M, Aleksandr S, Maryam Z. Prolactin and cortisol hormones level in patients with HIV and AIDS. *Int Sci Rev.* (2016) 21:74–8. Available online at: https://cyberleninka.ru/article/n/prolactin-and-cortisol-hormones-level-in-patients-with-hiv-and-aids
138. Collazos J, Ibarra S, Martinez E, Mayo J. Serum prolactin concentrations in patients infected with human immunodeficiency virus. *HIV Clin Trials.* (2002) 3:133–8. doi: 10.1310/QAQQ-XTCJ-8AL4-6F5P
139. Okeke CU, Agbasi PU, Okorie H, Ezeiruaku F. Effect of antiretroviral drugs on prolactin in HIV infected pregnant women. *Int J Biol Chem Sci.* (2014) 8:1234–8. doi: 10.4314/ijbcs.v8i3.34
140. Collazos J, Mayo J, Martínez E, Ibarra S. Serum cortisol in HIV-infected patients with and without highly active antiretroviral therapy. *AIDS.* (2003) 17:123–6. doi: 10.1097/00002030-200301030-00018
141. Esemu LF, Yuosembom EK, Fang R, Rasay S, Fodjo BA, Nguasong JT, et al. Impact of HIV-1 infection on the IGF-1 axis and angiogenic factors in pregnant Cameroonian women receiving antiretroviral therapy. *PLoS ONE.* (2019) 14:e0215825. doi: 10.1371/journal.pone.0215825
142. Laron Z. Insulin-like growth factor 1 (IGF-1): a growth hormone. *Mol Pathol.* (2001) 54:311. doi: 10.1136/mp.54.5.311
143. Mol BW, Roberts CT, Thangaratinam S, Magee LA, De Groot CJ, Hofmeyr GJ. Pre-eclampsia. *Lancet.* (2016) 387:999–1011. doi: 10.1016/S0140-6736(15)00070-7
144. Duley L, editor. The global impact of pre-eclampsia and eclampsia. In: *Seminars in Perinatology.* Bradford: Elsevier (2009). doi: 10.1053/j.semperi.2009.02.010

145. Moodley J, editor. Maternal deaths due to hypertensive disorders of pregnancy: data from the 2014-2016 Saving Mothers' Report. In: *Obstetrics and Gynaecology Forum*. Durban: In House Publications (2018).
146. Moodley J, Soma-Pillay P, Buchmann E, Pattinson R. Hypertensive disorders in pregnancy: 2019. National guideline. *S Afr Med J.* (2019) 109:12723. doi: 10.7196/SAMJ.2019.v109i3.14104
147. Anand S. Perinatal outcome in growth retarted babies born to normotensive and hypertensive mothers: a prospective study. *Peoples J Sci Res*. (2012) 5:24–8. Available online at: http://imsear.searo.who.int/handle/123456789/140314
148. Redman CW, Sargent IL. Immunology of pre-eclampsia. *Am J Reprod Immunol.* (2010) 63:534–43. doi: 10.1111/j.1600-0897.2010.00831.x
149. Udenze I, Amadi C, Awolola N, Makwe CC. The role of cytokines as inflammatory mediators in preeclampsia. *Pan Afr Med J.* (2015) 20:219. doi: 10.11604/pamj.2015.20.219.5317
150. Cakmak HA, Dincgez Cakmak B, Abide Yayla C, Inci Coskun E, Erturk M, Keles I. Assessment of relationships between novel inflammatory markers and presence and severity of preeclampsia: Epicardial fat thickness, pentraxin-3, and neutrophil-to-lymphocyte ratio. *Hypertens Pregnancy.* (2017) 36:233–9. doi: 10.1080/10641955.2017.1321016
151. Vilchez G, Londra L, Hoyos LR, Sokol R, Bahado-Singh R. Intrapartum mean platelet volume is not a useful predictor of new-onset delayed postpartum pre-eclampsia. *Int J Gynaecol Obstet.* (2015) 131:59–62. doi: 10.1016/j.ijgo.2015.04.037
152. Aggarwal R, Jain AK, Mittal P, Kohli M, Jawanjal P, Rath G. Association of pro- and anti-inflammatory cytokines in preeclampsia. *J Clin Lab Anal.* (2019) 33:e22834. doi: 10.1002/jcla.22834
153. AlSheeha MA, Alaboudi RS, Alghasham MA, Iqbal J, Adam I. Platelet count and platelet indices in women with preeclampsia. *Vasc Health Risk Manag.* (2016) 12:477. doi: 10.2147/VHRM.S120944
154. Lockwood CJ, Yen C-F, Basar M, Kayisli UA, Martel M, Buhimschi I, et al. Preeclampsia-related inflammatory cytokines regulate interleukin-6 expression in human decidual cells. *Am J Pathol.* (2008) 172:1571–9. doi: 10.2353/ajpath.2008.070629
155. Bramham K, Parnell B, Nelson-Piercy C, Seed PT, Poston L, Chappell LC. Chronic hypertension and pregnancy outcomes: systematic review and meta-analysis. *BMJ.* (2014) 348:g2301. doi: 10.1136/bmj.g2301
156. Maharaj NR, Phulukdaree A, Nagiah S, Ramkaran P, Tiloke C, Chuturgoon AA. Pro-inflammatory cytokine levels in HIV infected and uninfected pregnant women with and without preeclampsia. *PLoS ONE.* (2017) 12:e0170063. doi: 10.1371/journal.pone.0170063
157. Kalumba VM, Moodley J, Naidoo TD. Is the prevalence of pre-eclampsia affected by HIV/AIDS? A retrospective case-control study. *Cardiovasc J Afr.* (2013) 24:24–7. doi: 10.5830/CVJA-2012-078
158. Raman RT, Manimaran D, Rachakatla P, Bharathi K, Afroz T, Sagar R. Study of basic coagulation parameters among HIV patients in correlation to CD4 counts and ART status. *J Clin Diagn Res.* (2016) 10:EC04–6. doi: 10.7860/JCDR/2016/17459.7718
159. Possomato-Vieira JS, Khalil RA. Mechanisms of endothelial dysfunction in hypertensive pregnancy and preeclampsia. *Adv Pharmacol.* (2016) 77:361–431. doi: 10.1016/bs.apha.2016.04.008
160. Ciccone M, Carbonara R, Giardinelli F, Zito A, Ricci G, Dentamaro I, et al. Gestational hypertension: endothelial dysfunction as a marker of pre-eclampsia. *Eur Heart J.* (2017) 38:ehx502.P2632. doi: 10.1093/eurheartj/ehx502.P2632
161. Roberts JM, Pearson G, Cutler J, Lindheimer M. Summary of the NHLBI working group on research on hypertension during pregnancy. *Hypertension.* (2003) 41:437–45. doi: 10.1161/01.HYP.0000054981.03589.E9
162. Thadhani RI, Johnson RJ, Karumanchi SA. Hypertension during pregnancy: a disorder begging for pathophysiological support. *Am Heart Assoc.* (2005) doi: 10.1161/01.HYP.0000188701.24418.64
163. Roberts J. Gammill HS: preeclampsia: recent insights. *Hypertension.* (2005) 46:1243–9. doi: 10.1161/01.HYP.0000188408.49896.c5
164. Granger JP, Alexander BT, Llinas MT, Bennett WA, Khalil RA. Pathophysiology of hypertension during preeclampsia linking placental ischemia with endothelial dysfunction. *Hypertension.* (2001) 38:718–22. doi: 10.1161/01.HYP.38.3.718
165. Adu-Bonsaffoh K, Antwi DA, Gyan B, Obed SA. Endothelial dysfunction in the pathogenesis of pre-eclampsia in Ghanaian women. *BMC Physiol.* (2017) 17:5. doi: 10.1186/s12899-017-0029-4
166. Germain AM, Romanik MC, Guerra I, Solari S, Reyes MaS, Johnson RJ, et al. Endothelial dysfunction: a link among preeclampsia, recurrent pregnancy loss, and future cardiovascular events? *Hypertension.* (2007) 49:90–5. doi: 10.1161/01.HYP.0000251522.18094.d4
167. Chambers JC, Fusi L, Malik IS, Haskard DO, De Swiet M, Kooner JS. Association of maternal endothelial dysfunction with preeclampsia. *JAMA.* (2001) 285:1607–12. doi: 10.1001/jama.285.12.1607
168. Carbillon L. Uterine artery Doppler and changes in endothelial function before clinical disease in preeclamptic women. *Hypertension.* (2006) 47:e16. doi: 10.1161/01.HYP.0000208994.69007.3e
169. Saleh L, Verdonk K, Visser W, van den Meiracker AH, Danser AH. The emerging role of endothelin-1 in the pathogenesis of pre-eclampsia. *Ther Adv Cardiovasc Dis.* (2016) 10:282–93. doi: 10.1177/1753944715624853
170. Jain A. Endothelin-1: a key pathological factor in pre-eclampsia? *Reprod Biomed Online.* (2012) 25:443–9. doi: 10.1016/j.rbmo.2012.07.014
171. Verdonk K, Saleh L, Lankhorst S, Smilde JI, Van Ingen MM, Garrelds IM, et al. Association studies suggest a key role for endothelin-1 in the pathogenesis of preeclampsia and the accompanying renin–angiotensin–aldosterone system suppression. *Hypertension.* (2015) 65:1316–23. doi: 10.1161/HYPERTENSIONAHA.115.05267
172. Bakrania B, Duncan J, Warrington JP, Granger JP. The endothelin type A receptor as a potential therapeutic target in preeclampsia. *Int J Mol Sci.* (2017) 18:522. doi: 10.3390/ijms18030522
173. Granger JP, Alexander BT, Llinas MT, Bennett WA, Khalil RA. Pathophysiology of preeclampsia: linking placental ischemia/hypoxia with microvascular dysfunction. *Microcirculation.* (2002) 9:147–60. doi: 10.1038/sj.mn.7800137
174. Roberts JM, Von Versen-Hoeynck F. Maternal fetal/placental interactions and abnormal pregnancy outcomes. *Hypertension.* (2007) 49:15–6. doi: 10.1161/01.HYP.0000251523.44824.02
175. Taylor RN, Varma M, Teng NN, Roberts JM. Women with preeclampsia have higher plasma endothelin levels than women with normal pregnancies. *J Clin Endocrinol Metab*. (1990) 71:1675–7. doi: 10.1210/jcem-71-6-1675
176. Powe CE, Levine RJ, Karumanchi SA. Preeclampsia, a disease of the maternal endothelium: the role of antiangiogenic factors and implications for later cardiovascular disease. *Circulation.* (2011) 123:2856–69. doi: 10.1161/CIRCULATIONAHA.109.853127
177. Cipolla MJ. Cerebrovascular function in pregnancy and eclampsia. *Hypertension.* (2007) 50:14–24. doi: 10.1161/HYPERTENSIONAHA.106.079442
178. Euser AG, Cipolla MJ. Cerebral blood flow autoregulation and edema formation during pregnancy in anesthetized rats. *Hypertension.* (2007) 49:334–40. doi: 10.1161/01.HYP.0000255791.54655.29
179. Lind Malte A, Uldbjerg N, Wright D, Torring N. Prediction of severe pre-eclampsia/HELLP syndrome by combination of sFlt-1, CT-pro-ET-1, and blood pressure: exploratory study. *Ultrasound Obstet Gynecol.* (2018) 51:768–74. doi: 10.1002/uog.17561
180. Morris R, Spencer S-K, Kyle PB, Williams JM, Harris As, Owens MY, et al. Hypertension in an animal model of HELLP syndrome is associated with activation of endothelin 1. *Reprod Sci.* (2016) 23:42–50. doi: 10.1177/1933719115592707
181. Brewer J, Martin J, Armstrong A, Blake P, Morris R, Owens M, et al. 775: posterior reversible encephalopathy syndrome (PRES) associated with eclampsia: the variable effects of therapeutic agents to accelerate safe recovery. *Am J Obstetr Gynecol.* (2012) 206:S342. doi: 10.1016/j.ajog.2011.10.793
182. Funderburg NT, Mayne E, Sieg SF, Asaad R, Jiang W, Kalinowska M, et al. Increased tissue factor expression on circulating monocytes in chronic HIV infection: relationship to in vivo coagulation and immune activation. *Blood.* (2010) 115:161–7. doi: 10.1182/blood-2009-03-210179
183. Hansen L, Parker I, Sutliff RL, Platt MO, Gleason RL. Endothelial dysfunction, arterial stiffening, and intima-media thickening in large arteries from HIV-1 transgenic mice. *Ann Biomed Eng.* (2013) 41:682–93. doi: 10.1007/s10439-012-0702-5
184. Taremwa IM, Muyindike WR, Muwanguzi E, Boum Y. Prevalence of HIV-related thrombocytopenia among clients at Mbarara Regional Referral Hospital, Mbarara, southwestern Uganda. *J Blood Med.* (2015) 6:109. doi: 10.2147/JBM.S80857

185. Jiang J, Fu W, Wang X, Lin PH, Yao Q, Chen C. HIV gp120 induces endothelial dysfunction in tumour necrosis factor-α-activated porcine and human endothelial cells. *Cardiovasc Res.* (2010) 87:366–74. doi: 10.1093/cvr/cvq013
186. Solages A, Vita JA, Thornton DJ, Murray J, Heeren T, Craven DE, et al. Endothelial function in HIV-infected persons. *Clin Infect Dis.* (2006) 42:1325–32. doi: 10.1086/503261
187. Rajendran P, Rengarajan T, Thangavel J, Nishigaki Y, Sakthisekaran D, Sethi G, et al. The vascular endothelium and human diseases. *Int J Biol Sci.* (2013) 9:1057. doi: 10.7150/ijbs.7502
188. Lafeuillade A, Alessi M, Poizot-Martin I, Boyer-Neumann C, Zandotti C, Quilichini R, et al. Endothelial cell dysfunction in HIV infection. *J Acquir Immune Defic Syndr.* (1992) 5:127–31.
189. Shen Y-MP, Frenkel EP. Thrombosis and a hypercoagulable state in HIV-infected patients. *Clin Appl Thromb Hemost.* (2004) 10:277–80. doi: 10.1177/107602960401000311
190. Szpera-Gozdziewicz A, Majcherek M, Boruczkowski M, Gozdziewicz T, Dworacki G, Wicherek L, et al. Circulating endothelial cells, circulating endothelial progenitor cells, and von Willebrand factor in pregnancies complicated by hypertensive disorders. *Am J Reprod Immunol.* (2017) 77:e12625. doi: 10.1111/aji.12625
191. Vinayagam V, Bobby Z, Habeebullah S, Chaturvedula L, Bharadwaj SK. Plasma markers of endothelial dysfunction in patients with hypertensive disorders of pregnancy: a pilot study in a South Indian population. *J Matern Fetal Neonatal Med.* (2016) 29:2077–82. doi: 10.3109/14767058.2015.1075200

Conflict of Interest: The author declares that the research was conducted in the absence of any commercial or financial relationships that could be construed as a potential conflict of interest.

frontiers in Cardiovascular Medicine

ORIGINAL RESEARCH
published: 21 May 2021
doi: 10.3389/fcvm.2021.632728

Impact of Syndecan-2-Selected Mesenchymal Stromal Cells on the Early Onset of Diabetic Cardiomyopathy in Diabetic db/db Mice

*Kathleen Pappritz[1,2,3], Fengquan Dong[2], Kapka Miteva[2,4], Arpad Kovacs[5], Muhammad El-Shafeey[1,2,3,6], Bahtiyar Kerim[2], Lisa O'Flynn[7], Stephen Joseph Elliman[7], Timothy O'Brien[8], Nazha Hamdani[5,9,10], Carsten Tschöpe[1,2,3,11] and Sophie Van Linthout[1,2,3]**

[1] Berlin Institute of Health at Charité – Universitätmedizin Berlin, BIH Center for Regenerative Therapies (BCRT), Berlin, Germany, [2] Berlin-Brandenburg Center for Regenerative Therapies, Charité, Universit4tsmedizin Berlin, Berlin, Germany, [3] German Center for Cardiovascular Research (DZHK), Partner site Berlin, Berlin, Germany, [4] Division of Cardiology, Foundation for Medical Research, Department of Medicine Specialized Medicine, Faculty of Medicine, University of Geneva, Geneva, Switzerland, [5] Institute of Physiology, Ruhr University Bochum, Bochum, Germany, [6] Medical Biotechnology Research Department, Genetic Engineering and Biotechnology Research Institute (GEBRI), City of Scientific Research and Technological Applications, Alexandria, Egypt, [7] Orbsen Therapeutics, National University of Ireland Galway, Galway, Ireland, [8] Regenerative Medicine Institute and Department of Medicine, National University of Ireland Galway, Galway, Ireland, [9] Molecular and Experimental Cardiology, Ruhr University Bochum, Bochum, Germany, [10] Department of Cardiology, St. Josef-Hospital, Ruhr University Bochum, Bochum, Germany, [11] Department of Cardiology, Charit9 - Universit4tsmedizin Berlin, Campus Virchow Klinikum, Berlin, Germany

OPEN ACCESS

Edited by:
Modar Kassan, University of Tennessee Health Science Center (UTHSC), United States

Reviewed by:
Daniela Sorriento, University of Naples Federico II, Italy
Michele Ciccarelli, University of Salerno, Italy

***Correspondence:**
Sophie Van Linthout
sophie.van-linthout@charite.de

Specialty section:
This article was submitted to Hypertension, a section of the journal Frontiers in Cardiovascular Medicine

Received: *25 November 2020*
Accepted: *02 March 2021*
Published: *21 May 2021*

Citation:
Pappritz K, Dong F, Miteva K, Kovacs A, El-Shafeey M, Kerim B, O'Flynn L, Elliman SJ, O'Brien T, Hamdani N, Tschöpe C and Van Linthout S (2021) Impact of Syndecan-2-Selected Mesenchymal Stromal Cells on the Early Onset of Diabetic Cardiomyopathy in Diabetic db/db Mice. Front. Cardiovasc. Med. 8:632728. doi: 10.3389/fcvm.2021.632728

Background: Mesenchymal stromal cells (MSCs) are an attractive cell type for cell therapy given their immunomodulatory, anti-fibrotic, and endothelial-protective features. The heparin sulfate proteoglycan, syndecan-2/CD362, has been identified as a functional marker for MSC isolation, allowing one to obtain a homogeneous cell product that meets regulatory requirements for clinical use. We previously assessed the impact of wild-type (WT), $CD362^-$, and $CD362^+$ MSCs on local changes in protein distribution in left ventricular (LV) tissue and on LV function in an experimental model of early-onset diabetic cardiomyopathy. The present study aimed to further explore their impact on mechanisms underlying diastolic dysfunction in this model.

Materials: For this purpose, 1×10^6 WT, $CD362^-$, or $CD362^+$ MSCs were intravenously (i.v.) injected into 20-week-old diabetic BKS.Cg-m+/+$Lepr^{db}$/BomTac, i.e., db/db mice. Control animals (db+/db) were injected with the equivalent volume of phosphate-buffered saline (PBS) alone. After 4 weeks, mice were sacrificed for further analysis.

Results: Treatment with all three MSC populations had no impact on blood glucose levels in db/db mice. WT, $CD362^-$, and $CD362^+$ MSC application restored LV nitric oxide (NO) and cyclic guanosine monophosphate (cGMP) levels in db/db mice, which correlated with a reduction in cardiomyocyte stiffness. Furthermore, all stromal cells were able to increase arteriole density in db/db mice. The effect of $CD362^+$ MSCs on NO and cGMP levels, cardiomyocyte stiffness, and arteriole density was less pronounced than in mice treated with WT or $CD362^-$ MSCs. Analysis of collagen I and III protein expression revealed that fibrosis had not yet developed at this stage of experimental

diabetic cardiomyopathy. All MSCs reduced the number of cardiac $CD3^+$ and $CD68^+$ cells in db/db mice, whereas only splenocytes from $CD362^-$- and $CD362^+$-db/db mice exhibited a lower pro-fibrotic potential compared to splenocytes from db/db mice.

Conclusion: $CD362^+$ MSC application decreased cardiomyocyte stiffness, increased myocardial NO and cGMP levels, and increased arteriole density, although to a lesser extent than WT and $CD362^-$ MSCs in an experimental model of early-onset diabetic cardiomyopathy without cardiac fibrosis. These findings suggest that the degree in improvement of cardiomyocyte stiffness following $CD362^+$ MSC application was insufficient to improve diastolic function.

Keywords: type 2 diabetes, diabetic cardiomyopathy, syndecan-2/$CD362^+$-selected stromal cells, immunomodulation, cardiomyocyte stiffness, cardiac fibrosis, angiogenesis

INTRODUCTION

Diabetes mellitus is a global health problem, and despite enormous advances in therapy options and patient self-management, over 600 million people worldwide are expected to be affected by 2045 (1). Diabetic cardiomyopathy is an own clinical entity, which is characterized by structural and functional alterations of the heart (2), including interstitial inflammation (3), cardiac fibrosis (4), impaired cardiac vascularization (5), and cardiomyocyte stiffness (6). Due to excessive collagen deposition (7, 8) and cardiomyocyte stiffness (9, 10), left ventricular (LV) function is impaired, although cardiomyocyte stiffness alone is sufficient to induce LV diastolic dysfunction without any involvement of collagen (10, 11). Alterations in the NO–cyclic guanosine monophosphate (cGMP)–protein kinase (PK)G-titin phosphorylation pathway have been identified as underlying mechanisms of abnormal cardiomyocyte stiffness in diabetic mice (11, 12), rats (13, 14), and patients suffering from heart failure with preserved ejection fraction (13–15).

Bone marrow-derived mesenchymal stromal cells (MSCs) are an attractive tool to treat diabetic cardiomyopathy due to their immunomodulatory properties (16, 17), their capacity to home to damaged tissues (17), their low immunogenic nature (18), and their anti-diabetic properties (19, 20). With respect to cardiac repair, MSCs have been demonstrated to differentiate into cardiomyocytes, endothelial cells, and smooth muscle cells (21), but their cardioprotective effects, including immunomodulatory (22–24), anti-fibrotic (17), and pro-angiogenic effects (11) have mainly been attributed to their paracrine actions. This also includes the ability of MSCs to restore impaired titin phosphorylation and hereto-related cardiomyocyte stiffness and diastolic dysfunction (11, 25).

A potential concern in the use of MSCs as a therapeutic cellular product is the isolation technique, which relies on the plastic adherence of bone marrow mononuclear cells (MNCs) and leads to a heterogeneous population. Although minimal criteria for MSC characterization have been defined (26), this still heterogeneous human MSC population may not be sufficiently pure to meet emerging regulatory requirements for Advanced Therapeutic Medicinal Products for clinical use. Syndecan-2/CD362, a heparin sulfate proteoglycan, is expressed on the surface of a subpopulation of human MSCs and allows the selective isolation of these cells via fluorescence-activated cell sorting.

In experimental *Escherichia coli*-induced pneumonia, Masterson et al. (27) demonstrated that $CD362^+$-selected MSCs decreased pneumonia severity and that their efficacy was at least comparable with that of heterogeneous MSCs. We recently assessed local changes in protein distribution in myocardial tissue in response to wild-type (WT), $CD362^+$, and $CD362^-$-selected cell application in db/db mice (25). Subsequent investigations of the phosphorylation state of titin in the heart revealed that only WT and $CD362^-$-selected MSCs restored all-titin phosphorylation and downstream PKG activity in db/db mice, which were paralleled with an improvement in parameters of diastolic function.

With $CD362^+$-selected MSCs being a homogeneous cell product that meets regulatory requirements for clinical use, the present study aimed to gain further insights into the impact of $CD362^+$-selected MSC application on the pathogenesis of experimental diabetic cardiomyopathy, especially on the mechanisms underlying diastolic dysfunction. To this end, $CD362^+$, $CD362^-$, and WT MSCs were intravenously (i.v.) administrated in type 2 diabetic db/db mice and their impact on cardiomyocyte stiffness, myocardial NO and cGMP levels, cardiac fibrosis, cardiac immune cell presence, and angiogenesis was analyzed.

MATERIALS AND METHODS

Mesenchymal Stromal Cell Preparation

As described in detail previously (25, 27), bone marrow-derived WT MSCs (WT), $CD362^-$ MSCs ($CD362^-$), and $CD362^+$ MSCs ($CD362^+$) were obtained from Orbsen Therapeutics Ltd. (Galway, Ireland). Via Ficoll density gradient centrifugation (GE Health Care Bio-Sciences, Buckinghamshire, UK), MNCs were isolated, followed by lysis of erythrocytes using commercially available ACK lysis buffer (Life Technologies, California, USA). Subsequently, cells were stained with antibodies directed against CD23 (eBioscience, Hatfield, UK), CD45 (BD Biosciences, Oxford, UK), CD271 (Miltenyi Biotec, Bergisch Gladbach, Germany), and CD362 (R&D Systems, Abingdon, UK). As

a marker for cell viability, Sytox Blue (Life Technologies, California, USA) was used. On a BD FACS Aria (BD Biosciences, Oxford, UK), cells were sorted and plated afterwards for further expansion. At passage 2, the different cell types were cryopreserved and shipped to the consortia partners for further experiments. Informed consent was obtained for all bone marrow samples (Ethics Ref. C.A.02/08).

Model of Experimental Type 2 Diabetes Mellitus-Associated Diabetic Cardiomyopathy

As a common model for human type 2 diabetes mellitus, leptin receptor (Lepr) knockout mice, commonly known as db/db mice, were used. In detail, 8-week-old, male heterozygous (db+/db) and homozygous (db/db) BKS.Cg-m+/+Lepr^{db}/BomTac mice were purchased from Taconic (Skensved, Denmark) and housed in the animal facilities of the Charité-Universitätsmedizin Berlin under standard housing conditions (12-h light/dark cycle, 50–70% humidity, 19–21°C) with free access to food and water. At the age of 20 weeks, db+/db and db/db mice were randomly divided over the groups and administered with 1×10^6 WT, CD362$^-$, or CD362$^+$ MSCs in 200 µl of phosphate-buffered saline (PBS) via i.v. injection. Control animals received the same volume (200 µl) of PBS alone (Life Technologies, Darmstadt, Germany). The respective n-number of each group is indicated in the figure legends. Four weeks after cell or PBS application, at the age of 24 weeks, mice were anesthetized with a mixture of buprenorphine [0.05 mg/kg bodyweight (BW)] and urethane [0.8–1.2 g/kg BW] to enable subsequent characterization of LV function (25). After functional characterization, mice were sacrificed via cervical dislocation under anesthesia. Subsequently, organs of interest were harvested for further analysis. All experimental procedures were performed according to the European legislation (Directive 2010/63/EU) and approved by the local animal welfare committee (Landesamt für Gesundheit und Soziales, Berlin, Germany, G0254/13).

Blood Glucose and Determination of Glycated Hemoglobin

Before and once a week after cell application, blood glucose (BG) was measured using the Accu-Chek Aviva® (Roche Diabetes Care Deutschland GmbH, Mannheim, Germany) after 4-h fasting. To quantify the glycated hemoglobin fraction HbA_{1c} in whole blood samples, the Helena GLYCO-Tek kit (Helena Laboratories, Texas, USA) was used. In accordance with the manufacturer's protocol, blood samples were hemolyzed with the hemolysate reagent and subsequently vortexed. Next, samples were loaded on special GLYCO-Tek affinity columns placed on collection tubes. Columns were washed with Developer A, and non-glycated hemoglobin (GHb) was eluted by adding 4 ml of Developer A afterwards. The resulting eluate was adjusted to 15 ml with deionized water containing non-GHb. Subsequently, Developer B was used to extract GHb from the same sample. After three times' inversion, the solution of the collection tubes was transferred to a cuvette and measured photometrically at 415 nm on a Spectra Max 340PC microplate reader (Molecular Devices, Biberach an der Riß, Germany). The calculated percentage (%) of GHb was transferred into the percentage (%) of HbA_{1c} using the provided algorithm.

Tissue Preparation

After hemodynamic measurement (25), blood was taken and stored on ice until centrifugation. Additionally, the respective tissues were harvested and immediately snap frozen in liquid nitrogen. For flow cytometry, spleens were collected and stored on ice until further processing.

Assessment of Human Mesenchymal Stromal Cells After Application in Different Organs

In accordance to McBride et al. (28), the enrichment of the human MSCs in different organs was investigated by Alu-PCR. Genomic DNA from frozen LV, lung, kidney, liver, spleen, and pancreas was extracted. As previously described (11, 29), human genomic DNA obtained from human umbilical vein endothelial cells served as standard, which was serially diluted over a 100,000-fold range, into murine spleen genomic DNA. To perform real-time PCR, 800 ng of target DNA, Alu-specific primers, and a fluorescent probe were used. Consistent with findings of Lee et al. (30), human DNA was not detectable 4 weeks after application in any of the analyzed organs/tissues (data not shown).

Passive Force Measurements of Isolated Cardiomyocytes

To record passive force ($F_{passive}$) of skinned cardiomyocyte preparations, frozen LV samples were first mechanically disrupted in relaxing solution, containing 1.0 mM of Mg^{2+}, 100 mM of KCl, 2.0 mM of EGTA, 4.0 mM of Mg-ATP, and 10 mM of imidazole (all Sigma-Aldrich, Munich, Germany), followed by incubation in relaxing solution supplemented with 0.5% Triton X-100 for 5 min. Next, five times' washing in relaxing solution was performed. Under an inverted microscope (Zeiss Axiovert 135, 40× objective; Carl Zeiss AG Corp., Oberkochen, Germany), single cardiomyocytes were selected and subsequently fixed in a "Permeabilized Myocyte Test System" (1600A; with force transducer 403A; Aurora Scientific, Aurora, ON, Canada) using silicone adhesive. $F_{passive}$ was measured in relaxing buffer by stepwise stretching of the cardiomyocytes within a sarcomere length (SL) range between 1.8 and 2.4 µm. All measurements were performed at room temperature. For data presentation and analysis, force values were normalized to myocyte cross-sectional area (12).

Determination of Myocardial Nitric Oxide Levels

To determine the concentration of myocardial NO, a colorimetric assay kit (BioVision Inc., Milpitas, CA, USA) was used. As described previously (12), frozen LV samples were first treated with trichloroacetic acid (Sigma-Aldrich), washed with 1 ml of 0.2% dithiothreitol, and subsequently homogenized in 1% sodium dodecyl sulfate (SDS) sample buffer, containing tri-distilled water, glycerol, SDS, Tris-HCl, brome-phenol blue, and

DTT (all purchased from Sigma-Aldrich). After centrifugation at 14,000*g* for 15 min (2–8°C), absorbance of the supernatants was measured at 570 nm. As standard curve, an assay buffer was used from which the absorbance of the samples could be translated into nitrate/nitrite concentrations (15).

Determination of Myocardial Cyclic Guanosine Monophosphate Concentration

Cardiac cGMP levels were investigated by the use of the commercially available parameter cGMP assay immunoassay kit (R&D systems, Minneapolis, MN, USA). In brief, homogenates of frozen LV samples were prepared and subsequently diluted in cell lysis buffer to a concentration of 0.025 μg/L. In accordance with the manufacturer's protocol, 100 μl of the homogenate was assayed by which the amount of cGMP present in the homogenate competed with fixed amount of horseradish peroxidase-labeled cGMP for sites on a rabbit polyclonal antibody. All samples were analyzed in duplicate, and cGMP concentration was expressed in pmol/ml (14).

Immunohistochemistry

Frozen LV samples were embedded in Tissue-Tek OCT (Sakura, Zoeterwoude, NL) and cut into 5-μm-thick sections. Subsequently, immunohistological stainings using the avidin–biotin complex (ABC) method or the EnVision® method were performed. To this end, the following antibodies were used: anti-collagen I (dilution 1:350; Chemicon, Limburg, Germany), anti-collagen III (dilution 1:200; Calbiochem, Merck Millipore, Darmstadt, Germany), anti-CD3 (dilution 1:35; Santa Cruz Biotechnology, Heidelberg, Germany), anti-CD4 (dilution 1:50; BD Bioscience/Pharmigen, Heidelberg, Germany), anti-CD8a (dilution 1:50; BioLegend, Koblenz, Germany), and anti-CD68 (dilution 1:600; Abcam, Cambridge, Germany). The EnVision® method was used to investigate cardiac collagen I, collagen III, and α-SMA expression. To determine the presence of inflammatory cells such as CD3, CD4, CD8a, and CD68 in LV tissue samples, the ABC method was performed. In general, specific epitopes of the stained structure are colored red, and the heart area (HA) was counterstained with Heamalaun (blue). Quantitative analysis of all stainings was performed at 200× magnification in a blinded manner by digital image analysis on a Leica DM2000 light microscope (Leica Microsystems, Wetzlar, Germany). For this purpose, special macros were created to assess the number of cells/HA (mm^2) or the positive area (%)/HA (mm^2). In total, a minimum of 50 pictures from two LV sections from different cutting levels for each animal were recorded and analyzed. To assess artery and arteriole density, an anti-α-smooth muscle actin (α-SMA) antibody (dilution 1:200; Abcam) was used. In 10 high-power field (hpf), arteries and arterioles were counted at 100× magnification and presented as number of arteries or arterioles per hpf.

Flow Cytometry

Splenocytes were isolated according to Van Linthout et al. (22). In brief, collected spleens of PBS- and cell-treated mice were positioned in a petri dish containing Roswell Park Memorial Institute (RPMI) media (Life Technologies). Next, spleens were mashed through a 70-μm cell strainer, followed by washing with 1% fetal bovine serum (FBS; Biochrom, Berlin, Germany) in PBS (Life Technologies). After centrifugation, supernatant was carefully aspirated, and the remaining pellet was resuspended in ACK lysis buffer (Life Technologies). Erythrocyte lysis was stopped by adding RPMI (Life Technologies), and the cell suspension was subsequently passed through a 40-μm cell strainer. Next, the cell suspension was again centrifuged, and the remaining cell pellet was resuspended for subsequent staining.

To assess the number of splenic (apoptotic; Annexin V^+) regulatory T cells (Tregs; $CD4^+CD25^+FoxP3^+$ cells), splenocytes were incubated with anti-CD4 FITC (dilution 1:20; Miltenyi Biotec), anti-CD25 PE (dilution 1:20; Miltenyi Biotec), and anti-Annexin V V450 (dilution 1:20; BD Bioscience, Heidelberg, Germany) antibodies for 20 min at 4°C in the dark. Subsequently, cells were washed and resuspended in fixation/permeabilization solution (BD Biosciences, New Jersey, USA). Finally, incubation with an anti-FoxP3 APC (dilution 1:10; Miltenyi Biotec) antibody followed. To determine the percentage of IL-10 and IFN-γ expressing $CD4^+$ and $CD8^+$ cells, splenocytes were stimulated after isolation with Iscove medium (Sigma-Aldrich) containing 50 ng/ml of phorbol 12-myristate 13-acetate (PMA; BD Biosciences, Heidelberg, Germany), 500 ng/ml of Ionomycin (BD Biosciences), and GolgiStop™ (dilution 1:1,500; BD Biosciences) prior to staining with anti-CD4 FITC and anti-CD8 VioBlue (both dilution 1:10; both Miltenyi). Afterwards, cells were fixated and permeabilized before they were incubated with the respective anti-IFN-γ APC and IL-10 PE (both dilution 1:10; both Miltenyi) antibodies.

After the respective staining was finished, cells were resuspended in PBS and measured on a MACSQuant Analyzer (Miltenyi Biotec). For data analysis, the FlowJo software version 8.8.6 (Tree Star Inc.) was used.

RNA Isolation From Left Ventricular Tissue and Gene Expression Analysis

As previously published (23), RNA was isolated using the TRIzol™ method (Invitrogen, Heidelberg, Germany). To this end, frozen LV tissue was homogenized in TRIzol™ reagent, followed by chloroform extraction. Next, RNA was precipitated and subsequently purified using the NucleoSpin® RNA mini kit (Macherey-Nagel GmbH, Düren, Germany) according to the manufacturer's protocol. The concentration of RNA was measured at the absorbance of 260 nm by using a NanoDrop 1000 (Thermo Scientific, Erlangen, Germany). For subsequent cDNA transcription, 1 μg of RNA and the High Capacity cDNA Reverse Transcription Kit from Applied Biosystems (Life Technologies GmbH) was used. Expression levels of the respective target genes were examined on a 7900HT real-time system (Applied Biosystems). Therefore, gene reporter assays from Applied Biosystems for lysyl oxidase (Lox; Mm00495386_m1), lysyl oxidase like (Loxl)-2 (Mm00804740_m1), transforming growth factor-β (TGF-β; Mm00441724_m1), and GAPDH (Mm99999915_g1) as a housekeeping gene were used. To examine the n-fold change, mRNA levels were further normalized to the db+/db group set as 1.

Co-culture of Fibroblasts With Splenocytes

To determine the impact of splenocytes on collagen production in fibroblasts, splenocytes of the different experimental groups were co-cultured with murine C4 fibroblasts. According to Van Linthout et al. (11), fibroblasts were plated at a density of 10,000 cells per well in Iscove Basal Medium (Sigma-Aldrich) containing 10% FBS and 1% penicillin/streptomycin (both Biochrom). Twenty-four hours later, isolated splenocytes were added at a ratio of 1 to 10 (fibroblasts to splenocytes) in Iscove medium (Sigma) supplemented with 10% FBS and 1% penicillin/streptomycin (both Biochrom) in the presence of 50 ng/ml of PMA and 500 ng/ml of Ionomycin (both BD Biosciences). After 24-h co-culture, splenocytes were removed, and fibroblasts were fixed with cold methanol. Subsequently, Sirius red staining was performed. For photometric analyses at 540 nm, the Spectra Max 340PC microplate reader (Molecular Device GmbH) was used.

Statistical Analysis

All data are illustrated as mean ± SEM, and statistical analysis was performed using the GraphPad Prism 9 Software (GraphPad Software, La Jolla, USA). Differences were considered significant at $p < 0.05$ using one-way ANOVA with Fisher's least significant difference (LSD) *post hoc* test (parametric data) or Brown–Forsythe and Welch-ANOVA followed by unpaired *t*-test with Welch's correction (non-parametric data).

RESULTS

Application of Wild-Type, CD362^{-}, and CD362^{+} Mesenchymal Stromal Cells Does Not Affect Blood Glucose and HbA_{1c} Levels of db/db Mice

BG (**Supplementary Figures 1A,B**) and HbA_{1c} levels (**Supplementary Figure 1C**) were elevated in db/db mice compared with db+/db mice. None of the applied MSCs reduced BG or HbA_{1c} levels in db/db mice (**Supplementary Figures 1B,C**).

Application of Wild-Type, CD362^{-}, and CD362^{+} Mesenchymal Stromal Cell Reduces Cardiomyocyte Stiffness in db/db Mice

Previous studies have shown that application of WT and CD362^{-} MSCs improves diastolic function in db/db mice, whereas application of CD362^{+} MSCs does not (25). To gain further insights into the mechanisms underlying their impact on diastolic dysfunction, *ex vivo* measurements of cardiomyocyte stiffness were performed (**Figure 1A**). In accordance with the literature (12), db/db mice showed increased $F_{passive}$ in isolated cardiomyocytes compared with control animals. Interestingly, all cell types reduced $F_{passive}$. This reduction was the most pronounced in the db/db CD362^{-} group and less prominent in the db/db CD362^{+} group. Since regulation of titin phosphorylation via NO-cGMP-PKG signaling (12) is important for proper diastolic function (14), we therefore measured the levels of myocardial NO and cGMP (**Figures 1B,C**). db/db mice displayed reduced NO and cGMP levels than did db+/db animals, which correlates with the higher $F_{passive}$ values observed in db/db mice. Intravenous administration of WT, CD362^{-}, and CD362^{+} MSCs restored the reduction of NO and cGMP levels in db/db mice (**Figures 1B,C**), by which this effect was less pronounced in db/db mice receiving CD362^{+} MSCs.

Application of Wild-Type, CD362^{-}, and CD362^{+} Mesenchymal Stromal Cell Does Not Influence Cardiac Collagen Expression in db/db Mice

Given the importance of cardiac fibrosis in diabetic cardiomyopathy (3) and diastolic dysfunction (7) and the anti-fibrotic potential of MSCs (17), the impact of MSC application on cardiac fibrosis was analyzed (**Figure 2** and **Supplementary Figure 2**). Quantitative analysis of collagen I and III revealed no significant changes in collagen I and III protein expression between db/db and db+/db control mice (**Figures 2A,B**), indicative of no developed cardiac fibrosis at this stage in db/db mice. However, the collagen I/III protein ratio was increased in db/db animals vs. db+/db mice, showing alterations in the extracellular matrix composition (**Supplementary Figure 2A**). Application of WT, CD362^{-}, and CD362^{+} MSCs resulted in a higher LV collagen I protein expression compared with db+/db mice, whereas WT and CD362^{-} MSCs reduced LV collagen III protein expression than did db+/db controls (**Figures 2A,B**). The collagen I/III protein ratio was increased in db/db mice, which received WT, CD362^{-}, and CD362^{+} MSCs as compared with db+/db mice (**Supplementary Figure 2A**). In addition to cardiac collagen content, the gene expression of known fibrosis mediator TGF-β (**Supplementary Figure 2B**) and the collagen crosslinking enzymes Lox (**Supplementary Figure 2C**) and LoxL-2 (**Supplementary Figure 2D**) were also determined. In comparison with db+/db mice, TGF-β, Lox, and LoxL-2 mRNA levels were elevated in db/db animals. None of the different stromal cells reduced TGF-β, Lox, and LoxL-2 gene expression in db/db mice.

Application of Wild-Type, CD362^{-}, and CD362^{+} Mesenchymal Stromal Cell Increases Arteriole Density in db/db Mice

Since impaired vascularization underlies diastolic dysfunction (8, 31) and MSCs are known for their pro-angiogenic properties (11), we next evaluated the impact of WT, CD362^{-}, and CD362^{+} MSC application on artery and arteriole density in LV sections of db/db mice (**Figure 3**). There was no decrease in artery and arteriole density in db/db mice compared with db+/db mice (**Figures 3A,B**). Administration of WT, CD362^{-}, and CD362^{+} MSCs resulted in a higher arteriole density in db/db mice and was the most pronounced in db/db WT and db/db CD362^{-}-treated mice (**Figure 3B**).

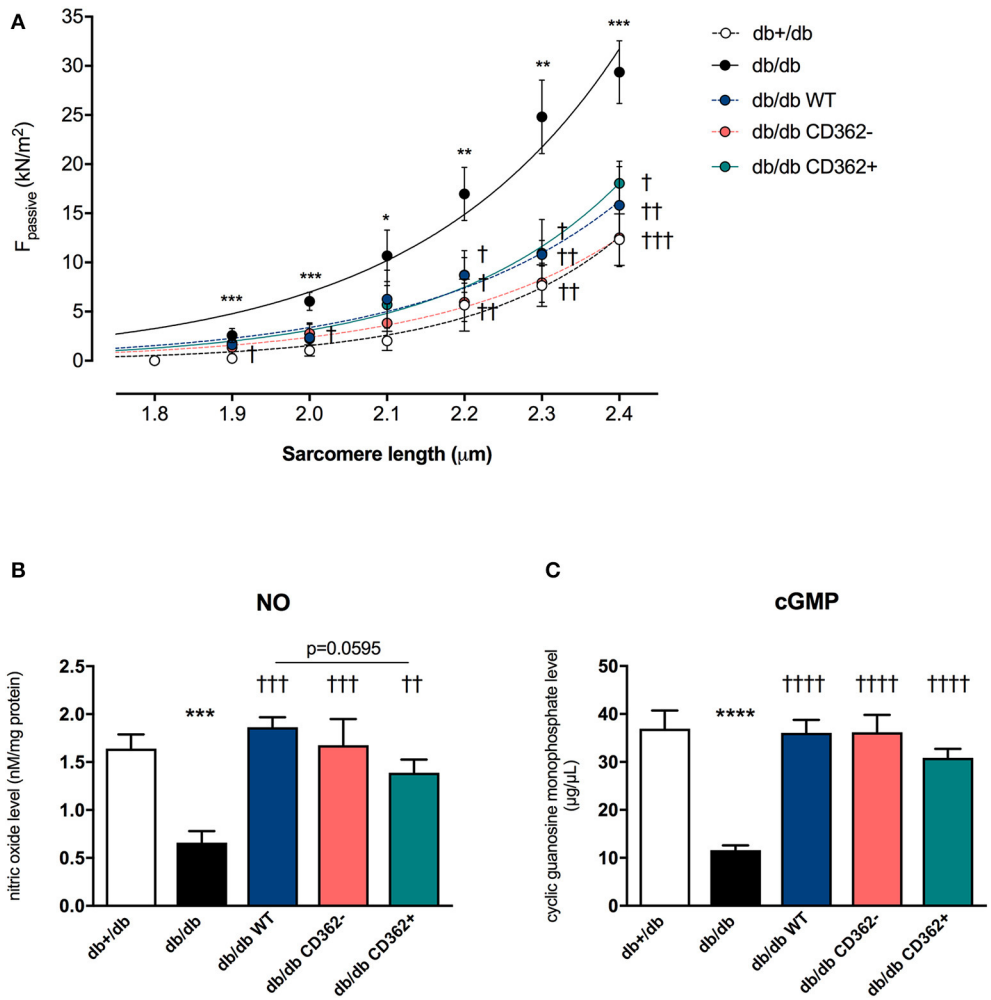

FIGURE 1 | Application of wild-type (WT), CD362$^-$, and CD362$^+$ mesenchymal stromal cells (MSCs) reduces cardiomyocyte stiffness in db/db mice. **(A)** Passive force ($F_{passive}$; in kN/m^2) measurements in single cardiomyocytes at different sarcomere length (1.8–2.4 μm). To further investigate the underlying NO-cGMP-PKG pathway, cardiac nitric oxide (NO; **B**; in nM/mg protein) and cyclic guanosine monophosphate (cGMP; **C**; in μg/μl) concentration in left ventricular (LV) tissue homogenates were measured. Bar graphs represent the mean ± SEM and were analyzed with one-way ANOVA or Welch-ANOVA (*$p < 0.05$, **$p < 0.01$, ***$p < 0.001$, ****$p < 0.0001$ vs. db+/db; $^{\dagger}p < 0.05$, $^{\dagger\dagger}p < 0.01$, $^{\dagger\dagger\dagger}p < 0.001$, $^{\dagger\dagger\dagger\dagger}p < 0.0001$ vs. db/db; with $n = 8$/group for **A**; $n = 5$/group for **B,C**).

Application of Wild-Type, CD362$^-$, and CD362$^+$ Mesenchymal Stromal Cell Influences Cardiac Immune Cell Presence in db/db Mice

Given the importance of cardiac inflammation in diabetic cardiomyopathy (32) and the immunomodulatory properties of MSCs (33), we next evaluated the impact of i.v. WT, CD362$^-$, and CD362$^+$ MSC application on cardiac immune cell presence. Therefore, the number of CD3$^+$, CD4$^+$, CD8a$^+$, and CD68$^+$ cells was assessed in the myocardium of the different groups (**Figure 4** and **Supplementary Figure 3**). Compared with db+/db mice, db/db animals displayed an increased number of CD3$^+$ (**Figure 4A**), CD4$^+$ (**Supplementary Figure 3A**), CD8a$^+$ (**Supplementary Figure 3B**), and CD68$^+$ (**Figure 4B**) cells in the heart. Administration of WT, CD362$^-$, and CD362$^+$ MSCs abrogated the number of cardiac CD3$^+$ and CD68$^+$ cells in db/db animals to levels similar to those of non-diabetic db+/db mice (**Figures 4A,B**), whereas none of the stromal cells resulted in lower CD4$^+$ and CD8a$^+$ cells in db/db mice (**Supplementary Figures 3A,B**).

Application of Wild-Type, CD362$^-$, and CD362$^+$ Mesenchymal Stromal Cell Modulates Splenic Immune Cells in db/db Mice

Based on the knowledge that the cardiosplenic axis, which describes the homing of immune cells from the spleen toward the heart, has an impact on the progression of heart failure (34), we further evaluated whether WT, CD362$^-$, and CD362$^+$ MSC application affects splenic immune cells in db/db mice (**Figure 5**). By an unchanged percentage of splenic CD4$^+$CD25$^+$FoxP3$^+$ cells (Tregs) (**Figure 5A**), db/db

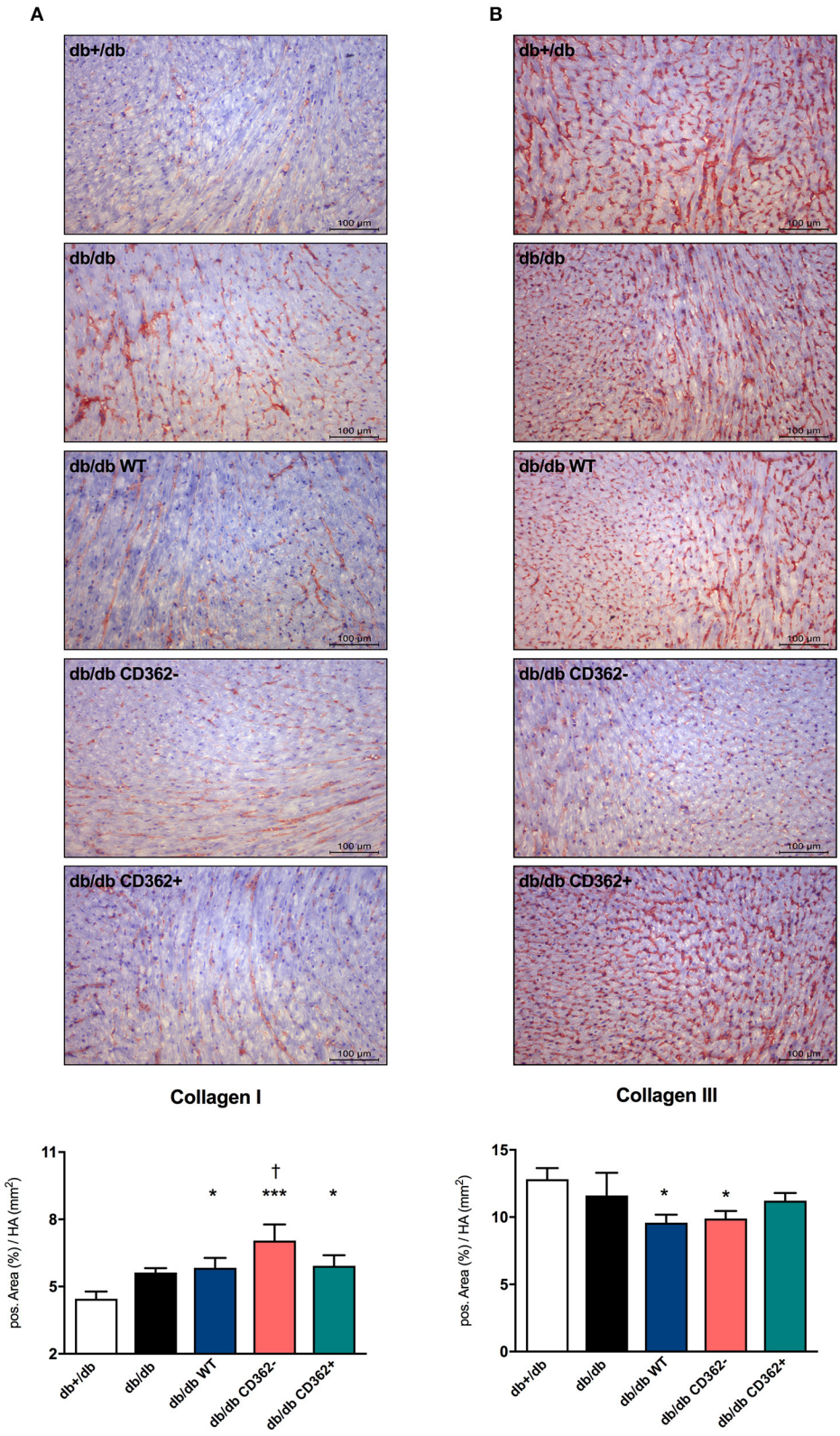

FIGURE 2 | Application of wild-type (WT), CD362^{-}, and CD362^{+} mesenchymal stromal cells (MSCs) does not influence cardiac collagen expression in db/db mice. Representative images (scale bar = 100 µm) of the cardiac collagen I **(A)** and collagen III **(B)** staining and the corresponding quantification of the positive area (%)/heart area (HA; mm^2). Data are depicted as mean ± SEM and analyzed with one-way ANOVA or Welch-ANOVA (*$p < 0.05$, ***$p < 0.001$, vs. db+/db; $^{\dagger}p < 0.05$ vs. db/db; with $n = 11$ for db+/db, $n = 9$ for db/db, $n = 9$ for db/db WT, $n = 9$ for db/db CD362^{-}, and $n = 10$ for db/db CD362^{+}).

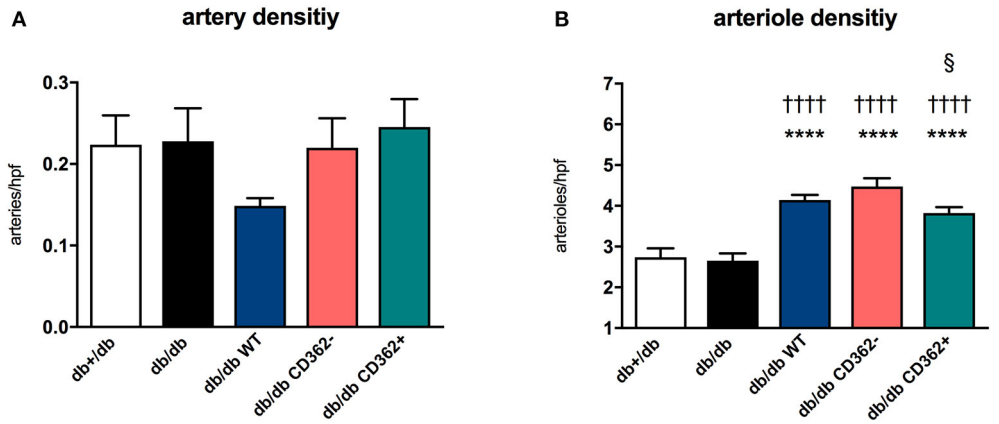

FIGURE 3 | Application of wild-type (WT), CD362$^-$, and CD362$^+$ mesenchymal stromal cells (MSCs) increases arteriole density in db/db mice. **(A)** Artery and **(B)** arteriole density per high-power field (hpf) in db+/db, db/db, and db/db mice injected with WT, CD362$^-$, or CD362$^+$ cells. Bar graphs represent the mean ± SEM and were analyzed with one-way ANOVA or Welch-ANOVA (****$p < 0.0001$ vs. db+/db; ††††$p < 0.0001$ vs. db/db; §$p < 0.05$ vs. db/db CD362$^-$ with $n = 8$ for db+/db, $n = 9$ for db/db, $n = 8$–9 for db/db WT, $n = 9$–10 for db/db CD362$^-$, and $n = 10$–11 for db/db CD362$^+$ group).

mice exhibited a higher percentage of splenic apoptotic Tregs vs. db+/db mice (**Figure 5B**). Furthermore, the amount of anti-inflammatory CD4$^+$IL-10$^+$ and CD8$^+$IL-10$^+$ cells was lower in the spleen of db/db mice vs. db+/db animals (**Figures 5C,E**), which was paralleled by an increased amount of splenic pro-inflammatory CD4$^+$IFN-γ^+ and CD8$^+$IFN-γ^+ cells (**Figures 5D,F**). Application of WT, CD362$^-$, and CD362$^+$ MSC cell in db/db mice resulted in a lower percentage of apoptotic Tregs compared with db/db mice (**Figure 5B**). WT and CD362$^+$ cells resulted in a higher number of splenic CD4$^+$IL-10$^+$ and CD8$^+$IL-10$^+$ cells in db/db mice, whereas CD362$^-$ cells did not alter those cell populations (**Figures 5C,E**). In contrast, a decrease in CD4$^+$IFN-γ^+ and CD8$^+$IFN-γ^+ cells was the most pronounced after CD362$^-$ MSC administration (**Figures 5D,F**).

Knowing that splenocytes play an important role in cardiac remodeling (34) and the above-described systemic immunomodulation, we finally evaluated the impact of MSC application on the pro-fibrotic potential of splenocytes (**Supplementary Figure 4**). Therefore, splenocytes of the different groups were co-cultured with fibroblasts, and their subsequent impact on collagen production was determined (**Supplementary Figure 4A**). Upon co-culture, collagen production was increased in fibroblasts supplemented with splenocytes from db/db mice compared with fibroblasts supplemented with splenocytes from db+/db mice (**Supplementary Figure 4B**). Interestingly, only splenocytes isolated from db/db CD362$^-$ and db/db CD362$^+$ mice led to a lower collagen production upon co-culture with fibroblasts vs. splenocytes from db/db animals.

DISCUSSION

The salient findings of the present study are that all the MSC populations tested in this experimental model of type 2 diabetes mellitus-associated diabetic cardiomyopathy, characterized by diastolic dysfunction and absence of cardiac fibrosis, are able to reduce cardiomyocyte stiffness and restore the impaired underlying NO-cGMP signaling cascade. Interestingly, these effects tended to be less pronounced after CD362$^+$ MSC application. Additionally, increased arteriole density was more pronounced after WT and CD362$^-$ MSCs compared with CD362$^+$ MSC application to db/db mice; however, all MSCs exerted systemic immunomodulatory effects and resulted in reduced immune cell presence in the heart. These observations together with our previous findings showing an improvement in diastolic dysfunction only after WT and CD362$^-$ MSC application in db/db mice (25) indicate that in a model of diastolic dysfunction in the absence of cardiac fibrosis, a specific degree of decrease in cardiomyocyte stiffness and restoration of the underlying NO-cGMP-PKG-titin phosphorylation pathway is required to ameliorate diastolic dysfunction.

Evidence from a rodent model of the metabolic syndrome and from type I diabetic mice (11) indicates that dysregulation of the sarcomere protein titin is sufficient to induce diastolic dysfunction, even in the absence of cardiac fibrosis (9, 35). We previously showed lower PKG levels and titin hypophosphorylation in db/db mice, which is reflected in diastolic dysfunction (25). Assessment of NO and cGMP levels and cardiomyocyte stiffness in the present study corroborates the hypothesis that impaired NO-cGMP-PKG signaling leads to titin hypophosphorylation and cardiomyocyte stiffness (12, 14), as indicated by the high $F_{passive}$ in isolated cardiomyocytes of db/db mice. Unaltered collagen I and III protein expression compared with non-diabetic db/db+ mice further illustrates that the diastolic dysfunction in this model of early diabetic cardiomyopathy occurs in the absence of cardiac fibrosis. With respect to stromal cell application, we recently demonstrated that only application of WT and CD362$^-$ MSCs normalized PKG activity and titin phosphorylation in db/db mice and was associated with restored diastolic performance in these animals (25). Based on our previous findings illustrating that impaired NO bioavailability, a hallmark of endothelial dysfunction (13, 36,

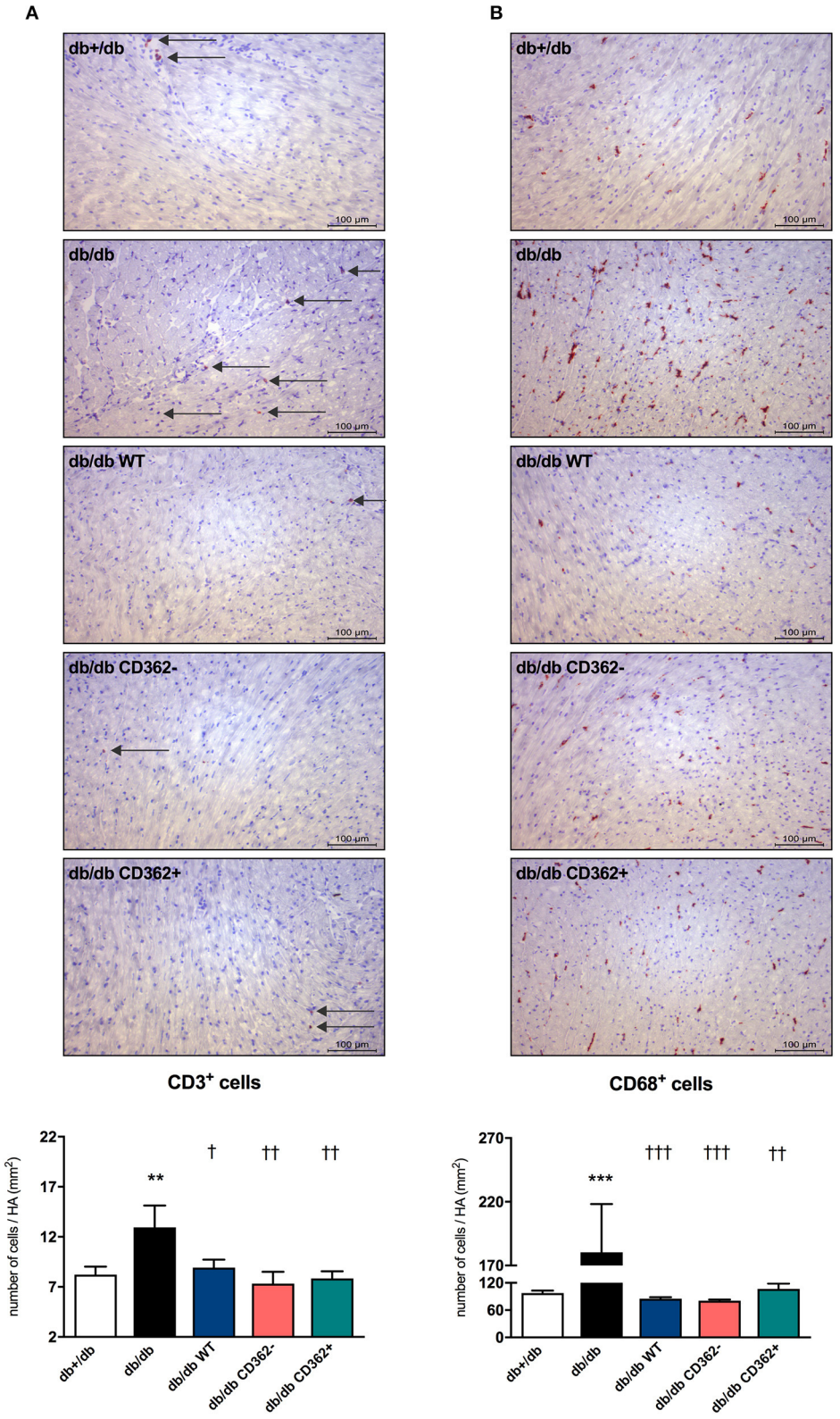

FIGURE 4 | Application of wild-type (WT), CD362^{-}, and CD362^{+} mesenchymal stromal cells (MSCs) influences cardiac presence of CD3^{+} and CD68^{+} immune cells in db/db mice. Characterization of the immune cells present within the myocardium 4 weeks after stromal cell administration. Top: representative immunohistological

(Continued)

FIGURE 4 | stainings (scale bar = 100 μm) of $CD3^+$ **(A)** and $CD68^+$ **(B)** cells. The specific epitopes are colored red and indicated by the arrows. Bottom: the respective quantification performed via digital image analysis is depicted. Bar graphs represent the mean ± SEM of the number of cells/heart area (HA; mm^2) and were analyzed with one-way ANOVA or Welch-ANOVA (**$p < 0.01$, ***$p < 0.001$ vs. db+/db; $^{\dagger}p < 0.05$, $^{\dagger\dagger}p < 0.01$, $^{\dagger\dagger\dagger}p < 0.001$ vs. db/db with $n = 10$–11 for db+/db, $n = 6$–7 for db/db, $n = 7$–9 for db/db WT, $n = 7$–8 for db/db $CD362^-$, and $n = 11$ for db/db $CD362^+$ group).

37), could be increased by i.v. application of placenta-derived stromal cells (11), we suggested that the improved diastolic performance following WT and $CD362^-$ MSC administration (25) was caused by changes of the NO-cGMP-PKG pathway. Supporting this hypothesis, we observed normalized NO and cGMP levels in db/db mice upon cell application; however, this effect was less pronounced in $CD362^+$ MSC-treated db/db mice. Beyond NO-dependent PKG activation, vascularization can also be increased by MSCs (11). Accordingly, increased arteriole density was detected in db/db mice injected with WT, $CD362^-$, and $CD362^+$ MSCs. In parallel to the smaller increase in NO and cGMP levels, db/db mice that received $CD362^+$ MSCs displayed a lower number of arterioles than did the db/db $CD362^-$ group. This finding is supported by the study of De Rossi et al. (38), who demonstrated that released syndecan-2 (=CD362) induces anti-angiogenic effects. It further suggests that less pronounced pro-angiogenic/endothelial-protective effects of $CD362^+$ MSCs compared with WT and $CD362^-$ MSCs underlie the lower PKG activity, subsequent titin hypophosphorylation, lower improvement in cardiomyocyte stiffness, and failure to improve diastolic function in db/db mice.

Given the well-accepted concept of crosstalk between inflammation and cardiac fibrosis on the one hand (39) and the immunomodulatory properties of MSCs on the other hand (17, 22), we investigated the impact of MSC application on cardiac and splenic immune cell presence. In agreement with their ability to decrease the number of immune cells in the heart (17), WT as well as $CD362^-$ and $CD362^+$ MSCs reduced cardiac $CD3^+$ and $CD68^+$ cell presence in db/db mice. Furthermore, application of all MSC populations led to fewer apoptotic Tregs within the spleen; however, only $CD362^+$ MSCs increased the percentage of splenic Tregs in db/db mice. In line with observations in ob/ob mice (40), db/db animals displayed higher numbers of splenic pro-inflammatory $CD4^+$IFN-γ^+ and $CD8^+$IFN-γ^+ cells, whereas the numbers of anti-inflammatory $CD4^+$IL-10^+ and $CD8^+$IL-10^+ cells were reduced. MSC application modulated the percentages of these specific immune cells in the spleen, with the observed effects differing depending on the applied MSC population. The immunomodulatory effects observed following WT and $CD362^+$ MSC application were similar; both cell populations increased the anti-inflammatory splenic $CD4^+$IL-10^+ and $CD8^+$IL-10^+ cells in db/db mice, whereas $CD362^-$ MSCs led to a decrease. Injection with $CD362^-$ MSCs also led to the largest reduction of pro-inflammatory cells in the MSC-treated db/db animals. Since syndecans are known to interact with immune cells (41), the absence of CD362 may explain the differences in those immunomodulatory effects following $CD362^-$ vs. WT and $CD362^+$ MSC application. However, further investigations beyond the scope of this study are needed to support this hypothesis. In general, a reduction in systemic and cardiac inflammatory cells was observed after MSC application, which might in part be explained by the MSC-mediated increase in Tregs and/or Tregs quality (reduction in apoptotic Tregs) (42). However, a direct MSC/CD362-mediated effect on the specific analyzed T cells cannot be excluded.

Given the relevance of the cardiosplenic axis in the pathogenesis of heart failure, we investigated the pro-fibrotic potential of splenocytes derived from the different groups. Similar to splenocytes isolated from streptozotocin-induced diabetic cardiomyopathy mice (11), db/db-derived splenocytes increased the collagen production of fibroblasts upon co-culture. Interestingly, splenocytes from $CD362^-$ and $CD362^+$ db/db mice exhibited a lower pro-fibrotic potential than did splenocytes of db/db mice. Given the early-onset model of experimental diabetic cardiomyopathy without cardiac fibrosis, we hypothesize that the $CD362^-$- and $CD362^+$-mediated immunomodulatory and anti-fibrotic effects may be reflected in a reduction in cardiac fibrosis at a later stage.

Importantly, all the abovementioned effects following the different applied stromal cells in db/db mice occurred in the absence of changes in BG or HbA_{1c} levels. This is in contrast to previous studies in humans (43–45) and rodents (19, 20, 46) in which a therapeutic effect on glycemic control after stromal cell treatment was found. This phenomenon was explained by the regenerative properties of MSCs, including their capacity to differentiate into insulin-producing cells (19) and their ability to repair pancreatic β-cells in a paracrine manner (47, 48). Most of these studies were performed with murine MSCs or with human MSCs in immunodeficient [severe combined immunodeficiency (SCID)] mice. We suggest that absence of alterations in BG or HbA_{1c} levels after MSC application in db/db mice might be explained by the xenogenic approach in non-immunocompromised mice, leading to a lower regenerative capacity.

CONCLUSION

The i.v. application of $CD362^+$ MSCs resulted in reduced cardiomyocyte stiffness paralleled by elevated NO and cGMP levels and increased arteriole density in a model of early-onset diabetic cardiomyopathy without fibrosis. These effects were less pronounced than after WT and $CD362^-$ MSC administration, known to improve diastolic performance in db/db mice (25). These findings indicate that the $CD362^+$ MSC-mediated decrease in cardiomyocyte stiffness and increase in NO-cGMP levels were insufficient to improve diastolic function in this model.

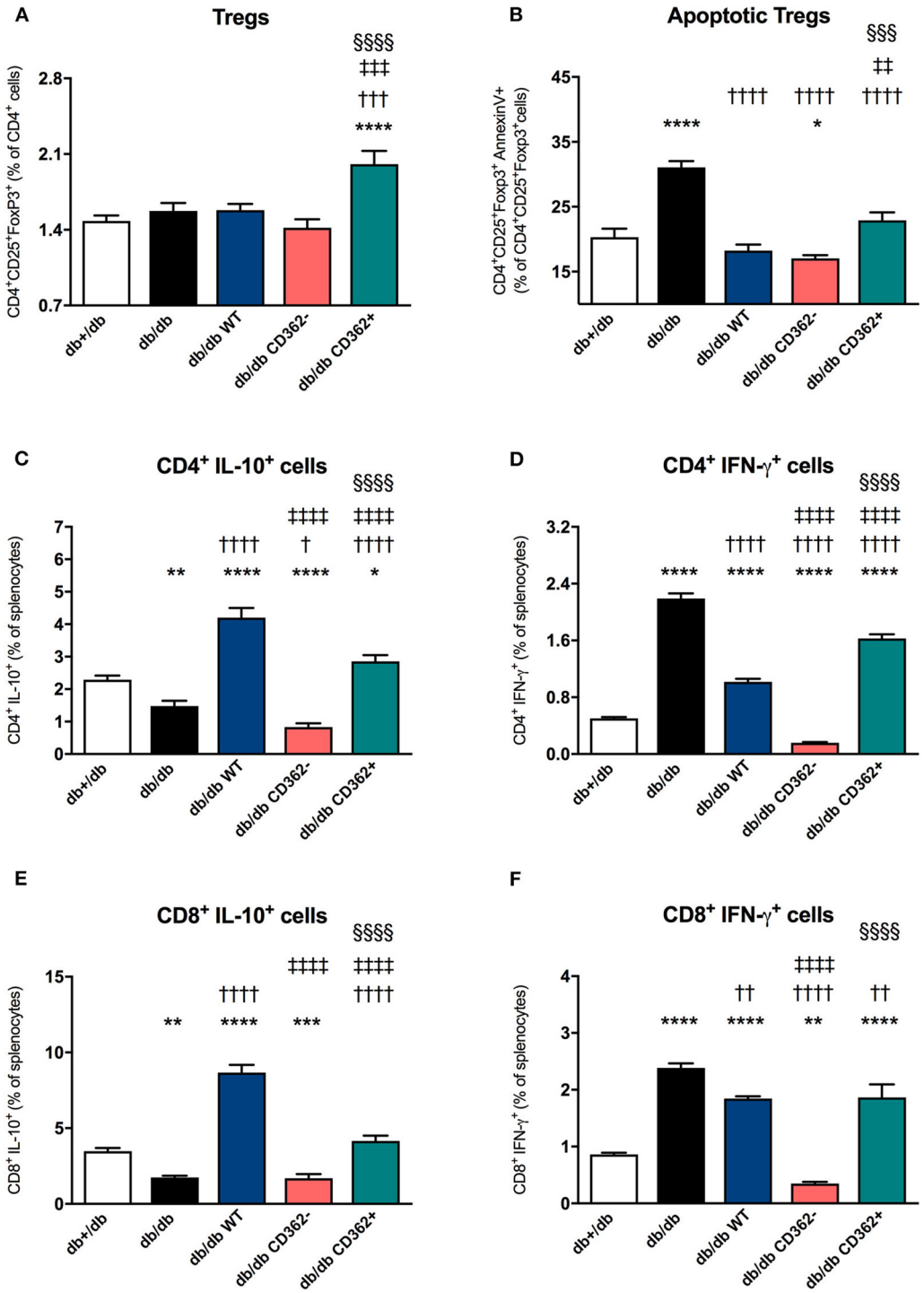

FIGURE 5 | Application of wild-type (WT), CD362^{-}, and CD362^{+} mesenchymal stromal cells (MSCs) modulates the composition of splenic immune cells in db/db mice. To investigate if stromal cell application influences splenic immunomodulation, flow cytometry was performed; and the % of regulatory T cells (Tregs; **A**) and apoptotic Tregs **(B)** was determined. Additionally, anti-inflammatory CD4^{+}IL-10^{+} **(C)** and CD8^{+}IL-10^{+} **(D)** cells and their pro-inflammatory counterparts, CD4^{+}IFN-γ^{+} **(E)**, and CD8^{+}IFN-γ^{+} **(F)** cells were analyzed by flow cytometry. Data are depicted as mean ± SEM and analyzed with one-way ANOVA or Welch-ANOVA (*$p < 0.05$, **$p < 0.01$, ***$p < 0.001$, ****$p < 0.0001$ vs. db+/db; $^{\dagger}p < 0.05$, $^{\dagger\dagger}p < 0.01$, $^{\dagger\dagger\dagger}p < 0.001$, $^{\dagger\dagger\dagger\dagger}p < 0.0001$ vs. db/db; $^{\ddagger\ddagger}p < 0.01$, $^{\ddagger\ddagger\ddagger}p < 0.001$, $^{\ddagger\ddagger\ddagger\ddagger}p < 0.0001$ vs. db/db WT; $^{\S\S\S}p < 0.001$, $^{\S\S\S\S}p < 0.0001$ vs. db/db CD362^{-} with $n = 5$–6/group).

DATA AVAILABILITY STATEMENT

The original contributions presented in the study are included in the article/**Supplementary Material**, further inquiries can be directed to the corresponding author/s.

ETHICS STATEMENT

The animal study was reviewed and approved by the Landesamt für Gesundheit und Soziales, Berlin, Germany (G0254/13).

AUTHOR CONTRIBUTIONS

KP wrote the manuscript and substantially contributed to data acquisition including data analysis and interpretation, and intellectual content. FD, KM, AK, ME-S, and BK contributed to data acquisition and data analysis. LO'F and SE provided the human MSCs used in the study, including data of cell characterization. NH, SE, and TO'B revised the manuscript. CT coordinated funding and revised the manuscript. SVL performed conception of the study, data analysis and interpretation, coordinated funding, and revised the manuscript. All authors revised the manuscript for intellectual content and gave their final approval for publication.

FUNDING

This study was supported by the European 7th Framework Consortium REDDSTAR (Grant: HEALTH.2012.2.4.3-1) to SE, TO'B, CT, and SVL.

ACKNOWLEDGMENTS

We would like to acknowledge Annika Koschel, Gwendolin Matz, Kerstin Puhl, and Marzena Sosnowski for excellent technical support. We further acknowledge the assistance of the BCRT Flow Cytometry Lab. In addition, we acknowledge support from the German Research Foundation (DFG) and the Open Access Publication Funds of the Charité-Universitätsmedizin Berlin. Furthermore, we would like to thank Nicola Brindle for scientific language check and editing.

SUPPLEMENTARY MATERIAL

The Supplementary Material for this article can be found online at: https://www.frontiersin.org/articles/10.3389/fcvm.2021.632728/full#supplementary-material

REFERENCES

1. Beckman JA, Creager MA, Libby P. Diabetes and atherosclerosis: epidemiology, pathophysiology, and management. *JAMA.* (2002) 287:2570–81. doi: 10.1001/jama.287.19.2570
2. Rubler S, Dlugash J, Yuceoglu YZ, Kumral T, Branwood AW, Grishman A. New type of cardiomyopathy associated with diabetic glomerulosclerosis. *Am J Cardiol.* (1972) 30:595–602. doi: 10.1016/0002-9149(72)90595-4
3. Van Linthout S, Spillmann F, Riad A, Trimpert C, Lievens J, Meloni M, et al. Human apolipoprotein A-I gene transfer reduces the development of experimental diabetic cardiomyopathy. *Circulation.* (2008) 117:1563–73. doi: 10.1161/CIRCULATIONAHA.107.710830
4. Tschope C, Walther T, Koniger J, Spillmann F, Westermann D, Escher F, et al. Prevention of cardiac fibrosis and left ventricular dysfunction in diabetic cardiomyopathy in rats by transgenic expression of the human tissue kallikrein gene. *FASEB J.* (2004) 18:828–35. doi: 10.1096/fj.03-0736com
5. Chen JX, Zeng H, Reese J, Aschner JL, Meyrick B. Overexpression of angiopoietin-2 impairs myocardial angiogenesis and exacerbates cardiac fibrosis in the diabetic db/db mouse model. *Am J Physiol Heart Circ Physiol.* (2012) 302:H1003–12. doi: 10.1152/ajpheart.00866.2011
6. Kruger M, Kotter S, Grutzner A, Lang P, Andresen C, Redfield MM, et al. Protein kinase G modulates human myocardial passive stiffness by phosphorylation of the titin springs. *Circ Res.* (2009) 104:87–94. doi: 10.1161/CIRCRESAHA.108.184408
7. Westermann D, Lindner D, Kasner M, Zietsch C, Savvatis K, Escher F, et al. Cardiac inflammation contributes to changes in the extracellular matrix in patients with heart failure and normal ejection fraction. *Circ Heart Fail.* (2011) 4:44–52. doi: 10.1161/CIRCHEARTFAILURE.109.931451
8. Tschope C, Van Linthout S. New insights in (inter)cellular mechanisms by heart failure with preserved ejection fraction. *Curr Heart Fail Rep.* (2014) 11:436–44. doi: 10.1007/s11897-014-0219-3
9. Hamdani N, Franssen C, Lourenco A, Falcao-Pires I, Fontoura D, Leite S, et al. Myocardial titin hypophosphorylation importantly contributes to heart failure with preserved ejection fraction in a rat metabolic risk model. *Circ Heart Fail.* (2013) 6:1239–49. doi: 10.1161/CIRCHEARTFAILURE.113.000539
10. Hamdani N, Paulus WJ. Myocardial titin and collagen in cardiac diastolic dysfunction: partners in crime. *Circulation.* (2013) 128:5–8. doi: 10.1161/CIRCULATIONAHA.113.003437
11. Van Linthout S, Hamdani N, Miteva K, Koschel A, Muller I, Pinzur L, et al. Placenta-derived adherent stromal cells improve diabetes mellitus-associated left ventricular diastolic performance. *Stem Cells Transl Med.* (2017) 6:2135–45. doi: 10.1002/sctm.17-0130
12. Hamdani N, Hervent AS, Vandekerckhove L, Matheeussen V, Demolder M, Baerts L, et al. Left ventricular diastolic dysfunction and myocardial stiffness in diabetic mice is attenuated by inhibition of dipeptidyl peptidase 4. *Cardiovasc Res.* (2014) 104:423–31. doi: 10.1093/cvr/cvu223
13. Franssen C, Chen S, Unger A, Korkmaz HI, De Keulenaer GW, Tschope C, et al. Myocardial microvascular inflammatory endothelial activation in heart failure with preserved ejection fraction. *JACC Heart Fail.* (2016) 4:312–24. doi: 10.1016/j.jchf.2015.10.007
14. Kolijn D, Pabel S, Tian Y, Lodi M, Herwig M, Carrizzo A, et al. Empagliflozin improves endothelial and cardiomyocyte function in human heart failure with preserved ejection fraction via reduced pro-inflammatory-oxidative pathways and protein kinase Galpha oxidation. *Cardiovasc Res.* (2021) 117:495–507. doi: 10.1093/cvr/cvaa123
15. van Heerebeek L, Hamdani N, Falcao-Pires I, Leite-Moreira AF, Begieneman MP, Bronzwaer JG, et al. Low myocardial protein kinase G activity in heart failure with preserved ejection fraction. *Circulation.* (2012) 126:830–9. doi: 10.1161/CIRCULATIONAHA.111.076075
16. Aggarwal S, Pittenger MF. Human mesenchymal stem cells modulate allogeneic immune cell responses. *Blood.* (2005) 105:1815–22. doi: 10.1182/blood-2004-04-1559
17. Savvatis K, van Linthout S, Miteva K, Pappritz K, Westermann D, Schefold JC, et al. Mesenchymal stromal cells but not cardiac fibroblasts exert beneficial systemic immunomodulatory effects in experimental myocarditis. *PLoS ONE.* (2012) 7:e41047. doi: 10.1371/journal.pone.0041047
18. Hare JM, Traverse JH, Henry TD, Dib N, Strumpf RK, Schulman SP, et al. A randomized, double-blind, placebo-controlled, dose-escalation study of intravenous adult human mesenchymal stem cells (prochymal) after acute myocardial infarction. *J Am Coll Cardiol.* (2009) 54:2277–86. doi: 10.1016/j.jacc.2009.06.055

19. Lee RH, Seo MJ, Reger RL, Spees JL, Pulin AA, Olson SD, et al. Multipotent stromal cells from human marrow home to and promote repair of pancreatic islets and renal glomeruli in diabetic NOD/scid mice. *Proc Natl Acad Sci USA.* (2006) 103:17438–43. doi: 10.1073/pnas.0608249103
20. Ezquer FE, Ezquer ME, Parrau DB, Carpio D, Yanez AJ, Conget PA. Systemic administration of multipotent mesenchymal stromal cells reverts hyperglycemia and prevents nephropathy in type 1 diabetic mice. *Biol Blood Marrow Transplant.* (2008) 14:631–40. doi: 10.1016/j.bbmt.2008.01.006
21. Quevedo HC, Hatzistergos KE, Oskouei BN, Feigenbaum GS, Rodriguez JE, Valdes D, et al. Allogeneic mesenchymal stem cells restore cardiac function in chronic ischemic cardiomyopathy via trilineage differentiating capacity. *Proc Natl Acad Sci USA.* (2009) 106:14022–7. doi: 10.1073/pnas.0903201106
22. Van Linthout S, Savvatis K, Miteva K, Peng J, Ringe J, Warstat K, et al. Mesenchymal stem cells improve murine acute coxsackievirus B3-induced myocarditis. *Eur Heart J.* (2011) 32:2168–78. doi: 10.1093/eurheartj/ehq467
23. Miteva K, Pappritz K, El-Shafeey M, Dong F, Ringe J, Tschope C, et al. Mesenchymal stromal cells modulate monocytes trafficking in coxsackievirus B3-induced myocarditis. *Stem Cells Transl Med.* (2017) 6:1249–61. doi: 10.1002/sctm.16-0353
24. Miteva K, Pappritz K, Sosnowski M, El-Shafeey M, Muller I, Dong F, et al. Mesenchymal stromal cells inhibit NLRP3 inflammasome activation in a model of Coxsackievirus B3-induced inflammatory cardiomyopathy. *Sci Rep.* (2018) 8:2820. doi: 10.1038/s41598-018-20686-6
25. Pappritz K, Klein O, Dong F, Hamdani N, Kovacs A, O'Flynn L, et al. MALDI-IMS as a tool to determine the myocardial response to syndecan-2-selected mesenchymal stromal cell application in an experimental model of diabetic cardiomyopathy. *Proteomics Clin Appl.* (2021) 15:e2000050. doi: 10.1002/prca.202000050
26. Dominici M, Le Blanc K, Mueller I, Slaper-Cortenbach I, Marini F, Krause D, et al. Minimal criteria for defining multipotent mesenchymal stromal cells. The International Society for Cellular Therapy position statement. *Cytotherapy.* (2006) 8:315–7. doi: 10.1080/14653240600855905
27. Masterson C, Devaney J, Horie S, O'Flynn L, Deedigan L, Elliman S, et al. Syndecan-2-positive, bone marrow-derived human mesenchymal stromal cells attenuate bacterial-induced acute lung injury and enhance resolution of ventilator-induced lung injury in rats. *Anesthesiology.* (2018) 129:502–16. doi: 10.1097/ALN.0000000000002327
28. McBride C, Gaupp D, Phinney DG. Quantifying levels of transplanted murine and human mesenchymal stem cells in vivo by real-time PCR. *Cytotherapy.* (2003) 5:7–18. doi: 10.1080/14653240310000038
29. Miteva K, Van Linthout S, Pappritz K, Muller I, Spillmann F, Haag M, et al. Human endomyocardial biopsy specimen-derived stromal cells modulate angiotensin II-induced cardiac remodeling. *Stem Cells Transl Med.* (2016) 5:1707–18. doi: 10.5966/sctm.2016-0031
30. Lee RH, Pulin AA, Seo MJ, Kota DJ, Ylostalo J, Larson BL, et al. Intravenous hMSCs improve myocardial infarction in mice because cells embolized in lung are activated to secrete the anti-inflammatory protein TSG-6. *Cell Stem Cell.* (2009) 5:54–63. doi: 10.1016/j.stem.2009.05.003
31. Paulus WJ, Tschope C. A novel paradigm for heart failure with preserved ejection fraction: comorbidities drive myocardial dysfunction and remodeling through coronary microvascular endothelial inflammation. *J Am Coll Cardiol.* (2013) 62:263–71. doi: 10.1016/j.jacc.2013.02.092
32. Tschope C, Walther T, Escher F, Spillmann F, Du J, Altmann C, et al. Transgenic activation of the kallikrein-kinin system inhibits intramyocardial inflammation, endothelial dysfunction and oxidative stress in experimental diabetic cardiomyopathy. *FASEB J.* (2005) 19:2057–9. doi: 10.1096/fj.05-4095fje
33. Ren G, Zhang L, Zhao X, Xu G, Zhang Y, Roberts AI, et al. Mesenchymal stem cell-mediated immunosuppression occurs via concerted action of chemokines and nitric oxide. *Cell Stem Cell.* (2008) 2:141–50. doi: 10.1016/j.stem.2007.11.014
34. Ismahil MA, Hamid T, Bansal SS, Patel B, Kingery JR, Prabhu SD. Remodeling of the mononuclear phagocyte network underlies chronic inflammation and disease progression in heart failure: critical importance of the cardiosplenic axis. *Circ Res.* (2014) 114:266–82. doi: 10.1161/CIRCRESAHA.113.301720
35. Pappritz K, Grune J, Klein O, Hegemann N, Dong F, El-Shafeey M, et al. Speckle-tracking echocardiography combined with imaging mass spectrometry assesses region-dependent alterations. *Sci Rep.* (2020) 10:3629. doi: 10.1038/s41598-020-60594-2
36. Camici PG, Tschope C, Di Carli MF, Rimoldi O, Van Linthout S. Coronary microvascular dysfunction in hypertrophy and heart failure. *Cardiovasc Res.* (2020) 116:806–16. doi: 10.1093/cvr/cvaa023
37. Van Linthout S, Rimoldi O, Tschope C, Camici PG. Coronary microvascular dysfunction in heart failure with preserved ejection fraction - adding new pieces to the jigsaw puzzle. *Eur J Heart Fail.* (2020) 22:442–4. doi: 10.1002/ejhf.1720
38. De Rossi G, Evans AR, Kay E, Woodfin A, McKay TR, Nourshargh S, et al. Shed syndecan-2 inhibits angiogenesis. *J Cell Sci.* (2014) 127 (Pt 21):4788–99. doi: 10.1242/jcs.153015
39. Van Linthout S, Miteva K, Tschope C. Crosstalk between fibroblasts and inflammatory cells. *Cardiovasc Res.* (2014) 102:258–69. doi: 10.1093/cvr/cvu062
40. Spillmann F, De Geest B, Muthuramu I, Amin R, Miteva K, Pieske B, et al. Apolipoprotein A-I gene transfer exerts immunomodulatory effects and reduces vascular inflammation and fibrosis in ob/ob mice. *J Inflamm.* (2016) 13:25. doi: 10.1186/s12950-016-0131-6
41. Carey DJ. Syndecans: multifunctional cell-surface co-receptors. *Biochem J.* (1997) 327 (Pt 1):1–16. doi: 10.1042/bj3270001
42. Pappritz K, Savvatis K, Miteva K, Kerim B, Dong F, Fechner H, et al. Immunomodulation by adoptive regulatory T-cell transfer improves Coxsackievirus B3-induced myocarditis. *FASEB J.* (2018) 32:fj201701408R. doi: 10.1096/fj.201701408R
43. Bhansali A, Asokumar P, Walia R, Bhansali S, Gupta V, Jain A, et al. Efficacy and safety of autologous bone marrow-derived stem cell transplantation in patients with type 2 diabetes mellitus: a randomized placebo-controlled study. *Cell Transplant.* (2014) 23:1075–85. doi: 10.3727/096368913X665576
44. Bhansali A, Upreti V, Khandelwal N, Marwaha N, Gupta V, Sachdeva N, et al. Efficacy of autologous bone marrow-derived stem cell transplantation in patients with type 2 diabetes mellitus. *Stem Cells Dev.* (2009) 18:1407–16. doi: 10.1089/scd.2009.0164
45. Estrada EJ, Valacchi F, Nicora E, Brieva S, Esteve C, Echevarria L, et al. Combined treatment of intrapancreatic autologous bone marrow stem cells and hyperbaric oxygen in type 2 diabetes mellitus. *Cell Transplant.* (2008) 17:1295–304. doi: 10.3727/096368908787648119
46. Hao H, Liu J, Shen J, Zhao Y, Liu H, Hou Q, et al. Multiple intravenous infusions of bone marrow mesenchymal stem cells reverse hyperglycemia in experimental type 2 diabetes rats. *Biochem Biophys Res Commun.* (2013) 436:418–23. doi: 10.1016/j.bbrc.2013.05.117
47. Van Linthout S, Spillmann F, Schultheiss HP, Tschope C. Effects of mesenchymal stromal cells on diabetic cardiomyopathy. *Curr Pharm Des.* (2011) 17:3341–7. doi: 10.2174/138161211797904163
48. Cao Y, Xu W, Xiong S. Adoptive transfer of regulatory T cells protects against Coxsackievirus B3-induced cardiac fibrosis. *PLoS ONE.* (2013) 8:e74955. doi: 10.1371/journal.pone.0074955

Conflict of Interest: SE is the Chief Scientific Officer and LO'F is the Head of Process Development at Orbsen Therapeutics Ltd. (Galway, Ireland), a company that is developing the CD362+ MSC for therapeutic purposes.

The remaining authors declare that the research was conducted in the absence of any commercial or financial relationships that could be construed as a potential conflict of interest.

frontiers in Cardiovascular Medicine

ORIGINAL RESEARCH
published: 04 June 2021
doi: 10.3389/fcvm.2021.644797

α-Ketoglutarate Upregulates Collecting Duct (Pro)renin Receptor Expression, Tubular Angiotensin II Formation, and Na^+ Reabsorption During High Glucose Conditions

Aarón Guerrero[1†], Bruna Visniauskas[2†], Pilar Cárdenas[1], Stefanny M. Figueroa[3], Jorge Vivanco[1], Nicolas Salinas-Parra[1], Patricio Araos[3], Quynh My Nguyen[4], Modar Kassan[5], Cristián A. Amador[3], Minolfa C. Prieto[2] and Alexis A. Gonzalez[1]*

[1] Instituto de Química, Pontificia Universidad Católica de Valparaíso, Valparaíso, Chile, [2] Department of Physiology, School of Medicine, Tulane University, New Orleans, LA, United States, [3] Laboratory of Renal Physiopathology, Institute of Biomedical Sciences, Universidad Autónoma de Chile, Santiago, Chile, [4] Skaggs School of Pharmacy and Pharmaceutical Sciences, University of California, San Diego, San Diego, CA, United States, [5] Department of Physiology, College of Medicine, University of Tennessee Health Science Center, Memphis, TN, United States

OPEN ACCESS

Edited by:
Brett M. Mitchell,
Texas A&M Health Science Center,
United States

Reviewed by:
Carmen De Miguel,
University of Alabama at Birmingham,
United States
Dulce Elena Casarini,
Federal University of São Paulo, Brazil

***Correspondence:**
Alexis A. Gonzalez
alexis.gonzalez@pucv.cl

[†] These authors have contributed equally to this work

Specialty section:
This article was submitted to Hypertension, a section of the journal Frontiers in Cardiovascular Medicine

Received: 21 December 2020
Accepted: 13 April 2021
Published: 04 June 2021

Citation:
Guerrero A, Visniauskas B, Cárdenas P, Figueroa SM, Vivanco J, Salinas-Parra N, Araos P, Nguyen QM, Kassan M, Amador CA, Prieto MC and Gonzalez AA (2021) α-Ketoglutarate Upregulates Collecting Duct (Pro)renin Receptor Expression, Tubular Angiotensin II Formation, and Na^+ Reabsorption During High Glucose Conditions. Front. Cardiovasc. Med. 8:644797. doi: 10.3389/fcvm.2021.644797

Diabetes mellitus (DM) causes high glucose (HG) levels in the plasma and urine. The (pro)renin receptor (PRR) is a key regulator of renal Na^+ handling. PRR is expressed in intercalated (IC) cells of the collecting duct (CD) and binds renin to promote angiotensin (Ang) II formation, thereby contributing to Na^+ reabsorption. In DM, the Kreb's cycle is in a state of suppression in most tissues. However, in the CD, expression of glucose transporters is augmented, boosting the Kreb's cycle and consequently causing α-ketoglutarate (αKG) accumulation. The αKG receptor 1 (OXGR1) is a Gq-coupled receptor expressed on the apical membrane of IC cells of the CD. We hypothesize that HG causes αKG secretion and activation of OXGR1, which increases PRR expression in CD cells. This effect then promotes intratubular AngII formation and Na^+ reabsorption. To test this hypothesis, streptozotocin (STZ)-induced diabetic mice were treated with or without montelukast (ML), an OXGR1 antagonist, for 6 days. STZ mice had higher urinary αKG and PRR expression along with augmented urinary AngII levels and Na^+ retention. Treatment with ML prevented all these effects. Similarly, primary cultured inner medullary CD cells treated with HG showed increased PRR expression, while OXGR1 antagonist prevented this effect. αKG increases PRR expression, while treatments with ML, PKC inhibition, or intracellular Ca^{2+} depletion impair this effect. *In silico* analysis suggested that αKG binds to mouse OXGR1. These results indicate that HG conditions promote increased levels of intratubular αKG and OXGR1-dependent PRR upregulation, which impact AngII formation and Na^+ reabsorption.

Keywords: prorenin receptor, diabetes, angiotensin, collecting duct, Kreb's cycle

INTRODUCTION

A hallmark of diabetic disease is the activation of the intrarenal renin–angiotensin system (RAS) (1–3). This system contributes to the development of hypertension by increasing intratubular angiotensin II (AngII)-dependent activation of Na^+ transporters and thereby stimulating tubular renal Na^+ reabsorption (4, 5). In most of the cases, patients with diabetes mellitus (DM) develop hypertension, which further increases their risk of kidney disease (6). Despite the suppressed plasma renin activity (PRA) observed in these patients, treatment with RAS inhibitors slows the progression of hypertension (7). Patients with DM show high plasma prorenin instead of active renin (8–10); indeed, plasma prorenin does not correlate with plasma renin concentrations and might predict microvascular damage (11). Animal models of type I DM showed augmented expression of prorenin in the renal collecting duct (CD) (2) and upregulation of the (pro)renin receptor (PRR) in the kidney (12, 13).

PRR binding to renin or prorenin induces a fourfold increase in the catalytic renin efficiency to convert angiotensinogen (AGT) to AngI and fully activates the non-enzymatically active prorenin (14). This suggests that upregulation of PRR in the CD results in further intratubular AngII formation. Increased expression and secretion of AGT by the proximal tubule cells (15, 16), as well as prorenin (2) and CD PRR (12) in diabetic conditions, further support this idea. Rats fed a high fat diet and given a low dose of streptozotocin (STZ) developed high blood pressure (17). Endothelial dysfunction STZ mice has been reported having mild effect on blood pressure during early phase of diabetes (18).

Diabetic conditions cause suppression of the tricarboxylic acid cycle (or Kreb's cycle) because oxaloacetate, an important component in the cycle, is instead channeled toward gluconeogenesis in the liver. Accumulation of nicotinamide adenine dinucleotide (NADH) also decreases the activity of α-ketoglutarate (αKG) dehydrogenase, leading to αKG accumulation and release (19). STZ-induced type I diabetic rats show increased urinary levels of αKG, citrate, and succinate in urine (19). Interestingly, diabetic rats show increased expression of facilitative glucose transporter GLUT1 in the CD (20). Upregulation of GLUT1 under high glucose (HG) conditions causes accelerated glucose uptake, glycolysis, and Kreb's cycle leading to a higher metabolic rate and accumulation of intermediaries of the Kreb's cycle such as succinate and αKG (21).

The recently deorphanized receptor for α-ketoglutarate (OXGR1) (22, 23) has been shown to increase intracellular Ca^{2+} (24). In mice, OXGR1 is expressed predominantly in kidney CD cells in the apical side of type B and non-A–non-B intercalated cells where it co-localizes with PRR (25). We have shown that PRR is upregulated by the activation of the AngII type 1 receptor (AT1R), a Gq-coupled receptor (26). As such, it is likely that the increased levels of plasma and urinary α-ketoglutarate described under HG conditions might reach the CD at physiological concentrations high enough to activate OXGR1, therefore stimulating signaling pathways to induce the expression of PRR.

In this study, we propose that in the early phase of STZ-induced diabetic hyperglycemia, αKG is augmented in the urine, activating ORXG1 receptor and consequently leading to the upregulation of PRR. This ultimately contributes to intratubular generation of AngII impacting on Na^+ handling.

MATERIALS AND METHODS

Experimental Animals and Sample Collections

All methods were performed in accordance with the Tulane Institutional Animal Care and the Bioethical Committee of the Pontificia Universidad Católica de Valparaiso, under international guidelines and regulations for animal use. Twelve-week-old male C57BL/6 mice were placed under the following conditions: light–dark cycle (12 h), temperature of 21°C, humidity of 50%, adequate ventilation, noise free, and food and water *ad libitum*. Mice were divided randomly into four groups: control (saline injection, normoglycemic mice, $n = 9$), streptozotocin-induced diabetic mice (200 mg/kg, single i.p. injection, $n = 9$), mice treated with OXGR1 antagonist montelukast (ML) (27) (5 mg/kg/day, i.p. and 4 h previous to STZ, $n = 9$), and STZ + ML ($n = 9$). STZ was injected after a 6-h fasting. Six hours was determined to be appropriate because a more prolonged fast may be inappropriate in mice, as it induces metabolic stress and enhances insulin action (28). Mice were considered diabetic if three consecutive blood glucose readings exceeded 250 mg/dl. Blood glucose was directly (not diluted) measured using ONETOUCH Ultra glucometer (LifeScan, catalog no. ZJZ8158JT, Milpitas, CA; reported result ranged 20–600 mg/dl) and also compared with regular glucometer Prodigy© (https://www.prodigymeter.com/) demonstrating no differences in plasma glucose measurements. Renal tissue samples were analyzed after 6 days. Plasma and 24-h urine samples were collected from metabolic cages on day 6. A saline challenge was performed on day 5 to evaluate the effect of STZ or STZ plus OXGR1 antagonism on Na^+ balance. Mice were injected i.p. with a volume of warmed isotonic saline equivalent to 10% of their body weight and placed immediately afterward in metabolic cages for urine collection. Results are expressed as the percentage of the injected sodium excreted over 5 h. On day 6, the animals were euthanized, and blood and kidneys were harvested. Urine samples from nine animals were collected into tubes containing an inhibitor cocktail [5 mmol/L of ethylenediaminetetraacetic acid (EDTA), 20 μmol/L of pepstatin A, 10 μmol/L of phenylmethylsulfonyl fluoride (PMSF), 20 μmol/L of enalaprilat, and 1.25 mmol/L of 1,10-phenanthroline]. After centrifugation at 4°C for 10 min at 1,000 *g*, urine was separated and applied to phenyl-bonded solid-phase extraction columns that had been prewashed with methanol followed by water. After sample application, angiotensin peptides were eluted from the solid-phase extraction column with 90% methanol. The eluates were collected, evaporated to dryness under vacuum, and stored at −20°C until radioimmunoassay was performed (29, 30). Angiotensin II was measured by using EIA Kit, Cayman, catalog no. A05880. The results are expressed in

fmol/h. The α KG in urine samples and cell culture media was measured by Abcam α-ketoglutarate Assay Kit ab83431 (Abcam, Cambridge, UK). Creatinine was measured using Creatinine Analyzer 2 (Beckman Coulter, Inc., Fullerton, CA). Calphostin C and thapsigargin (Sigma-Aldrich) were used at 10 and 1 nM, respectively.

Systolic Blood Pressure Measurements

Animals were trained daily for 4 days to become accustomed to the tail-cuff procedure using photoplethysmography. Eight to 12 consecutive pulse readings were recorded for each mouse in each measurement at day 0, 3, and 6 of treatment. All data were recorded using BP-2000 series II Blood Pressure Analysis System (Visitech System Inc.) before daily Montelukast injection as previously described above.

Primary Cultures of Mouse IMCD Cells

In a different group of mice, after kidney excision, inner medullary tissues were digested in 10 ml of Dulbecco's modified Eagle's medium (DMEM)–Ham F-12, 20 mg of collagenase B, 7 mg of hyaluronidase, 80 mmol/L of urea, and 130 mmol/L of NaCl and incubated at 37°C under continuous agitation for 90 min. After centrifugation, the pellet was washed in prewarmed culture medium without enzymes [DMEM–Ham F-12, 80 mmol/L of urea, 130 mmol/L of NaCl, 10 mmol/L of HEPES, 2 mmol/L of L-glutamine, penicillin-streptomycin (10,000 U/ml), 50 nmol/L of hydrocortisone, 5 pM 3,3,5-triiodothyronine, 1 nmol/L of sodium selenate, and 5 mg/L of transferrin, without fetal bovine serum (FBS) (pH 7.4; 640 mosmol/kg of H_2O)]. The resulting inner medullary collecting duct (IMCD) cell suspension was seeded in 3-mm Petri dishes. IMCD were divided and treated with normal glucose (5 mM D-glucose, NG), HG (25 mM), and mannitol (25 mM) during 24 h. No effects on PRR or GLUT1 expression levels were observed in mannitol-treated group (data not shown). We continued to explore the effect of NG or HG in the following experiments. Two hours before changing to HG conditions, the IMCD cells were pretreated with and without ML (10^{-7} M; Sigma Chemical Co.), which was dissolved in dimethyl sulfoxide (DMSO) and diluted to the final concentrations with phosphate-buffered saline (31). Experiments of αKG measurements in supernatant were assessed after 24 h incubation in NG or HG and measured by Abcam α-ketoglutarate Assay Kit ab83431 (Abcam, Cambridge, UK). A single dose of 0.2 mM of αKG was used for the acute experiments in IMCD cells (32).

PRR and GLUT1 Transcripts Quantitation by Real-Time qRT-PCR

Total messenger RNA (mRNA) was isolated from mouse renal medullas or IMCD cells using RNeasy Mini Kit (Qiagen, Valencia, CA) according to the manufacturer's protocol. Total RNA was quantified using NanoDrop system. Quantitative real-time RT-PCR (qRT-PCR) was performed using the following primers: GLUT1, 5′-CAG CTG TCG GGT ATC AAT GC-3′, 3′-TCC AGC TCG CTC TAC AAC AA-5′; PRR, 5′-CAC AAG GGA TGT GTC GAA TG-3′, 3′-TTT GGA TGA ACT TGG GAA GC-5′; β-actin, 5′-ATC ATG AAG TGT GAC GTT GA-3′, 3′-GAT CTT CAT GGT GCT AGG AGC-5′. Results were presented as the fold change ratio between the levels of mRNA of the interest gene against β-actin ("housekeeping" gene) compared to control group ($n = 6$). Primers were obtained from IDT Company (https://www.idtdna.com).

Immunoblotting Analyses

Forty micrograms of protein samples was electrophoretically separated on a precast NuPAGE 10% Bis-Tris gel (Novex) at 200 V for 45 min followed by semi-dry transference to a nitrocellulose membrane (Invitrogen) using iBlot (Invitrogen, Carlsbad, CA, USA). Blots were blocked at room temperature (RT) for 3 h, incubated overnight with specific primary antibody at 4°C, subsequently incubated with the corresponding secondary antibodies (1:5,000 dilutions), at RT for 45 min, and then analyzed by normalization against β-actin, which was used as a housekeeping gene. PRR protein levels were detected using a polyclonal rabbit anti-PRR (*ATP6AP2*, 1:200; Cat. no. HPA003156, Sigma-Aldrich) that recognizes the intracellular segment and the ectodomain (33). GLUT1 was detected using rabbit anti-GLUT1 (1:200; Cat. no. SAB4200519, Sigma-Aldrich). For characterization of IMCD, we used anti- aquaporin (AQP)-2 antibody at 1:400 dilutions (Cat. no. 178612 Calbiochem, San Diego, CA) and NKCC cotransporter 1:500 dilutions (Cat. no. 51791, Abcam, UK). Immunoblots are presented in each figure as representative images. Results are presented as the ratio of PRR or GLUT1 vs. β-actin as fold change of control. Tissue analysis was performed by using six animals per group and three to five independent experiments for Western blot analysis.

Immunofluorescence in Kidney Tissues and Primary Cultures of IMCD Cells

Three-micrometer kidney slides were fixed and stained with anti-PRR at 1:200 dilutions (ATP6AP2, Cat. no. HPA003156, Sigma-Aldrich, MO, USA), anti-GLUT1 1:100 dilutions (Cat. no. SAB4200519, Sigma-Aldrich), and anti-OXGR-1 1:100 dilutions (Cat. no. PA5-67872, Invitrogen, CA). For cultured cell immunofluorescence, 50–60% subconfluent IMCD cells cultured in chamber slides (Nalge Nunc) were fixed in cold methanol for 20 min, blocked with PBS-Tween (0.1%) plus bovine serum albumin (BSA) (3%) for 1 h, stained with the following antibodies: anti-aquaporin-2, AQP-2 (Cat. no. 178612, Calbiochem, San Diego, CA), anti-PRR (ATP6AP2, 1:100 dilutions; Cat. no. HPA003156, Sigma-Aldrich, MO, USA), anti-anion exchanger type 1, AE1 (Cat. no. AE11-A, Alpha Diagnostic Intl, San Antonio, TX), and anti-OXGR-1, 1:100 dilutions (Cat. no. PA5-67872, Invitrogen, CA) and detected with Alexa Fluor 488 or 594 conjugated to antirabbit immunoglobulin G (IgG) (Invitrogen, Life Science, Co.). The slides were mounted with ProLong® Gold with 4,6-diamidino-2-phenylindole dihydrochloride (DAPI) for nuclei staining. The images were obtained using a Nikon Eclipse-50i immunofluorescence microscope (Nikon Eclipse-50i, Japan) and were digitalized using the NIS-Elements BR version 4.0 from

Nikon). Negative controls were obtained by omission of the specific primary antibody.

In vitro Ca^{2+} Measurements

Cell suspensions (8×10^5 cells/ml) were loaded with Fura-2 AM (5 μM) and incubated for 30 min at room temperature and protected from light and 37°C. Then, cells were washed with 1× PBS and suspended. A volume of 500 μl was added in a quartz cell to measure fluorescence in Fluoromax-2 spectrofluorometer (Instruments SA, Edison, NJ). The $[Ca^{2+}]$ was calculated as: $[Ca^{2+}]i\ (nM) = Kd \times [(R - R_{min})/R_{max} - R)] \times Sfb$, where Kd (for Ca^{2+} binding to Fura-2 at 37°C) = 225 nM, R = 340/380 ratio, R_{max} = 340/380 ratio under Ca^{2+}-saturating conditions, R_{min} = 340/380 ratio under Ca^{2+}-free conditions, and Sfb = ratio of baseline fluorescence (380 nm) under Ca^{2+}-free and Ca^{2+}-bound conditions.

In silico Analysis of the Interaction of αKG and Mouse OXGR1

In silico analysis was performed to evaluate the interaction of αKG and mouse OXGR1 (GPR99) using the free-online servers I-TASSER, ProSA-Web, and MolProbidity (Duke University) for structure modeling, since there is no available structure for mouse GPR99. Docking model (αKG and mouse OXGR1 interaction) was performed using free-online software Swiss-Dock. Multiple sequence alignment of GPR99 and GPR91 was performed using software Clustal Omega (https://www.ebi.ac.uk/Tools/msa/clustalo).

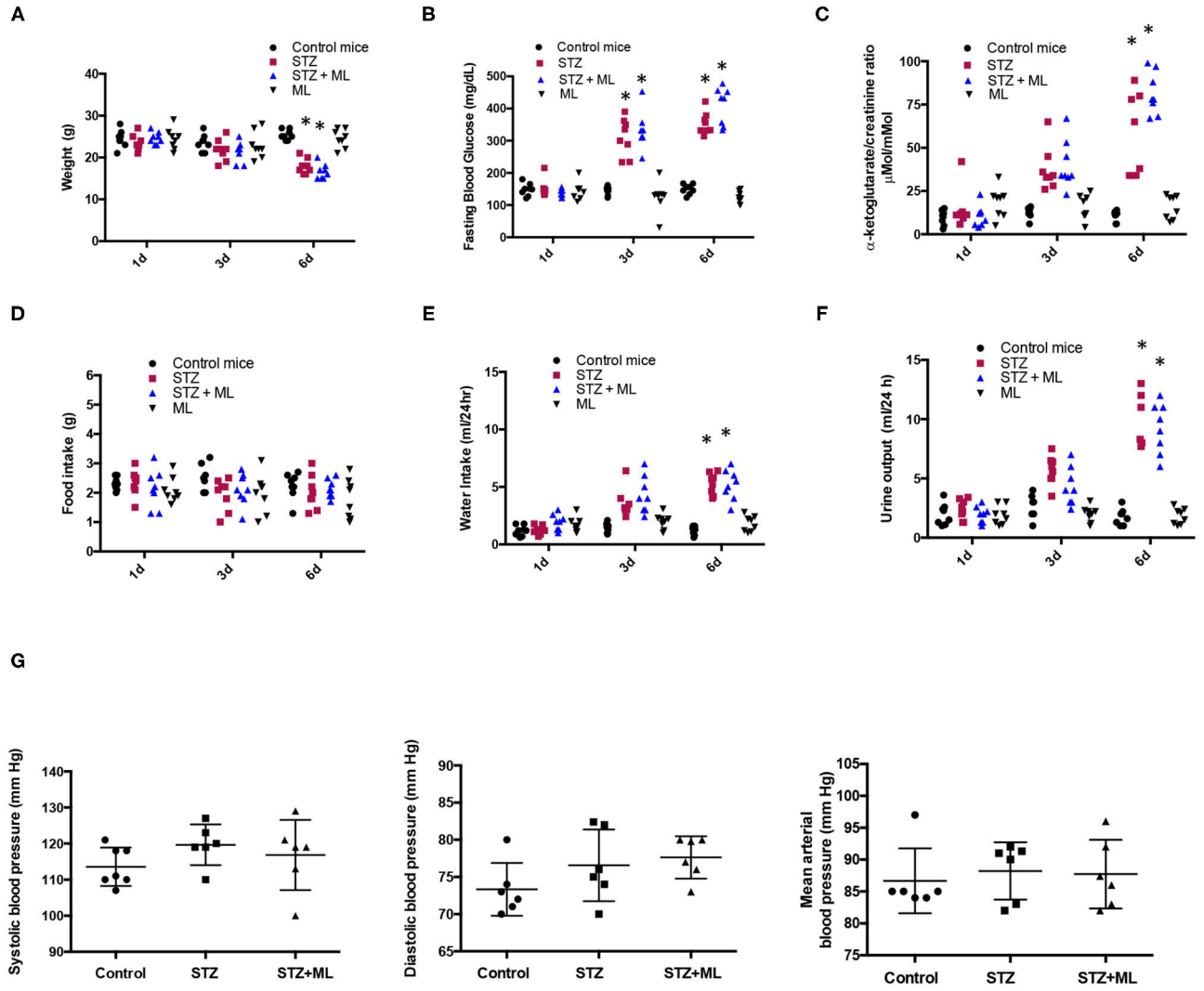

FIGURE 1 | Physiological parameters in control mice and streptozotocin-induced diabetic mice with or without treatment with montelukast (ML), an OXGR1 antagonist. **(A)** Body weight was reduced after 6 days of streptozotocin (STZ) treatment. **(B)** Fasting glucose levels were augmented on days 3 and 6 in STZ and STZ + ML mice. **(C)** After 6 days, a significant increase in urinary levels of αKG (assessed by αKG/creatinine ratio) was detected in STZ and STZ + ML mice. **(D)** A slight but not significant reduction was observed in food intake. **(E)** Water intake was augmented in STZ and STZ + ML groups. **(F)** Urine output was also augmented in STZ and STZ + ML group. **(G)** Systolic, diastolic, and mean arterial blood pressure was not changed at the end of the treatment. *$p < 0.05$ vs. control group (n = 7–9).

Statistical Analyses

Results are expressed as mean ± SEM. Grubb's test was used to detect outliers in univariate data assumed to have come from a normally distributed population. Comparisons between groups were performed using one-way ANOVA and Tukey's posttest. $p \leq 0.05$ values were considered statistically significant.

RESULTS

STZ-Induced Hyperglycemia Is Associated With Increased Urinary α-Ketoglutarate

As shown in **Figure 1A**, STZ mice have reduced body weight at day 6 (17.8 ± 0.8 vs. control mice, 23.3 ± 0.4 g, $p < 0.05$). Mice treated with the OXGR1 antagonist ML also showed a significant reduction in body weight (16.2 ± 0.6 g, $p < 0.05$ vs. control mice). Reduction in body weight was also confirmed and standardized by measuring body weight vs. tibia–length ratio. The data showed a less evident loss in body weight in STZ mice (STZ, 1.153 ± 0.017 vs. control, 1.333 ± 0.045, $p < 0.05$) and in STZ + ML group (STZ + ML, 1.193 ± 0.042 vs. control, 1.333 ± 0.045, $p = 0.23$). Mice treated only with ML did not show changes in body weight (24.5 ± 0.7 g, $p = 0.23$ vs. control mice). Fasting blood glucose levels were significantly higher on day 6 in STZ-induced hyperglycemic mice (354 ± 12 mg/dl, $p < 0.05$ vs. controls) and STZ + ML mice (410 ± 20 mg/dl, $p < 0.01$ vs. controls) compared to controls (149 ± 5 mg/dl). Fasting blood glucose was not altered in mice treated with ML when compared to normoglycemic control mice (**Figure 1B**). Urinary levels of αKG assessed by αKG/creatinine ratio were significantly augmented in STZ and STZ + ML groups on day 6 as compared to controls (**Figure 1C**). No differences in plasma creatinine (controls, 0.45 ± 0.11; STZ, 0.53 ± 0.13; STZ + ML, 0.47 ± 0.05 mg/dl, $p = 0.40$) or blood urea nitrogen (controls, 12.5 ± 2.8; STZ, 20.1 ± 4.6; STZ + ML, 19.1 ± 5.7 mg/dl, $p = 0.33$) were found among the groups. Urine protein/creatinine ratio was not different among groups (controls, 2.2 ± 0.3; STZ, 4.7 ± 3.3; STZ + ML, 2.2 ± 1.3 mg/dl, $p = 0.21$). No effects were observed in ML group.

Since STZ animals had reduced body weight, we evaluated food intake in 24 h metabolic cages measurements. No differences were found in food intake on days 1, 3, and 6 between controls, STZ, and STZ plus ML (**Figure 1D**). As shown in **Figure 1E**, water intake was significantly greater in diabetic mice (STZ alone and STZ + ML treatment) compared to control mice on day 6. No effect was observed in the ML group. Of note, diuresis was significantly higher in STZ mice and STZ + ML group (**Figure 1F**) showing a negative 24-h water intake vs. urine output balance at day 6. The treatment with ML alone did not affect urinary volume. Finally, a new set of experiments was performed to measure systolic and diastolic blood pressure. We observed

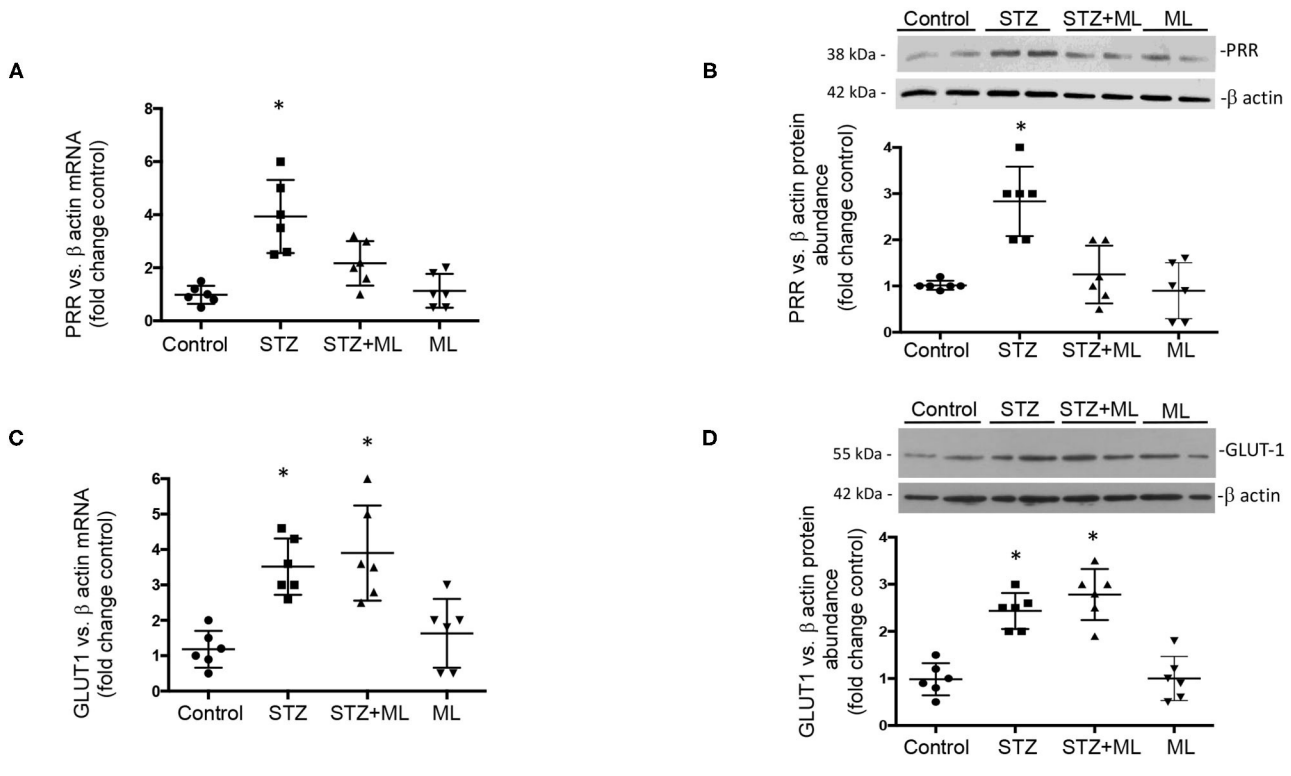

FIGURE 2 | (A) After 6 days of a single streptozotocin (STZ) administration, (pro)renin receptor (PRR) messenger RNA (mRNA) levels were augmented in the renal medulla of STZ mice. **(B)** Same effect was observed in PRR protein abundance. Treatment with OXGR antagonist montelukast (ML) in STZ mice prevented the upregulation of PRR mRNA and protein. **(C)** GLUT1 mRNA and **(D)** protein levels were increased in the renal medulla of STZ mice, as well as in STZ and STZ + ML groups. ML alone did not show significant changes on PRR or GLUT expression. *$p < 0.05$ vs. control group ($n = 6$).

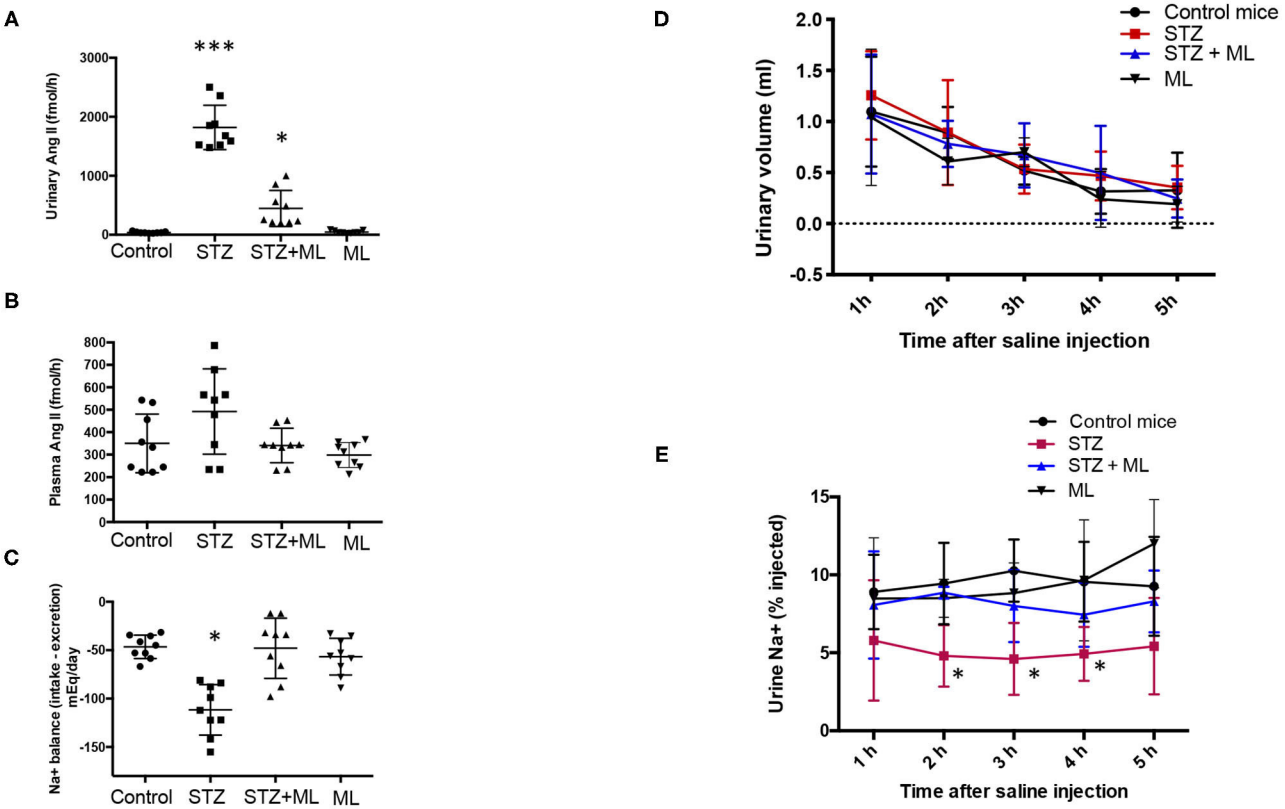

FIGURE 3 | Streptozotocin (STZ) mice showed augmented urinary AngII excretion and Na^+ retention that was prevented by OXGR1 pharmacological blockade. **(A)** AngII was significantly augmented in STZ mice ($p < 0.001$ vs. control group). Although mice treated with the OXGR1 antagonist montelukast (ML) also showed significant increases in AngII levels, this effect was less evident ($p < 0.05$). Treatment with ML alone in normoglycemic mice did not significantly change AngII excretion. **(B)** No changes were observed in plasma AngII. **(C)** Na^+ balance assessed on day 6 demonstrated that STZ mice retained Na^+. ML treatment in STZ mice blunted this effect. Saline challenge was performed to determine the percentage of injected Na^+ that would be excreted. **(D)** Urine samples collected every hour showed a continuous decrease in total volume with no significant differences between controls and STZ or STZ + ML treated mice. **(E)** Na^+ concentration of these samples was measured in order to calculate the percentage of Na^+ excreted after saline (0.9% NaCl) injection. STZ mice showed a reduced percentage of injected Na^+ in urine samples, demonstrating increased Na^+ retention. This effect was less evident in STZ + ML group. Significant values were observed only at 2, 3, and 4 h as compared to controls. $^*p < 0.05$ vs. control group, $^{***}p < 0.001$ vs. control group, $n = 9$.

a slight but not statistically significant ($p = 0.081$) increase in systolic blood pressure in STZ mice (**Figure 1G**).

Increased mRNA and Protein Levels of PRR in Renal Medullary Tissues of STZ Mice Are Blunted by OXGR1 Antagonism

After 6 days of single STZ administration, PRR mRNA levels were augmented in STZ mice (3.7 ± 0.6 vs. control 1.0 ± 0.1, $p < 0.05$), while ML prevented the increase in PRR transcript levels (1.7 ± 0.4, $p = 0.08$ vs. controls, **Figure 2A**). The same effect was observed in PRR protein abundance (STZ, 3.8 ± 0.5 vs. controls, 1.0 ± 0.2, $p < 0.05$). Treatment with OXGR antagonist ML in STZ mice prevented the upregulation of PRR protein (1.7 ± 0.4, $p = 0.32$ vs. controls, **Figure 2B**). We next evaluated the expression of GLUT1 in STZ-induced HG conditions in the renal medulla and the effect of OXGR1 antagonist ML. Both treatments STZ and STZ + ML caused an increase in the mRNA (3.5 ± 0.5 vs. 1.1 ± 0.2, $p < 0.05$) and protein levels (2.4 ± 0.2 vs. 1.0 ± 0.1, $p < 0.05$) of GLUT1. ML alone did not show significant changes on GLUT1 abundance (**Figures 2C,D**).

Augmentation of Urinary AngII and Decreased Na^+ Excretion Was Attenuated by OXGR1 Antagonism in STZ Mice

Because downregulation of PRR expression in the collecting ducts may decrease intratubular AngII formation, we evaluated urinary AngII excretion. AngII levels were greatly augmented in STZ mice (STZ, 1890 ± 178 fmol/h vs. controls, 40 ± 7 fmol/h, $p < 0.05$). This augmentation effect was not seen in mice that received ML treatment (560 ± 130 fmol/h, $p < 0.05$ vs. STZ group). Treatment with ML alone in normoglycemic mice did not show significant changes in AngII excretion (**Figure 3A**). Because intratubular AngII formation may impact on intratubular Na^+ handling, we evaluate the balance between Na^+ intake and excretion on day 6. STZ causes Na^+ retention, while ML prevented this effect (**Figure 3B**). We next performed a

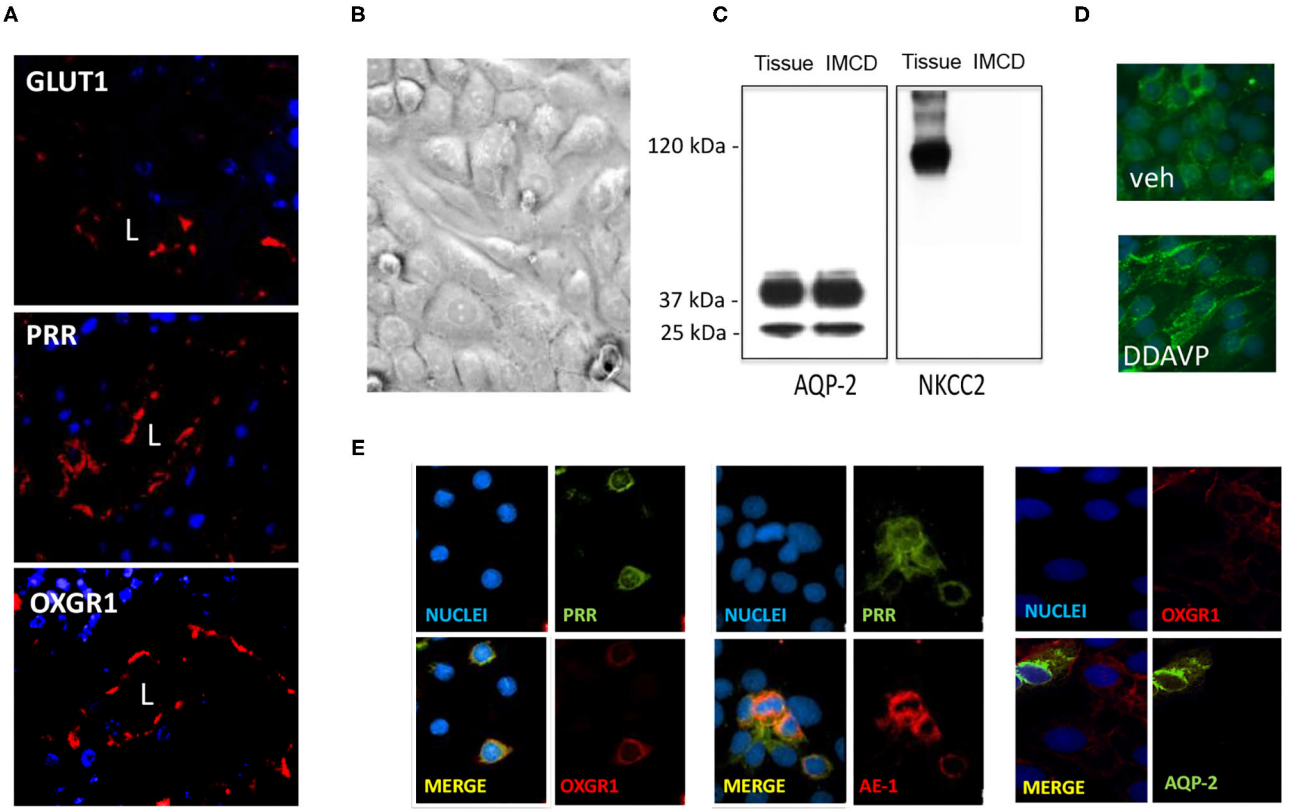

FIGURE 4 | (A) Staining of whole kidney sections showed the presence of GLUT1, (pro)renin receptor (PRR), and OXGR1 (red staining). L indicates lumen. Nuclei are stained with 4,6-diamidino-2-phenylindole dihydrochloride (DAPI). **(B)** Inner medullary collecting duct (IMCD) cells were grown until reach confluence and assessed for the presence of NKCC to rule out the presence of cortical tissues cells. Western blot analysis showed the presence of aquaporin (AQP)-2 in homogenates of total kidney tissue and IMCD cells. **(C)** NKCC was absent in IMCD. Functional IMCD cells were assessed by the activation of the vasopressin V2 with a V2 receptor agonist (DDAVP, 10^{-8} M). **(D)** After 45 min, AQP-2 immunofluorescence was mostly detected in plasma membrane. Coimmunostaining demonstrated the coexistence of OXGR1 and PRR, which also co-localizes with AE-1, a marker of intercalated cell. **(E)** OXGR1 did not co-localizes with AQP-2, a marker of principal cell.

saline challenge to determine the percentage of injected Na^+ that could be excreted by normoglycemic mice, STZ mice, and mice subjected to STZ plus ML treatment. As shown in **Figure 3C**, urine samples collected every hour showed a progressive decrease in total volume. Na^+ concentration of these samples was measured to calculate the percentage of Na^+ excreted after saline (0.9% NaCl) injection. As shown in **Figure 3D**, STZ mice had lower percentages of injected Na^+ in their urine, suggesting increased Na^+ retention. This effect was less evident in STZ + ML group. Significant values were observed only at 2 and 3 h as compared to controls.

OXGR1 Co-localizes With PRR in Inner Medullary Collecting Duct Cells

GLUT1, PRR, and OXGR1 were detected in inner medullary tissues (**Figure 4A**). IMCD cells were grown until confluence (**Figure 4B**) and assessed for the presence of sodium potassium 2-chloride transporter, NKCC, to rule out the presence of cortical tissues cells. Western blot analysis showed the presence of AQP-2 in homogenates of total kidney tissue and IMCD cells. NKCC was absent in IMCD (**Figure 4C**). To further evaluate the functional responses of IMCD cells to the activation of the vasopressin V2 receptor treatment, IMCD cells were treated with desmopressin (DDAVP, 10^{-8} M). After 45 min AQP-2 immunofluorescence was mostly detected in plasma membrane (**Figure 4D**). Coimmunostaining demonstrated the coexistence of PRR and OXGR1 and PRR, which also co-localizes with AE-1, a marker of intercalated cell. As observed in **Figure 4E**, 35–40% of the total cells in each microscopic correspond to intercalated cells as described by Kim et al. (34), which explains why PRR and OXGR1 are present only in few cells in the microscopic culture's fields. OXGR1 did not co-localizes with AQP-2, a marker of principal cell (**Figure 4E**).

Treatment With αKG Increases Intracellular Ca^{2+} During Normal Glucose Conditions and HG Promotes αKG Accumulation in Cell Culture Media From Inner Medullary Collecting Duct Cells

Because OXGR1 is a Gq-coupled receptor that stimulates intracellular Ca^{2+} release, we evaluated the responses of cultures

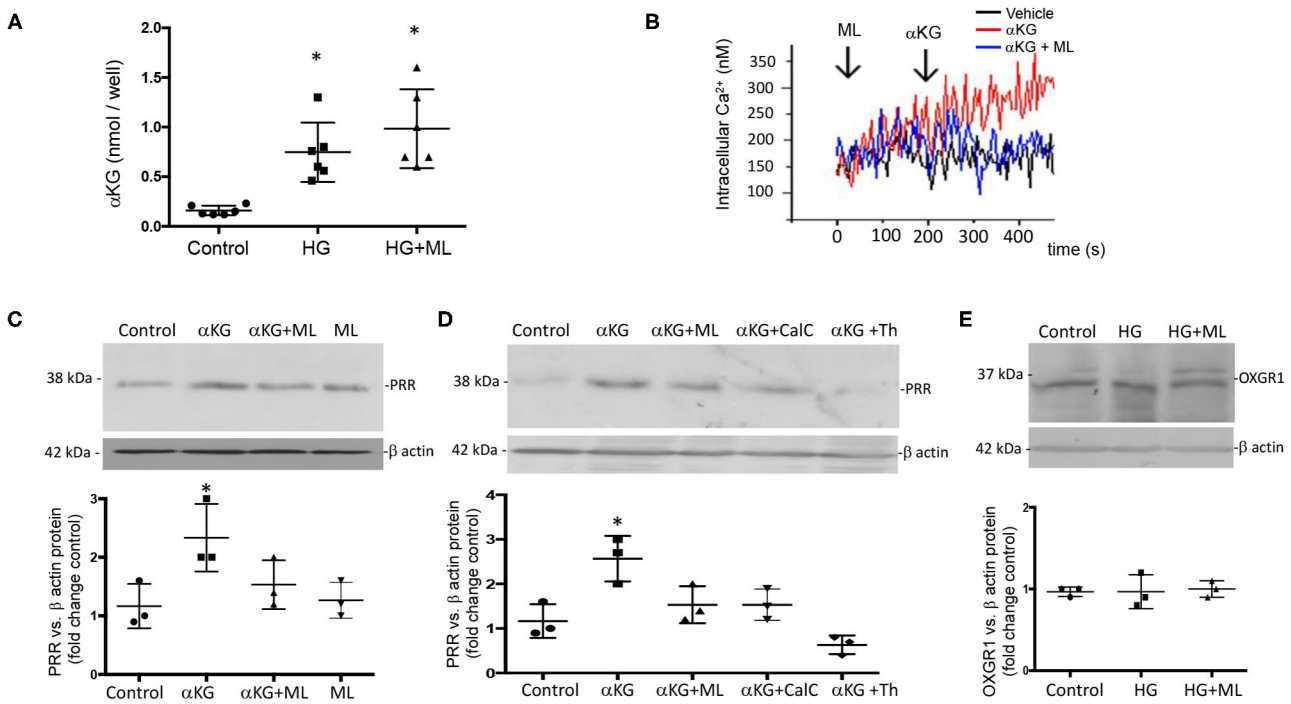

FIGURE 5 | Evidence of the effect of αKG on (pro)renin receptor (PRR) expression and intracellular signaling pathways. **(A)** Incubations with HG during 24 h increased in αKG accumulation in inner medullary collecting duct (IMCD) cell culture media. HG + ML did not cause αKG accumulation (*$p < 0.05$ vs. control group, $n = 5$). **(B)** Functional assessment of cultured IMCD cells demonstrated that αKG induced a rise in intracellular Ca^{2+} that was blunted by OXGR1 antagonist montelukast (ML). This suggest that the mechanism involves the activation of OXGR1. **(C)** IMCD incubated with αKG 0.2 mM for 16 h showed increased levels of PRR; this effect was blunted by ML. **(D)** Increased PRR levels was suppressed by PKC inhibitor calphostin C (10 nM) or intracellular Ca^{2+} depletion using thapsigargin (1 μM). **(E)** OXGR1 expression did not change in HG conditions. For Panels **(C–E)**; *$p < 0.05$ vs. control group, $n = 3$.

from IMCD cells to αKG treatment (10^{-7} M) on intracellular Ca^{2+} concentrations by using IMCD cells preloaded with Fura-2 AM (see *Methods* for details). As shown in **Figure 5A**, αKG treatment at 180 s causes an increase in intracellular Ca^{2+} concentrations from ∼150 to ∼300 nM at 400 s. IMCD cells previously treated with ML did not show increased intracellular Ca^{2+}. No effects were seen in the presence of ML alone (data not shown). Then, we evaluated the effect of 24-h incubations under HG conditions on αKG levels in cell culture media. **Figure 5B** shows that αKG secretion is increased in the HG group (0.82 ± 0.35 nmol/well vs. control 0.22 ± 0.02 nmol/well, $p < 0.05$), as well as in HG + ML group (1.23 ± 0.42 nmol/well vs. control 0.22 ± 0.02 nmol/well, $p < 0.05$). ML alone has no effect on αKG levels. We next evaluated the effect of αKG treatment on PRR expression after 24 h. As shown in **Figure 5C**, αKG increased PRR protein abundance (2.6 ± 0.2 vs. 1.1 ± 0.2, $p < 0.05$), while pretreatment with ML blunted this effect (1.6 ± 0.2, $p = 0.23$ vs. control). OXGR1 activates PKC signaling pathways (35). We block the activity of PKC by using 10 nM of calphostin C, 30 min before αKG treatment. As shown in **Figure 5D**, Calphostin C prevented the increase in PRR (1.5 ± 0.2, $p = 0.13$ vs. control). Since IMCD cells express mostly calcium-dependent PKC, we use thapsigargin (1 μM), a non-competitive inhibitor of the sarco-endoplasmic reticulum Ca-ATPase (SERCA) to deplete cytoplasmatic Ca^{2+}. As shown in **Figure 5D**, previous treatment with thapsigargin blocked the induction of PRR mediated by αKG (0.6 ± 0.1, $p = 0.21$ vs. control).

In silico Studies Suggested Binding of αKG to Mouse OXGR1

OXGR1 (GPR99) is a seven-transmembrane receptor. Due to the absence of a three-dimensional structure for mice, we used online server Phyre2, I-TASSER, and ProSA-Web and MolProbidity (**Figure 6A**). The model was used for docking studies of αKG to OXGR1 using the server Swiss-Dock (**Figure 6B**). As observed in the dotted line in **Figure 6B**, there are several binding sites located mainly at the extracellular side of the receptor. It should be mentioned that docking was performed using a rigid form of the receptor, which does not usually happen in nature. **Figure 6C** highlights the presence of a large pocket inside the OXGR1 (blue color) in which ARG110, HIS114, ARG228, and ARG261 are the most important residues interacting with αKG. OXGR1 shares a high identity with the P2Y receptor family, which can be activated by AMP and adenosine (36), as well as by αKG (22). By making a multiple alignment analysis with rat, mice, and human GPR99 (OXGR1) and GPR91 as shown in **Figure 6D**, the residues R99, H103, R252, and R281 of GPR91 are the same residues present in the hydrophobic pocket of OXGR1 (as seen in the magnification of the image in **Figure 6C**).

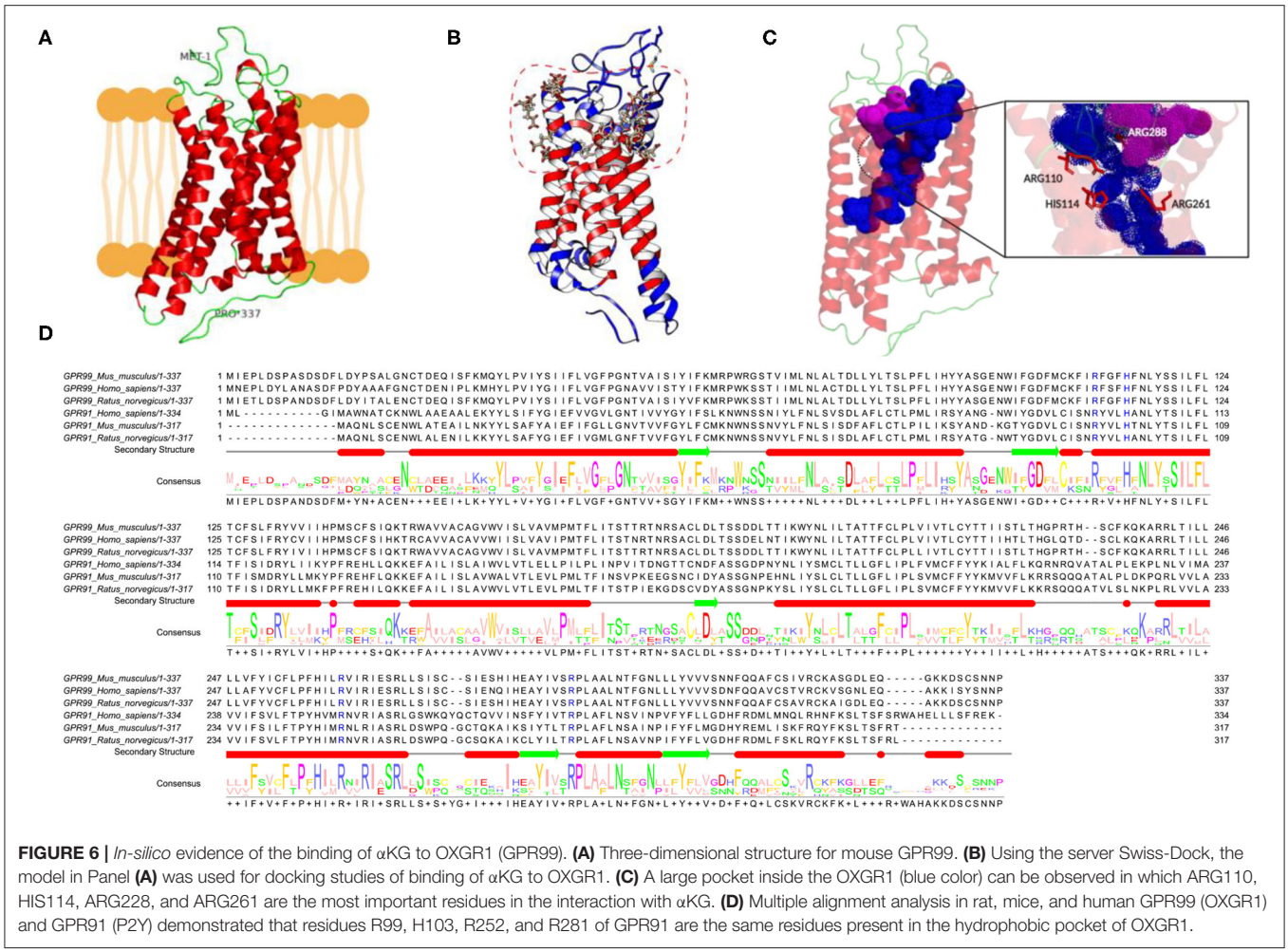

FIGURE 6 | *In-silico* evidence of the binding of αKG to OXGR1 (GPR99). **(A)** Three-dimensional structure for mouse GPR99. **(B)** Using the server Swiss-Dock, the model in Panel **(A)** was used for docking studies of binding of αKG to OXGR1. **(C)** A large pocket inside the OXGR1 (blue color) can be observed in which ARG110, HIS114, ARG228, and ARG261 are the most important residues in the interaction with αKG. **(D)** Multiple alignment analysis in rat, mice, and human GPR99 (OXGR1) and GPR91 (P2Y) demonstrated that residues R99, H103, R252, and R281 of GPR91 are the same residues present in the hydrophobic pocket of OXGR1.

OXGR1 Antagonism Suppressed HG-Dependent Induction of PRR in Inner Medullary Collecting Duct Cells

Finally, we evaluate the effect of HG conditions (25 mM) on GLUT1 and PRR expression in cultured IMCD cells subjected to OXGR1 pharmacological blockade. As shown in **Figures 7A,B**, PRR mRNA and protein levels were augmented by 24-h HG treatment (4.8 ± 0.9 vs. control 1.0 ± 0.1, $p < 0.05$), while pretreatment with 10^{-7} M of ML blunted the induction of PRR expression (1.2 ± 0.2, $p = 0.08$ vs. control). IMCD cells showed an increase in GLUT1 mRNA and protein (**Figures 7C,D**) levels under HG conditions (3.5 ± 0.5 vs. control 1.0 ± 0.2, $p < 0.05$). This phenomenon was not altered by the pretreatment with ML (3.6 ± 0.5, $p < 0.05$ vs. control). ML alone has no effect on GLUT1 or PRR expression as compared to controls.

DISCUSSION

We demonstrated that mice with 6 days of STZ-induced hyperglycemia exhibit augmentation of αKG in urine along with increased expression of PRR in medullary collecting ducts and augmented urinary AngII levels and Na^+ retention. We also showed that pharmacological blockade of the αKG receptor, OXGR1, with ML *in vivo* and *in vitro* prevented the upregulation of PRR in medullary collecting duct cells observed during HG conditions. Moreover, blunted upregulation of PRR by ML was accompanied by attenuated increases in urinary excretion of AngII and increased natriuresis. These effects were independent of changes in blood pressure.

In the present study, we have used a model of early diabetic conditions to trigger with no gross kidney damage. Six days of hyperglycemia was chosen because longer periods implicate nephropathy and further damage (e.g., including collagen deposition in glomerular, tubulointerstitial, and perivascular areas) in rat (37) and mice kidneys after 3 and 5 weeks post-STZ injection, respectively (38). Furthermore, it is possible that ML treatment in STZ-induced diabetic mice for a longer period of time would result in further protection against PRR augmentation and PRR-related signaling pathways related to fibrosis; however, longer treatments (>6 days of single STZ dose) showed structural evidence of acute tubular necrosis in mice (39). We performed 24-h incubations with HG in primary cultures of IMCD cells because it has been reported that longer periods of

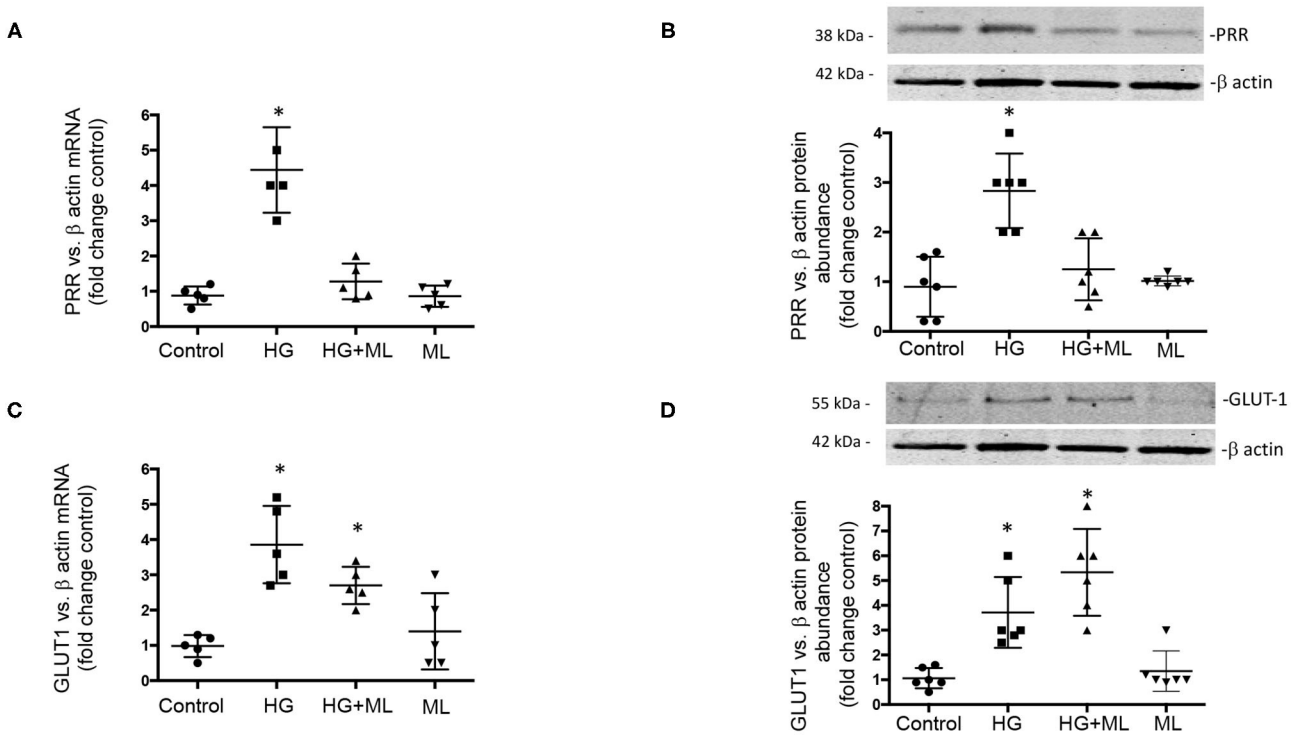

FIGURE 7 | Effect of high glucose (HG) conditions (25 mM) on GLUT1 and (pro)renin receptor (PRR) expression in cultured inner medullary collecting duct (IMCD) cells subjected or not to OXGR1 pharmacological blockade. **(A)** PRR messenger RNA (mRNA) and **(B)** protein levels were augmented by 24-h HG treatment while pretreatment with 10^{-7} M of montelukast (ML) blunted the induction of PRR expression. Augmentation of GLUT1 at **(C)** mRNA and **(D)** protein levels was not altered by the pretreatment with ML. *$p < 0.05$ vs. control group, $n = 5$. Reblotting of blot **(B)** is shown in Panel **(D)**, and same representative β-actin loading control was used.

incubation with HG significantly decreases the number of viable cells in cultured kidney cells (40). Additionally, our model of primary cultures of IMCD cells allows for experiments lasting up to 5 days. Beyond this time point, cells reach confluence and impair further treatment. Despite this, OXGR1 expression was not altered under HG conditions. However, prolonged exposure to high levels of αKG or HG *in vivo* may promote complex pathways that include receptor internalization and tissue damage.

PRR is a multifunctional protein (41) that is part of the multisubunit complex, vacuolar H^+-ATPase, which plays a key role in intracellular acidification (42, 43), autophagy (44), and kidney development (45). PRR increases renin activity and fully activates prorenin (33, 46). Increased renin activity under pathological conditions has been further supported by *in vivo* data from different models of experimental hypertension demonstrating that PRR in the CD is required for the local formation of AngII (47, 48). Furthermore, Kang et al. demonstrated that CD is the main source of prorenin in STZ diabetic mice (2). More recent evidence has also shown that prorenin and renin levels are increased in the plasma and kidneys in diabetes (8, 11, 49). Our data corroborate the results of previous studies by demonstrating PRR augmentation in mesangial cells during HG conditions (50) and in CD during diabetes (51). HG was also shown to stimulate polarized translocation of PRR to the apical plasma membrane in proximal tubular HK-2 cells (52).

OXGR1 participates in paracrine communication between different parts of the renal tubules and is necessary for maintaining the systemic acid–base balance (53). We have shown that STZ treatment stimulates metabolic pathways that enhance αKG formation in CD. Since PRR is part of the vacuolar H^+-ATPase, changes in its abundance may play an essential role in distal urine acidification and phenotype of intercalated cells, as described previously (54), which seems to be independent of changes in GLUT1 expression. Furthermore, ML treatment prevented increases in PRR expression in medulla and specifically intercalated cells but did not cause changes in GLUT1 expression, which may have otherwise altered intercalated cell function. Since αKG concentration in CD decreases in acute acidosis and increases in acute alkalosis, αKG/OXGR1 could be considered as a paracrine system allowing proximal and distal parts of the nephron to communicate. Furthermore, OXGR1 activation stimulate HCO_3– secretion and also contributes to NaCl reabsorption in earlier segments such as proximal tubules (55).

Because both PRR and renin are both increased in CD cells in diabetes, it is reasonable that both may contribute to distal AngII formation. Furthermore, levels of angiotensinogen, the substrate for renin, are also increased and secreted under diabetic conditions (56) contributing to AngI and AngII formation

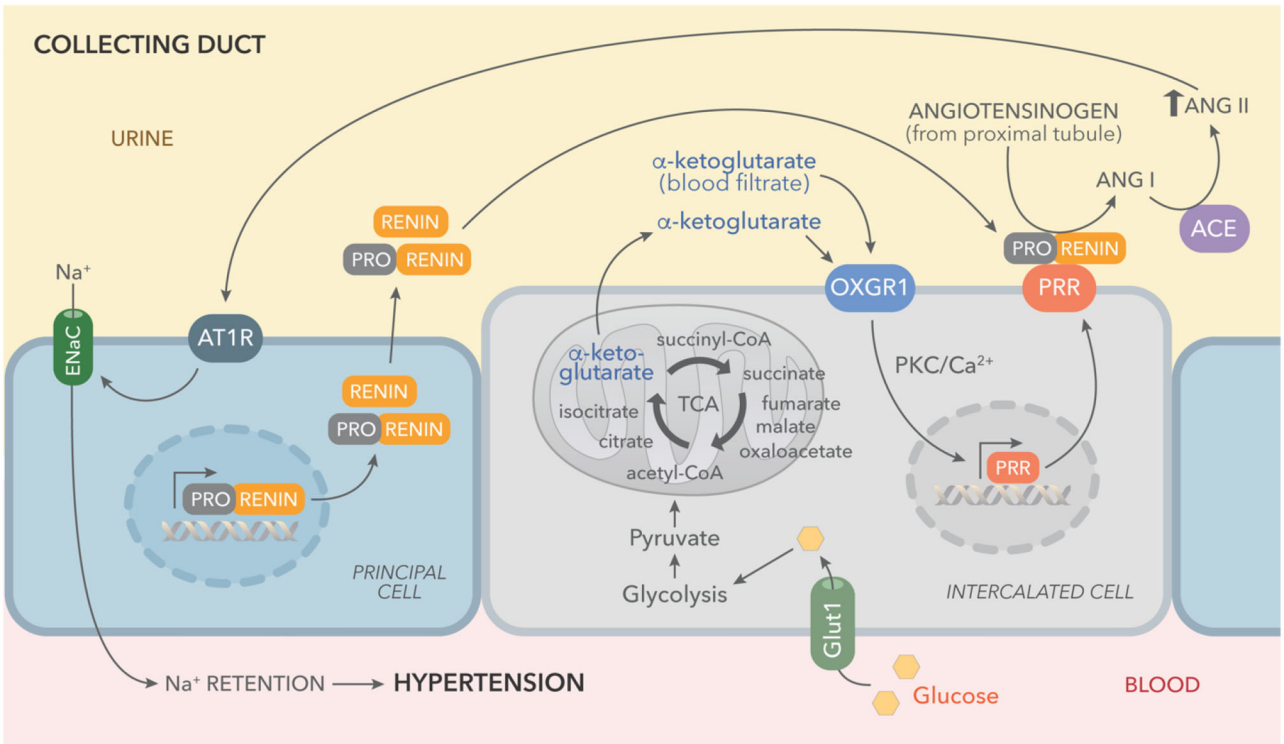

FIGURE 8 | Working hypothesis representing the effects of high glucose on the activation of tricarboxylic acid (TCA) cycle and accumulation of αKG leading to OXGR1 activation. Elevated plasma glucose levels and increased expression of GLUT1 boost glycolysis and TCA cycle, causing αKG accumulation and secretion. Prorenin (and renin) released into the lumen by the principal cell, binds to (pro)renin receptor (PRR), consequently increasing renin activity and activating enzymatic activity of prorenin. Angiotensinogen in the urine (secreted by proximal tubules or coming from blood filtrate) is cleaved by activated prorenin or renin. Since ACE activity is present along the nephron, this intratubular RAS activation ends with AngII intratubular formation and angiotensin type 1 receptor (ATR1)-dependent stimulation of sodium reabsorption through epithelial sodium channels (ENaC).

in the distal nephron. The concomitant augmented excretion of renin and increased expression of PRR leading to newly formed AngII supports the concept that intratubular RAS, which may have a differential expression between cortex and medulla in renal damage (57), confabulates to promote Na^+ reabsorption impacting on blood pressure. Despite our evidence demonstrating that STZ mice exhibit Na^+ retention, we were unable to demonstrate significant increases in arterial blood pressure on day 6 (**Figure 1G**). A slight but not significant increase was observed in systolic and diastolic blood pressure on day 6. This mild impact on blood pressure may be explained by an apparent negative body fluid balance, as suggested by the significant body weight loss on day 6 that was correlated with massive urine output in diabetic mice. Indeed, although body weight was reduced in STZ mice, weight gain evidenced by measuring body weight vs. tibia length may not explain the significant reduction in body mass. Furthermore, food intake was not altered by STZ treatment. Taken all together, it is possible that the increases in blood pressure may be clinically relevant after longer periods of diabetic disease, such that tubular damage is more evident as described previously (39). Despite this, it is clear that PRR upregulation in high glucose conditions may favor tubular RAS activation.

Despite the evidence of PRR upregulation in mesangial cells under HG conditions (13, 50, 58), the precise mechanisms involved in the regulation of PRR in the CD are not well-understood. Although tubular fluid under physiological conditions is virtually glucose free by the time it reaches the CD, basolateral uptake of glucose by GLUT1 facilitative transporters in the CD may stimulate the Kreb's cycle under diabetic conditions with consequent accumulation and secretion of Kreb's intermediaries (59). This idea is supported by studies showing that in STZ-diabetic rats, both the expression of GLUT1 in the CD and the levels of αKG in the urine are augmented (60).

In 2002, a new G-protein-coupled receptor with homology to a new subgroup of nucleotide receptors was described and called GPR99 (which is also known as 2-oxoglutarate receptor 1 or OXGR1) (22). Studies to deorphanize the OXGR1 revealed that αKG activates OXGR1 through Gq to increase intracellular Ca^{2+} (24). The EC50 of OXGR1 for αKG is in the millimolar range, similar to the concentration of αKG in the circulation (25), indicating that the ligand–receptor interaction is physiologically significant. Evidence has demonstrated that OXGR1 effects can be specifically inhibited by leukotriene receptor antagonists such as ML (23). In mice, OXGR1 is expressed only in the testes, smooth muscle cells, and predominantly in kidney CD

cells (23). Double-labeling immunohistochemistry demonstrated the colocalization of OXGR1 in type B and non-A–non-B intercalated cells of the B1 subunit isoform of vacuolar H^+-ATPase (25). PRR immunoreactivity is detected at the apical aspect of type A intercalated cells and non-A, non-B intercalated CD cells (61). Tokonami et al. demonstrated that millimolar concentrations of αKG act in a paracrine manner on type B and non-A–non-B intercalated cells stimulating NaCl reabsorption (25). These effects were induced by apical but not basolateral application of αKG and mediated by OXGR1. Based on this, it is likely that the increased levels of plasma and urine αKG described in diabetic animals can reach the CD at physiological concentrations high enough to activate OXGR1, stimulating signaling pathways to induce the expression of PRR. Furthermore, a recent revision from Peterdi et al. pointed out evidence of Kreb's cycle activation in the CD by HG (21) through enhanced GLUT1 expression (20), which in turn contributes to αKG secretion and augmented intratubular concentrations.

This concept was supported by our results, which show increased levels of αKG in urine samples of STZ diabetic mice and in cultured IMCD cells (**Figures 1**, **5**). We have reported that PRR is stimulated by the receptor 1 of AngII (AT1R), which is also a Gq-coupled receptor linked to protein kinase C activation and intracellular Ca^{2+} release (62). Higher levels of αKG might stimulate apical OXGR1, a Gq-coupled receptor that increases intracellular raising Ca^{2+} (**Figure 5**) and PKC activity (35). Thus, αKG coming from the filtrate and accumulation in collecting duct cells is able to stimulate OXGR1-dependent activation of PKC/Ca^{2+} pathways, which are responsible for the increased expression of PRR and further intratubular AngII formation (**Figure 8**).

This was further demonstrated in the experiments in which cultured IMCD cells were treated with physiological concentrations of αKG and consequently had increased intracellular Ca^{2+}. We further confirmed these observations by blocking OXGR1 with ML. Preincubation with ML prevented the increase in intracellular Ca^{2+} levels in response to αKG treatment (**Figure 5B**). Furthermore, OXGR1 blockade prevented the increase in PRR mRNA and protein levels (**Figure 5C**). Interestingly, OXGR1 blockade did not affect GLUT1 expression in STZ mice or in cultured IMCD cells. Finally, we demonstrated that PKC inhibition and Ca^{2+} depletion impairs αKG-dependent augmentation of PRR (**Figure 5D**). Importantly, blockade of OXGR1 partially blunted the Na^+ retention observed in STZ mice. This effect was observed during the first 3 h of the saline challenge test (**Figure 3E**). This was also accompanied by a partial reduction in urinary AngII formation observed in STZ mice (**Figure 3**).

Our data highlight the importance of the distal nephron segments in RAS activation and formation of intratubular AngII under conditions of HG. Our evidence also demonstrates that metabolic pathways might be involved in the regulation of intratubular RAS components.

DATA AVAILABILITY STATEMENT

The original contributions presented in the study are included in the article/**Supplementary Material**, further inquiries can be directed to the corresponding author/s.

ETHICS STATEMENT

The animal study was reviewed and approved by Bioethical Committee of the Pontificia Universidad Católica de Valparaiso.

AUTHOR CONTRIBUTIONS

AG, BV, PC, SF, JV, PA, and NS-P performed experiments. QN and MK performed experiments and analyzed the data. CA and MP supervised the experiments. AG wrote the manuscript, supervised the experiments, and analyzed the data. CA, MP, QN, and MK approved the final form of the manuscript. All authors contributed to the article and approved the submitted version.

FUNDING

This work was supported by Fondo Nacional de Desarrollo Científico y Tecnológico (FONDECYT) of Chile No. 1191006 to AG and No. 1201251 to CA, CONICYT-ANID 3201016 to PA; 5R01HL150360-03, AHA 18CDA34030155 to MK and and the National Institute of Diabetes and Digestive and Kidney (NIDDK; No.DK104375), Tulane School of Medicine Faculty Research Pilot Funds Program, and Carol Lanvin-Bernick Faculty Grant to MP.

ACKNOWLEDGMENTS

We would like to thank Dr. L. Gabriel Navar (Chairman Department of Physiology, Tulane University School of Medicine) for his critical advice and thoughtful insights. We thank KIMEN Design4Research for the graphic design of **Figure 8**.

SUPPLEMENTARY MATERIAL

The Supplementary Material for this article can be found online at: https://www.frontiersin.org/articles/10.3389/fcvm.2021.644797/full#supplementary-material

REFERENCES

1. Zimpelmann J, Kumar D, Levine DZ, Wehbi G, Imig JD, Navar, et al. Early diabetes mellitus stimulates proximal tubule renin mRNA expression in the rat. *Kidney Int.* (2000) 58:2320–30. doi: 10.1046/J.1523-1755.2000.00416.X
2. Kang JJ, Toma I, Sipos A, Meer EJ, Vargas, Peti-Peterdi SL. The collecting duct is the major source of prorenin in diabetes. *Hypertension.* (2008) 51:1597–604. doi: 10.1161/Hypertensionaha.107.107268
3. Persson, Lu F X, Rossing P, Garrelds IM, Danser AHJ, Parving H-H. Urinary renin and angiotensinogen in type 2 diabetes: added

value beyond urinary albumin? *J Hypertens.* (2013) 31:1646–52. doi: 10.1097/HJH.0b013e328362217c
4. Mamenko M, Zaika O, Ilatovskaya DV, Staruschenko, Pochynyuk AO. Angiotensin II increases activity of the epithelial Na+ channel (ENaC) in distal nephron additively to aldosterone. *J Biol Chem.* (2012) 287:660–71. doi: 10.1074/jbc.M111.298919
5. Mamenko M, Zaika O, Prieto MC, Jensen VB, Doris PA, Navar, et al. Chronic Angiotensin II infusion drives extensive aldosterone-independent epithelial Na+ channel activation. *Hypertension.* (2013) 62:1111–22. doi: 10.1161/Hypertensionaha.113.01797
6. Ritz E, Adamczak, Zeier M. Kidney M, and hypertension - Causes. *Herz.* (2003) 28:663–7. doi: 10.1007/s00059-003-2509-5
7. Price DA, Porter LE, Gordon M, Fisher NDL, De'Oliveira JMF, Laffel LMB, et al. The paradox of the low-renin state in diabetic nephropathy. *J Am Soc Nephrol.* (1999) 10:2382–91. doi: 10.1681/ASN.V10112382
8. Franken AA, Derkx FH, Blankestijn PJ, Janssen JA, Mannesse CK, Hop W, et al. Plasma prorenin as an early marker of microvascular disease in patients with diabetes-mellitus. *Diabetes Metab.* (1992) 18:137–43.
9. Franken AA, Derkx FH, Schalekamp MA, Man in t'Veld AJ, Hop WC, van Rens, et al. Association of high plasma prorenin with diabetic-retinopathy. *J Hypertens.* (1988) 6:S461–3. doi: 10.1097/00004872-198812040-00145
10. Franken AA, Dullaart RPF, Derkx FHM, Schalekamp MADH. Plasma prorenin and progression of albuminuria in type-i diabetic-patients - a 2 years follow-up. *Diabetologia.* (1992) 35:A146.
11. Chiarelli F, Pomilio M, De Luca FA, Vecchiet, Verrotti JA. Plasma prorenin levels may predict persistent microalbuminuria in children with diabetes. *Pediatr Nephrol.* (2001) 16:116–20. doi: 10.1007/s004670000514
12. Siragy, Huang HM. Renal (pro)renin receptor upregulation in diabetic rats through enhanced angiotensin AT(1) receptor and NADPH oxidase activity. *Exp Physiol.* (2008) 93:709–14. doi: 10.1113/expphysiol.2007.040550
13. Huang, Siragy JQ. Regulation of (Pro) renin receptor expression by glucose-induced mitogen-activated protein kinase, nuclear factor-kappa b, and activator protein-1 signaling pathways. *Endocrinology.* (2010) 151:3317–25. doi: 10.1210/en.2009-1368
14. Nabi AH, Kageshima. A., Uddin MN, Nakagawa T, Park, Suzuki EYF. Binding properties of rat prorenin and renin to the recombinant rat renin/prorenin receptor prepared by a baculovirus expression system. *Int J Mol Med.* (2006) 18:483–8. doi: 10.3892/ijmm.18.3.483
15. Kamiyama M, Garner MK, Farragut KM, Sofue T, Hara T, Morikawa T, et al. Detailed localization of augmented angiotensinogen mRNA and protein in proximal tubule segments of diabetic kidneys in rats and humans. *Int J Biol Sci.* (2014) 10:530–42. doi: 10.7150/ijbs.8450
16. Kamiyama M, Zsombok, Kobori AH. Urinary angiotensinogen as a novel early biomarker of intrarenal renin-angiotensin system activation in experimental type 1 diabetes. *J Pharmacol Sci.* (2012) 119:314–23. doi: 10.1254/jphs.12076fp
17. Danda RS, Habiba NM, Rincon-Choles H, Bhandari BK, Barnes JL, Abboud HE, et al. Kidney involvement in a nongenetic rat model of type 2 diabetes. *Kidney Int.* (2005) 68:2562–71. doi: 10.1111/j.1523-1755.2005.00727.x
18. Nacci C, Tarquinio M, De Benedictis L, Mauro A, Zigrino A, Carratù MR, et al. Endothelial dysfunction in mice with streptozotocin-induced type 1 diabetes is opposed by compensatory overexpression of cyclooxygenase-2 in the vasculature. *Endocrinology.* (2009) 150:849–61. doi: 10.1210/en.2008-1069
19. Guan M, Xie L, Diao C, Wang N, Hu W, Zheng Y, et al. Systemic perturbations of key metabolites in diabetic rats during the evolution of diabetes studied by urine metabonomics. *PLoS ONE.* (2013) 8:e60409. doi: 10.1371/journal.pone.0060409
20. Linden KC, DeHaan CL, Zhang Y, Glowacka S, Cox AJ, Kelly DJ, et al. and localization of the facilitative glucose transporters GLUT1 and GLUT12 in animal models of hypertension and diabetic nephropathy. *Am J Physiol-Renal.* (2006) 290:F205–13. doi: 10.1152/ajprenal.00237.2004
21. Peti-Peterdi J. High glucose and renin release: the role of succinate and GPR91. *Kidney Int.* (2010) 78:1214–7. doi: 10.1038/ki.2010.333
22. Wittenberger T, Hellebrand S, Munck A, Kreienkamp, H.-J., Chica Schaller H, et al. GPR99, a new G protein-coupled receptor with homology to a new subgroup of nucleotide receptors. *Bmc Genomics.* (2002) 3:17. doi: 10.1186/1471-2164-3-17
23. Kanaoka Y, Maekawa, Austen AKF. Identification of GPR99 protein as a potential third cysteinyl leukotriene receptor with a preference for leukotriene E4 ligand. *J Biol Chem.* (2013) 288:10967–72. doi: 10.1074/jbc.C113.453704
24. He W, Miao FJ-P, Lin DC-H, Schwandner RT, Wang Z, Gao J, et al. Citric acid cycle intermediates as ligands for orphan G-protein-coupled receptors. *Nature.* (2004) 429:188–93. doi: 10.1038/nature02488
25. Tokonami N, Morla L, Centeno G, Mordasini D, Ramakrishnan SK, Nikolaeva S, et al. alpha-Ketoglutarate regulates acid-base balance through an intrarenal paracrine mechanism. *J Clin Invest.* (2013) 123:3166–71. doi: 10.1172/JCI67562
26. Gonzalez AA, Womack JP, Liu L, Seth, Prieto DM. Angiotensin II increases the expression of (pro)renin receptor during low-salt conditions. *Am J Med Sci.* (2014) 348:416–22. doi: 10.1097/MAJ.0000000000000335
27. Bankova LG, Lai J, Yoshimoto E, Boyce JA, Austen KF, Kanaoka Y, et al. Leukotriene E4 elicits respiratory epithelial cell mucin release through the G-protein-coupled receptor, GPR99. *Proc Natl Acad Sci U S A.* (2016) 113:6242–7. doi: 10.1073/pnas.1605957113
28. McGuinness OP, Ayala JE, Laughlin, Wasserman MR. NIH experiment in centralized mouse phenotyping: the Vanderbilt experience and recommendations for evaluating glucose homeostasis in the mouse. *Am J Phys Endocr Metab.* (2009) 297:E849–55. doi: 10.1152/ajpendo.90996.2008
29. Shao W, Seth DM, Prieto MC, Kobori, Navar H. Activation of the renin-angiotensin system by a low-salt diet does not augment intratubular angiotensinogen and angiotensin II in rats. *Am J Phys Renal Phys.* (2013) 304:F505–14. doi: 10.1152/ajprenal.00587.2012
30. Reverte V, Gogulamudi VR, Rosales CB, Musial DC, Gonsalez SR, Parra-Vitela AJ, et al. Urinary angiotensinogen increases in the absence of overt renal injury in high fat diet-induced type 2 diabetic mice. *J Diabetes Compl.* (2020) 34:107448. doi: 10.1016/j.jdiacomp.2019.107448
31. Lin, Y.-C., Huang, M.-Y., Lee, M.-S., et al.-C., Kuo, H.-F., Kuo, C.-H., Hung, et al. Effects of montelukast on M2-related cytokine and chemokine in M2 macrophages. *J Microb Immunol Infect.* (2018) 51:18–26. doi: 10.1016/j.jmii.2016.04.005
32. Yao K, Yin Y, Li X, Xi P, Wang J, Lei J, et al. Alpha-ketoglutarate inhibits glutamine degradation and enhances protein synthesis in intestinal porcine epithelial cells. *Amino Acids.* (2012) 42:2491–2500. doi: 10.1007/s00726-011-1060-6
33. Gonzalez AA, Lara LS, Luffman C, Seth, Prieto DMMC. Soluble form of the (pro) renin receptor is augmented in the collecting duct and urine of chronic angiotensin ii-dependent hypertensive rats. *Hypertension.* (2011) 57:859–64. doi: 10.1161/Hypertensionaha.110.167957
34. Kim J, Kim YH, Cha JH, Tisher, Madsen CCKM. Intercalated cell subtypes in connecting tubule and cortical collecting duct of rat and mouse. *J Am Soc Nephrol.* (1999) 10:1–12.
35. Lazo-Fernandez Y, Welling SM, Wall PA. alpha-Ketoglutarate stimulates pendrin-dependent Cl(-) absorption in the mouse CCD through protein kinase C. American journal of physiology. *Renal Phys.* (2018) 315:F7–F15. doi: 10.1152/ajprenal.00576.2017
36. Abbracchio MP, Burnstock G, Boeynaems, J.-M., Barnard EA, Boyer JL, et al. The recently deorphanized GPR80 (GPR99) proposed to be the P2Y15 receptor is not a genuine P2Y receptor. *Trends Pharmacol Sci.* (2005) 26:8–9. doi: 10.1016/j.tips.2004.10.010
37. Fujisawa G, Okada K, Muto S, Fujita N, Itabashi N, Kusano E, et al. Spironolactone prevents early renal injury in streptozotocin-induced diabetic rats. *Kidney Int.* (2004) 66:1493–502. doi: 10.1111/j.1523-1755.2004.00913.x
38. Noshahr ZS, Salmani H, Khajavi Rad, Sahebkar AA. Animal models of diabetes-associated renal injury. *J Diabetes Res.* (2020) 2020:9416419. doi: 10.1155/2020/9416419
39. Tay YC, Wang Y, Kairaitis L, Rangan GK, Zhang C, Harris, et al. Can murine diabetic nephropathy be separated from superimposed acute renal failure? *Kidney Int.* (2005) 68:391–8. doi: 10.1111/j.1523-1755.2005.00405.x
40. Peres GB, Schor N, Michelacci YM. Impact of high glucose and AGEs on cultured kidney-derived cells. Effects on cell viability, lysosomal enzymes and effectors of cell signaling pathways. *Biochimie.* (2017) 135:137–48. doi: 10.1016/j.biochi.2017.02.004
41. Ichihara A, Yatabe MS. The (pro)renin receptor in health and disease. *Nat Rev Nephrol.* (2019) 15:693–712. doi: 10.1038/s41581-019-0160-5

42. Ludwig J, Kerscher S, Brandt U, Pfeiffer K, Getlawi F, Apps DK, et al. and characterization of a novel 9.2-kDa membrane sector-associated protein of vacuolar proton-ATPase from chromaffin granules. *J Biol Chem.* (1998) 273:10939–47. doi: 10.1074/Jbc.273.18.10939
43. Advani A, Kelly DJ, Cox AJ, White KE, Advani SL, Thai K, et al. The (Pro) renin receptor site-specific and functional linkage to the vacuolar H(+)-ATPase in the kidney. *Hypertension.* (2009) 54:261–U129. doi: 10.1161/Hypertensionaha.109.128645
44. Ichihara. (Pro)renin receptor A, and autophagy in podocytes. *Autophagy.* (2012) 8:271–2. doi: 10.4161/auto.8.2.18846
45. Yosypiv IV. Renin-angiotensin system in ureteric bud branching morphogenesis: insights into the mechanisms. *Pediatr Nephrol.* (2011) 26:1499–512. doi: 10.1007/s00467-011-1820-2
46. Wang F, Lu X, Liu M, Feng Y, Zhou, S.-F., et al. Renal medullary (pro)renin receptor contributes to angiotensin II-induced hypertension in rats via activation of the local renin-angiotensin system. *Bmc Med.* (2015) 13. doi: 10.1186/S12916-015-0514-1
47. Ramkumar N, Stuart D, Calquin M, Quadri S, Wang S, Van Hoek AN, et al. Nephron-specific deletion of the prorenin receptor causes a urine concentration defect. *Am J Phys Renal Phys.* (2015) 309:F48–56. doi: 10.1152/ajprenal.00126.2015
48. Peng K, Lu X, Wang F, Nau A, Chen R, Zhou, et al. Collecting duct (pro)renin receptor targets ENaC to mediate angiotensin II-induced hypertension. *Am J Phys Renal Phys.* (2017) 312:F245–F253. doi: 10.1152/ajprenal.00178.2016
49. Deinum J, Tarnow L, van Gool JM, de Bruin RA, Derkx FHM, Schalekamp, et al. Plasma renin and prorenin and renin gene variation in patients with insulin-dependent diabetes mellitus and nephropathy. *Nephr Dialy Transpl.* (1999) 14:1904–11. doi: 10.1093/ndt/14.8.1904
50. Huang HM, Siragy JQ. Glucose promotes the production of interleukine-1 beta and cyclooxygenase-2 in mesangial cells via enhanced (Pro)Renin receptor expression. *Endocrinology.* (2009) 150:5557–5565. doi: 10.1210/en.2009-0442
51. Matavelli LC, Huang HM, Siragy JQ. (Pro)renin receptor contributes to diabetic nephropathy by enhancing renal inflammation. *Clin Exp Pharmacol P.* (2010) 37:277–82. doi: 10.1111/j.1440-1681.2009.05292.x
52. Sautin YY, Lu M, Gaugler A, Zhang SL, Gluck L. Phosphatidylinositol 3-kinase-mediated effects of glucose on vacuolar H+-ATPase assembly, translocation, and acidification of intracellular compartments in renal epithelial cells. *Mol Cell Biol.* (2005) 25:575–89. doi: 10.1128/MCB.25.2.575-589.2005
53. Diehl J, Gries B, Pfeil U, Goldenberg A, Mermer P, Kummer W, et al. and localization of GPR91 and GPR99 in murine organs. *Cell Tissue Res.* (2016) 364:245–62. doi: 10.1007/s00441-015-2318-1
54. Chen L, Lee JW, Chou, C.-L., Nair AV, Battistone MA, et al. Transcriptomes of major renal collecting duct cell types in mouse identified by single-cell RNA-seq. *Proc Natl Acad Sci USA.* (2017) 114:E9989–98. doi: 10.1073/pnas.1710964114
55. Bobulescu OW, Moe IA. Luminal Na(+)/H (+) exchange in the proximal tubule. *Pflugers Archiv Europ J Phys.* (2009) 458:5–21. doi: 10.1007/s00424-008-0595-1
56. Zhuang Z, Bai Q, A L, Liang Y, Zheng D, Wang, et al. Increased urinary angiotensinogen precedes the onset of albuminuria in normotensive type 2 diabetic patients. *Int J Clin Exp Pathol.* (2015) 8:114 64–69.
57. Figueroa SM, Lozano M, Lobos C, Hennrikus MT, Gonzalez AA, Amador, et al. Upregulation of cortical renin and downregulation of medullary (pro)renin receptor in unilateral ureteral obstruction. *Front Pharmacol.* (2019) 10:1314. doi: 10.3389/fphar.2019.01314
58. Huang JQ, Gildea HM, Siragy J. Transcriptional regulation of prorenin receptor by high glucose in mesangial cells via PKC-MAPK-c-Jun axis. *Hypertension.* (2007) 50:E76.
59. Peti-Peterdi J, Gevorgyan H, Lam A, Riquier-Brison L. Metabolic control of renin secretion. *Pflug Arch Eur J Phy.* (2013) 465:53–58. doi: 10.1007/s00424-012-1130-y
60. Shibata K. Urinary excretion of 2-oxo acids is greater in rats with streptozotocin-induced diabetes. *J Nutr Sci Vitam.* (2018) 64:292–5. doi: 10.3177/jnsv.64.292
61. Gonzalez AA, Luffman C, Bourgeois CR, Vio MC, Prieto CP. Angiotensin II-independent upregulation of cyclooxygenase-2 by activation of the (Pro)renin receptor in rat renal inner medullary cells. *Hypertension.* (2013) 61:443–9. doi: 10.1161/HYPERTENSIONAHA.112.196303
62. Gonzalez AA, Liu L, Lara LS, Bourgeois CRT, Ibaceta-Gonzalez C, Salinas-Parra N, et al. PKC-alpha-dependent augmentation of cAMP and CREB phosphorylation mediates the angiotensin II stimulation of renin in the collecting duct. *Am J Phys Renal Phys.* (2015) 309:F880–8. doi: 10.1152/ajprenal.00155.2015

Conflict of Interest: The authors declare that the research was conducted in the absence of any commercial or financial relationships that could be construed as a potential conflict of interest.

frontiers in Physiology

ORIGINAL RESEARCH
published: 17 June 2021
doi: 10.3389/fphys.2021.615443

Acute Effect of Enhanced External Counterpulsation on the Carotid Hemodynamic Parameters in Patients With High Cardiovascular Risk Factors

*Yahui Zhang[1,2,3], Zhouming Mai[1], Jianhang Du[1,3], Wenjuan Zhou[1], Wenbin Wei[1], Hui Wang[4], Chun Yao[1,2], Xinxia Zhang[1,3], Hui Huang[1,3] and Guifu Wu[1,2,3]**

[1] Department of Cardiology, The Eighth Affiliated Hospital of Sun Yat-sen University, Shenzhen, China, [2] National Health Commission (NHC) Key Laboratory of Assisted Circulation, Sun Yat-sen University, Guangzhou, China, [3] Guangdong Innovative Engineering and Technology Research Center for Assisted Circulation, Shenzhen, China, [4] Department of Cardiac Ultrasound, The Eighth Affiliated Hospital, Sun Yat-sen University, Shenzhen, China

OPEN ACCESS

Edited by:
Soo-Kyoung Choi,
Yonsei University College of Medicine, South Korea

Reviewed by:
Antoine Bergel,
UMR 7587 Institut Langevin Ondes et Images (Institut Langevin), France
Mohamed Lamine Freidja,
University of M'sila, Algeria

***Correspondence:**
Guifu Wu
wuguifu@mail.sysu.edu.cn

Specialty section:
This article was submitted to Vascular Physiology, a section of the journal Frontiers in Physiology

Received: *09 October 2020*
Accepted: *21 May 2021*
Published: *17 June 2021*

Citation:
Zhang Y, Mai Z, Du J, Zhou W, Wei W, Wang H, Yao C, Zhang X, Huang H and Wu G (2021) Acute Effect of Enhanced External Counterpulsation on the Carotid Hemodynamic Parameters in Patients With High Cardiovascular Risk Factors. Front. Physiol. 12:615443. doi: 10.3389/fphys.2021.615443

Purpose: Enhanced external counterpulsation (EECP) can improve carotid circulation in patients with coronary artery disease. However, the response of carotid hemodynamic parameters induced by EECP in patients with high cardiovascular risk factors remains to be clarified. This study aimed to investigate the acute effect of EECP on the hemodynamic parameters in the carotid arteries before, during, and immediately after EECP in patients with hypertension, hyperlipidemia, and type 2 diabetes.

Methods: Eighty-three subjects were recruited into this study to receive 45-min EECP, including patients with simple hypertension (n = 21), hyperlipidemia (n = 23), type 2 diabetes (n = 18), and healthy subjects (n = 21). Hemodynamic parameters in both common carotid arteries (CCAs) were measured and calculated from Doppler ultrasound images. Peak systolic velocity (PSV), end-diastolic velocity (EDV), mean inner diameter (ID), systolic/diastolic flow velocity ratio (VS/VD), flow rate (FR), and resistance index (RI) were monitored before, during, and immediately after 45-min EECP.

Results: EDV and VS/VD were significantly reduced, while RI of CCAs was significantly increased among four groups during EECP (all $P < 0.01$). Additionally, the ID of CCAs and the FR of left CCA increased in patients with hyperlipidemia during EECP ($P < 0.05$). PSV of left CCA was reduced in patients with type 2 diabetes ($P < 0.05$). Moreover, immediately after EECP, ID was significantly higher in patients with hyperlipidemia. The RI of patients with hypertension and PSV and VS/VD of patients with type 2 diabetes were significantly lower compared with baseline (all $P < 0.05$).

Conclusion: EECP created an acute reduction in EDV, PSV, and VS/VD, and an immediate increase in the RI, FR, and ID of CCAs among the four groups. Additionally, a single 45-min session of EECP produced immediate improvement in the ID of patients

with hyperlipidemia, the RI of patients with hypertension, and the PSV and VS/VD of patients with type 2 diabetes. The different hemodynamic responses induced by EECP may provide theoretical guidance for making personalized plans in patients with different cardiovascular risk factors.

Keywords: enhanced external counterpulsation, hemodynamic responses, cardiovascular risks, Doppler ultrasound images, common carotid artery

INTRODUCTION

Enhanced external counterpulsation (EECP) is a non-invasive FDA-approved treatment that reduces angina and improves myocardial ischemia in patients with coronary heart disease (CHD) (Masuda et al., 2001; Gloekler et al., 2010). EECP includes sequential inflation and deflation of compressible cuffs wrapped around the participant's calves, lower thighs, and upper thighs. Compressed air pressure is used by the cuffs to the lower extremities in a sequence synchronized with the cardiac cycle *via* identifying ECG signals. Studies have also reported that EECP was beneficial for peripheral vascular function (e.g., blood pressure (BP) and blood flow) in patients with CHD (Michaels, 2002; Braith et al., 2010). However, the effects of EECP on cardiovascular function in patients with different cardiovascular risk factors, such as hypertension, hyperlipidemia, and type 2 diabetes, remains controversial.

Bondesson et al. (2010) found that EECP treatment decreased BP in patients with refractory angina pectoris. By contrast, Lin et al. (2012) found that EECP significantly increased the mean BP of stroke patients (12.84%). Sardina et al. (2016) reported that EECP decreased advanced glycation end product (AGE/RAGE) concentrations, oxidative stress, and inflammation in patients with type II diabetes mellitus, but it is unclear how EECP will influence those parameters. Martin et al. (2013) found that the benefits of EECP therapy in people with abnormal glucose tolerance may contribute to microvascular function. Other studies showed that EECP improved vascular endothelial function and wave reflection characteristics and reduced arterial stiffness (Nichols et al., 2006), while a study found that EECP cannot reduce arterial stiffness (Dockery et al., 2004).

Acute intervention is an effective method of investigating the peripheral hemodynamic parameter responses to external stimuli (Liu et al., 2015; Zhang et al., 2018). Michaels (2002) found that average peak velocity significantly increased during EECP, and coronary flow showed a 28% increase during EECP compared with baseline. Gurovich and Braith (2013) reported that EECP acutely improves endothelium-dependent vasodilation in both femoral and brachial arteries in young people (Gurovich and Braith, 2013). Levenson et al. (2007) showed that EECP exerts vascular relaxation effects on both large and small arteries of the carotid circulation in patients with coronary artery disease immediately after EECP. To date, however, little attention has been paid to the acute impact of EECP on carotid vascular function in patients with high cardiovascular risk factors.

The responses of peak systolic velocity (PSV), resistance index (RI), mean inner diameter (ID), end-diastolic velocity (EDV), and blood flow in the left and right common carotid arteries (CCAs) may exhibit different prognostic values in the investigated population (Lee et al., 2011; Loizou et al., 2015) and are closely related to cardiovascular events (Bai et al., 2007; Ozari et al., 2012; Chuang et al., 2016). Kallikazaros et al. (1999) and Sedaghat et al. (2018) found that the ID of the carotid artery was closely related to CHD based on large samples. However, few studies focused on the acute effect of EECP on carotid hemodynamics. Moreover, the mechanisms of acute responses, which can highlight the responses of cardiovascular disease, have not yet been clarified (Levenson et al., 2007; Zhang et al., 2007, 2018).

This study aimed to investigate the acute effect of EECP on the hemodynamic parameters in CCAs before, during, and immediately after EECP in patients with hypertension, hyperlipidemia, and type 2 diabetes and healthy controls. Meanwhile, we try to find out sensitive hemodynamic parameters reflecting different cardiovascular risk factors and then explore the response mechanism induced by EECP.

MATERIALS AND METHODS

Participants

Patients with simple hypertension (n=21), simple hyperlipidemia (n=23), and simple type 2 diabetes (n=18) were included who had enrolled in the Cardiovascular Medicine of Eighth Affiliated Hospital of Sun Yat-sen University (SYSU). In addition, healthy controls (n=21) were enrolled from the Health Examination Center of the Eighth Affiliated Hospital of SYSU. Before the experiment, informed consent forms were signed by all of the subjects. The study was approved by the local medical ethics committee of the Eighth Affiliated Hospital of SYSU.

Experiment Scheme

Before this experiment, all participants were required not to ingest any food or flavonoid-containing beverages and ethanol after midnight, and to avoid alcohol, caffeine, and EECP or exercise for at least 24 h prior to the measurements. Their carotid hemodynamic data were collected in the Enhanced External Counterpulsation Center. The baseline measurements were performed for each group in the supine position after 10 min of relaxation. All subjects were received a 45-min session EECP treatment with the PSK P-ECP/TM Oxygen Saturation Monitoring EECP Instrument (made in Chongqing, China). These participants lay supine on the EECP treatment bed with their legs and buttocks wrapped in cuffs, which were sequentially inflated from the lower thigh to the upper thigh and buttocks

TABLE 1 | Base characteristics, clinic information and risk factors of study population.

	Hypertension	Hyperlipidemia	Type 2 diabetes	Health	*P*-value
Number (No.)	21	23	18	21	0.272
Age (years old)	58.86 ± 9.75	60.48 ± 7.48	60.11 ± 6.92	53.95 ± 8.44	0.196
Gender (female/%)	5 (23.8)	16 (69.6)	15 (83.3)	15 (71.4)	0.063
Height (cm)	167.1 ± 7.1	163.85 ± 6.68	158.35 ± 7.62	161.3 ± 9.5	0.196
Weight (kg)	68.93 ± 8.75	62.35 ± 9.76	58.41 ± 11.61	65.3 ± 59.24	0.311
SV (ml)	80.22 ± 15.81	71.2 ± 10.16	77 ± 16.43	64 ± 20.92	0.260
EF (%)	69.2 ± 5.53	69.8 ± 3.91	67.33 ± 8.09	67.25 ± 7.09	0.190
LVIDD (mm)	48.4 ± 4.38	46.7 ± 3.02	49.17 ± 5.85	45 ± 4.72	0.619
Blood sugar (mmol/L)	4.68 ± 0.9	4.18 ± 0.66	7.6 ± 1.05	4.17 ± 0.64	0.045
Triglyceride (mmol/L)	1.33 ± 0.39	1.75 ± 0.72	1.19 ± 0.34	1.83 ± 1.16	0.037
LDL_cholesterol (μmmol/L)	3.02 ± 0.65	3.97 ± 0.52	3.37 ± 0.78	3.09 ± 0.63	0.254
Total cholesterol (mmol/L)	4.93 ± 0.8	6.31 ± 0.49	5.34 ± 0.98	5.17 ± 0.91	0.000
Glycosylated Hemoglobin (%)	5.76 ± 0.48	5.58 ± 0.23	6.54 ± 0.79	5.57 ± 0.39	0.008
Smoking	3 (14.3)	2 (8.7)	0 (0)	0 (0)	0.153
Drinking	0 (0)	1 (4.3)	1 (5.6)	4 (19)	0.096

SV, stroke volume; LVEF, left ventricle ejection fraction; LVDD, left ventricular end diastolic diameter.

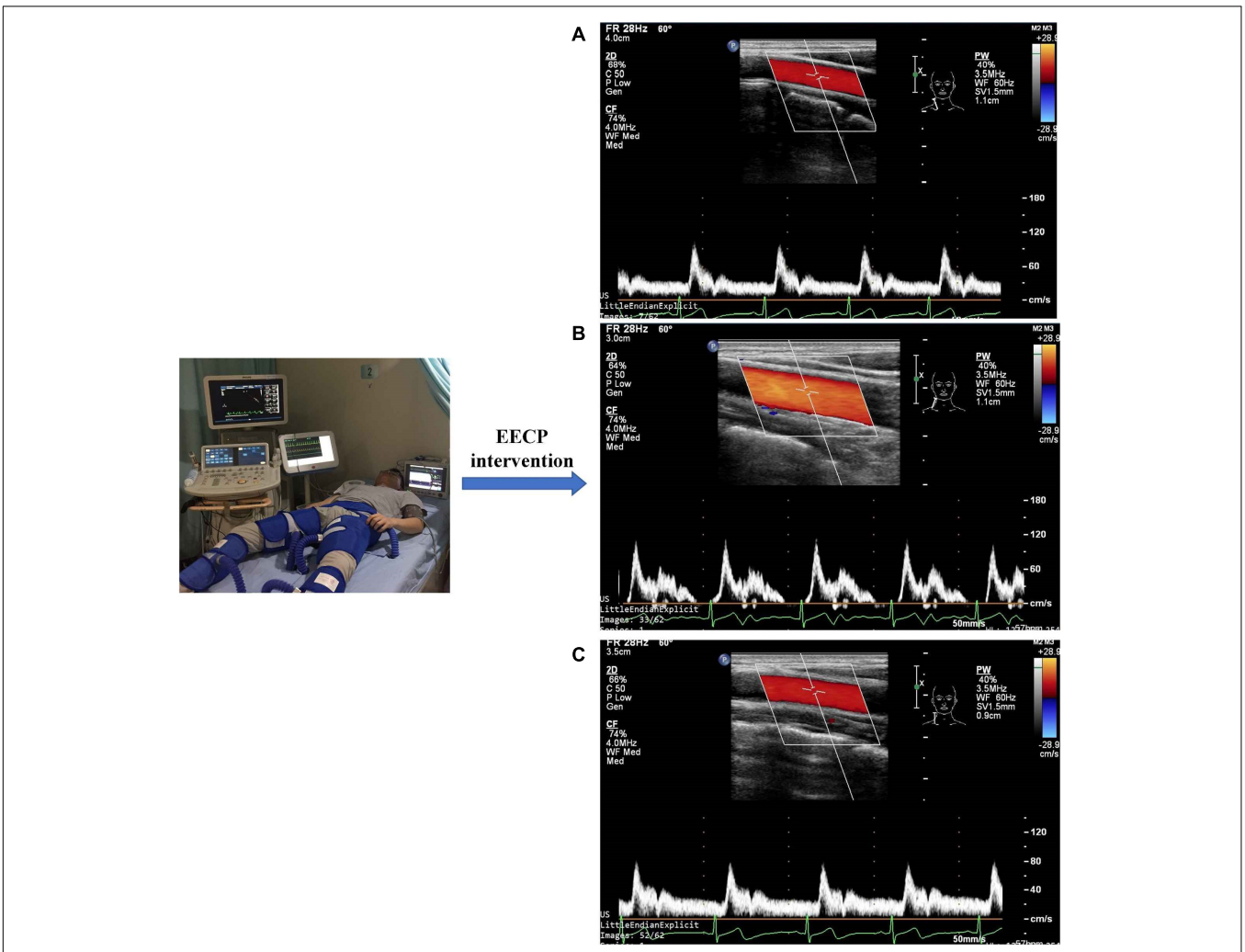

FIGURE 1 | Measurement of blood flow velocity spectrum in the right common carotid artery before **(A)**, during **(B)**, and immediately after EECP **(C)**.

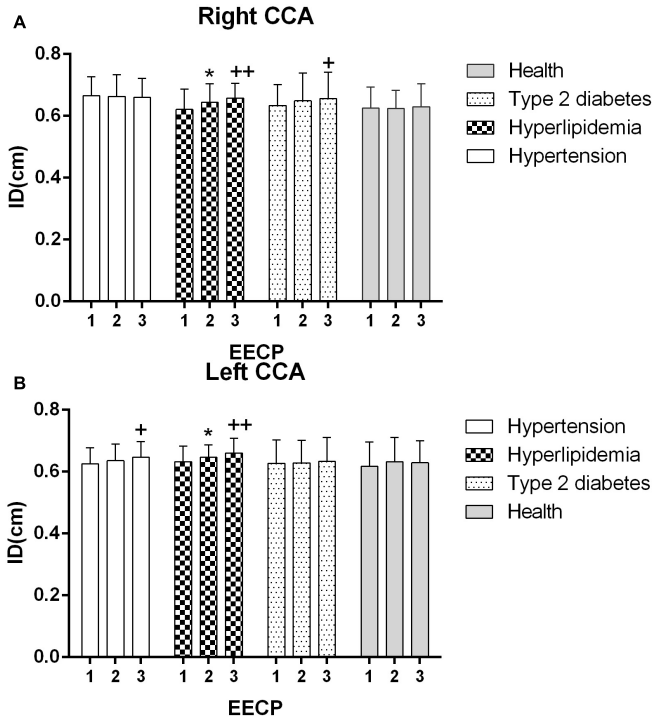

FIGURE 2 | Averaged inner diameters (IDs) in the right **(A)** and left **(B)** common carotid artery (CCA) in four groups before, during and after 45-min EECP. $^{*}P < 0.05$ during EECP vs. pre-EECP, $^{**}P < 0.01$; $^{++}P < 0.05$ post-EECP vs. pre EECP, $^{++}P < 0.01$.

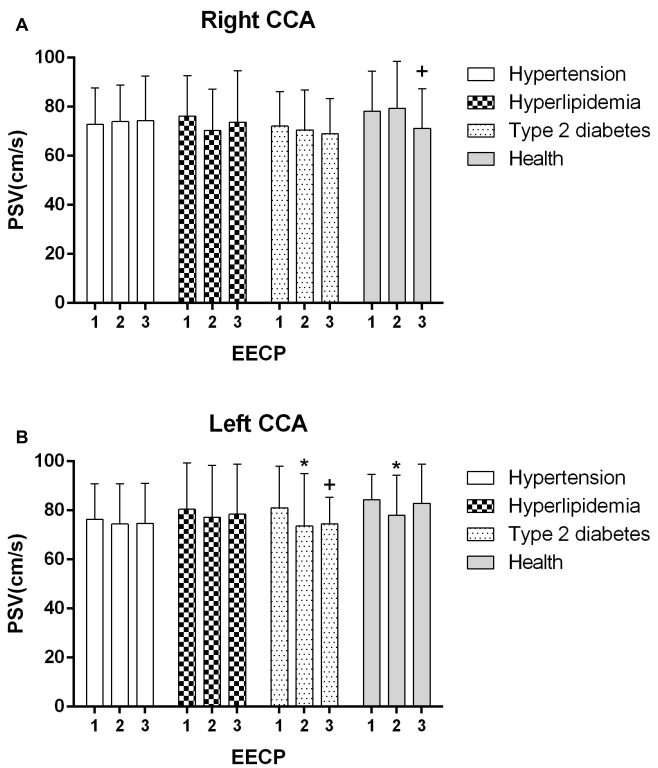

FIGURE 3 | Peak systolic velocity (PSV) in the right **(A)** and left **(B)** common carotid artery (CCA) in four groups before, during and after 45-min EECP. $^{*}P < 0.05$ during EECP vs. pre-EECP; $^{+}P < 0.05$ post-EECP vs. pre-EECP.

at the beginning of the diastolic phase, followed by a quick, simultaneous deflation of all cuffs just prior to the onset of systole. The EECP treatment pressure was set as 0.028–0.033 MPa. Color Doppler Ultrasound (GE Logiq E, Universal Imaging, Wayne, NJ, United States) was used to measure at rest, 15–25 min during EECP and immediately after 45 min of EECP. The right and left CCAs were examined with 1.5 cm proximal to the bifurcation of the vessels.

Parameter Calculation

Parameters, PSV, RI, peak diastolic velocity (VD), PSV/VD (VS/VD), and velocity-time integral (VTI) in the CCAs were continuously recorded for 10 s and then were calculated for mean value.

The mean IDs of all arteries were calculated as:

$$ID = (ID_{dia} + ID_{sys})/2; \quad (1)$$

where ID_{sys} and ID_{dia} are the systolic and diastolic diameters, respectively.

RI was analyzed only in the carotid arteries because, as a measure of cerebral resistance, it is closely associated with cardiovascular risk was calculated as:

$$RI = (PSV - EDV)/PSV, \quad (2)$$

where PSV is the peak systolic velocity (PSV), and EDV is the end-diastolic velocity (EDV).

Flow rate (FR) was calculated from the vessel diameter, cardiac period, and velocity-time integral as:

$$Flow\ rate = (\frac{1}{4}\pi ID^2 \times VTI)/T, \quad (3)$$

where VTI is the averaged velocity-time integral, and T is the averaged cardiac cycle time.

Statistical Analysis

ID, PSV, EDV, RI, and VS/VD are the mean values of area under the envelope curve in a cardiac cycle. Results are shown as means ± SD. Normal distribution for all the carotid

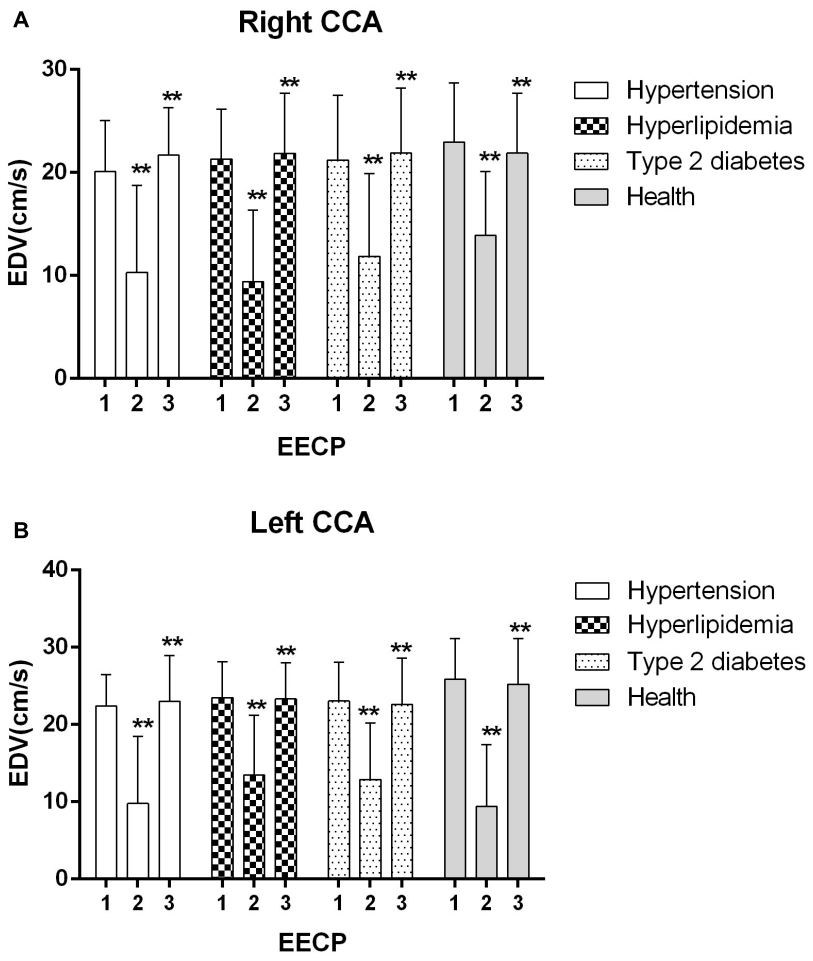

FIGURE 4 | Effect of EECP on the end-diastolic velocity (EDV) of the right **(A)** and left **(B)** common carotid artery (CCA) in four groups before, during and after 45-min EECP. $^{**}P < 0.01$ during EECP vs. pre-EECP.

hemodynamic variables was evaluated by the Kolmogorov–Smirnov test (at least one test $P > 0.05$). The difference of basic characteristics among the four groups was performed by one-way ANOVA. The repeated ANOVAs comparing carotid hemodynamic parameters before, during, and immediately after EECP and between patients with cardiovascular risks and healthy controls were performed. Fisher's least significant difference was conducted as *post-hoc analysis.* All statistical tests were conducted by SPSS version 20.0 (IBM SPSS Statistics, Chicago, IL, United States), and $P < 0.05$ was taken as a measure of statistical significance.

RESULTS

Table 1 shows the base information (age, gender, height, and weight), clinical information (stroke volume (SV), left ventricle ejection fraction (LVEF), left ventricular end diastolic diameter (LVDD), blood sugar, and blood lipids), and risk factors (smoking and drinking) among the four groups. There were significant differences in blood sugar, triglyceride, total cholesterol, and glycosylated hemoglobin ($P < 0.05$), while age, gender, height, weight, SV, LVEF, LVDD, smoking, and drinking had no significant differences in each group at baseline ($P > 0.05$).

Ultrasound pictures and Doppler spectrum of right CCA before, during, and immediately after EECP are presented in **Figure 1**. The effect of EECP on the hemodynamic variables varied in CCAs as did the differences among the four groups. The results are illustrated in **Figures 2–7** and summarized in S1 **Table 2**, which compares the effects of EECP for CCAs in each group separately, and **Table 3**, which allows multiple comparisons among the four groups.

Mean ID

The ID of the right CCA was significantly higher in patients with hypertension at baseline compared with patients with hyperlipidemia and healthy controls (both $P < 0.05$), while it had no significant differences in each group during and immediately after EECP ($P > 0.05$). The ID of CCAs was significantly increased only in patients with hyperlipidemia during EECP, and it was continuously increased in patients with hyperlipidemia and type 2 diabetes ($P < 0.05$, **Figure 2**). Immediately after EECP, the ID of left CCA was also markedly increased in patients with hypertension ($P < 0.05$, **Figure 2B**).

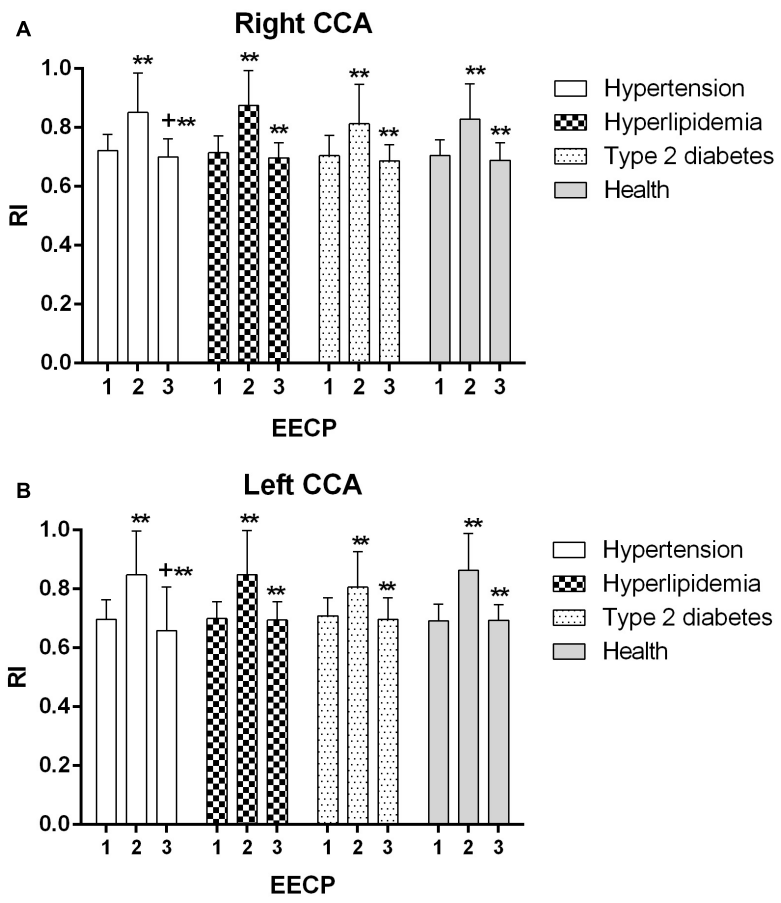

FIGURE 5 | Resistance index (RI) of the right **(A)** and left **(B)** common carotid artery (CCA) in four groups before, during and after 45-min EECP. $^{**}P < 0.01$ during EECP vs. pre-EECP; $^{+}P < 0.05$ post-EECP vs. pre-EECP.

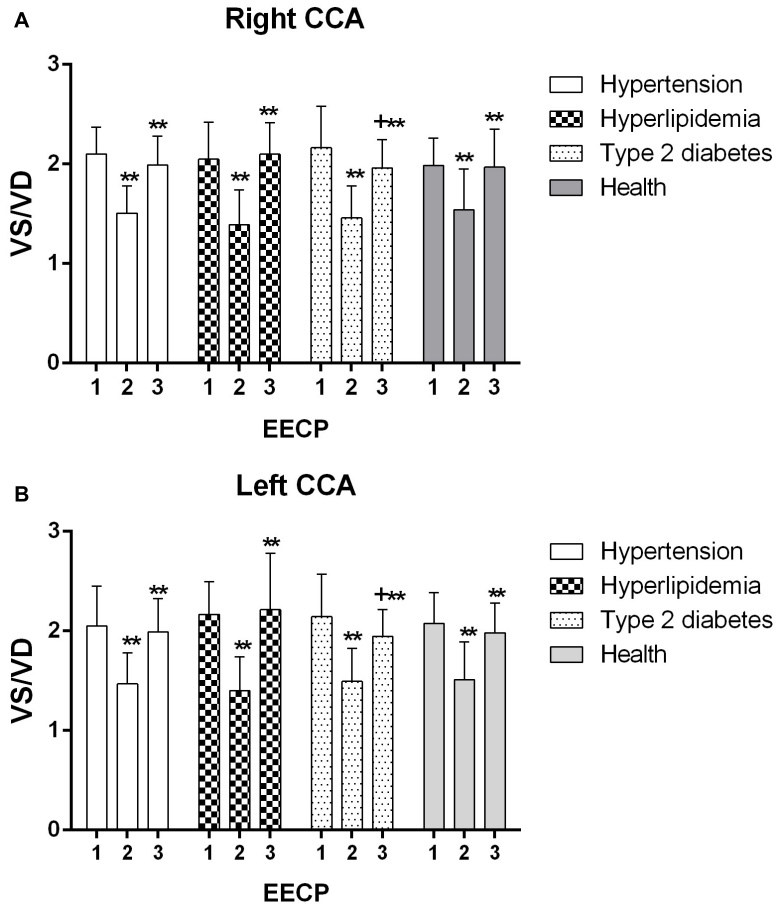

FIGURE 6 | VS/VD of the right **(A)** and left **(B)** common carotid artery (CCA) in four groups before, during and after 45-min EECP. $^{**}P < 0.01$ during EECP vs. pre-EECP; $^{+}P < 0.05$ post-EECP vs. pre-EECP.

PSV

During EECP, the PSV of the left CCAs was significantly reduced in healthy controls and patients with type 2 diabetes ($P < 0.05$, **Figure 3B**). Immediately after EECP, PSV of right CCA and left CCA was markedly decreased in healthy controls and patients with type 2 diabetes, respectively ($P < 0.05$, **Figure 3**).

EDV

EDV of the left CCA was significantly lower in patients with hypertension at baseline, while during EECP, EDV of the right CCA was markedly lower in patients with type 2 diabetes compared with healthy controls ($P < 0.05$). EDV of the CCAs was significantly reduced during EECP and then increased immediately after EECP in each group (all $P < 0.01$, **Figure 4B**).

RI

RI of the CCAs was significantly increased during EECP and then markedly decreased immediately after EECP among four groups (all $P < 0.01$, **Figure 5**). Only in patients with hypertension was RI significantly reduced immediately after EECP (both $P < 0.01$, **Figure 5**).

Ratio of PSV to Diastolic Velocity

VS/VD of the CCAs was significantly decreased during EECP and then markedly increased immediately after EECP among four groups (all $P < 0.01$, **Figure 6**). Immediately after EECP, VS/VD was significantly higher compared with baseline only in patients with type 2 diabetes (both $P < 0.01$, **Figure 6**). Additionally, VS/VD of left CCA was lower in patients with type 2 diabetes compared with that in patients with hyperlipidemia immediately after EECP ($P < 0.05$).

Mean FR

The FR of the left CCA was significantly increased in patients with hypertension and hyperlipidemia during EECP (both $P < 0.05$, **Figure 7B**). In addition, FR of right CCA was markedly lower in healthy controls during EECP compared with immediately after EECP ($P < 0.05$, **Figure 7A**).

DISCUSSION

The present study was designed to investigate carotid hemodynamic responses during and immediately EECP in

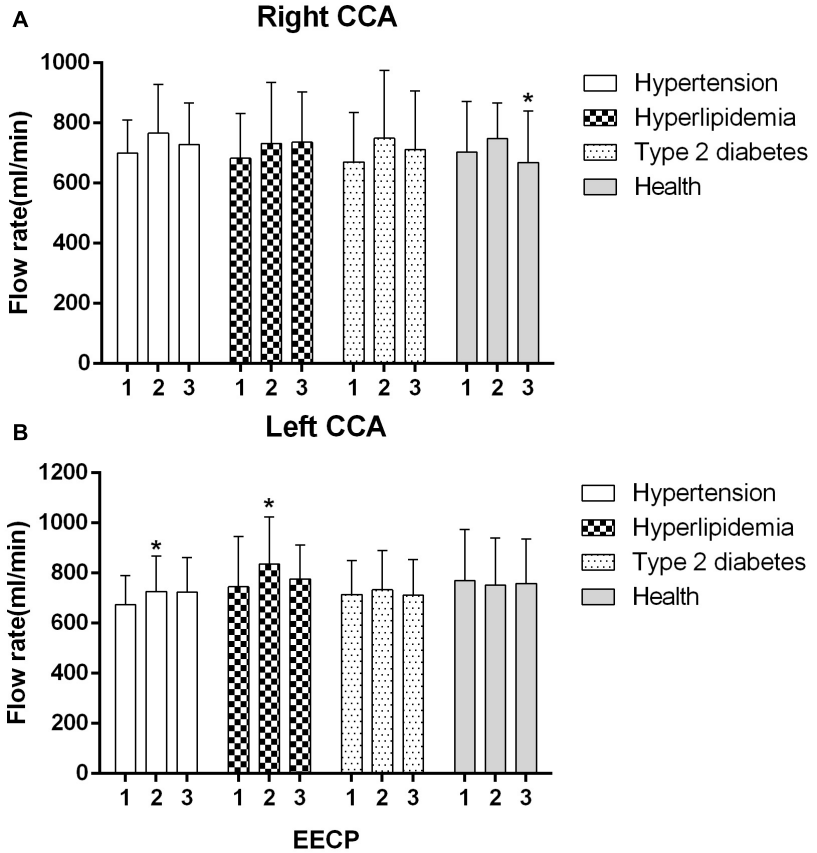

FIGURE 7 | Mean flow rate (FR) of the four groups before, during and after 45-min EECP. *$P < 0.05$ during EECP vs. pre-EECP.

patients with different cardiovascular risks. Two interesting findings were summarized: first, EECP creates an acute reduction in EDV and VS/VD and an immediate increase in RI of CCAs among four groups. Additionally, the ID of CCAs and FR of left CCA were increased in patients with hyperlipidemia during EECP. PSV of left CCA was reduced in patients with type 2 diabetes; second, a single 45-min EECP intervention produces acute improvement on the ID of patients with hyperlipidemia, RI of patients with hypertension, and PSV and VS/VD of patients with type 2 diabetes.

Few studies have investigated the acute effect of EECP on these hemodynamic parameters in patients with hyperlipidemia. A study had reported that EECP exerts clear arterial effects on large and small vessels of the carotid circulation in CAD patients (Levenson et al., 2007). Our results are consistent, at least by some parameters, with the study of Levenson et al. (2007) ID, EDV, and FR in the CCAs were significantly improved by 45-min EECP intervention. EECP as well as physical training may also activate catecholamines and/or metabolic vasodilator pathways. In addition, a possible mechanism is the reduction of arterial pressure (Armentano et al., 1991).

Picard et al. found that EECP can reduce BP and improve cardiac fitness and arterial stiffness (Picard et al., 2018). By contrast, a study reported that EECP induced the augmentation in cerebral BP in both stroke patients and control (Werner et al., 2003). In the present study, although there was a negative change in RI and EDV in patients with hypertension during EECP, it was a better response immediately after EECP in comparison with baselines in this study. We also found that only in patients with hypertension was RI reduced immediately after EECP. The reduced RI which is strongly associated with cerebrovascular resistance can predict the degree of atherosclerosis (Frauchiger et al., 2001), which is also beneficial to the increase of blood flow.

It showed that the RI reduced immediately after EECP, which was conducive to increasing the perfusion. This finding was consistent with a study that EECP treatment reduces distal brain resistance and increases cerebral perfusion (Lin et al., 2012). A study found that EECP creates an immediate improvement in carotid mean blood flow (Levenson et al., 2007). The other study also found that cerebral blood flow of ischemic stroke patients was increased during EECP, but it does not change in healthy subjects (Lin et al., 2012). Cerebral autoregulation played a part in guaranteeing the constancy of cerebral perfusion during and immediately after EECP (Markus, 2004).

Mean blood flow was significantly elevated in patients with hyperlipidemia during EECP, but it had no significant change immediately after EECP. It was consistent with the findings

TABLE 2 | Hemodynamic variables in the CCAs before, during and immediately after EECP in each group.

Part	Variable	EECP	Hypertension (n = 21)	P-value	Hyperlipidemia (n = 23)	P-value	Type 2 diabetes (n = 18)	P-value	Controls (n = 21)	P-value
RC	ID	Before	0.666 ± 0.061		0.621 ± 0.066	0.019	0.634 ± 0.067		0.625 ± 0.069	
		During	0.663 ± 0.070		0.644 ± 0.060		0.649 ± 0.09		0.624 ± 0.059	
		After	0.660 ± 0.062		0.658 ± 0.048	0.000	0.656 ± 0.085	0.038	0.63 ± 0.074	
	PSV	Before	72.816 ± 14.801		76.216 ± 16.428		72.136 ± 13.955		78.203 ± 16.234	
		During	73.943 ± 14.887		70.34 ± 16.819		70.546 ± 16.256		79.382 ± 19.123	
		After	74.270 ± 18.24		73.729 ± 21.016		69.014 ± 14.323		71.217 ± 16.056	0.019
	EDV	Before	20.077 ± 4.983	0.000	21.321 ± 4.831	0.000	21.2 ± 6.275	0.001	22.94 ± 5.773	0.000
		During	10.276 ± 8.453	0.000	9.39 ± 6.965	0.000	11.852 ± 8.051	0.000	13.905 ± 6.189	0.000
		After	21.708 ± 4.605		21.857 ± 5.847		21.889 ± 6.294		21.895 ± 5.796	
	RI	Before	0.721 ± 0.551	0.000	0.715 ± 0.057	0.000	0.705 ± 0.068	0.000	0.705 ± 0.053	0.000
		During	0.851 ± 0.134	0.000	0.875 ± 0.119	0.000	0.813 ± 0.133	0.000	0.829 ± 0.120	0.000
		After	0.7 ± 0.614	0.039	0.697 ± 0.051		0.686 ± 0.056		0.689 ± 0.059	
	VS/VD	Before	2.099 ± 0.271	0.000	2.05 ± 0.368	0.000	2.165 ± 0.416	0.000	1.987 ± 0.275	0.000
		During	1.506 ± 0.274	0.000	1.39 ± 0.35	0.000	1.459 ± 0.319	0.000	1.541 ± 0.408	0.000
		After	1.99 ± 0.29		2.10 ± 0.316		1.962 ± 0.285	0.026	1.968 ± 0.382	
	FR	Before	700.381 ± 110.343		682.831 ± 148.092		670.356 ± 163.890	0.049	703.709 ± 167.713	
		During	766.445 ± 161.586		732.16 ± 202.638		749.64 ± 225.135		747.538 ± 118.619	0.039
		After	728.576 ± 138.115		736.31 ± 167.714		711.346 ± 195.599		668.411 ± 171.023	
LC	ID	Before	0.626 ± 0.051		0.632 ± 0.05	0.036	0.627 ± 0.076		0.617 ± 0.079	
		During	0.636 ± 0.053		0.647 ± 0.04		0.628 ± 0.073		0.632 ± 0.079	
		After	0.646 ± 0.051	0.027	0.66 ± 0.048	0.001	0.634 ± 0.077		0.629 ± 0.071	
	PSV	Before	76.335 ± 14.528		80.45 ± 18.933		81.023 ± 16.954	0.043	84.29 ± 10.339	0.048
		During	74.483 ± 16.344		77.126 ± 21.259		73.608 ± 21.309		77.997 ± 16.346	
		After	74.699 ± 16.290		78.444 ± 20.471		74.494 ± 10.838	0.022	82.878 ± 15.877	
	EDV	Before	22.415 ± 4.021	0.000	23.486 ± 4.617	0.000	23.055 ± 5.041	0.000	25.867 ± 5.269	0.000
		During	9.797 ± 8.646	0.000	13.463 ± 7.734	0.000	12.876 ± 7.325	0.000	9.424 ± 7.966	0.000
		After	22.974 ± 5.938		23.315 ± 4.666		22.594 ± 5.996		25.217 ± 5.891	
	RI	Before	0.696 ± 0.068	0.000	0.7 ± 0.057	0.000	0.709 ± 0.061	0.000	0.692 ± 0.057	0.000
		During	0.848 ± 0.149	0.000	0.848 ± 0.15	0.000	0.806 ± 0.121	0.000	0.863 ± 0.126	0.000
		After	0.658 ± 0.149	0.044	0.695 ± 0.062		0.696 ± 0.074		0.694 ± 0.052	
	VS/VD	Before	2.049 ± 0.399	0.000	2.167 ± 0.326	0.000	2.144 ± 0.427	0.000	2.076 ± 0.31	0.000
		During	1.469 ± 0.311	0.000	1.398 ± 0.341	0.000	1.493 ± 0.332	0.000	1.51 ± 0.38	0.000
		After	1.99 ± 0.333		2.213 ± 0.568		1.945 ± 0.271	0.047	1.982 ± 0.298	
	FR	Before	673.992 ± 115.073	0.046	745.701 ± 201.169	0.005	714.45 ± 135.201		770.708 ± 202.409	
		During	726.992 ± 141.483		835.49 ± 188.825		733.362 ± 155.955		751.516 ± 188.786	
		After	723.051 ± 138.335		776.145 ± 135.881		711.132 ± 142.346		758.736 ± 177.745	

RC and LC are the right carotid and left carotid arteries, respectively. The letters in the p-value column indicate significant differences between variables measured before and during EECP; between during and after EECP; and between before and immediately after EECP.

of Levenson et al. (2007) showing that EECP increased FR in the carotid artery. The related mechanism was caused by a reduction in the regional vascular resistance which was in turn caused by the tone of the vascular smooth muscle (Lincoln et al., 2001; Rybalkin et al., 2003). The other exploration was shown that EECP may have training effects, such as exercise (Levenson et al., 2007). Moreover, a study reported that regulation of blood flow was related to carotid diameters and blood flow velocity (Levenson et al., 1985). Furthermore, another study found that mean carotid artery blood flow did not change due to the decreased systolic blood flow, although blood flow during diastole was significantly increased during intra-aortic balloon pump (Applebaum et al., 1998).

A study reported that blood flow velocity is associated with the regulation of blood flow (Schmidt-Trucksass et al., 1999). In the present study, PSV was reduced in patients with type 2 diabetes during EECP. However, Werner et al. (2003) reported that cerebral flow velocity in systole was elevated during EECP in both patients and healthy controls. It is attributed to decreased SBP and pronounced vascular autoregulation (Werner et al., 2003). Other studies found that increased carotid circulation was associated with a decrease of arterial stiffness and arterial resistance in the carotid artery, which was decreased by shear stress generated by EECP, arterial pressure, and modulation of smooth muscle (Levenson et al., 2007). A study also suggested that PSV is related to arterial diameters and blood flow, which is used to evaluate atherosclerotic risk factors

TABLE 3 | Differences of Hemodynamic variables in the common carotid artery among four groups before, during and immediately after 45 min-EECP.

Label	Groups	Variables		*P*-value		*P*-value		*P*-value
		RC-ID	**Before**		**During**		**After**	
1	Hypertension (*n* = 21)		0.666 ± 0.061		0.663 ± 0.07		0.66 ± 0.062	
2	Hyperlipidemia (*n* = 23)		0.621 ± 0.066	0.026 (1–2)	0.644 ± 0.06		0.658 ± 0.048	
3	Type 2 diabetes (*n* = 18)		0.634 ± 0.067		0.649 ± 0.09		0.656 ± 0.085	
4	Healthy controls (*n* = 21)		0.625 ± 0.069	0.043 (1–4)	0.624 ± 0.059		0.63 ± 0.074	
		PSV	**Before**		**During**		**After**	
1	Hypertension (*n* = 21)		72.816 ± 14.801		73.943 ± 14.887		74.270 ± 18.24	
2	Hyperlipidemia (*n* = 23)		76.216 ± 16.428		70.34 ± 16.819		73.729 ± 21.016	
3	Type 2 diabetes (*n* = 18)		72.136 ± 13.955		70.546 ± 16.256		69.014 ± 14.323	
4	Healthy controls (*n* = 21)		78.203 ± 16.234		79.382 ± 19.123		71.217 ± 16.056	
		EDV	**Before**		**During**		**After**	
1	Hypertension (*n* = 21)		20.077 ± 4.983		10.276 ± 8.453		21.708 ± 4.605	
2	Hyperlipidemia (*n* = 23)		21.321 ± 4.831		9.39 ± 6.965		21.857 ± 5.847	
3	Type 2 diabetes (*n* = 18)		21.2 ± 6.275		11.852 ± 8.051		21.889 ± 6.294	
4	Healthy controls (*n* = 21)		22.94 ± 5.773		13.905 ± 6.189	0.048 (2–4)	21.895 ± 5.796	
		RI	**Before**		**During**		**After**	
1	Hypertension (*n* = 21)		0.721 ± 0.551		0.851 ± 0.134		0.7 ± 0.614	
2	Hyperlipidemia (*n* = 23)		0.715 ± 0.057		0.875 ± 0.119		0.697 ± 0.051	
3	Type 2 diabetes (*n* = 18)		0.705 ± 0.068		0.813 ± 0.133		0.686 ± 0.056	
4	Healthy controls (*n* = 21)		0.705 ± 0.053		0.829 ± 0.120		0.689 ± 0.059	
		VS/VD	**Before**		**During**		**After**	
1	Hypertension (*n* = 21)		2.099 ± 0.271		1.506 ± 0.274		1.99 ± 0.29	
2	Hyperlipidemia (*n* = 23)		2.05 ± 0.368		1.39 ± 0.35		2.10 ± 0.316	
3	Type 2 diabetes (*n* = 18)		2.165 ± 0.416		1.459 ± 0.319		1.962 ± 0.285	
4	Healthy controls (*n* = 21)		1.987 ± 0.275		1.541 ± 0.408		1.968 ± 0.382	
		FR	**Before**		**During**		**After**	
1	Hypertension (*n* = 21)		700.381 ± 110.343		766.445 ± 161.586		728.576 ± 138.115	
2	Hyperlipidemia (*n* = 23)		682.831 ± 148.092		732.16 ± 202.638		736.31 ± 167.714	
3	Type 2 diabetes (*n* = 18)		670.356 ± 163.890		749.64 ± 225.135		711.346 ± 195.599	
4	Healthy controls (*n* = 21)		703.709 ± 167.713		747.538 ± 118.619		668.411 ± 171.023	
		LC-ID	**Before**		**During**		**After**	
1	Hypertension (*n* = 21)		0.666 ± 0.061		0.663 ± 0.07		0.66 ± 0.062	
2	Hyperlipidemia (*n* = 23)		0.621 ± 0.066		0.644 ± 0.06		0.658 ± 0.048	
3	Type 2 diabetes (*n* = 18)		0.634 ± 0.067		0.649 ± 0.09		0.656 ± 0.085	
4	Healthy controls (*n* = 21)		0.625 ± 0.069		0.624 ± 0.059		0.63 ± 0.074	
		PSV	**Before**		**During**		**After**	
1	Hypertension (*n* = 21)		72.816 ± 14.801		73.943 ± 14.887		74.270 ± 18.24	
2	Hyperlipidemia (*n* = 23)		76.216 ± 16.428		70.34 ± 16.819		73.729 ± 21.016	
3	Type 2 diabetes (*n* = 18)		72.136 ± 13.955		70.546 ± 16.256		69.014 ± 14.323	
4	Healthy controls (*n* = 21)		78.203 ± 16.234		79.382 ± 19.123		71.217 ± 16.056	
		EDV	**Before**		**During**		**After**	
1	Hypertension (*n* = 21)		20.077 ± 4.983		10.276 ± 8.453		21.708 ± 4.605	
2	Hyperlipidemia (*n* = 23)		21.321 ± 4.831		9.39 ± 6.965		21.857 ± 5.847	
3	Type 2 diabetes (*n* = 18)		21.2 ± 6.275		11.852 ± 8.051		21.889 ± 6.294	
4	Healthy controls (*n* = 21)		22.94 ± 5.773	0.021 (1–4)	13.905 ± 6.189		21.895 ± 5.796	

(Continued)

TABLE 3 | Continued

Label	Groups	Variables		*P*-value		*P*-value	*P*-value
		RI	**Before**		**During**	**After**	
1	Hypertension (*n* = 21)		0.721 ± 0.551		0.851 ± 0.134	0.7 ± 0.614	
2	Hyperlipidemia (*n* = 23)		0.715 ± 0.057		0.875 ± 0.119	0.697 ± 0.051	
3	Type 2 diabetes (*n* = 18)		0.705 ± 0.068		0.813 ± 0.133	0.686 ± 0.056	
4	Healthy controls (*n* = 21)		0.705 ± 0.053		0.829 ± 0.120	0.689 ± 0.059	
		VS/VD	**Before**		**During**	**After**	
1	Hypertension (*n* = 21)		2.099 ± 0.271		1.506 ± 0.274	1.99 ± 0.29	
2	Hyperlipidemia (*n* = 23)		2.05 ± 0.368		1.39 ± 0.35	2.10 ± 0.316	
3	Type 2 diabetes (*n* = 18)		2.165 ± 0.416		1.459 ± 0.319	1.962 ± 0.285	0.034 (2–3)
4	Healthy controls (*n* = 21)		1.987 ± 0.275		1.541 ± 0.408	1.968 ± 0.382	
		FR	**Before**		**During**	**After**	
1	Hypertension (*n* = 21)		700.381 ± 110.343		766.445 ± 161.586	728.576 ± 138.115	
2	Hyperlipidemia (*n* = 23)		682.831 ± 148.092		732.16 ± 202.638	0.039 (1–2) 736.31 ± 167.714	
3	Type 2 diabetes (*n* = 18)		670.356 ± 163.890		749.64 ± 225.135	711.346 ± 195.599	
4	Healthy controls (*n* = 21)		703.709 ± 167.713		747.538 ± 118.619	668.411 ± 171.023	

RC, LC, RB, and RF are the right carotid, left carotid, brachial and femoral arteries, respectively.
PSV, peak systolic velocity; ID, mean inner diameter; FR, mean flow rate; EDV, end-diastolic velocity; RI, resistance index.

(Schmidt-Trucksass et al., 1999). In our study, the decreased PSV in healthy subjects during EECP may be caused by a better vascular function response.

Meanwhile, the response of PSV in patients with diabetes influenced the change in the VS/VD during and immediately after EECP. EECP creates an acute reduction in VS (PSV)/VD in patients with type 2 diabetes. During EECP, the counterpulsation wave of EECP treatment was superposed in VD, resulting in the change of VS/VD. Few studies have reported on VS/VD in patients with diabetes during EECP. Martin et al. (2013) found that EECP improved the microvascular function in subjects with abnormal glucose tolerance. Blood flow velocity in diastole of the brachial artery is increased by 132%, which led to the increase in brachial artery wall shear stress (WSS) (Zhang et al., 2007). The acute increase of WSS can cause the production of NO, which plays a critical role in vessel relaxation, while chronic NO production because the increased laminal shear stress may serve as an anti-inflammatory and antiatherogenic molecule (Klein-Nulend et al., 1998). Moreover, eNOS, which is regarded as a rate-limiting enzyme essential for NO synthesis and with shear stress-responsive elements in its gene promotor region, may serve as a mechanosensory coupling NO release to hemodynamic responses (Rudic et al., 1998).

Some limitations of the present study should be emphasized. Firstly, the sample size of each group is relatively small. Secondly, we just measure the blood flow data of carotid Doppler ultrasound, which are closely related to cardiovascular events. Thirdly, in order to explore the acute responses of hemodynamics, carotid hemodynamic parameters during and immediately EECP are analyzed in this study. Our results need to be further verified for long-term EECP treatment (36-h EECP intervention).

CONCLUSION

EECP created an acute reduction in EDV and VS/VD and an immediate increase in the RI of CCAs among the four groups examined in this study. In addition, the ID of CCAs and FR of the left CCA were increased in patients with hyperlipidemia during EECP. PSV of the left CCA was reduced in patients with type 2 diabetes. Moreover, a single 45-min EECP intervention produces immediate improvement on the ID of patients with hyperlipidemia, RI of patients with hypertension, and PSV and VS/VD of patients with type 2 diabetes. These findings indicate that the different hemodynamic parameters induced by EECP are highlighted in different patients. Moreover, EECP can regulate the vascular and blood flow characteristics of carotid arteries and further improve the carotid function in patients with high cardiovascular risk factors.

DATA AVAILABILITY STATEMENT

The original contributions presented in the study are included in the article/supplementary material, further inquiries can be directed to the corresponding author/s.

ETHICS STATEMENT

The studies involving human participants were reviewed and approved by the Eighth Affiliated Hospital of Sun Yat-sen University. The patients/participants provided their written informed consent to participate in this study. Written informed consent was obtained from the individual(s) for the publication of any potentially identifiable images or data included in this article.

AUTHOR CONTRIBUTIONS

YZ and GW proposed the scientific problems. YZ, GW, and JD designed the experiments. YZ, ZM, CY, and WZ collected the experimental data. YZ and ZM processed and calculated the data. YZ conducted the statistical analysis and wrote the draft manuscript. JD, XZ, HH, and GW contributed to the revision and final version of the manuscript. All authors contributed to the article and approved the submitted version.

FUNDING

This work was, in part, supported by the National Natural Science Foundation of China (Grant Nos. 819770367, 81670417, 81500361, and 81370389), the National Key Research and Development Program of China (No. 2020YFC2004400), and an Open Grant by National Health Commission Key Laboratory of Assisted Circulation (Sun Yat-sen University) (No. cvclab201901).

REFERENCES

Applebaum, R. M., Wun, H. H., Katz, E. S., Tunick, P. A., and Kronzon, I. (1998). Effects of intraaortic balloon counterpulsation on carotid artery blood flow. *Am. Heart J.* 135(Pt 1), 850–854. doi: 10.1016/s0002-8703(98)70045-6

Armentano, R., Simon, A., Levenson, J., Chau, N. P., Megnien, J. L., and Pichel, R. (1991). Mechanical pressure versus intrinsic effects of hypertension on large arteries in humans. *Hypertension* 18, 657–664. doi: 10.1161/01.hyp.18.5.657

Bai, C. H., Chen, J. R., Chiu, H. C., and Pan, W. H. (2007). Lower blood flow velocity, higher resistance index, and larger diameter of extracranial carotid arteries are associated with ischemic stroke independently of carotid atherosclerosis and cardiovascular risk factors. *J. Clin. Ultrasound* 35, 322–330. doi: 10.1002/jcu.20351

Bondesson, S., Pettersson, T., Ohlsson, O., Hallberg, I. R., Wackenfors, A., and Edvinsson, L. (2010). Effects on blood pressure in patients with refractory angina pectoris after enhanced external counterpulsation. *Blood Press.* 19, 287–294. doi: 10.3109/08037051003794375

Braith, R. W., Conti, C. R., Nichols, W. W., Choi, C. Y., Khuddus, M. A., Beck, D. T., et al. (2010). Enhanced external counterpulsation improves peripheral artery flow-mediated dilation in patients with chronic angina: a randomized sham-controlled study. *Circulation* 122, 1612–1620. doi: 10.1161/circulationaha.109.923482

Chuang, S. Y., Bai, C. H., Cheng, H. M., Chen, J. R., Yeh, W. T., Hsu, P. F., et al. (2016). Common carotid artery end-diastolic velocity is independently associated with future cardiovascular events. *Eur. J. Prev. Cardiol.* 23, 116–124. doi: 10.1177/2047487315571888

Dockery, F., Rajkumar, C., Bulpitt, C. J., Hall, R. J., and Bagger, J. P. (2004). Enhanced external counterpulsation does not alter arterial stiffness in patients with angina. *Clin. Cardiol.* 27, 689–692. doi: 10.1002/clc.4960271206

Frauchiger, B., Schmid, H. P., Roedel, C., Moosmann, P., and Staub, D. (2001). Comparison of carotid arterial resistive indices with intima-media thickness as sonographic markers of atherosclerosis. *Stroke* 32, 836–841. doi: 10.1161/01.str.32.4.836

Gloekler, S., Meier, P., de Marchi, S. F., Rutz, T., Traupe, T., Rimoldi, S. F., et al. (2010). Coronary collateral growth by external counterpulsation: a randomised controlled trial. *Heart* 96, 202–207. doi: 10.1136/hrt.2009.184507

Gurovich, A. N., and Braith, R. W. (2013). Enhanced external counterpulsation creates acute blood flow patterns responsible for improved flow-mediated dilation in humans. *Hypertens Res* 36, 297–305. doi: 10.1038/hr.2012.169

Kallikazaros, I., Tsioufis, C., Sideris, S., Stefanadis, C., and Toutouzas, P. (1999). Carotid artery disease as a marker for the presence of severe coronary artery disease in patients evaluated for chest pain. *Stroke* 30, 1002–1007. doi: 10.1161/01.str.30.5.1002

Klein-Nulend, J., Helfrich, M. H., Sterck, J. G. H., MacPherson, H., Joldersma, M., Ralston, S. H., et al. (1998). Nitric oxide response to shear stress by human bone cell cultures is endothelial nitric oxide synthase dependent. *Biochem. Biophys. Res. Commun.* 250, 108–114. doi: 10.1006/bbrc.1998.9270

Lee, S. W., Hai, J. J., Kong, S. L., Lam, Y. M., Lam, S., Chan, P. H., et al. (2011). Side differences of carotid intima-media thickness in predicting cardiovascular events among patients with coronary artery disease. *Angiology* 62, 231–236. doi: 10.1177/0003319710379109

Levenson, J., Simon, A., Megnien, J. L., Chironi, G., Gariepy, J., Pernollet, M. G., et al. (2007). Effects of enhanced external counterpulsation on carotid circulation in patients with coronary artery disease. *Cardiology* 108, 104–110. doi: 10.1159/000095949

Levenson, J. A., Simon, A. C., and Safar, M. E. (1985). Vasodilatation of small and large arteries in hypertension. *J. Cardiovasc. Pharmacol.* 7(Suppl. 2), S115–S120.

Lin, W., Xiong, L., Han, J., Leung, T. W., Soo, Y. O., Chen, X., et al. (2012). External counterpulsation augments blood pressure and cerebral flow velocities in ischemic stroke patients with cerebral intracranial large artery occlusive disease. *Stroke* 43, 3007–3011. doi: 10.1161/strokeaha.112.659144

Lincoln, T. M., Dey, N., and Sellak, H. (2001). Invited review: cGMP-dependent protein kinase signaling mechanisms in smooth muscle: from the regulation of tone to gene expression. *J. Appl. Physiol. (1985)* 91, 1421–1430. doi: 10.1152/jappl.2001.91.3.1421

Liu, H. B., Yuan, W. X., Qin, K. R., and Hou, J. (2015). Acute effect of cycling intervention on carotid arterial hemodynamics: basketball athletes versus sedentary controls. *Biomed. Eng. Online* 14(Suppl. 1):S17.

Loizou, C. P., Nicolaides, A., Kyriacou, E., Georghiou, N., Griffin, M., and Pattichis, C. S. (2015). A comparison of ultrasound intima-media thickness measurements of the left and right common carotid artery. *IEEE J. Transl. Eng. Health Med.* 3:1900410. doi: 10.1109/jtehm.2015.2450735

Markus, H. S. (2004). Cerebral perfusion and stroke. *J. Neurol. Neurosurg. Psychiatry* 75, 353–361. doi: 10.1136/jnnp.2003.025825

Martin, J. S., Beck, D. T., and Braith, R. W. (2013). Peripheral resistance artery blood flow in subjects with abnormal glucose tolerance is improved following enhanced external counterpulsation therapy. *Appl. Physiol. Nutr. Metab.* 39, 596–599. doi: 10.1139/apnm-2013-0497

Masuda, D., Nohara, R., Hirai, T., Kataoka, K., Chen, L., Hosokawa, R., et al. (2001). Enhanced external counterpulsation improved myocardial perfusion and coronary flow reserve in patients with chronic stable angina. Evaluation by13N-ammonia positron emission tomography. *Eur. Heart J.* 22, 1451–1458. doi: 10.1053/euhj.2000.2545

Michaels, A. D. (2002). Left ventricular systolic unloading and augmentation of intracoronary pressure and doppler flow during enhanced external counterpulsation. *Circulation* 106, 1237–1242. doi: 10.1161/01.cir.0000028336.95629.b0

Nichols, W. W., Estrada, J. C., Braith, R. W., Owens, K., and Conti, C. R. (2006). Enhanced external counterpulsation treatment improves arterial wall properties and wave reflection characteristics in patients with refractory angina. *J. Am. Coll. Cardiol.* 48, 1208–1214. doi: 10.1016/j.jacc.2006.04.094

Ozari, H. O., Oktenli, C., Celik, S., Tangi, F., Ipcioglu, O., Terekeci, H. M., et al. (2012). Are increased carotid artery pulsatility and resistance indexes early signs of vascular abnormalities in young obese males? *J. Clin. Ultrasound* 40, 335–340. doi: 10.1002/jcu.21927

Picard, F., Panagiotidou, P., Wolf-Pütz, A., Buschmann, I., Buschmann, E., Steffen, M., et al. (2018). Usefulness of individual shear rate therapy, new treatment option for patients with symptomatic coronary artery disease. *Am. J. Cardiol.* 121, 416–422. doi: 10.1016/j.amjcard.2017.11.004

Rudic, R. D., Shesely, E. G., Maeda, N., Smithies, O., Segal, S. S., and Sessa, W. C. (1998). Direct evidence for the importance of endothelium-derived nitric oxide in vascular remodeling. *J. Clin. Invest.* 101, 731–736. doi: 10.1172/jci1699

Rybalkin, S. D., Yan, C., Bornfeldt, K. E., and Beavo, J. A. (2003). Cyclic GMP phosphodiesterases and regulation of smooth muscle function. *Circ. Res.* 93, 280–291. doi: 10.1161/01.res.0000087541.15600.2b

Sardina, P. D., Martin, J. S., Dzieza, W. K., and Braith, R. W. (2016). Enhanced external counterpulsation (EECP) decreases advanced glycation end products

and proinflammatory cytokines in patients with non-insulin-dependent type II diabetes mellitus for up to 6 months following treatment. *Acta Diabetol.* 53, 753–760. doi: 10.1007/s00592-016-0869-6

Schmidt-Trucksass, A., Grathwohl, D., Schmid, A., Boragk, R., Upmeier, C., Keul, J., et al. (1999). Structural, functional, and hemodynamic changes of the common carotid artery with age in male subjects. *Arterioscler. Thromb. Vasc. Biol.* 19, 1091–1097. doi: 10.1161/01.atv.19.4.1091

Sedaghat, S., van Sloten, T. T., Laurent, S., London, G. M., Pannier, B., Kavousi, M., et al. (2018). Common carotid artery diameter and risk of cardiovascular events and mortality: pooled analyses of four cohort studies. *Hypertension* 72, 85–92. doi: 10.1161/hypertensionaha.118.11253

Werner, D., Marthol, H., Brown, C. M., Daniel, W. G., and Hilz, M. J. (2003). Changes of cerebral blood flow velocities during enhanced external counterpulsation. *Acta Neurol. Scand.* 107, 405–411. doi: 10.1034/j.1600-0404.2003.00074.x

Zhang, Y., He, X., Chen, X., Ma, H., Liu, D., Luo, J., et al. (2007). Enhanced external counterpulsation inhibits intimal hyperplasia by modifying shear stress responsive gene expression in hypercholesterolemic pigs. *Circulation* 116, 526–534. doi: 10.1161/circulationaha.106.647248

Zhang, Y., Jiang, Z., Qi, L., Xu, L., Sun, X., Chu, X., et al. (2018). Evaluation of cardiorespiratory function during cardiopulmonary exercise test in untreated hypertensive and healthy subjects. *Front. Physiol.* 9:1590. doi: 10.3389/fphys.2018.01590

Conflict of Interest: The authors declare that the research was conducted in the absence of any commercial or financial relationships that could be construed as a potential conflict of interest.

frontiers in Cardiovascular Medicine

ORIGINAL RESEARCH
published: 17 June 2021
doi: 10.3389/fcvm.2021.637437

Birth Weight and Adult Obesity Index in Relation to the Risk of Hypertension: A Prospective Cohort Study in the UK Biobank

Yi Zhang[1†], Jingjia Liang[1†], Qian Liu[1†], Xikang Fan[2], Cheng Xu[1], Aihua Gu[1‡], Wei Zhao[3*‡] and Dong Hang[2*‡]*

[1] State Key Laboratory of Reproductive Medicine, Institute of Toxicology, Nanjing Medical University, Nanjing, China, [2] Department of Epidemiology and Biostatistics, Jiangsu Key Lab of Cancer Biomarkers, Prevention and Treatment, Collaborative Innovation Center for Cancer Personalized Medicine, School of Public Health, Nanjing Medical University, Nanjing, China, [3] Jinling Hospital Department of Reproductive Medical Center affiliated School of Medicine, Nanjing University, Nanjing, China

Objectives: To investigate the association between birth weight and the risk of hypertension, and to examine the interaction between birth weight and the adult obesity index.

Methods: We included 199,893 participants who had birth weight data and no history of hypertension at baseline (2006–2010) from the UK Biobank. A multivariate cubic regression spline was used to visually explore the dose-response relationship. Multivariate Cox proportional hazard regression models were used to calculate hazard ratios (HRs) and 95% confidence intervals (CIs).

Results: We observed a nonlinear inverse association between birth weight and hypertension. The risk for hypertension decreased as birth weight increased up to approximately 3.80 kg. Compared with the participants with the fourth quintile of birth weight (3.43–3.80 kg), those with the first quartile of birth weight (<2.88 kg) were associated with a 25% higher risk of hypertension [HR 1.25; 95% CI (1.18–1.32)]. In addition, the participants with birth weight <2.88 kg and body mass index ≥30 kg/m^2 had the highest risk [HR 3.54; 95% CI (3.16–3.97); p for interaction <0.0001], as compared with those with birth weight between 3.43–3.80 kg and body mass index between 18.5–25.0 kg/m^2. These associations were largely consistent in the stratified and sensitivity analyses.

Conclusion: Our findings indicate that lower birth weight is nonlinearly correlated with higher risk of hypertension, and birth weight between 3.43–3.80 kg might represent an intervention threshold. Moreover, lower birth weight may interact with adult obesity to significantly increase hypertension risk.

Keywords: birth weight, adult obesity index, hypertension, blood pressure, epidemiology, prospective study

OPEN ACCESS

Edited by:
Soo-Kyoung Choi, Yonsei University College of Medicine, South Korea

Reviewed by:
Jane A. Leopold, Brigham and Women's Hospital and Harvard Medical School, United States
Elise Peery Gomez-Sanchez, University of Mississippi Medical Center, United States

***Correspondence:**
Dong Hang
hangdong@njmu.edu.cn
Wei Zhao
zhaowei0714@nicemice.cn
Aihua Gu
aihuagu@njmu.edu.cn

[†] These authors have contributed equally to this work and share first authorship

[‡] These authors have contributed equally to this work and share last authorship

Specialty section:
This article was submitted to Hypertension, a section of the journal Frontiers in Cardiovascular Medicine

Received: *03 December 2020*
Accepted: *12 May 2021*
Published: *17 June 2021*

Citation:
Zhang Y, Liang J, Liu Q, Fan X, Xu C, Gu A, Zhao W and Hang D (2021) Birth Weight and Adult Obesity Index in Relation to the Risk of Hypertension: A Prospective Cohort Study in the UK Biobank. Front. Cardiovasc. Med. 8:637437. doi: 10.3389/fcvm.2021.637437

INTRODUCTION

Fetal malnutrition, the primary indicator of which is low birth weight, can permanently alter organ structure and function in a way that predisposes the offspring to cardiovascular disease (CVD) in adulthood (1, 2). Growing evidence has suggested that low birth weight increases the risk of hypertension (3–5).

Although some epidemiological studies have suggested a nonlinear inverse association between birth weight and hypertension (6–9), the intervention threshold of birth weight for hypertension remains undetermined. A previous meta-analysis including 4,335,149 participants suggested that those with birth weight of 4.0–4.5 kg had the lowest risk (10). However, the meta-analysis contained significant heterogeneity that limited the validity of summary estimates, and the ability to control for potential confounders (e.g., maternal smoking) was insufficient. In addition, previous results are mixed regarding the association between high birth weight and hypertension risk. Some studies reported higher birth weight in relation to increased hypertension risk (11–13), whereas other studies did not find such an association (14, 15). These conflicting results might be attributed to the differences in sample sizes and confounder adjustments (13). Furthermore, low birth weight and obesity in adulthood can both stimulate the sympathetic nervous system and alter renal function (16, 17). Few studies have examined potential interaction between birth weight and the adult obesity index on hypertension risk, although there is evidence showing an effect on CVD risk (18, 19).

Therefore, for the current study we used data from the UK Biobank, a large prospective cohort study conducted in UK, to investigate the dose-response association of birth weight with hypertension and blood pressure. Moreover, we examined potential interactions between birth weight and the adult obesity index.

METHODS AND MATERIALS

Study Population

The UK Biobank is a prospective cohort study recruiting half a million participants aged 37–73 years between 2006 and 2010 (20). At baseline, participants were asked to provide electronically signed consent, answer touch-screen questionnaires, and complete physical and anthropometric measurements. Follow-up with the UK Biobank was performed on an ongoing basis through study visits and linkage to national health records, death registers, and primary care records, as described previously (21). The UK Biobank has received ethical approvals from the UK Biobank Research Ethics Committee and Human Tissue Authority.

In the current study, we excluded participants who self-reported a history of hypertension or were taking antihypertensive medication at baseline (n = 147,989). We further excluded 151,078 individuals with missing birth weight data and 3,661 individuals with missing values on the main covariables. Finally, a total of 199,893 participants were included (**Supplementary Figure 1**). The basic characteristics of the excluded participants were similar to those included (**Supplementary Table 1**).

Abbreviations: BMI, body mass index; CVD, cardiovascular disease; WHR, waist-to-hip ratio; SBP, systolic blood pressure; DBP, diastolic blood pressure; LRT, likelihood ratio test; MET, metabolic equivalent of task; SD, standard deviation; HR, hazard ratio; CI, confidence interval; Ref, reference; NA, not applicable.

Birth Weight and Physical Measurements

Participants were asked to report their own birth weight (either in kilograms directly, or in imperial pounds and ounces). Standing height was measured using a Seca202 device. Body mass index (BMI) was defined as weight divided by height squared (m^2). Waist and hip circumferences were measured with a Seca200 measuring tape using standard procedures, and waist-to-hip ratio (WHR) was the ratio of waist circumference to hip circumference.

Systolic blood pressure (SBP) and diastolic blood pressure (DBP) measurements were taken in a seated position after a few minutes of rest using an Omron 705 IT electronic blood pressure monitor. A manual sphygmometer was used if the standard automated device could not be employed. Further details of these measurements can be found in the UK Biobank online protocol (https://biobank.ndph.ox.ac.uk/showcase/showcase/docs/Bloodpressure.pdf" https://biobank.ndph.ox.ac.uk/showcase/showcase/docs/Bloodpressure.pdf). Means of SBP and DBP from two automated or two manual blood pressure measurements were calculated.

Assessment of Hypertension

The date and cause of hospital admissions were confirmed by electronic health records linkage to health episode statistics (England and Wales) and Scottish morbidity records (Scotland). Date of death was obtained from death certificates held by the National Health Service Information Center (England and Wales) and the National Health Service Central Register Scotland (Scotland) (22). The primary outcome was incident hypertension, which was defined according to the International Classification of Diseases edition 10 (ICD-10) codes I10-I15.

Statistical Analysis

Person-time of follow-up was calculated for each participant from the age in months at the return date of the baseline questionnaire (2006–2010) until the age in months at the date of first diagnosis of hypertension or the end of follow-up (November 30, 2016, in Edinburgh, Scotland, and January 31, 2018, in England or Wales), whichever came first. Cox proportional hazards regression models with age as the time scale were used to analyze the association between birth weight and hypertension, reporting hazard ratio (HR) and 95% confidence intervals (CI).

A multivariate restricted cubic spline with four knots was used to visually explore the nonlinear association of birth weight with hypertension. We used a likelihood ratio test (LRT) to compare the model with only the linear term of birth weight to the model with both the linear and the cubic spline terms, with a p-value <0.05 denoting significant nonlinearity.

In the multivariate analysis of hypertension, we adjusted for age, sex, and early life events, including maternal smoking, breastfeeding, part of a multiple birth, and birthplace (Model 1). We also further adjusted for the Townsend deprivation index, college or university degree, BMI, summed metabolic equivalent of task hours per week (MET-hours/week) for physical activity, smoking status, alcohol intake frequency, intake of vegetables and fruit, family history of hypertension, and prevalence of diabetes (Model 2). Multivariate linear regression analysis was conducted to examine the associations between birth weight and SBP and DBP separately (n = 199,765). Birth weight was treated as a categorical (the quintiles) or continuous (per SD increment) variable.

Stratified analyses were conducted according to sex (male, female), maternal smoking (yes, no), breastfeeding (yes, no), physical activity (<median, ≥median), and smoking status (never, former, current). We tested the interaction between birth weight and each of the stratification variables using LRT, comparing a model with and without interaction terms.

In the joint analysis of birth weight and BMI, the fourth quintile of birth weight (3.43–3.80 kg) and BMI in adulthood between 18.5–25.0 kg/m^2 was treated as the reference group. P for interaction was assessed by a Wald test for the cross-product terms between birth weight and BMI (continuous). Sensitivity analyses were performed by excluding individuals who were part of multiple births (n = 5,431).

All statistical tests were two-sided, and SAS version 9.4 (SAS Institute) was used for all analyses. P <0.05 was defined as statistically significant.

RESULTS

During a median follow-up of 8.8 (interquartile range: 8.1–9.4) years, 12,333 hypertension events occurred among 199,893 participants. The basic characteristics of participants according to the quintile of birth weight are shown in **Table 1.** Those with lower birth weight were more likely to be part of a multiple birth and exposed to maternal smoking around birth, and were less likely to be breastfed.

A nonlinear inverse association between birth weight and hypertension is observed in **Figure 1**. The risk of hypertension decreased as birth weight increased up to approximately 3.80 kg (p for nonlinearity = 0.0004).

In the fully adjusted models, compared with the fourth quintile of birth weight (3.43–3.80 kg), the first quartile (<2.88 kg) was associated with a 25% higher risk of hypertension [HR 1.25; 95% CI (1.18–1.32)] (**Table 2**).

Table 3 shows the association between birth weight and blood pressure. A unit increase per SD increment in birth weight was associated with lower SBP [β coefficient = −1.07; 95% CI (−1.14 to −1.00)] and lower DBP [β coefficient = −0.47; 95% CI (−0.51 to −0.44)].

In the stratified analysis (**Supplementary Figure 2**), the association between birth weight and hypertension was largely consistent across subgroups, except that the association was stronger in females (p for interaction = 0.004).

A multiplicative interaction between birth weight and obesity index was observed in the joint analysis for birth weight and adult BMI in relation to hypertension risk (**Figure 2**). Compared with the reference group (birth weight between 3.43–3.80 kg and BMI between 18.5–25 kg/m^2), participants with low birth weight and adult obesity (birth weight <2.88 kg and BMI ≥30 kg/m^2) had the highest risk of hypertension [HR 3.54; 95% CI (3.16, 3.97); p for interaction <0.0001]. A similar pattern of correlations was observed between birth weight, WHR, and hypertension (**Supplementary Figure 3**).

Sensitivity analysis by excluding 5,431 participants who were part of a multiple birth showed similar associations between birth weight and hypertension (**Supplementary Table 2**).

DISCUSSION

In this large prospective cohort study, we observed a nonlinear association between birth weight and hypertension risk. Moreover, we observed a multiplicative interaction between birth weight and obesity index, and participants with low birth weight and adult obesity had the highest risk of hypertension.

Most previous studies investigating the association between birth weight and hypertension risk were based on predefined categories of birth weight. The lowest risk for hypertension was observed in different ranges of birth weight, such as 2.5–3.5 kg, ≥4.5 kg, 4.0–4.5 kg, and ≥4.0 kg (5, 6, 10, 23). A multivariate restricted cubic spline can display more information than the categorical data, and in the current study a nonlinear inverse association was found between birth weight and hypertension. The risk of hypertension decreased as birth weight increased, up to approximately 3.80 kg. Our data indicated that higher birth weight did not increase the hypertension risk, in line with the results from previous studies (14, 24). The World Health Organization defined low birth weight as <2.50 kg (25). The cutoff was based on epidemiological observations that infants with birth weight <2.50 kg had a higher mortality risk than ≥2.50 kg (26). Nevertheless, it may not be the optimal target for mitigating the increasing epidemic of hypertension. Our findings suggested that birth weight between 3.43–3.80 kg might represent a potential threshold for reducing hypertension risk.

Epidemiological evidence has shown an association between low birth weight and obesity in adulthood (27). Consistently, we found that individuals with lower birth weight were more likely to have a higher BMI or waist-to-hip ratio in the UK biobank (data not shown). When we adjust for potential confounders, including BMI or waist-to-hip ratio, the association between birth weight and hypertension remained stable. We also found an inverse association between birth weight and blood pressure, in line with the results from previous observational studies (3, 28, 29). Furthermore, a Mendelian randomization study, which took advantage of genetic variants as instrumental variables for birth weight, supported an inverse association between birth weight and blood pressure (30). However, several studies reported that birth weight was inversely associated with SBP only (31, 32). This might be attributed to the limited statistical power of these studies to identify the relatively small effects of birth weight on

TABLE 1 | Basic characteristics of study participants according to birth weight.

Characteristics	Birth weight quintiles				
	Q1 (<2.88kg)	Q2 (2.88–3.18kg)	Q3 (3.19–3.42kg)	Q4 (3.43-3.80 kg)	Q5 (>3.80 kg)
Participants, No. (%)	39,042 (19.53)	43,780 (21.90)	36,948 (18.48)	40,493 (20.26)	39,630 (19.83)
Perinatal					
Female, No. (%)	28,740 (73.61)	29,709 (67.86)	23,790 (64.39)	23,623 (58.34)	20,757 (52.38)
White, No. (%)	37,252 (95.70)	42,165 (96.56)	36,104 (97.92)	39,399 (97.52)	38,674 (97.80)
Part of a multiple birth, No. (%)	3,880 (9.95)	806 (1.84)	366 (0.99)	228 (0.56)	151 (0.38)
Breastfeeding, No. (%)	20,987 (60.98)	27,614 (69.76)	24,015 (70.23)	26,538 (71.44)	25,581 (72.49)
Maternal smoking around birth, No. (%)	11,988 (34.32)	11,577 (29.33)	9,167 (27.43)	9,260 (25.26)	8,843 (24.83)
Baseline					
Age, mean (SD), year	54.32 (8.09)	54.32 (8.13)	53.71 (7.87)	53.30 (7.96)	54.41 (8.13)
Townsend deprivation index <0, No. (%)	28,312 (72.52)	32,683 (74.65)	27,611 (74.73)	30,302 (74.83)	29,517 (74.48)
BMI, mean (SD), kg/m^2	26.39 (4.57)	26.25 (4.35)	26.39 (4.34)	26.60 (4.40)	27.06 (4.49)
Physical activity, mean (SD), MET-hours/week	44.85 (44.71)	44.62 (44.09)	44.57 (44.23)	44.26 (44.52)	45.79 (46.00)
Current smoking, No. (%)	3,985 (10.24)	4,246 (9.72)	3,875 (10.52)	4,116 (10.19)	4,325 (10.95)
Alcohol intake daily or almost daily, No. (%)	6,291 (16.12)	8,360 (19.11)	7,313 (19.81)	8,157 (20.16)	8,421 (21.26)
Family history of hypertension, No. (%)	19,139 (52.42)	21,099 (51.13)	18,251 (52.08)	19,469 (50.89)	18,341 (49.40)
Vegetable intake, mean (SD), serving/day	2.25 (2.13)	2.23 (2.14)	2.24 (2.09)	2.23 (2.08)	2.23 (2.21)
Fruit intake, mean (SD), serving/day	2.24 (1.57)	2.23 (1.51)	2.24 (1.53)	2.23 (1.54)	2.25 (1.57)
DBP, mean (SD), mmHg	80.89 (9.74)	80.52 (9.68)	80.57 (9.60)	80.50 (9.60)	80.73 (9.57)
SBP, mean (SD), mmHg	134.32 (17.94)	133.48 (17.60)	132.89 (17.06)	132.42 (17.01)	133.24 (16.93)

BMI, body mass index (calculated as weight in kilograms divided by height in meters squared); MET, metabolic equivalent of task; DBP, diastolic blood pressure; SBP, systolic blood pressure; SD, standard deviation.

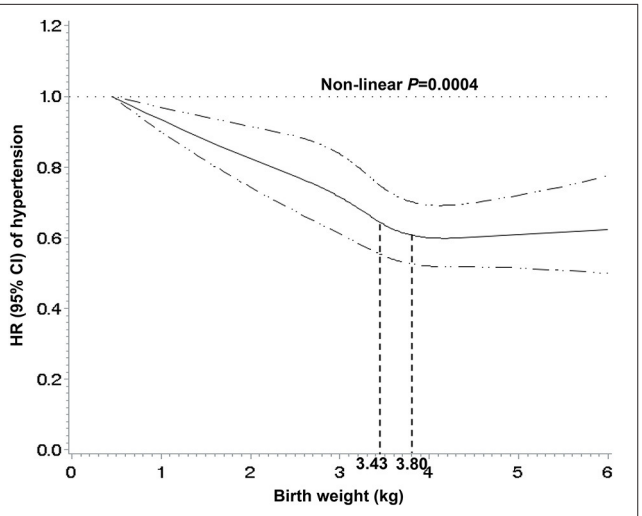

FIGURE 1 | Nonlinear associations between birth weight and risk of hypertension. The associations were examined by multivariate Cox regression models based on restricted cubic splines. Participants with birth weight >6 kg were not included (n = 147). Solid line represents estimates of hazard ratios and dashed line represents 95% confidence intervals.

DBP (31). The current study confirmed that the magnitude of the association for DBP was smaller than that for SBP.

Joint analysis indicated that participants with low birth weight and adult obesity had the highest risk of hypertension. Consistently, previous studies have shown that low-birth-weight children with obesity now tend to have higher values of systolic blood pressure than those who are obese with normal birth weight (33, 34). It is plausible that individuals with an abnormal intrauterine environment (such as poor nutrition) are more sensitive to the adverse effects of adult obesity on hypertension risk. Our study is the first to suggest that low birth weight might interact with adult obesity to increase hypertension risk in adult life. Targeting interventions and prevention of obesity, especially for those with low birth weight, might be given high priority.

Biological mechanisms by which low birth weight affects the development of hypertension are complex and remain equivocal. The proposed mechanisms are mostly related to reduced nephron counts, sympathetic hyperactivity, and impairment of vascular structure and function (17). In addition, intrauterine growth restriction may lead to impaired function of the hypothalamic-pituitary-adrenal axis and increased activity of renin angiotensin aldosterone system, thereby elevating the risk for hypertension (35, 36). Animal studies have also found that fetal exposure to maternal protein restriction lead to an increase in renal inflammation, indicating an important role of inflammatory processes caused by low birth weight in the development of hypertension (37).

STRENGTHS AND LIMITATIONS OF THE STUDY

Our study has several strengths, including a large sample size, long-term follow-up, and strict adjustment for potential confounders. We also estimated the joint effects of birth weight

TABLE 2 | Associations between birth weight and hypertension.

Hypertension	Birth weight quintiles, HR (95% CI)					*P* for non-linearity
	Q1 (< 2.88 kg)	Q2 (2.88–3.18 kg)	Q3 (3.19–3.42 kg)	Q4 (3.43–3.80 kg)	Q5 (> 3.80 kg)	
No. of cases/ person years	2,803/332,781.46	2,729/374,124.06	2,115/317,483.58	2,247/347,241.82	2,439/339,481.78	NA
Model 1[a]	1.27 (1.20–1.35)	1.08 (1.02–1.15)	1.03 (0.97–1.09)	Ref (1)	1.00 (0.94–1.06)	< 0.0001
Model 2[b]	1.25 (1.18–1.32)	1.11 (1.05–1.17)	1.04 (0.98–1.11)	Ref (1)	0.95 (0.9–1.01)	0.0004

HR, hazard ratio; CI, confidence interval; Ref, reference; NA, not applicable.
[a]Model 1: adjusted for age, sex, maternal smoking, breastfeeding, birth place, part of a multiple birth.
[b]Model 2: model 1 plus Townsend deprivation index, college or university degree, body mass index, physical activity (MET-hours/week), smoking status, alcohol intake frequency, intake of vegetables and fruit, family history of hypertension, prevalent diabetes.

TABLE 3 | Associations between birth weight and blood pressure.

Blood pressure	Birth weight quintiles, β coefficient (95% CI)					Per SD increase β coefficient (95% CI)
	Q1 (< 2.88 kg)	Q2 (2.88–3.18 kg)	Q3 (3.19–3.42 kg)	Q4 (3.43–3.80 kg)	Q5 (> 3.80 kg)	
No. (%)	39,005 (19.53)	43,754 (21.90)	36,923 (18.48)	40,468 (20.26)	39,615 (19.83)	NA
SBP						
Model 1[a]	2.27 (2.04 to 2.49)	1.03 (0.81 to 1.24)	0.62 (0.39 to 0.85)	Ref (0)	−0.4 (−0.62 to −0.18)	−0.93 (−1.01 to −0.86)
Model 2[b]	2.36 (2.14 to 2.58)	1.23 (1.01 to 1.44)	0.72 (0.5 to 0.94)	Ref (0)	−0.69 (−0.9 to −0.47)	−1.07 (−1.14 to −1.00)
DBP						
Model 1[a]	0.91 (0.78 to 1.04)	0.31 (0.18 to 0.44)	0.28 (0.14 to 0.41)	Ref (0)	−0.11 (−0.24 to 0.02)	−0.36 (−0.40 to −0.32)
Model 2[b]	0.99 (0.86 to 1.11)	0.50 (0.37 to 0.62)	0.38 (0.25 to 0.50)	Ref (0)	−0.36 (−0.49 to −0.24)	−0.47 (−0.51 to −0.44)

CI, confidence interval; Ref, reference; NA, not applicable; DBP, diastolic blood pressure; SBP, systolic blood pressure.
[a]Model 1: adjusted for age, sex, maternal smoking, breastfeeding, birth place, part of a multiple birth.
[b]Model 2: model 1 plus Townsend deprivation index, college or university degree, body mass index, physical activity (MET-hours/week), smoking status, alcohol intake frequency, intake of vegetables and fruit, family history of hypertension, prevalent diabetes. SD = 0.65.

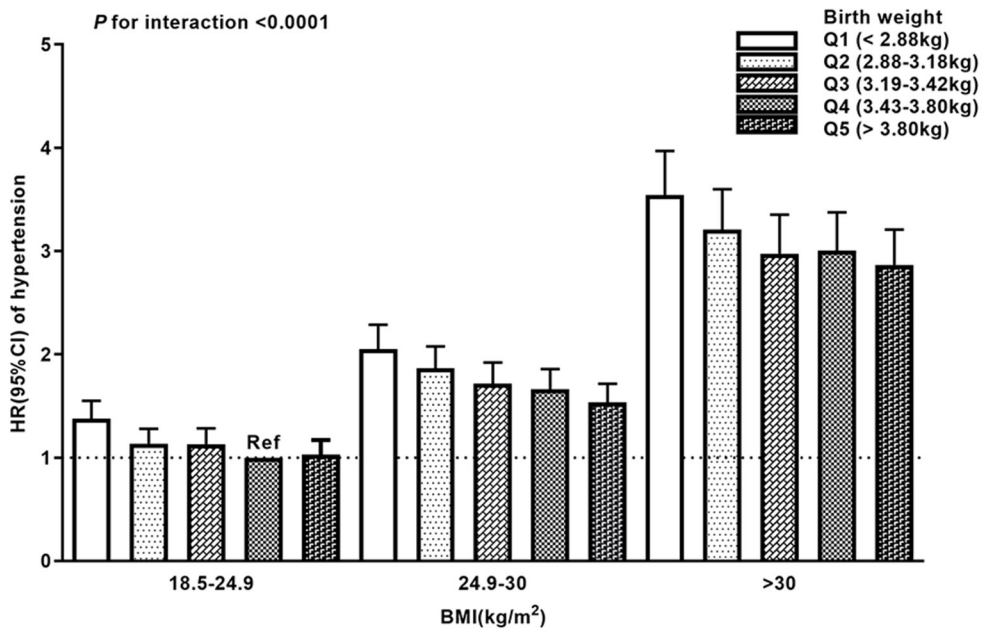

FIGURE 2 | Joint analysis of birth weight and body mass index (BMI) in the full model. The participants with birth weight in group Q4 (3.43–3.80 kg) and BMI in adult between 18.5–25.0 kg/m^2 were treated as the reference group (Ref). Error bars represent 95% confidence intervals of the hazard ratios.

and adult obesity. Several limitations need to be acknowledged (12). First, early life exposures were based on self-reporting, which could lead to recall bias. However, we calculated the weighted Kappa correlation coefficients of self-reported birth weight between baseline and first (n = 12,171) and second follow-up (n = 4,272), which were 0.82 and 0.81, respectively, indicating a good reliability of self-reported birth weight in the UK biobank. In addition, a previous study of the UK Biobank estimated the associations of self-reported birth weight with sex, deprivation index, multiple births, and maternal smoking, and supported the validity of self-reported birth weight (38). Some other studies also confirmed the validity of self-reported birth weight by comparing it with mothers' recall or hospital birth records (39, 40). Second, residual confounding could still exist in the observational study, and we were thus unable to make causal inferences. Finally, most of the UK Biobank participants were of caucasian race, which limits the generalizability of our findings to other ethnic populations.

CONCLUSIONS

The current study indicates a nonlinear inverse association between birth weight and hypertension and suggests birth weight between 3.43–3.80 kg as a threshold for reducing disease risk. Low birth weight may interact with adult obesity to increase hypertension risk in adult life. Further studies are warranted to explore underlying mechanisms.

DATA AVAILABILITY STATEMENT

The raw data supporting the conclusions of this article will be made available by the authors, without undue reservation.

AUTHOR CONTRIBUTIONS

DH, AG, and WZ contributed to the conception and design of the study. YZ and DH have full access to all the data in the study and take responsibility for the integrity of the data and the accuracy of the data analysis. YZ, JL, and QL did the statistical analysis and drafted the manuscript. XF and CX critically revised the manuscript for important intellectual content. All authors reviewed and approved the final manuscript.

FUNDING

This study was funded by the National Natural Science Foundation of China (81973127, 91839102, and 81722040), the National Key Research and Development Program of China (2019YFA0802701 and 2017YFC0908300), and the Science Foundation for Excellent Young Scholars of Jiangsu (BK20190083). The sponsors or funders had no involvements in any parts of this study. All authors confirm the independence of researchers from funding sources.

ACKNOWLEDGMENTS

We are grateful to the UK Biobank participants. This research has been conducted using the UK Biobank resource under application number 55858.

SUPPLEMENTARY MATERIAL

The Supplementary Material for this article can be found online at: https://www.frontiersin.org/articles/10.3389/fcvm.2021.637437/full#supplementary-material

REFERENCES

1. Miranda JO, Ramalho C, Henriques-Coelho T, Areias JC. Fetal programming as a predictor of adult health or disease: the need to reevaluate fetal heart function. *Heart Fail Rev.* (2017) 22:861–77. doi: 10.1007/s10741-017-9638-z
2. Lane RH. Fetal programming, epigenetics, and adult onset disease. *Clin Perinatol.* (2014) 41:815–31. doi: 10.1016/j.clp.2014.08.006
3. Chen W, Srinivasan SR, Berenson GS. Amplification of the association between birthweight and blood pressure with age: the Bogalusa Heart Study. *J Hypertens.* (2010) 28:2046–52. doi: 10.1097/HJH.0b013e32833cd31f
4. Huxley R, Neil A, Collins R. Unravelling the fetal origins hypothesis: is there really an inverse association between birthweight and subsequent blood pressure? *Lancet.* (2002) 360:659–65. doi: 10.1016/S0140-6736(02)09834-3
5. Li Y, Ley SH, VanderWeele TJ, Curhan GC, Rich-Edwards JW, Willett WC, et al. Joint association between birth weight at term and later life adherence to a healthy lifestyle with risk of hypertension: a prospective cohort study. *BMC Med.* (2015) 13:175. doi: 10.1186/s12916-015-0409-1
6. Xia Q, Cai H, Xiang YB, Zhou P, Li H, Yang G, et al. Prospective cohort studies of birth weight and risk of obesity, diabetes, and hypertension in adulthood among the Chinese population. *J Diabetes.* (2019) 11:55–64. doi: 10.1111/1753-0407.12800
7. Andersson SW, Lapidus L, Niklasson A, Hallberg L, Bengtsson C, Hulthen L. Blood pressure and hypertension in middle-aged women in relation to weight and length at birth: a follow-up study. *J Hypertens.* (2000) 18:1753–61. doi: 10.1097/00004872-200018120-00008
8. Pocobelli G, Dublin S, Enquobahrie DA, Mueller BA. Birth weight and birth weight for gestational age in relation to risk of hospitalization with primary hypertension in children and young adults. *Matern Child Health J.* (2016) 20:1415–23. doi: 10.1007/s10995-016-1939-7
9. Curhan GC, Chertow GM, Willett WC, Spiegelman D, Colditz GA, Manson JE, et al. Birth weight and adult hypertension and obesity in women. *Circulation.* (1996) 94:1310–5. doi: 10.1161/01.CIR.94.6.1310
10. Knop MR, Geng TT, Gorny AW, Ding R, Li C, Ley SH, et al. Birth weight and risk of type 2 diabetes mellitus, cardiovascular disease, and hypertension in adults: a meta-analysis of 7 646 267 participants from 135 studies. *J Am Heart Assoc.* (2018) 7:e008870. doi: 10.1161/JAHA.118.008870
11. Tian JY, Cheng Q, Song XM, Li G, Jiang GX, Gu YY, et al. Birth weight and risk of type 2 diabetes, abdominal obesity and hypertension among Chinese adults. *Eur J Endocrinol.* (2006) 155:601–7. doi: 10.1530/eje.1.02265
12. Bowers K, Liu G, Wang P, Ye T, Tian Z, Liu E, et al. Birth weight, postnatal weight change, and risk for high blood pressure among Chinese children. *Pediatrics.* (2011) 127:e1272–9. doi: 10.1542/peds.2010-2213
13. Kuciene R, Dulskiene V, Medzioniene J. Associations between high birth weight, being large for gestational age, and high blood pressure among adolescents: a cross-sectional study. *Eur J Nutr.* (2018) 57:373–81. doi: 10.1007/s00394-016-1372-0
14. Johnsson IW, Haglund B, Ahlsson F, Gustafsson J. A high birth weight is associated with increased risk of type 2 diabetes and obesity. *Pediatr Obes.* (2015) 10:77–83. doi: 10.1111/ijpo.230

15. Wei JN, Li HY, Sung FC, Lin CC, Chiang CC, Li CY, et al. Birth weight correlates differently with cardiovascular risk factors in youth. *Obesity.* (2007) 15:1609–16. doi: 10.1038/oby.2007.190
16. Seravalle G, Grassi G. Obesity and hypertension. *Pharmacol Res.* (2017) 122:1–7. doi: 10.1016/j.phrs.2017.05.013
17. Alexander BT, Dasinger JH, Intapad S. Fetal programming and cardiovascular pathology. *Comprehen Physiol.* (2015) 5:997–1025. doi: 10.1002/cphy.c140036
18. Tian J, Qiu M, Li Y, Zhang X, Wang H, Sun S, et al. Contribution of birth weight and adult waist circumference to cardiovascular disease risk in a longitudinal study. *Sci Rep.* (2017) 7:9768. doi: 10.1038/s41598-017-10176-6
19. Lawlor DA, Ronalds G, Clark H, Smith GD, Leon DA. Birth weight is inversely associated with incident coronary heart disease and stroke among individuals born in the 1950s: findings from the Aberdeen Children of the 1950s prospective cohort study. *Circulation.* (2005) 112:1414–8. doi: 10.1161/CIRCULATIONAHA.104.528356
20. Collins R. What makes UK Biobank special? *Lancet.* (2012) 379:1173–4. doi: 10.1016/S0140-6736(12)60404-8
21. Honigberg MC, Patel AP, Lahm T, Wood MJ, Ho JE, Kohli P, et al. Association of premature menopause with incident pulmonary hypertension: a cohort study. *PLoS ONE.* (2021) 16:e0247398. doi: 10.1371/journal.pone.0247398
22. Sudlow C, Gallacher J, Allen N, Beral V, Burton P, Danesh J, et al. UK biobank: an open access resource for identifying the causes of a wide range of complex diseases of middle and old age. *PLoS Med.* (2015) 12:e1001779. doi: 10.1371/journal.pmed.1001779
23. Tan M, Cai L, Ma J, Jing J, Ma Y, Chen Y. The association of gestational age and birth weight with blood pressure among children: a Chinese national study. *J Hum Hypertens.* (2018) 32:651–9. doi: 10.1038/s41371-018-0084-8
24. Dong YH, Zou ZY, Yang ZP, Wang ZH, Jing J, Luo JY, et al. Association between high birth weight and hypertension in children and adolescents: a cross-sectional study in China. *J Hum Hypertens.* (2017) 31:737–43. doi: 10.1038/jhh.2017.22
25. Blencowe H, Krasevec J, de Onis M, Black RE, An X, Stevens GA, et al. National, regional, and worldwide estimates of low birthweight in 2015, with trends from 2000: a systematic analysis. *Lancet Global Health.* (2019) 7:e849–e60. doi: 10.1016/S2214-109X(18)30565-5
26. Kramer MS. Determinants of low birth weight: methodological assessment and meta-analysis. *Bull World Health Org.* (1987) 65:663–737.
27. Barker DJ. The developmental origins of chronic adult disease. *Acta Paediatr Suppl.* (2004) 93:26–33. doi: 10.1111/j.1651-2227.2004.tb00236.x
28. Bustos P, Amigo H, Bangdiwala SI, Pizarro T, Rona RJ. Does the association between birth weight and blood pressure increase with age? A longitudinal study in young adults. *J Hypertens.* (2016) 34:1062–7. doi: 10.1097/HJH.0000000000000912
29. Hovi P, Vohr B, Ment LR, Doyle LW, McGarvey L, Morrison KM, et al. Blood pressure in young adults born at very low birth weight: adults born preterm international collaboration. *Hypertension.* (2016) 68:880–7. doi: 10.1161/HYPERTENSIONAHA.116.08167
30. Warrington NM, Beaumont RN, Horikoshi M, Day FR, Helgeland Ø, Laurin C, et al. Maternal and fetal genetic effects on birth weight and their relevance to cardio-metabolic risk factors. *Nat Genet.* (2019) 51:804–14. doi: 10.1038/s41588-019-0403-1
31. Hardy R, Wadsworth ME, Langenberg C, Kuh D. Birthweight, childhood growth, and blood pressure at 43 years in a British birth cohort. *Int J Epidemiol.* (2004) 33:121–9. doi: 10.1093/ije/dyh027
32. Järvelin MR, Sovio U, King V, Lauren L, Xu B, McCarthy MI, et al. Early life factors and blood pressure at age 31 years in the 1966 northern Finland birth cohort. *Hypertension.* (2004) 44:838–46. doi: 10.1161/01.HYP.0000148304.33869.ee
33. Lurbe E, Carvajal E, Torro I, Aguilar F, Alvarez J, Redon J. Influence of concurrent obesity and low birth weight on blood pressure phenotype in youth. *Hypertension.* (2009) 53:912–7. doi: 10.1161/HYPERTENSIONAHA.109.129155
34. Leon DA, Koupilova I, Lithell HO, Berglund L, Mohsen R, Vagero D, et al. Failure to realise growth potential in utero and adult obesity in relation to blood pressure in 50 year old Swedish men. *BMJ.* (1996) 312:401–6. doi: 10.1136/bmj.312.7028.401
35. Rasyid H, Bakri S. Intra-uterine growth retardation and development of hypertension. *Acta Med Indones.* (2016) 48:320–4. https://pubmed.ncbi.nlm.nih.gov/28143994/
36. Seckl JR. Prenatal glucocorticoids and long-term programming. *Eur J Endocrinol.* (2004) 151 (Suppl 3):U49–62. doi: 10.1530/eje.0.151u049
37. Lurbe E, Ingelfinger J. Developmental and early life origins of cardiometabolic risk factors: novel findings and implications. *Hypertension.* (2021) 77:308–18. doi: 10.1161/HYPERTENSIONAHA.120.14592
38. Tyrrell JS, Yaghootkar H, Freathy RM, Hattersley AT, Frayling TM. Parental diabetes and birthweight in 236 030 individuals in the UK biobank study. *Int J Epidemiol.* (2013) 42:1714–23. doi: 10.1093/ije/dyt220
39. Troy LM, Michels KB, Hunter DJ, Spiegelman D, Manson JE, Colditz GA, et al. Self-reported birthweight and history of having been breastfed among younger women: an assessment of validity. *Int J Epidemiol.* (1996) 25:122–7. doi: 10.1093/ije/25.1.122
40. Walton KA, Murray LJ, Gallagher AM, Cran GW, Savage MJ, Boreham C. Parental recall of birthweight: a good proxy for recorded birthweight? *Eur J Epidemiol.* (2000) 16:793–6. doi: 10.1023/A:1007625030509

Conflict of Interest: The authors declare that the research was conducted in the absence of any commercial or financial relationships that could be construed as a potential conflict of interest.

frontiers in Physiology

ORIGINAL RESEARCH
published: 23 June 2021
doi: 10.3389/fphys.2021.614532

Intensity of Glycemic Exposure in Early Adulthood and Target Organ Damage in Middle Age: The CARDIA Study

Yifen Lin[1,2†], Xiangbin Zhong[1,2†], Zhenyu Xiong[1,2], Shaozhao Zhang[1,2], Menghui Liu[1,2], Yongqiang Fan[1,2], Yiquan Huang[1,2], Xiuting Sun[1,2], Huimin Zhou[1,2], Xingfeng Xu[1,2], Yue Guo[1,2], Yuqi Li[1,2], Daya Yang[1,2], Xiaomin Ye[1,2], Xiaodong Zhuang[1,2] and Xinxue Liao[1,2]**

[1] Department of Cardiology, First Affiliated Hospital of Sun Yat-sen University, Guangzhou, China, [2] NHC Key Laboratory of Assisted Circulation, Sun Yat-sen University, Guangzhou, China

OPEN ACCESS

Edited by:
Gerald A. Meininger,
University of Missouri, United States

Reviewed by:
Sushil Kumar Mahata,
VA San Diego Healthcare System, United States
Aaron J. Trask,
The Research Institute at Nationwide Children's Hospital, United States

***Correspondence:**
Xinxue Liao
liaoxinx@mail.sysu.edu.cn
Xiaodong Zhuang
zhuangxd3@mail.sysu.edu.cn

[†]These authors have contributed equally to this work

Specialty section:
This article was submitted to Vascular Physiology, a section of the journal Frontiers in Physiology

Received: 06 October 2020
Accepted: 19 March 2021
Published: 23 June 2021

Citation:
Lin Y, Zhong X, Xiong Z, Zhang S, Liu M, Fan Y, Huang Y, Sun X, Zhou H, Xu X, Guo Y, Li Y, Yang D, Ye X, Zhuang X and Liao X (2021) Intensity of Glycemic Exposure in Early Adulthood and Target Organ Damage in Middle Age: The CARDIA Study. Front. Physiol. 12:614532. doi: 10.3389/fphys.2021.614532

Aim: To determine whether long-term intensity of glycemic exposure (IGE) during young adulthood is associated with multiple target organs function at midlife independent of single fasting glucose (FG) measurement.

Methods: We included 2,859 participants, aged 18–30 years at Y0, in the Coronary Artery Risk Development in Young Adults (CARDIA) Study. IGE was calculated as the sum of (average FG of two consecutive examinations × years between the examinations) over 25 years. Target organs function was indicated by cardiac structure, left ventricular (LV) systolic function, LV diastolic function, coronary artery calcium (CAC), and urine albumin-to-creatinine ratio (UACR) at Y25. We evaluated the associations between IGE with target organs function using linear regression models and estimated the associations between IGE with numbers of organs involved (0, 1, or ≥ 2 organs) using multinomial logistic regression models.

Results: A 1-SD increment of IGE was significantly associated with worse target organs function after multivariable adjustment: left ventricular mass (β [SE], 5.468 [1.175]); global longitudinal strain (β [SE], 0.161 [0.071]); E/e' ratio (β[SE], 0.192 [0.071]); CAC score (β [SE], 27.948 [6.116]); and log UACR (β [SE], 0.076 [0.010]). Besides, IGE was independently associated with having ≥ 2 organs involved in both overall population (OR [95% CI], 1.48 [1.23, 1.41], $P < 0.001$) and subgroups stratified by diabetes at Y25.

Conclusion: Higher intensity of glycemic exposure during young adulthood was independently associated with subclinical alterations of target organs function at midlife. Our findings highlight the importance of early screening and management of IGE in youth.

Keywords: hyperglycemia, left ventricular hypertrophy, cardiac dysfunction, coronary artery calcium, albuminuria

INTRODUCTION

Individuals with long-term exposure to hyperglycemia underwent chronic injuries to multiple organ systems. Previous studies have confirmed strong correlations between elevated blood glucose with coronary artery disease (CAD), diabetic cardiomyopathy, and diabetic nephropathy in late life (Devereux et al., 2000; Rossing et al., 2004; Cosentino et al., 2020). Since chronic exposure to glycemia shows detrimental impacts on target organs, a life-course evaluation of glycemic exposure considering both the magnitude and duration of exposure to hyperglycemia should be established for comprehensive assessment of its toxicity. Attempts have been made to investigate the long-term impact of glycemic exposure based on the long-term blood glucose trajectory, which was associated with mortality and cardiovascular disease (Lee et al., 2018; Ogata et al., 2019). However, long-term trajectories simply clustered the subjects into different groups based on the change tendency of blood glucose, leading to inaccurate assessment of glycemic exposure (Nagin and Odgers, 2010). Hence, the association between increased intensity of glycemic exposure (IGE) in young adulthood with target organ damages (TOD) in midlife deserves investigation.

Subclinical target organ damages of hyperglycemia, indicated by coronary artery calcium (CAC), early cardiac deformation, and dysfunction as well as albuminuria in our study, are efficient markers and well precursors of adverse clinical outcomes (BMJ, 2012; Yeboah et al., 2016; Medvedofsky et al., 2018). The Coronary Artery Risk Development in Young Adults (CARDIA) Study, which only enrolled young adults aged 18–30 years at baseline and underwent six blood glucose monitoring over 25 years, offers the opportunity to assess the impact of IGE on subclinical indicators of organ dysfunction in the life-course pattern since young adulthood.

In this study, we aimed to determine how the intensity of glycemic exposure from young adulthood to middle adulthood affects target organ function in 2,859 CARDIA study participants. We firstly assessed the associations between IGE with clinical measures of coronary artery calcification, cardiac deformation, and dysfunction as well as albuminuria. We also evaluated the association between IGE and the number of target organs involved.

MATERIALS AND METHODS

Study Population

The datasets of the CARDIA study were obtained at the CARDIA Coordinating Center[1] according to the application procedure required.

The CARDIA study was a prospective and observational investigation of 5,115 healthy black and white adults from 4 U.S. metropolitan communities (Birmingham, AL; Chicago, IL; Minneapolis, MN; and Oakland, CA). Briefly, men and women aged 18–30 years were recruited at 1985–1986 (Y0) and reexamined after 2 (Y2), 5 (Y5), 7 (Y7), 10 (Y10), 15 (Y15), 20 (Y20), and 25 (Y25) years. Further details of the CARDIA study have been published previously (Friedman et al., 1988). Institutional Review Boards approved the CARDIA study protocols, and all participants provided written informed consent at each examination.

For this analysis, we evaluated 3,498 participants who attended reexamination at Y25 and excluded those who had race other than white or black (n = 11), those with missing data on blood glucose at Y0 and Y25 (n = 75), and those with missing data on covariates (n = 553). Finally, 2,859 participants were included in our analysis. Baseline characteristics at examination in Y0 of individuals who were included and excluded are summarized in **Supplementary Table 1**.

Intensity of Glycemic Exposure Assessment and Incident Diabetes

Participants were asked to fast > 8 h for measurements of fasting glucose at Y0, Y7, Y10, Y15, Y20, and Y25. Fasting glucose was measured using the hexokinase ultraviolet method by American Bio-Science Laboratories at baseline and hexokinase coupled to glucose-6-phosphate dehydrogenase at the following reexamination. Intensity of glucose exposure from young to middle adulthood was evaluated by the sum of (average blood glucose of two consecutive examinations years between the examinations) (**Supplementary Figure 1**). A similar approach was also used to assess the deleterious effects of elevated cumulative exposure to blood pressure in early adulthood (Kishi et al., 2015; Mahinrad et al., 2020). We determined diabetes based on any one of the following: self-report of hypoglycemic medications (measured at Y0, Y7, Y10, Y15, Y20, and Y25); fasting glucose levels $\geq$ 7.0 mmol/L or $\geq$ 126 mg/dL (measured at Y0, Y7, Y10, Y15, Y20, and Y25); 2-h post-load blood glucose $\geq$ 11.1 mmol/L or $\geq$ 200 mg/dL in 75 g oral glucose tolerance test (measured at Y10, Y20, and Y25); or glycated hemoglobin $\geq$ 6.5% (measured at Y20 and Y25).

Outcome Measurements

Cardiac structure and function were assessed by echocardiographic measurements in standardized methods following American Society of Echocardiography guidelines across all field centers at Y25, as described previously (Armstrong et al., 2015; Lang et al., 2015). Echocardiographic images were collected using a commercially available cardiac ultrasound machine (Artida; Toshiba Medical Systems) by trained sonographers and were interpreted using a standard offline image analysis system (Digisonics, TX). For cardiac structure assessment, left ventricular mass (LVM) was estimated from the Devereux formula and relative wall thickness (RWT) was calculated as (diastolic interventricular septal + diastolic left ventricular [LV] posterior wall thickness)/diastolic internal LV diameter. For LV systolic function assessment, left ventricular ejection fraction (LVEF) was evaluated based on LV end-systolic and end-diastolic volumes. Global longitudinal strain (GLS), a more sensitive and prognostic index of LV systolic function, was measured using speckle-tracking echocardiography and

[1]https://www.cardia.dopm.uab.edu/

calculated as the systolic change of segmental length divided by the segmental length at end-diastole (in percentile) (Potter and Marwick, 2018). Peak velocities in mitral inflow at early (E), late diastole (A), and early peak diastolic mitral annular velocity (e') were measured for assessment of E/A ratio and E/e' ratio to reflect LV diastolic function.

Coronary artery calcium (CAC) was measured by multidetector computed tomography (CT) scanner in all centers using standardized approach at Y25 (Carr et al., 2005). The analysts in CARDIA Reading Center who were blinded to participants' information analyzed the images and calculated a CAC score using on modified Agatston method (Agatston et al., 1990). Briefly, the total CAC score in Agatston units (AU) was determined based on numbers, areas, and maximal computed tomographic numbers of the lesions. Besides, albuminuria was assessed by measurement of urine albumin to creatinine ratio (UACR). Urine albumin and urine creatinine levels were measured using nephelometry-based assay at Y25 examination according to the standardized exam protocol available at cardia.dopm.uab.edu.

For categorical analyses of significant target organ dysfunction, we defined left ventricular hypertrophy (LVH) as increased LVM > 224 g for men and > 162 g for women (Kirkpatrick et al., 2007). Concentric remodeling was defined as increased RWT > 0.42 (Lang et al., 2015). LV systolic dysfunction was defined by decreased LVEF (<50%) or abnormal GLS (>90th percentile) (Kishi et al., 2017). LV diastolic dysfunction was defined as abnormal filling patterns (E/A ratio $\leq$ 0.8 or $\geq$ 2) or increased filling pressure (E/e' ratio > 15) (Kishi et al., 2015; Nagueh et al., 2016). We also defined CAC as an Agatston score > 0 and albuminuria as UACR > 30 mg/g.

Covariates Measurements

Demographic characteristics, clinical history, medication use, and anthropometric and laboratory data were collected based on standardized approaches as reported in the study protocol (Friedman et al., 1988). Age, gender, race, educational attainment, and smoking and drinking status were self-reported. Smoking status and drinking status were recorded as ever/never smoking and ever/never drinking, respectively. Educational attainment was evaluated by years in school. Height and weight were measured in light clothing, and body mass index (BMI) was calculated as the ratio of weight (kg) to the square of height (m^2). After 5 min of quiet rest, seated blood pressure (BP) in the right arm was measured three times with 1-min intervals using validated Omron HEM907XL oscillometric BP monitor at Y25 and the mean of the second and third readings was used for analysis. Plasma insulin level at Y0 and Y25 was detected via immunoassay method. Total cholesterol, high-density lipoprotein cholesterol (HDL-c) were enzymatically determined and low-density lipoprotein cholesterol (LDL-c) was calculated using the Friedewald equation.

Statistical Analysis

Participants eligible in our analysis were subdivided into three categories based on tertiles of IGE. Baseline characteristics of participants at Y25 were compared using one-way ANOVA (continuous variables), χ^2 tests (categorical variables), and the Kruskal-Wallis test as appropriate. Urine albumin to creatinine ratio was log-transformed due to skewed distribution. We also compared the baseline characteristics of participants in CARDIA study who were included in the final analysis with those excluded. Data were presented as means $\pm$ SD or median (interquartile range) for continuous variables and frequencies (percentages) for categorical variables.

Multivariable linear regression models were performed to evaluate the longitudinal associations between IGE over 25 years with target organs function at Y25, including cardiac structure and function, CAC, and albuminuria. Multivariable models were adjusted for covariates at Y25: model 1 included age, gender, race; model 2 was additionally adjusted for smoking, drinking, BMI, and educational attainment; model 3 was further adjusted for systolic BP, LDL-c, HDL-c, and Y25 blood glucose; and model 4 was additionally adjusted for aspirin, medication for lower cholesterol, HTN, and DM. The covariates included in the model were determined based on a P value < 0.05 in univariable model and clinical knowledge (**Supplementary Table 2**). The effects were assessed by calculating the estimates (βs) and standard errors (SEs) for per 1-SD increment on IGE. The powers of multivariable linear regression models based on unconditional model were shown in **Supplementary Table 3**. Multivariable linear regression model was performed to assess the association between IGE with insulin level and left ventricular mass index (LVMI), calculated as LVM indexed to body surface area. To investigate the robustness of the associations, we additionally adjusted for average FG across follow-up examination instead of FG in Y25 in model 5 and number of measurements of FG in model 6 in sensitivity analysis. In an explorative analysis, we further performed categorical analyses to explore the effects on significantly clinical organ dysfunction. Multivariable logistic regression models were used to evaluate the association between per 1-SD increment on IGE with target organs dysfunction, including CAC, LVH, concentric remodeling, impaired LVEF, abnormal GLS, abnormal filling patterns, increased filling pressures, and albuminuria. In logistic models, we accounted for the same covariates as in linear models and presented the effects using odds ratios (ORs) and 95% confidential intervals (95% CIs).

For further analysis in the prevalence of TOD derived from LGE, we defined numbers of TODs as the sum of the presence of cardiac deformation (LVH or concentric remodeling), cardiac systolic dysfunction (impaired LVEF or abnormal GLS), cardiac diastolic dysfunction (abnormal filling patterns or increased filling pressures), CAC, and albuminuria, ranging from 0 to 5. Multinomial logistic regression models were performed to explore the relationship between IGE and numbers of TODs (0, 1, or $\geq$ 2). We adjusted for traditional cardiovascular risk factors at Y25, including age, gender, race, smoking, drinking, BMI, educational attainment, SBP, LDL-c, HDL-c, Y25 blood glucose, aspirin, medication for lower cholesterol, HTN, and DM. We also compared the effects of IGE on numbers of TOD stratified by the presence of DM.

All statistical analyses were performed using SPSS version 18.0. A two-tailed $P < 0.05$ was considered statistically significant.

RESULTS

Baseline characteristics of 2,859 eligible participants in the CARDIA study were summarized in **Table 1**. Overall, the mean age at Y25 was 50.0 ± 3.6 years; 43.4% of the participants were male (n = 1,240) and 44.6% were black (n = 44.6). The average intensity of glycemic exposure was 2237.5 ± 324.7 mg/dl Yrs over 25 years in total eligible population (ranged 1717.0 to 5713.0 mg/dl Yrs). Participants with higher IGE were more frequently male, had higher BMI, SBP, DBP, fasting glucose at Y0 and Y25 (all $P < 0.001$). Among them, only very few participants (n = 10, 0.3%) had diabetes at Y0 and 373 participants (13.0%) developed diabetes up to Y25. **Supplementary Table 4** described the baseline characteristics of participants who had diabetes and remained free from diabetes at Y25. Participants who developed diabetes were more likely black and had higher IGE, BMI, SBP, and DBP.

IGE and Target Organ Function

As shown in **Figure 1**, higher deciles of IGE produced higher LVM, GLS, E/e' ratio, CAC score, UACR, and lower E/A ratio. **Table 2** represented the associations between IGE over 25 years with target organs function parameters in linear regression models. In model 1, a 1-SD-increment higher IGE was significantly associated with higher LVM, E/e' ratio, CAC score, log UACR, and lower E/A (all $P < 0.001$). Further adjustments for smoking, drinking, BMI, and educational attainment in model

TABLE 1 | Baseline Characteristics for 2,859 CARDIA participants.

Characteristic	Total (N = 2,859)	Intensity of Glycemic exposure			
		Group 1 (N = 953)	Group 2 (N = 956)	Group 3 (N = 950)	P-value
IGE (mg/dl Yrs)	2237.5 ± 324.7	2016.4 ± 72.2	2183.2 ± 42.1	2514.0 ± 426.5	<0.001
Age, years	50.0 ± 3.6	49.4 ± 3.7	50.0 ± 3.6	50.6 ± 3.4	<0.001
Male	1240 (43.4)	213 (22.4)	442 (46.2)	585 (61.6)	<0.001
Black	1275 (44.6)	436 (45.8)	382 (40.0)	457 (48.1)	0.001
BMI, kg/m2	29.9 ± 6.8	27.7 ± 6.2	29.8 ± 6.5	32.2 ± 6.8	<0.001
SBP, mmHg	118.2 ± 15.3	115.3 ± 15.3	118.1 ± 14.7	121.3 ± 15.2	<0.001
DBP, mmHg	73.6 ± 10.8	71.6 ± 11.1	73.7 ± 10.5	75.4 ± 10.4	<0.001
FG at Y0, mg/dl	81.9 ± 10.4	76.6 ± 6.0	81.8 ± 7.4	87.2 ± 13.2	<0.001
FG at Y25, mg/dl	98.6 ± 27.0	86.5 ± 6.6	94.0 ± 7.6	115.3 ± 40.5	<0.001
Insulin at Y0, uU/mL	10.4 ± 7.2	8.9 ± 5.8	9.8 ± 6.0	12.3 ± 9.0	<0.001
Insulin at Y25, uU/mL	11.0 ± 9.7	8.0 ± 5.7	10.7 ± 7.8	14.4 ± 12.9	<0.001
DM at Y0	10 (0.3%)	0	3 (0.3)	7 (0.7)	0.011
DM at Y25	373 (13.0%)	20 (2.1)	57 (6.0)	296 (31.2)	<0.001
Smoking	1541 (53.9)	491 (51.5)	512 (53.6)	538 (56.6)	0.079
Drinking	2253 (78.8)	750 (78.7)	772 (80.8)	731 (76.9)	0.126
Educational attainment	14.8 ± 1.8	14.9 ± 1.8	14.9 ± 1.8	14.5 ± 1.9	<0.001
LDL-c, mg/dl	111.8 ± 32.6	109.4 ± 30.5	113.9 ± 31.8	112.0 ± 35.3	0.011
HDL-c, mg/dl	58.5 ± 18.0	65.2 ± 18.4	57.8 ± 17.4	52.6 ± 15.7	<0.001
DM medication	201 (7.0)	7 (0.7)	16 (1.7)	178 (18.7)	<0.001
HTN medication	761 (26.6)	164 (17.2)	236 (24.7)	361 (38.0)	<0.001
Lipid medication	437 (15.3)	79 (8.3)	117 (12.2)	241 (25.4)	<0.001
Aspirin use	480 (16.8)	97 (10.2)	146 (15.3)	237 (24.9)	<0.001
Echocardiographic parameters					
LVM (n = 2553)	167.3 ± 51.9	148.5 ± 44.4	168.8 ± 48.5	186.8 ± 55.5	<0.001
RWT (n = 2549)	0.4 ± 0.1	0.3 ± 0.1	0.4 ± 0.1	0.4 ± 0.1	0.005
LVEF (n = 2553)	69.8 ± 8.0	69.9 ± 7.4	69.9 ± 7.8	69.6 ± 8.8	0.773
GLS (n = 2497)	−15.1 ± 2.4	−15.2 ± 2.3	−15.2 ± 2.3	−14.5 ± 2.5	<0.001
E/A (n = 2810)	1.3 ± 0.4	1.4 ± 0.4	1.3 ± 0.3	1.2 ± 0.4	<0.001
E/e' (n = 2785)	9.0 ± 2.7	8.8 ± 2.6	8.8 ± 2.7	9.3 ± 2.9	<0.001
CAC score, AU (n = 2616)	0.0 (0.0, 3.9)	0.0 (0.0, 0.0)	0.0 (0.0, 1.9)	0.0 (0.0, 29.0)	<0.001
UACR, mg/g (n = 2794)	4.7 (3.3, 8.1)	4.7 (3.3, 7.5)	4.4 (3.1, 7.1)	5.1 (3.4, 10.2)	<0.001

Data are presented as mean ± SD, number (percentage), or median (interquartile range), as appropriate. Sample characteristics were drawn from examination 8 at Y25 unless otherwise indicated. IGE, intensity of glycemic exposure; BMI, body mass index; SBP, systolic blood pressure; DBP, diastolic blood pressure; FG, fasting glucose; DM, diabetes mellitus; HDL-C, high-density lipoprotein cholesterol; LDL-C, low-density lipoprotein cholesterol; CAC, coronary artery calcium; LVM, left ventricular mass; RWT, relative wall thickness; LVEF, left ventricular ejection fraction; GLS, global longitudinal peak strain; UACR, urine albumin to creatinine ratio.

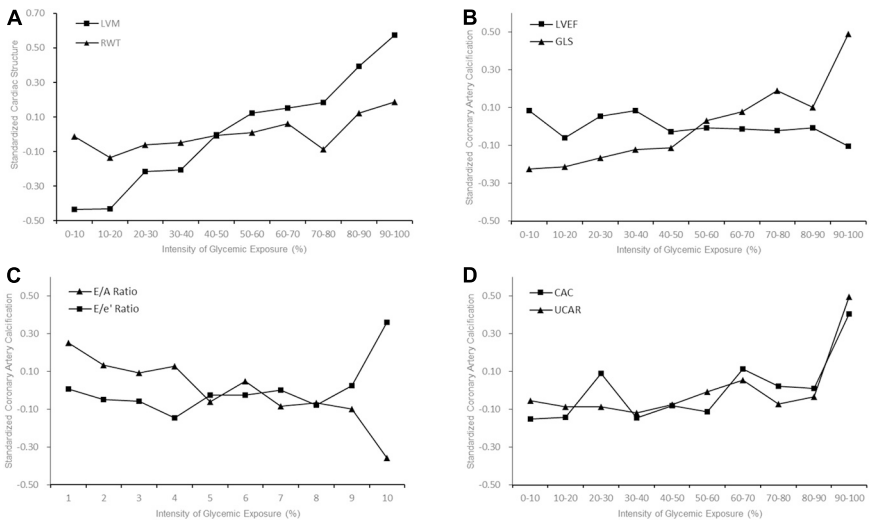

FIGURE 1 | Early Adulthood Intensity of Glycemic Exposure and Middle-Age Target Organ Function. The trajectory slopes showed indices of target organs function with increasing decile of intensity of glycemic exposure (IGE). **(A)** Cardiac structure; **(B)** Left ventricular (LV) systolic function; **(C)** LV diastolic function; **(D)** Coronary artery calcium (CAC) and albuminuria. Higher deciles of IGE produced higher level of left ventricular mass (LVM) **(A)**, global longitudinal strain (GLS), CAC and urine albumin to creatinine ratio (UACR).

2 did not alter the results. The association between E/A ratio with IGE dissipated after further adjustments in model 3, while other associations remained significant. A 1-SD increment of IGE were still positively associated with LVM (β [SE], 5.468 [1.175]), GLS (β [SE], 0.161 [0.071]), E/e' ratio (β[SE], 0.192 [0.071]), CAC score (β [SE], 27.948 [6.116]), and log UACR (β [SE], 0.076 [0.010]) after full adjustment in model 4. IGE over 25 years was positively associated with serum insulin and LVMI at Y25 (**Supplementary Table 5**). Sensitivity analysis with additional adjustment for average blood glucose in model 5 and number of measurements of FG in model 6 demonstrated consistent results (**Supplementary Table 6**).

Supplementary Table 7 presented multivariable logistic regression models to further investigate the impacts of IGE on subclinical target organ dysfunction. For cardiac structural and functional outcomes, per 1-SD increment of IGE was significantly associated with a higher prevalence of LVH (OR [95% CI], 1.25 [1.09, 1.43]) and abnormal GLS (OR [95% CI], 1.22 [1.02, 1.45]) in a fully adjusted model. In contrast, IGE was not related to clinical diastolic dysfunction, including abnormal filling patterns and increased filling pressure after full adjustments. Besides, per 1-SD increment of IGE showed correlations with higher prevalence of subclinical atherosclerosis (OR [95% CI], 1.24 [1.08, 1.43]) and albuminuria (OR [95% CI], 1.40 [1.20, 1.63]).

IGE and Number of TOD

Prevalence of TOD (0, 1, or ≥ 2 organs damaged) in the overall population and subgroups stratified by incident diabetes were shown in **Figure 2**. Compared with the non-diabetes population, those with DM at Y25 had a higher prevalence of 2 or more damaged organs, indicating a greater vulnerability to target organ damages in the diabetes population. **Figure 2** presented the odds ratio of having 1 or ≥ 2 organs damaged by long-term IGE in multivariable multinomial logistic regression models. A 1-SD increment of IGE was independently associated with having ≥ 2 organs involved in overall population (OR [95% CI], 1.48 [1.23, 1.41]; $P < 0.001$; **Figure 2**), suggesting the higher the levels of IGE, the more advanced the target organs involvement. It should be noted that the association were statistically significant in both DM and non-DM subgroups.

DISCUSSION

In this prospective cohort of young adults followed up over 25 years, we demonstrated greater IGE during young adulthood was associated with unfavorable impairment of multiple target organs, including subclinical cardiac structural and functional impairment, subclinical atherosclerosis, and albuminuria independent of fasting glucose at Y25. The long-term IGE was associated with the prevalence of TOD and the higher IGE tended to involve more target organs, which remained consistent even among those free from diabetes at Y25.

Previous researches have established that diabetes is responsible for multiple target organs injury (De Simone et al., 2017). Diabetic cardiomyopathy is characterized by myocardial hypertrophy and myocardial remodeling, manifested as diastolic dysfunction in the earlier and systolic dysfunction during disease progression (Boudina and Abel, 2007). Besides, individuals with diabetes are also at increased risk of atherosclerosis and diabetic nephropathy in later life (Rossing et al., 2004; Raffield et al., 2018). Overall, these prior studies suggested that diabetes is a strong predictor of adverse clinical events in later life. However, previous studies always investigated the detrimental impacts of hyperglycemia based on measurement of blood glucose at a single time point and whether lifespan exposure to hyperglycemia

TABLE 2 | Linear regression models to examine the associations between intensity of glycemic exposure during young adulthood with target organ function in midlife.

Variables	Per 1 SD increment of IGE (standardized value)			
	Model 1	Model 2	Model 3	Model 4
	β (SE)	β (SE)	β (SE)	β (SE)
Cardiac structure and function				
Structure				
LVM (*n* = 2553)	8.359(0.890)***	4.139(0.829)***	5.293(1.085)***	5.468(1.175)***
RWT (*n* = 2549)	0.002(0.001)	0.000(0.001)	−0.001(0.002)	−0.002(0.002)
Systolic Function				
LVEF (*n* = 2553)	−0.071(0.157)	−0.075(0.161)	−0.100(0.215)	−0.024(0.233)
GLS (*n* = 2497)	0.398(0.049)***	0.318(0.050)***	0.214(0.067)**	0.161(0.071)*
Diastolic Function				
E/A (*n* = 2810)	−0.048(0.007)***	−0.030(0.007)***	−0.017(0.009)	−0.007(0.010)
E/e' (*n* = 2785)	0.367(0.051)***	0.260(0.051)***	0.207(0.066)**	0.192(0.071)**
Subclinical Atherosclerosis				
CAC score (*n* = 2616)	35.315(4.303)***	34.917(4.393)***	30.161(5.707)***	27.948(6.116)***
Renal Function				
Log UACR (*n* = 2794)	0.115(0.007)***	0.111(0.007)***	0.085(0.010)***	0.076(0.010)***

*IGE, intensity of glycemic exposure. All models were adjusted for covariates measured at Y25. Model 1 was adjusted for age, gender, race; Model 2 was additionally adjusted for smoking, drinking, BMI, educational attainment; Model 3 was additionally adjusted for SBP, LDL-c, HDL-c, Y25 blood glucose; Model 4 was additionally adjusted for aspirin, medication for lower cholesterol, HTN, and DM. ***P < 0.001; **P < 0.01; *P < 0.05.*

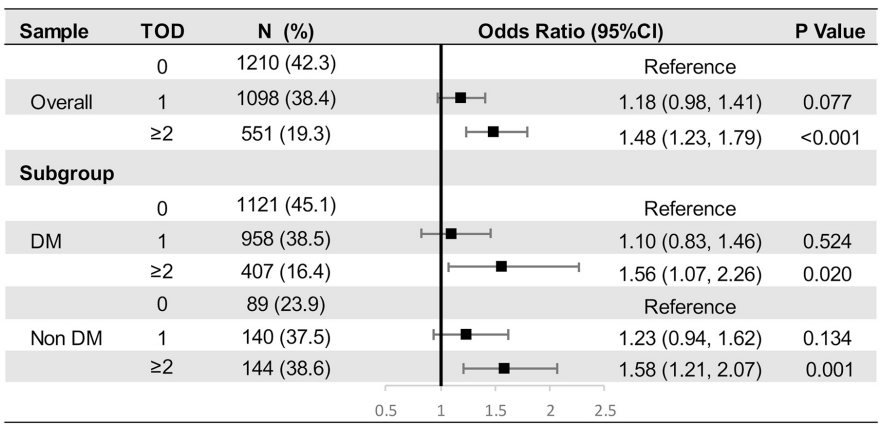

FIGURE 2 | Multinomial Logistic Regression Models to Examine the Odds Ratio of Having 0, 1 or ≥ 2 Target Organ Damages by Intensity of Glycemic Exposure.

derived subclinical adverse effects earlier is still unknown. To the best of our knowledge, our study was the first to comprehensively focus on the chronic impacts of the long-term intensity of glycemic exposure during young adulthood on multiple target organs in midlife, accounting for the magnitude and duration of glycemic exposure simultaneously. Our findings extended the prior studies by showing that higher IGE over the 2nd, 3rd, and 4th decade of life was associated with earlier target organs dysfunction at the 5th decade. Besides, our results also suggested that the numbers of target organs involved depended on the cumulative effects of IGE, even in a non-diabetic subset of participants who were younger with fewer clinical comorbidities.

Prior to our study, there have been several metrics concerning the effect of long-term glycemic exposure. Visit-to-visit FG variability in young adulthood was correlated with incident cardiovascular disease and all-cause mortality in the CARDIA study (Bancks et al., 2019b). Visit-to-visit FG variability mediates the effect of long-term glycemic exposure in part; however, it does not capture the impact derived from the magnitude of glycemic exposure. Duration of diabetes, associated with atherosclerosis and adverse outcome, was a surrogate measurement of lifespan glycemia exposure but was not available for subclinical hyperglycemia assessment (Fox et al., 2004; Kim et al., 2015). Besides, based on group-based trajectory modeling, participants with three or more FG measurements were clustered into distinct groups, each with a specific trajectory (Nagin and Odgers, 2010; Yuan et al., 2018). Bancks et al. (2019a) developed trajectory curves to visualize the long-term FG tendency in the CARDIA study, observing impaired LV structure and diastolic function in both moderate-increasing and

high-stable FG trajectory groups compared to the low-stable FG group. Nevertheless, the classification for distinctive groups was roughly based on the FG tendency and not precise enough for clinical assessment (Jennings and Muniz, 2016). In trajectory methodology, the grouping is automatically assumed to exist and the findings were data-driven, so the conclusion needs to be interpreted with great caution (Jennings and Muniz, 2016). In the present study, IGE seems to be a more concrete and accurate indicator for long-term glycemic exposure assessment.

The underlying pathophysiologic pathways that link higher long-term IGE with target organs impairment may share common pathogenic mechanisms. Studies have shown that hyperglycemia induces and accelerates the deposition and accumulation of glycosylation products within myocardium and arterial wall, leading to cardiac and vascular injury (Naka et al., 2004; Boudina and Abel, 2007; West et al., 2009). Besides, endothelial dysfunction is also a main pathogenic factor contributing to diabetic vascular impairment, e.g., initiating the pathogenesis of atherosclerosis (Calles-Escandon and Cipolla, 2001). Furthermore, hyperglycemia and insulin resistance also promote myocardial collagen deposition and myocyte hypertrophy, causing myocardial remodeling (Kishi et al., 2017). Some other mechanisms may also involve the pathogenesis, including oxidative stress, altered substrate metabolism, mitochondrial dysfunction, inflammation activation, and so on (Boudina and Abel, 2007; Ceriello and Testa, 2009; Donath and Shoelson, 2011).

For cardiac functional measurements, it has been demonstrated that global longitudinal strain is a sensitive marker of systolic dysfunction than ejection fraction and provides additional prognostic value on adverse outcomes (Russo et al., 2014; Potter and Marwick, 2018). Meanwhile, previous studies indicated that E/e' ratio was more predictive for primary cardiac events than E/A ratio (Sharp et al., 2010). In our study, we noted associations between long-term IGE with worse global longitudinal strain but not ejection fraction. We also found that IGE over young adulthood was associated with a worse E/e' ratio rather than E/A. Therefore, GLS and E/e' ratio seemed to be powerful in showing the adverse effects of IGE that classical echocardiographic indicators failed to identify, which may be explained by a young age of CARDIA population with a lower prevalence of clinical organ dysfunction at advanced stage. Similarly, IGE was also associated with CAC and albuminuria, the well-known and powerful precursors of adverse outcomes (Detrano et al., 2008; BMJ, 2012). In fact, identification of the predisposing factors for subclinical organ dysfunction provides insight toward the long-term risk of organ dysfunction. From a disease-prevention perspective, given the independent prognostic significance of TOD, it would make sense to establish screening strategies on IGE and implement intensive blood glucose management during young adulthood, avoiding irreversible organ damage (BMJ, 2012; Yeboah et al., 2016; Medvedofsky et al., 2018).

An unexpected finding was that long-term IGE showed subclinical adverse effects on target organs in both diabetes and non-diabetes subgroups, which highlights the need to investigate the cumulative effects of glycemic exposure in participants below the diagnostic criteria of diabetes. Indeed, even in examination at Y25, only a minority of participants (13.0%) were diagnosed as diabetes and the FG level in the non-diabetes population was on average below the current threshold of prediabetes (92.8 $\pm$ 9.1 mg/dl, **Supplementary Table 4**), suggesting exposure to subclinical hyperglycemia over young adulthood could precipitate organ dysfunction. A prospective study may be warranted to determine the optimal cut-off points for evaluation of the subclinical impacts of cumulative glycemic exposure. On the other hand, given the subclinical hyperglycemia is a modifiable factor, the optimal glycemic control target remains controversial despite several randomized controlled trials (RCTs) published (UK Prospective Diabetes Study (UKPDS) Group, 1998; Gerstein et al., 2008; Holman et al., 2008; Patel et al., 2008). UKPDS trial demonstrated a great microvascular benefit from intensive glucose control therapy, which was confirmed in subsequent ADVANCE and ACCORD trials. However, whether intensive glucose control therapy reduces the risk of macrovascular events is still disputed. Indeed, the participants in these RCTs were characterized by old age, long duration of diabetes, and poor glycemic control. Irreversible subclinical organ impairment in these participants may weaken the effects of intensive glucose control therapy and lead to unclear macrovascular benefit. Thus, further research is needed to clarify whether intensive glucose control in young patients with subclinical hyperglycemia can prevent or delay the early organ dysfunction, ultimately improving prognosis. Nevertheless, the accompanying risk of adverse reaction, especially hypoglycemic episodes, should be carefully assessed.

Our study results are strengthened by a population-based cohort with a large sample size; regular screening fasting glucose using standardized protocols over 25 years, facilitating assessment of the cumulative intensity of glycemic exposure; a cohort of young adults with fewer comorbidities, almost non-diabetic population, was optimal for exploring the subclinical effects of IGE on target organs and providing evidence on prevention of diabetes-induced end-organ damage. However, several limitations in our study need to be considered. First, cardiac function and CAC were measured in detail until examination in Y25, hindering further assessment of the long-term changes of target organs function from young adulthood to midlife. Hence, we can only assume that the measurements in Y25 could reflect the decline in organ function. Second, only approximately half of participants in CARDIA performed echocardiographic measurements and CAC assessment in Y25, thus our analysis may be subjected to selection bias. To address this issue, we further compared the baseline characteristics between the analyzed sample with the excluded sample (**Supplementary Table 1**). The participants who were excluded in our study were more frequently male, black, smokers, have lower educational attainment, and higher FG and SBP levels. In fact, the participants included in our analysis may have a lower risk of target organs impairment than those excluded, which likely creates bias toward the null and may underestimate the deleterious effects of IGE. Third, owing to the calculation method of IGE, each individual had unequal number of measurements of FG, and those who were less measured may have inaccurate

evaluation of glycemic exposure. Indeed, more than 80% of individuals completed all 6 measurements of FG and we observed consistent associations when additionally adjusted for number of measurements (**Supplementary Table 6**). Fourth, given the nature of the observational study, our findings may be susceptible to reverse causation and residual confounding. Last but not least, CARDIA is a biracial cohort including white and black individuals, so that our findings required external validation in other ethnic populations, e.g., Asians.

CONCLUSION

In conclusion, our study finds associations between the long-term intensity of glycemic exposure during young adulthood with subclinical impairment of cardiac structure and function, CAC, and albuminuria at midlife. Higher IGE is also associated with increased numbers of target organs involvement, even in non-diabetic populations. Our findings emphasize the importance of screening and management of subclinical hyperglycemia in youth, thus preventing or delaying the early organ dysfunction and ultimately improving the prognosis.

DATA AVAILABILITY STATEMENT

The raw data supporting the conclusions of this article will be made available by the authors, without undue reservation.

ETHICS STATEMENT

Ethical review and approval was not required for the study on human participants in accordance with the local legislation and institutional requirements. The patients/participants provided their written informed consent to participate in this study.

AUTHOR CONTRIBUTIONS

XL and XZhu conceived and designed the study, obtained funding, and acquired the data. YiL and XZho conceived and designed the study, performed all analysis and interpretation of data, and drafted the manuscript. ZX, SZ, and ML advised on statistical analysis methods and critically revised the manuscript for important content. YF, YH, and XS interpreted the data and critically revised the manuscript for important content. HZ, XX, YG, YuL, DY, and XY critically revised the manuscript for important content and contributed to the discussion. XL was the guarantor of this work and, as such, had full access to all the data in the study and took responsibility for the integrity of the data and the accuracy of the data analysis. All authors contributed to the article and approved the submitted version.

FUNDING

This work was supported by the National Natural Science Foundation of China (81600206 to XZha and 81870195 to XL) and Natural Science Foundation of Guangdong Province (2016A030310140 to XZha and 2016A020220007 and 2019A1515011582 to XL). The funders had no role in study design, data collection and analysis, decision to publish, or preparation of the manuscript. The Coronary Artery Risk Development in Young Adults Study (CARDIA) is conducted and supported by the National Heart, Lung, and Blood Institute (NHLBI) in collaboration with the University of Alabama at Birmingham (HHSN268201800005I and HHSN268201800007I), Northwestern University (HHSN268201800003I), University of Minnesota (HHSN268201800006I), and Kaiser Foundation Research Institute (HHSN268201800004I).

ACKNOWLEDGMENTS

We thank the staff and participants of the CARDIA Study for their important contributions. This manuscript has been released as a pre-print at Research Square, https://www.researchsquare.com/article/rs-72341/v1.

SUPPLEMENTARY MATERIAL

The Supplementary Material for this article can be found online at: https://www.frontiersin.org/articles/10.3389/fphys.2021.614532/full#supplementary-material

REFERENCES

Agatston, A. S., Janowitz, W. R., Hildner, F. J., Zusmer, N. R., Viamonte, M. Jr., and Detrano, R. (1990). Quantification of coronary artery calcium using ultrafast computed tomography. *J. Am. Coll. Cardiol.* 15, 827–832.

Armstrong, A. C., Ricketts, E. P., Cox, C., Adler, P., Arynchyn, A., Liu, K., et al. (2015). Quality control and reproducibility in M-mode, two-dimensional, and speckle tracking echocardiography acquisition and analysis: the CARDIA study, year 25 examination experience. *Echocardiography* 32, 1233–1240. doi: 10.1111/echo.12832

Bancks, M. P., Carnethon, M. R., Chow, L. S., Gidding, S. S., Jacobs, D. R. Jr., Kishi, S., et al. (2019a). Fasting glucose and insulin resistance trajectories during young adulthood and mid-life cardiac structure and function. *J. Diabetes Complicat.* 33, 356–362. doi: 10.1016/j.jdiacomp.2019.01.005

Bancks, M. P., Carson, A. P., Lewis, C. E., Gunderson, E. P., Reis, J. P., Schreiner, P. J., et al. (2019b). Fasting glucose variability in young adulthood and incident diabetes, cardiovascular disease and all-cause mortality. *Diabetologia* 62, 1366–1374. doi: 10.1007/s00125-019-4901-6

Boudina, S., and Abel, E. D. (2007). Diabetic cardiomyopathy revisited. *Circulation* 115, 3213–3223. doi: 10.1161/circulationaha.106.679597

BMJ (2012). Low eGFR and high albuminuria predict end stage kidney disease and death at all ages. *BMJ* 345:e7478. doi: 10.1136/bmj.e7478

Calles-Escandon, J., and Cipolla, M. (2001). Diabetes and endothelial dysfunction: a clinical perspective. *Endocr. Rev.* 22, 36–52. doi: 10.1210/edrv.22.1.0417

Carr, J. J., Nelson, J. C., Wong, N. D., Mcnitt-Gray, M., Arad, Y., Jacobs, D. R. Jr., et al. (2005). Calcified coronary artery plaque measurement with cardiac CT in population-based studies: standardized protocol of multi-ethnic study of atherosclerosis (MESA) and Coronary artery risk development in young adults (CARDIA) study. *Radiology* 234, 35–43. doi: 10.1148/radiol.2341040439

Ceriello, A., and Testa, R. (2009). Antioxidant anti-inflammatory treatment in type 2 diabetes. *Diabetes Care* 32(Suppl. 2), S232–S236.

Cosentino, F., Grant, P. J., Aboyans, V., Bailey, C. J., Ceriello, A., Delgado, V., et al. (2020). 2019 ESC Guidelines on diabetes, pre-diabetes, and cardiovascular diseases developed in collaboration with the EASD. *Eur. Heart J.* 41, 255–323.

De Simone, G., Wang, W., Best, L. G., Yeh, F., Izzo, R., Mancusi, C., et al. (2017). Target organ damage and incident type 2 diabetes mellitus: the Strong Heart Study. *Cardiovasc. Diabetol.* 16:64.

Detrano, R., Guerci, A. D., Carr, J. J., Bild, D. E., Burke, G., Folsom, A. R., et al. (2008). Coronary calcium as a predictor of coronary events in four racial or ethnic groups. *N. Engl. J. Med.* 358, 1336–1345. doi: 10.1056/nejmoa072100

Devereux, R. B., Roman, M. J., Paranicas, M., O'grady, M. J., Lee, E. T., Welty, T. K., et al. (2000). Impact of diabetes on cardiac structure and function: the strong heart study. *Circulation* 101, 2271–2276. doi: 10.1161/01.cir.101.19.2271

Donath, M. Y., and Shoelson, S. E. (2011). Type 2 diabetes as an inflammatory disease. *Nat. Rev. Immunol.* 11, 98–107.

Fox, C. S., Sullivan, L., D'agostino, R. B. Sr., and Wilson, P. W. (2004). The significant effect of diabetes duration on coronary heart disease mortality: the Framingham Heart Study. *Diabetes Care* 27, 704–708. doi: 10.2337/diacare.27.3.704

Friedman, G. D., Cutter, G. R., Donahue, R. P., Hughes, G. H., Hulley, S. B., Jacobs, D. R. Jr., et al. (1988). CARDIA: study design, recruitment, and some characteristics of the examined subjects. *J. Clin. Epidemiol.* 41, 1105–1116. doi: 10.1016/0895-4356(88)90080-7

Gerstein, H. C., Miller, M. E., Byington, R. P., Goff, D. C. Jr., Bigger, J. T., Buse, J. B., et al. (2008). Effects of intensive glucose lowering in type 2 diabetes. *N. Engl. J. Med.* 358, 2545–2559. doi: 10.1056/nejmoa0802743

Holman, R. R., Paul, S. K., Bethel, M. A., Matthews, D. R., and Neil, H. A. (2008). 10-year follow-up of intensive glucose control in type 2 diabetes. *N. Engl. J. Med.* 359, 1577–1589. doi: 10.1056/nejmoa0806470

Jennings, W., and Muniz, C. (2016). *Group-Based Trajectory Modeling*. Oxford: Oxford Handbooks.

Kim, J. J., Hwang, B. H., Choi, I. J., Choo, E. H., Lim, S., Kim, J. K., et al. (2015). Impact of diabetes duration on the extent and severity of coronary atheroma burden and long-term clinical outcome in asymptomatic type 2 diabetic patients: evaluation by Coronary CT angiography. *Eur. Heart J. Cardiovasc. Imaging* 16, 1065–1073. doi: 10.1093/ehjci/jev106

Kirkpatrick, J. N., Vannan, M. A., Narula, J., and Lang, R. M. (2007). Echocardiography in heart failure: applications, utility, and new horizons. *J. Am. Coll. Cardiol.* 50, 381–396.

Kishi, S., Gidding, S. S., Reis, J. P., Colangelo, L. A., Venkatesh, B. A., Armstrong, A. C., et al. (2017). Association of insulin resistance and glycemic metabolic abnormalities with LV structure and function in middle age: the CARDIA study. *JACC Cardiovasc. Imaging* 10, 105–114. doi: 10.1016/j.jcmg.2016.02.033

Kishi, S., Teixido-Tura, G., Ning, H., Venkatesh, B. A., Wu, C., Almeida, A., et al. (2015). cumulative blood pressure in early adulthood and cardiac dysfunction in middle age: the CARDIA study. *J. Am. Coll. Cardiol.* 65, 2679–2687. doi: 10.1016/j.jacc.2015.04.042

Lang, R. M., Badano, L. P., Mor-Avi, V., Afilalo, J., Armstrong, A., Ernande, L., et al. (2015). Recommendations for cardiac chamber quantification by echocardiography in adults: an update from the American Society of Echocardiography and the European Association of Cardiovascular Imaging. *J. Am. Soc. Echocardiogr.* 28, 1–39.e14.

Lee, C. L., Sheu, W. H., Lee, I. T., Lin, S. Y., Liang, W. M., Wang, J. S., et al. (2018). Trajectories of fasting plasma glucose variability and mortality in type 2 diabetes. *Diabetes Metab.* 44, 121–128. doi: 10.1016/j.diabet.2017.09.001

Mahinrad, S., Kurian, S., Garner, C. R., Sedaghat, S., Nemeth, A. J., Moscufo, N., et al. (2020). Cumulative blood pressure exposure during young adulthood and mobility and cognitive function in midlife. *Circulation* 141, 712–724. doi: 10.1161/circulationaha.119.042502

Medvedofsky, D., Maffessanti, F., Weinert, L., Tehrani, D. M., Narang, A., Addetia, K., et al. (2018). 2D and 3D echocardiography-derived indices of left ventricular function and shape: relationship with mortality. *JACC Cardiovasc. Imaging* 11, 1569–1579. doi: 10.1016/j.jcmg.2017.08.023

Nagin, D. S., and Odgers, C. L. (2010). Group-based trajectory modeling in clinical research. *Annu. Rev. Clin. Psychol.* 6, 109–138. doi: 10.1146/annurev.clinpsy.121208.131413

Nagueh, S. F., Smiseth, O. A., Appleton, C. P., Byrd, B. F. III, Dokainish, H., Edvardsen, T., et al. (2016). Recommendations for the evaluation of left ventricular diastolic function by echocardiography: an update from the american society of echocardiography and the european association of cardiovascular imaging. *J. Am. Soc. Echocardiogr.* 29, 277–314. doi: 10.1016/j.echo.2016.01.011

Naka, Y., Bucciarelli, L. G., Wendt, T., Lee, L. K., Rong, L. L., Ramasamy, R., et al. (2004). RAGE axis: animal models and novel insights into the vascular complications of diabetes. *Arterioscler. Thromb. Vasc. Biol.* 24, 1342–1349. doi: 10.1161/01.atv.0000133191.71196.90

Ogata, S., Watanabe, M., Kokubo, Y., Higashiyama, A., Nakao, Y. M., Takegami, M., et al. (2019). Longitudinal trajectories of fasting plasma glucose and risks of cardiovascular diseases in middle age to elderly people within the general japanese population: the suita study. *J. Am. Heart Assoc.* 8:e010628.

Patel, A., Macmahon, S., Chalmers, J., Neal, B., Billot, L., Woodward, M., et al. (2008). Intensive blood glucose control and vascular outcomes in patients with type 2 diabetes. *N. Engl. J. Med.* 358, 2560–2572. doi: 10.1056/nejmoa0802987

Potter, E., and Marwick, T. H. (2018). Assessment of left ventricular function by echocardiography: the case for routinely adding global longitudinal strain to ejection fraction. *JACC Cardiovasc. Imaging* 11, 260–274.

Raffield, L. M., Cox, A. J., Criqui, M. H., Hsu, F. C., Terry, J. G., Xu, J., et al. (2018). Associations of coronary artery calcified plaque density with mortality in type 2 diabetes: the diabetes heart study. *Cardiovasc. Diabetol.* 17:67.

Rossing, K., Christensen, P. K., Hovind, P., Tarnow, L., Rossing, P., and Parving, H. H. (2004). Progression of nephropathy in type 2 diabetic patients. *Kidney Int.* 66, 1596–1605.

Russo, C., Jin, Z., Elkind, M. S., Rundek, T., Homma, S., Sacco, R. L., et al. (2014). Prevalence and prognostic value of subclinical left ventricular systolic dysfunction by global longitudinal strain in a community-based cohort. *Eur. J. Heart Fail.* 16, 1301–1309. doi: 10.1002/ejhf.154

Sharp, A. S., Tapp, R. J., Thom, S. A., Francis, D. P., Hughes, A. D., Stanton, A. V., et al. (2010). Tissue doppler E/E' ratio is a powerful predictor of primary cardiac events in a hypertensive population: an ASCOT substudy. *Eur. Heart J.* 31, 747–752. doi: 10.1093/eurheartj/ehp498

UK Prospective Diabetes Study (UKPDS) Group (1998). Intensive blood-glucose control with sulphonylureas or insulin compared with conventional treatment and risk of complications in patients with type 2 diabetes (UKPDS 33). UK Prospective Diabetes Study (UKPDS) Group. *Lancet* 352, 837–853. doi: 10.1016/s0140-6736(98)07019-6

West, N. A., Hamman, R. F., Mayer-Davis, E. J., D'agostino, R. B. Jr., Marcovina, S. M., Liese, A. D., et al. (2009). Cardiovascular risk factors among youth with and without type 2 diabetes: differences and possible mechanisms. *Diabetes Care* 32, 175–180. doi: 10.2337/dc08-1442

Yeboah, J., Young, R., Mcclelland, R. L., Delaney, J. C., Polonsky, T. S., Dawood, F. Z., et al. (2016). Utility of nontraditional risk markers in atherosclerotic cardiovascular disease risk assessment. *J. Am. Coll. Cardiol.* 67, 139–147. doi: 10.1016/j.jacc.2015.10.058

Yuan, Z., Yang, Y., Wang, C., Liu, J., Sun, X., Liu, Y., et al. (2018). Trajectories of long-term normal fasting plasma glucose and risk of coronary heart disease: a prospective cohort study. *J. Am. Heart Assoc.* 7:e007607.

Conflict of Interest: The authors declare that the research was conducted in the absence of any commercial or financial relationships that could be construed as a potential conflict of interest.

Advantages of publishing in Frontiers

OPEN ACCESS
Articles are free to read for greatest visibility and readership

FAST PUBLICATION
Around 90 days from submission to decision

HIGH QUALITY PEER-REVIEW
Rigorous, collaborative, and constructive peer-review

TRANSPARENT PEER-REVIEW
Editors and reviewers acknowledged by name on published articles

Frontiers
Avenue du Tribunal-Fédéral 34
1005 Lausanne | Switzerland

Visit us: www.frontiersin.org
Contact us: frontiersin.org/about/contact

REPRODUCIBILITY OF RESEARCH
Support open data and methods to enhance research reproducibility

DIGITAL PUBLISHING
Articles designed for optimal readership across devices

FOLLOW US
@frontiersin

IMPACT METRICS
Advanced article metrics track visibility across digital media

EXTENSIVE PROMOTION
Marketing and promotion of impactful research

LOOP RESEARCH NETWORK
Our network increases your article's readership